Advances in Intelligent Systems and Computing 335

Kedar Nath Das · Kusum Deep
Millie Pant · Jagdish Chand Bansal
Atulya Nagar *Editors*

Proceedings of Fourth International Conference on Soft Computing for Problem Solving

SocProS 2014, Volume 1

Springer

Advances in Intelligent Systems and Computing

Volume 335

Series editor

Janusz Kacprzyk, Polish Academy of Sciences, Warsaw, Poland
e-mail: kacprzyk@ibspan.waw.pl

About this Series

The series "Advances in Intelligent Systems and Computing" contains publications on theory, applications, and design methods of Intelligent Systems and Intelligent Computing. Virtually all disciplines such as engineering, natural sciences, computer and information science, ICT, economics, business, e-commerce, environment, healthcare, life science are covered. The list of topics spans all the areas of modern intelligent systems and computing.

The publications within "Advances in Intelligent Systems and Computing" are primarily textbooks and proceedings of important conferences, symposia and congresses. They cover significant recent developments in the field, of both foundational and applicable character. An important characteristic feature of the series is the short publication time and world-wide distribution. This permits a rapid and broad dissemination of research results.

Advisory Board

More information about this series at http://www.springer.com/series/11156

Kedar Nath Das · Kusum Deep
Millie Pant · Jagdish Chand Bansal
Atulya Nagar
Editors

Proceedings of Fourth International Conference on Soft Computing for Problem Solving

SocProS 2014, Volume 1

Springer

Editors
Kedar Nath Das
Department of Mathematics
National Institute of Technology Silchar
Silchar, Assam
India

Jagdish Chand Bansal
Department of Mathematics
South Asian University
New Delhi
India

Kusum Deep
Department of Mathematics
Indian Institute of Technology Roorkee
Roorkee
India

Atulya Nagar
Department of Computer Science
Liverpool Hope University
Liverpool
UK

Millie Pant
Department of Paper Technology
Indian Institute of Technology Roorkee
Roorkee
India

ISSN 2194-5357 ISSN 2194-5365 (electronic)
Advances in Intelligent Systems and Computing
ISBN 978-81-322-2216-3 ISBN 978-81-322-2217-0 (eBook)
DOI 10.1007/978-81-322-2217-0

Library of Congress Control Number: 2014957312

Springer New Delhi Heidelberg New York Dordrecht London

Printed on acid-free paper

Springer (India) Pvt. Ltd. is part of Springer Science+Business Media (www.springer.com)

Preface

SocProS, which stands for 'Soft Computing for Problem Solving', is entering its fourth edition as an established and flagship international conference. This particular annual event is a joint collaboration between a group of faculty members from institutes of repute like NIT Silchar, IIT Roorkee, South Asian University, Delhi and Liverpool Hope University, UK.

The first in the series of SocProS started in 2011 and was held from 20 to 22 December at the IIT Roorkee Campus with Prof. Deep (IITR) and Prof. Nagar (Liverpool Hope University) as the General Chairs. JKLU Jaipur hosted the second SocProS from 28 to 30 December 2012. Coinciding with the Golden Jubilee of the IIT Roorkee's Saharanpur Campus, the third edition of this international conference, which has by now become a brand name, took place at the Greater Noida Extension Centre of IIT Roorkee during 26–28 December 2013.

Like earlier SocProS conferences, the focus of SocProS 2014 is on Soft Computing and its applications to real-life problems arising in diverse areas of medical and healthcare, supply chain management, signal processing and multimedia, industrial optimisation, image processing, cryptanalysis, etc. SocProS 2014 attracted a wide spectrum of thought-provoking articles. A total of 103 high-quality research papers were selected for publication in the form of this two-volume proceedings.

We hope that the papers contained in this proceeding will prove helpful towards improving the understanding of Soft Computing at the teaching and research levels and will inspire more and more researchers to work in the field of Soft Computing.

The editors express their sincere gratitude to the SocProS 2014 Patron, Plenary Speakers, Invited Speakers, Reviewers, Programme Committee Members, International Advisory Committee, and Local Organizing Committee; without whose support, the quality and standards of the Conference could not be maintained. We express special thanks to Springer and its team for this valuable support in the publication of this proceedings.

Over and above, we express our deepest sense of gratitude to 'National Institute of Technology (NIT) Silchar' for facilitating the hosting of this conference. Our sincere thanks to all the sponsors of SocProS' 2014.

Silchar, India — Kedar Nath Das
Roorkee, India — Kusum Deep
Roorkee, India — Millie Pant
New Delhi, India — Jagdish Chand Bansal
Liverpool, UK — Atulya Nagar

Contents

About the Editors

Dr. Kedar Nath Das is now working as an Assistant Professor in the Department of Mathematics, National Institute of Technology Silchar, Assam, India. Over the last 10 years, he has contributed immensely towards research in 'soft computing'. He has many papers to his credit in national and international journals of repute. His areas of interest include Evolutionary and Bio-inspired algorithms for optimization.

Prof. Kusum Deep is working as a Full-time Professor in the Department of Mathematics, Indian Institute of Technology Roorkee, Roorkee, India. Over the last 25 years, her research is increasingly well-cited making her a central International figure in the area of Nature Inspired Optimization Techniques, Genetic Algorithms and Particle Swarm Optimization.

Dr. Millie Pant is an Associate Professor at the Department of Paper Technology, Indian Institute of Technology Roorkee, Roorkee, India. She has to her credit several research papers in journals of national and international repute and is a well-known figure in the field of Swarm Intelligence and Evolutionary Algorithms.

Dr. Jagdish Chand Bansal is an Assistant Professor with the South Asian University, New Delhi, India. Holding an excellent academic record, he is an excellent researcher in the field of Swarm Intelligence at the national and international level, having several research papers in journals of national and international repute.

Prof. Atulya Nagar holds the Foundation Chair as Professor of Mathematical Sciences and is the Dean of Faculty of Science, at Liverpool Hope University, Liverpool, UK. Professor Nagar is an internationally recognised scholar working at the cutting edge of theoretical computer science, applied mathematical analysis, operations research and systems engineering and his work is underpinned by strong complexity-theoretic foundations.

Solving 0/1 Knapsack Problem Using Hybrid TLBO-GA Algorithm

A.J. Umbarkar, P.D. Sheth and S.V. Babar

Abstract The 0/1 knapsack problem is attempted to solve using various soft computing methods till date. This paper proposes hybrid TLBO-GA algorithm which is hybrid of teaching learning-based optimization (TLBO) algorithm with genetic algorithm (GA). The 0/1 knapsack problem is a combinatorial optimization problem. The 0/1 knapsack problem aims to maximize the benefit of objects in a knapsack without exceeding its capacity as a constraint. In the literature, it is found that TLBO works for real-coded or real-valued problems. Hybrid TLBO-GA combines evolutionary process of TLBO and binary chromosome representation of GA for solving the knapsack problem (KP). Hybrid TLBO-GA combines advantages of both TLBO and GA. Results are taken on random as well as standard date sets using hybrid TLBO-GA for 0/1 knapsack problem. Hybrid TLBO-GA results are compared with the results obtained using simple genetic algorithm (SGA) on the same data sets. The results obtained using hybrid TLBO-GA are found satisfactory.

Keywords Function optimization · Teaching learning-based optimization · TLBO · Knapsack problem · Genetic algorithm

1 Introduction

0/1 knapsack problem is a non-deterministic polynomial (NP) problem [1] with ample significance in practical life. It has high economic value. The decision function problems such as goods dispatching problems and containers loading

A.J. Umbarkar (✉) · P.D. Sheth · S.V. Babar
Department of Information Technology, Walchand College of Engineering, Sangli, Maharashtra, India
e-mail: anantumbarkar@rediffmail.com

P.D. Sheth
e-mail: pranalisheth@gmail.com

S.V. Babar
e-mail: sonalikababarvh@gmail.com

K.N. Das et al. (eds.), *Proceedings of Fourth International Conference on Soft Computing for Problem Solving*, Advances in Intelligent Systems and Computing 335,
DOI 10.1007/978-81-322-2217-0_1

problems have knapsack problem generically. This problem was proved to be NP-complete. Its original search space has $2n$ possible values, and therefore, an exhaustive search would take $O(2n)$ time to find a solution in the worst case. Solving the knapsack problem can be seen as a way to study some large problems in number theory as well. Its high exponential complexity allows to be getting used into some public-key cryptosystem. Therefore, much effort has been made in order to find the techniques which could lead to practical algorithms with reasonable running times. Followed by extensive survey for solving combinatorial optimization problem using various algorithms, it is decided to explore its application area based on existing meta-heuristic model.

TLBO algorithm searches good solutions to the problem among a large number of possible solutions. TLBO was proposed by R.V. Rao et al. in 2011 [2, 3]. It works on the philosophy of teaching and learning. This mechanism is well suited to resolve a variety of practical problems and computational problems in other fields such as optimization, manufacturing, machine learning, economics, social system, and so on.

The literature of TLBO has shown that it is well suited for high-quality solutions to NP problems. It is the most efficient way for finding an approximate optimal solution for optimization problems [2, 3].

This paper proposes hybrid TLBO-GA algorithm to solve the 0/1 knapsack problem. Several experiments are carried out on the random data set and standard data set to test the performance of the proposed algorithm.

2 Hybrid TLBO-GA

TLBO begins with a set of candidate solutions called population. A new population is created from the solutions of an old population for getting better candidate solutions in new population. Candidate parents are chosen according to their fitness value to produce solutions in the next generation. Each time, heuristic factor of TLBO, i.e., teacher factor, is added to the old solution to get a better solution. This process is repeated until a particular condition is satisfied.

TLBO is based on elements populations (P_old), fitness function ($F(x)$), teacher factor (TF), difference factor (Df), design variables (X), mean value (P_Mean), best solution (P_Best), and random value (r). TF is a teacher factor that decides the value of the mean to be changed. The value of TF can be either 1 or 2 which is again a heuristic step and decided randomly with equal probability as given in Eq. (1) [2, 3].

$$\mathrm{TF} = \mathrm{round}[1 + \mathrm{rand}(0, 1)\{2 - 1\}] \tag{1}$$

TLBO requires a fitness function to calculate fitness of each individual solution in the current population. Random value (r) is a value between 0 and 1. Mean value

Fig. 1 Outline of basic TLBO

Procedure TLBO
Start: Randomly generate a population of size N.
Teacher_Phase
1. Calculate Mean
2. Calculate Difference factor
3. Find Best Solution
4. Create New Population
5. Calculate Fitness
6. Replace the current population with the new population.

Learner_Phase
1. Create New Population
2. Compare Fitness
3. Replace the current population with the new population.

Test:
Test whether the end condition is satisfied. If yes, stop. If no, return to the best solution in current population and go to the Teacher Phase again.
End

(P_Mean) provides mean of the solutions obtained during each run of the algorithm. P_Mean is calculated by using Eq. (2) [2, 3].

$$\text{P\_Mean} = \frac{\text{Sum of all the solutions in the populations}}{\text{Population size}} \tag{2}$$

The solution is updated by difference factor (Df) according to the difference between the existing and the new mean. Df is calculated by using the Eq. (3) [2, 3].

$$\text{Df} = r * (\text{P\_Best} - (\text{Tf} * \text{P\_Mean})) \tag{3}$$

Figure 1 shows the outline of basic TLBO algorithm. The knapsack problem is combinatorial as well as decision problem. Therefore, initial population must contain the selected as well as the rejected items. Thus, binary string representation is perfectly suitable for the representation of candidate solutions of population. The basic TLBO in Fig. 1 is modified to hybrid TLBO-GA, and its algorithm is explained in Fig. 2 (The flow chart of TLBO-GA is given in Fig. 3).

3 Implementation of the 0/1 KP Using hybrid TLBO-GA

3.1 Representation of the Items

Items	0	1	2	3
	20|30	5|10	10|20	40|50

Fig. 2 Hybrid TLBO-GA algorithm

```
Algorithm: Hybrid TLBO-GA
Begin
    g = 0
    Initialize_Population (P, pop_size)
    Evaluate(P) {Calculate_Fitness(P)}
    Repeat
    {Teacher Phase}
    Calculate Tf
    Xmean = Calculate_Mean_Vector(P)
    Xteacher = Best_Solution(P)
    Difference_Vector =  (Xteacher OR Xmean))
    P_New_i = (P_old_i )X-OR Difference_Vector
    Evaluate(P_New) {Calculate_Fitness(P)}
     If P_New_i better than Xold_i
                then{Compare_Fitness(P)}
                P_old_i = P_New_i
    end if
    {End of Teacher Phase}
    {Learner Phase}
    Randomly select 2 solutions i.e. X_i, X_j{X_i≠X_j }
    If X_i better than X_j
     then
                P_New_i = (X_i OR X_j)
    else
                P_New_i= (X_i X-OR X_j)
    end if
    Evaluate(P_New_i) {Calculate_Fitness()}
    If P_New_ibetter than P_old_i
                then {Compare_Fitness()}
                P_old_i = P_New_i
    end if
    {End of Learner Phase}
    g = g + 1
    until(g≠num_gen)
    {Termination_Condition}
    Print_Best_Result(P)
End
```

3.2 Solution or Population Representation

A solution in population can be represented as an array having size equal to the number of items (in our example of size 4). Each element of the array denotes whether an item is included in the knapsack (‘1’) or not (‘0’). For example, the following solution indicates that the 1st and the 4th items are included in the knapsack.

0	1	2	3
1	0	0	1

3.3 Termination Conditions

The algorithm terminates, when an optimal solution is found or after the given predefined number of generations.

3.4 Fitness Function

It calculates the fitness of each solution by summing the benefits of the items that are added in the knapsack, while checking the constraint of the capacity of the knapsack. If the volume of the solution is greater than the capacity of the knapsack, then we ignore that solution and create a new solution again.

4 Knapsack Problem

Knapsack problem (KP) seeks for a best solution from among many other solutions. It is a combinatorial optimization problem. Knapsack problem can be explained as for given some items, the knapsack is packed to get the maximum total value. Each item has some weight and some value. Formulation of KP is given in Eq. 4. Total weight that we can carry is no more than some fixed capacity W. The problem is to find

$$\begin{aligned} &\text{Max} \sum_{i \in T} b_i \\ &\text{subject to} \sum_{i \in T} w_i \leq W \end{aligned} \tag{4}$$

where w_i is weight and b_i is benefit of ith item.

Example of a 0/1 KP
Suppose there is a knapsack of capacity ($W = 13$) and there are several items of different sizes and different benefits. The knapsack is supposed to put items that are high in total

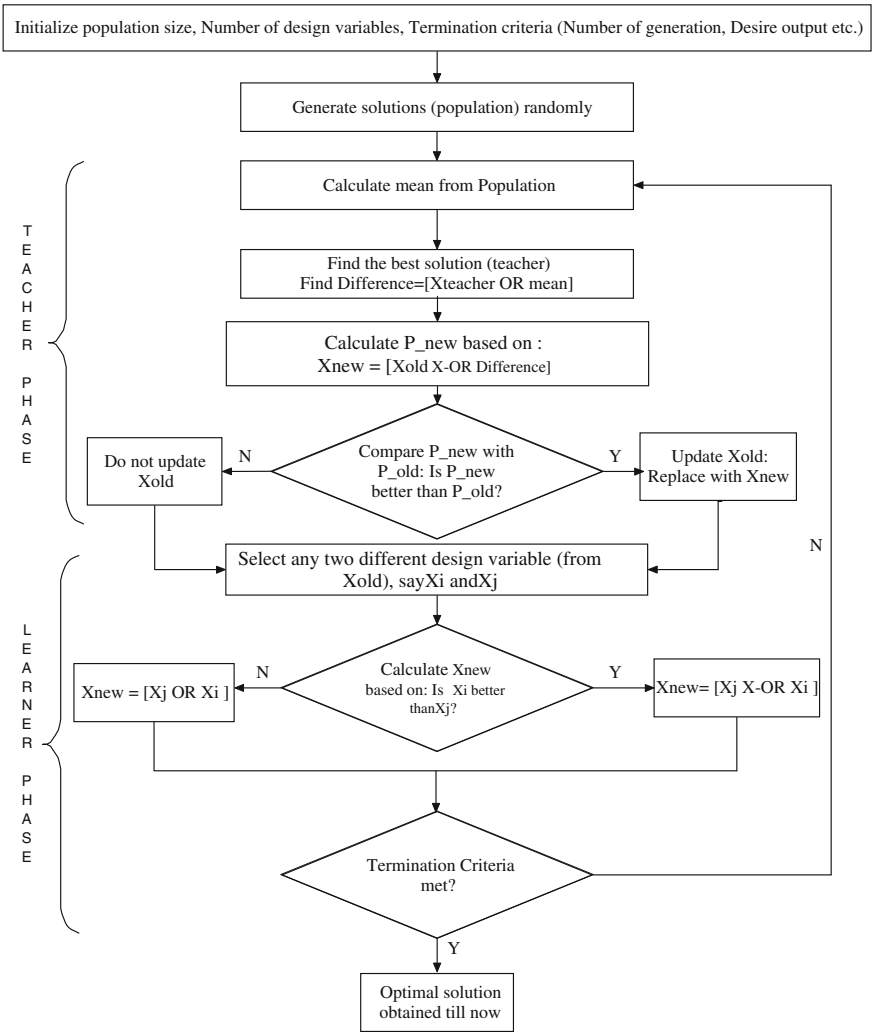

Fig. 3 Flowchart of hybrid TLBO-GA for solving 0/1 knapsack problem

benefit within the constraints on the capacity of the knapsack. There are three potential items labeled A, B, and C. The volumes and benefits of KP are as follows:

Item	A	B	C
Benefit	4	3	5
Volume	6	7	12

Table 1 Possible solutions for the example problem

A	B	C	Volume of the set	Benefit of the set
0	0	0	0	0
0	*0*	*1*	*8*	*5*
0	*1*	*0*	*7*	*3*
0	1	1	15	–
1	*0*	*0*	*6*	*4*
1	0	1	14	–
1	*1*	*0*	*13*	*7*
1	1	1	21	–

We aim to maximize the total benefit:

$$\sum BiXi = 4X1 + 3X2 + 5X3 \tag{5}$$

Subject to the constraints:

$$\begin{aligned} &\sum ViXi = 4X1 + 3X2 + 5X3 \\ &X_i \in \{0, 1\}, \quad \text{for } i = 1, 2, \ldots, n \end{aligned} \tag{6}$$

In order to find the best solution, it requires identifying a subset that meets the constraints and has the maximum total benefit. Only rows given in italics in Table 1 satisfy the constraint. The optimal benefit for the given constraint ($W = 13$) can only be obtained by selecting one quantity of A, one quantity of B, and zero quantity of C, and it is 7.

5 Results and Discussion

The algorithm is implemented in Java on Intel Dual-Core CPU 2.80 GHz with 1 GB of main memory and 150 GB hard disk.

5.1 Random Data Set (Data Set 1)

Results are taken using random data set. The random data are generated using random number generator on test machine. These randomly generated numbers become weight and benefit of every object. They act as input to the knapsack algorithm. The randomly generated data are as follows:

Weights = {14, 29, 13, 36, 15, 19, 33, 36, 13, 36, 36, 31, 43, 26, 16, 16, 23, 30, 24, 27}
Benefits = {19, 19, 11, 11, 11, 4, 11, 15, 18, 14, 2, 15, 9, 14, 9, 3, 7, 14, 8, 6}

5.2 Standard Data Set (Data Set 2)

Standard data set 1 for solving 0/1 knapsack problem is taken from [4].

Weights = {135, 139, 149, 150, 156, 163, 173, 184, 192, 201, 210, 214, 221, 229, 240}
Benefits = {70, 73, 77, 80, 82, 87, 90, 94, 98, 106, 110, 113, 115, 118, 120}.

5.3 Standard Data Set (Data Set 3)

Standard data set 3 for solving 0/1 knapsack problem is taken from [5].

Weights = {56, 59, 80, 64, 75, 17}
Benefits = {50, 50, 64, 46, 50, 5}

Experimentation of hybrid TLBO-GA algorithm is carried on three on different data sets. The results taken on three data sets are shown in Tables 2, 3, and 4, respectively.

Table 2 Parameter settings and results for random data set 1

Parameter settings for random data				
Dimension	20	Capacity 400	Population size	20
Standard benefit	200		Generation No.	50
Knapsack benefit and weight				
S. No.	Weight	Benefit		
1	385	178		
2	375	153		
3	324	146		
4	356	167		
5	390	164		
6	324	169		
7	347	167		
8	386	147		
9	347	150		
10	380	173		
Statistical analysis				
Benefit	SGA [6]	Hybrid TLBO-GA		
Mean	193.10	161.40		
SD	6.43	10.87		
SEM	2.03	3.43		

Table 3 Parameter settings and results for standard data set 2

Parameter settings for random data				
Dimension	15	Capacity 750	Population size	20
Standard benefit	395		Generation No.	50
Knapsack benefit and weight				
S. No.	Weight	Benefit		
1	745	391		
2	747	393		
3	750	389		
4	746	390		
5	743	392		
6	747	391		
7	748	390		
8	748	395		
9	747	393		
10	749	390		
Statistical analysis				
Benefit	SGA [6]		Hybrid TLBO-GA	
Mean	394.70		391.40	
SD	0.67		1.7435	
SEM	0.15		0.5513	

Table 4 Parameter settings and results for standard data set 3

Parameter settings for random data				
Dimension	6	Capacity 190	Population size	20
Standard benefit	150		Generation No.	50
Knapsack benefit and weight				
S. No.	Weight	Benefit		
1	190	150		
2	190	150		
3	190	150		
4	190	150		
5	190	150		
6	190	150		
7	190	150		
8	190	150		
9	190	150		
10	190	150		
Statistical analysis				
Benefit	SGA [6]		Hybrid TLBO-GA	
Mean	142.60		150	
SD	12.57		0	
SEM	3.97		0	

From the experimental results, it is observed that the mean value obtained for knapsack benefit using hybrid TLBO-GA algorithm is better for data set 3 over the mean value obtained using SGA.

6 Conclusion

The paper proposes hybrid TLBO-GA for solving 0/1 knapsack problem. Hybrid TLBO-GA can be successfully applied to problems where the candidates are represented in binary format. Proposed algorithm gives satisfactory solutions compared to solutions shown by simple genetic algorithm (SGA). The experimentation shows that though the TLBO algorithm works on real coding, it can also be suitable to solve problems in which representation of solution is binary. In future scope, the hybrid TLBO-GA could improve performance by selecting good population for hybrid TLBO-GA algorithm.

References

1. Hristakeva, M., Shrestha, D: Solving the 0-1 knapsack problem with genetic Algorithms. In: Proceedings of the 37th Midwest Instruction and Computing Symposium, Morris, MN (2004)
2. Rao, R., Savsani, V., Vakharia, D.: Teaching–learning-based optimization: a novel method for constrained mechanical design optimization problems. Comput. Aided Des. **43**(3), 303–315 (2011)
3. Rao, R.V., Savsani, V.J., Vakharia, D.P.: Teaching–learning-based optimization: an optimization method for continuous non-linear large scale problems. Inf. Sci. **183**(1), 1–15 (2012)
4. KNAPSACK_01—Data for the 01 knapsack problem. http://people.sc.fsu.edu/~jburkardt/datasets/knapsack_01/p07_c.txt. 8 Sept 2014
5. https://github.com/jkdeveyra/CMSC-170-KnapsackGA/tree/master/src/main/java/dataset. 12 Aug 2013
6. Umbarkar, A., Joshi, M.: 0/1 knapsack problem using diversity based dual population genetic algorithm. Int. J. Intell. Syst. Appl. (IJISA) **6**(10), 34–40 (2014). doi:10.5815/ijisa.2014.10.05

Cluster Head Selection Using Modified ACO

Varsha Gupta and Shashi Kumar Sharma

Abstract WSNs have limited computation power, battery life, and memory resources. In this paper, an approach is introduced to selection cluster head by using swarm intelligence. This proposed approach is based on LEACH clustering algorithm. Modified version of ant colony optimization by using residual energy as a parameter is employed over LEACH algorithm for effective cluster head selection. This approach reduces the amount of energy consumption. The proposed technique work in three stages: Cluster members transmit their data directly to their cluster heads, cluster heads transmit their data to leader, and leader transmits data to the base station. The result shows that LEACH-MA algorithm improves the average energy consumption effectively.

Keywords LEACH · ACO · Pheromone · Sensors

1 Introduction

A wireless sensor network (WSN) is a large collection of tiny self-aware, analyzable sensor devices that can perceive environmental parameters and detecting emergency events in various different applications. The three key elements of WSN, i.e., monitoring, computing, and communication whose combination in one sensor device provides ample number of remote sensing applications [1, 2]. Due to its vast and distinguishable applications, efficient design and implementation of WSNs [3, 4] makes it an influential area of research. In sensor network, there are three main components which are the sink, monitored events, and sensor nodes from a few to

V. Gupta (✉) · S.K. Sharma
Department of Computer Science and Engineering, Graphic Era Hill University, Dehradun, India
e-mail: varsha.gupta647@gmail.com

S.K. Sharma
e-mail: 12sksharma@gmail.com

K.N. Das et al. (eds.), *Proceedings of Fourth International Conference on Soft Computing for Problem Solving*, Advances in Intelligent Systems and Computing 335,
DOI 10.1007/978-81-322-2217-0_2

several hundreds or even more than hundreds. Due to mobility of node, routing of data becomes more challenging since stability of route is more important factor, in addition to energy, bandwidth, etc. A sensor network device consists of different components: a radio transceiver with an internal and an external antenna, a memory unit, an electronic circuit for interfacing with the sensors and a power source, and generally a lithium (Li-ion) battery which is non-renewable. A sensor node may change in size and cost, depending on the complexity and some factor such as energy, memory, computational speed, and communications bandwidth of the individual sensor nodes.

Base station provides strong processing unit and storage capacity, and it acts as an access point to each sensor node in the network. The aim of WSN is to sense environment, collect data, and communicate that data to the base station or sink node. The remaining paper is distributed as follows: Sect. 2 described related work, Sect. 3 explained the background, Sect. 4 discussed proposed algorithm and its implementation, and Sect. 5 presented simulations and results analysis, and conclusions are provided in the last section.

2 Related Work

Numbers of important issues are related to develop low power wireless sensor application, i.e., using available energy in the most efficient way, without compromising performance [5]. Sensor nodes use batteries as power source and have quite limited lifetime. So efficiency of energy management becomes a key requirement in wireless sensor network design [6]. Due to the nodes of WSN have limited power constrain and WSN are deployed in challenging conditions, a radio device is employed for wireless communication to transmission of data to sink node [1]. The routing protocols in sensor networks could be classified into three categories: flat-based, hierarchical-based, and location-based routing. LEACH protocol is grouped in hierarchical routing approaches of wireless sensors networks [7]. LEACH [8] protocol is an organizing, by itself, robust clustering protocol [7]. LEACH is the earliest proposed single-hop cluster routing protocol in WSN; it can save network energy greatly compared with the non-cluster routing algorithm [9]. The effectiveness of LEACH protocol in cluster head selection is not optimized because of the probability model. An improved clustering algorithm is proposed which takes node's residual energy and location information into account, optimizes the selection method of the threshold for electing cluster head, and improves optimal cluster head selection strategy, that is, normal nodes select the effective cluster head on the basis of cost function [9]. If the number of cluster heads can be optimized, the energy consumption of the sensor nodes can be more evenly distributed in the WSNs. It can avoid extra energy consumption of single node to untimely death, which directly affects the network life cycle [10]. Ant colony algorithms (ACOs) are speculative procedures for searching. The essential component of ACO is the pheromone model, which is used to equally sample the search

space [11]. Ant colony algorithm is applied on routing mechanism for finding the best path from cluster heads to base station by which the energy consuming of cluster heads node was decreased [12]. Applying the concept of an enhanced ant colony in WSNs, for finding the optimal paths from the source nodes to the base station, where each node maintains its probabilistic routing table, because of that, it also called as pheromone tables [13]. On the basis of the death of first node, ant colony applied on LEACH protocol in the WSN [14]. Proposed algorithm is dedicated to the survival of the network lifetime, which affects the performance of LEACH protocols in terms of energy consumption.

3 Background

3.1 Ant Colony Algorithm

The basic concept of ACO [11] is taken from the behavior of real ants. Initially, each ant traverses the area surrounding their ant hill in random manner while searching for food. When ant finds a food source, then they estimate the quantity and the quality of the food and carry some of food back. While going back to their ant hill, each ant deposits a chemical pheromone on the path. The amount of pheromone is deposited, which may depend on the quantity and quality of the food. This pheromone amount will guide other ants to find the food source. As a result of this phenomenon, the optimal solution derives rapidly [13]. By using this behavior of the ants, optimal cluster head can be selected.

3.2 Network Environment

A sensor network can be considered as a directed graph G(V,E), where V is the set of sensors nodes and E is the set of path connecting nodes in the network.

In this paper, the number of assumptions is adopted which are given below:

1. 100 sensor nodes are uniformly distributed within a monitoring area. Each sensor nodes has its unique identification.
2. All sensor nodes are static, or there is less mobility factor after being deployed.
3. The sensor nodes energy is non-renewable.
4. Sensor nodes are unaware from their exact location; there should not be any computation for finding the location.
5. Data transmission is performing on a node-to-node link.

4 Implementation and Proposed Algorithm

Using the concept of ant colony algorithm in WSNs, each node calculates its probability by using the pheromone to be elected as a cluster head.

In this section of paper, the basic idea of proposed algorithm is summarized. Initially, modified ant colony optimization is explained, and then, proposed LECH-MA algorithm is described.

4.1 Modified Ant Colony Algorithm

As explained in Sect. 1, wireless sensors devices are power constraint, i.e., the cluster head selections should be determined not only in terms of probability, but also in terms of the power and distance between node and the base station. For an instance, it would be preferable to choose a longer distance node with high energy than a shorter distance node with very low energy.

According to proposed algorithm, the working of ants is given below: First of all, each ant selects its next cluster head on the basis of initial rule, and then, each ant elects the optimal cluster head by the use of revising rule.

1. Initial rule:
   Suppose the ant is placed on cluster head node i, the probability of an ant choosing the next node j as cluster head according to Eqs. (1) and (2):

$$\mathrm{Prob_i}(t) = \frac{\mathrm{dist_i} * \alpha + [ph_i(t)] * \beta}{\sum_{1=0}^{N_i} \mathrm{dist_i} * \alpha + [ph_i(t)] * \beta} \tag{1}$$

   where

   Prob_i gives the probability of each node to be selected as a cluster head;
   dist_i is the distance of node.

$$\mathrm{ph}_i = \frac{\tau_{i.j}^{\alpha} * [\eta_i(t)]^{\beta}}{\sum_{1=0}^{N_i} \tau_{i.j}^{\alpha} * [\eta_i(t)]^{\beta}} \tag{2}$$

   $\tau_{ij}\ (t)$ is the pheromone intensity;
   N_i is set of nodes in the cluster;
   α and β are control parameters; and
   η_{ij} is a heuristic function, and it can be defined as Eq. (3)

$$\eta_i = \frac{1}{I\mathrm{e} - e} \tag{3}$$

where

I_e is the initial energy level of the nodes;

e is the actual energy level of nodes. This enables an ant to make a decision according to residual energy that means if a node has a low power, then it has low probability to be chosen as the head of cluster

2. Revising Rule:

When ants traverse in search of next possible cluster head, the amount of pheromone on the elected node $\tau_{i,j}$ (t) is revised according to Eq. (4).

$$\tau_{i,j}(t+1) = (1-\rho)\tau_{i,j}(t) + \rho\Delta\tau_{i,j}(t) \tag{4}$$

where

ρ is the parameter for the local pheromone corrosion;

$\Delta\tau_{ij}$ (t) is pheromone enhancement.

4.2 Description of LEACH-MA

Proposed algorithm low energy adaptive cluster hierarchy routing based on modified ACO (LEACH-MA) is improvement over LEACH protocol. LEACH uses a probability model for taking the decision of cluster head selection. In proposed approach, the distances as well as energy as parameters are combined to judge an effective cluster head on dual stage.

The proposed algorithm has the following steps:
For each round:

1. According to LEACH [8], CHs and the CNs are selected from each cluster.
2. Each node has to calculate its pheromone value that depends on the energy of the node and find the probability which depends on the pheromone and the distance to chosen as CH.
3. Update final set of cluster heads on the basis of comparison between the probability and threshold factor of CH and the CNs of the cluster.
4. Update pheromone value of selected CHs.
5. TDMA schedule is assigned to each node by its CHs, assigned time schedule is used to transfer the data from CNs to CHs.
6. Find maximum probability of CHs and select CH as CH Leader.
7. CH sends data to their CH leader.
8. CH leader transmitted data to the sink node.

5 Analysis of Simulations Results

In this section, we have discussed the analysis of simulations results.

5.1 Simulation Environment

The proposed algorithm is simulated using MATLAB.

The simulation is tested for random 100 node network. The location of base station was selected at (50,175) in network.

The reference network used in simulation has 100 nodes, in a 10 × 10 square field. Each node has 0.5 J of initial energy. The packet size is 2,000 bits, and 0.05 % of the nodes are selected as cluster heads.

5.2 Simulation Results

To prove the advantage of the proposed algorithm, we have compared it with LEACH. The results of simulation for the system lifetime and energy consumption as a function of round are shown in Figs. 1 and 2. Table 1 shows the comparison of lifetime of both approaches, and Table 2 shows the comparison of energy consumption by using both algorithms (Figs. 3 and 4).

The proposed approach proved that slow energy consumption of the network and it increases the lifetime of the network.

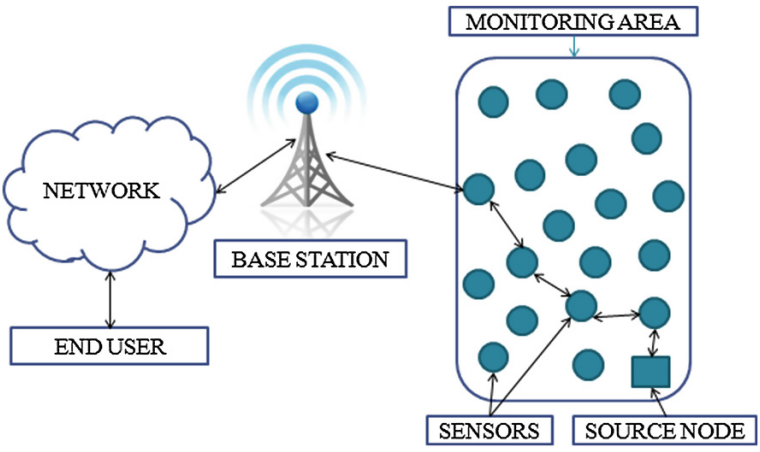

Fig. 1 Architecture of WSN

Fig. 2 Flow diagram

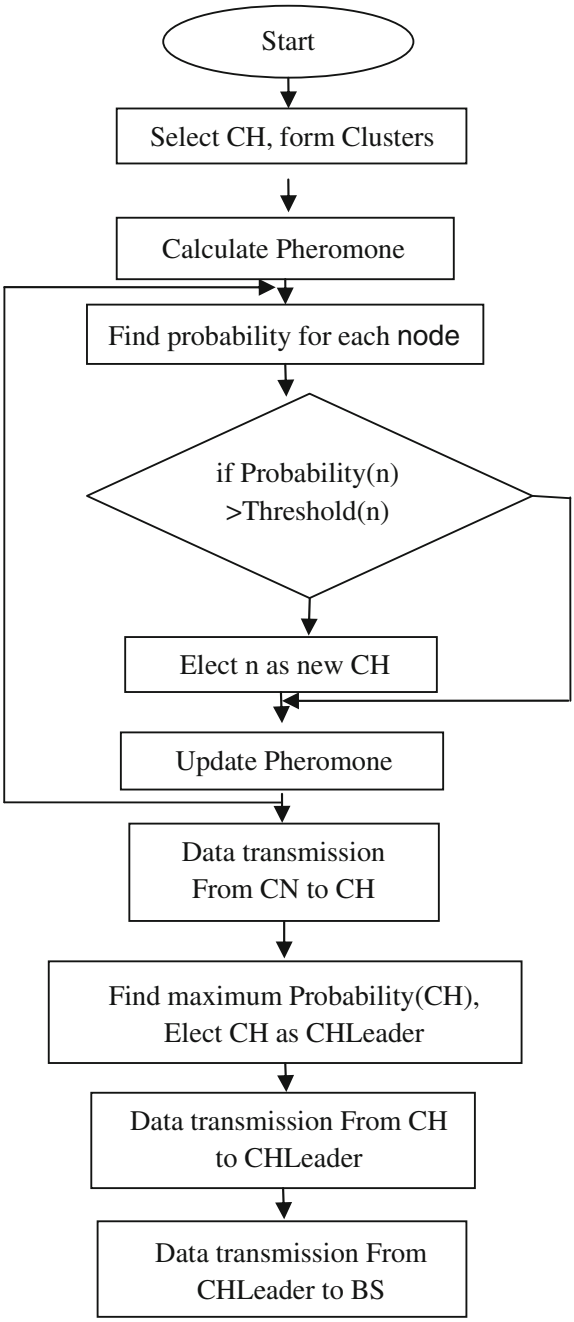

Table 1 Lifetime of network

Methodologies	Number of rounds		
	First node die	Half node die	Last node die
LEACH	55	165	230
LEACH-MA	100	260	345

Table 2 Energy consumption

Methodologies	Number of rounds
LEACH	225
LEACH-MA	280

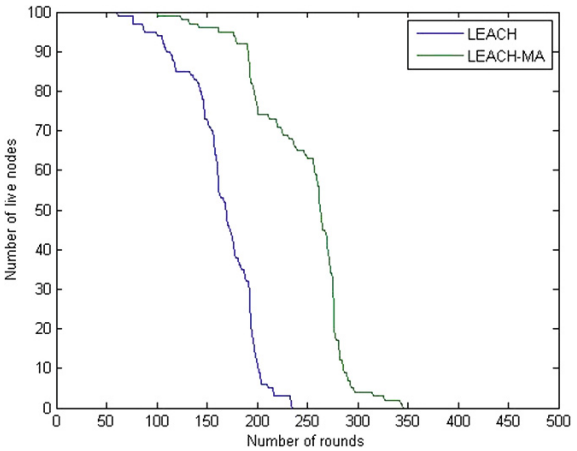

Fig. 3 Comparison between numbers of live nodes versus number of rounds in terms of network lifetime

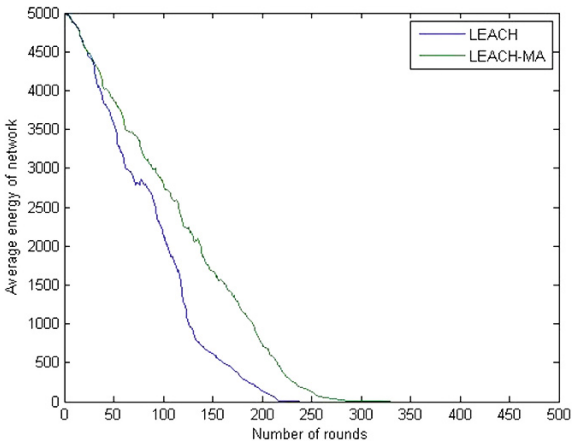

Fig. 4 Comparison of average energy of network versus number of rounds the energy consumption

6 Conclusion and Future Work

On the basis of LEACH protocol, this paper proposes a modified ant-based cluster head selection algorithm for effective cluster head selection on dual phase. This algorithm considers the residual energy and distance factors as parameters, to improve cluster head selection. The main goal of LEACH-MA is to enhance network lifetime as well as to improve the power consumption of the network. Simulation results show that LEACH-MA is more energy efficient than LEACH. As the WSN has data redundancy, how to design and realize routing protocol with optimal data aggregation will be our future research work.

Acknowledgments We heartily thankful to Suryakant, Ritu Yadav, and Shilpi Saxena for their valuable time that they spent with us in discussion of subjects strictly related to this paper. Additionally, we wish to thanks our member of family for their moral and mental support.

References

1. Akyildiz, I.F., Su, W., Sankarasubramaniam, Y., Cayirci, E.: A survey on sensor networks. IEEE Commun. Mag. **40**(8), 102–114 (2002)
2. Puccinelli, D., Haenggi, M.: Wireless sensor networks: applications and challenges of ubiquitous sensing. IEEE Circ. Syst. Mag. **5**(3), 19–31 (2005)
3. Hac, A.: Wireless Sensor Network Designs. Wiley, New York (2003)
4. Raghavendra, C., Sivalingam, K.M., Znati, T.: Wireless Sensor Networks. Springer, Berlin (2006)
5. Srivastava, N.: Challenges of next-generation wireless sensor networks and its impact on society. J. Telecommun. **1**(1), 128–133 (2010)
6. Tang, C.: Comprehensive energy efficient algorithm for WSN. Int. J. Comput. Commun. 9 (2):209–216. ISSN 1841-98369 (2014)
7. Khan, A.G., Rahman, A., Bisht, N.: Classification of hierarchical based routing protocols for wireless sensor networks. In: International Journal of Innovations in Engineering and Technology, ISSN: 2319-1058 (Special Issue ICAECE-2013)
8. Heinzelman, W.R., Chandrakasan, A., Balakrishnan, H.: Energy-efficient communication protocol for wireless microsensor networks. In: Proceedings of the 33rd Hawaii International Conference on System Sciences, vol. 8, p. 8020. Citeseer (2000)
9. Liao, Q., Zhu, H.: An energy balanced clustering algorithm based on LEACH protocol. In: Proceedings of the 2nd International Conference on Systems Engineering and Modeling (ICSEM-13) (2013)
10. Chen, H., Zhang, C., Zong, X., Wang, C.: LEACH-G: an optimal cluster-heads selection algorithm based on LEACH. J. Soft. **8**(10), 2660–2667 (2013)
11. Dorigo, M., Blum, C.: Ant colony optimization theory: a survey. Theoret. Comput. Sci. **344**, 243–278 (2005)
12. Wang, G., Wang, Y., Tao, X.: An ant colony clustering routing algorithm for wireless sensor networks. In: 2009 Third International Conference on Genetic and Evolutionary Computing, IEEE. ISSN 978-0-7695-3899-0/092009

13. Sun, Y., Zhou, W., Shao, H.: An energy efficient routing based on improved ant colony algorithm. In: 2012 International Conference on Mechanical Engineering and Automation Advances in Biomedical Engineering, vol. 10. ISSN 978-1-61275-028-6/10
14. Agarwal, T., Kumar, D., Prakash, N.R.: Prolonging network lifetime using ant colony optimization algorithm on LEACH protocol for wireless sensor networks. In: Meghanathan, N. et al., (eds.) NeCoM, WiMoN, and WeST 2010, CCIS, vol. 90, pp. 634–641. Springer, Berlin (2010)

Application of Artificial Intelligence Methods to Spot Welding of Commercial Aluminum Sheets (B.S. 1050)

Biranchi Narayan Panda, M.V.A. Raju Babhubalendruni, B.B. Biswal and Dheerendra Singh Rajput

Abstract Artificial intelligence (AI) methods exhibit surprising ability to capture nonlinear relationship and interaction effect with great success. Due to complicacy during the welding and lots of interferential factors, especially short-time property of the spot welding process, of late, AI methods are used more frequently by the researchers to estimate output responses of the process. The present study is aimed at investigating failure load of spot-welded B.S. 1050 aluminum sheets using two most commonly used AI methods such as adaptive neuro-fuzzy inference system (ANFIS) and support vector machine (SVM). Data generated from an experimental study is fed into the paradigm of ANFIS and SVR for the formulation of mathematical model between input and output process parameters. Based on the input data, AI models estimate the failure load of welded joint and results are compared in terms of percentage of relative error. The details of experimentation, model development, and comparisons of modeling methods are summarized in this paper which will guide welders about the proper setting of the process parameters for a strong weld joint.

Keywords Support vector machine (SVM) · Failure load prediction · Resistance spot welding (RSW) · Adaptive neuro-fuzzy inference system (ANFIS)

B.N. Panda (✉) · M.V.A.R. Babhubalendruni · B.B. Biswal · D.S. Rajput
Department of Industrial Design, National Institute of Technology Rourkela, Rourkela 769008, Odisha, India
e-mail: biranchi.panda3@gmail.com

M.V.A.R. Babhubalendruni
e-mail: bahubalindruni@gmail.com

B.B. Biswal
e-mail: bibhuti.biswal@gmail.com

D.S. Rajput
e-mail: dhirendra.kds@gmail.com

K.N. Das et al. (eds.), *Proceedings of Fourth International Conference on Soft Computing for Problem Solving*, Advances in Intelligent Systems and Computing 335,
DOI 10.1007/978-81-322-2217-0_3

1 Introduction

In the recent decade, artificial intelligence (AI) methods are being increasingly used to predict the performance of various welding process such as resistance welding, arc welding, tungsten inert gas (TIG), and metal inert gas (MIG) welding. Spot welding is one of the versatile resistance welding processes widely used for the fabrication of sheet metal assemblies owing to its excellent techno-economic advantages such as low cost, high speed, and flexibility to automation for high-volume production. It is used to weld various sheet metals within thickness range of (0.5–3.0 mm) instead of rivets, screws, soldering, and brazing [1, 2]. In resistance spot welding, two or more metal sheets are joined together by passing an electric current through them. The current is conducted through electrodes pressed against the metal surfaces to hold the parts to be welded tightly together. The heat produced by the flowing current melts the metal, and a welding spot is formed [3]. The amount of heat released in the spot is determined by the amplitude and duration of the current. The current and duration are chosen to match the material, the sheet thickness, and type of electrodes. Literature reveals that welding input parameters play very significant role in determining the quality of a weld joint. A common problem faced by welder is controlling the process input parameters to obtain a welded joint with required strength. Thus, appropriate selection of the input parameters is of great interest for successful implementation of RSW in related industrial application.

By using design of experiment (DOE) and response surface methodology (RSM), some researchers [4–14] have tried to develop mathematical relationships between different weld quality indicators and process parameters. But due to nonlinearity of process and restrictions of the regression analysis, the results were found to be not so satisfactory. To overcome this issue, several well-known computational intelligence (CI) methods such as artificial neural networks (ANNs), fuzzy logic, adaptive-network-based fuzzy inference system, genetic programming (GP), and support vector regression (SVR) have been applied to improve the performance of RSW process [15–20]. Among these methods, artificial neural networks (ANN) are used most frequently to model various welding techniques as they can capture nonlinear mapping and complex relationship in which the regression methods have their limitations. Ates [21] used artificial neural networks (ANNs) to model gas metal arc welding process. The proposed ANN predicts mechanical properties of the weldment which found to be in good agreement with the measured data. Based on experimental results, Cevika et al. [22] proposed an ANN to determine the ultimate capacity of arc spot welding. The results of the neural network model are later compared with results of existing literature and found to be more accurate. Tseng [23] also took the support of artificial neural network to approximate the model and genetic algorithms (GA) to solve the model to obtain optimum welding parameters. Bouyousfi et al. [24] studied the effect of spot welding process parameters on mechanical properties and characteristics of the spot joints between two stainless steel sheets (304 ASS) having same thickness.

Microhardness and tensile test results have shown that the weld resistance is important and highly correlated with the value of the process parameters especially the applied load. Nizamettin [25] focused his study on the influence of welding parameters on the joint strength of resistance spot-welded titanium sheets. The results indicated that increasing current time and electrode force increased the tensile shear strength, and the joint obtained under the argon atmosphere gave better strength. Waller [26] studied the relationship between the quality of resistance welding spots and signal curves measured during the welding cycle. One parameter has been used to study the relationship between the variables which allows the examination of the effects of different variables on the diameter in the form of easily understandable probabilities. Fratini et al. [27] used ANN with finite element model (FEM) to estimate average grain size values in the friction stir welding (FSW) process. Martin et al. [28] studied pitting corrosion behavior (PCB) of resistance spot welding (RSW) joints of AISI 304 austenitic stainless steel (ASS) and formulated a model through artificial neural network. In another study, Martín et al. [29] proposed an ANN to predict the tensile shear strength of the 304 ASS RSW welded joints. They investigated the effect of three process parameters, namely welding time, welding current, and electrode force, on the tensile shear strength.

Although artificial intelligence methods have been applied extensively, the choice of an appropriate one is unclear among a wide range of alternative options and conflicting criteria. Traditional practice in industry is to perform extensive tests to obtain sufficient data sets for design purpose. To do so, it requires a time-consuming trial and error development effort, with weld input parameters chosen by the experience of weld operator and using welding data handbooks. Consequently, it is costly to develop a meaningful and useful database. So a verified, simple, systematic mathematical tool would be very useful to guide decision makers in considering a number of selection criteria and significantly reduce the number of test required and thus the cost involved.

In support of this, present work introduces and compares the performance of two most commonly used AI techniques ANFIS and SVM in modeling RSW process. The advantage of implementing ANFIS is that it combines benefits of both neural network (NN) and fuzzy theory for predicting failure load, whereas SVM avoids overfitting problem in the data by adjusting the regularization parameter. In this study, soft computing techniques are applied on the outcomes of experimental runs. Welding current, electrode force, welding time, and metal sheet thickness are chosen as input parameters, and failure load that can withstand the joint is chosen as the output parameter. Using the experimental data set, ANFIS, and SVM, models are developed and then their performances were compared.

The remainder of this paper is outlined as follows: Sect. 2 discusses in brief about the RSW experimental setup and data preparation. Section 3 introduces two artificial intelligence methods: SVR and ANFIS. Section 4 provides statistical comparison of models. Finally, Sect. 5 concludes with recommendations for future work.

2 Experimental Details

The material used in the study was B.S. 1050 commercially pure aluminum sheets having 0.5, 1, 1.5, 2, and 2.5 mm thickness. A Meriut pedestal spot welding machine incorporating a single-phase AC power supply was used for the involved specimens. Before starting the experimental study, the welding current, electrode force, and welding time have been computed. The calculated resistances for 0.5 and 2.5 mm aluminum sheet thickness are 3.663×10^{-4} and 3.691×10^{-4} Ω, respectively. Based on the linear relationship between the sheet thickness and the average sheet resistance, the resistances of 1, 1.5, and 2 mm thickness were found to be 3.671×10^{-4}, 3.678×10^{-4}, and 3.685×10^{-4} Ω, respectively. The four process input parameters, each having five levels considered, are listed in Table 1. The power consumption (P) in the spot welding is calculated according to the following formula:

$$P = I^2RT \tag{1}$$

where
I is the welding current in amperes,
R is the welding resistance in ohms, and
T is the welding time in seconds

Twenty-five sets of combinations have been generated using the data (Table 1) for the experimental purpose, and the average of failure loads for each set has been given in a tabular form shown in Table 2. In this work, Kennard and Stone algorithm [30] is used for proper selection of training and testing data sets. Twenty samples are chosen as training data, while remaining as a set of test samples. Training data sets are used for formulating the models where the testing sets are used to check the extrapolation ability of the model.

Table 1 Process input parameters with five levels

Factor	Symbol	Unit	Level				
			Lowest	Low	Middle	High	Highest
Welding current	A	A	13860.3	15236.32	16612.33	17988.35	19364.36
Electrode force	B	N	756.56	980.65	1204.746	1428.84	1652.93
Welding time	C	ms	75	140	205	270	335
Thickness	D	mm	0.5	1	1.5	2	2.5

Table 2 Experimental conditions and average failure load

Current (A)	Electrode force (N)	Welding time (ms)	Thickness (mm)	Failure load (N)
15,236	1428.8	270	1.0	705.30
17,988	1428.8	140	1.0	831.30
15,236	980.7	270	2.0	706.30
15,236	980.7	140	1.0	737.70
17,988	980.7	270	1.0	973.00
17,988	1428.8	270	2.0	960.30
17,988	980.7	140	3.0	1198.00
15,236	1428.8	140	2.0	589.30
16,612	1204.7	205	1.50	911.85
17,988	980.7	140	1.0	936.00
15,236	1428.8	140	1.0	705.70
15,236	980.7	270	1.0	735.70
17,988	1428.8	270	1.0	918.70
15,236	980.7	140	2.0	758.30
17,988	1428.8	140	2.0	927.30
17,988	980.7	270	2.0	1053.30
15,236	1428.8	270	2.0	855.70
13,860	1204.7	205	1.50	681.00
19,364	1204.7	205	1.50	1357.30
16,612	756.6	205	1.50	1075.30
16,612	1652.9	205	1.50	762.00
16,612	1204.7	75	1.50	760.00
16,612	1204.7	335	1.50	973.30
16,612	1204.7	205	0.50	369.00
16,612	1204.7	205	2.50	772.70

3 Artificial Intelligence Methods

3.1 Support Vector Regression (SVR)

Support vector machine (SVM) is a very promising artificial intelligence method applied extensively for solving the classification problems. SVR method came from the support vector machine (SVM), which has been applied to solve regression problems of various functional domains [31, 32]. SVR known for providing generalization ability to the model has become promising area of research when compared to other regression techniques.

The idea of SVR method is based on statistical learning theory and structural risk minimization. Firstly, the lower-dimensional input variable space x is projected into higher-dimensional space using nonlinear function in SVR. So that

nonlinear regression problem is transformed into linear regression problems in higher-dimensional space. To attain such transformation, different types of non-linear mapping or transfer function can be used.

The SVR model is formed from the N training data where x_i is the input vector and y_i is the actual value (failure load). The SVR model is expressed as follows:

$$y = z(x) = \sum_{i=1}^{N} w_i \rho_i(x) + b = w^H \rho(x) + b \tag{2}$$

where the function $\rho_i(x)$ is the transformed higher-dimensional space

$$w = [w_1 w_2 \ldots w_N]^H \quad \text{and} \quad \rho = [\rho_1 \rho_2 \ldots \rho_N]^H$$

The surface of the nonlinear regression model given by Eq. (2) is projected over the original input variable space. The model given by $\rho(x)$ is linear in nature and is a converted form of original nonlinear model in higher-dimensional space. The kernel machine learns from the data and minimizes the regularized risk function (L_r). Parameters w (weight) and b (bias) are estimated by minimizing this risk function L_r.

$$L_r(w) = \frac{1}{2} w^T w + \lambda \sum_{i=1}^{N} |y_i - z(x)|_e \tag{3}$$

where

$$|y_i - z(x)|_e = \begin{cases} 0, & \text{if } |y_i - z(x)| < \varepsilon \\ |y_i - z(x)| - \varepsilon, & \text{otherwise} \end{cases}$$

The regularization parameter controls the trade-off between the approximation error and the weight vector norm. An increase in (λ) or weight vector norm leads to decrease of approximation error, but improper control of k may lead to overfitting of model. Values of λ and ε (tolerance level) are user-specified parameters. ε-insensitive loss function $\left(|y_i - z(x)|_e\right)$ given by Eq. (3) is minimized so as to estimate the parameters. If the values predicted by the SVR model $z(x)$ lies within the defined tolerance level ε, the values of loss function is zero, and for the points outside ε, it is the magnitude of the difference between the values predicted by the SVR model and tolerance level ε. The points on the margin lines $(y = z(x) \pm \varepsilon)$ are called support vectors, whereas those outside are known as error set (see Fig. 1).

In the present work, least square–support vector machines (LS-SVM) toolbox [33] built for MATLAB has been used on data (see Table 1) for the application of SVR in predicting the failure load in spot welding process. The suitable radial basis function (RBF) parameters k and r are determined using a combination of coupled simulated annealing (CSA) and a grid search method. The performance of the SVR model on testing data is discussed in Sect. 4.

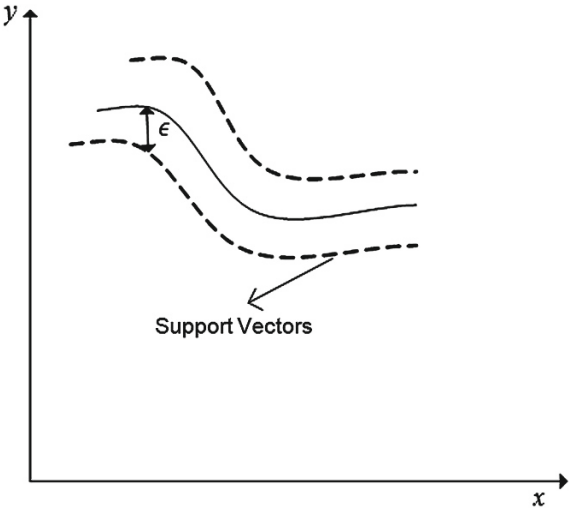

Fig. 1 ε-Insensitive width in the SVR model

3.2 Adaptive Neuro-Fuzzy Inference System (ANFIS)

Adaptive neuro-fuzzy inference system (ANFIS), introduced by Jang [34], is a fuzzy inference system implemented in the framework of an adaptive neural network. By using a hybrid learning procedure, it can map inputs through input membership functions and associated parameters, and then through output membership functions and associated parameters to outputs. In ANFIS system, membership function parameters are estimated using either a back-propagation algorithm alone or in combination with a least squares type of method by using a given data set. It includes the training, testing, and checking of data sets for model validation. Figure 2 shows a typical ANFIS architecture with two inputs (x and y), the linguistic labels (A_1, A_2, B_1, and B_2) associated with this node function, the

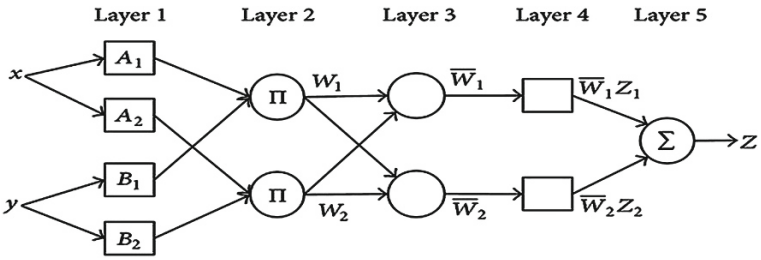

Fig. 2 ANFIS architecture

normalized firing strengths (w_i), and the node label. The neural network structure consists of five layers (see Fig. 1) as follows:

Layer 1 It is the fuzzification layer in which each node in this layer generates a membership grade of a linguistic label. The membership relationship between the output and input functions of this layer can be expressed as follows:

$$O_{1,i} = \mu A_i(x) \quad (i = 1, 2)$$
$$O_{1,j} = \mu B_j(y) \quad (j = 1, 2)$$

where $O_{1,i}$ and $O_{1,j}$ denote the output functions and $\mu A_i(x)$ and $\mu B_j(y)$ denote the membership functions. Usually, $\mu A_i(x)$ is to be selected as bell shaped with maximum equal to 1 and minimum equal to 0.

Layer 2 It is the product layer that consists of two nodes labeled as π and whose output is the product of all the incoming signals; outputs of this layer can be presented as follows:

$$O_{2,i} = w_i = \mu A_i(x) \cdot \mu B_j(y) \quad (i = 1, 2)$$

where $O_{2,i}$ denotes second layer and w_i is the weight function of second layer.

Layer 3 It is the normalization where weight function is normalized based on the equation given by

$$O_{3,j} = \bar{w} = \frac{w_i}{w_1 + w_2} \quad (i = 1, 2)$$

Here, $O_{3,j}$ denotes layer 3 output.

Layer 4 It is the defuzzification layer, where output of each node (adaptive node) is simply the product of the normalized firing strength and a first order polynomial. The defuzzy relationship between the input and output of this layer can be defined as follows:

$$O_{4,j} = \bar{w}_i f_i = w_i(p_i x + q_i y + r_i) \quad (i = 1, 2)$$

Here, $O_{4,j}$ denotes the Layer 4 output.

Layer 5 It is the output layer, whose node is labeled as $\sum$. The overall output computed as the summation of all incoming signals can be written as follows:

$$O_{5,i} = \frac{\sum_i w_i f_i}{\sum_i w_i} \quad (i = 1, 2)$$

In this study, the ANFIS toolbox [34] built in MATLAB is applied on the data to predict failure load of the welded joint.

4 Performance Evaluation of Artificial Intelligence Methods

The results obtained from the two prediction modeling methods, ANFIS and SVR, have been compared. The best prediction method that gives highest accuracy has been determined by calculating relative percentage error between the predicted values of these methods and the experimental values. The relative error is given by

$$\text{Relative error}\,(\%) = \frac{|M_i - Y_i|}{Y_i} \times 100$$

Here, M_i is the value predicted by a model and Y_i is the actual value of the output. The box plots of relative error (%) for the two methods on the training and testing data of failure load are shown in Figs. 3 and 4 respectively.

The box plot shown in Fig. 3 indicates that the two models SVR and ANFIS have lower mean relative error of 0.59 and 1.46 %, respectively, which shows that they have been able to capture the relationship between process variables satisfactorily. The box plot shown in Fig. 4 depicts that the performance of the SVR model on the testing data is better than those of the ANFIS model since it has lower mean relative error of 3.52 %. From the above discussion, it is clear that both

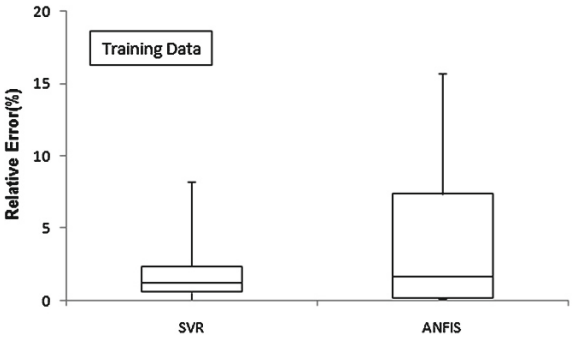

Fig. 3 Box plot showing relative error (%) of two methods on training data of failure load

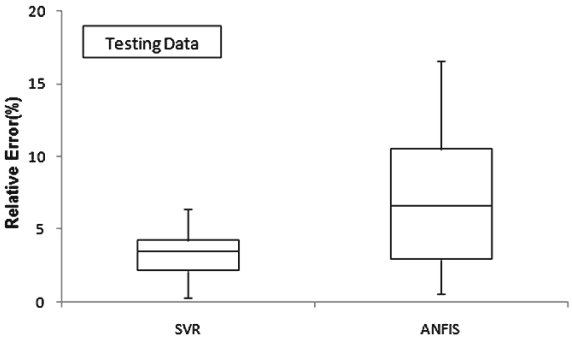

Fig. 4 Box plot showing relative error (%) of two methods on testing data of failure load

models are statically fit for modeling spot welding process; however, SVR has shown best performance among them as it is able to catch dynamics and complex interaction of the process satisfactorily.

5 Conclusion

This study was carried out to develop predictive models to measure failure load of spot welding process using SVR and ANFIS. The performance of these potential AI methods was compared in terms of relative error obtained from box plots. The statistical comparison in Sect. 4 concludes that SVR has outperformed ANFIS. Hence, deployment of generalized SVR models will significantly save the computational time for running additional set of experiments. This SVR model can also be further optimized, and the optimal input of spot welding settings can be determined to maximize the failure load of the joint.

References

1. Jou, M.: Real time monitoring weld quality of resistance spot welding for the fabrication of sheet metal assemblies. J. Mater. Process. Technol. **132**, 102–113 (2003)
2. Aslanlar, S., Ogur, A., Ozsarac, U., Ilhan, E.: Welding time effect on mechanical properties of automotive sheets in electrical resistance spot welding. J. Mater Des. **29**, 1427–1431 (2008)
3. Tsai, C.L., Jammal, O.A., Papritan, J.L., Dickinson, D.W.: Modelling of resistance spot weld nugget growth. Welding J. Res. Suppl. **71**, 47–54 (1992)
4. Muhammad, N., Manurang, H.P.Y.: Design parameters selection and optimization of weld zone development in resistance spot welding. World Acad. Sci. Eng. Technol. **71**, 1220 (2012)
5. Muhammad, N., Manurung, Y., Hafidzi, M., Abas, S.K., Tham, G., Rahim, M.R.: A quality improvement approach for resistance spot welding using multi-objective Taguchi method and response surface methodology. Int. J. Adv. Sci. Eng. Inf. Technol. **2**, 2088–5334 (2012)
6. Muhammad, N., Manurung, Y., Hafidzi, M., Abas, S.K., Tham, G., Haruman, E.: Optimization and modeling of spot welding parameters with simultaneous multiple response consideration using multi-objective Taguchi method and RSM. J. Mech. Sci. Technol. **26**(8), 2365–2370 (2012)
7. Muhammad, N., Manurung, Y., Hafidzi, M., Abas, S.K., Tham, G., Haruman, E.: Model development for quality features of resistance spot welding using multi-objective Taguchi method and response surface methodology. J. Intell. Manuf. (2012). doi:10.1007/s1084506483
8. Zhao, D., Wang, Y., Sheng, S., Lin, Z.: Multi-objective optimal design of small scale resistance spot welding process with principal component analysis and response surface methodology. J. Intell. Manuf. doi:10.1007/s10845(2013)0733-2
9. Zhao, D., Wang, Y., Wang, X., Wang, X., Chen, F., Liang, D.: Process analysis and optimization for failure energy of spot welded titanium alloy. J. Mater. Des. **60**, 479–489 (2014)
10. Kim, I.S., Park, C.E., Jeong, Y.J., Son, J.S.: Development of an intelligent system for selection of the process variables in gas metal arc welding processes. Int. J. Adv. Manuf. Technol. **18**, 98–102 (2001)

11. Tzeng, Y.-F., Chen, F.-C.: Effects of operating parameters on the static properties of pulsed laser welded zinc-coated steel. Int. J. Adv. Manuf. Technol. **18**, 641–647 (2001)
12. Darwish, S.M., Al-Dekhial, S.D.: Statistical models for spot welding of commercial aluminium sheets. Int. J. Mach. Tools Manuf. **39**, 1589–1610 (1999)
13. Gunaraj, V., Murugan, N.: Application of response surface methodology for predicting weld bead quality in submerged arc welding of pipes. J. Mater. Process. Technol. **88**, 266–275 (1999)
14. Elangovan, K., Balasubramaniam, V., Babu, S.: Predicting tensile strength of friction stir welded AA6061 aluminium alloys joints by a mathematical model. Mater. Des. **30**, 188–193 (2009)
15. Gill, S., Singh, J.: Artificial intelligent modeling to predict tensile strength of inertia friction-welded pipe joints. Int. J. Adv. Manuf. Technol. **69**, 2001–2009 (2013)
16. Singh, J., Singh, S.G.: Modeling for tensile strength of friction welded aluminium pipes by ANFIS. J. Intell. Eng. Inf **1**(1), 3–20 (2010)
17. Tran, H.T., Kim, K.Y., Yang, H.J.: Weldability prediction of AHSS stack ups using support vector machines. Int. J. Comput. Electr. Eng. **6**(3), 207–210 (2014)
18. Shuangsheng, G., Xingwei, T., Shude, J., Zhitao, Y.: Prediction of mechanical properties of welded joints based on support vector regression. J. Proc. Eng. **29**, 1471–1475 (2012)
19. Na, M.G., Kim, J.W., Lim, D.H., Kang, Y.: Residual stress prediction of dissimilar metals welding at NPPs using support vector regression. Nucl. Eng. Des. **238**(7), 1503–1510 (2008)
20. Nagesh, D.S., Datta, G.L.: Genetic algorithm for optimization of welding variables for height to width ratio and application of ANN for prediction of bead geometry for TIG welding process. Appl. Soft Comput. **10**, 897–907 (2010)
21. Ates, H.: Prediction of gas metal arc welding parameters based on artificial neural networks. J. Mater. Des. **28**, 2015–2023 (2007)
22. Cevika, A., Kutuk, A.M., Erklig, A., Guzelbey, I.H.: Neural network modeling of arc spot welding. J. Mater. Process Technol. **202**, 137–449 (2008)
23. Tseng, H.Y.: Welding parameters optimization for economic design using neural approximation and genetic algorithm. Int. J. Adv. Manuf. Technol. **27**, 897–901 (2006)
24. Bouyousfi, B., Sahraoui, T., Guessasma, S., Chaouch, K.T.: Effect of process parameter on physical characteristic of spot weld joints. J. Mater. Des. **28**, 414–419 (2003)
25. Nizamettin, K.: The influence of welding parameters on the joints of strength of resistance spot welded. J. Mater. Des. **28**, 421–427 (2007)
26. Waller, D.N., Knowlson, P.M.: Electrode separation applied to quality control in resistance welding. Weld. J. **44**(12), 168-s–174-s (1965)
27. Fratini, L., Buffa, G., Palmeri, D.: Using a neural network for predicting the average grain size in friction stir welding processes. J. Comput. Struct. **87**, 1166–1174 (2009)
28. Martin, O., Tiedra, P.D., Lopez, M.: Artificial neural networks for pitting potential prediction of resistance spot welding joints of AISI 304 austenitic stainless steel. J. Corros. Sci. **52**, 2397–2402 (2010)
29. Martin, O., Tiedra, P.D., Lopez, M., Manuel, S.J., Cristina, G., Fernando, M.: Quality prediction of resistance spot welding joints of 304 austenitic stainless steel. J. Mater. Des. **30**, 68–77 (2009)
30. Kennard, R.W., Stone, L.A.: Computer aided design of experiments. Technometrics **11**, 137–148 (1969)
31. Kecman, V.: Learning and Soft Computing: Support Vector Machines, Neural Networks, and Fuzzy Logic Models. MIT Press, Cambridge (2001)
32. Andrés, E., Salcedo-Sanz, S., Monge, F., Pérez-Bellido, A.M.: Efficient aero-dynamic design through evolutionary programming and support vector regression algorithms. Expert Syst. Appl. **39**, 10700–10708 (2012)

33. Pelckmans, K., Suykens, J.A.K., Vangestel, T., De Brabanter, J., Lukas, L., Hamers, B., et al.: LS SVMlab: a MATLAB/c toolbox for least squares support vector machines. Tutorial. KU Leuven-ESAT, Leuven (2002)
34. Jang, J.S.R.: Adaptive-network-based fuzzy inference system (ANFIS). IEEE Trans. Syst. Man Cybern. **23**, 665–685 (1993)

A Fuzzy Multi-criteria Decision-making Model for Green Electrical Discharge Machining

Jagadish and Amitava Ray

Abstract This paper aims to combine fuzzy and technique for order preference by simulation of ideal solution (TOPSIS) to solve the multi-response parameters optimization problem in green manufacturing. From the viewpoint of health and environment, tap water is used as working fluid, since it does not release the harmful gases. This work considers discharge current, pulse width/pulse interval ratio, gap voltage, and lifting height are the input parameters and output parameters have been identified as material removal rate (MRR), electrode wear ratio (EWR), and surface roughness (SR). In this paper, initially, an experiment was performed using Taguchi experimental technique. Thereafter, fuzzy-TOPSIS is used to convert multi-response parameters into a single response parameter. Finally, the ranking of the parameter decides the best experimental setup and optimized the input-process parameters. In this work, weighting factors for the output parameters are determined using triangular fuzzy number which influences correlation coefficient values for finding the finest experimental setup. Additionally, an attempt has been made to compare the proposed methodology with the gray relational analysis (GRA). The numerical result shows that the optimum process parameters are A_1 (4.5 A), B_1 (30:70 μs), C_3 (30 V), and D_4 (6 mm) and using tap water machining Ti-6Al-4V material can produce high MRR, decrease the machining cost, and have no harmful to the operators and environment.

Keywords Fuzzy · TOPSIS · Green manufacturing (GM) · Process parameters

Jagadish (✉)
Department of Mechanical Engineering, National Institute of Technology Silchar, Silchar 788010, Assam, India
e-mail: jagadishbaridabad.s@gmail.com

A. Ray
Department of Training and Placement, Jalpaiguri Government Engineering College, Jalpaiguri 735102, India
e-mail: amitavaray.siliguri@gmail.com

K.N. Das et al. (eds.), *Proceedings of Fourth International Conference on Soft Computing for Problem Solving*, Advances in Intelligent Systems and Computing 335,
DOI 10.1007/978-81-322-2217-0_4

1 Introduction

EDM is non-traditional machining process, which is extensively used in machining hard, high strength, and complex geometry in a contact less manner. The material is removed from the workpiece by generating the electric spark between electrode tool and workpiece [1–5]. Ti-6Al-4V is widely used in aerospace, automobile, chemical, and biomedical fields, because it has exceptional merits such high strength to weight ratio, good temperature-resistance, and prominent corrosion resistance. However, it is a hard to cut material with high melting point and low thermal conductivity, and it is not suitable for cutting by traditional machining. Therefore, non-traditional machining process has been used to machine this alloy.

Green manufacturing deals with environmental principle and plays an important role in reduction of environmental burdens [6, 7]. Friction during the machining process of Ti-6Al-4V alloy results in the heat generation. The effect of this heat generated decrease the MRR, increase the SR, and increase the electrode wear ratio (EWR) and also releases numerous amounts of harmful components in the form of solid, liquid, and gas wastes resulting in serious occupational health and environmental issues. These toxic substances are very harmful and create serious problems to the operator through ingestion, inhalation, and skin contact. The amount of waste generated and its output parameters of process are strongly affects the input-process parameters. Therefore to mitigate this, optimization of process parameters is a key role to improve the EDM, MRR, SR, reduce the EWR, and look for optimal machining parameters attains the green EDM. Green manufacturing not only improves the efficiency but also saves the resources.

The selection of optimum process parameters is a multi-criteria decision-making (MCDM) selection problem. The literature survey [8–15] reveals the use of various MCDM methods employed in solving engineering problems. Authors suggested that in all these MCDM methods, the ranking of the alternatives is influenced by the criteria weights. Several researchers [16–23] used these MCDM methods for optimization in green manufacturing. Much research has been conducted to attempt green manufacturing parameters for EDM using different types of dielectric fluid. Several researchers have proposed in the literature to study the influence of various process parameters on EDM operation [24–29]. The machining D2 tool steeled in tap water and deionized water with brass and bronze electrode, and the results reveal that by using 75 % tap water and 25 % deionized water mixture, the dielectric can obtain the maximum MRR and the minimum EWR [30]. Study has been conducted on EDM with dielectric-water-in-oil, kerosene, a urea with water, and low-sensitivity deionized water to attempt high MRR and low EWR [31–33]. Graphite, electrolytic copper, aluminum, and copper–tungsten material were researched as EDM electrodes in order to obtain surface integrity of Ti-6Al-4V [34, 35, 36]. The fundamental study on the Ti-6Al-4V alloy properties and improving the capabilities of EDM using Powder-mixed EDM has been made to

improve the MRR [37, 38]. The relationship between residual stresses and white layer has been made with different types of EDM dielectric [39, 40]. A comparative study on different machining techniques [41–44] such as ultrasonic, vibratory, and rotary and magnetic field has been made to determine the optimal machining parameters in EDM. Machining performance in the EDM process can be improved effectively through optimal machining parameters [45–48]. Using kerosene in the machining releases numerous amounts of harmful components in the form of solid, liquid, and gases wastes resulting in serious occupational health and environmental issues. These toxic substances are very harmful and create serious problems to the operator through ingestion, inhalation, and skin contact [49].

Tang et al. [50] developed a combined method of Taguchi coupled with GRA to optimize the process parameters and machining of Ti-6Al-4V alloy under tap water as dielectric medium. In this work, an author has determined the optimal parameters and improves the green manufacturing parameters without considering the relative weights of the response parameters. But in actual practice, the response parameters are solely dependence on the input parameters with their relative importance. The effect of weights on the performance parameters will lead to error in decision making and methodology will not produce the optimal result. Therefore, in this paper, fuzzy theory [51, 52] has been used to overcome this. Fuzzy set theory deals effectively with this type of uncertainty data, thus allowing linguistic variables (such as low, high, very high, and very low) to be employed for approximate reasoning. Generally, triangular and trapezoidal fuzzy numbers are used for representing linguistic variables.

Among the MCDM methods, TOPSIS [49, 53], which can handle multi-response problems with both continuous and discrete data, is the most suitable technique in engineering applications. The basic principle of TOPSIS is to select the best alternative that has the shortest distance from the positive ideal solution and the farthest distance from the negative ideal solution.

The objective of this research is to optimize the process parameters of Ti-6Al-4V alloy green EDM. In this paper, an integrated approach has been projected to handle the multi-response parameters optimization problems. The experiments are designed using Taguchi (L9) orthogonal array and optimized the process parameters by developing methodology. Weighting factors associated with each of the output parameters are determined using triangular fuzzy number and the most paramount factor level combination is identified utilizing TOPSIS approach. The goal was to attain high efficiency; high quality and pollution-free environment during the machining meets the modern industrial requirements.

The rest of the following sections are organized as follows: Section 2 explores the input-process-output parameters for green EDM; Sect. 3 describes the materials and research design in detail; In Sect. 4, result and discussion have been highlighted. Finally, conclusions are described in Sect. 5.

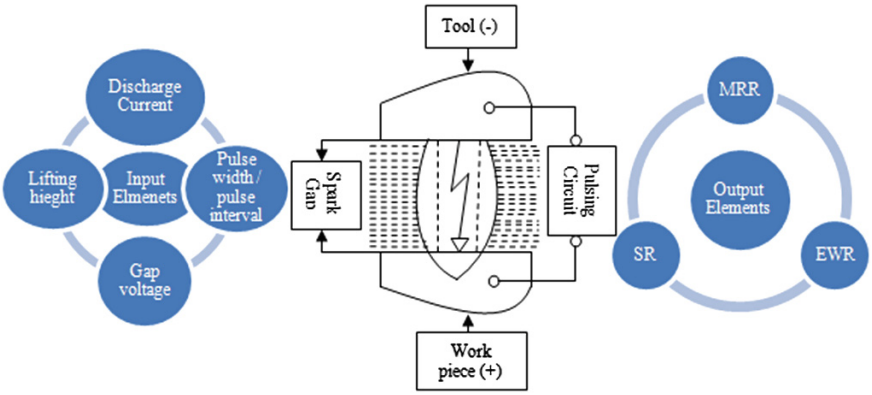

Fig. 1 Input-process-output for Green EDM

2 Input-Process-Output Diagram of Green EDM

The main theory of the EDM process is an electric arc struck between two electrodes produces the energy required for the material removal [6]. The relationship between input and output parameters is shown in Fig. 1.

3 Materials and Methods

3.1 Determination of Response Parameters

The response parameters are determined by means of valid experiential setup on CNC ACTSPARK EDM machine. The detailed explanation of experimental setup and material chemical composition has been explored in the literature [50]. The work considers four input parameters and three output parameters. The number of experimental runs is carried out using L9 (3^4) orthogonal array. The input-process parameters and three levels for the design are shown in Table 1. The results of the experiments are depicted in Table 2.

Table 1 Input parameters and their levels [50]

Symbol	Control parameters	Level 1	Level 2	Level 3
A	Discharge current (A)	11	16	20
B	Pulse width/pulse interval (Ton/Toff) (μs)	30:70	50:50	70:30
C	Gap voltage (V)	20	25	30
D	Lifting height (mm)	3	6	9

Table 2 Experimental results [50]

Exp. No.	Input parameters				Output parameters		
	A	B	C	D	MRR (mm^3/min)	EWR (mm^3/min)	SR(μs)
1	1	1	1	1	2.96	0.21	2.17
2	1	2	2	2	1.28	0.14	2.37
3	1	3	3	3	1.73	0.16	2.83
4	2	1	2	3	3.27	0.30	2.19
5	2	2	3	1	4.30	0.30	2.61
6	2	3	1	2	4.07	0.28	2.86
7	3	1	3	2	5.90	0.41	2.15
8	3	2	1	3	6.62	0.41	2.65
9	3	3	2	1	6.36	0.41	4.27

3.2 Optimization Using Fuzzy-TOPSIS

In this paper, fuzzy coupled with TOPSIS is developed to compute the optimal process parameters for green EDM. The relative weights of the output parameters are assigned in terms of linguistic variables as shown in Table 3. The triangular fuzzy number is used to describe the linguistics variables. A committee with four experts is made to act as decision maker. Each decision maker rated each attribute weights with respect to linguistics variables, and aggregated fuzzy weights are tabulated in Table 4.

Thereafter, TOPSIS method is used for optimizing the process parameters. This method begins with normalized performance matrix. The normalized performance matrix is expressed using the following equation:

$$p_{ij} = \frac{x_{ij}}{\sqrt{\sum_{i=1}^{m} x_{ij}^2}} \tag{1}$$

where x_{ij} represents the actual values of ith attributes with jth experimental run, p_{ij} represents the corresponding normalized performance values, and m indicates the

Table 3 Linguistic variables for each output criterion

Importance	Fuzzy weight
Extremely low (EL)	(0, 0, 0.1)
Very low (VL)	(0, 0.1, 0.3)
Low (L)	(0.1, 0.3, 0.5)
Medium (M)	(0.3, 0.5, 0.7)
High (H)	(0.5, 0.7, 0.9)
Very high (VH)	(0.7, 0.9, 1)
Extremely high (EH)	(0.9, 1, 1)

Table 4 Importance of output responses and Fuzzy weights

Output response	Decision maker				Fuzzy weights
	DM1	DM2	DM3	DM4	
MRR	H	H	VH	H	0.55, 0.75, 0.925
EWR	VL	L	L	VL	0.05, 0.2, 0.4
Ra	M	H	M	L	0.75, 0.925, 1

number of experimental runs. The normalized performance values are then multiplied with respective relative weights of each output parameter thus yielding the weighted normalized matrix N. The weighted normalized matrix is expressed as follows:

$$N_{ij} = p_{ij} \times w_j \quad j = 1, 2, \ldots n \;\; i = 1, 2, \ldots m \tag{2}$$

The ideal and nadir ideal solutions are determined using Eqs. (3) and (4), respectively:

$$N_j^+ = \left\{ \left(\underset{i}{\text{Max}} N_{ij} \middle| j \in K \right), \left(\underset{i}{\text{Min}} N_{ij} \middle| j \in K^1 \right) \right\} \tag{3}$$

$$N_j^- = \left\{ \left(\underset{i}{\text{Min}} N_{ij} \middle| j \in K \right), \left(\underset{i}{\text{Max}} N_{ij} \middle| j \in K^1 \right) \right\} \tag{4}$$

where K is the index set of benefit criteria and K^1 is the index set of non-benefit criteria.

The distances from the ideal and nadir solutions are measured. The two Euclidean distances for each alternative are determined as given in Eqs. (5) and (6), respectively:

$$V_i^+ = \left\{ \sum_{j=1}^{n} \left(N_{ij} - N_j^+ \right)^2 \right\}^{0.5} \quad j = 1, 2, \ldots n \quad i = 1, 2, \ldots m \tag{5}$$

$$V_i^- = \left\{ \sum_{j=1}^{n} \left(N_{ij} - N_j^- \right)^2 \right\}^{0.5} \quad j = 1, 2, \ldots n \quad i = 1, 2, \ldots m \tag{6}$$

The closeness coefficient to the ideal solution is calculated as shown in following equation

$$CC_i = \frac{V_i^-}{V_i^+ + V_i^+} \quad i = 1, 2, \ldots m \quad 0 \leq CC_i \leq 1 \tag{7}$$

The higher values of CC_i mean that the rank is better.

4 Results and Discussion

At first, closeness coefficient values for each of the experiments of the (L9) orthogonal array are calculated as discussed in the previous section (Table 5). The result reveals that experiment No. 2 yields the highest clones coefficient value. Therefore, the experiment No. 2 has the optimal machining parameters setting for the desirable output responses among the nine experiments.

Additionally, this research also analyzes the response of input parameters using the response table obtained from Taguchi method by calculating the average closeness coefficient for each level of the input parameter. The process consists of two major steps, as follows: (i) Group the closeness coefficient values by factor level for each column in the orthogonal array and (ii) average of closeness coefficient values. The mean closeness coefficient values for each of the process parameters are shown in Table 6.

The influence of each input parameters can be clearly presented by means of closeness coefficient graph. It shows that the change in the response when value of the parameters factor goes for their level 1–3. The response graph is shown in Fig. 2.

The higher closeness coefficient values show the optimum input parameters for the green EDM. The optimal comparability sequence is obtained as $A_1B_1C_3D_2$ and they are shown in Table 6. Therefore, the optimal parameters that minimize the manufacturing and environmental components are the A_1 (4.5 A), B_1 (30:70 µs), C_3

Table 5 Closeness coefficient values

Exp. No	A	B	C	D	Closeness coefficient (CC_i)	Rank
1	1	1	1	1	0.7225	3
2	1	2	2	2	0.9594	1
3	1	3	3	3	0.8548	2
4	2	1	2	3	0.6620	4
5	2	2	3	1	0.4903	6
6	2	3	1	2	0.5077	5
7	3	1	3	2	0.3443	7
8	3	2	1	3	0.2498	8
9	3	3	2	1	0.0434	9

Table 6 Response table of closeness coefficients

	Average closeness coefficients			Max–Min	Rank
Input parameters	Level 1	Level 2	Level 3		
A	**0.84557**	0.55333	0.21250	0.63307	1
B	**0.57627**	0.56650	0.46863	0.10763	3
C	0.49333	0.55493	**0.56313**	0.06980	4
D	0.41873	**0.60380**	0.58887	0.18507	2

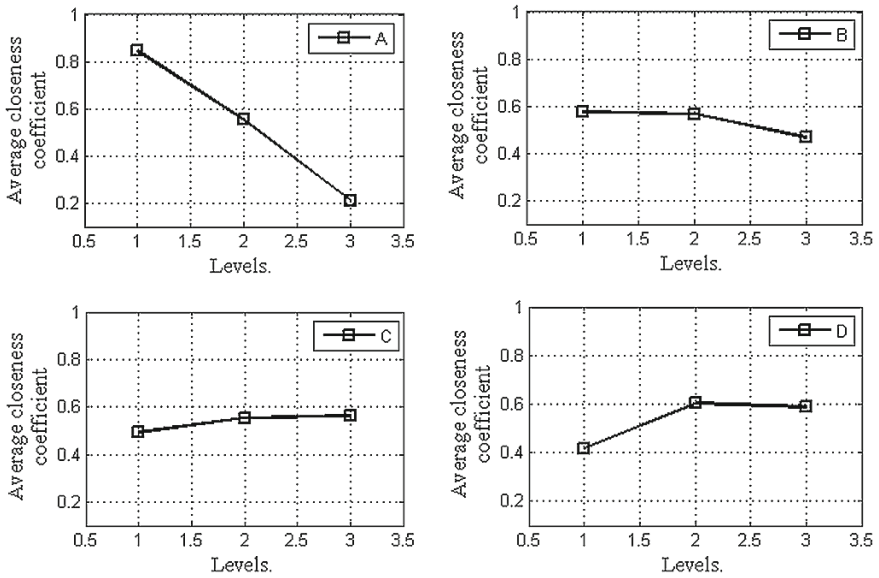

Fig. 2 Effects of process parameters on closeness coefficient

Fig. 3 Comparison of the results

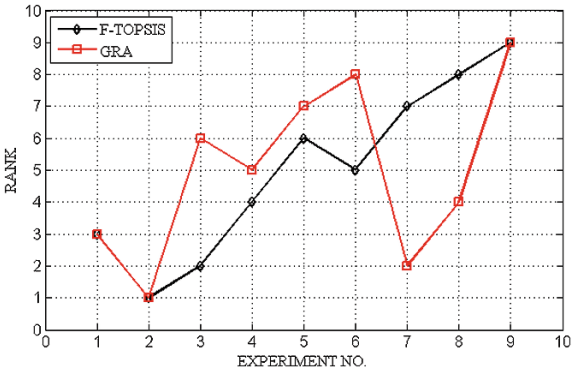

(30 V), and D_4 (6 mm). The most significant factor is identified (Table 6) by determining the difference between the maximum and the minimum values of the closeness coefficient of the EDM parameters. The value indicated that discharge current (A) has strong effect on the output parameters. Finally, Fuzzy-TOPSIS result is compared with the results of GRA [50] model. The observed results are same for all the cases which are as shown in Fig. 3.

5 Conclusion

The present manufacturing industries is considered as one of the main sources of environmental pollution. How to minimize the environmental pollution is an important topic for the entire manufacturer. The novel Ti-6Al-4V with tap water is explored in this paper. The fuzzy-TOPSIS is used to optimize the process parameters and to improve the multiple performances of the EWR, MRR, and SR in the EDM. There are three conclusions gained as follows:

- The result shows that experiment No. 2 yields the highest closeness coefficient value. Therefore, experiment No. 2 has the optimal machining paramagnets setting for the desirable output responses among the nine experiments.
- The optimal parameters that minimize the manufacturing and environmental components are the A_1 (4.5 A), B_1 (30:70 μs), C_3 (30 V), and D_4 (6 mm). The most significant factor is identified by determining the difference between the maximum and the minimum values of the closeness coefficient of the EDM parameters. The value indicated that discharge current (A) has strong effect on the output parameters.
- The fuzzy-TOPSIS result is compared with the published results of GRA model and indicated that the proposed methodology is validated and it can be used for multi-objective parameters optimization in green electrical discharge machining Ti-6Al-4V alloy with tap water.

Using tap water machining, Ti-6Al-4V alloy has high MRR, has less environmental pollution, and the also decrease the machining cost.

References

1. Pandey, A., Singh, S.: Current research trends in variants of electrical discharge machining: a review. Int. J. Eng. Sci. Technol. **2**(6), 2172–2191 (2010)
2. Leao, F.N., Pashby, I.R.: A review on the use of environmentally friendly dielectric fluids in electrical discharge machining. J. Mater. Process. Technol. **149**(1–3), 341–346 (2004)
3. Abbas, N.M., Solomon, D.G., Bahari, M.F.: A review on current research trends in electrical discharge machining (EDM). Int. J. Mach. Tools Manuf. **47**(7–8), 1214–1228 (2007)
4. Singh, S., Bhardwaj, A.: Review to EDM by using water and powder-mixed dielectric fluid. J. Min. Mater. Charact. Eng. **10**(2), 199–230 (2011)
5. Abbas, N.M., Yusoff, N.: Electrical discharge machining (EDM): practices in Malaysian industries and possible change towards green manufacturing. Procedia Eng. **41**, 1684–1688 (2012)
6. Sheng, P., Srinivasan, M.: Multi-objective process planning in environmentally conscious manufacturing: a feature-based approach. Ann. CIRP **44**(1), 433–437 (1995)
7. Abbas, N.M., Solomon, D.G., Bahari, M.F.: A review on current research trends in electrical discharge machining (EDM). Int. J. Mach. Tool Manuf. **47**, 1214–1228 (2007)
8. Saaty, T.L.: The Analytic Hierarchy Process. McGraw-Hill, New York (1980)
9. Roy, B.: Decision-aid and decision-making. Eur. J. Oper. Res. **45**, 324–331 (1990)
10. Kumar, R., Jagadish, Ray, A.: Selection of material for optimal design using multi-criteria decision making. Procedia Material Science. (2014) (Accepted for publication)

11. Caliskan, H., Kursuncu, B., Kurbanoglu, C., Guven, Y.S.: Material selection for the tool holder working under hard milling conditions using different multi criteria decision making methods. Mater. Des. **45**, 473–479 (2013)
12. Kumar, R., Jagadish, Ray, A.: Selection of material: a multi-objective decision making approach. Presented at the international conference on industrial engineering, SVNIT, and Surat, India. Proceeding of ICIE-2013 with ISBN 978-93-83083-37-4,162-165 (2013)
13. Kumar, R., Jagadish, Ray, A.: Selection of cutting tool materials: a holistic approach. Presented at the 1st International Conferences on Mechanical Engineering. Emerging Trends For Sustainability, MANIT, vol. 5028. Bhopal, India. pp. 447–452 (2014)
14. Saket, S., Purbey, V., Jagadish, Ray, A.: Multi attributes decision making for mobile phone selection. Int. J. Res. Eng. Technol. **03**(03), 497–501 (2014)
15. Deng, J.L.: Introduction to grey system. J. Grey Syst. **1**(1), 1–24 (1989)
16. Tan, X.C., Liu, F., Cao, H.J., Zhang, H.: A decision-making framework model of cutting fluid selection for green manufacturing and a case study. J. Mater. Process. Technol. **129**, 467–470 (2002)
17. Yeo, S.H., New, A.K.: A method for green process planning in EDM. Int. J. Adv. Manuf. Technol. **15**, 287–291 (1999)
18. Abbas, N.M., Yusoff, N., Wahab, R.M.: Electrical discharge machining (EDM): practices in Malaysian industries and possible change towards green manufacturing. Proc. Eng. **41**, 1684–1688 (2012)
19. Jagadish, Ray, A. Cutting fluid selection for sustainable design for manufacturing: an integrated theory. Procedia Material Science. (2014) (Accepted for publication)
20. Ray, Jagadish: A. Green cutting fluid selection using MOOSRA method. Int. J. Res. Eng. Technol. **03**(03), 559–563 (2014)
21. Pradhan, M.K.: Estimating the effect of process parameters on surface integrity of EDMed AISI D2 tool steel by response surface methodology coupled with grey relational analysis. Int. J. Adv. Manuf. Technol. **67**, 2051–2062 (2013)
22. Jagadish, Ray, A.: Green cutting fluid selection using multi-attribute decision making approach. J. Inst. Eng. India Ser C (2014) doi:10.1007/s40032-014-0126-0
23. Jagadish, Ray, A. Multi-objective optimization of green EDM: an integrated theory. J. Inst. Eng. India Ser C (2014) doi:10.1007/s40032-014-0142-0
24. Mandal, D., Pal, S.K., Saha, P.: Modeling of electrical discharge machining process using back propagation neural network and multi-objective optimization using non-dominating sorting genetic algorithm-II. J. Mater. Process. Technol. **186**(1–3), 154–162 (2007)
25. Dvivedi, A., Kumar, P., Singh, I.: Experimental investigation and optimisation in EDM of Al 6063 SiCp metal matrix composite. Int. J. Mach. Machb. Mater. **3**(3–4), 293–308 (2008)
26. Kanagarajan, D., Karthikeyan, R., Palanikumar, K., Sivaraj, P.: Influence of process parameters on electric-discharge machining of WC/30 %Co composites. P I Mech. Eng. B-J Eng. **222**(7), 807–815 (2008)
27. Chiang, K.: Modeling and analysis of the effects of machining parameters on the performance characteristics in the EDM process of Al_2O_3 + TiC mixed ceramic. Int. J. Adv. Manuf. Technol. **37**(5–6), 523–533 (2008)
28. Kuppan, P., Rajadurai, A., Narayanan, S.: Influence of EDM process parameters in deep hole drilling of Inconel 718. Int. J. Adv. Manuf. Technol. **38**(1–2), 74–84 (2007)
29. Pradhan, M.K., Biswas, C.K.: Multi-response optimisation of EDM AISI D2 tool steel using response surface methodology. Int. J. Mach. Machb. Mater. **9**(1–2), 66–85 (2011)
30. Medellin, H.I., De Lange, D.F., Morales, J., Flores, A.: Experimental study on electro discharge machining in water of D2 tool steel using two different electrode materials. Proc. Inst. Mech. Eng. Part B J. Eng. Manuf. **223**(11), 1423–1430 (2009)
31. Chen, S.L., Yan, B.H., Huang, F.Y.: Influence of kerosene and distilled water as dielectrics on the electric discharge machining characteristics of Ti-6Al-4V. J. Mater. Process. Technol. **87**, 107–111 (1999)
32. Zhang, Y., Liu, Y., Ji, R., Cai, B., Shen, Y.: Sinking EDM in water in-oil emulsion. Int. J. Adv. Manuf. Technol. **65**(5–8), 705–716 (2013)

33. Yan, B.H., Tsai, H.C., Huang, F.Y.: The effect in EDM of a dielectric of a urea solution in water on modifying the surface of titanium. Int. J. Mach. Tools Manuf. **45**(2), 194–200 (2005)
34. Nguyen, M.D., Rahman, M., Wong, Y.S.: An experimental study on micro-EDM in low-resistivity deionized water using short voltage pulses. Int. J. Adv. Manuf. Technol. **58**(5–8), 533–544 (2012)
35. Hascalık, A., Caydas, U.: Electrical discharge machining of titanium alloy (Ti-6Al-4V). Appl. Surf. Sci. **253**, 9007–9016 (2007)
36. Gu, L., Li, L., Zhao, W., Rajurkar, K.P.: Electrical discharge machining of Ti6Al4V with a bundled electrode. Int. J. Mach. Tools Manuf. **53**, 100–106 (2012)
37. Kansal, H.K., Singh, S., Kumar, P.: Technology and research developments in powder mixed electric discharge machining (PMEDM). J. Mater. Process. Technol. **184**, 32–41 (2007)
38. Kansal, H.K., Singh, S., Kumar, P.: Numerical simulation of powder mixed electric discharge machining (PMEDM) using finite element method. Math. Comput. Model. **47**, 1217–1237 (2008)
39. Ekmekci, B.: Residual stresses and white layer in electric discharge machining (EDM). Appl. Surf. Sci. **253**, 9234–9240 (2007)
40. Zhang, Y., Liu, Y., Ji, R., Cai, B.: Study of the recast layer of a surface machined by sinking electrical discharge machining using water-in-oil emulsion as dielectric. Appl. Surf. Sci. **257** (14), 5989–5997 (2011)
41. Kumar, J., Khamba, J.S.: Modeling the material removal rate in ultrasonic machining of titanium using dimensional analysis. Int. J. Adv. Manuf. Technol. **48**(1–4), 103–119 (2010)
42. Ghoreishi, M., Atkinson, J.: A comparative experimental study of machining characteristics in vibratory, rotary and vibro-rotary electro-discharge machining. J. Mater. Process. Technol. **120** (1–3), 374–384 (2002)
43. Abdullah, A., Shabgard, M.R.: Effect of ultrasonic vibration of tool on electrical discharge machining of cemented-tungsten carbide (WC-Co). Int. J. Adv. Manuf. Technol. **38**, 1137–1147 (2008)
44. Kibria, G., Sarkar, B.R., Pradhan, B.B., Bhattacharyya, B.: Comparative study of different dielectrics for micro-EDM performance during microhole machining of Ti-6Al-4V alloy. Int. J. Adv. Manuf. Technol. **48**(5–8), 557–570 (2010)
45. Teimouri, R., Baseri, H.: Experimental study of rotary magnetic field-assisted dry EDM with ultrasonic vibration of workpiece. Int. J. Adv. Manuf. Technol. **67**(5–8), 1371–1384 (2013)
46. Chattopadhyay, K.D., Satangi, P.S., Verma, S., Sherma, P.C.: Analysis of rotary electrical discharge machining characteristics in reversal magnetic field for copper-en8 steel system. Int. J. Adv. Manuf. Technol. **38**, 925–937 (2008)
47. Lin, J.L., Lin, C.L.: The use of the orthogonal array with grey relational analysis to optimize the electrical discharge machining process with multiple performance characteristics. Int. J. Mach. Tools Manuf. **42**(2), 237–244 (2002)
48. Tzeng, C.J., Lin, Y.H., Yang, Y.K., Jeng, M.C.: Optimization of turning operations with multiple performance characteristics using the Taguchi method and grey relational analysis. J. Mater. Process. Technol. **209**(6), 2753–2759 (2009)
49. Sivapirakasam, S.P., Mathew, J., Surianarayanan, M.: Multi attribute decision making for green electrical discharge machining. Expert Syst. Appl. **38**(7), 8370–8374 (2011)
50. Tang, L., Du, Y.T.: Experimental study on green electrical discharge machining in tap water of Ti-6Al-4V and parameters optimization. Int. J. Adv. Manuf. Technol. **70**, 469–475 (2014)
51. Zadeh, L.A.: Fuzzy sets. Inf. Control **8**(3), 338–353 (1965)
52. Bortolan, G., Degami, R.: A review of some methods for ranking fuzzy subset. Fuzzy Set Syst. **15**(1), 1–19 (1985)
53. Tong, L.I., Su, C.T.: Optimizing multi-response problems in the Taguchi method by fuzzy multiple attribute decision making. Int. Qual. Reliab. Eng. **13**, 25–34 (1997)

Two-Warehouse Reverse Logistic Inventory Model for Deteriorating Item under Learning Effect

S.R. Singh and Himanshu Rathore

Abstract Sustainability of environment requires more concentration on reverse logistics. Keeping this in mind, in this article, we have developed a two-warehouse reverse logistic model with finite rate of production and remanufacturing. A forward and reverse supply chain is considered for deteriorating items. During different cycles, remanufactured and fresh products are stored in owned warehouse (OW) which has limited storage space. For the excess amount, supplier hire rented warehouse (RW) at a high cost of holding than the holding cost of OW. Main objective of this study is to find optimal value of total relevant cost. Numerical illustration and sensitivity analysis is given at the end of this paper.

Keywords Two warehouse · Remanufacturing · Production · Reverse logistics · Deterioration

1 Introduction

In today's global world, recycling becomes very important due to environmental changes as well as in economic perspective. Recycling is a recovery process of used items. In this process, used items are collected from customer's end and send to the remanufacturing unit for the recovery. This whole process of forward and backward supply chain is known as reverse logistics. In recent years, many authors have focused on reverse logistics. It is also promoted by the governments to save the environment and human life.

S.R. Singh (✉)
Department of Mathematics, D. N. College, Meerut, Uttar Pradesh, India
e-mail: shivrajpundir@gmail.com

H. Rathore
Banasthali University, Banasthali, Rajasthan, India
e-mail: rathorehimanshu2003@gmail.com

K.N. Das et al. (eds.), *Proceedings of Fourth International Conference on Soft Computing for Problem Solving*, Advances in Intelligent Systems and Computing 335,
DOI 10.1007/978-81-322-2217-0_5

Reverse logistic is applicable in many cases, for example, electronic items, spare parts, etc. In the literature, the concept of reverse logistics is first introduced by Schrady [1]. He developed an EOQ model for recoverable items with the concept of reverse logistics and instantaneous rate of production and repairing. Further many authors have extended his work like Nahmias and Rivera [2], Fleischmann et al. [3], El Saadany and Jaber [4], etc. Recently, many authors have studied the concept of reverse logistics for deteriorating items. For further review, we can go through the work of Alamri [5], Singh and Saxena [6], Singh et al. [7], Singh and Saxena [8, 9], etc.

Storage space is an important factor in different aspects. In the literature, many authors have studied the two-warehouse inventory problems. Hartley [10] is the first who studied the two-warehouse problem. The concept of limited storage capacity of owned warehouse (OW) is first introduced by Sarma [11]. Further many authors have concentrated on the concept of two-warehouse problem like Kumari et al. [12], and Singh et al. [13] have studied the two-warehouse inventory problem for deteriorating items.

It is very often seen that through a repetitive process, everything get fine and fine shape. An organization and their employee perform the same process repeatedly; through this repetitive process, they get experience. As the experience increases, the costs associated with repetitive process decreases. So one can say the production and remanufacturing cost decreases as these processes performed repeatedly just because of learning effect. In recent years, many authors have focused on the effect of learning in modeling of inventory problems. Chin and Chen [14], Kuo and Yang [15], Jaber et al. [16], and Singh et al. [17] have studied the effect of learning.

In this paper, we have developed an inventory model for repairable items with constant rate of demand, production, remanufacturing collection, and deterioration of items. We have considered the concept of two warehouses with limited storage capacity of owned warehouse and infinite storage capacity at production unit and collection unit. Effect of learning is studied on production and remanufacturing cost. The diagrammatic representation of forward and backward flow of products is shown in Fig. 1.

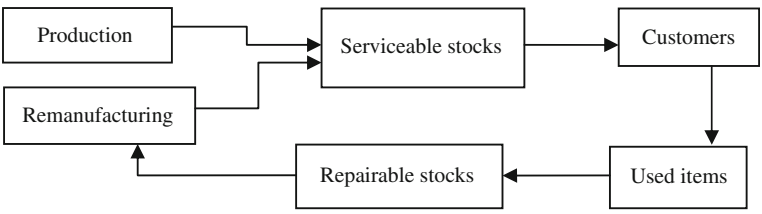

Fig. 1 Flow of inventory in forward and backward supply chain

2 Assumptions and Notations

The assumptions and notations which are used in mathematical model formulation are given as below.

2.1 Notations

In this paper, subscript 'm' is used for the manufacturing cycle, and subscripts 'r' and 'c' are used for remanufacturing cycle and collection (returned items) cycle, respectively.

- P_m, P_r are the finite production and remanufacturing rate, respectively.
- R_c: rate of returning items.
- θ: deterioration rate.
- D: demand rate.
- T: total cycle length.
- K_m: setup cost for manufacturing.
- K_r: setup cost for remanufacturing.
- K_c: setup cost for collection.
- h_0 (t): holding cost (per unit per unit time) of owned warehouse.
- h_R (t): holding cost (per unit per unit time) of rented warehouse.
- $h_c(t)$: cost for holing returned items per unit per unit time.
- S_m: unit procurement cost.
- C_m: unit production cost.
- C_r: unit remanufacturing cost.
- C_c: unit acquisition cost.
- q_1: maximum inventory level during remanufacturing.
- q_2: maximum inventory level during manufacturing.
- t_i: time intervals for $i = 1, 2, \ldots, 7$.
- $I_{mi}(t)$: inventory level during manufacturing, $i = 1, 2, \ldots, 5$.
- $I_{ri}(t)$: inventory level during remanufacturing, $i = 1, 2, \ldots, 5$.
- $I_{ci}(t)$: inventory level during collection cycle, $i = 1, 2$.

2.2 Assumptions

- Items are returnable, and retuned items are remanufactured. In quality, both manufactured and remanufactured products are of same quality.
- System is proposed for single item only.
- Deterioration rate is constant.
- Items are produced/remanufactured at a finite rate of production and remanufacturing. First, w amount of items is stored in owned warehouse (OW). The

quantity exceeding w amount is stored in rented warehouse (RW) which is hired by supplier at high cost of holding than OW.

- Demand is satisfied by both fresh and remanufactured products. Products of RW are sold first and then products of OW.
- Cycle length is infinite, but we have discussed only a typical cycle of length T. All other cycles are identical to the cycle T.
- $C_r + C_r^{'}/n^{\beta}$ is the remanufacturing cost under the effect of learning where $\beta > 0$ is the learning coefficient.
- $C_m + C_m^{'}/n^{\gamma}$ is the manufacturing cost under the effect of learning where $\gamma > 0$ is the learning coefficient.
- Holding costs (per unit per unit time) of both OW and RW are linear function of time $h_o\ (t) = h_1 + h_2 t$, $h_R\ (t) = h_3 + h_4 t$ such that $h_o(t) < h_R\ (t)$.
- Holding cost (per unit per unit time) for collected items is $h_C(t) = h_5 + h_6 t$.

3 Mathematical Model Formulation

The inventory depletion is governed by the following differential equations and graphically represented in Fig. 2. During the time period $[0, t_1]$ and $[t_1, t_2]$, returned items are remanufactured and stored in owned warehouse and rented warehouse,

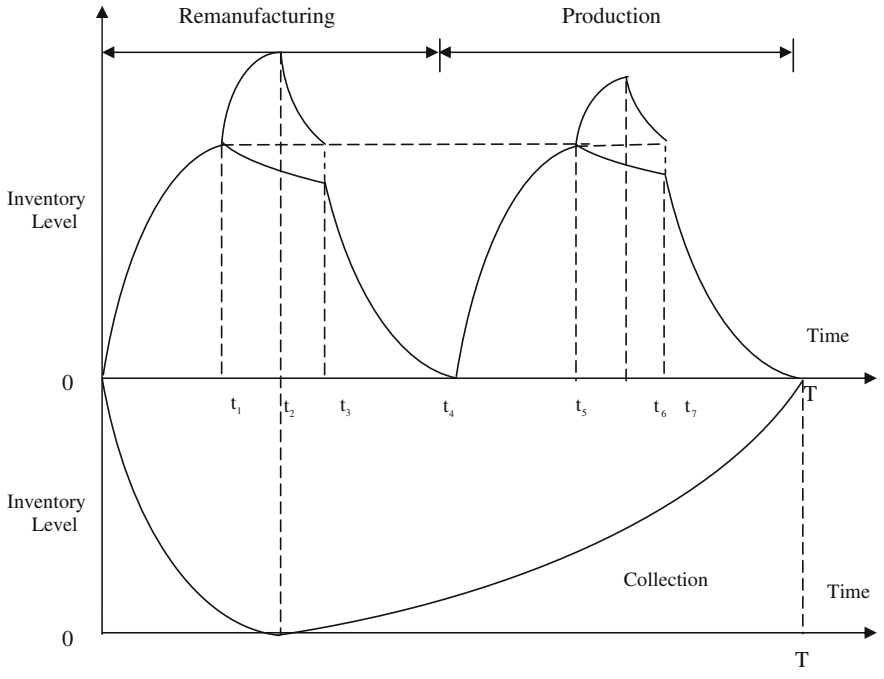

Fig. 2 Graphical representation of inventory depletion during $[0, T]$

respectively. At time $t_{2,}$ inventory level of returned items becomes zero, and at this instant, remanufacturing process ceases. During time intervals $[t_2, t_3]$ and $[t_3, t_4]$, inventory depleted due to combine effect of demand and deterioration in rented and owned warehouse, respectively. Similarly, functioning of inventory in production cycle during $[t_4, T]$ is shown Fig. 2.

Remanufacturing Cycle

$$\frac{\mathrm{d}I_{\mathrm{r}1}(t)}{\mathrm{d}t} + \theta I_{\mathrm{r}1}(t) = P_{\mathrm{r}} - D; \quad I_{\mathrm{r}1}(t=0) = 0, I_{\mathrm{r}1}(t=t_1) = w, \quad 0 \le t \le t_1 \tag{1}$$

$$\frac{\mathrm{d}I_{\mathrm{r}2}(t)}{\mathrm{d}t} + \theta I_{\mathrm{r}2}(t) = P_{\mathrm{r}} - D; \quad I_{\mathrm{r}2}(t=t_1) = 0, I_{\mathrm{r}2}(t=t_2) = q_1 - w, \quad t_1 \le t \le t_2 \tag{2}$$

$$\frac{\mathrm{d}I_{\mathrm{r}3}(t)}{\mathrm{d}t} + \theta I_{\mathrm{r}3}(t) = -D; \quad I_{\mathrm{r}3}(t=t_3) = 0, I_{\mathrm{r}3}(t=t_2) = I_{\mathrm{r}2}(t=t_2), \quad t_2 \le t \le t_3 \tag{3}$$

$$\frac{\mathrm{d}I_{\mathrm{r}4}(t)}{\mathrm{d}t} + \theta I_{\mathrm{r}4}(t) = 0; \quad I_{\mathrm{r}4}(t=t_1) = w, I_{\mathrm{r}4}(t=t_3) = I_{\mathrm{r}5}(t=t_3), \quad t_1 \le t \le t_3 \tag{4}$$

$$\frac{\mathrm{d}I_{\mathrm{r}5}(t)}{\mathrm{d}t} + \theta I_{\mathrm{r}5}(t) = -D; \quad I_{\mathrm{r}5}(t=t_4) = 0, I_{\mathrm{r}4}(t=t_3) = I_{\mathrm{r}5}(t=t_3), \quad t_3 \le t \le t_4 \tag{5}$$

Manufacturing Cycle

$$\frac{\mathrm{d}I_{\mathrm{m}1}(t)}{\mathrm{d}t} + \theta I_{\mathrm{m}1}(t) = P_{\mathrm{m}} - D; \quad I_{\mathrm{m}1}(t=t_4) = 0, I_{\mathrm{m}1}(t=t_5) = w, \quad t_4 \le t \le t_5 \tag{6}$$

$$\frac{\mathrm{d}I_{\mathrm{m}2}(t)}{\mathrm{d}t} + \theta I_{\mathrm{m}2}(t) = P_{\mathrm{m}} - D; \quad I_{\mathrm{m}2}(t=t_5) = 0, I_{\mathrm{m}2}(t=t_6) = q_2 - w, \quad t_5 \le t \le t_6 \tag{7}$$

$$\frac{\mathrm{d}I_{\mathrm{m}3}(t)}{\mathrm{d}t} + \theta I_{\mathrm{m}3}(t) = -D; \quad I_{\mathrm{m}3}(t=t_7) = 0, I_{\mathrm{m}3}(t=t_6) = I_{\mathrm{m}2}(t=t_6), \quad t_6 \le t \le t_7 \tag{8}$$

$$\frac{\mathrm{d}I_{\mathrm{m}4}(t)}{\mathrm{d}t} + \theta I_{\mathrm{m}4}(t) = 0; \quad I_{\mathrm{m}4}(t=t_5) = w, I_{\mathrm{m}4}(t=t_7) = I_{\mathrm{m}5}(t=t_7), \quad t_5 \le t \le t_7 \tag{9}$$

$$\frac{dI_{m5}(t)}{dt} + \theta I_{m5}(t) = -D; \quad I_{m5}(t = T) = 0, I_{m4}(t = t_7) = I_{m5}(t = t_7), \quad t_7 \le t \le T \tag{10}$$

Collection Cycle

$$\frac{dI_{C1}(t)}{dt} + \theta I_{C1}(t) = R_C - P_r; \quad I_{C1}(t = t_2) = 0, \qquad t_4 \le t \le t_5 \tag{11}$$

$$\frac{dI_{C2}(t)}{dt} + \theta I_{C2}(t) = R_C; \quad I_{C2}(t = t_2) = 0, I_{C2}(t = T) = I_{C1}(t = 0), \quad t_5 \le t \le t_6 \tag{12}$$

Now solving above (1)–(10), respectively, we get

Remanufacturing Cycle

$$I_{r1}(t) = \left(\frac{P_r - D}{\theta}\right)\left[e^{\theta t_1} - 1\right]e^{-\theta t} \tag{13}$$

$$I_{r2}(t) = \left(\frac{P_r - D}{\theta}\right)\left[e^{\theta t_2} - e^{\theta t_1}\right]e^{-\theta t} \tag{14}$$

$$I_{r3}(t) = \left(\frac{-D}{\theta}\right)\left[e^{\theta t_3} - e^{\theta t_2}\right]e^{-\theta t} \tag{15}$$

$$I_{r4}(t) = we^{\theta(t_1 - t)} \tag{16}$$

$$I_{r5}(t) = \left(\frac{-D}{\theta}\right)\left[e^{\theta t_4} - e^{\theta t_3}\right]e^{-\theta t} \tag{17}$$

Using continuity of inventory functions, we get

$$t_1 = \left(\frac{P_r - D}{w}\right);$$

$$t_2 = \left(\frac{q_1 - w}{P_r - D} + \frac{P_r - D}{w}\right);$$

$$t_3 = \left[\left(\frac{(P_r - D)^2}{Dw}\right) + \left(\frac{2D - P_r}{D}\right)\left(\frac{q_1 - w}{P_r - D} + \frac{P_r - D}{w}\right)\right];$$

$$t_4 = \left[\left(-\frac{w}{D} - \frac{P_r - D}{w}\right) + \left(\frac{w\theta}{D}\right)\left(\left(\frac{(P_r - D)^2}{Dw}\right) + \left(\frac{2D - P_r}{D}\right)\left(\frac{q_1 - w}{P_r - D} + \frac{P_r - D}{w}\right)\right)\right];$$

Manufacturing Cycle

$$I_{m1}(t) = \left(\frac{P_m - D}{\theta}\right)\left[e^{\theta t_5} - e^{\theta t_4}\right]e^{-\theta t} \tag{18}$$

$$I_{m2}(t) = \left(\frac{P_m - D}{\theta}\right)\left[e^{\theta t_6} - e^{\theta t_5}\right]e^{-\theta t} \tag{19}$$

$$I_{m3}(t) = \left(\frac{-D}{\theta}\right)\left[e^{\theta t_7} - e^{\theta t_6}\right]e^{-\theta t} \tag{20}$$

$$I_{m4}(t) = we^{\theta(t_5 - t)} \tag{21}$$

$$I_{m5}(t) = \left(\frac{-D}{\theta}\right)\left[e^{\theta T} - e^{\theta t_7}\right]e^{-\theta t} \tag{22}$$

Using continuity of inventory functions, we get

$$t_5 = \left(\frac{P_m - D}{w}\right) + \left[\left(-\frac{w}{D} - \frac{P_r - D}{w}\right) + \left(\frac{w\theta}{D}\right)\left(\left(\frac{(P_r - D)^2}{Dw}\right) + \left(\frac{2D - P_r}{D}\right)\left(\frac{q_1 - w}{P_r - D} + \frac{P_r - D}{w}\right)\right)\right];$$

$$t_6 = \left(\frac{q_2 - w}{P_m - D}\right) + \left(\frac{P_m - D}{w} + \left(-\frac{w}{D} - \frac{P_r - D}{w}\right)\right.$$
$$\left. + \left(\frac{w\theta}{D}\right)\left(\left(\frac{(P_r - D)^2}{Dw}\right) + \left(\frac{2D - P_r}{D}\right)\left(\frac{q_1 - w}{P_r - D} + \frac{P_r - D}{w}\right)\right)\right);$$

$$t_7 = \left[\left(\frac{(P_m - D)^2}{Dw} + \frac{P_m - D}{D}\left(\left(-\frac{w}{D} - \frac{P_r - D}{w}\right)\right.\right.\right.$$
$$\left.\left.\left. + \left(\frac{w\theta}{D}\right)\left(\left(\frac{(P_r - D)^2}{Dw}\right) + \left(\frac{2D - P_r}{D}\right)\left(\frac{q_1 - w}{P_r - D} + \frac{P_r - D}{w}\right)\right)\right)\right)\right]$$
$$+ \left[\left(\frac{2D - P_m}{D}\right)\left(\frac{q_2 - w}{P_m - D}\right) + \left(\frac{P_m - D}{w} + \left(-\frac{w}{D} - \frac{P_r - D}{w}\right)\right.\right.$$
$$\left.\left. + \left(\frac{w\theta}{D}\right)\left(\left(\frac{(P_r - D)^2}{Dw}\right) + \left(\frac{2D - P_r}{D}\right)\left(\frac{q_1 - w}{P_r - D} + \frac{P_r - D}{w}\right)\right)\right)\right];$$

$$T = \left[\left(1 + \frac{w\theta}{D}\right)t_7 - \frac{w\theta}{D}t_5 - \frac{w}{D}\right]$$

Collection Cycle

$$I_{C1}(t) = \left(\frac{R_C - P_r}{\theta}\right)\left[e^{\theta t_2} - 1\right]e^{-\theta t} \tag{23}$$

$$I_{C2}(t) = \left(\frac{R_C}{\theta}\right)\left[e^{\theta T} - e^{\theta t_2}\right]e^{-\theta t} \tag{24}$$

Now acceptable returned quantity for used items is

$$Q = R_C T$$

Now using continuity of inventory function, we get

$$\int_0^T R_C \mathrm{d}t = \int_0^{t_2} P_r \mathrm{d}t \Rightarrow R_C T = P_r t_2$$

Total cost function includes following cost parameters:

1. Procurement (POC) and Acquisitions (AC) cost is

$$= S_m \int_{t_4}^{t_6} P_m \mathrm{d}t + C_C \int_0^T R_C \mathrm{d}t = S_m P_m (t_6 - t_4) + C_C R_C T \tag{25}$$

2. Production (PC) and Remanufacturing (RC) cost is

$$\begin{aligned} &= \left(C_m + \frac{C'_m}{n^\gamma}\right) \int_{t_4}^{t_6} P_m \mathrm{d}t + \left(C_r + \frac{C'_r}{n^\beta}\right) \int_0^{t_2} P_r \mathrm{d}t \\ &= \left(C_m + \frac{C'_m}{n^\gamma}\right) P_m (t_6 - t_4) + \left(C_r + \frac{C'_r}{n^\beta}\right) P_r t_2 \end{aligned} \tag{26}$$

3. Holding = Cost is HC [Holding cost for remanufactured items + Holding cost for manufactured items + Holding cost for collected items]

$$\begin{aligned} = &\left| \int_0^{t_1} (h_1 + h_2 t) I_{r1}(t) \mathrm{d}t + \int_{t_1}^{t_3} (h_1 + h_2 t) I_{r4}(t) \mathrm{d}t + \int_{t_3}^{t_4} (h_1 + h_2 t) I_{r5}(t) \mathrm{d}t \right. \\ &\left. + \int_{t_1}^{t_2} (h_3 + h_4 t) I_{r2}(t) \mathrm{d}t + \int_{t_2}^{t_3} (h_3 + h_4 t) I_{r3}(t) \mathrm{d}t \right] \\ &+ \left[\int_{t_4}^{t_5} (h_1 + h_2 t) I_{m1}(t) \mathrm{d}t + \int_{t_5}^{t_7} (h_1 + h_2 t) I_{m4}(t) \mathrm{d}t + \int_{t_7}^{T} (h_1 + h_2 t) I_{r5}(t) \mathrm{d}t \right. \\ &\left. + \int_{t_5}^{t_6} (h_3 + h_4 t) I_{m2}(t) dt + \int_{t_6}^{t_7} (h_3 + h_4 t) I_{m3}(t) \mathrm{d}t + + \int_{t_5}^{t_6} (h_3 + h_4 t) I_{m2}(t) \mathrm{d}t \right] \end{aligned}$$

$$
\begin{aligned}
&= (P_{\mathrm{r}} - D)\left[h_1 t_1^2 + (h_2 - \theta h_1)\frac{t_1^3}{2} - \frac{\theta h_2 t_1^4}{3}\right] \\
&\quad + w\mathrm{e}^{\theta t_1}\left[h_1(t_3 - t_1) + (h_2 - \theta h_1)\frac{\left(t_3^2 - t_1^2\right)}{2} - \frac{\theta h_2\left(t_3^3 - t_1^3\right)}{3}\right] \\
&\quad + D(t_3 - t_4)\left[h_1(t_4 - t_3) + (h_2 - \theta h_1)\frac{\left(t_4^2 - t_3^2\right)}{2} - \frac{\theta h_2\left(t_4^3 - t_3^3\right)}{3}\right] \\
&\quad + (P_{\mathrm{r}} - D)(t_2 - t_1)\left[h_3(t_2 - t_1) + (h_4 - \theta h_3)\frac{\left(t_2^2 - t_1^2\right)}{2} - \frac{\theta h_4\left(t_2^3 - t_1^3\right)}{3}\right] \\
&\quad + (D)(t_2 - t_3)\left[h_3(t_3 - t_2) + (h_4 - \theta h_3)\frac{\left(t_3^2 - t_2^2\right)}{2} - \frac{\theta h_4\left(t_3^3 - t_2^3\right)}{3}\right] \\
&\quad + (P_{\mathrm{m}} - D)(t_5 - t_4)\left[h_1(t_5 - t_4) + (h_2 - \theta h_1)\frac{\left(t_5^2 - t_4^2\right)}{2} - \frac{\theta h_2\left(t_5^3 - t_4^3\right)}{3}\right] \\
&\quad + w\mathrm{e}^{\theta t_5}\left[h_1(t_7 - t_5) + (h_2 - \theta h_1)\frac{\left(t_7^2 - t_5^2\right)}{2} - \frac{\theta h_2\left(t_7^3 - t_5^3\right)}{3}\right] \\
&\quad + D(t_7 - T)\left[h_1(T - t_7) + (h_2 - \theta h_1)\frac{\left(T^2 - t_7^2\right)}{2} - \frac{\theta h_2\left(T^3 - t_7^3\right)}{3}\right] \\
&\quad + (P_{\mathrm{m}} - D)(t_6 - t_5)\left[h_3(t_6 - t_5) + (h_4 - \theta h_3)\frac{\left(t_6^2 - t_5^2\right)}{2} - \frac{\theta h_4\left(t_6^3 - t_5^3\right)}{3}\right] \\
&\quad + (D)(t_6 - t_7)\left[h_3(t_7 - t_6) + (h_4 - \theta h_3)\frac{\left(t_7^2 - t_6^2\right)}{2} - \frac{\theta h_4\left(t_7^3 - t_6^3\right)}{3}\right] \\
&\quad + (R_{\mathrm{C}} - P_{\mathrm{r}})\left[h_5 t_2^2 + (h_6 - \theta h_5)\frac{t_2^3}{2} - \frac{\theta h_6 t_2^4}{3}\right] \\
&\quad + R_{\mathrm{C}}(T - t_2)\left[h_5(T - t_2) + (h_6 - \theta h_5)\frac{\left(T^2 - t_2^2\right)}{2} - \frac{\theta h_6\left(T^3 - t_2^3\right)}{3}\right]
\end{aligned}
\tag{27}
$$

Now using continuity functions for values of t_1, t_2, t_3, t_4, t_5, t_6, and t_7, T is the total cost function. Hence, total cost function per unit time is

$$\mathrm{TC}\ (q_1,\ q_2,\ Q)\ =\ (1/T)\left[K_{\mathrm{r}} + K_{\mathrm{m}} + K_{\mathrm{C}} + \mathrm{POC} + \mathrm{AC} + \mathrm{PC} + \mathrm{RC} + \mathrm{HC}\right] \tag{28}$$

To minimize total relevant cost, we differentiate TC (t_1, T, ξ) w. r. t to t_1, T and ξ, and for optimal value, necessary conditions are

$$\frac{\partial TC(q_1, q_2, Q)}{\partial q_1} = 0;\ \frac{\partial TC(q_1, q_2, Q)}{\partial q_2} = 0;\ \frac{\partial TC(q_1, q_2, Q)}{\partial Q} = 0$$

Provided the determinant of principal minor of hessian matrix is positive definite, i.e., det($H1$) > 0, det($H2$) > 0, and det($H3$) > 0 where H1, H2, and H3 are the principal minor of the Hessian matrix. Hessian matrix of the total cost function is as follows:

$$\begin{bmatrix} \frac{\partial^2 \mathrm{TC}}{\partial q_1^2} & \frac{\partial^2 \mathrm{TC}}{\partial q_1 \partial q_2} & \frac{\partial^2 \mathrm{TC}}{\partial q_1 \partial Q} \\ \frac{\partial^2 \mathrm{TC}}{\partial q_2 \partial q_1} & \frac{\partial^2 \mathrm{TC}}{\partial q_2^2} & \frac{\partial^2 \mathrm{TC}}{\partial q_2 \partial Q} \\ \frac{\partial^2 \mathrm{TC}}{\partial Q \partial q_1} & \frac{\partial^2 \mathrm{TC}}{\partial Q \partial q_2} & \frac{\partial^2 \mathrm{TC}}{\partial Q^2} \end{bmatrix}$$

4 Numerical Example and Sensitivity Analysis

For the numerical illustration, following numerical values are used to calculate optimal value of total cost $K_m = 150$, $K_{r-} = 80$, $K_c = 100$, $h_1 = 1$, $h_2 = 0.2$, $h_3 = 2$, $h_4 = 0.5$, $h_5 = 1$, $h_6 = 0.2$, $R_c = 6$, $D = 10$, $P_m = 20$, $P_r = 12$, $w = 50$, $\theta = 0.005$, $S_m = 8$, $C_m = 3$, $C_m^{'} = 3.2$, $C_r = 2$, $C_r^{'} = 2.2$, $n = 6$, $C_c = 2$, with the help of mathematical software Mathematica7, and optimal values are as follows: TC* = 1,764.33 × 10^3, $Q^* = 878.619$, $q_1^* = 620.614$, $q_2^* = 2{,}420.87$, $T^* = 2.77388$ (Figs. 3, 4, and 5).

The keen observations of Table 1 are as follows:

- Increment in D results in increment in T^*, q_2^*, and TC*, while decrement in q_1^*.
- Increment in P_m results in increment in q_2^* and q_1^*, while decrement in T^* and TC*.

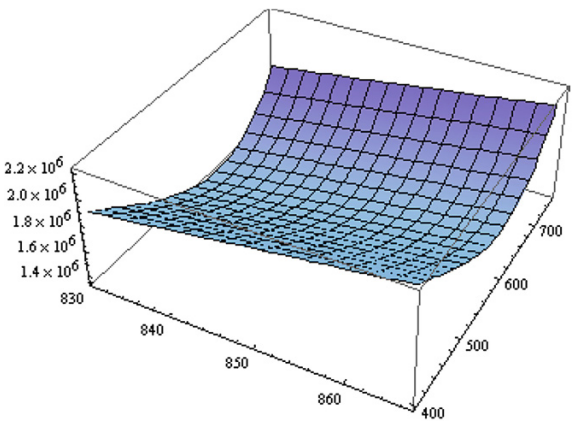

Fig. 3 Convexity of TC* w. r. t. Q^* and q_1^*

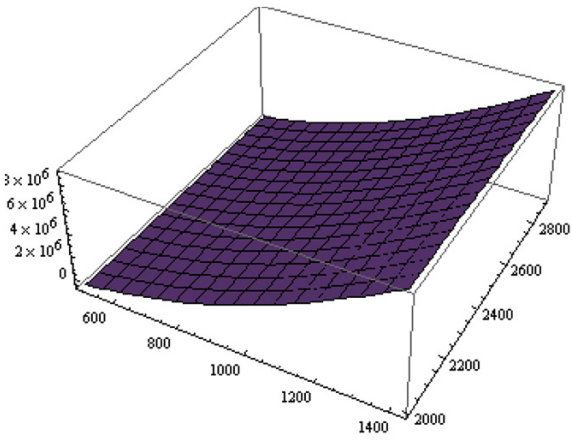

Fig. 4 Convexity of TC* w. r. t. Q^* and q_2^*

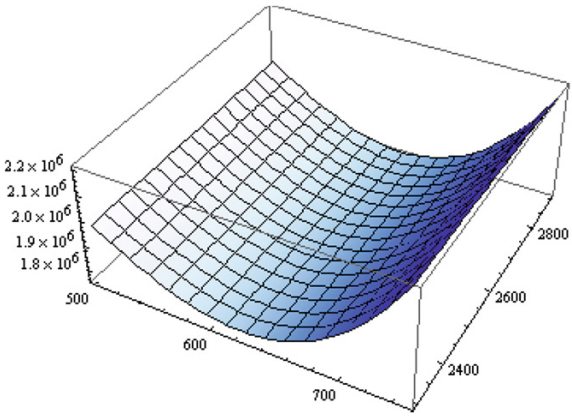

Fig. 5 Convexity of TC* w. r. t. q_1^* and q_2^*

- Increment in P_r results in increment in T^*, q_1^*, and Q^*, while decrement in q_2^*, TC*.
- Increment in P_m results in increment in Q^*, while decrement in TC*.
- Increment in γ and β results in decrement TC*.

Table 1 Sensitivity analysis

D	T^*	Q^*	q_1^*	q_2^*	$TC^* \times 10^3$
10.2	1.746645	878.619	555.804	4,203.53	1,873.17
10.6	2.03134	878.619	550.136	8,344.36	9,582.65
10.8	2.41801	878.619	483.456	8,587.5	1,6536.4
11	2.77.476	878.619	394.624	8,610.74	2,1087.6
P_m	T^*	Q^*	q_1^*	q_2^*	$TC^* \times 10^3$
20.1	1.58964	878.619	621.208	2,319	1,750.41
20.2	1.57528	878.619	622.129	2,291.79	1,742.57
20.3	1.56418	878.619	623.484	2,348.1	1,740.05
20.4	1.53656	878.619	632.789	2,909.53	1,706.06
P_r	T^*	Q^*	q_1^*	q_2^*	$TC^* \times 10^3$
12.1	2.933474	886.44	676.07	2,379.16	2,710.34
12.2	2.95737	894.002	749.723	2,331.53	1,776.21
12.3	2.97855	901.318	861.101	2,278.69	1,672.74
12.4	2.99507	908.403	1060.34	2,224.35	1,281.53
R_c	T^*	Q^*	q_1^*	q_2^*	$TC^* \times 10^3$
6.1	2.77388	863.729	620.614	2420.87	1761.17
6.2	2.77388	869.444	620.614	2420.87	1733.43
6.3	2.77388	873.758	620.614	2420.87	1700.79
6.4	2.77388	876.784	620.614	2420.87	1655.59
γ	T^*	Q^*	q_1^*	q_2^*	$TC^* \times 10^3$
0.021	2.77388	878.619	620.614	2,420.76	1,764.3
0.03	2.77388	878.619	620.608	2,419.76	1,764.07
0.04	2.77388	878.619	620.603	2,418.66	1,763.81
0.05	2.77388	878.619	620.597	2,417.59	1,763.56
β	T^*	Q^*	q_1^*	q_2^*	$TC^* \times 10^3$
0.03	2.77388	878.619	620.62	2420.86	1,764.2
0.04	2.77388	878.619	620.625	2,420.85	1,764.07
0.05	2.77388	878.619	620.631	2,420.84	1,763.95
0.06	2.77388	878.619	620.636	2,420.83	1,763.8

5 Conclusion

In this article, we studied concept of reverse logistics under the effect of learning. We have developed a two-warehouse inventory model for deteriorating items in forward and backward supply chain. The optimal values of total cost TC*, maximum level of returned item Q^*, maximum level of remanufactured products q_1^*, and maximum level of manufactured products q_2^* are calculated by using mathematical software Mathematica7. The numerical illustration and sensitivity analysis

is given. This study is applicable in case of electronic items, spare parts, and other recoverable items. For the future research, we can incorporate some other parameters of inventory control system.

References

1. Schrady, D.A.: A deterministic inventory model for repairable items. Naval Res. Logistics Q. **14**(3), 391–398 (1967)
2. Nahmias, S., Rivera, H.: A deterministic model for repairable item inventory system with finite repair rate. Int. J. Prod. Res. **17**(3), 215–221 (1979)
3. Fleischmann, M., Bloemhof-Ruwaard, J.M., Dekker, R., Van Der Laan, E., Van Nunen, J.A.E. E., Van Wassenhove, L.N.: Quantitative models for reverse logistics: a review. Eur. J. Oper. Res. **103**(1), 1–17 (1997)
4. El Saadany, A.M.A., Jaber, M.Y.: A production/remanufacturing inventory model with price and quality dependent return rate. Comput. Ind. Eng. **58**(3), 352–362 (2010)
5. Alamri, A.A.: Theory and methodology on the global optimal solution to a general reverse logistics inventory model for deteriorating items and time varying rates. Comput. Ind. Eng. **60** (2), 236–247 (2010)
6. Singh, S.R., Saxena, N.: An optimal returned policy for a reverse logistics inventory model with backorders. Adv. Decis. Sci. Article ID 386598, 21 (2012)
7. Singh, S.R., Prasher, L., Saxena, N.: A centralized reverse channel structure with flexible manufacturing under the stock out situation. Int. J. Ind. Eng. Comput. **4**, 559–570 (2013)
8. Singh, S.R., Saxena, N.: A closed loop supply chain system with flexible manufacturing and reverse logistics operation under shortages for deteriorating items. Procedia Technol. **10**, 330–339 (2013)
9. Singh, S.R., Saxena, N.: An integrated inventory model with remanufacturing of secondary material under shortages. In: Proceedings of 3rd International Conference on Recent Trends in Engineering & Technology, pp. 354–359. Elsevier, India (2014)
10. Hartley, R.V.: Operations Research—A Managerial Emphasis. Good Year Publishing Company, Culver City (1976)
11. Sarma, K.V.S.: A deterministic order level inventory model for deteriorating items with two storage facilities. Eur. J. Oper. Res. **29**, 70–73 (1987)
12. Kumari, R., Singh, S.R., Kumar, N.: Two-warehouse inventory model for deteriorating items with partial backlogging under the conditions of permissible delay in payments. Int. Trans. Math. Sci. Comput. **1**(1), 123–134 (2008)
13. Singh, S.R., Rathore, H., Saxena, N.: A two warehouse inventory model for deteriorating items with shortages under inflationary environment. In: Proceedings of 3rd International Conference on Recent Trends in Engineering & Technology, pp. 385–391. Elsevier, India (2014)
14. Chiu, H.N., Chen, H.M.: An optimal algorithm for solving the dynamic lot-sizing model with learning and forgetting in setups and production. Int. J. Prod. Econ. **95**(2), 179–193 (2005)
15. Kuo, W.-H., Yang, D.-L.: Minimizing the total completion time in a single-machine scheduling problem with a time-dependent learning effect. Eur. J. Oper. Res. **174**(2), 1184–1190 (2006)
16. Jaber, M.Y., Goyal, S.K., Imran, M.: Economic production quantity model for items with imperfect quality subject to learning effects. Int. J. Prod. Econ. **115**, 143–150 (2008)
17. Singh, S.R., Jain, S., Pareek, S.: An imperfect quality items with learning and inflation under two limited storage capacity. Int. J. Ind. Eng. Comput. **4**, 1–12 (2013)

An Integrated Approach of Logarithmic Transformation and Histogram Equalization for Image Enhancement

Saurabh Chaudhury, Sudhankar Raw, Abhradeep Biswas and Abhshek Gautam

Abstract Logarithmic transformation and histogram equalization (HE) are well-known image enhancement techniques in spatial domain. These techniques are very popular for contrast enhancement because the methods are simple and effective. The basic idea of HE is to remap the gray levels of an image. However, HE tends to introduce some annoying artifacts and unnatural enhancement. Here, we propose an integration of the two techniques at pixel level, doing first the HE and then using logarithmic transformation for mapping purpose. Both the *global HE* and *local HE* are preformed on the input image pixels. The histogram equalization has been performed in the MATLAB environment. We have experimented the proposed techniques over a number of sample images and found to produce much better results compared to image enhancement using the inbuilt MATLAB function *histeq.*

Keywords Image processing · Logarithmic transformation · Histogram equalization · Contrast enhancement · Histeq

1 Introduction

Image enhancement is among the simplest and most appealing areas of digital image processing. Basically, the idea behind enhancement techniques [1] is to bring out detail that is obscured, or simply to highlight certain features of interest in an image. It is important to keep in mind that enhancement is a very subjective area of image processing. Image enhancement can be carried out in two domains: spatial domain and frequency domain. Histogram and its equalization fall under spatial domain techniques, so also the logarithmic transformation. Logarithmic transformation is a

S. Chaudhury (✉) · S. Raw · A. Biswas · A. Gautam
Department of Electrical Engineering, National Institute of Technology Silchar, Silchar 788010, Assam, India
e-mail: saurabh1971@gmail.com

K.N. Das et al. (eds.), *Proceedings of Fourth International Conference on Soft Computing for Problem Solving*, Advances in Intelligent Systems and Computing 335,
DOI 10.1007/978-81-322-2217-0_6

non-linear basic gray-level transformation function which maps a narrow range of low gray values to a wider range of output levels and thus enhancing the contrast levels and brightness of the image. A histogram, on the other hand, is the estimation of the probability distribution of a particular type of data. An image histogram is a type of histogram which offers a graphical representation of the total distribution of the gray values in a digital image. For an 8-bit grayscale image, there are 256 different possible intensities, and so the histogram will graphically display 256 numbers showing the distribution of pixels among those grayscale values. By viewing the image's histogram, we can analyze the frequency of appearance of the different gray levels (intensities) contained in the image. Each colour or gray level is represented as a point on x-axis and y-axis represents the number of instances of a colour level that repeat in the image. Each color level (gray value) is represented as a point on *x*-axis, and on *y*-axis is the number instance of a color level repeats in the image. Histogram may be viewed or plotted with MATLAB *imhist* command.

Sometimes all the important information in an image lies only in a small region of colors; hence, it is usually difficult to extract information out of that image. There comes the need for histogram equalization. A good histogram is that which covers all the possible values in the grayscale used. This type of histogram suggests that the image has good contrast and that details in the image may be observed more easily.

1.1 Logarithmic Transformation

Log transformations are one of the elementary image enhancement techniques of the spatial domain that can be effectively used for contrast enhancements of dark images. The log transform is essentially a gray-level transform which means that the gray levels of image pixels are altered. This transformation maps a narrow range of low gray-level values in the input image to a wider range of output levels. The opposite is true for higher input gray levels. Thus, the dark input values are spread out into the higher gray level values which improve the overall contrast and brightness of the image. The general form of the log transformation can be mathematically represented as

$$s = c \ \log\left(1 + r\right) \tag{1}$$

where s is the output gray level, r is the input gray level, and c is a constant. It is assumed that $r \geq 0$. Figure 1 shows such a transformation function. This transformation is used to expand the dark pixels in an image while compressing the higher level pixel values as illustrated in Fig. 2 where the hidden diffraction pattern becomes prominent and clearly visible.

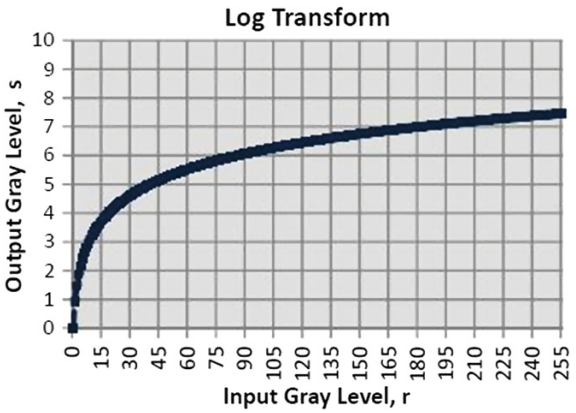

Fig. 1 Logarithmic transformation function

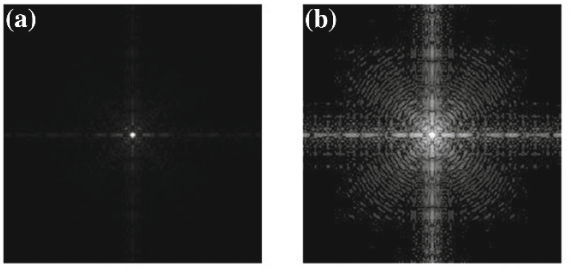

Fig. 2 Diffraction pattern enhanced through log transformation

1.2 Histogram Equalization (HE)

Various enhancement schemes are used for enhancing an image which includes grayscale manipulation, filtering, and histogram equalization (HE) [2–6]. Histogram equalization is one of the well-known image enhancement techniques. It has become a popular technique for contrast enhancement because this method is simple and effective. In the latter case, preserving the input brightness of the image is required to avoid the generation of non-existing artifacts in the output image. The basic idea of HE method is to remap the gray levels of an image. HE tends to introduce some annoying artifacts and unnatural enhancement.

1.3 Adaptive Histogram

This is an extension of traditional histogram equalization technique. It enhances the contrast of an image by transforming the values in the intensity image *I*. Unlike *histeq*, it operates on small data regions (tiles), rather than the entire image. Each tile's contrast is enhanced, so that the histogram of the output region approximately

matches the specified histogram. The neighboring tiles are then combined using bilinear interpolation in order to eliminate artificially induced boundaries. The contrast, especially in homogeneous areas, can be limited in order to avoid amplifying the noise which might be present in the image.

1.4 Histogram Equalization Techniques

There are a number of different types of histogram equalization exist, such as cumulative histogram equalization, normalized cumulative histogram equalization, and localized equalization. A detailed list of histogram equalization techniques and their advantages and disadvantages is explained in [7]. *Histogram expansion* is a simple technique that enhances the contrast levels of an image. But it has the disadvantage that if there are gray values that are physically far apart from each other in the image, then this method fails. *LAHE* offers an excellent image enhancement technique in terms of contrast level but has the disadvantage that it is computationally very slow and requires a high number of operations per pixel. *Par sectioning* on the other hand is easy to implement and better suits in hardware level, whereas *odd sectioning* offers a good image contrast but has problems with histograms which cover almost the full grayscale.

An advanced contrast enhancement using partially overlapped sub-block histogram equalization has been presented in [6]. This technique uses a low pass filter (as a mask) to get a non-overlapped sub-block histogram equalization which can produce high contrast associated with local histogram but can take advantage of simplicity of global equalization. In [8], a method to evaluate the performance of an enhancement technique is presented which they termed as EME on contrast. A modified histogram equalization is presented in [9] to avoid certain details which wash out after enhancement due to quantum jump of cumulative distribution function in histogram. Contrast enhancement using recursive mean-separate histogram equalization for scalable brightness preservation has been presented in [10]. A multi-histogram equalization technique has been presented in [11] which decomposes the image into several sub-images and then apply the classical HE process to each one. This way it performs a less intensive image contrast enhancement, and the output image presents a more natural look. Contrast enhancement for digital image using histogram equalization [12] on the other hand takes grayscale image enhancement by multi-histogram equalization, whereas for color images, it applies a hue-preserving HE for image enhancement.

Image histogram and histogram equalization find applications not only in image enhancement but also in other higher level processing such as in thresholding, adaptive thresholding [13], image segmentation [14], super-resolution, image quality, and image restoration. A histogram-based thresholding approach might be used to create a histogram of the image pixel intensities and it takes the valley point as the threshold. The histogram approach assumes that there is some average values

for both the background and object pixels, but that the actual pixel values have some variation around these average values.

The paper is organized as follows: Section 2 illustrates the proposed algorithms, the integrated global histogram equalization, and local histogram equalization, respectively, which include the mapping function to be the logarithmic transformation and techniques behind such processing. In Sect. 3, we present our observation on the results of exhaustive experimentation of the proposed techniques on some sample images, and finally, Sect. 4 concludes the paper.

2 Proposed Algorithms

The image enhancement (precisely, the contrast) using an integrated approach of Histogram Equalization and logarithmic transformation has been proposed here. The log transformation used here acts as the mapping function. Two algorithms have been proposed—global histogram equalization and local histogram equalization. The algorithms and flowchart are discussed in the following subsections and are implemented using MATLAB.

2.1 Integrated Global Histogram Equalization with Log Transformation

The flowchart (Fig. 3) depicts the different steps that were followed during the global histogram equalization.

Consider a discrete grayscale image $\{x\}$ and let n_i be the number of occurrences of gray level i. The probability of an occurrence of a pixel of level in the image is as follows:

$$p_x(i) = p(x = i) = n_i/n, \quad 0 \leq I < L \tag{3}$$

L being the total number of gray levels in the image, n being the total number of pixels in the image, and $p_x(i)$ being in fact the image's histogram for pixel value i,

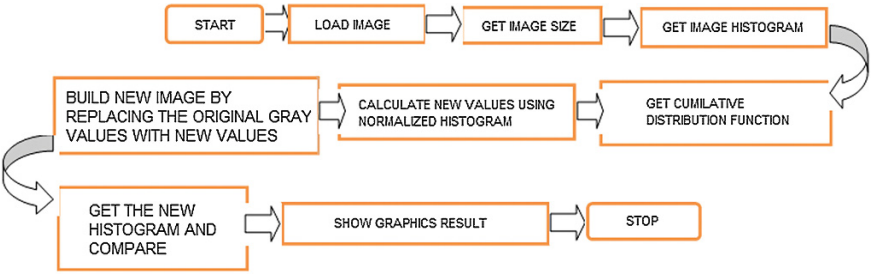

Fig. 3 Flow chart showing global histogram equalization technique

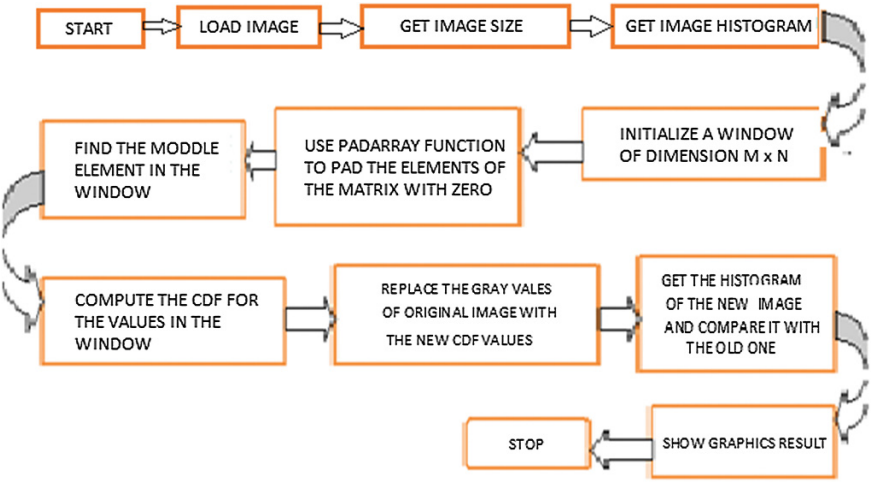

Fig. 4 Flow chart showing the proposed algorithm on local histogram equalization

normalized to [0,1]. The cumulative distribution function is defined corresponding to p_x as $\mathrm{cdf}_x(i) = \sum_{j=0}^{j=i} p(j)$ where p is a function of x which is also the image's accumulated normalized histogram. We would like to create a transformation of the form $y = T(x)$ to produce a new image $\{y\}$, such that its CDF will be linearized

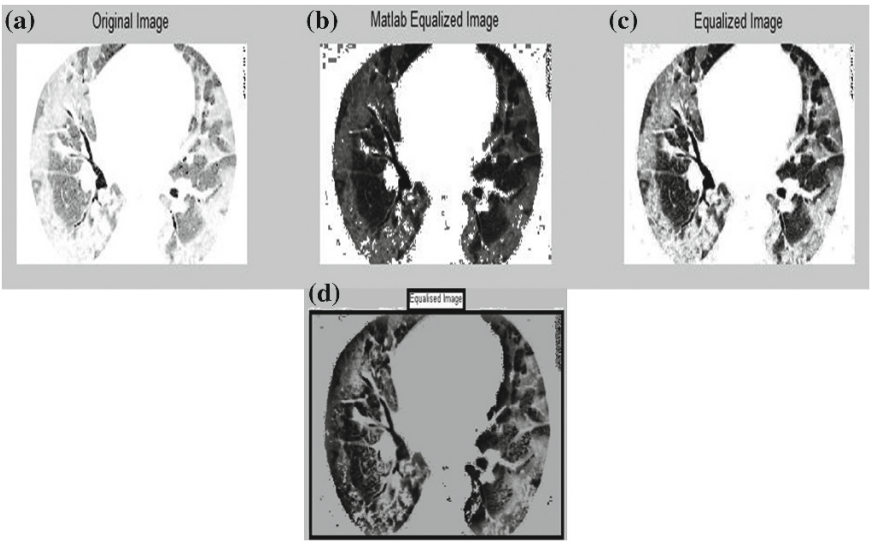

Fig. 5 **a** Image of human lungs; **b–d** are the images after MATLAB, integrated global HE, and local HE

across the value range, i.e., $\text{cdf}_x(i) = iK$ for some constant K. The properties of the CDF allow us to perform such a transform. For logarithmic transformation, this can be defined as follows:

$$y = T(x) = \log\{1 + \text{cdf}(x)\} \tag{4}$$

We notice here that T maps the gray levels in the image into the range [0,1] in a logarithmic way such that a large range of input gray levels can be confined to a narrow range of output gray levels. In order to map the values back into their original range, the following simple transformation needs to be applied on the result:

$$y' = y \cdot \{\max\{x\} - \min\{x\}\} + \min\{x\}.$$

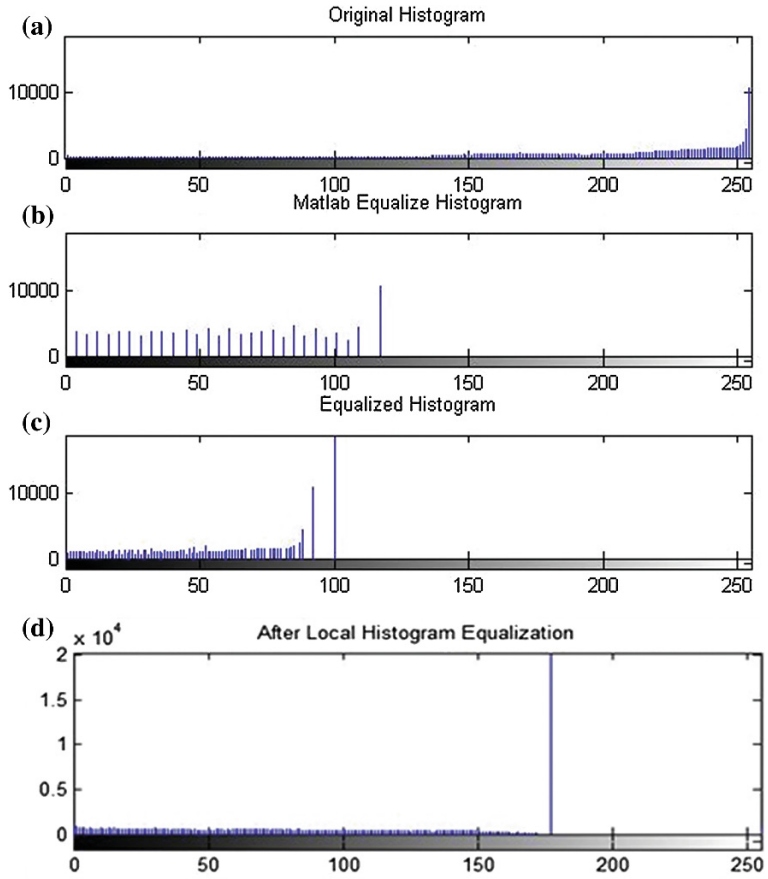

Fig. 6 **a** Histogram of lung image and **b–d** equalized histograms

2.2 Integrated Local Histogram Equalization with Log Transformation

The flowchart as shown in Fig. 4 depicts the algorithmic steps that have been implemented in the proposed approach for local histogram equalization.

- The input image is loaded, and the histogram is obtained by using the function *imhist* [15].
- A window of our own chosen size is initialized.
- CDF values for the pixels in the image are computed.
- The middle values for each window is computed, and the CDF value is calculated.
- The pixels in the original image are replaced by the new CDF values which depend on the value of the CDF of the middle element.
- Img(i,j) = round (cdf(ele)/(M * N) * 255).
- The histogram of the equalized image is obtained.
- Histograms of new and original images are compared.
- Print the graphic results.

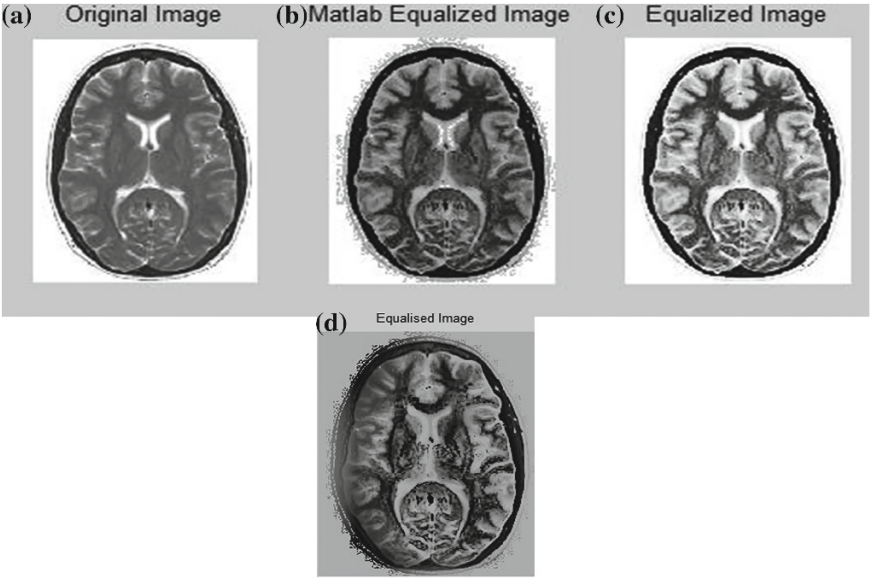

Fig. 7 **a** Human brain; **b–d** are MATLAB equalized, integrated global-logarithmic, and local-logarithmic equalized brain image

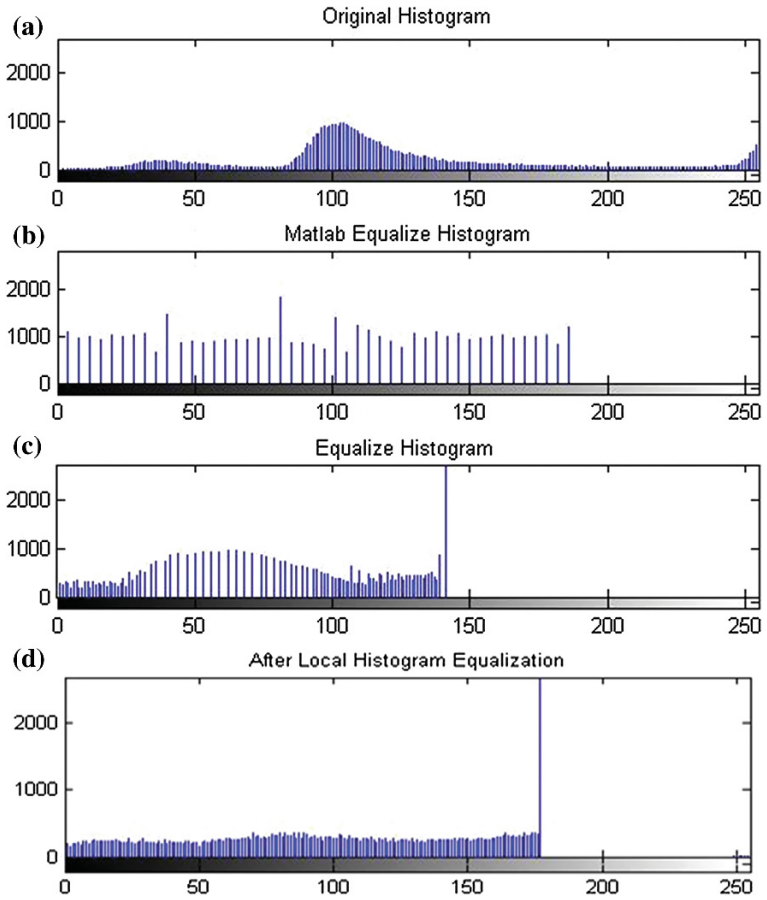

Fig. 8 **a** Histogram of brain image and **b–d** equalized histograms

3 Observations and Results

In this work, we have chosen three different types of images. Each image has its own characteristic features and differs from each other in terms of their detail, contrast levels, background, and the amount of noise. Figure 5a shows the image of human lungs. The MATLAB equalized image and the proposed global and local histogram equalized images are shown in Fig. 5b–d, respectively. The original black and white image is of high contrast and difficult to diagnose whether any damage has taken place or not. MATLAB equalized on the other hand gives a dark image with a lot of noise content in the image and clearly not suitable for medical diagnosis. However, integrated logarithmic global histogram equalized image implementing the proposed algorithm, clearly enhance the quality of image in terms of the contrast levels, in noise contents, and easy for diagnosis. Locally equalized

image with log transformation, however, is better than MATLAB equalized image but definitely, not better than global one.

Figure 6 shows the histograms of the lung image. The original image has got high contrasts, and so the pixels are distributed more toward the higher levels. Whereas both the MATLAB equalized and the integrated global equalized image show a constricted intensity distribution, thus bringing out the detail more clearer and is best in case of integrated global equalized image. The integrated local equalized image is definitely not better in quality than the integrated global equalization.

The image of Fig. 7 is an MRI view of the human brain showing the left and right brain and other cortical regions. Here, we observe that the original image has poor contrast levels, and the intensity distribution is not uniform as can be observed from the histograms in Fig. 8. We cannot categorize the image into a bright foreground and a dark background. The MATLAB equalized image has a better contrast but the various parts in the cross section cannot be easily distinguished. Moreover, it introduces undesirable noises in the image. Proposed algorithms using integrated global equalization show a significant change in the contrast levels and the details of the image are much clearer, easy for diagnostics and without introducing any noise. Local equalization is also carried out for the same image. However, the contrast is not as good as integrated global one but definitely better than the MATLAB equalized image. In fact the integrated global histogram equalization method scores above all other techniques referred here.

In case of satellite image of Fig. 9, both the MATLAB equalized image and the global histogram equalized image are better contrast image than the original low

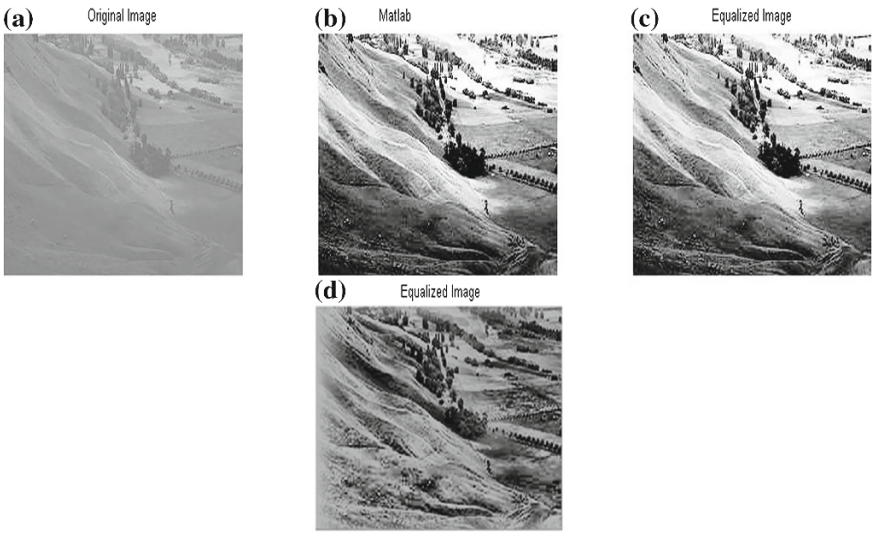

Fig. 9 **a** Satellite captured image, **b–d** are the images after MATLAB, integrated global-logarithmic, and local-logarithmic equalization

contrast image obtained from the satellite. The integrated global equalized image differs from the MATLAB equalized image in the regions in the lower left of the landscape as it brings out better contrast than the MATLAB image which can be depicted from the histogram of Fig. 10. On the other hand, locally equalized image exposes much more details than the global histogram equalized one throughout the image. The image has exposed details such as trees and fields in the right half of the image, and stones and other objects in dark regions. Also, the higher intensity distributions at the edges are brought down to a lower value because of log transformation along with local equalization which is not expected in local equalization only (where the gray levels of the boundary pixels get over-amplified).

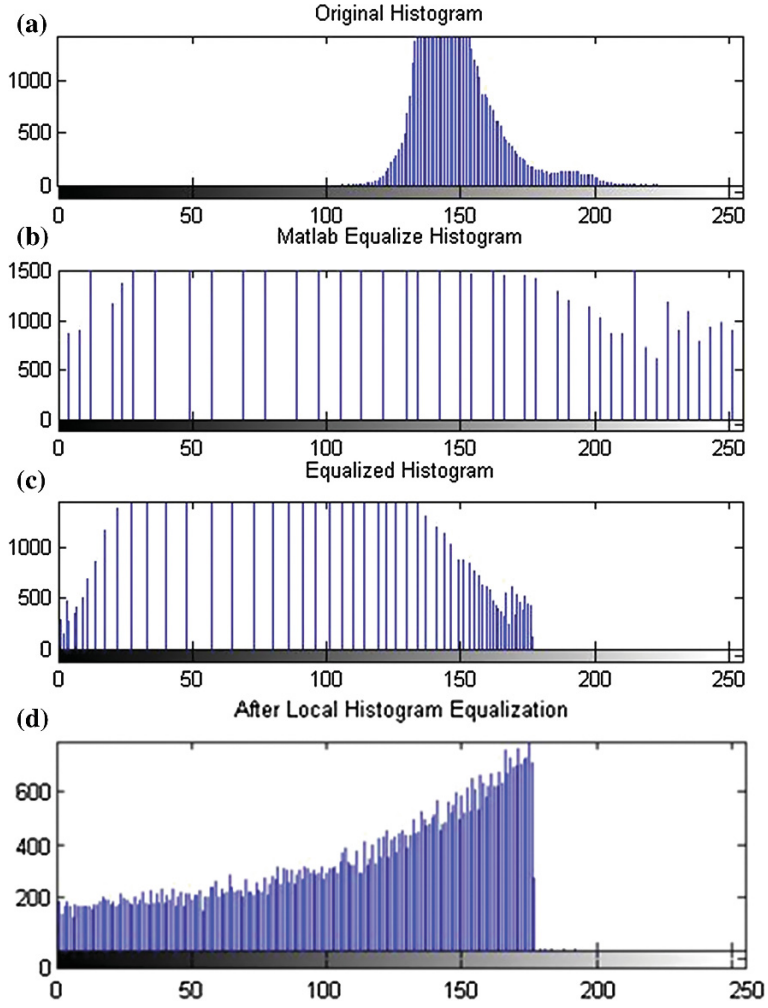

Fig. 10 **a** Histogram of satellite image and **b–d** equalized histograms

4 Conclusion

In this paper, we have presented two algorithms for histogram equalization, namely the integrated global and local HE; wherein, we have used the logarithmic transformation for mapping the image. We have observed that for most of the medical images, integrated global HE works well compared to integrated local HE. This is because of the fact that in such images, there is a little variation in contrast levels of different details in the image. Moreover, the technique is simple and takes less time for computation. However, in case of satellite captured image, there are different levels of contrasts among different objects, and hence, the integrated local HE works well as it can be observed from the image of Fig. 9d.

References

1. Maini, R., Agarwal, H.: A comprehensive review of image enhancement techniques. J. Comput. **2**(3). ISSN 2151-9617 (2010)
2. Garg, R., Mittal, B., Garg, S.: Histogram Equalization Techniques for Image Enhancement. H. I.T., Sonepat
3. Mark, E., David, M.: Histogram equalization using neighborhood metrics. Department of Computer Science, 110 Science Place, Saskatoon, SK, Canada
4. Mokhtar, N.R., Nor Hazlyna, H., Yusoff, M., Mashor, P.D., Roseline, H., Mustafa, N., Adollah, R., Adilah, H., Nashrul, F., Nasir, M.: Image enhancement techniques using local, global, bright, dark and partial contrast stretching for acute leukemia images. In: Proceedings of the World Congress on Engineering, Vol. I (2009)
5. Robert, K., David, T.: Histogram equalization. Technical Report, Microcontroller Solutions Group, Guadalajara
6. Kim, J.-Y., Kim, L.-S., Hwang, S.-H.: An advanced contrast enhancement using partially overlapped sub-block histogram equalization. IEEE Trans. Circuits Syst. Video Technol. **11** (4), 475 (2001)
7. Freescale : http://cache.freescale.com/files/dsp/doc/app_note/AN4318.pdf
8. Lavania, K.K., Kumar, R.: A comparative study of image enhancement using histogram approach. Int. J. Comput. Appl. **32**(5), 1–6 (2011)
9. Naushad Ali, M.M., Abdullah- Al-Waded, M.: Image Enhancement Using a Modified Histogram Equalization, pp. 17–24. Springer, Berlin (2012)
10. Chen, S.D., Ramli, A.R.: Contrast enhancement using recursive mean-separate histogram equalization for scalable brightness preservation," IEEE Trans. Consum. Electron. **49**(4), 1301 (2003)
11. Menotti, D., Najman, L., Facon, J., de Araujo, A.A.: Multi-histogram equalization methods for contrast enhancement and brightness preserving. IEEE Trans. Consum. Electron. **53**(3), 1186 (2007)
12. Menotti, D., de Araujo, A.A., Pappa, G.L., Najman, L., Facon, J.: Contrast enhancement in digital imaging using histogram equalization. VII Workshop of Theses, 2008-esiee.fr
13. Gonzalvez, R.C., Woods, R.E.: Digital Image Processing. Pearson Education Inc., New Delhi (2002). ISBN 81-7808-629-8
14. Shapiro, L.G., Stockman, G.C.: Computer Vision. Prentice Hall, Upper Saddle River (2002). ISBN 0-13-030796-3
15. Khan, S.D.: Image Processing in Matlab: An Introductory Approach. Khwarzimic Science Society, Lahore

Genetic Algorithms, a Nature-Inspired Tool: Review of Applications in Supply Chain Management

Sunil Kumar Jauhar and Millie Pant

Abstract The use of genetic algorithm for supply chain management with its ability to evolve solutions, handle uncertainty, and perform optimization remains to be a leading field of study. The growing body of publications over the last two decades means that it can be difficult to keep track of what has been done previously, what has worked, and what really needs to be addressed. Hence, this paper presents a review of existing research activities inspired by the genetic algorithm application in supply chain management (SCM) aimed at presenting key research themes, trends, and directions of future research.

Keywords Genetic algorithm · Supply chain management · Manufacturing flow management · Order fulfillment · Demand management

1 Introduction

Supply chain management (SCM) is a multipart and intricate practice comprising of many sub-processes that require suitable techniques for their solution. Out of the various methods available for dealing with various aspects of SCM, genetic algorithms (GAs) have emerged as one of the most popular ones. This trend is particularly visible during the last decade when a lot of research work in the area of SCM involves GA. Some of the reasons for the popularity of GA include the following (i) simple structure, (ii) independent of mathematical nature of the problem, (iii) their parallel structure, which makes the search procedure faster, (iv) ability to determine the global optimal solution, and (v) wide applicability, etc.

S.K. Jauhar (✉) · M. Pant
Indian Institute of Technology Roorkee, Roorkee, India
e-mail: suniljauhar.iitr@gamil.com

M. Pant
e-mail: millidma@gamil.com

K.N. Das et al. (eds.), *Proceedings of Fourth International Conference on Soft Computing for Problem Solving*, Advances in Intelligent Systems and Computing 335,
DOI 10.1007/978-81-322-2217-0_7

GA is heuristics whose applications are being stated at a speeded up rate. This motivation of this research article is to review the applications of GA to SCM practices. The paper explores the current research trends and tries to identify the opportunities for future work.

This research article is organized in six sections. Subsequent to the introduction in Sect. 1, genetic algorithms and SCM are briefed in Sects. 2 and 3, respectively. Section 4 refers to the research methodology used in this research article. Section 5 discusses and examines the existing research of applying GAs to different fields of SCM. Conclusions and future research drawn from the current review are given in Sect. 6.

2 Genetic Algorithm

GAs are perhaps the oldest and the most popular direct search method used for dealing with complex real-life problems. Based on the Darwin's theory of survival of the fittest, GAs have emerged as powerful optimization technique in the past few decades. GAs were conceptualized by John Holland and his colleagues of Michigan State University in mid-1960s. The idea of correlating natural genetics as potential problem-solving tools fascinated scientists and researchers, and soon GAs were known for their robustness for solving difficult problems that were otherwise difficult to solve by traditional methods. Some pioneering work in GA can be found in [1–9].

3 Supply Chain Management (SCM)

SCM is the management of upstream and downstream associated with vendors and customers to provide high-class client value at lowest possible cost to the supply chain as a whole [10]. Reference [11] defined the SCM as a strategy as well as governor of all the practices that tie allies in a supply chain together in order to come across client's necessities. Its aim is to produce and allocate the products and services in the right amount, to the right place, and at the right time so as to reduce inclusive asking price, however, retaining client satisfaction [12].

4 Methodology

The present study deals with the review of research articles dealing with the use of GA to the related processes of SCM. The study is inspired by Ko et al. [13], we have considered eight practices of SCM as given by Council of SCM Professionals (CSCMF), and these practices are as follows:

1. Manufacturing flow management (MFM)
   (a) *Inventory management*
   (b) *Supply chain planning*
   (c) *Production planning*
2. Order fulfillment (OF)
   (a) *Logistics network design/planning*
   (b) *Vehicle routing/assignment*
   (c) *Other issues*
3. Demand management (DM)
   (a) *Sales forecasting*
   (b) *Bullwhip effect*
4. Supplier relationship management (SRM)
5. Product development and commercialization (PDC)
6. Returns management (RM)
7. Customer service management (CSM)
8. Customer relationship management (CRM)

These practices are explained one-by-one in a sequential order in the following sub-sections.

4.1 Manufacturing Flow Management (MFM)

MFM is the SCM process that contains all activities needed to travel goods through the plants and to acquire, implement, and manage manufacturing flexibility in the supply chain which imitates the ability to produce a wide range of goods in a timely manner at lowest possible price [14] as revealed in Fig. 1. Production planning has drawn researchers' leading attention. Mainly, there are 15 pieces of study aiming on production planning, which make up 52 % of all research articles within the MFM processes. Table 1 shows the number of papers in MFM.

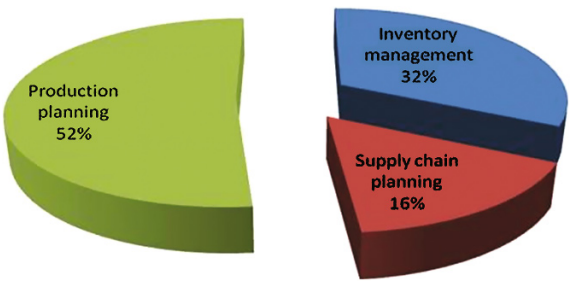

Fig. 1 Distribution of papers in sub-processes of MFM

Table 1 Number of papers in MFM

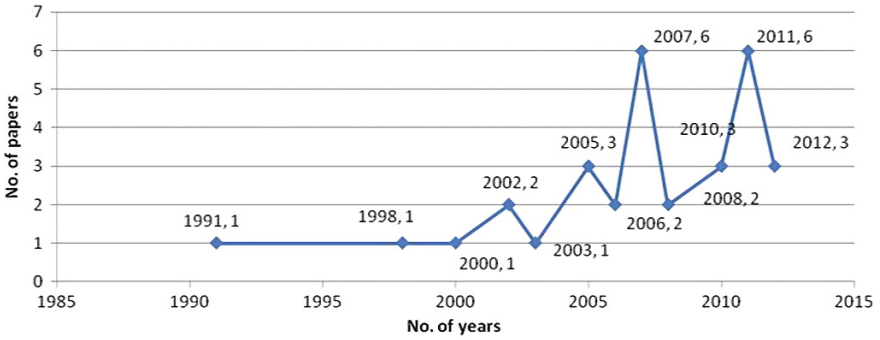

(a) Inventory Management

Inventory management in SCM is a unified method for the planning and control of inventory, all over the whole network of collaborating enterprises from the source of supply to the end user [15]. The economic lot-size scheduling difficulties were resolved by a GA-based heuristic tactic [16]. Further inventory-related problems solved by researchers consist of vendor managed inventory difficulties, such as modeling and optimizing a vendor managed replenishment system using machine learning and GAs [17], and GAs for optimum operational parameters of vendor managed inventory system in a two-echelon supply chain [18]. Furthermore, Ref. [19] suggested a GA-neural network technique to lessen spare parts logistics overhead.

Reference [20] proposed a parameter-tuned GA for multi-product economic production quantity model with space constraint, discrete delivery orders, and shortages, as Ref. [21] aids the knowledge of calibrating emission inventory for a chemical transport model with GA. Reference [22] research implements GA for searching optimal parameters in crisp and fuzzy vendor managed inventory (VMI) models. Later, Pasandideh et al. [23] proposed that economic order quantity (EOQ) model of this study relates to a two-level supply chain comprising of a single vendor and a single retailer that works underneath vendor managed inventory (VMI) system. Reference [24] presents GA to optimize two-echelon continuous review inventory practices efficiently.

(b) Supply Chain Planning

In most enterprises, supply chain planning is the admin of supply-facing and demand-facing actions to decrease disparities of supply chain as a whole [25].

GAs have been used to derive optimum resolutions for collaborative supply chain planning [26]. References [27, 28] present united process planning and scheduling model for resource allocation in multi-plant supply chain; furthermore, Huin et al. [29] proposed a knowledge-based model for resource planning.

Afterward, Huang et al. [30] considered a supply chain model to incorporate production and supply sourcing decisions.

(c) **Production Planning**

Production planning is a vital concern that together directly as well as indirectly affects the performance of the facility [31]. Reference [32] added realistic constraints and used multi-objective GA. Constrained GAs are also used in scheduling problem [33]. The general capacitated lot-sizing problem was solved by Xie and Dong [34] at first. Reference [35] suggested a heuristic algorithm to optimize the sequence of consumer orders in production line. Additionally, Ossipov [36] dedicated to simulation-based sequencing and lot-size optimization; however, Bjork and Carlsson [37] studied the influence of flexible lead times by developing a combined production and inventory model. Also, lot scheduling [38] and batch manufacturing problems [39] were analyzed, where researchers developed a GA specially aimed for job-shop problems.

Reference [40] developed an effective GA on the value of an optimum schedule. As Ref. [41] shows a new GA which created the manufacturing schedule for each factory and transport operation schedule very quickly, Chiou et al. [42] then proposed an adaptive GA to resolve the job-shop planning and scheduling complications for the single-piece, small-batch, custom production mode. Subsequently, Musharavati and Hamouda [43] tested the simple GA (SGA) and a modified GA (MGA), in creating manufacturing process plans. Reference [44] presented GA as well as tabu search for resolving the aggregate production planning model aimed at two-phase production systems problem. Reference [45] presented a GA embedded using the earliest due date (EDD) dispatching rule (a GA-EDD algorithm) for scheduling dual flow shops. Furthermore, Zamarripa et al. [46] proposed GA as a computing efficient alternative to deal with the combinatorial explosion of alternatives associated with the consideration of different production scenarios.

4.2 Order Fulfillment (OF)

Developing more responsive OF processes is generally recognized as being desirable [47]. As illustrated in Table 2, the number of research articles concerning OF increased gradually, with some rise and fall, between 1998 and 2003. On the other hand, a histrionic development can be witnessed from 2003 to 2007.

Out of the 37 articles on the sub-processes of OD in SCM, 62 % of the researchers focused on logistics network design and planning problems; however; the others motivated on vehicle routing and assignment and other issues, as revealed in Fig. 2.

(a) **Logistics Network Design/Planning**

Reference [48] uses genetic algorithms to solving network design problems which can be quite general in nature. GAs have been applied to resolve dynamic

Table 2 Number of papers in OD

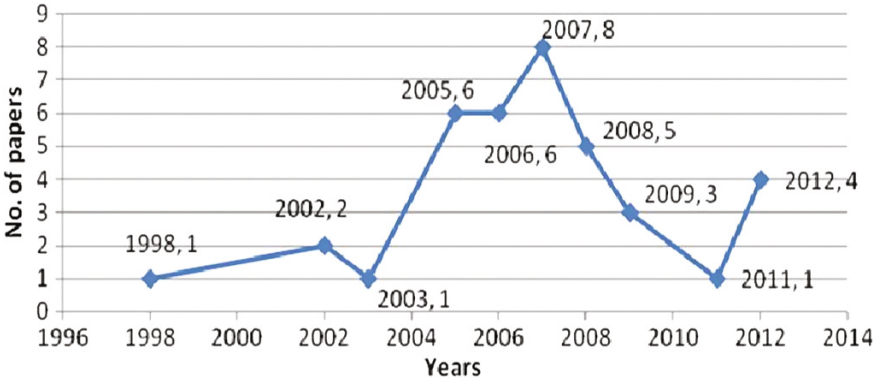

Fig. 2 Distribution of papers in sub-processes of OD

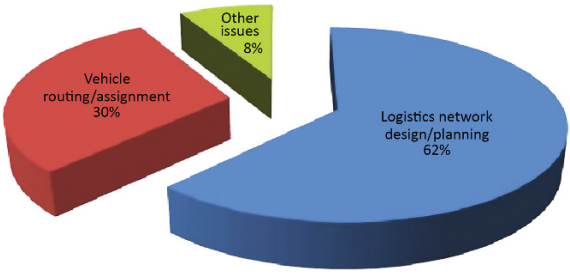

logistics network design as well as planning problems, such as multi-stage logistic network design and optimization [49–55], freight transportation planning [56, 57], multi-time period production and distribution planning [58, 59], logistic process optimization [60, 61], and vehicle transshipment planning in seaport terminal [62], and network design problems [63, 64].

Further researchers focused on truckload assignment [65], container shipping and repositioning [66], concrete distribution [67], and 3PLs services integration [68, 69]. Reference [70] study a GA approach is presented to develop a collaborative supply chain network so as to attain improved collaboration and better collaborative performance.

(b) **Vehicle Routing/Assignment**

The basic vehicle routing problem (VRP) comprises of a number of clients, each demanding a definite load of products to be delivered [71]. Reference [72] justified that a GA-based methodology is competent to find quality solution to meet the growing demands on flexible and speedy transportation services. Afterward, Ref. [73–75] founds that a hybrid genetic algorithm is extra encouraging in reducing

transportation cost in a simple supply chain. References [76, 77] presented an promising outcome on vehicle routing problem with pickup and delivery sequence constraints as well as resolve similar difficulties with multiple depots.

Reference [78] developed three heuristics to solve bi-objective vehicle routing difficulties by forced backhauls (BVFB), as Ref. [79] proposed a new Hybrid Genetic Search with Advanced Diversity Control to expertly address a large class of vehicle routing problem with time window (VRPTW) variants. Subsequently, Yucenur and Demirel [80] proposed a new type of geometric shape-based genetic clustering algorithm. Furthermore, Refs. [80–82] present a hybrid tactic that combines a GA with an iterated local search (ILS) to resolve the location routing problem (LRP) expertly.

(c) **Other issues**

References [83, 84] set up an optimum solution, by considering total transit time and shipping cost at the same time, to assign clients to accessible warehouses or distribution centers by GA. Reference [85] recommended an evolutionary algorithm to regulate the optimum arrangement of shipping alternatives to minimize total logistics costs.

4.3 Demand Management (DM)

DM plays a critical role within supply chain management. As pointed out by Kuo [86], a reliable demand forecast can improve the quality of organizational strategy.

(a) **Sales Forecasting**

In many researches, GAs are used to determine the model parameters for given forecasting models [87–91].

(b) **Bullwhip Effect**

The Bullwhip effect is an observed phenomenon whereby a minor variation in the demand from end consumer effects in huge deviations as it drives upstream [92].

It seems that there is a deficiency of research articles addressing-related problems in this process.

4.4 Supplier Relationship Management (SRM)

SRM is a practice involved in dealing ideal vendors and finding new ones at the same time as reducing prices, making procurement foreseeable and repeatable, pooling purchaser experience, and take out the profits of vendor partnerships [93–97].

Reference [98] proposed a GA technique for optimization of incentive system to achieve performance of supply chain allies to ensure the long-term tactical relations, whereas Ref. [99] presents a stochastic demand multi-product vendor selection model with service level and budget constraints using GA. Moreover, Yeh and Chuang [100] applied two multi-objective genetic algorithms to find the set of pareto-optimal solutions, which utilized the weighted sum tactic that can produce more number of solutions.

4.5 Product Development and Commercialization (PDC)

It seems that there is an insufficiency of research articles addressing related problems in this process.

4.6 Returns Management (RM)

RM is the SCM practice by which activities associated with returns; reverse logistics, gate keeping, and avoidance are managed within the enterprise and through crucial associates of the supply chain [101].

References [102, 103] suggested a GA-based method to resolve reverse logistics difficulties of handling returned goods. In addition, Lieckens and Vandaele [104] established an optimum solution to resolve the reverse logistics network design difficulties, whereas Min and Ko [105] solved the similar difficulties from 3rd-party logistics service providers' viewpoint.

4.7 Customer Service Management (CSM)

CSM deals with a service-focused management interface between client and service provider [106]. It seems that there is a dearth of research articles addressing related issues in this area.

4.8 Customer Relationship Management (CRM)

CRM is an extensively applied model for management of a company's interactions with customers, clients, and sales scenarios [107]. It seems that there is a deficiency of research articles addressing related problems in this process.

5 Discussion

5.1 Distribution of Research Articles in Subject Processes

As demonstrated in Table 3, many research articles have contributed to seven wide-ranging processes of SCM. The OD is the utmost prevalent process targeted by genetic algorithm applications. The research articles about MFM are more common than the articles concerning DM. It is clear as a result that articles aimed at those three key processes in SCM are significantly more than those in other processes. Additionally, Fig. 3 shows the proportion of articles focusing in major subject processes. It reveals that OD, which makes up 47 %, is the most popular subject in SCM to attract researchers' attention. There are 39 and 5 % of research articles concentrating on MFM and DM, respectively.

5.2 The Research Articles Published by Main Journals

As shown in Table 4, 16 of these research articles were published by Expert systems with applications while 12 of total articles were published by European journal of operational research and 10 articles by International Journal of

Table 3 GA applied to respective subject processes

Processes	Genetic algorithm
MFM	31
OD	37
DM	4
SRM	3
PDC	0
RM	4
CSM	0
CRM	0
Total	78

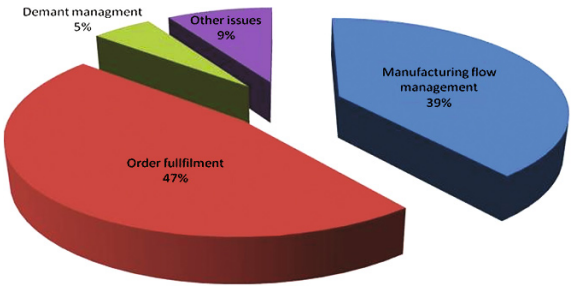

Fig. 3 Proportion of research articles in major subject processes

Table 4 Research articles published by main journals

Journals title	No. of research articles
Expert Systems with Applications	15
Computers and Industrial Engineering	13
European Journal of Operational Research	7
International Journal of Production Economics	7
Computers and Operations Research	5
Industrial Management and Data Systems	3
Applied Mathematics and Computation	2
International Journal of Physical Distribution and Logistics Management	2
Others	24
Total	78

Production Economics. Computers and Industrial Engineering, Computers and Operations Research, Journal of Operations Research, Industrial Management and Data Systems, International Journal of Physical Distribution, and Logistics Management and Journal of Manufacturing Technology Management are also the key journals recognized by researchers.

5.3 The Growing Trends of Research in SCM

As demonstrated in Table 5, there were only a small number of research articles in the SCM field applying genetic algorithm in early 1990s. Then, the produced

Table 5 Number of research articles in SCM using GA

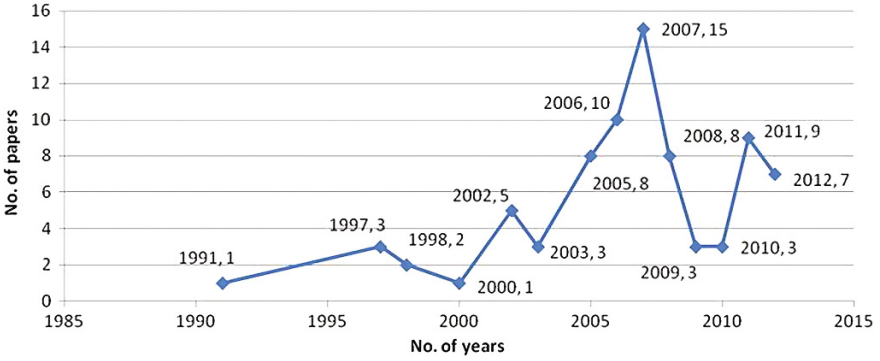

research articles varied to some extent from 1997 to 2013, looking at the general trend, and the number of research articles can be anticipated to rise in the upcoming years.

6 Conclusions and Future Research

Genetic algorithms are the most widespread practice implemented to resolve SCM difficulties, predominantly in MFM, OD, and DM processes, and the indication appears to be strong that the problems in SCM have appealed a rising concern. It could be acknowledged that there has been a substantial rising tendency of relating genetic algorithms to resolve different SCM difficulties since 2000. The motives may not simply be that new studies have been involved in old-fashioned supply chain field, but besides fresh researches have been advanced in novel processes such as SRM.

Some practices in SCM that have hardly been uncovered in current research articles, such as PDC, CSM, and CRM, are as a result put forward for future study.

References

1. Davis, L.: Handbook of Genetic Algorithms. Nostrand Reinhold, New York (1991)
2. Eshelman, L.: The CHC adaptive search algorithm. In: Rawlins, G (ed.) Foundations of Genetic Algorithms, pp. 256–283. Morgan-Kaufmann, Burlington (1991)
3. Forrest, S.: Genetic algorithms. ACM Comput. Surv. **28**(1), 77 (1996)
4. Grefenstette, J.J.: Optimization of control parameters for genetic algorithms. IEEE Trans. Syst. Man Cybern. **16**(1), 122–128 (1986)
5. Mitchell, M., Forrest, S., Holland, J. H.: The royal road for genetic algorithms: fitness landscapes and GA performance. In: Varela, F.J., Bourgine, P. (ed.) Toward a Practice of Autonomous Systems: Proceedings of the First European Conference on Artificial Life. MIT Press/Bradford Books, Cambridge (1992)
6. Koza, J.R.: Genetic Programming: A Paradigm for Genetically Breeding Populations of Com-puter Programs to Solve Problems. Stanford University Computer Science Department technical report STAN-CS-90-1314 (1990)
7. Schaffer, J.D. (ed.): Proceedings of the Third International Conference on Genetic Algorithms. Morgan Kaufmann, San Mateo (1989)
8. DeJong, K.A.: Genetic-algorithm based learning. Mach. Learn. **3**, 611–638 (1990)
9. Back, T., Hammel, U., Schwefel, H.P.: Evolutionary computation: comments on the history and current state. IEEE Trans. Evol. Comput. **1**(1), 3–17 (1997)
10. Christopher, M.: Logistics and Supply Chain Management, 2nd edn. Prentice Hall, Norfolk (2004)
11. Harrison, A., Hoek, R.: Logistics Management and Strategy, 2nd edn. Prentice Hall, Essex (2005)
12. Jeong, B., Junga, H.S., Parkb N.K.: A computerized causal forecasting system using genetic algorithms in supply chain management. J. Syst. Softw. **60**, 223–237 (2002)
13. Ko, M., Tiwari, A., Mehnen, J.A.: Review of soft computing applications in supply chain management. Appl. Soft Comput. **10**, 661–674 (2010)

14. Douglas, M., Lambert, Terrance, L.P.: Supply chain metrics. Int. J. Logistics Manage. **12**(1), 1–19 (2001)
15. Verwijmeren, M., Vlist, P., Donselaar, K.: Networked inventory management I formation systems: materializing supply chain management. Int. J. Phys. Distrib. Logistics Manage. **26** (6), 16–31 (1996)
16. Chang, P., Yao, M., Huang, S., Chen, C.: A genetic algorithm for solving a fuzzy economic lot-size scheduling problem. Int. J. Prod. Econ. **102**(2), 265–288 (2006)
17. Chi, H., Ersoy, O.K., Moskowitz, H., Ward, J.: Modeling and optimizing a vendor managed replenishment system using machine learning and genetic algorithms. Eur. J. Oper. Res. **180** (1), 174–193 (2007)
18. Nachiappan, S.P., Jawahar, N.: A genetic algorithm for optimal operating parameters of VMI system in a two echelon supply chain. Eur. J. Oper. Res. **182**(3), 1433–1452 (2007)
19. Wu, M., Hsu, Y.: Design of BOM configuration for reducing spare parts logistic costs. Expert Syst. Appl. **34**(4), 2417–2423 (2008)
20. Pasandideh, S.H.R., Niaki, S.T.A., Yeganeh, J.A.: A parameter-tuned genetic algorithm for multi-product economic production quantity model with space constraint, discrete delivery orders and shortage. Adv. Eng. Softw. **41**, 306–314 (2010)
21. Li, M.J., Chen, D.S., Cheng, S.Y., Wang, F., Li, Y., Zhou, Y., Lang JL.: Optimizing emission inventory for chemical transport models by using genetic algorithm. Atmos. Environ. **44**, 3926–3934 (2010)
22. Lin, K.P., Chang, P.T., Hung, K.C., Pai, P.F.: A simulation of vendor managed inventory dynamics using fuzzy arithmetic operations with genetic algorithms. Expert Syst. Appl. **37**, 2571–2579 (2010)
23. Pasandideh, S.H.R., Niaki, S.T.A., Nia, A.R.: A genetic algorithm for vendor managed inventory control system of multi-product multi-constraint economic order quantity model. Expert Syst. Appl. **38**, 2708–2716 (2011)
24. Pasandideh, S.H.R., Niaki, S.T.A., Tokhmehchi, N.: A parameter-tuned genetic algorithm to optimize two-echelon continuous review inventory systems. Expert Syst. Appl. **38**, 11708–11714 (2011)
25. Braunscheidel, M.J., Suresh, N.C.: The organizational antecedents of a firm's supply chain agility for risk mitigation and response. J. Oper. Manage. **27**, 119–140 (2009)
26. Han, C., Damrongwongsiri, M.: Stochastic modeling of a two-echelon multiple sourcing supply chain system with genetic algorithm. J. Manuf. Technol. Manage. **16**(1), 87–108 (2005)
27. Moon, C., Kim, J., Hur, S.: Integrated process planning and scheduling with minimizing total tardiness in multi-plants supply chain. Comput. Ind. Eng. **43**(1–2), 331–349 (2002)
28. Moon, C., Lee, Y.H., Jeong, C.S., Yun, Y.: Integrated process planning and scheduling in a sup-ply chain. Comput. Ind. Eng. **54**(4), 1048–1061 (2008)
29. Huin, S.F., Luong, L.H.S., Abhary, K.: Knowledge-based tool for planning of enterprise resources in ASEAN SMEs. Robot. Comput. Integr. Manuf. **19**(5), 409–414 (2003)
30. Huang, G.Q., Zhang, X.Y., Liang, L.: Towards integrated optimal configuration of platform products, manufacturing processes, and supply chains. J. Oper. Manage. **23**(3–4), 267–290 (2005)
31. Nasab, M.K., Konstantaras, I.: A random search heuristic for a multi-objective production planning. Comput. Ind. Eng. **62**, 479–490 (2012)
32. Candido, M.A.B., Khator, S.K., Barcia, R.M.: A genetic algorithm based procedure for more realistic job shop scheduling problems. Int. J. Prod. Resour. **36**(13), 3437–3457 (1998)
33. Maraghy, H., Patel, V., Abdallah, I.B.: Scheduling of manufacturing systems under dual-resource constraints using genetic algorithms. J. Manuf. Syst. **19**(3), 186–201 (2000)
34. Xie, J., Dong, J.: Heuristic genetic algorithms for general capacitated lot-sizing problems. Comput. Math. Appl. **44**(1–2), 263–276 (2002)
35. Ossipov, P.: Heuristic optimization of sequence of customer orders. Appl. Math. Comput. **162**(3), 1303–1313 (2005)

36. Kampf, M., Kochel, P.: Simulation-based sequencing and lot size optimisation for a production-and-inventory system with multiple items. Int. J. Prod. Econ. **104**(1), 191–200 (2006)
37. Bjork, K., Carlsson, C.: The effect of flexible lead times on a paper producer. Int. J. Prod. Econ. **107**(1), 139–150 (2007)
38. Chatfield, D.C.: The economic lot scheduling problem: a pure genetic search approach. Comput. Oper. Res. **34**(10), 2865–2881 (2007)
39. Li, Y., Chen, J., Cai, X.: Heuristic genetic algorithm for capacitated production planning problems with batch processing and remanufacturing. Int. J. Prod. Econ. **105**(2), 301–317 (2007)
40. Engin, O., Ceran, Yilmaz, M.K.: An efficient genetic algorithm for hybrid flow shop scheduling with multiprocessor task problems. Appl. Soft Comput. **11**, 3056–3065 (2011)
41. Ławrynowicz, A.: Advanced scheduling with genetic algorithms in supply networks. J. Manuf. Technol. Manage. **22**(6), 748–769 (2011)
42. Chiou, C.W., Chen, W.M., Liu, C.M., Wu M.C.: A genetic algorithm for scheduling dual flow shops. Expert Syst. Appl. **39**, 1306–1314 (2012)
43. Musharavati, F., Hamouda, A.S.M.: Modified genetic algorithms for manufacturing process planning in multiple parts manufacturing lines. Expert Syst. Appl. **38**, 10770–10779 (2011)
44. Ramezanian, R., Rahmani, D., Barzinpour, F.: An aggregate production planning model for two phase production systems: solving with genetic algorithm and tabu search. Expert Syst. Appl. **39**, 1256–1263 (2012)
45. Chiou, C.W., Chen, W.M., Liu, C.M., Wu, M.C.: A genetic algorithm for scheduling dual flow shops. Expert Syst. Appl. **39**, 1306–1314 (2012)
46. Zamarripa, M., Silvente, J., Espuña, A.: Supply chain planning under uncertainty using genetic algorithms. Comput. Aided Chem. Eng. **30**, 457–461 (2012)
47. Kritchanchai, D., MacCarthy, B.L.: Responsiveness of the order fulfilment process. Int. J. Oper. Prod. Manage. **19**(8), 812–833 (1999)
48. Berry, L.M., Murtagh, B.A., McMahon, G.B., Sugden, S.J., Welling L.D.: Genetic algorithms in the design of complex distribution networks. Int. J. Phys. Distrib. Logistics Manage. **28**(5), 377 (1998)
49. Syarif, A., Yun, Y., Gen, M.: Study on multi-stage logistic chain network: a spanning tree-based genetic algorithm approach. Comput. Ind. Eng. **43**(1–2), 299–314 (2002)
50. Xu, H., Xu, R., Ye, Q.: Optimization of unbalanced multi-stage logistics systems based on prufer number and effective capacity coding. Tsinghua Sci. Technol. **11**(1), 96–101 (2006)
51. Xu, J., Liu, Q., Wang, R.: A class of multi-objective supply chain networks optimal model under random fuzzy environment and its application to the industry of Chinese liquor. Inf. Sci. **178**(8), 2022–2043 (2008)
52. Xu, T., Wei, H., Wang, Z.: Study on continuous network design problem using simulated annealing and genetic algorithm. Expert Syst. Appl. **36**(2), 1322–1328 (2009)
53. Farahani, R.Z., Elahipanah, M.: A genetic algorithm to optimize the total cost and service level for just-in-time distribution in a supply chain. Int. J. Prod. Econ. **111**(2), 229–243 (2008)
54. Altiparmak, F., Gen, M., Lin, L., Karaoglan, I.: A steady-state genetic algorithm for multi-product supply chain network design. Comput. Ind. Eng. **56**(2), 521–537 (2009)
55. Jawahar, N., Balaji, A.N.: A genetic algorithm for the two-stage supply chain distribution problem associated with a fixed charge. Eur. J. Oper. Res. **194**(2), 496–537 (2009)
56. Ma, H., Davidrajuh, R.: An iterative approach for distribution chain design in agile virtual environment. Ind. Manage. Data Syst. **105**(6), 815–834 (2005)
57. Jo, J., Li, Y., Gen, M.: Nonlinear fixed charge transportation problem by spanning tree-based genetic algorithm. Comput. Ind. Eng. **53**(2), 290–298 (2007)
58. Gen, M., Syarif, A.: Hybrid genetic algorithm for multi-time period production/distribution planning. Comput. Ind. Eng. **48**(4), 799–809 (2005)

59. Aliev, R.A., Fazlollahi, B., Guirimov, B.G., Aliev, R.R.: Fuzzy-genetic approach to aggregate production–distribution planning in supply chain management. Inf. Sci. **177**(20), 4241–4255 (2007)
60. Silva, C.A., Sousa, J.M.C., Runkler, T.A.: Optimization of logistic systems using fuzzy weighted aggregation. Fuzzy Sets Syst. **158**(17), 1947–1960 (2007)
61. Silva, C.A., Sousa, J.M.C., Runkler, T.A.: Rescheduling and optimization of logistic processes using GA and ACO. Eng. Appl. Artif. Intell. **21**(3), 343–352 (2008)
62. Fischer, T., Gehring, H.: Planning vehicle transhipment in a seaport automobile terminal using a multi-agent system. Eur. J. Oper. Res. **166**(3), 726–740 (2005)
63. Lau, H.C.W., Ning, A., Pun, K.F., Chin, K.S., Ip, W.H.: A knowledge-based system to support procurement decision. J. Knowl. Manage. **9**(1), 87–100 (2005)
64. Altiparmak, F., Gen, M., Lin, L., Paksoy, T.: A genetic algorithm approach for Multiobjective optimization of supply chain networks. Comput. Ind. Eng. **51**(1), 196–215 (2006)
65. Caputo, A.C., Fratocchi, L., Pelagagge, P.M.: A genetic approach for freight transportation plan-ning. Ind. Manage. Data Syst. **106**(5), 719–738 (2006)
66. Shintani, K., Imai, A., Nishimura, E., Papadimitriou, S.: The container shipping network de-sign problem with empty container repositioning. Transport. Res. Part E: Logistics Transport. Rev. **43**(1), 39–59 (2007)
67. Naso, D., Surico, M., Turchiano, B., Kaymak, U.: Genetic algorithms for supply-chain scheduling: a case study in the distribution of ready-mixed concrete. Eur. J. Oper. Res. **177** (3), 2069–2099 (2007)
68. Ko, H.J., Ko, C.S., Kim, T.: A hybrid optimization/simulation approach for a distribution net-work design of 3PLS. Comput. Ind. Eng. **50**(4), 440–449 (2006)
69. Ko, H.J., Evans, G.W.: A genetic algorithm-based heuristic for the dynamic integrated for-ward/reverse logistics network for 3PLs. Comput. Oper. Res. **34**(2), 346–366 (2007)
70. Lam, C.Y., Chan, S.L., Ip, W.H., Lau, C.W.: Supply chain network using embedded genetic algorithms. Ind. Manage. Data Syst. **108**(8), 1101–1110 (2008)
71. Baker, B.M., Ayechew, M.A.: A genetic algorithm for the vehicle routing problem. Comput. Oper. Res. **30**, 787–800 (2003)
72. Pankratz, G.: Vehicle routing by means of a genetic algorithm. Int. J. Phys. Distrib. Logistics Manage. **35**(5), 362–383 (2005)
73. Torabi, S.A., Ghomi, S.M.T.F., Karimi, B.: A hybrid genetic algorithm for the finite horizon economic lot and delivery scheduling in supply chains. Eur. J. Oper. Res. **173**(1), 173–189 (2006)
74. Fu, L., Sun, D., Rilett, L.R.: Heuristic shortest path algorithms for transportation applications: state of the art. Comput. Oper. Res. **33**(11), 3324–3343 (2006)
75. Yang, V., Ji, X., Gao, Z., Li, K.: Logistics distribution centers location problem and algorithm under fuzzy environment. J. Comput. Appl. Math. **208**(2), 303–315 (2007)
76. Ganesh, K., Narendran, T.T.: CLOVES: a cluster-and-search heuristic to solve the vehicle routing problem with delivery and pick-up. Eur. J. Oper. Res. **178**(3), 699–717 (2007)
77. Ho, W., Ho, G.T.S., Ji, P., Lau, H.C.W.: A hybrid genetic algorithm for the multi-depot vehicle routing problem. Eng. Appl. Artif. Intell. **21**(4), 548–557 (2008)
78. Anbuudayasankar, V., Ganesh, P.X., Koh, S.C.L., Ducq, Y.: Modified savings heuristics and genetic algorithm for bi-objective vehicle routing problem with forced backhauls. Expert Syst. Appl. **39**, 2296–2305 (2012)
79. Vidal, T., Crainic, T.G., Gendreaud, M., Prins C.: A hybrid genetic algorithm with adaptive diversity management for a large class of vehicle routing problems with time-windows, Comput. Oper. Res. (1999). http://dx.doi.org/10.1016/j.cor.2012.07.018
80. Yucenur, G.N., Demirel, N.C.: A new geometric shape-based genetic clustering algorithm for the multi-depot vehicle routing problem. Expert Syst. Appl. **38**, 11859–11865 (2011)
81. Chung-Cheng, L., Vincent, F.Y.: Data envelopment analysis for evaluating the efficiency of genetic algorithms on solving the vehicle routing problem with soft time windows. Comput. Ind. Eng. **63**, 520–529 (2012)

82. Derbel, H., Jarboui, B., Hanafi, S., Chabchoub, H.: Genetic algorithm with iterated local search for solving a location-routing problem. Expert Syst. Appl. **39**, 2865–2871 (2012)
83. Zhou, G., Min, H., Gen, M.: The balanced allocation of customers to multiple distribution centers in the supply chain network: a genetic algorithm approach. Comput. Ind. Eng. **43**(1–2), 251–261 (2002)
84. Zhou, G., Min, H., Gen, M.: A genetic algorithm approach to the bi-criteria allocation of customers to warehouses. Int. J. Prod. Econ. **86**(1), 35–45 (2003)
85. Dullaert, W., Maes, B., Vernimmen, B., Witlox, F.: An evolutionary algorithm for order split-ting with multiple transport alternatives. Expert Syst. Appl. **28**(2), 201–208 (2005)
86. Kuo, R.J.: A sales forecasting system based on fuzzy neural network with initial weights generated by genetic algorithm. Eur. J. Oper. Res. **129**(3), 496–517 (2001)
87. Hadavandi, E., Shavandia, H., Ghanbarib, A.: An improved sales forecasting approach by the integration of genetic fuzzy systems and data clustering: case study of printed circuit board. Expert Syst. Appl. **38**, 9392–9399 (2011)
88. Chiraphadhanakul, S., Dangprasert, P., Avatchanakorn V.: Genetic algorithms in forecasting commercial banks deposit. In: Proceedings of the IEEE International Conference on Intelligent Processing Systems (1997)
89. Ju, Y.K., Kim, C., Shim, J.C.: Genetic based fuzzy models: interest rate forecasting problem. Comput. Ind. Eng. **33**, 561–564 (1997)
90. Kim, D., Kim, C.: Forecasting time series with genetic fuzzy predictor ensemble. IEEE Trans. Fuzzy Syst. **5**, 523–535 (1997)
91. Jeong, B., Junga, H.S., Parkb N.K.: A computerized causal forecasting system using genetic algorithmsin supply chain management. J. Syst. Softw. **60**, 223–237 (2002)
92. Kristianto, Y., Helo, P., Jiao, J., Sandhu, M.: Adaptive fuzzy vendor managed inventory control for mitigating the Bullwhip effect in supply chains. Eur. J. Oper. Res. **216**, 346–355 (2012)
93. Herrmann, J., Hodgson B.: SRM: leveraging the supply base for competitive advantage In: Proceedings of the SMTA International Conference, Chicago, Illinois, 1 Oct 2001
94. Jauhar, S.K., Pant. M.: Recent trends in supply chain management: a soft computing approach. In: Proceedings of Seventh International Conference on Bio-Inspired Computing: Theories and Applications (BIC-TA 2012). Springer, India (2013)
95. Jauhar, S.K., Pant. M., Deep. A.: An approach to solve multi-criteria supplier selection while considering environmental aspects using differential evolution. Swarm, Evolutionary, and Memetic computing, pp. 199–208. Springer International Publishing, Switzerland (2013)
96. Jauhar, S.K., Pant, M., Abraham, A.: A novel approach for sustainable supplier selection using differential evolution: a case on pulp and paper industry. In: Intelligent Data analysis and Its Applications, vol. II, pp. 105–117. Springer International Publishing, Switzerland (2014)
97. Jauhar, S., Pant, M., Deep, A.: Differential evolution for supplier selection problem: a DEA based approach. In: Proceedings of the Third International Conference on Soft Computing for Problem Solving, pp. 343–353. Springer, India (2014)
98. Chiadamrong, N., Prasertwattana, K.: A comparative study of supply chain models under the traditional centralized and coordinating policies with incentive schemes. Comput. Ind. Eng. **50**(4), 367–384 (2006)
99. Yang, P.C., Wee, H.M., Pai, S., Tseng, Y.F.: Solving a stochastic demand multi-product supplier selection model with service level and budget constraints using Genetic Algorithm. Expert Syst. Appl. **38**, 14773–14777 (2011)
100. Yeh, W.C., Chuang, M.C.: Using multi-objective genetic algorithm for partner selection in green supply chain problems. Expert Syst. Appl. **38**, 4244–4253 (2011)
101. Rogers, D.S., Lambert, D.M., Croxton, K.L., García-Dastugue, S.J.: The returns management process. Int. J. Logistics Manage. **13**(2), 1–18 (2002)
102. Min, H., Ko, C.S., Ko, H.J.: The spatial and temporal consolidation of returned products in a closed-loop supply chain network. Comput. Ind. Eng. **51**(2), 309–320 (2006)

103. Min, H.: Jeong ko, H., Seong Ko C.: A genetic algorithm approach to developing the multi-echelon reverse logistics network for product returns. Omega: Int. J. Manage. Sci. **34**(1), 56–69 (2006)
104. Lieckens, K., Vandaele, N.: Reverse logistics network design with stochastic lead times. Comput. Oper. Res. **34**(2), 395–416 (2007)
105. Min, H., Ko, H.: The dynamic design of a reverse logistics network from the perspective of third-party logistics service providers. Int. J. Prod. Econ. **113**(1), 176–192 (2008)
106. Langer, M., Loidl, S., Nerb M.: Customer service management: towards a management information base for an IP connectivity service. In: The Fourth IEEE Symposium on Computers and Communications, Red Sea, Egypt, pp. 149–155 (1999)
107. Robert S.: Computer Aided Marketing & Selling. Butterworth, Heinemann (1991). ISBN 978-0-7506-1707-9

Data Mining in Market Segmentation: A Literature Review and Suggestions

Saibal Dutta, Sujoy Bhattacharya and Kalyan Kumar Guin

Abstract The importance of data mining techniques for market segmentation is becoming indispensable in the field of marketing research. This is the first identified academic literature review of the available data mining techniques related to market segmentation. This research paper provides surveys of the available literature on data mining techniques in market segmentation. A categorization has been provided based on the available data mining techniques used in market segmentation. Eight online journal databases were used for searching, and finally, 103 articles were selected and categorized into 13 groups based on data mining techniques. The utility of data mining techniques and suggestions are also discussed. The findings of this study show that neural networks is the most used method, and kernel-based method is the most promising data mining techniques. Our research work provides a comprehensive understanding of past, present as well as future research trend on data mining techniques in market segmentation. We hope this paper provides reasonable insight and clear understating to both industry as well as academic researchers.

Keywords Market segmentation · Data mining · Literature review · Classification

1 Introduction

Market segmentation is one of the important concepts both in marketing theory and in practice. In the last few decades, market segmentation has become a central issue in marketing theory. In marketing theory literature, many researchers have proposed

S. Dutta (✉) · S. Bhattacharya · K.K. Guin
Indian Institute of Technology Kharagpur, Kharagpur, India
e-mail: saibal.13@gmail.com

S. Bhattacharya
e-mail: sujoy.research@gmail.com

K.K. Guin
e-mail: kalyan@vgsom.iitkgp.ernet.in

K.N. Das et al. (eds.), *Proceedings of Fourth International Conference on Soft Computing for Problem Solving*, Advances in Intelligent Systems and Computing 335,
DOI 10.1007/978-81-322-2217-0_8

different techniques but still proper market segmentation is a burning problem among market researchers. The concept of market segmentation was first proposed by American marketing researcher Smith [45] and then was further developed by many researchers. Market segmentation is the process of differentiating a large market into some groups or the clusters of customers from available market information or similar behavior customer [18, 23, 31, 45, 46, 51]. The groups or subset may be demographic, economic, and choice based.

This research paper surveys the development of data mining techniques in market segmentation. Data mining is the process of discovering pattern in data, and market researchers are frequently used for understanding the behavior pattern in marketing data. Nowadays, data mining is becoming one of the emerging fields of research due to explosion of data.

The aim of this paper is to present a comprehensive review of literature which published in academic journals related to the application of data mining techniques in market segmentation. The classification of framework is adopted here as per previous literature [42, 43]. The paper is organized as follows: First, the research methodology of the study is presented; second, introduced available list of data mining techniques which used for market segmentation and are also presented into several groups; third, articles about data mining in market segmentation are analyzed, and the results of the classification are showed through table; and finally, the conclusions, limitations of the study, and suggestion are discussed.

2 Research Methodology

Nowadays, the nature of research in market segmentation becomes multidisciplinary and many researchers across the different field worked on and have published relevant materials in various journals. The following online journal databases were used for searching comprehensive bibliography of academic literature on market segmentation.

1. Science Direct
2. ABI/INFORM Database
3. Emerald Full Text
4. IEEE Transaction
5. JSTOR
6. Springer
7. Google Scholar
8. Wiley Online Library.

The above academic literature was searched with key word “market segmentation” or “target marketing” or “data mining and market segmentation,” and originally around 750 articles were produced. Each full-text article was reviewed carefully and eliminated those articles which were not related to data mining techniques in market segmentation or those were not having main focus for improvement of market

segmentation. Below criteria followed for selection and the number reduced to 103 articles which are related to data mining techniques and development of methodologies in market segmentation. Those articles have been included which were published in above-mentioned academic journal. Doctoral thesis, master thesis, conferences, and unpublished work are avoided as per previous literature [43].

Each article has been carefully reviewed and separately classified into several categories of data mining techniques. Although this search tried to cover all the available used data mining techniques so far, this paper will serve as a comprehensive base of data mining research in market segmentation area and will give a broad view of available techniques in marker segmentation.

3 Classification Method

The reviewed research papers were classified into thirteen categories, and each category also consists of several single or hybrid data mining techniques. Each categorywise several data mining techniques presented into table with reference papers.

3.1 Classification Framework for Data Mining Techniques

This paper surveys and classifies different market segmentation techniques into thirteen broad categories as follows:

1. Neural network
2. Evolutionary algorithm
3. Fuzzy theory
4. RFM analysis
5. Hierarchical clustering
6. K-means
7. Bagged clustering
8. Kernel methods
9. Multidimensional scaling
10. Taguchi method
11. Model-based clustering
12. Rough set
13. Others.

Early 1960s and 1970s researchers had started K-means and hierarchical cluster analysis for market segmentation [44]. Even today also, many researchers successfully used K-means clustering for market segmentation [8, 33]. But above traditional clustering techniques have some drawbacks. For example, K-means algorithm cannot handle noise and outliers data [5, 6, 47]. K-means algorithm also

failed to give any exact or initial number of cluster and the statistical validity of the cluster formed [37], and hence, clustering falls into local minima [15, 35]. To address the above issue, the researcher combined K-means with genetic algorithm to reach the global minima [3, 36, 40].

To classify the complex consumer pattern in market, researchers also introduced other different approaches such as evolutionary algorithm, kernel methods, rough set, Taguchi method, etc. Nowadays, the above approaches are quite popular among the market researchers, and also these approaches are able to perform better market segmentation than traditional one [24]. Other important market segmentation techniques such as multidimensional scaling, random forest, RFM analysis, bagged clustering, etc., are also found in academic literature [10, 48].

3.2 Classification Process

Each of the selected research papers were reviewed carefully and classified into one of the thirteen categories according to the proposed classification framework. The research papers were analyzed by year of publication and distribution of journal. The classification process is adopted here as per previous literature [42, 43]:

- Online academic literature search
- First-phase classification by the researcher
- Second-phase classification of initial classification result
- Final verification and classification of result.

4 Classification of the Articles

The distributions of 103 articles have been done according to the proposed classification model which is shown in Table 1. Articles are categorized into thirteen broad methodologies, and then, each methodology is further divided into major data mining techniques. Most of the data mining techniques used in market segmentation have been included here.

4.1 Distribution by Journals

The distribution of articles by journal has been shown in Table 2. Articles related to application of data mining techniques in market segmentation are distributed across 45 journals. The top three journals are as follows: Expert Systems with Applications, Journal of Marketing Research, and Management Science.

Table 1 Distribution of articles according to the proposed classification model

Method	Major methodology
Neural network	Self-organizing map [7, 29, 32, 39]
	Multilayer perceptron and K-means [26]
	FSCL algorithm [4]
	Neural network Hopfield dNN [9]
	Adaptive resonance theory (ART2) neural network [14]
	Neural network and Monte Carlo [41]
Evolutionary algorithm	Genetic algorithm [30, 33]
	Artificial immune system and simulated annealing algorithm [1, 13]
Fuzzy theory	Fuzzy clustering [55]
RFM analysis	RFM model [16]
	LRFM model [53]
Hierarchical clustering	Hierarchical clustering [38]
K-means	K-means [34]
Bagged clustering	Bagged clustering [11]
Kernel methods	Kernel-based clustering algorithm [24, 50]
Multidimensional scaling	Multidimensional scaling [48]
	Bilinear multidimensional scaling [22]
Rough set	Rough set [54]
Taguchi method	Taguchi method [27]
Model-based clustering	Model-based clustering [28]
Others	Chi-square automatic interaction (CHAID) [17]
	Choice-based conjoint analysis [20]
	Multicriterion clusterwise regression [13]
	Regression model [2]
	Metric conjoint segmentation [49]
	Clusterwise linear regression [52]
	Constrained market segmentation [21]
	CRISP: Customer response-based iterative segmentation [19]

The above journals covered more than 45 % of the total number of articles published. However, other important journals are as follows: Decision Support Systems, European Journal of Operational Research, and Tourism Management.

4.2 Distribution of Articles by Year of Publication

The distribution of articles by year of publication is shown in Fig. 1. Last 12 years has taken for consideration. The amount of publication increased significantly from 2001 to 2012. More research work would be expected in the future.

Table 2 Distribution of articles by journal

Journal title	Amount	Percentage (%)
Expert Systems with Applications	38	36.89
Journal of Marketing Research	5	4.85
Management Science	4	3.88
European Journal of Operational Research	4	3.88
Tourism Management	3	2.91
Decision Support Systems	3	2.91
Marketing Letters	3	2.91
Computational Statistics & Data Analysis	2	1.94
Journal of Classification	2	1.94
Management Science	2	1.94
Marketing Science	2	1.94
International Journal of Research in Marketing	2	1.94
Computer-Aided Design,	1	0.97
Computers & Operations Research	1	0.97
Journal of Marketing	1	0.97
European Journal of Economic and Social Systems	1	0.97
International Marketing Review	1	0.97
Journal of Direct Marketing	1	0.97
Journal of Engineering Design	1	0.97
Journal of Organizational Computing and Electronic Commerce	1	0.97
Powder Technology	1	0.97
Psychometrika	1	0.97
Transportation Research	1	0.97
Applied Mathematical Modeling	1	0.97
Advanced Engineering Informatics	1	0.97
Annals of Tourism Research	1	0.97
Australian Marketing Journal	1	0.97
Journal of Econometrics	1	0.97
Omega	1	0.97
Computer-Aided Design	1	0.97
Computers & Operations Research	1	0.97
Decision Sciences	1	0.97
Fuzzy Sets and Systems	1	0.97
Housing Studies	1	0.97
International Journal of Applied Science and Engineering	1	0.97
International Journal of Intelligent Systems in Accounting, Finance and Management	1	0.97
Iranian Acc. Aud. Rev	1	0.97
Journal of International Consumer Marketing	1	0.97

(continued)

Table 2 (continued)

Journal title	Amount	Percentage (%)
Journal of Management Information Systems	1	0.97
Journal of Strategic Marketing	1	0.97
Journal of the American Society for Information Science and Technology	1	0.97
Knowledge-Based Systems	1	0.97
Neurocomputing	1	0.97
Quality & Quantity	1	0.97
The International Journal of Management Science	1	0.97

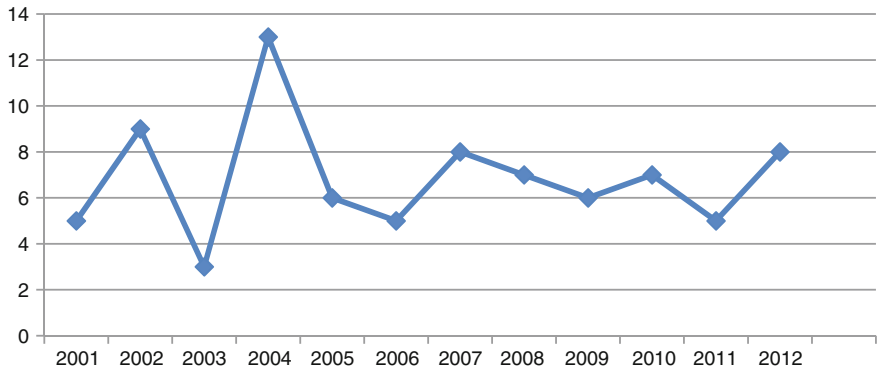

Fig. 1 Distribution of articles by year of publication

4.3 Distribution of Articles According to the Proposed Classification Model

The distribution of articles according to the major data mining techniques is shown in Table 3. Twenty-two major data mining techniques found in literature. The top six data mining techniques are as follows: neural network, evolutionary algorithm, fuzzy theory, RFM analysis, hierarchical clustering, and K-means.

More than 75 % of the total articles have published using above techniques. Researcher also used hybrid techniques for the better result and another reason was to overcome shortfall of another techniques. In last few years, many advance techniques are proposed for market segmentation.

Table 3 Distribution of articles by data mining techniques

Data mining techniques	Amount
Neural network	30
Evolutionary algorithm	17
Fuzzy theory	12
RFM analysis.	10
Hierarchical clustering	5
K-means	5
Bagged clustering	3
Kernel methods	3
Multidimensional scaling	3
Taguchi method	3
Rough set.	2
Model-based clustering	1
Chi-square automatic interaction (CHAID)	1
Choice-based conjoint analysis	1
Simulated annealing algorithm	1
Multicriterion clusterwise regression	1
Regression model	1
Metric conjoint segmentation	1
Clusterwise linear regression	1
Combinatorial optimization approaches to constrained market segmentation	1
CRISP: customer response-based iterative segmentation	1
Total	103

5 Discussions, Limitations, and Suggestions

5.1 Discussions

This is the first identified research paper on data mining techniques in market segmentation. This paper covers available data mining techniques used in market segmentation so far. Eight online journal databases were used for searching. After careful analysis of several research papers on market segmentation, we found that various researchers adopted different data mining techniques in the last few decades. The development of methodologies on marketing research can be divided into two phases. In the first phase, early researchers who worked on market segmentation generally used K-means and hierarchical clustering. But after 2000, market researchers are motivated to use advanced data mining techniques that can handle complex consumer behavior pattern. Hybrid algorithms are found in literature to increase the performance of exiting one. Some examples of hybrid algorithm include multilayer perceptron and K-means, genetic algorithm and K-means, particle swarm optimization and K-means, and self-organizing map and K-means. Neural network-based market segmentation is quite popular among the researcher.

5.2 Limitations

This paper might have some limitations. A widespread comprehensive literature review of data mining techniques in market segmentation has been presented. This research paper tries to incorporate all the available data mining techniques without time bound. However, this work surveyed those articles which were extracted based on the keyword "market segmentation" or "target marketing" or "data mining and market segmentation." In order to find out how data mining techniques for market segmentation developed, the categorization is done based on keyword index, abstract, and article methodology part. Articles without keyword index could not be extracted. This research work limited search for articles to 8 online databases. There might be the presence of other useful academic journals which can provide other important data mining techniques for market segmentation. We believe that many companies practice advanced techniques for market segmentation but failed to include here due to limited resource. In this study, we do not consider other non-English publications. However, other languages may have important techniques for market segmentation. Another major limitation is as the quality of market segmentation not only depends on good data mining techniques but also on the selection of proper segmentation variables [51]. Normally, researchers used general variables because general variables are easy to use [25]. The review of segmentation variable in market segmentation is out of scope of this paper.

5.3 Suggestions

1. Research on the application of data mining techniques in market segmentation is becoming an emerging field as shown in the Fig. 1 and Table 1, and the number of publication in term of research on the application of data mining in the market segmentation will gradually increase in the future.
2. Neural network-based market segmentation is the most used data mining technique. Neural network is used for classification, clustering, and prediction purpose. Many researchers preferred self-organizing map neural network model for visualization and determination number of cluster.
3. The result of market segmentation can easily improve with combination of good data mining techniques and proper selection of segmentation variable.
4. The K-means and hierarchical clustering are still preferred data mining techniques for market segmentation.
5. Kernel-based market segmentation is one of the promising techniques for robust market segmentation and also performed better than tradition techniques.
6. Many hybrid data mining techniques are used to increase the performance. For example, researchers used K-means with combination genetic algorithm for better performance.

7. Market segmentation is becoming more complex gradually and researchers are also working on development of more advanced data mining techniques that can handle outlier, noise, and big data-related problem.
8. Many data mining techniques are used from last few decades, but still there is always scope of improvement. Future researchers can improve the available algorithm for better performance in market segmentation. Some examples of such data mining techniques include kernel-based method, probabilistic fuzzy c-means, random forest, evolutionary algorithm.

6 Conclusion

Market segmentation is one of the primary and most critical parts of market research. This research work identified 103 articles which were published in 8 online databases. Our aim is to provide brief summary on available all data mining techniques which are most popular and successfully used so far. However, the research work cannot claim to be exhaustive. We believe that this work does provide reasonable insight of market segmentation and would help to give a clear picture for those who interested to work and research on this area.

References

1. Abdi, K., Fathian, M., Safari, E.: A novel algorithm based on hybridization of artificial immune system and simulated annealing for clustering problem. Int. J. Adv. Manuf. Technol. **60**(5–8), 723–732 (2012)
2. Wildt, Albert R., McCann, John M.: Multicriterion market segmentation: a new model, implementation, and evaluation. J. Mark. Res. **17**(3), 335–340 (1980)
3. Babu, G.P., Murty, M.N.: A near-optimal initial seed value selection in K-means algorithm using a genetic algorithm. Pattern Recogn. Lett. **14**(10), 763–769 (1993)
4. Balakrishnan, P.V., Cooper, M.C., Jacob, V.S., Lewis, P.A.: Comparative performance of the FSCL neural net and K-means algorithm for market segmentation. Eur. J. Oper. Res. **93**, 346–357 (1996)
5. Bezdek, J.C., Pal, N.R.: Some new indexes of cluster validity. IEEE Trans. Syst. Man Cybern. Part B: Cybern. **28**(3), 301–315 (1998)
6. Blatt, M., Wiseman, S., Domany, E.: Clustering data through an analogy to the potts model. Adv. Neural Inf. Process. Syst. **8**, 416–422 (1996)
7. Bloom, J.Z.: Tourist market segmentation with linear and non-linear techniques. Tour. Manage. **25**, 723–733 (2004)
8. Boone, D.S., Roehm, M.: Retail segmentation using artificial neural networks. Int. J. Res. Mark. **19**(3), 287–301 (2002)
9. Boone, D.S., Roehm, M.: Evaluating the appropriateness of market segmentation solutions using artificial neural networks and the membership clustering criterion. Market. Lett. **13**(4), 317–333 (2002)

10. Brida, J.G., Disegna, M., Osti, L.: Segmenting visitors of cultural events by motivation: A sequential non-linear clustering analysis of Italian Christmas market visitors. Expert Syst. Appl. **39**, 11349–11356 (2012)
11. Brida, J.G., Disegna, M., Scuderi, R.: Visitors of two types of museums: a segmentation study. Expert Syst. Appl. **40**(6), 2224–2232 (2012)
12. Bursco, M.J., Cradit, J.D., Stahl, S.: A simulated annealing heuristic for a bicriterion partitioning problem in marketing segmentation. J. Mark. Res. **39**(1), 99–109 (2002)
13. Bursco, M.J., Cradit, J.D., Stahl, S.: Multicriterion cluster wise regression for joint segmentation settings: an application to customer value. J. Mark. Res. **40**(2), 225–234 (2002)
14. Chen, C.H., Khoo, C.L., Yan, W.: A strategy for acquiring customer requirement patterns using laddering technique and ART2 neural network. Adv. Eng. Inform. **16**, 229–240 (2002)
15. Chen, M.C., Wu, H.P.: An association-based clustering approach to order batching considering customer demand patterns. Omega **33**(4), 333–343 (2005)
16. Cheng, C.H., Chen, Y.S.: Classifying the segmentation of customer value via RFM model and RS theory. Expert Syst. Appl. **36**, 4176–4184 (2009)
17. Chung, K.Y., Oh, S.Y., Kim, S.S., Han, S.Y.: Three representative market segmentation methodologies for hotel guest room customers. Tour. Manag. **25**(4), 429–441 (2004)
18. Croft, M.J.: Market Segmentation: A Step-by-Step Guide to Profitable New Business. Routledge, London, New York (1994)
19. Desarbo, W.S., Ramaswamy, V.: CRISP: customer response based iterative segmentation procedures for response modeling in direct marketing. J. Direct Market. **8**, 7–20 (1994)
20. Desarbo, W.S., Ramaswamy, V., Cohen, S.H.: market segmentation with choice-based conjoint analysis. Market. Lett. **6**(2), 137–147 (1995)
21. DeSarbo, W.S., Grisaffe, D.: Combinatorial optimization approaches to constrained market segmentation: an application to industrial market segmentation. Market. Lett. **9**, 115–134 (1998)
22. Desarbo, W.S., Grewal, R., Scott, C.J.: A cluster wise bilinear multidimensional scaling methodology for simultaneous segmentation and positioning analyses. J. Mark. Res. **45**, 280–292 (2008)
23. Frank, R.E., Massy, W.F., Wind, Y.: Market segmentation. Prentice Hall, Englewood Cliffs (1972)
24. Huang, J.H., Tzeng, G.H., Ong, C.S.: Marketing segmentation using support vector clustering. Expert Syst. Appl. **32**, 313–317 (2007)
25. Hammond, K., Ehrenberg, A.S.C., Goodhardt, G.J.: Market segmentation for competitive brands. Eur. J. Mark. **30**(12), 39–49 (1996)
26. Hruschka, H., Natter, M.: Comparing performance of feedforward neural nets and K-means for cluster-based market segmentation. Eur. J. Oper. Res. **114**, 346–353 (1999)
27. Hong, C.W.: Using the Taguchi method for effective market segmentation. Expert Syst. Appl. **39**, 5451–5459 (2012)
28. Kamakura, W.A., Russell, G.J.: A probabilistic choice model for market segmentation and elasticity structure. J. Market. Res. **26**, 379–390 (1989)
29. Kauko, T., Hooimeijer, P., Hakfoort, J.: Capturing housing market segmentation: an alternative approach based on neural network modeling. Hous. Stud. **17**(6), 875–894 (2002)
30. Kim, Y., Street, W.N.: An intelligent system for customer targeting: a data mining approach. Decis. Support Syst. **37**(2), 215–228 (2004)
31. Kotler, P., Gordon, M.: Principles of Market. Prentice Hall, Canada (1983)
32. Kuo, R.J., Ho, L.M., Hu, C.M.: Integration of self-organizing feature map and K-means algorithm for market segmentation. Comput. Oper. Res. **29**(11), 1475–1493 (2002)
33. Kuo, R.J., Chang, K., Chien, S.Y.: Integration of self-organizing feature maps and genetic algorithm- based clustering method for market segmentation. J. Organ. Comput. Electron. Commer. **14**(1), 43–60 (2004)
34. Li, Z., Wang, W., Yang, C., Ragland, D.R.: Bicycle commuting market analysis using attitudinal market segmentation approach. Transport. Res. Part A: Policy Pract. **47**, 56–68 (2013)

35. Maroosi, A., Amiri, B.: A new clustering algorithm based on hybrid global optimization based on a dynamical systems approach algorithm. Expert Syst. Appl. **37**(8), 5645–5652 (2010)
36. Maulik, U., Bandyopadhyay, S.: Genetic algorithm-based clustering technique. Pattern Recogn. **33**(9), 1455–1465 (2000)
37. Maulik, U., Bandyopadhyay, S.: Performance evaluation of some clustering algorithms and validity indices. IEEE Trans. Patt. Anal. Mach. Intell. **24**(12), 1650–1654 (2002)
38. Miguéis, V.L., Camanho, A.S., Falcão e Cunha, J.: Customer data mining for lifestyle segmentation. Expert Syst. Appl. **39**, 9359–9366 (2012)
39. Mostafa, M.M.: Clustering the ecological footprint of nations using Kohonen's self-organizing maps. Expert Syst. Appl. **37**, 2747–2755 (2010)
40. Murthy, C.A., Chowdhury, N.: In search of optimal clusters using genetic algorithms. Pattern Recogn. Lett. **17**(8), 825–832 (1996)
41. Natter, M.: Conditional market segmentation by neural networks: a Monte-Carlo study. J. Retail. Consum. Serv. **6**(4), 237–248 (1999)
42. Ngai, E.W., Xiu, L., Chau, D.C.K.: Application of data mining techniques in customer relationship management: A literature review and classification. Expert Syst. Appl. **36**(2), 2592–2602 (2009)
43. Park, D.H., Kim, H.K., Choi, I.Y., Kim, J.K.: A literature review and classification of recommender systems research. Expert Syst. Appl. **39**(11), 10059–10072 (2012)
44. Punj, G., Stewart, D.W.: Cluster analysis in marketing research: review and suggestions for application. J. Market. Res. **20**, 134–148 (1983)
45. Smith, W.R.: Product differentiation and market segmentation as an alternative marketing strategy. J. Market. **21**, 3–8 (1956)
46. Vellido, A., Lisboa, P.J.G., Vaughan, J.: Neural networks in business: a survey of applications (1992–1998). Expert Syst. Appl. **17**(1), 51–70 (1999)
47. Vesanto, J., Alhoniemi, E.: Clustering of the self-organizing map. IEEE Trans. Neural Netw. **11**(3), 586–600 (2000)
48. Vishwanath, A., Chen, H.: Technology clusters: using multidimensional scaling to evaluate and structure technology clusters. J. Am. Soc. Inform. Sci. Technol. **57**(11), 1451–1460 (2006)
49. Vriens, M., Wedel, M., Wilms, T.: Metric conjoint segmentation methods: a Monte Carlo comparison. J. Mark. Res. **33**, 73–85 (1996)
50. Wang, C.H.: Apply robust segmentation to the service industry using kernel induced fuzzy clustering techniques. Expert Syst. Appl. **37**, 8395–8400 (2010)
51. Wedel, M., Kamakura, W.A.: Market segmentation: conceptual and methodological foundations. Kluwer Academic, Boston (2000)
52. Wedel, M., Kistemaker, C.: Consumer benefit segmentation using cluster wise linear regression. Int. J. Res. Mark. **6**, 241–258 (1989)
53. Wei, J.T., Lin, S.Y., Weng, C.C., Wu, H.H.: A case study of applying LRFM model in market segmentation of a children's dental clinic. Expert Syst. Appl. **39**(5), 5529–5533 (2012)
54. Wu, W.W.: Segmenting and mining the ERP users' perceived benefits using the rough set approach. Expert Syst. Appl. **38**, 6940–6948 (2011)
55. Zhang, Y., Jiao, J., Ma, Y.: Market segmentation for product family positioning based on fuzzy clustering. J. Eng. Des. **18**(3), 227–241 (2007)

Cuckoo Search Optimization for Job Shop Scheduling Problem

Shekhar Singh and Krishna Pratap Singh

Abstract In this paper, a novel hybrid algorithm incorporating the cuckoo search optimization (CSO) technique and an Assorted Individual Enhancement Scheme is proposed to solve the ob shop scheduling problem (JSSP) with an objective to minimize the makespan. The proposed hybrid algorithm is applied to 20 job shop problem instances available in OR-Library and the results are compared with simple CSO. Analysis suggests that the hybrid approach is more effective and robust toward JSSP than simple CSO technique.

Keywords Job shop scheduling problem · Makespan · Cuckoo search optimization · Random key encoding · Assorted Individual Enhancement

1 Introduction

Operations research (OR) is a field full of real-world complex decision-making problems and deals with study of efficient algorithms/techniques to solve such problems. The goal is to arrive at an optimal or say near-optimal acceptable solution. Scheduling problems are an important component in study of OR. There are several scheduling problems studied in literature, and all the problems are designed to model some real-world scenario. In this paper, the focus is on job shop scheduling problem (JSSP). JSSP is a combinatorial optimization problem and is NP-hard in strong sense.

As mentioned, the JSSP is NP-hard in nature. So there is no polynomial time algorithm for this problem which guarantees an optimal solution. Meta-heuristics [1] are widely used to solve some hard optimization problems. Meta-heuristic

S. Singh (✉) · K.P. Singh
Indian Institute of Information Technology, Allahabad 211012, Uttar Pradesh, India
e-mail: shekhar.singh1729@gmail.com

K.P. Singh
e-mail: kpsinghiitr@gmail.com

K.N. Das et al. (eds.), *Proceedings of Fourth International Conference on Soft Computing for Problem Solving*, Advances in Intelligent Systems and Computing 335,
DOI 10.1007/978-81-322-2217-0_9

techniques in general are problem-independent approaches and do not guarantee an optimal solution. But with comparatively lesser computations, these techniques provide a near-optimal but practically acceptable solution for a given JSSP. In recent years, significant amount of research is being done toward application of certain meta-heuristics for solving the JSSP. Several meta-heuristic algorithms such as genetic algorithm [2, 3], ant colony optimization [4], particle swarm optimization [5–8], artificial immune system [7], artificial bee colony [9], tabu Search [3, 4], simulated annealing [6, 8], differential evolution [5], and more have already been applied. Initial research involved application of a single meta-heuristic technique, but now the focus has shifted and a meta-heuristic approach is usually embedded with some other techniques. As for some techniques, the global search capability is better than the local search and vice versa. So, with hybridized approach, the idea is to enhance the optimization capability. Recently, Yang and Deb [10] formulated a new nature-inspired meta-heuristic algorithm, cuckoo search (CS). In nature-inspired computing, the focus is on modeling some peculiar natural phenomenon and coming up with an algorithmic technique which can be advantageous in solving real-world (optimization) problems. By meticulously observing and then algorithmically modeling the breeding behavior of cuckoo, Yang and Deb [10] came up with a novel meta-heuristic optimization technique called the cuckoo search optimization (CSO). This technique is based upon the obligate brood parasitic nature of cuckoo. Current paper applies CS optimization technique with assorted individual enhancement to minimize makespan for a given JSSP.

The remainder of this paper is categorized as follows: Sects. 2 and 3 give an introduction to the JSSP and CSO, respectively. Sections 4 and 5 give a detailed description of using CSO for the JSSP and Assorted Individual Enhancement Scheme, respectively. Then, proposed hybrid algorithm is discussed in Sect. 6. Experimental results and related discussion is done in Sect. 7. Finally, in Sect. 8, this paper is summarized and some related future scope is also mentioned.

2 Job Shop Scheduling Problem

Formally, let us assume that there are n jobs and m machines; then, in basic model of this general $n \times m$ JSSP, it is essential that each of these n jobs require some m number of operations in order to get completed. As per convention, it is assumed that a particular operation/task $i, 1 \leq i \leq m$ can be performed only on machine i. Also, each job $j, 1 \leq i \leq n$ has a technological constraint associated with it in a manner that it requires the available m machines in a particular order, i.e., m operations have to be performed in a certain order for each job to get finished. The ordering preference associated with each job has to be followed strictly, and then for execution of each job operation (on a particular machine), some processing time is required. So the requirement is to obey the constraint posed by given job shop and try to optimize given objective(s).

There can be several objectives associated with a JSSP, but the one most widely studied is *makespan minimization*. In simple terms, makespan means the span of time required to complete/manufacture a set of jobs or tasks. So if a certain set of jobs have to be done on a certain set of machines, then there is a time, say $t = 0$, when this process starts and then at some time, all the jobs are completed. Now the time span from $t = 0$ to the completion point is amount of time spent to do or perform all the set of jobs and this is termed as makespan. The objective is to keep the *makespan* as *small* as possible. The completion time for a job is the time at which the last operation of that particular job gets executed or the job gets processed/visited at the last required machine. So if completion time for *j*th job is called C_j, then automatically the makespan is Max C_j, for $1 \leq j \leq n$ value. Clearly, $\text{Max}(C_1, C_2, \ldots, C_n)$ in general gives the makespan. So the makespan objective can be formally written as $\text{Minimize}\{\text{Max } C_j, \text{ for } 1 \leq j \leq n\}$.

3 Cuckoo Search Optimization (CSO)

CSO starts with a randomly chosen nest. A nest in CSO technique comprises of potential solutions to the optimization problem in consideration. Now a nest in itself contains several hosts so precisely each host is a solution to the optimization problem. A nest contains several such solutions, and when the algorithm converges, the best or, say the fittest host, is the final solution to the optimization problem being solved. Choice of number of hosts in a nest depends upon the problem. If the number of hosts is large, then firstly there are those many solution seed to start with and accordingly the coverage area is also increased. So there will be certain number of hosts available in system. A cuckoo will lay one egg at a time and dump it in host nests. Then probabilistically, it will be decided that whether the host bird will discover cuckoo's egg in its nest or not. It should be noted that an egg in CSO refers to a potential solution to the optimization problem under consideration. From implementation perspective, the two major components in CSO technique are discussed below.

3.1 Get a Solution from Cuckoo via Levy Flight

In CSO technique, for getting a solution from cuckoo, Yang and Deb [10, 11] utilized the concept of *Levy flight.* A Levy flight can be described as a random walk in which the step length is decided by certain probability distribution functions which are heavily tailed. In this paper to simulate the pattern of Levy flight [12], the *Mantegna's algorithm* is used.

As per the Mantegna's algorithm, step size can be computed using the expression:

$$\text{step} = \frac{u}{|v|^{1/\beta}} \tag{1}$$

Here, u and v are derived from normal distributions:

$$u \sim N\left(0, \sigma_u^2\right), \quad v \sim N\left(0, \sigma_v^2\right) \tag{2}$$

with

$$\sigma_u = \left\{ \frac{\Gamma(1+\beta)\sin(\pi\beta/2)}{\Gamma[(1+\beta)/2]\beta 2^{(\beta-1)/2}} \right\}^{1/\beta}, \tag{3}$$

$$\sigma_v = 1 \tag{4}$$

and $0 < \beta \leq 2$. Current work assumes $\beta = 3/2$ for evaluating step size.

3.2 Empty Discovered Host Nests

If the host bird discovers that the egg (solution) in its nest is dumped by some other species, then it simply abandons its nest. From implementation point of view abandoning or disowning a nest means, replace the current solution string in discovered host nest with some new solution string generated randomly. While modeling CSO technique, Yang and Deb [10, 11] refer that with some pre-defined probability p_a, a host nest will be discovered. It can be interpreted as a fraction of p_a hosts will be replaced during an iteration of algorithm.

4 CSO for Job Shop Scheduling Problem

4.1 Representation of a Host

CSO is designed for general optimization problem(s) where the solution string can be a continuously defined real-valued set. As JSSP is a discrete optimization problem, so there should be a well-defined technique for mapping the potential solution string (which is continuously defined real values) from each host in nest to discrete values which suggest a job sequence and can be easily interpreted as a schedule solving JSSP. The length of solution string depends upon the dimension of optimization function. In $n \times m$ JSSP, each of these n jobs have m number of operations, so each job needs to go exactly once on each machine to complete all its operations. Therefore, the dimension of the solution string is nm. A *random key encoding* [8] scheme is generally used for mapping $n \times m$ dimensional continuous real-valued solution space to $n \times m$ dimensional discrete-valued job sequence.

4.2 Random Key Encoding Scheme

Each host in CSO is *nm*-dimensional string and contains some continuously defined real values. For example, let us consider a 3 × 3 job shop, then some arbitrarily chosen host (*original host* in Fig. 1) is a 9 (3 × 3) dimensional vector. As per the random key encoding scheme, the values in host are transformed to discrete values in set $[1, (nm)]$. In this paper, the mapping technique replaces the elements of original host with the indices of elements when they are sorted in ascending order. Say if an element α_k, $1 \leq k \leq (nm)$ present at index δ is the smallest element in host vector, then the first element of modified host vector is index δ. In Fig. 1, the *modified host* shows this transformation The random key encoding is applied to each and every host present in the nest in similar manner. Now host vector holds discrete values in range $[1, (nm)]$ but for it to be a valid job shop schedule each element in host vector must be in range $[1, n]$ and also each element should get repeated m number of times. As the modulus operation on some arbitrary integer (say) N returns discrete values in range $[0, (N-1)]$. To map the elements of host vector in range $[1, n]$ (for given $n \times m$ JSSP), on every element γ_k, $1 \leq k \leq (nm)$, following operation can be performed: $(\gamma_k n) + 1$ with $1 \leq k \leq (nm)$. The *encoded sequence* in Fig. 1 is obtained using this operation. So modified host is processed further by applying the modulus operation in aforementioned manner on each element of host. Now as desired, each element in encoded sequence is in range $[1, n]$ and also getting repeated m number of times. So this seems to be a genuine schedule, but one more detail is required regarding several occurrences of a single job index. If there is $n \times m$ JSSP, then an operation can be represented as O_{ji} $(1 \leq j \leq n, 1 \leq i \leq m)$; it shows the ith operation of job j. So the repeated occurrence can be understood more precisely in terms of formal notations; if first value in encoded sequence is index j, $1 \leq j \leq n$, then this should be read as the first operation of job j, i.e., O_{j1} now second occurrence of same job index j represents second operation of job j, i.e., O_{j2} and so on. Using this rule, the encoded sequence is transformed into corresponding *operations sequence* which represents a valid machine schedule as shown in Fig. 1. In this manner, a host containing continuous real-valued elements can be transformed to an operations sequence. This operations sequence vector can be easily employed for evaluating the makespan for JSSP under consideration.

Original Host	0.69	0.54	0.50	0.90	0.68	0.88	0.94	0.22	0.24
Index	1	2	3	4	5	6	7	8	9
Sorted Host	0.22	0.24	0.50	0.54	0.68	0.69	0.88	0.90	0.94
Modified Host	**8**	**9**	**3**	**2**	**5**	**1**	**6**	**4**	**7**
Encoded Sequence	**3**	**1**	**1**	**3**	**3**	**2**	**1**	**2**	**2**
Operations Sequence	O_{31}	O_{11}	O_{12}	O_{32}	O_{33}	O_{21}	O_{13}	O_{22}	O_{23}

Fig. 1 Random key encoding scheme $(n = 3, m = 3)$

5 Assorted Individual Enhancement Scheme

To enhance the local and global search ability of an optimization technique, Lin et al. [8] discuss a *multi-type individual enhancement scheme*. On similar lines in this paper, Assorted Individual Enhancement Scheme is used. The scheme is termed as assorted individual enhancement; there are four different types of enhancements, namely *swapping, insertion, inversion,* and *long-distance movement*. The enhanced solution string returned by an enhancement scheme will be considered only if it increases the fitness (i.e., minimizes the makespan). In the following discussion, the working of these four different enhancements is explained and later on Algorithm 1 gives its implementation from perspective of CSO technique.

Swapping operation generates two random integers, say a, b, within the range $[1, (nm)]$ such that $a \neq b$, and then simply swaps the elements present at these two indices. Figure 2 illustrates this operation for an arbitrary host vector (for a given 3×2 job shop) processed using *random key encoding*. *Insertion operation* also generates two random integers, say a, b, within the range $[1, (nm)]$ such that $a \neq b$ and then picks up the element at index a and inserts it at location pointed by index b. When the element at dimension a is inserted at dimension referred by b, an empty space is created at dimension a. So the remaining elements in host vector are contiguously shifted left or right depending upon the location of a. Figure 3 shows how the original host vector (for a given 3×2 job shop) is enhanced using this operation. To perform the *inversion operation,* in this paper two (slightly) different ways are defined. First method to perform inversion operation generates two random integers, say a, b, within the range $[1, (nm)]$ such that $a \neq b$. Then, all the elements in contiguous location between dimension a and b are inverted, i.e., the host sub-string between index a and b is simply reversed. In second type of inversion operation, the entire host string is reversed. So it can be said that the second type of inversion is a special case of first method with $a = 1$ and $b = (nm)$. The decision regarding which of these two methods is to be used is done by generating a uniformly distributed random number in range $[0, 1]$ as Algorithm 1 illustrates it later. Figure 4 represents *inversion operation* of *type I* for an arbitrary host vector (for a given 3×2 job shop). In contrast to previously discussed three operation schemes, *long-distance movement operation* generates three random integers, say a, b and c, with certain constraints. Firstly, a and b are generated such that $1 \leq a,\ b \leq (nm)$ with $a \neq b$ and $\min(a, b) \neq 1$ AND $\max(a, b) \neq (nm)$. Then, once a and b are generated, third random integer (say) c is generated such that $1 \leq c \leq (nm)$ with $c \neq a$ and $c \neq b$ and also $c \notin [a, b]$, i.e., $c < \min(a, b)$ OR $c > \max(a, b)$. Now in long-distance movement operation, the host sub-string from index a to b is copied contiguously and this sub-string is inserted at index pointed out by integer c. Once the host vector sub-string in range $[a, b]$ is removed, then there will be some empty cells in original host vector. So the neighboring values are accordingly shifted occupying the space created by movement of selected sub-string. Figure 5 shows how the original host vector (for a given 3×2 job shop) is enhanced using *long-distance movement operation*. These enhancement operations are not applied at once, i.e., one particular enhancement

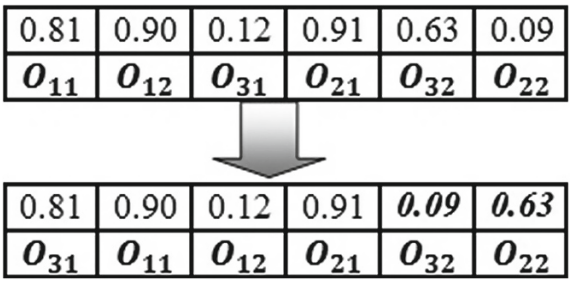

Fig. 2 Swapping operation (assuming $a = 5$, $b = 6$)

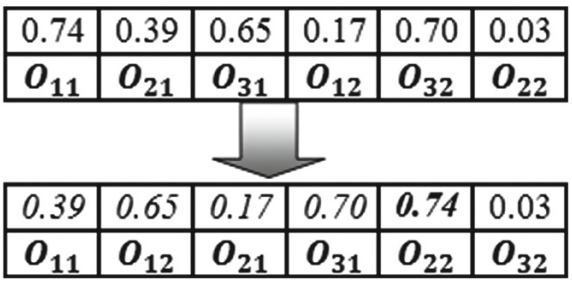

Fig. 3 Insertion operation (assuming $a = 1$, $b = 5$)

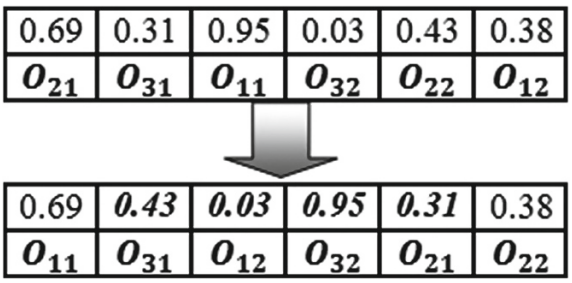

Fig. 4 Inversion operation of *type I* (assuming $a = 2$, $b = 5$)

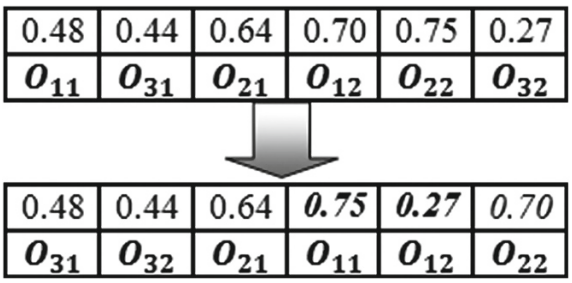

Fig. 5 Long-distance movement operation (assuming $a = 5$, $b = 6$ and $c = 4$)

scheme is selected and applied at a time. To make the process of selection of a particular enhancement scheme smooth and fair, different probability is assigned to all the available operations as Algorithm 1 below explains this further. Suppose $\text{prob}_{\text{swap}}$, $\text{prob}_{\text{insert}}$, $\text{prob}_{\text{invert}}$ and $\text{prob}_{\text{long}}$ is the probability of execution of swapping operation, insertion operation, inversion operation, and long-distance movement operation, respectively.

Input: Original *nest* developed using CSO, a *fitness* vector containing the fitness of all the hosts in *nest*, $prob_{swap}$, $prob_{insert}$, $prob_{invert}$ and $prob_{long}$.

Output: Modified *nest* with hosts having better or at least equal fitness value as the original *nest* and accordingly an updated *fitness* vector.

for all the *hosts* in input *nest* $(1 \le i \le num_{hosts})$
  generate a uniformly distributed random number in range $[0, 1]$ and store it in variable $perform_{oper}$
  if $perform_{oper} \ge 0$ *AND* $perform_{oper} \le prob_{swap}$ then execute *Swapping Operation* on $host(i)$
  else if $perform_{oper} > prob_{swap}$ *AND* $perform_{oper} \le (prob_{swap} + prob_{insert})$ then execute *Insertion Operation* on $host(i)$
  else if $perform_{oper} > (prob_{swap} + prob_{insert})$ *AND* $perform_{oper} \le (prob_{swap} + prob_{insert} + prob_{invert})$
    generate a uniformly distributed random number in range $[0, 1]$ and store it in variable $invert_{type}$
    if $invert_{type} \le 0.5$ then execute *Inversion Operation* of *type I* on $host(i)$
    else execute *Inversion Operation* of *type II* on $host(i)$ end if
  else execute the *Long-distance Movement Operation* on $host(i)$ end if
  compute fitness value of $host(i)$ and store it in variable $fitness_{new}$
  if $fitness_{new} \ge fitness(i)$ then update $nest(i)$ with current solution string in $host(i)$ and also update $fitness(i)$ with value $fitness_{new}$
end for

6 Hybridization of CSO and Assorted Individual Enhancement

As discussed, the Assorted Individual Enhancement Scheme is designed to enhance the search ability of an optimization algorithm. In current paper, CSO technique is hybridized with Assorted Individual Enhancement Scheme to increase the search space and also to boost up the optimization process. Now with some suitable exposure to CSO and Assorted Individual Enhancement Scheme, a formal algorithm can be proposed tying both of them together. Algorithm 2 below gives a general algorithm for hybridization of CSO and Assorted Individual Enhancement. Suppose an optimization problem with fitness function, say $F(x_1, \ldots, x_d)$, is to be solved; here, d represents the dimension of problem. Assume that a constrained optimization is to be performed between certain given lower bound (LB) and an upper bound (UB).

Input: Number of hosts (population size): num_{hosts}, probability of discovery p_a, $prob_{swap}$, $prob_{insert}$, $prob_{invert}$, and $prob_{long}$, an objective function for optimization: $F(x_1, \ldots, x_d)$.

Output: Best host (d dimensional solution string): $best_{host}$ providing an optimal (near) value for given objective function.

initialize a *nest* (having dimension $num_{hosts}Xd$) with uniformly distributed random numbers in range $[LB, UB]$
compute fitness of each host (solution string) in initialized nest and store it in column vector: *fitness* (having dimension $num_{hosts}X1$)
perform assorted individual enhancement using *Algorithm 1* on initialized *nest*, get an updated *nest* and *fitness* vector
rank *fitness* vector to get current best solution string and assign it to a row vector: $best_{host}$
while ($maximumiteration$) *OR* ($convergencecriteria$)
    get new set of solutions in $levy_{nest}$ (having dimension $num_{hosts}Xd$) generated using the Mantegna's algorithm for Levy noise; ensuring all the hosts in $levy_{nest}$ are within $[LB, UB]$
    retain $best_{host}$ and replace other hosts in $nest(i)$ $(1 \leq i \leq num_{hosts})$ with better hosts from $levy_{nest}(i)$
    accordingly update in $fitness(i)$ the fitness value of $host(i)$
    rank *fitness* vector to get the (new) current best solution and assign it to $best_{host}$
    replace p_a fraction of hosts in current *nest* by generating new set of solutions in new_{solns} (having dimension $num_{hosts}Xd$); ensuring all the hosts in new_{solns} are within $[LB, UB]$

```
    replace hosts in nest(i) (1 ≤ i ≤ num_hosts) with better
    hosts from new_solns(i) accordingly update in fitness(i)
    the fitness value of host(i)
    perform assorted individual enhancement using
    Algorithm 1 on current nest, get an updated nest
    and fitness vector
    rank updated fitness vector to get the (new)
    current best solution string and assign it to
    best_host_new
    if fitness value of best_host_new > best_host then make
    best_host_new as best_host
end while
```

7 Experimental Results and Discussion

The proposed algorithms are implemented in MATLAB and simulated in Windows environment. OR-Library [13] is a standard library containing datasets for several OR problems. Out of several job shop problem instances available in OR-Library [14], the current paper focuses on 20 such instances as test benchmarks for testing the efficiency of proposed algorithms. 3 problems, namely *ft06*, *ft10,* and *ft20* are due to *Fisher and Thompson*. Remaining 17 problem instances, namely *la01*, *la02*, …, *la17* are due to *Lawrence*. On basis of experimental results and some tuning, the parameters chosen for CSO in current paper are $\text{num}_{\text{hosts}} = 40, p_a = 0.25$ also current work does not assume any LB or, UB for optimization. The probabilities used (for 4 different types of operations) are as follows: $\text{prob}_{\text{swap}} = 0.4$, $\text{prob}_{\text{insert}} = 0.4$, $\text{prob}_{\text{invert}} = 0.1$ and $\text{prob}_{\text{long}} = 0.1$ Each job shop problem instance is solved by executing the algorithm 30 times. With 30 trials of same problem instance, one can compute the *minimum*, *mean,* and *standard deviation*. The *minimum* value out of these 30 runs provides the best value for corresponding job shop problem instance. In this paper, the results obtained for CSO (with Mantegna's algorithm for Levy noise) are compared with hybridized CSO algorithm. Table 1 tabulates the results obtained for makespan optimization using simple CSO technique and CSO algorithm hybridized with Assorted Individual Enhancement Scheme. It is evident from Table 1 that CSO with Mantegna's algorithm for Levy flight is only able to attain the best known solution (BKS) for 11 problems out of 20. But when same algorithm is hybridized with Assorted Individual Enhancement Scheme, then the technique becomes more effective, and out of 20 job shop instances, 17 BKS is attained. Another important observation is that for hybrid approach, standard deviation (SD) is pretty low, so hybrid approach is more robust in nature. It is also apparent with hybrid approach that for 13 instances the value of SD is zero, so for all 30 runs, the algorithm is returning BKS for that instance which is fairly commendable. Figures 6 and 7 represent the relative percentage error (RPE) for all 20

Table 1 Makespan optimization results for FT and LA test instances

Instance	Size ($n \times m$)	BKS in literature	CSO minimum (best)	CSO mean (average)	CSO standard deviation	CSO (hybrid) minimum (best)	CSO (hybrid) mean (average)	CSO (hybrid) standard deviation
ft06	6 × 6	**55**	***55***	55	0	***55***	55	0
ft10	10 × 10	**930**	1,058	1,111	21.7	961	984	12.73
ft20	20 × 5	**1,165**	1,374	1,410	19.13	1,185	1,216	15.96
la01	10 × 5	**666**	***666***	667	2.5	***666***	666	0
la02	10 × 5	**655**	672	688	9.68	***655***	658	4.01
la03	10 × 5	**597**	617	637	7.03	***597***	606	5.35
la04	10 × 5	**590**	607	616	4.8	***590***	593	3.26
la05	10 × 5	**593**	***593***	593	0	***593***	593	0
la06	15 × 5	**926**	***926***	926	0	***926***	926	0
la07	15 × 5	**890**	900	931	12.5	***890***	890	0
la08	15 × 5	**863**	***863***	880	10.81	***863***	863	0
la09	15 × 5	**951**	***951***	952	3.1	***951***	951	0
la10	15 × 5	**958**	***958***	958	0	***958***	958	0
la11	20 × 5	**1,222**	***1,222***	1,228	6.14	***1,222***	1,222	0
la12	20 × 5	**1,039**	***1,039***	1,040	2.96	***1,039***	1,039	0
la13	20 × 5	**1,150**	***1,150***	1,153	4.55	***1,150***	1,150	0
la14	20 × 5	**1,292**	***1,292***	1,292	0	***1,292***	1,292	0
la15	20 × 5	**1,207**	*1,281*	1,321	19.13	***1,207***	1,207	0
la16	10 × 10	**945**	*1,008*	1,042	15.5	*946*	974	10.78
la17	10 × 10	**784**	*838*	864	13.35	***784***	792	2.67

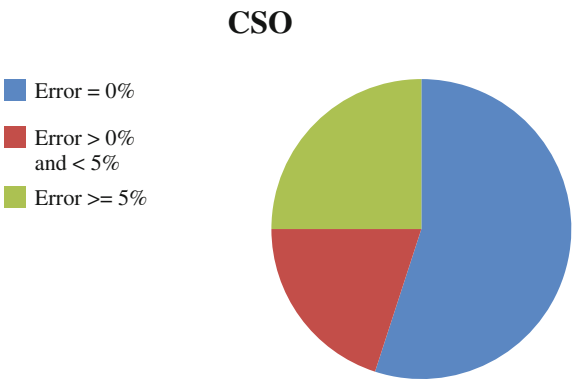

Fig. 6 Pie chart showing RPE of 20 instances for simple CSO technique

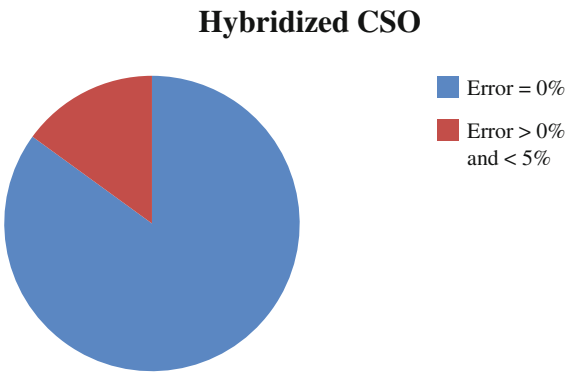

Fig. 7 Pie chart showing RPE of 20 instances for hybridized CSO technique

instances. RPE is computed using the Minimum value for an instance and the BKS for that instance as: RPE = ((MinimumValue − BKS)/BKS) × 100. Cleary, for majority of instances, the RPE is zero (i.e., Minimum Value = BKS) in case of hybrid approach as compared to simple CSO.

8 Conclusion

In this paper, a new hybrid approach is proposed for solving the makespan optimization problem in basic job shop scheduling environment. CSO technique is mixed with a set of assorted individual enhancements to increase its search ability. Major advantage of CSO lies in its simplicity as just two parameters are required for its implementation: probability of discovery p_a and population size $\text{num}_{\text{hosts}}$. To apply CSO and also to perform individual enhancements, random key encoding is used so as to transform a real-valued vector to discrete values representing a genuine schedule. As it is evident from experimental results, the hybrid approach is

better than simple CSO technique. Although the proposed algorithm is able to attain the BKS for majority of problems, still it is missing the best solution for some of the instances and can be further improved.

References

1. Yang, X.-S.: Nature-inspired Metaheuristic Algorithms. Luniver Press, UK (2010)
2. Goncalves, J.F., et al.: A hybrid genetic algorithm for the job shop scheduling problem. Eur. J. Oper. Res. **167**(1), 77–95 (2005)
3. Meeran, S., Morshed, M.S.: A hybrid genetic tabu search algorithm for solving job shop scheduling problems: a case study. J. Intell. Manuf. **23**(4), 1063–1078 (2012)
4. Huang, K.-L., Liao, C.-J.: Ant colony optimization combined with taboo search for the job shop scheduling problem. Comput. Oper. Res. **35**(4), 1030–1046 (2008)
5. Tasgetiren, M.F., et al.: A particle swarm optimization and differential evolution algorithms for job shop scheduling problem. Int. J. Oper. Res. **3**(2), 120–135 (2006)
6. Ge, H., et al.: A hybrid algorithm based on particle swarm optimization and simulated annealing for job shop scheduling. In: Third International Conference on Natural Computation, 2007. ICNC 2007, pp. 715–719 (2007)
7. Ge, H.-W., et al.: An effective PSO and AIS-based hybrid intelligent algorithm for job-shop scheduling. IEEE Trans. Syst. Man Cybern. Part A Syst. Hum. **38**(2), 358–368 (2008)
8. Lin, T.-L., et al.: An efficient job-shop scheduling algorithm based on particle swarm optimization. Expert Syst. Appl. **37**(3), 2629–2636 (2010)
9. Banharnsakun, A., et al.: Job shop scheduling with the best-so-far ABC. Eng. Appl. Artif. Intell. **25**(3), 583–593 (2012)
10. Yang, X.-S., Deb, S.: Cuckoo search via Levy flights. In: World Congress on Nature Biologically Inspired Computing, 2009. NaBIC 2009, pp. 210–214 (2009)
11. Yang, X.-S., Deb, S.: Engineering optimisation by cuckoo search. Int. J. Math. Model. Numer. Optim. **1**(4), 330–343 (2010)
12. Leccardi M.: Comparison of three algorithms for Levy noise generation. In: Proceedings of Fifth EUROMECH Nonlinear Dynamics Conference (2005)
13. Beasley, J.E.: OR-Library: distributing test problems by electronic mail. J. Oper. Res. Soc. **41** (11), 1069 (1990)
14. OR-Library Job shop scheduling. http://people.brunel.ac.uk/~mastjjb/jeb/orlib/files/jobshop1.txt

Artificial Neural Network Technique for Solution of Nonlinear Elliptic Boundary Value Problems

Neha Yadav, Anupam Yadav and Kusum Deep

Abstract In this article, we present an artificial neural network technique to solve some of the two-point nonlinear elliptic boundary value problems arising in science and engineering. A trial solution of the differential equation is written in terms of a feed forward neural network with adjustable parameters weights or biases, and error function is prepared to use in the back-propagation algorithm to update the network parameters with momentum term. Comparison of the results obtained by the present method is done with analytical solution and other existing numerical methods which show the efficiency of Neural network method with high accuracy, fast convergence, and low use of memory for solving nonlinear elliptic boundary value problems. The main advantage of the proposed approach is that once the network is trained, it allows evaluation of the solution at any desired number of points instantaneously with spending negligible computing time.

Keywords Artificial neural network · Back-propagation algorithm · Boundary value problems · Nonlinear elliptic equations

AMS Subject Classifications: 65N20.

N. Yadav (✉)
Department of Applied Science, ITM University,
Sector 23 A, Gurgaon 122001, Haryana, India
e-mail: nehayad441@yahoo.co.in

A. Yadav
Department of Science and Humanities, National Institute of Technology Uttarakhand,
Garhwal 246174, Uttarakhand, India
e-mail: anupuam@gmail.com

K. Deep
Department of Mathematics, Indian Institute of Technology Roorkee,
Roorkee 247667, Uttarakhand, India
e-mail: kusumfma@iitr.ernet.in

K.N. Das et al. (eds.), *Proceedings of Fourth International Conference on Soft Computing for Problem Solving*, Advances in Intelligent Systems and Computing 335,
DOI 10.1007/978-81-322-2217-0_10

1 Introduction

Linear and Nonlinear phenomenon of differential equations are of fundamental importance in fields of science and engineering. A variety of problems in many scientific fields are modeled with the use of differential equations, e.g., problems arise in physics, chemistry, biology, economics, etc. The solution of linear differential equation is now not very difficult to solve, but the problems associated with nonlinear differential equation are still challenging for the researchers. There are many techniques available for the solution of nonlinear elliptic boundary value problems, e.g., homotopy perturbation method, finite difference method, finite element method, etc. [1–8].

In this paper, we consider two nonlinear elliptic boundary value problems which are reaction–diffusion equation and the equation arises in catalytic reactions in a flat particle. Nonlinear elliptic boundary value problems have been solved by various authors in [1, 2] which includes weak and convex solution. Existence and uniqueness of solutions to a nonlinear differential equation has also been discussed in [3]. Due to the complexity of analytical solutions, several numerical methods have been also developed for the solution of nonlinear elliptic boundary value problems [4–6]. Finite difference approximation of reaction–diffusion equation is given in [2]. Homotopy perturbation method has been presented in [7] for the numerical solution of some two-point nonlinear elliptic boundary value problems.

Neural network solution of a differential equation provides many advantages over the traditional methods [9–12]. The main advantage of the neural network method is that it provides a continuous solution over whole domain of integration while the other numerical methods provide solution only over discrete points and the solution between these points obtained using the method of interpolation. Another advantage of the neural network method is computational complexity, as it does not increase rapidly when the number of sampling point and the dimension of the problem increases.

The aim of this article is to apply the artificial neural network method for solving two-point nonlinear elliptic boundary value problems arising in steady-state reaction–diffusion and catalytic reactions of a flat particle. A neural network technique with gradient descent algorithm is used to optimize the network parameters in the neural network to solve both the given problems. The main advantage of using neural network technique for solution of nonlinear elliptic boundary value problems is that it does not require the linearization of problem. Hence, this method requires less calculus effort with negligible computing time. Performance of the neural network method is tested by finding the numerical solutions for a number of cases of the problems, and then, comparison has been presented with analytical solution presented in the literature.

The rest of this article is organized as follows: In Sect. 2, neural network formulation of reaction–diffusion equation is given. Artificial neural network technique for the solution of a nonlinear elliptic boundary value problem arising in catalytic reaction of a flat particle is presented in Sect. 3. In Sect. 4, numerical

simulations have been performed. Also, the results are compared with the exact solutions and some existing numerical solutions in this section. Finally, in Sect. 5, a conclusion is given which briefly summarizes the results.

2 Reaction–diffusion Equation

Consider the reaction–diffusion equation [7]

$$y'' + \lambda \exp\left[\frac{y}{(1+\alpha y)}\right] = 0, \quad t \in (0,1) \tag{1}$$

with the boundary conditions $y(0) = y(1) = 0$. The trial solution of Eq. (1) using neural network can be written as:

$$y_T = t\,(t-1)\,N(\bar{t},\bar{p}) \tag{2}$$

which satisfies the desired boundary condition at $t = 0$ and 1. The derivatives are then calculated with respect to input vector and weight parameters to minimize the error quantity.

3 Catalytic Reactions in a Flat Particle and Its Solution

This equation arises in a study of heat and mass transfer for a catalytic reaction within a porous catalyst flat particle [8]. If a flat geometry of the particle and conductive heat transfer is assumed negligible compared to convective heat transfer yields a differential equation which is a direct result of a material and energy balance as:

$$y'' = \lambda y \exp\left[\frac{\gamma\beta(1-y)}{1+\beta(1-y)}\right], \quad t \in [0,1] \tag{3}$$

with the boundary condition $y'(0) = 0$ and $y(1) = 1$. Parameters λ, β, and γ in the above Eq. (3) represent dimensionless energy of activation. The trial solution of Eq. (3) can be written as:

$$y_T(t,p) = 1 + \left(-8t^4 + 16t^3 - 8t^2\right)\left(\frac{N_0' - N_L'}{2}t^2 - N_0 + N\right) \tag{4}$$

which satisfies the desired boundary conditions at $y = 0$ and 1. Since

$$y_T(1,p) = 1 + (-8 + 16 - 8)\left(\frac{N_0' - N_L'}{2} - N_0 + N\right) = 0$$

and

$$\begin{aligned} y_T'(t,p) = (-8t^4 + 16t^3 - 8t^2)\left(\frac{N_0' - N_L'}{2}2t - N_0' + N'\right) \\ + (-32t^3 + 48t^2 - 16t)\left(\frac{N_0' - N_L'}{2}t^2 - N_0 + N\right) \end{aligned} \tag{5}$$

$$y_T'(0,p) = 0$$

The error quantity to be minimized is then given by

$$E(\bar{p}) = \sum \left\{ y_T'' - f(y_T, \lambda, \beta, \gamma) \right\}^2 \tag{6}$$

The approximate solution taken in Eq. (4) includes the term

$$N_0 = N(0,\bar{p})$$

which is the output of the ANN evaluated at $x = 0$ which depends on the network parameters $\bar{p}$ but not x. To calculate the approximate solution, N_0 is evaluated simply by plugging $x = 0$ into the ANN for the current value of the weight vector. The derivatives

$$N_0' = \left.\frac{\partial N}{\partial x}\right|_{x=0} \quad \text{and} \quad N_L' = \left.\frac{\partial N}{\partial x}\right|_{x=L} \tag{7}$$

are similarly evaluated at $x = 0$ and $x = L$, respectively. To train the ANN by gradient descent, these terms are dependent on the network weights.

4 Numerical Simulation

To illustrate the artificial neural network technique using gradient descent algorithm for solving two-point nonlinear elliptic boundary value problems, we have considered three-layered neural network with $h = 10$ number of hidden nodes and $N = 100$ (training points) to minimize the error term whose initial weights are chosen randomly. The ANN solution has been compared with the exact solution for different values of parameters α, β, γ, and λ for both the equations. Influence of one parameter to the other parameters and solution has also been presented in Fig. 4.

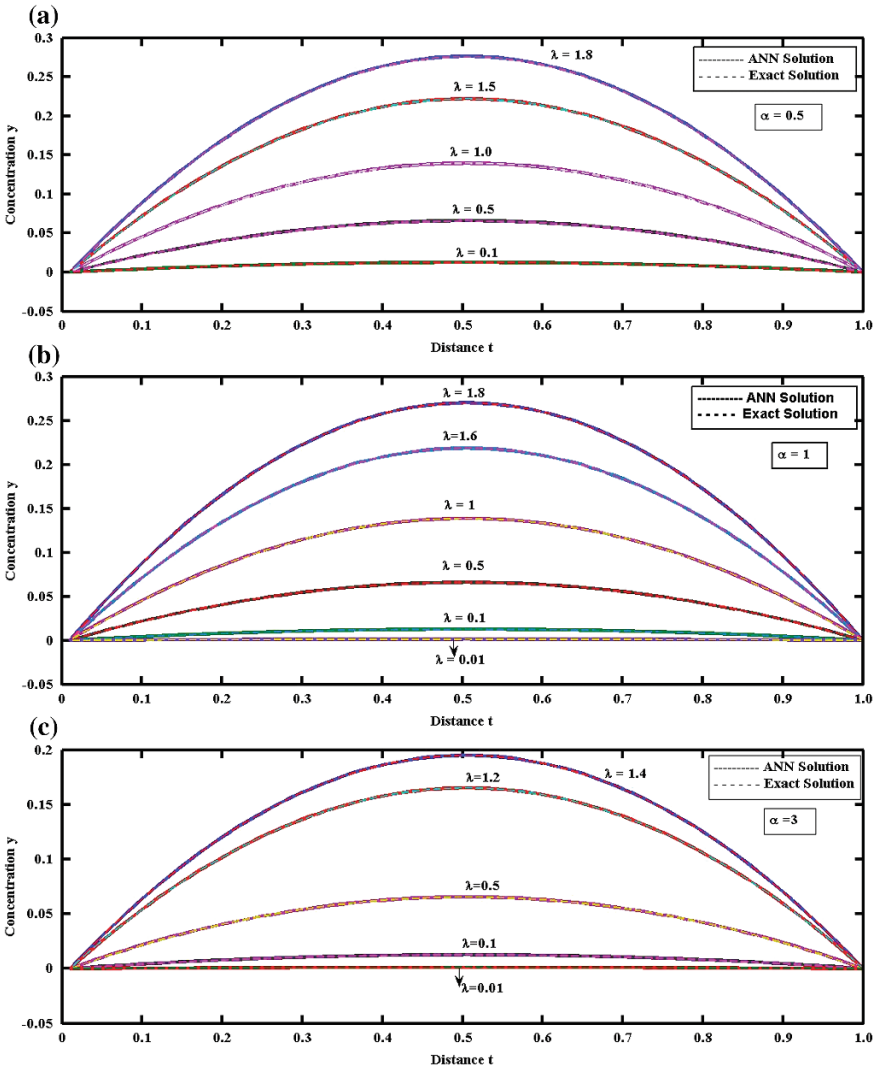

Fig. 1 Influence of λ on concentration $y(t)$ for $\alpha = 0.5$, 1, and 3 in reaction–diffusion equation using ANN

Figure 1 represents the influence of parameter λ on concentration $y(t)$ for different values of $\alpha = 0.5$, 1, and 3 for reaction–diffusion equation. From Fig. 1, it can be shown that the concentration $y(t)$ increases when the dimensionless parameter λ increases for the fixed values of α. Absolute errors have been computed for various

points lying inside the domain and tabulated as Table 1, where absolute error is given by:

$$\text{absolute error} = |y_{\text{exact}} - y_{\text{approx}}|$$

Figure 2 represents the influence of parameter α on concentration $y(t)$ for the fixed value of $\lambda = 0.3$ and 1. From the figure, it is clear that the concentration $y(t)$ decreases as the parameter α increases.

Equation (10) for the catalytic reactions in a flat particle has been solved using ANN technique, and the influence of one parameter on concentration has been observed while keeping other parameters fixed.

From Figs. 3a–d and 4a, b, it can be depicted that the concentration $y(t)$ decreases as the parameters γ, λ, and β increase for fixed value of other parameters.

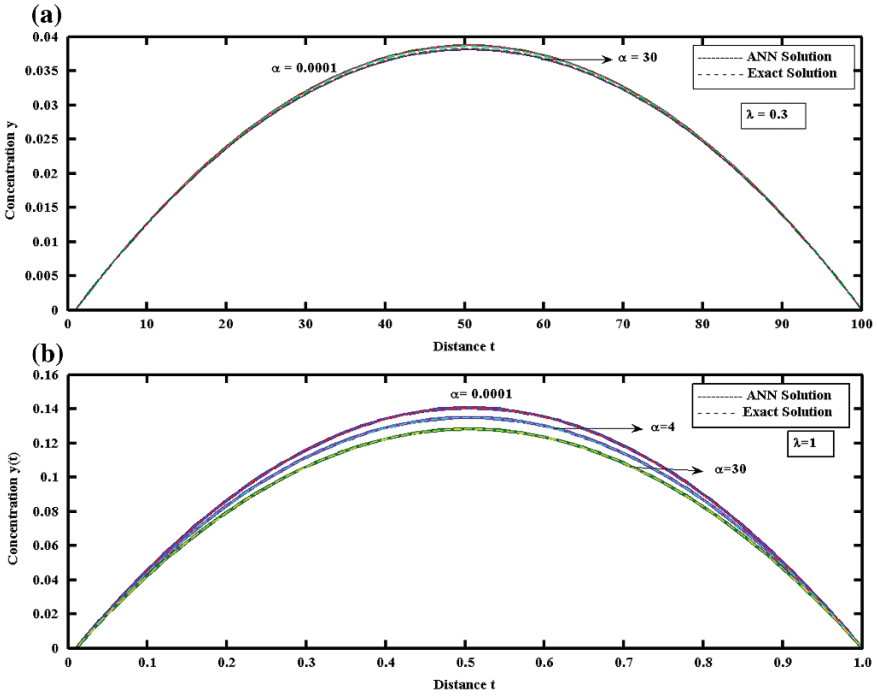

Fig. 2 Influence of α on concentration $y(t)$ for $\lambda = 0.3$ and 1 in reaction–diffusion equation using ANN

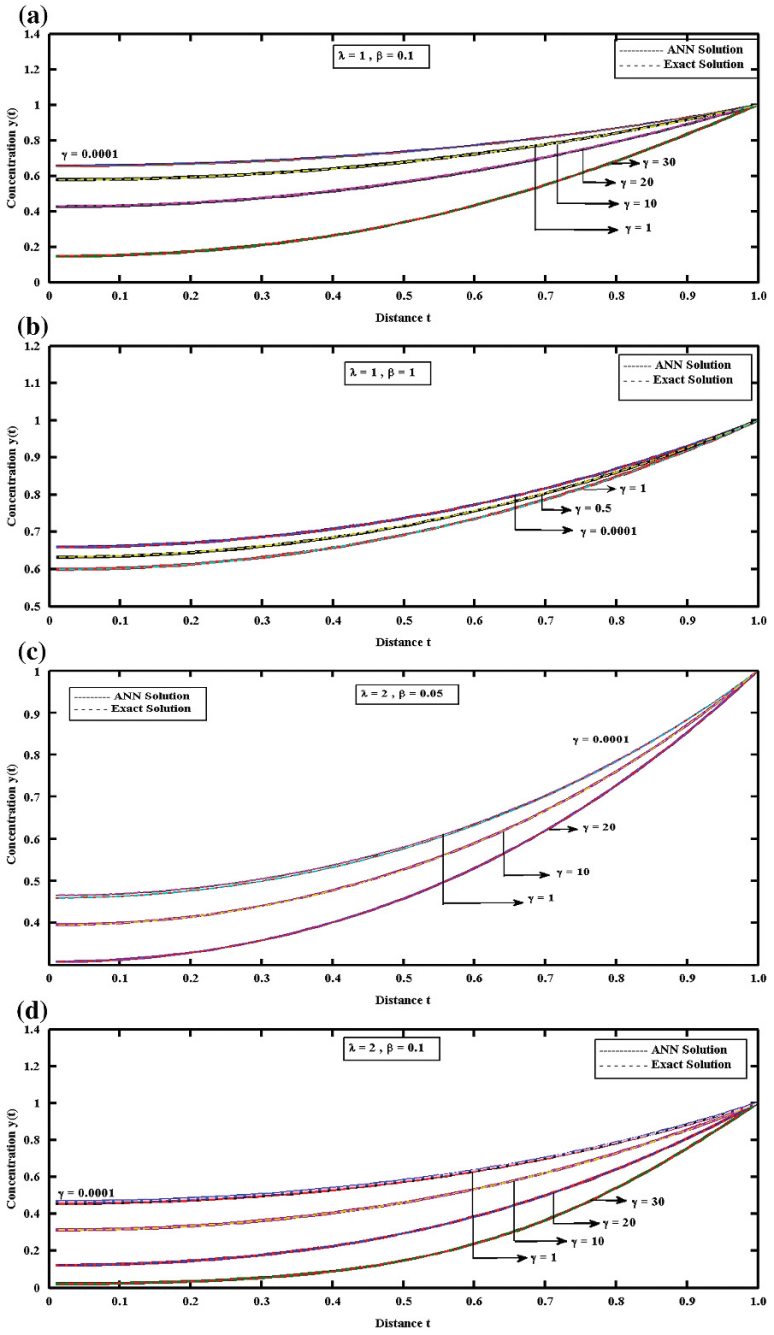

Fig. 3 Influence of parameter γ on concentration $y(t)$ for fixed value of the parameters **a** $\lambda = 1$, $\beta = 0.1$, **b** $\lambda = 1$, $\beta = 1$, **c** $\lambda = 2$, $\beta = 0.05$, **d** $\lambda = 2$, $\beta = 0.1$

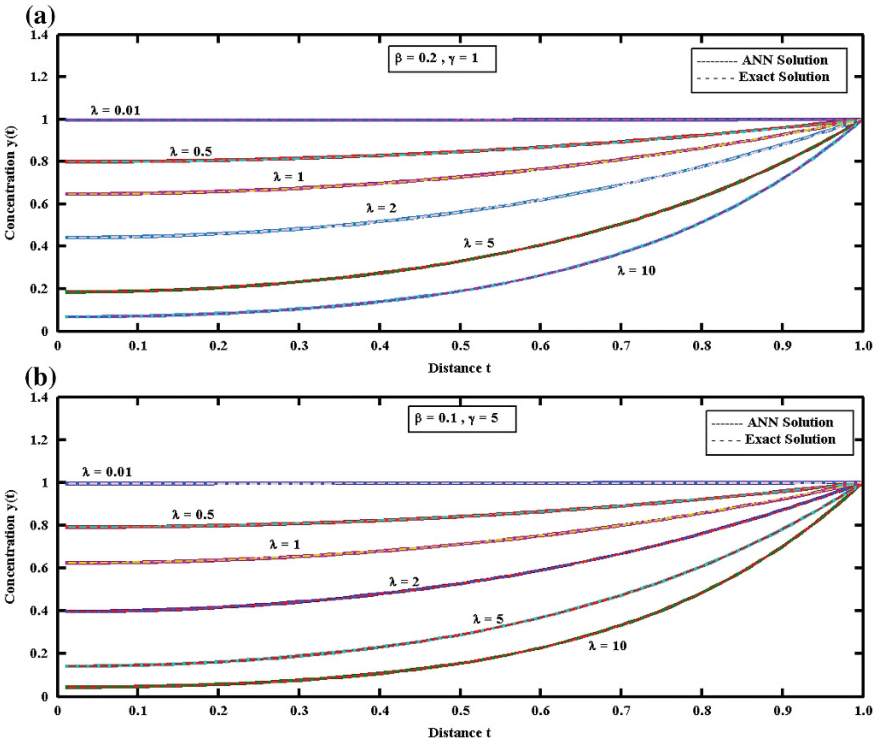

Fig. 4 Influence of parameter λ on concentration $y(t)$ for fixed value of the parameters **a** $= 0.2$, $\gamma = 1$, **b** $\beta = 0.1$, $\gamma = 5$

Table 1 Absolute error in the solution of reaction–diffusion equation for different values of λ with constant $\alpha = 3$

t	$\lambda = 0.01$	$\lambda = 0.1$	$\lambda = 0.5$	$\lambda = 1.2$	$\lambda = 1.4$
0.1	4.96535×10^{-6}	4.6302×10^{-5}	2.485×10^{-5}	1.2305×10^{-5}	1.1076×10^{-5}
0.2	3.1286×10^{-5}	4.8614×10^{-5}	3.4271×10^{-5}	1.0695×10^{-5}	1.8264×10^{-4}
0.3	3.0857×10^{-5}	3.8208×10^{-4}	4.9435×10^{-5}	1.1821×10^{-5}	2.0632×10^{-5}
0.4	3.9237×10^{-5}	3.4276×10^{-5}	1.0221×10^{-4}	2.3835×10^{-5}	2.8692×10^{-5}
0.5	2.4738×10^{-5}	4.3467×10^{-5}	2.3980×10^{-5}	1.2873×10^{-4}	1.3216×10^{-4}
0.6	2.1983×10^{-5}	1.2838×10^{-4}	2.0667×10^{-5}	1.76×10^{-4}	2.8642×10^{-4}
0.7	4.6650×10^{-5}	1.2690×10^{-5}	1.8532×10^{-4}	1.9243×10^{-4}	2.7147×10^{-4}
0.8	4.3852×10^{-5}	1.1741×10^{-5}	1.8391×10^{-4}	3.8216×10^{-5}	5.8838×10^{-4}
0.9	2.7036×10^{-4}	2.5472×10^{-4}	2.333×10^{-4}	6.3384×10^{-4}	2.864×10^{-5}
1.0	1.0831×10^{-4}	2.865×10^{-4}	1.269×10^{-4}	1.73×10^{-3}	2.634×10^{-4}

5 Conclusions

This paper presents an artificial neural network method with gradient descent algorithm for the solution of steady-state reaction–diffusion equation and equation arising in catalytic reaction in flat particle. It has been observed that for a given shape of the particle and given energy of activation, parameters λ, β, and γ in a catalytic reaction solution is dependent on the other parameter values. Numerical results show that the neural network method is comparable to the reported results of other numerical methods with less calculation efforts. From the results tabulated in Table 1 and depicted in Fig. 4, it can be seen that the neural network method is closed to the exact solution and provides less error. Moreover, an important property of this proposed scheme is that it does not require linearization to solve a nonlinear problem.

References

1. Korevaar, N.J.: Convex solutions to nonlinear elliptic and parabolic boundary value problems. Indiana Univ. Math. J. **32**(4), 603–614 (1983)
2. Wang, Y.M., Guo, B.Y.: Fourth-order compact finite difference method for fourth-order nonlinear elliptic boundary value problems. J. Comput. Appl. Math. **221**(1), 76–97 (2008)
3. Huseynov, A.: Existence and uniqueness of solutions to a nonlinear elliptic boundary value problem on time scales. Commun. Nonlinear Sci. Numer. Simul. **15**(5), 1124–1131 (2010)
4. Plum, M.: Numerical existence proofs and explicit bounds for solutions of nonlinear elliptic boundary value problems. Computing **49**(1), 25–44 (1992)
5. Pao, C.V.: Numerical methods for fourth-order nonlinear elliptic boundary value problems. Numer. Meth. Partial Differ. Equ. **17**(4), 347–368 (2001)
6. Wang, S.P., Lin, S.W., Chyan, C.J.: Nonlinear two-point boundary value problems on time scales. Math. Comput. Model. **53**(5–6), 985–990 (2011)
7. Ananthaswamy, V., Rajendran, L.: Analytical solutions of some two-point non-linear elliptic boundary value problems. Appl. Math. **3**, 1044–1058 (2012)
8. Hlavacek, V., Marek, M., Kubicek, M.: Modelling of chemical reactors, X: multiple solutions of enthalpy and mass balance for a catalytic reaction within a porous catalyst particle. Chem. Eng. Sci. **23**(9), 1083–1097 (1968)
9. Malek, A., Shekari Beidokhti, R.: Numerical solution for high order differential equations using a hybrid neural network-optimization method. Appl. Math. Comput. **183**, 260–271 (2006)
10. McFall, K.S., Mahan, J.R.: Artificial neural network method for solution of boundary value problems with exact satisfaction of arbitrary boundary conditions. IEEE Trans. Neural Networks **20**(8), 1221–1233 (2009)
11. Lagaris, I.E., Likas, A., Papageorgiou, D.G.: Neural network methods for boundary value problems with irregular boundaries. IEEE Trans. Neural Networks **11**(5), 1041–1049 (2000)
12. Shirvany, Y., Hayati, M., Moradian, R.: Multilayer perceptron neural network with novel unsupervised training method for the solution of partial differential equations. Appl. Soft Comput. **9**, 20–29 (2009)

Scene Classification Using Fuzzy Uncertainty Texture Spectrum

N.P. Rath, Swastika Mishra and Neeharika Naik

Abstract A method is proposed to discriminate rough and smooth scene images of various classes such as forest and coast, highway and inside city. The concept of fuzzy uncertainty texture spectrum (FUTS) is used. The fuzzy uncertainty parameter measures the uncertainty of the uniform surface in an image. Distribution of membership in a fuzzy image is called FUTS. The roughness or smoothness of a scene structure can be well explained by local texture information in a pixel and its neighborhood. Our proposed method uses the concept of FUTS to classify rough and smooth scene images. Probabilistic neural network (PNN) is used in the final stage to classify 150 images. This technique gives good result with less computational complexity.

Keywords FUTS · Texture · Triangular membership function · PNN

1 Introduction

Classification is the problem of identifying to which set of categories a new observation belongs to. Scene classification is an important aspect of computer vision. In a scene image, textural properties such as smoothness, coarseness, and regularity form the basis of classification [1]. Texture can be described as a repetitive pattern of local variations in image intensity. A typical problem faced in texture characterization is that the notion of texture is easy to grasp intuitively, whereas it is difficult to quantify [2]. Fuzzy logic is a form of many-valued logic; it

N.P. Rath (✉) · S. Mishra · N. Naik
ETC Department, VSSUT, Burla, India
e-mail: n_p_rath@hotmail.com

S. Mishra
e-mail: swastika.mishra91@gmail.com

N. Naik
e-mail: neeharikabputece@gmail.com

K.N. Das et al. (eds.), *Proceedings of Fourth International Conference on Soft Computing for Problem Solving*, Advances in Intelligent Systems and Computing 335,
DOI 10.1007/978-81-322-2217-0_11

deals with reasoning that is approximate rather than fixed and exact. Grau-Sanchez et al. [3] have proposed structured detection of texture through Fuzzy Texture Spectrum Analysis. Their model provides method for getting homogeneous, granulated, and structured texture image characterization. Lim and Chan [4] have introduced a method for Scene classification where they first adopted the fuzzy quantity space to model the training data, and secondly, they presented a novel weight function, 'w,' to train a fuzzy qualitative scene model in the fuzzy qualitative states. Finally, they introduce fuzzy qualitative partition to perform the scene classification. This process gives 80.5 % accuracy rate. Nedeljkovic [5] has proposed a method in which a priori knowledge about spectral information for certain land cover classes is used in order to classify satellite image in fuzzy logic manner. More specifically, input (image channels) and output variables (land classes) are introduced and membership functions are defined using results from supervised classification. Fuzzy logic inference rules are tested and verified through the simulation of classification procedure at random sample areas, and at the end, satellite image classification was conducted which has an average accuracy of 89 %. Mao et al. [6] have proposed a method using fuzzy rough neural network (FRNN) for classification of remote sensing images. In the FRNN classification algorithm, fuzzy set, rough set, and neural network technique are combined. Fuzzy rough function is used as membership function of the FRNN and integrates the ability of processing fuzzy and rough uncertainty information, which endow the FRNN classifier with better capability of learning and self-adapt and it has an accuracy of 92 %. Barcelo et al. [2] have introduced a texture characterization approach that uses the texture spectrum method and fuzzy techniques for defining 'texture unit boxes' which also takes care of vagueness introduced by noise. Najafi et al. [7] have proposed, a new enhanced conditional random field (CRF) for discriminating between different materials in natural scenes using terrestrial multispectral imaging. Most of the existing formulations of the CRF often suffer from over smoothing and loss of small detail, thereby deteriorating the information from the underlying unary classifier in areas with a high spatial frequency. Their work specifically addresses this issue by incorporating a new pairwise potential that is better at taking local context into account and this has average accuracy of 88.9 %. Dutt et al. [8] have proposed a method to classify real-world scenes in eight semantic groups of coast, forest, mountain, open country, street, tall building, and highway and inside city. Their approach takes into account the diagnostic information stored in the power spectrum of each category of images and through supervised learning separates characteristic feature vectors of each class in separate groups that helps assign a new test image to its respective group with around 80 % accuracy. Vassilis et al. [9] have proposed a scheme that has been developed to extract texture features from the fuzzy texture spectra in the chromatic and achromatic domains for a selected region of interest from each color component histogram of endoscopic images. The implementation of an advanced fuzzy inference neural network which combines fuzzy systems and artificial neural networks and the concept of fusion of multiple classifiers dedicated to specific feature parameters have also been adopted in their work. This has an accuracy of 91.43 %.

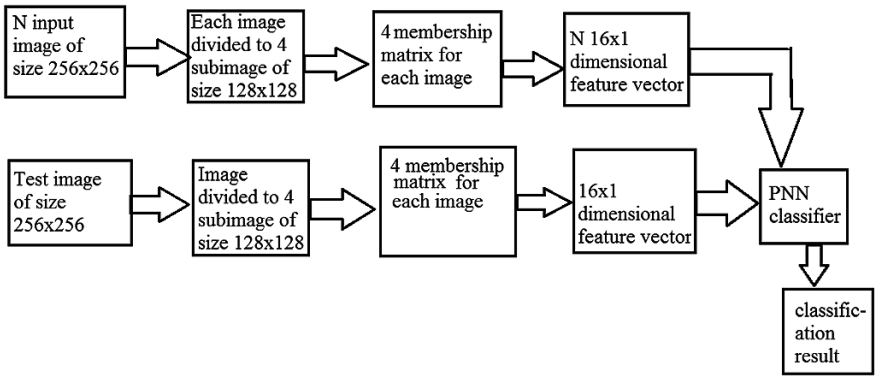

Fig. 1 Block diagram of classification through PNN

In this paper, a method is proposed, where images of different scene classes having varying degree of roughness are classified. An image is said to be smooth if large number of its pixels lies in uniform surface; otherwise, it is rough. In the first stage of the analysis, the scene images are converted to fuzzy images by triangular membership function. Then, the FUTS of images are found out. FUTS of similar type of scenes showed similar graphical results; thus, it can distinguish between rough and smooth scene images which forms basis of our experiment. In the first stage of our experiment, rough and smooth scene images are classified by sorting method. Then finally, we have used probabilistic neural network (PNN) to classify 150 images. The steps used in this experiment are shown in the block diagram given below in Fig. 1.

2 Fuzzy Uncertainty Texture Spectrum

Lee et al. [10] have proposed a method using fuzzy uncertainty, which measures the uncertainty of the uniform surface in an image. By the uncertainty definition, a grayscale image can be transformed into a fuzzy image. In texture analysis, we define *uniform surface uncertainty* (which ranges from 0 to 1) for a point in the texture as the degree to which it belongs to uniform physical surface (as defined by the neighborhood average intensity). The distribution of the membership in a measured fuzzy image, denoted by FUTS, is used as the texture feature for texture analysis. For a more rough texture, the intensity of pixels in its corresponding fuzzy image will cause a smaller value. So an image can be rough or smooth depending upon its pixel characteristics. A grayscale image f can be transformed into a fuzzy image by a fuzzification function. There are different types of fuzzification functions. It is the degree to which a pixel intensity represents a uniform physical surface. However, textural properties need neighborhood information about the

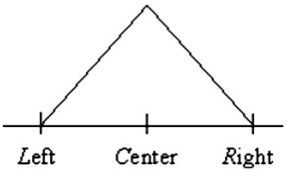

Fig. 2 Triangular membership function

pixel in order to define adequately membership functions. Here, a simplified triangular membership function is used (Fig. 2).

In general, the triangular membership function can be specified from the formula below [11]:

$$\mu_{\text{triangle}}(x) = \begin{cases} 0 & x < L \\ 1 - \frac{|c-x|}{(R-L)/2} & L < x < R \\ 0 & x > R \end{cases} \tag{1}$$

From the above formula, the uniform surface uncertainty is defined as:

$$\mu_{ij} = 1 - \left[\frac{\left| f(i,j) - \overline{f}(i,j) \right|}{\max_R f(i,j)} \right] \tag{2}$$

where $\max_R f(i,j)$ is the maximum intensity within the $\omega \times \omega$ surface region R centered at point (i, j) and the average intensity is given by (Fig. 3):

$$f(i,j) = \frac{1}{\omega \times \omega - 1} \sum_{m,n \neq i,j}^{R} f(i,j) \tag{3}$$

If $f(i, j)$ is equal to the average neighborhood intensity $\overline{f}(i,j)$, then $f(i, j)$ possesses 'full membership' to the surface region R. It defines that the pixel lies on uniform surface, alternatively, if $f(i, j)$ is significantly different than the average

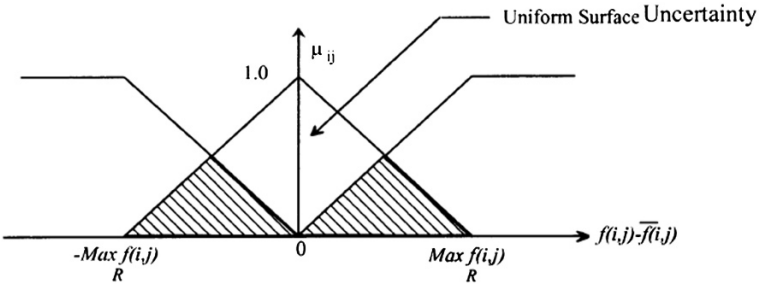

Fig. 3 Fuzzy membership function for a uniform surface

neighborhood intensity $\overline{f}(i,j)$, then $\mu_{ij} \to 0$. That means the pixel does not lie on uniform surface.

To analyze a texture image, we can transform it into its corresponding fuzzy image by using Eq. (2). As the value in fuzzy image represents the local aspect, the statistics of these values in the fuzzy image should gives its texture surface information. The occurrence distribution of these values is called the fuzzy uncertainty texture spectrum (FUTS), with the abscissa indicating the belief degree and the ordinate representing its occurrence frequency. In the practical application of classification, the uniform surface uncertainty values (range from 0 to 1) in a fuzzy image are uniformly quantized to L, levels to reduce the calculation time. All the elements of the membership matrix is multiplied with a scalar $(L-1)$. The minimum of this value (rounded toward zero) is taken. Formally, the unnormalized frequency is defined by:

$$s_j(\upsilon) = \#\left\{\upsilon = \left\lfloor \mu_{i,j} \times (L-1) \right\rfloor;\ (i,j) \in f\right\} \tag{4}$$

where # denotes the number of elements in the image f and $0 \leq \upsilon \leq L-1$.

2.1 Comparison of FUTS

To evaluate the performance of the extracted feature by using the proposed method, the FUTS for two textures T1 and T2 are taken out. The two textures are shown in Fig. 4a, b, and their corresponding FUTS are displayed in Fig. 4c, d. From Fig. 4c, d, we can find that the measured FUTS are distinguishable from each other, so they can serve as a good discriminating tool in texture classification. The FUTS of T2 shows a higher frequency than T1 when the measured uncertainty value is close to maximum value and this gives that the texture image T2 is more smooth than T1.

3 Probabilistic Neural Network

In this work, we have used PNN to classify scene images into different groups. The PNN algorithm represents the likelihood function of a given class as the sum of identical, isotropic Gaussians [12]. In practice, PNN is often an excellent pattern classifier, outperforming other classifiers including back propagation.

When an input is presented, the first layer computes distances from the input vector to the training input vectors, and produces a vector, whose elements indicate how close the input is to a training input. The second layer sums these contributions for each class of inputs to produce as its net output a vector of probabilities. Finally, a complete transfer function on the output of the second layer picks the maximum of these probabilities and produces a '1' for that class and a '0' for the other classes.

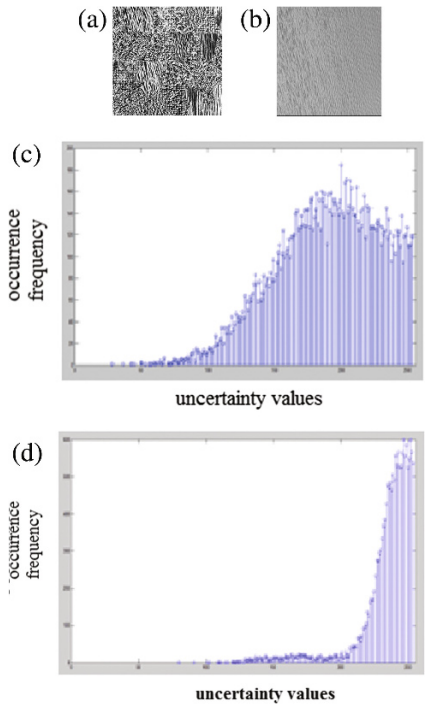

Fig. 4 **a** T1, **b** T2, **c** FUTS of T1, **d** FUTS of T2

In our experiment, the spread parameter of PNN is varied in order to get desired result.

4 Experimentation

Images of scenes are obtained from [13]. The database includes images of both natural and man-made scenes. Sample images belonging to various classes of scene images, i.e., coast, forest, mountain, inside city, highway, tall building, and open country, are shown in Fig. 5. Our proposed algorithm tends to differentiate between rough and smooth scene images; thus, we have experimented between scenes of forest and coast, high and inside city, and open country and forest.

Images taken in this work are of size 256 × 256. Computation of FUTS of scene image is the basis of our experiment. We have considered six scene images (two from each class, namely forest, coast, and inside city) as shown in Fig. 6.

Fig. 5 Sample images from open country, inside city, high way, forest, coast, and tall building

Fig. 6 **a**, **b** Coast images; **c**, **d** forest images; **e**, **f** inside city images. Scene images: 2 from each class, i.e. coast, forest, and inside city

4.1 Computation of FUTS

We have computed the FUTS of these scene images as below:

- In the image, each image pixel is taken as central pixel and a window is selected around the pixel. We have chosen the size of window to be 5 × 5.
- To process the border pixels, image is padded with 2 rows and 2 columns on both side making its size 260 × 260.
- Then in the 5 × 5 surface region, the average intensity is found out using Eq. (3).
- The maximum intensity in the window is found out.
- The uniform surface uncertainty value is obtained using Eq. (2). A matrix (size 256 × 256) of membership values is obtained. Thus, the image is converted into a fuzzy image.
- Then, the uniform surface uncertainty values (range from 0 to 1) are uniformly quantized to 300 levels. This is done using Eq. (4) resulting in a new matrix of size 256 × 256.
- Then, the FUTS of these six images are graphically represented in Fig. 7 where abscissa represents quantized uncertainty values and ordinate represents occurrence frequency.

FUTS of scene images belonging to same class are found to be similar to each other, which forms the basis of our experiment. It is observed that FUTS of two inside city images are found to be similar to one another and same is the case in forest and coast images.

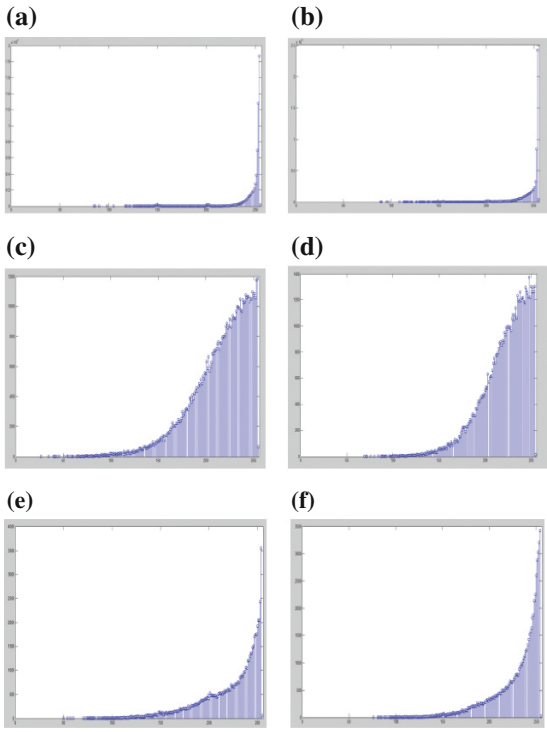

Fig. 7 **a**, **b** FUTSs of Fig. 6a, b. **c**, **d** FUTSs of Fig. 6c, d. **e**, **f** FUTSs of Fig. 6e, f

4.2 Computation of Feature Vector

- Each 256 × 256 size image is divided into 4 non-overlapping subimages each of size 128 × 128.
- In this case, the window size taken as 15 × 15 (for forest–coast) and 17 × 17 (for highway–inside city and open country–forest).
- Membership matrix of size 128 × 128 of each subimage is found out.
- The matrix of size 128 × 128 is down sampled to 2 × 2 matrix using Harr wavelet, and then, the 2 × 2 matrix was resized to 4 × 1 vector.

A feature vector was constructed by concatenating above four 4 × 1 vectors. Then, its size becomes 16 × 1.

In the first stage of our experiment, we have done two-class classification of 20 images (10 from each class). We have found the feature vector of 20 images. Among the 20 images, one image is taken as reference image. Then, euclidian distance is calculated between the feature vector of reference image and rest of images. Norm of these values is found out. Then, sorting is done according to increasing order of distance and images are ranked. The results are shown in Table 1, which shows the sorting results of forest and coast images. The image in the left most column is the reference scene image, whereas other scenes are arranged according to increasing distance, with respect to reference scene image,

Table 1 Classification result of coast and forest

Reference	Coast	Forest
C1	1, 10, 7, 5, 6, 3, 2, 4, 9, 8	18, 17, 15, 16, 20, 14, 13, 12, 19, 11
C2	2, 4, 8, 9, 3, 5, 10 ,1, 7, 6	18, 17, 16, 15, 20, 13, 14, 12, 19, 11
C3	3, 5, 2, 1, 4, 7, 9, 10, 8, 6	18, 17, 15, 16, 20, 13, 14, 12, 19, 11
C4	4, 9, 8, 2, 5, 10, 3, 1, 7, 6	18, 17, 16, 15, 20, 13, 14, 12, 19, 11
C5	5, 10, 3, 1, 7, 2, 4, 8, 9, 6	18, 17, 15, 16, 20, 14, 13, 12, 19, 11
C6	6, 1, 10, 5, 7, 2, 4, 8, 9, 3	18, 17, 15, 16, 20, 14, 13, 12, 19, 11
C7	7, 10, 1, 5, 3, 2, 6, 4, 9, 8	15, 18, 17, 16, 20, 14, 13, 12, 19, 11
C8	8, 4, 9, 2, 5, 10, 3, 1, 7, 6	18, 17, 16, 15, 20, 13, 14, 12, 19, 11
C9	9, 4, 8, 2, 5, 3, 10, 1, 7, 6	18, 17, 16, 15, 20, 13, 14, 12, 19, 11
C10	10, 7, 5, 1, 2, 4, 3, 8, 9, 6	18, 17, 15, 16, 20, 13, 14, 12, 19, 11
Reference	Forest	Coast
F1	11, 12, 19, 14, 13, 20, 15, 17, 16, 18	7, 6, 5, 1, 10, 3, 2, 4, 8, 9
F2	12, 19, 13, 14, 20, 17, 15, 11, 16, 18	7, 5, 6, 1, 10, 3, 2, 4, 8, 9
F3	13,17,20,14,12,15,19,16,11,18	5, 7, 6, 10, 1, 3, 2, 4, 8, 9
F4	14, 15, 13, 17, 20, 12, 19, 16, 11, 18	7, 5, 6, 1, 10, 3, 2, 4, 8, 9
F5	15,17,14,20,13,12,19,16,11,18	7, 5, 1, 10, 6, 3, 2, 4, 8, 9
F6	16, 17, 15, 20, 13, 14, 19, 12, 18, 5	11, 7, 10, 1, 3, 2, 4, 8, 9
F7	17, 13, 15, 20, 14, 16, 12, 19, 18, 11	5, 7, 6, 10, 1, 3, 2, 4, 8, 9
F8	18,17,13,16,20,6,15,10,5,14,	1, 7, 12, 4, 3, 8, 9, 19, 11
F9	19, 12, 14, 20, 13, 15, 17, 11, 16, 18	7, 5, 1, 3, 10, 6, 2, 4, 9, 8
F10	20, 17, 13, 14, 15, 12, 19, 16, 11, 18	7, 5, 6, 10, 1, 3, 2, 4, 8, 9

Fig. 8 These are images in order of the sorting result of coast–forest when 7th image is taken as reference image

from left to right in a row. It is observed that images belonging to the same class as reference image are grouped with the reference image, whereas images belonging other class are clustered farther, thus discriminating two classes of scene image. Similarly, we have experimented with highway versus inside city and open country versus forest scene images. We observed that our algorithm is able to distinguish between the respective classes (Fig. 8).

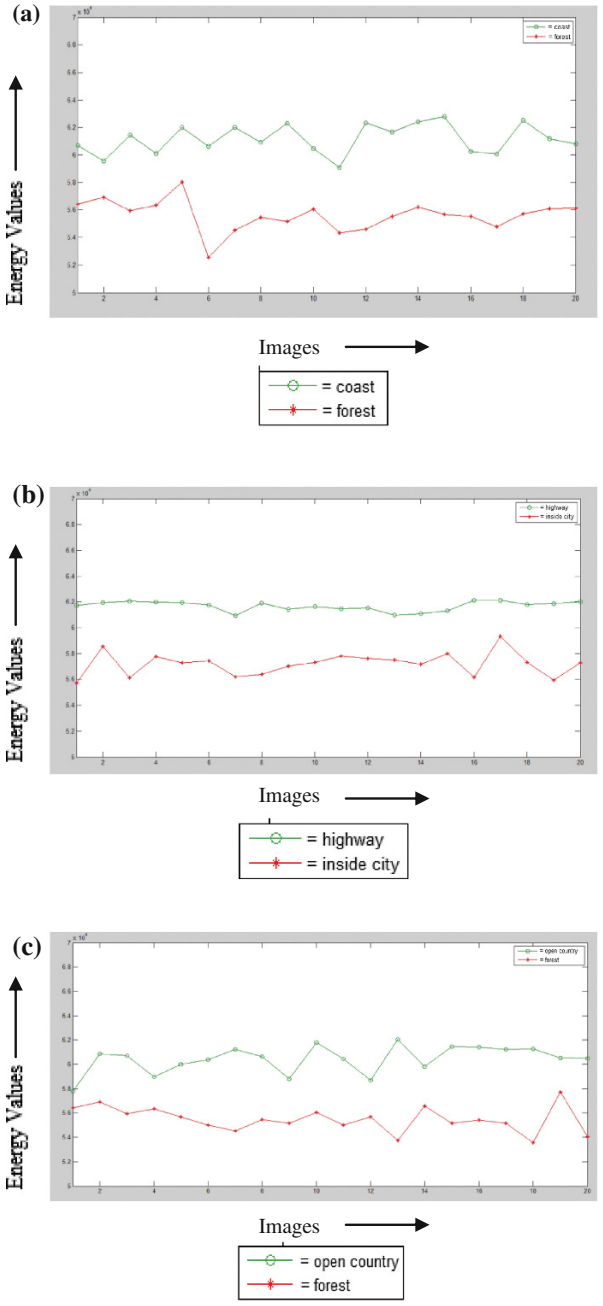

Fig. 9 **a**, **b**, **c** Graph showing energy values of images of two classes of each category. **a** Forest–coast, **b** highway–inside city, **c** open country–forest

We have also shown graphically the energy values of 20 images from each class, viz forest–coast, highway–inside city and open country–forest in Fig. 9 and found that they are distinct from each other.

In the second stage of the experiment, PNN is used. PNN is trained to classify the scenes into two classes. The feature vector is given as input to PNN. The classifier is tested by presenting unknown test image from each class (other than the training image) to it. 150 training images are taken, and also 150 images (other than training images) are tested. 75 images each of forest and coast were used as training. After using PNN, the images are classified to respective classes. If the test image was coast image, then it belonged to class 1, and if it is forest image, then it belonged to class 2. 93 % accuracy is found out. Similar experiment was done with another two classes, i.e. highway and inside city. It gives 92 % accuracy. Similarly, the classification of open country and forest showed 88.66 % accuracy. We have also experimented with three classes such as inside city, forest, and coast which showed less efficiency.

5 Conclusion

In this work, we have proposed a method where the concept of FUTS is used to classify the scenes with respect to their degree of roughness. We showed that the algorithm could segregate scenes belonging to forest (where the degree of roughness is high) and coast (where the degree of roughness is low). Similar is the case for the categories inside city and highway and open country and forest.

We also tested the algorithm for three-class problem, where the categories are inside city, forest, and coast. We found that the algorithm could not perform satisfactorily because the degree of roughness in forest and inside city images is similar. It is concluded that the proposed method is efficient for two-class classification, but its efficiency is less for multiple class. So this algorithm can be further developed for better results.

References

1. Srinivasan, G.N., Shobha, G.: Statistical texture analysis. In: Proceedings of World Academy of Science, Engineering and Technology, vol. 36, pp. 2070–3740. ISSN (2008)
2. Barcelo, A., Montesy, E., Sobervilla, P.: Fuzzy texture unit and fuzzy texture spectrum for texture characterization. Fuzzy sets Syst **158**, 239–252 (2007)
3. Grau-Sanchez, M., Sobrevilla, P., Montseny, E.: Structured detection through Fuzzy texture spectrum analysis. In: Proceedings of IPMU'08, pp. 1183–1190, 22–27 June 2008
4. Lim, C.H., Chan, C.S.: A fuzzy qualitative approach for scene classification. In: WCCI 2012 IEEE World Congress on Computational Intelligence, 10–15 June 2012
5. Nedeljkovic, I.: Image classification based on fuzzy logic. Commission VI, WG VI/1-3. Int. Arch. Photogrammetry Remote Sens. Spat. Inf. Sci. **34**(Part XXX)

6. Jianxu, M., Caiping, L., Yaonan, W.: Remote sensing images classification using fuzzy-rough neural network. In: 2010 IEEE Fifth International Conference on Bio-Inspired Computing: Theories and Applications (BIC-TA), pp. 23–26, Sept 2010. ISBN: 978-1-4244- 6437-1
7. Najafi, M., Namin, S.T., Petersson, L.: Classification of natural scene multi spectral images using a new enhanced CRF. In: Intelligent Robots and Systems (IROS), 3–7 Nov 2013. ISSN:2153-0858
8. Dutt, B.V.V.S.R., Agarwal, P., Nayak, S.: Scene classification in image. Project on computer vision. Unpublished
9. Kodogiannis, V.S., Lygouras, J.N.: Neuro-fuzzy classification system for wireless-capsule endoscopic images. World Acad Sci Eng Technol **21**, 23 Sept 2008
10. Lee, Y.G., Lee, G.H., Hsueh, Y.C.: Texture classification using fuzzy uncertainty texture spectrum. Neurocomputing **20**, 115–122 (1998)
11. Tsoukalas, L.H., Uhrig, R.E.: Fuzzy and Neural Approaches in Engineering (Chap. 4—Fuzzification technique). Wiley, New York (1993)
12. Montana, D.: A weighted probabilistic neural network. Supported by DARPA via ONR under Contract N00014-89-C-0264 part of the Artificial Neural Networks Initiative
13. Computation Visual Cognition Laboratory, Aude olive, PhD (http://cvcl.mit.edu/database.htm)

Parikh Matrices and Words Over Ternary Alphabet

Amrita Bhattacharjee and Bipul Syam Purkayastha

Abstract In this paper, Parikh matrices over ternary alphabet are investigated. Algorithm is developed to display Parikh matrices of words over ternary alphabet. A set of equations for finding ternary words from the respective Parikh matrix is discussed. A theorem regarding the relations of the entries of the 4×4 Parikh matrices is proved. Some other results in this regard are also discussed. Significance of graphical representation of binary amiable words is given. Extension of this notion for ternary amiable words is introduced.

Keywords Parikh matrix · Sub-word or scattered sub-word · Amiable words or M-ambiguous words · M-unambiguous word · Word line

1 Introduction

Several systems have been developed to solve complex problems of words over formal languages. Introduced in [1] by R.J. Parikh, Parikh mapping plays a very significant role in this context. The concept of Parikh matrix first introduced in [2] is an extension of Parikh mapping. The concept of sub-word is the basic idea behind this interesting notion of Parikh matrix. Since the introduction of it, a series of papers investigating these matrices has appeared studying various problems related to sub-words. We cite a few examples [3–13] which have used sub-word occurrences and Parikh matrix for solving the problems of word. Research on Parikh matrices are being extended from binary to higher ordered words. A word is a finite or infinite sequence of symbols taken from a finite set called alphabet. Parikh matrix which is a triangular matrix can be associated with every word over an ordered alphabet. Main diagonal of this matrix takes only the value 1, and every

A. Bhattacharjee (✉) · B.S. Purkayastha
Department of Computer Science, Assam University, Silchar 788011, India
e-mail: amritabhattacharjee10@gmail.com

B.S. Purkayastha
e-mail: bipulsyam@gmail.com

K.N. Das et al. (eds.), *Proceedings of Fourth International Conference on Soft Computing for Problem Solving*, Advances in Intelligent Systems and Computing 335,
DOI 10.1007/978-81-322-2217-0_12

entry below the main diagonal has the value 0, but the entries above the main diagonal provide information on the number of certain sub-words in w.

Organization of this paper is as follows. The following Sect. 2 recapitulates the basic preliminaries of Parikh matrix. Section 3 goes toward developing the algorithm for display Parikh matrix of a sequence over tertiary alphabet. In Sect. 3, result analysis is also presented. Section 4 gives characteristics of Parikh matrices on the ternary sequences corresponding to a given Parikh matrix. Section 5 goes toward the development of a set of equations to find out the ternary sequences corresponding to a given Parikh matrix. In Sect. 6, we have discussed representation of M-ambiguous words by graphical pictures. We conclude the paper in Sect. 7 by summarizing the observations.

2 Preliminaries

Ordered alphabet: An ordered alphabet is a set of symbols $\Sigma = \{a_1, a_2, a_3, \ldots, a_n\}$ where the symbols are arranged maintaining a relation of order ("<") on it. For example, if $a_1 < a_2 < a_3 < \cdots < a_n$, then we use notation: $\Sigma = \{a_1, a_2, a_3, \ldots, a_n\}$

Word: A word is a finite or infinite sequence of symbols taken from a finite set called an alphabet. Let $\Sigma = \{a_1, a_2, a_3, \ldots, a_n\}$ be the alphabet. The set of all words over Σ is Σ^*. The empty word is denoted by λ.

$|w|_{a_i}$: Let $a_i \in \Sigma = \{a_1, a_2, a_3, \ldots, a_n\}$ be a letter. The number of occurrences of a_i in a word $w \in \Sigma^*$ is denoted by $|w|_{a_i}$.

Sub-word: A word u is a sub-word of a word w, if there exists words $x_1 \ldots x_n$ and $y_0 \ldots y_n$ (some of them possibly empty), such that $u = x_1 \ldots x_n$ and $w = y_0 x_1 y_1 \ldots x_n y_n$.

For example, if $w = adbaabcacd$ is a word over the alphabet $\Sigma = \{a, b, c, d\}$, then $baca$ is a sub-word of w. Two occurrences of a sub-word are considered different if they differed by at least one position of some letter. In the word $w = adbaabcacd$, the number of occurrences of the word $baca$ as a sub-word of w is $|w|_{baca} = 2$.

Parikh matrix of a word: Let $\Sigma = \{a_1 < a_2 < a_3 \ldots < a_n\}$ be an nth ordered alphabet. The Parikh matrix of $a_1, a_2, a_3 \ldots, a_n$ are as follows:

$$\Psi_{M_n}(a_1) = \begin{pmatrix} 1 & 1 & \ldots & 0 & 0 \\ 0 & 1 & \ldots & 0 & 0 \\ \vdots & \vdots & \ldots & \vdots & \vdots \\ 0 & 0 & \ldots & 1 & 0 \\ 0 & 0 & \ldots & 0 & 1 \end{pmatrix}_{(n+1)\times(n+1)},$$

$$\Psi_{M_n}(a_2) = \begin{pmatrix} 1 & 0 & \ldots & 0 & 0 \\ 0 & 1 & 1 & \ldots & 0 \\ \vdots & \vdots & \ldots & \vdots & \vdots \\ 0 & 0 & \ldots & 1 & 0 \\ 0 & 0 & \ldots & 0 & 1 \end{pmatrix}_{(n+1)\times(n+1)}, \ldots,$$

$$\Psi_{M_n}(a_n) = \begin{pmatrix} 1 & 0 & \dots & 0 & 0 \\ 0 & 1 & \dots & 0 & 0 \\ \vdots & \vdots & \dots & \vdots & \vdots \\ 0 & 0 & \dots & 1 & 1 \\ 0 & 0 & \dots & 0 & 1 \end{pmatrix}_{(n+1)\times(n+1)}$$

Any word w over the nth order alphabet has a unique Parikh matrix. This matrix is given by

$$\Psi_{M_n}(w) = \begin{pmatrix} 1 & |w|_{a_1} & |w|_{a_1a_2} & \dots & |w|_{a_1a_2\dots a_{n-2}} & |w|_{a_1a_2\dots a_{n-1}} & |w|_{a_1a_2\dots a_n} \\ 0 & 1 & |w|_{a_2} & \dots & |w|_{a_2\dots a_{n-2}} & |w|_{a_2\dots a_{n-1}} & |w|_{a_2\dots a_n} \\ \vdots & \vdots & \vdots & \dots & \vdots & \vdots & \vdots \\ \vdots & \vdots & \vdots & \dots & \vdots & \vdots & \vdots \\ 0 & 0 & 0 & \dots & 1 & |w|_{a_{n-1}} & |w|_{a_{n-1}a_n} \\ 0 & 0 & 0 & \dots & 0 & 1 & |w|_{a_n} \\ 0 & 0 & 0 & \dots & 0 & 0 & 1 \end{pmatrix}_{(n+1)\times(n+1)}$$

where $|w|_{a_1\dots a_i}$ is the number of occurrences of $a_1\dots a_i$ in the word $w \in \Sigma^*$. Here $i \in [1, n]$.

Amiable or M-ambiguous words: Two words $\alpha, \beta \in \Sigma^*$ $(\alpha \neq \beta)$ over the same alphabet Σ may have the same Parikh matrix. Then, the words are called amiable or M-ambiguous.

3 Parikh Matrix of Ternary Sequence

3.1 Parikh Matrix of a Word Over Ternary Alphabet

Any word over the ternary alphabet has a unique Parikh matrix. This matrix can be obtained by simple matrix product of the respective Parikh matrices for *a, b, c*. This can also be obtained by using the theory of Parikh matrix which is

$$\Psi_{M_3}(w) = \begin{pmatrix} 1 & |w|_a & |w|_{ab} & |w|_{abc} \\ 0 & 1 & |w|_b & |w|_{bc} \\ 0 & 0 & 1 & |w|_c \\ 0 & 0 & 0 & 1 \end{pmatrix}$$

where $|w|_a$ denotes the number of scattered sub-word of *a,* and $|w|_{ab}$ denotes the number of Scattered sub-word of *ab* and so on.

But for larger words, the above processes are cumbersome, and to overcome this problem, the following algorithm is introduced. This algorithm gives instantly the Parikh matrix of a ternary sequence. Results are verified.

3.2 Algorithm

01 Initialise a word = 'w'
02 Set len = length of w
03 **For** $i = 0$ to len do
04 Calculate total number of a, ab, abc in w.
05 Calculate total number of b, bc in w.
06 Calculate total number of c in w.
07 **End**.
// create a matrix $\left(a_{ij}\right)$ of order $M\ (=4)$
08 **For** $i = 0$ to M do
09 **For** $j = 0$ to M do
10 **If** $(i = j)$
11 $a_{ij} = 1$
12 else **If** $(i > j)$
13 $a_{ij} = 0$
14 else
15 **If**$(i = 0 \,\&\, j = 1)$
16 $a_{ij} = \text{total number of } 'a'$
17 **If**$(i = 0 \,\&\, j = 2)$
18 $a_{ij} = \text{total number of } 'ab'$
19 **If**$(i = 0 \,\&\, j = 3)$
20 $a_{ij} = \text{total number of } 'abc'$
21 **If**$(i = 1 \,\&\, j = 2)$
22 $a_{ij} = \text{total number of } 'b'$
23 **If**$(i = 1 \,\&\, j = 3)$
24 $a_{ij} = \text{total number of } 'bc'$
25 **If**$(i = 2 \,\&\, j = 3)$
26 $a_{ij} = \text{total number of } 'c'$
27 **End**
28 **End**

3.3 Application of Above Algorithm

Example 1 The ternary word $\xi_2 = abc\underbrace{a\ldots a}_{10}\underbrace{b\ldots b}_{10}\underbrace{c\ldots c}_{10}abc$ has the Parikh matrix

$$\Psi_{M_3}(\xi_2) = \begin{pmatrix} 1 & 12 & 123 & 1234 \\ 0 & 1 & 12 & 123 \\ 0 & 0 & 1 & 12 \\ 0 & 0 & 0 & 1 \end{pmatrix}.$$

Example 2 The ternary word $\xi_3 = bb\underbrace{a\ldots a}_{50}\underbrace{b\ldots b}_{28}\underbrace{c\ldots c}_{10}abbcc$ has the Parikh matrix

$$\Psi_{M_3}(\xi_3) = \begin{pmatrix} 1 & 51 & 1502 & 17004 \\ 0 & 1 & 32 & 364 \\ 0 & 0 & 1 & 12 \\ 0 & 0 & 0 & 1 \end{pmatrix}$$

4 A Set of Equations for Finding Words Over Ternary Alphabet from the Respective Parikh Matrix

We propose a set of equations for finding the tertiary sequences corresponding to a given 4 × 4 Parikh matrix.

Let $\Sigma = \{a<b<c\}$ be a ternary ordered alphabet and $\xi \in \Sigma^*$ be a ternary sequence. If $|w|_a = l$, $|w|_b = m$, and $|w|_c = n$, then ξ can be represented in the following form:

$$\xi = a^{x_1}b^{y_1}c^{z_1}a^{x_2}b^{y_2}c^{z_2}\ldots a^{x_{l+m+n}}b^{y_{l+m+n}}c^{z_{l+m+n}}.$$

The Parikh matrix

$$\Psi_{M_3}(\xi) = \begin{pmatrix} 1 & l & p & r \\ 0 & 1 & m & q \\ 0 & 0 & 1 & n \\ 0 & 0 & 0 & 1 \end{pmatrix}$$

corresponds to this word if and only if x_i = either 0 or 1, y_j = either 0 or 1, and z_k = either 0 or 1, which is a solution of the following system of equations:

$$\sum_{i=1}^{l+m+n} x_i = l \tag{1}$$

$$\sum_{j=1}^{l+m+n} y_j = m \tag{2}$$

$$\sum_{k=1}^{l+m+n} z_k = n \tag{3}$$

$$\sum_{i=1}^{l+m+n} x_i \sum_{j=i}^{l+m+n} y_j = p \tag{4}$$

$$\sum_{j=1}^{l+m+n} y_j \sum_{k=j}^{l+m+n} z_k = q \tag{5}$$

$$\sum_{i=1}^{l+m+n} x_i \sum_{j=i}^{l+m+n} y_j \sum_{k=j}^{l+m+n} z_k = r \tag{6}$$

Example 1 For clear understanding, we take the example of the following Parikh matrix. Let

$$\Psi_{M_3}(\xi_1) = \begin{pmatrix} 1 & 1 & 0 & 0 \\ 0 & 1 & 1 & 0 \\ 0 & 0 & 1 & 0 \\ 0 & 0 & 0 & 1 \end{pmatrix}$$

be a Parikh matrix. Here, $|w|_a = 1$, $|w|_b = 1$, $|w|_c = 0$ and so on. Then, $\xi_1 \in \Sigma^*$ is a ternary sequence corresponds to the above matrix. Here, $l + m + n = 1 + 1 + 0 = 2$. So ξ_1 can be represented in the following form: $\xi_1 = a^{x_1} b^{y_1}\ c^{z_1} a^{x_2} b^{y_2} c^{z_2}$.

The Parikh matrix corresponds to this word if and only if x_i = either 0 or 1, y_j = either 0 or 1, z_k = either 0 or 1, which is a solution of the above system of equations. Now, from (1), we get $x_1 + x_2 = 1$, from (2), we get $y_1 + y_2 = 1$, from (5), we get$x_1(y_1 + y_2) + x_2 y_2 = 0 \Rightarrow x_1(1) + x_2 y_2 = 0$ [form (2)] $\Rightarrow y_2 = 0$ [using (1)] $\therefore y_1 = 1$, and again from (5) we have

$$x_1(y_1 + y_2) + x_2 y_2 = 0 \Rightarrow x_1(1 + 0) + x_2 \cdot 0 = 0 \Rightarrow x_1 = 0$$

So the word $\xi_1 = a^{x_1} b^{y_1} c^{z_1} a^{x_2} b^{y_2} c^{z_2}$ is $\xi_1 = a^0 b^1 c^0 a^1 b^0 c^0 = ba$

Example 2 For the Parikh matrix

$$\Psi_{M_3}(\xi_2) = \begin{pmatrix} 1 & 1 & 0 & 0 \\ 0 & 1 & 1 & 0 \\ 0 & 0 & 1 & 1 \\ 0 & 0 & 0 & 1 \end{pmatrix}$$

Applying the above processes we get

$$\xi_2 = a^{x_1}b^{y_1}c^{z_1}a^{x_2}b^{y_2}c^{z_2}a^{x_3}b^{y_3}c^{z_3} \Rightarrow \xi_2 = a^0b^0c^1a^0b^1c^0a^1b^0c^0 \Rightarrow \xi_2 = cba$$

This is how we can use the proposed set of equations to find the corresponding word from a 4 × 4 Parikh matrix.

5 Characteristics of Parikh Matrices

Every 4 × 4 matrix cannot be a Parikh matrix; the entries should maintain some relationship among themselves to make a Parikh matrix. For ternary words, the following theorem gives a useful rule regarding the same.

Theorem *If the Parikh matrix*

$$\Psi_{M_3}(\xi) = \begin{pmatrix} 1 & l & p & r \\ 0 & 1 & m & q \\ 0 & 0 & 1 & n \\ 0 & 0 & 0 & 1 \end{pmatrix}$$

corresponds to a ternary sequence, then $r \in [0, l \cdot m \cdot n]$.

Proof Let the Parikh matrix

$$\Psi_{M_3}(\xi) = \begin{pmatrix} 1 & l & p & r \\ 0 & 1 & m & q \\ 0 & 0 & 1 & n \\ 0 & 0 & 0 & 1 \end{pmatrix}$$

corresponds to a word $\xi \in \Sigma^+$. where $\Sigma = \{a < b < c\}$ is a ternary alphabet. ξ can be represented in the following form: $\xi = a^{x_1}b^{y_1}c^{z_1}a^{x_2}b^{y_2}c^{z_2} \ldots a^{x_{l+m+n}}b^{y_{l+m+n}}c^{z_{l+m+n}}$. Now by using Eqs. (1)–(3) and (6) we get, $l.m.n = \sum_{i=1}^{l+m+n} x_i \cdot \sum_{j=1}^{l+m+n} y_j \cdot \sum_{k=1}^{l+m+n} z_k > \sum_{i=1}^{l+m+n} x_i \sum_{j=i}^{l+m+n} y_j \sum_{k=j}^{l+m+n} z_k = r \therefore r \in [0, l.m.n]$

But the converse is not always true; this can be illustrated by the example of matrix $\begin{pmatrix} 1 & 1 & 1 & 0 \\ 0 & 1 & 1 & 1 \\ 0 & 0 & 1 & 1 \\ 0 & 0 & 0 & 1 \end{pmatrix}$. We can see that this upper triangular matrix does not have any corresponding ternary sequence. □

Remark In the Parikh matrix,

$$\Psi_{M_3}(\xi) = \begin{pmatrix} 1 & |w|_a & |w|_{ab} & |w|_{abc} \\ 0 & 1 & |w|_b & |w|_{bc} \\ 0 & 0 & 1 & |w|_c \\ 0 & 0 & 0 & 1 \end{pmatrix}$$

for a ternary sequence ξ whenever $|w|_{abc} = 0$ then either $|w|_{ab} = 0$ or $|w|_{bc} = 0$.

Examples The Parikh matrix corresponding to the ternary sequence *bca* is $\begin{pmatrix} 1 & 1 & 0 & 0 \\ 0 & 1 & 1 & 1 \\ 0 & 0 & 1 & 1 \\ 0 & 0 & 0 & 1 \end{pmatrix}$. We see that $|w|_{abc} = 0$, this matrix has a corresponding ternary sequence as here $|w|_{ab} = 0$, and again the Parikh matrix corresponding to the ternary sequence *cab* is $\begin{pmatrix} 1 & 1 & 1 & 0 \\ 0 & 1 & 1 & 0 \\ 0 & 0 & 1 & 1 \\ 0 & 0 & 0 & 1 \end{pmatrix}$.

We see that $|w|_{abc} = 0$, this matrix also has a corresponding ternary sequence as here $|w|_{bc} = 0$.

6 Graphical Representation of Words

In this section, the method to represent binary words in a two-dimensional area is discussed [13]. Two perpendicular axes X and Y (say) intersecting at a point (0, 0) are considered. In the X-axis, we take a's, and in the Y-axis, we take b's. Now, to draw the graph of the word, we start from (0, 0) and go on describing the word w as follows: If the first letter of the word is *a,* then we move to (1, 0), and if the second letter is *b,* then we move to (1, 1). But if the first letter of the word is *b,* then we move to (0, 1) and thus go on describing the path of the word in the two-dimensional graph. Let $M_\alpha = \begin{pmatrix} 1 & |w|_a & |w|_{ab} \\ 0 & 1 & |w|_b \\ 0 & 0 & 1 \end{pmatrix}$ be the Parikh matrix corresponding to the word w. Now, we draw two line segments. One line segment is parallel to the Y-axis through the point $\left(|w|_a, 0\right)$ and another line segment is parallel to the X-axis

through the point $(0, |w|_b)$. Thus, we shall get a closed bounded area. This area is either a square or a rectangle depending upon $|w|_a = |w|_b$ or $|w|_a \neq |w|_b$. Now, we divide the area into $|w|_a + |w|_b$ lines. We draw $|w|_a$ equidistant lines parallel to the *Y*-axis and $|w|_b$ equidistant lines parallel to the *X*-axis. These lines divide the prescribed area into $|w|_a \times |w|_b$ squares. The line traced by the word divides the rectangle in two parts. The upper part is bounded by the lines *Y*-axis, the line parallel to the *X*-axis through the point $(0, |w|_b)$, and the line traced by the word itself. The lower part is bounded by the lines *X*-axis, the line parallel to the *Y*-axis through the point $(|w|_a, 0)$, and the line traced by the word itself. For example, let us draw the words of the following Parikh matrices.

I. The two-dimensional representation of the matrix $M_{\alpha_1} = \begin{pmatrix} 1 & 3 & 5 \\ 0 & 1 & 3 \\ 0 & 0 & 1 \end{pmatrix}$ is given as follows:

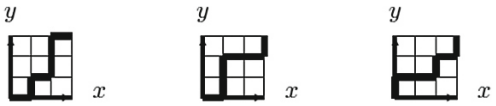

1.*ababba* 2.*abbaab* 3.*baabab*

II. The two-dimensional representation of the matrix $M_{\alpha_3} = \begin{pmatrix} 1 & 5 & 3 \\ 0 & 1 & 2 \\ 0 & 0 & 1 \end{pmatrix}$ is given as follows:

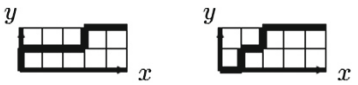

1.*baaabaa* 1.*ababaaa*

The line traced by the word is named as word line. The numbers of squares on the upper part are exactly equal to $|w|_{ab}$, and the number of squares on the lower part helps us to add some property in the field of amiable words. One can see that all the amiable words have the same area covered. Conversely, the words corresponding to the same area covered are M-ambiguous words. Two words with the same $|w|_a$ and $|w|_b$ will be amiable if the word lines drawn in the two-dimensional field in the same way defined above have the equal area covered.

To represent ternary words in a three-dimensional area, one have to draw three perpendicular axes *X*, *Y,* and *Z* (say) intersecting at *O*. It is considered that the coordinate of *O* is (0, 0, 0). In the *X*-axis, we take *a*'s, and in the *Y*-axis, we take *b*'s, and in the *Z*-axis, we take *c*'s. Now, we draw the graph of the word. This graph is named as word line. We start from (0, 0, 0), i.e., the intersection point of the three

axes and go on describing the word w as it is done in two-dimensional case and thus get the path of the word in the three-dimensional graph. Let

$$\Psi_{M_3}(w) = \begin{pmatrix} 1 & |w|_a & |w|_{ab} & |w|_{abc} \\ 0 & 1 & |w|_b & |w|_{bc} \\ 0 & 0 & 1 & |w|_c \\ 0 & 0 & 0 & 1 \end{pmatrix}$$

be the Parikh matrix corresponding to the word w. Now, we draw six plane segments. First, three are $x = 0, y = 0, z = 0$,, then one plane segment is perpendicular to the X-axis, and its equation is $x = |w|_a$ and another plane segment is perpendicular to the Y-axis, and its equation is $y = |w|_b$ another plane segment is perpendicular to the Z-axis and its equation is $z = |w|_c$. Thus, we shall get a closed bounded region. This region is either a cube or a cuboid depending upon $|w|_a = |w|_b = |w|_c$ or else. Now, we divide the region into $|w|_a + |w|_b + |w|_c$ planes. We draw $|w|_a$ equidistant planes perpendicular to the X-axis, $|w|_b$ equidistant planes perpendicular to the Y-axis, and $|w|_c$ equidistant planes perpendicular to the Z-axis. These planes divide the prescribed region into $|w|_a \times |w|_b \times |w|_c$ cubes.

7 Conclusion

This paper presents an algorithm showing Parikh matrix corresponding to a ternary word. A set of equations to determine the M-unambiguous words or amiable words corresponding to a particular Parikh matrix over ternary alphabet is presented. Using the proposed equations, some examples of ternary sequences are discussed. These equations give a new arena for investigation in this field. The condition for a 4×4 matrix to be a Parikh matrix is discussed in terms of theorem and results. The Problem of M-ambiguity is tried to be handled with the help of graphical representation of binary words. The area covered by line depicted by the word and the X-axis and the line parallel to the Y-axis though the point $(0, |w|_b)$ is the same for all M-ambiguous words corresponding to a 3×3 Parikh matrix. The number of squares covered by the word line, Y-axis, and the line parallel to the X-axis though the point is the same as the number $|w|_{ab}$. It is seen that if one word corresponding to a Parikh matrix is known, then those words which have the same area covered below the word line and with the same $|w|_a + |w|_b$ are all M-ambiguous words. The reason behind this property is yet to be investigated. The method of graphical representation of ternary sequences is introduced. Further investigation in this feature is an open problem.

References

1. Parikh, R.J.: On the context-free languages. J. Assoc. Comput. Mach. **13**, 570–581 (1966)
2. Mateescu, A., Salomaa, A., Salomaa, K., Yu, S.: A sharpening of the Parikh mapping theoret. Inf. Appl. **35**, 551–564 (2001)
3. Mateescu, A., Salomaa, A., Salomaa, K., Yu, S.: On an extension of the Parikh mapping. T.U. C.S Technical Report No. 364 (2000)
4. Subramanian, K.G., Huey, A.M., Nagar, A.K.: On Parikh matrices. Int. J. Found. Comput. Sci. **20**(2), 211–219 (2009)
5. Ding, C., Salomaa, A.: On some problems of Mateescu concerning sub word occurences. Fundamenta Informaticae **72**, 1–15 (2006)
6. Atanasiu, A., Vide, C.M., Mateescu, A.: On the injectivity of the Parikh matrix mapping Fundam. Informa **46**, 1–11 (2001)
7. Salomaa, A., et al.: Subword conditions and subword histories. Inf. Comput. **204**, 1741–1755 (2006)
8. Bhattacharjee, A., Purkayastha, B.S.: Parikh matrices and words over tertiary ordered alphabet. Int. J. Comput. Appl. **85**(4), 10–15 (2014)
9. Mateescu, A., Salomaa, A., Yu, S.: Subword histories and Parikh matrices. J. Comput. Syst. Sci. **68**, 1–21 (2004)
10. Atanasiu, A., Atanasiu, R., Petre, I.: Parikh matrices and amiable words. Theoret. Comput. Sci. **390**, 102–109 (2008)
11. Atanasiu, A.: Binary amiable words. Int. J. Found. Comput. Sci **18**(2), 387–400 (2007)
12. Bhattacharjee, A., Purkayastha, B.S.: Application of ratio property in searching of M-ambiguous words and its generalization. In: Proceedings of Third International Conference on Soft computing for Problem Solving, SocProS 2013, AISC, vol. 258, pp. 857–865. Springer, India (2014)
13. Bhattacharjee, A., Purkayastha, B.S.: Some alternative ways to find M-ambiguous binary words corresponding to a Parikh matrix. Int. J. Comput. Sci. Appl. AIRCC **4**(1), 53–64 (2014)

Neuro-genetic Approach to Predict Scour Depth Around Vertical Bridge Abutment

Abul Kashim Md Fujail, Shahin Ara Begum and Abdul Karim Barbhuiya

Abstract Scour is caused by the erosive action of flowing water. Although, different researchers have proposed various empirical models to predict the equilibrium local scour depth around bridge abutment, these are suitable to a particular abutment condition. In this study, an integrated model that combines genetic algorithms (GA) and multilayer perceptron (MLP) network, a class of artificial neural network (ANN), is developed to estimate the scour depth around vertical bridge abutment. The equilibrium scour depth was modeled as a function of four affecting parameters of scour, abutment length, median grain size, approaching flow depth, and average approach flow velocity, and these parameters are considered as input parameter to the MLP model. The efficiency of the developed models is compared with the empirical equations over a dataset collected from literature. The MLP is found to outperform the empirical equations for the dataset considered in the present study. The performance of the best case MLP is further improved by applying GA for weight initialization. The results indicate that the GA-based MLP is more effective in terms of accuracy of predicted results and is a promising approach compared to MLP as well as the previous empirical approaches in predicting the scour depth at bridge abutments.

Keywords Scour depth prediction · Artificial neural network · Genetic algorithm

A.K. Md Fujail · S.A. Begum (✉)
Department of Computer Science, Assam University, Silchar, Assam, India
e-mail: shahin.ara.begum@aus.ac.in

A.K. Md Fujail
e-mail: abul_fujail@yahoo.com

A.K. Barbhuiya
Department of Civil Engineering, National Institute of Technology, Silchar, Assam, India
e-mail: akbarbhuiya@yahoo.com

K.N. Das et al. (eds.), *Proceedings of Fourth International Conference on Soft Computing for Problem Solving*, Advances in Intelligent Systems and Computing 335,
DOI 10.1007/978-81-322-2217-0_13

1 Introduction

Scour is the process of removing underwater sediment from the base of a structure by waves and currents [1]. Due to the scouring action of the flow, bridge failures occur and a large amount of money is spent every year to repair or replace those bridges. The number of abutment is much more than the numbers of piers, as most of bridges are of single span, and hence, most of the repairing amount is spent toward abutment scour [2]. According to the report published by the Department of Scientific and Industrial Research of New Zealand [3], 50 % of total expenditure was made to repair and maintain bridge damage, out of which 70 % was spent to repair abutment scour. Thus, estimation of the depth of local scour around bridge abutments is an important issue in the design of bridges.

The empirical formulae [4–7] developed through experimental investigation for predicting scour depth around abutment are suitable to particular abutment instances and the results of each formula significantly differ with each other. Artificial Neural Networks (ANNs) are alternative method to overcome the variation of physical modeling and is a good function approximator. ANNs have been widely applied in modeling complex problems in civil engineering. A review shows that the available literature on the application of ANN to the scour at abutments is limited. Kheireldin [8] applied the ANN to predict the maximum local scour depth around bridge abutments. Begum et al. [9] developed Multilayer perceptron (MLP) to predict scour around semicircular abutment. It is reported that MLP performs better than the empirical formulae as well as the radial basis function network. Begum et al. [10] also developed genetic programming model to predict the depth of scour around vertical abutment. It is observed from the available literatures that the soft computing models provide more accurate results than the empirical formulae.

The main objective of this paper was to investigate the performance of GA-based MLP (GA-MLP) relative to MLP and empirical formulae. In this paper, MLP and GA-MLP networks are applied to existing experimental data for local scour.

The remainder of this paper is organized as follows: A brief introduction about equilibrium scour depth is given in Sect. 2. Section 3 includes the empirical formulae for local scour at bridge abutments. Methodology is given in Sect. 4. The MLP and GA-MLP models developed for scour depth prediction around abutment are introduced in Sects. 5 and 6, respectively. Section 7 concludes the paper.

2 Equilibrium Local Scour Depth Around Bridge Abutment

Local scour is caused by the erosion of bed material from the base of abutment. It can be either clear-water or live-bed scour. Clear-water scour occurs where there is no movement of bed material into a scour hole during the time of scour. On the

other hand, live-bed scour occurs when the scour hole is continuously fed with sediment by the approaching flow [11]. The dataset used in the present study involves clear-water condition.

Maximum equilibrium local scour depth around an abutment in a steady flow of uniform, cohesionless sediment depends on the fluid, flow, bed sediment, and abutment characteristics. Thus, the maximum equilibrium scour depth may be represented by the following functional relationship [12]:

$$d_{se} = f_1(U, \rho, \rho_s, g, l, v, h, d_{50}) \tag{1}$$

where U = average approach flow velocity, ρ = mass density of the fluid, ρ_s = mass density of the sediment, g = gravitational acceleration, l = abutment length, v = kinematic viscosity, h = approaching flow depth, d_{50} = median sediment size, and d_{se} = equilibrium scour depth.

For a given fluid condition, ρ, ρ_s, g, and v are constant and thus the relationship between d_{se} and its dependent variables can be expressed as follows:

$$d_{se} = f_2(l, d_{50}, h, U) \tag{2}$$

3 Empirical Formulae for Local Scour at Bridge Abutment

Four empirical formulae considered for evaluation in the present study are tabulated in Table 1.

In the above cases, abutment shape factor, K_s, is considered as 1 (one), which is the shape factor of vertical wall abutment.

Table 1 Empirical formulae for scour depth prediction around vertical bridge abutment

Author	Formula
Froehlich [4]	$\frac{d_{se}}{h} = 0.78 K_s K_\theta \left(\frac{l}{h}\right)^{0.63} F_r^{1.16} \left(\frac{h}{d}\right)^{0.43} \sigma_g^{-1.87} + 1$ where K_s = abutment shape factor, K_o = abutment alignment factor, F_r = approaching flow Froude number, σ_g = geometric standard deviation, and d = median diameter of sediment particles
Kandasamy and Melville [5]	$d_{se} = K_s K h^n l^{1-n}$ where K_s is the shape factor, K and n are coefficients that are determined as follows: $K = 5$ and $n = 1$ for $h/l \leq 0.04$; $K = 1$ and $n = 0.5$ for $0.04 < h/l < 1$; and $K = 1$ and $n = 0$ for $h/l > 1$
Melville and Coleman [6]	$d_{se} = K_{hl} K_I K_{d_{50}} K_s K_\theta K_G$ where K_{hl} represents the effects of flow depth and abutment length, K_I is the flow intensity factor, $K_{d_{50}}$ is abutment length and sediment size effects factor, K_G represents the approach channel geometry factor, and K_s and K_o are as defined in the previous equations
Dey and Barbhuiya [7]	$\frac{d_{se}}{l} = 7.281 F_e^{0.314} \left(\frac{h}{l}\right)^{0.128} \left(\frac{l}{d_{50}}\right)^{-0.167}$ where F_e = excess abutment Froude number.

4 Methodology

The ANN model development for scour depth prediction consists of 5 steps:

Step 1. The dataset for vertical wall abutment considered in the present study was collected from the literature [7, 12, 13]. It contains four independent parameters: length of the abutment, median grain size, depth of the flow, and average approaching flow and one dependent parameter, that is, depth of the scour. The dataset consists of 227 samples, out of which nine samples are removed as outlier.

Step 2. For effective training of the network, all data values were normalized within the range 0.1–0.9 with the following equation:

$$x_{\mathrm{N}} = \frac{0.9 - 0.1}{x_{\max} - x_{\min}}(x - x_{\min}) + 0.1 \tag{3}$$

where x is the data value, x_{N} is the normalized value of x, $x_{\max}$ is the maximum, and $x_{\min}$ is the minimum value in the original dataset. Next, the dataset was divided randomly into a training set and a testing set to train the network and assess the performance of the network, respectively. The training set consists of 80 % and the testing sets consists of 20 % data points.

Step 3. Network architectures and learning methods are selected. In the present study, MLP with single hidden layer is used which is shown in Fig. 1.

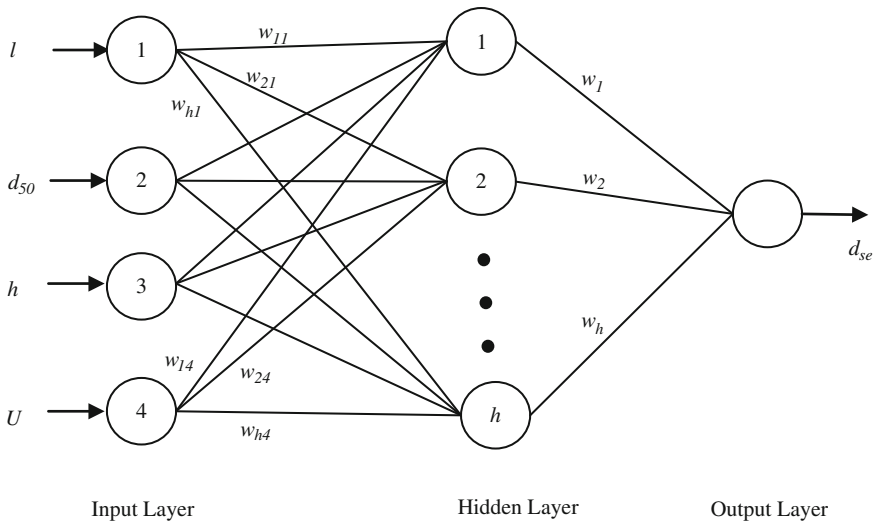

Fig. 1 MLP network

Step 4. Weights and other parameters, viz. learning rate (LR), momentum constant (MC), number of neuron in the hidden layer, and epochs are initialized. These parameters are modified with learning algorithms to get better performance of the network. Since there are four independent parameters that affect the extent of scour, the number of node in the input layer is four. There is only one output node that corresponds to the depth of scour. The networks have been trained several number of times to obtain the suitable number of nodes in the hidden layer, momentum values, learning rate, and number of iteration.

Step 5. Optimum network models are identified based on root mean square error (RMSE) and correlation coefficient (CC) between target and predicted values. The RMSE and CC are evaluated as follows:

$$\text{RMSE} = \sqrt{\frac{1}{n}\sum_{i=1}^{n}(o_i - t_i)^2} \tag{4}$$

$$\text{CC} = \frac{\sum_{i=1}^{n}(o_i - \bar{o})(t_i - \bar{t})}{\sqrt{\sum_{i=1}^{n}(o_i - \bar{o})^2 \sum_{i=1}^{n}(t_i - \bar{t})^2}} \tag{5}$$

where o_i and t_i are network and target output for the ith input pattern, $\bar{o}$ and $\bar{t}$ are the average of network and target outputs, and n is the total number of events considered.

To select the optimum architecture, each network is evaluated with testing dataset. The models with minimum RMSE and maximum CC during testing are selected as optimum.

5 Multilayer Perceptron

MLP is an important class of ANN. The schematic diagram of the implemented MLP models is shown in Fig. 1. The values of the independent parameters l, d_{50}, h, and U are fed in the network through the nodes in the input layer. The network is trained with Levenberg–Marquardt optimization algorithm and produces an expected result (d_{se}) in the output layer. The hidden layer of neurons enables the network to learn complex tasks by extracting meaningful features from the input patterns. The number of nodes in hidden layer is determined by trial and error method.

In Fig. 1, w_{11}, w_{21},…, w_{h4} are the weights between hidden and input layer and w_1, w_2, …, w_h are weight between hidden and output layer. The initial weights are generated by Nguyen–Widrow [14] method.

The network includes various activation functions in the hidden and output layer with different values of number of neurons, epochs, LR, and MC. The combinations

Table 2 MLP architectures

Activation function		No. of hidden neuron	Learning rate	Momentum	Epochs
Hidden layer	Output layer				
Log-sigmoid	Log-sigmoid	5–10	0.1–0.9	0.1 –0.9	1,000–7,000
Tan-sigmoid	Linear				

of different network parameters are tabulated in Table 2. The activation functions used in the present study are as follows:

$$f(x) = \frac{1}{(1 + \exp(-\mathrm{ax}))}, (\text{log-sigmoid}) \tag{6}$$

$$f(x) = \frac{(1 - \exp(-ax))}{(1 + \exp(-ax))}, (\text{hyperbolic tangent sigmoid (tan-sigmoid)}) \tag{7}$$

$$f(x) = x, (\text{linear}) \tag{8}$$

where a is the slope parameter of the sigmoid function which is considered as one.

The output (y_j) of the jth hidden node is given by

$$y_j = f\left(\sum_{i=1}^{n} w_{ji} x_i\right) \tag{9}$$

where x_i's are the input values, n is the number of input nodes, w_{ji} is the weight between ith input node and jth hidden node, and f is the activation function associated with jth hidden node.

The output of the network is derived by

$$d_{\mathrm{se}} = f\left(\sum_{j=1}^{h} w_j y_j\right) \tag{10}$$

where w_j is the weight between the jth hidden node and output unit and h is the number of hidden nodes.

Some training and testing cases of MLP for scour depth prediction around vertical bridge abutment are shortlisted in the Table 3. The shortlisting is done from 330 tested cases of MLP.

The best case of MLP is highlighted in Table 3. It was found with logistic sigmoid transfer function in the hidden as well as in the output layer with Nguyen and Widrow weight initialization method. The selected model of MLP had seven number of neurons in hidden layer, Epoch = 2,500, LR = 0.5, and MC = 0.6. It had very small RMSE during testing, that is, 0.0256, strong correlation value, that is, 0.9829 RMSE, and CC values of the corresponding training case are 0.0249 and 0.9834, respectively. The best case is graphically represented in the Fig. 2.

Table 3 Training and testing results of MLP (Neuron = 7, MC = 0.6)

Epoch	LR	Training		Testing	
		RMSE	CC	RMSE	CC
2,000	0.1	0.0272	0.9807	0.0270	0.9792
	0.2	0.0262	0.9832	0.0259	0.9825
	0.3	0.0264	0.9820	0.0320	0.9694
	0.4	0.0280	0.9792	0.0280	0.9785
	0.5	0.0265	0.9819	0.0340	0.9677
	0.6	0.0292	0.9770	0.0343	0.9662
	0.7	0.0257	0.9820	0.0356	0.9620
	0.8	0.0252	0.9842	0.0337	0.9653
	0.9	0.0263	0.9811	0.0367	0.9697
2,500	0.1	0.0247	0.9841	0.0383	0.9557
	0.2	0.0262	0.9811	0.0340	0.9708
	0.3	0.0310	0.9751	0.0342	0.9673
	0.4	0.0257	0.9825	0.0272	0.9794
	0.5	**0.0249**	**0.9834**	**0.0256**	**0.9829**
	0.6	0.0284	0.9781	0.0308	0.9776
	0.7	0.0280	0.9788	0.0328	0.9734
	0.8	0.0262	0.9815	0.0356	0.9660
	0.9	0.0249	0.9835	0.0322	0.9730
3,000	0.1	0.0278	0.9812	0.0290	0.9746
	0.2	0.0277	0.9792	0.0354	0.9623
	0.3	0.0256	0.9834	0.0257	0.9826
	0.4	0.0264	0.9815	0.0309	0.9719
	0.5	0.0253	0.9840	0.0377	0.9685
	0.6	0.0279	0.9802	0.0361	0.9627
	0.7	0.0276	0.9803	0.0356	0.9642
	0.8	0.0268	0.9809	0.0274	0.9805
	0.9	0.0267	0.9817	0.0347	0.9676

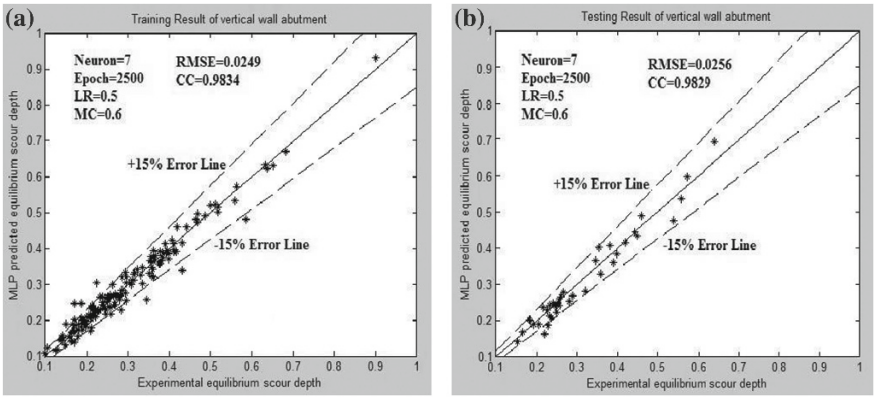

Fig. 2 ANN predicted versus experimental scour depth for vertical wall abutment

Table 4 ANN versus empirical formulae

Method	RMSE	CC
MLP	**0.0256**	**0.9829**
Froehlich [4]	0.1732	0.7047
Kandasamy and Melville [5]	0.0991	0.8802
Melville and Coleman [6]	0.0843	0.9136
Dey and Barbhuiya [7]	0.2078	0.7530

The results of selected MLP model and empirical formulae are tabulated in Table 4. The table shows that the neural network models are capable of predicting scour depth more accurately than the empirical formulae. The performance of MLP is further enhanced by initializing the weights with GA which is discussed in the next section.

6 Weight Optimization Using GA

GAs are computerized search and optimization algorithms based on the mechanics of natural genetics and natural selection [15]. GAs start with a random population of possible solutions to a problem called chromosomes. The individual components within a chromosome are referred to as genes. All chromosomes are then evaluated according to a fitness function. In this study, the average deviation between target and predicted values of scour depth is considered as the fitness function. Once the fitness values are calculated, new chromosomes are created by selecting two chromosomes and applying crossover and mutation operations. The process is repeated until some predefined termination criteria are satisfied [16, 17].

The application of genetic algorithm for weight optimization in MLP consists of three major phases. In the first phase, connection weights of each neuron are represented as gene segments.

In the next step, fitness of these connection weights is evaluated by constructing the corresponding neural network. The inverse of the error function as shown below is considered as the fitness function.

$$E = \frac{1}{2}\sum_{p=1}^{N}(t^p - y^p)^2 \tag{11}$$

where t^p *and* y^p are target and network output for pth training pattern and N is the total number of training patterns.

The third phase is to apply the genetic operators such as selection, crossover, and mutation. The process of selection, crossover, and mutation is repeated until the error is smaller than a predefined value.

The hybrid network learning process consists of two stages: Firstly, GA is employed to search for sub-optimal connection weights for the MLP network. Next,

Table 5 Training and testing results of GA-MLP

Epoch	Training		Testing	
	RMSE	CC	RMSE	CC
170	0.0317	0.9685	0.0351	0.9653
180	0.0292	0.9715	0.0305	0.9697
190	0.0268	0.9796	0.0291	0.9754
200	**0.0203**	**0.9875**	**0.0213**	**0.9864**
210	0.0231	0.9857	0.0239	0.9843
220	0.0218	0.9860	0.0227	0.9851

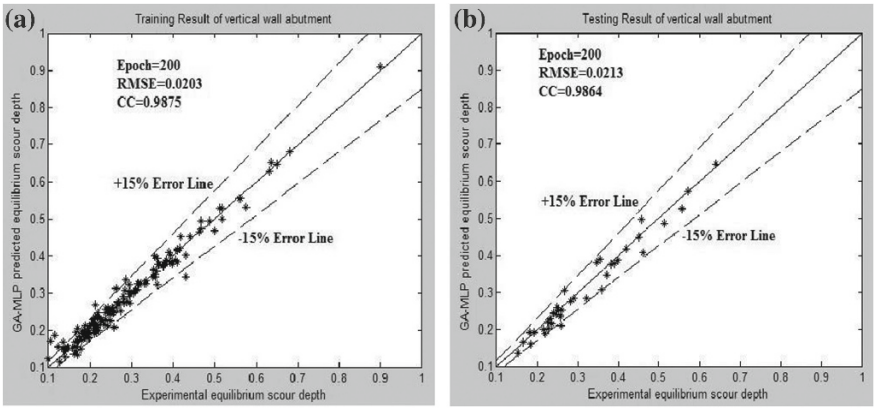

Fig. 3 GA-MLP predicted versus experimental scour depth

MLP with backpropagation algorithm (BP) is used to adjust the final weights. Some training and testing cases are tabulated in Table 5.

From Tables 4 and 5, it is observed that hybrid GA-MLP model provides more accurate result than the empirical as well as MLP model. The best case of GA-MLP is highlighted in Table 5 and graphically represented in Fig. 3. The initial population size was 60, and MLP was run by one iteration for each individual chromosome (i.e., weights). Based on the fitness value, the GA operations were performed and the process is repeated by 80 numbers of times. Finally, MLP was run with BP for 200 iterations. In the above table, epoch represents the number of iterations. MLP was run after applying the GA operations.

7 Conclusion

In the present study, MLP have been implemented to predict the maximum equilibrium scour depth around bridge abutment and found to be suitable for prediction of scour depth around bridge abutment. It is observed that the neural network

prediction of scour depth is much more accurate than the existing empirical formulae. The performance of best MLP model has further been improved by combining with GA which performed network connection weight optimization. In the dataset under consideration for vertical wall abutment, the hybrid models provide better result compared to MLP model.

The present study has been carried out using MLP with a single hidden layer and hybrid genetic algorithm-based MLP. Further experimentation needs to be carried out with other soft computing models like neuro-fuzzy model over different datasets.

References

1. Jeng, D.S., Bateni, S.M., Lockett, E.: Neural network assessment for scour depth around bridge piers. Research Report No R855, Department of Civil Engineering, Environmental Fluids/Wind Group, The University of Sydney (2005)
2. Richardson, E.V., Harrison, L J., Richardson, J.R., Davies, S.R.: Evaluating scour at bridges. Publ. FHWA-IP-90-017, Federal Highway Administration, US Department of Transportation, Washington, DC (1993)
3. Macky, G.H.: Survey of roading expenditure due to scour. CR 90_09, Department of Scientific and Industrial Research, Hydrology Centre, Christchurch, New Zealand (1990)
4. Froehlich, D.C. Local scour at bridge abutments. In: Proceedings of National Conference on Hydraulic Engineering, New Orleans, LA, pp. 13–18. American Society of Civil Engineering (1989)
5. Kandasamy, J.K., Melville, B.W.: Maximum local scour depth at bridge piers and abutments. J. Hydraul. Res. **36**(2), 183–198 (1998)
6. Melville, B.W., Coleman, S.E.: Bridge Scour. Water Resources Publications, Highlands Ranch (2000)
7. Dey, S., Barbhuiya, A.K.: Time variation of scour at abutments. J. Hydraul. Eng. **131**(1), 11–23 (2005)
8. Kheireldin, K.A.: Neural network modeling for clear water scour around bridge abutments. J. Water Sci. **25**(4), 42–51 (1999)
9. Begum, S.A., Md Fujail, A.K., Barbhuiya, A.K.: Artificial neural network to predict equilibrium local scour depth around semicircular bridge abutments. In: 6th SASTech, Malaysia, Kuala Lumpur (2012)
10. Begum, S.A., Md Fujail, A.K., Barbhuiya, A.K.: Genetic programming for prediction of local scour at vertical bridge abutment. Int. J. Res. Eng. Technol. 2(2), 74–77. ISSN-2321-7308 (2013)
11. Lombard, P.J., Hodgkins, G.A.: Comparison of observed and predicted abutment scour at selected bridges in Maine. Scientific Investigations Report 2008–5099, U.S. Department of the Interior, U.S. Geological Survey, (2008)
12. Coleman, S.E., Lauchlan, C.S., Melville, B.: Clear-water scour development at bridge abutments. J. Hydraul. Res. **41**(5), 521–531 (2003)
13. Ballio, F., Teruzzi, A., Radice, A.: Constriction effects in clear-water scour at abutments. J. Hydraul. Eng. **135**(2), 140–145 (2009)
14. Nguyen, D., Widrow, B.: Improving the learning speed of 2-layer neural networks by choosing initial values of the adaptive weights. In: Proceedings of the International Joint Conference on Neural Networks, vol. 3, pp. 21–26 (1990)

15. Rajasekaran, S., Vijayalakshmi Pai, G.A.: Neural Networks, Fuzzy Logic and Genetic Algorithms. Prentice Hall, New Delhi (2003) (Eastern Economy Edition)
16. Irani, R., Shahbazian, M., Nasimi, R.: Evolving neural network using real coded genetic algorithm for permeability estimation of the reservoir. Expert Syst. Appl. **38**:9862 (2011)
17. Sedki, A., Ouazar, D., Mazoudi, E.El: Evolving neural network using real coded genetic algorithm for daily rainfall–runoff forecasting. Expert Syst. Appl. **36**, 4523–4527 (2009)

Rough Fuzzy Classification for Class Imbalanced Data

Riaj Uddin Mazumder, Shahin Ara Begum and Devajyoti Biswas

Abstract This paper presents a new rough fuzzy classification approach for class imbalanced data. Here, interval type-2 fuzzy granulation of input features is formulated, various combinations of rough set extension-based methods are used to perform class imbalance learning, and *K*-nearest neighbor (KNN) classifier is used for data classification. The experimental results on the UCI data sets are reported to demonstrate the effectiveness of the proposed rough fuzzy classification model. Performance evaluation measures viz *F*-measure and geometric mean (*G*-mean) are used for analyzing classifier's performance and suitability of the developed model for class imbalance learning.

Keywords Interval type-2 fuzzy granulation · Rough set · Feature selection

1 Introduction

In many real-world classification problems, the data sets are typically imbalanced and the class distribution is not uniform among the classes. The problem of class imbalance is a supervised classification technique [1]. The imbalanced data sets consist of two classes: the majority (negative) class and the minority (positive) class. Data sets with imbalanced class distribution usually suffer from class overlapping, small sample size, or small disjuncts, which is difficult for classifier learning [2, 3]. In data analysis, class imbalance problems are used to adjust the class distribution of a data set (i.e., the ratio between the different class representations).

To improve the performance of learning technique, a balanced class distribution is needed [4]. The main aim in class imbalance learning is to increase the accuracy

R.U. Mazumder · D. Biswas
Department of Mathematics, Assam University, Silchar, India

S.A. Begum (✉)
Department of Computer Science, Assam University, Silchar, India
e-mail: shahin.begum.ara@gmail.com

K.N. Das et al. (eds.), *Proceedings of Fourth International Conference on Soft Computing for Problem Solving*, Advances in Intelligent Systems and Computing 335,
DOI 10.1007/978-81-322-2217-0_14

of minority class, but at the same time not to decrease the accuracy of majority class too much. In class imbalance learning, re-sampling technique is used to balance the classes of the original data set by either over-sampling the minority class or by under-sampling the majority class, until the classes are equally represented [5]. The level of imbalance is reduced by both techniques and balanced training set give better results [4]. Under-sampling requires lesser training time and is computationally efficient, whereas over-sampling increases size of the training data and thus requires more training time and over fitting because of repetition of minority class samples [5]. Fuzzy granulation has been used as an important concept in fuzzy set theory, rough set theory, and the combination of both [6]. Generally speaking, the process of fuzzy granulation can be divided in two main categories such as class dependent and class independent. In class-independent fuzzy granulation, each feature vector is described with its fuzzy membership values over the whole space as investigated by Pal et al. [7]. With class-dependent fuzzy granulation, individual class information is restored by the generated fuzzy granules.

Rough set theory is a powerful mathematical model proposed by Pawlak [8] of imperfect information and finds application in many real-world problems especially in the field of machine learning. Rough set theory can be used with the discretized data which may affect the learning process for information loss. To address this problem, rough sets extension-based methods viz neighborhood rough set model [9, 10] and exponential kernel-based fuzzy rough set model [11] are found suitable that can deal with mixtures of data without the process of discretization. In the present work, a new approach for rough fuzzy classification model for class-imbalanced data is presented where interval type-2 fuzzy granulation of input features is used with various combinations of rough set extension-based methods to perform class imbalance learning and *K*-nearest neighbor (KNN) classifier is used for data classification.

Rest of the paper is organized as follows: In Sect. 2, some basic concept of rough set extensions and fuzzy granulation is presented. In Sect. 3, rough fuzzy classification model is introduced. In Sect. 4, comparison of rough- and fuzzy set-based methods for class imbalance learning is presented. Experimental results and discussion are demonstrated in Sect. 5. Section 6 concludes the paper.

2 Rough Set Extensions and Fuzzy Granulation

The present work focuses on the use of equivalence relation based and their generalized approaches. In the following subsections, the preliminary concept of Pawlak's rough sets and two rough set extensions viz neighborhood rough sets and exponential kernel-based fuzzy rough sets is briefly described.

2.1 Pawlak's Rough Sets

Rough set theory provides a mathematical tool to deal with both uncertainty and vagueness [8, 12] and provides efficient algorithms for discovering hidden patterns in the data. According to Pawlak [12] and Skowron [13], an information system $\mathrm{IS} = \langle U, A, V, f \rangle$ is a pair, where U is a non-empty finite set of objects (the universe) and A is a non-empty finite set of attributes such that $a: U \rightarrow V_a$ for every $a \in A$. The set V_a is the set of values that attribute a may take and is called the domain of a. Any subset of attributes $B \subseteq A$ defines an equivalence relation (an indiscernibility relation) on U. This relation is defined as:

$$IND(B) = \left\{(x, y) \in U^2 | for\ every\ a \in B, a(x) = a(y)\right\}$$

The elements of U, generated by $\mathrm{IND}(B)$, are objects with the same values for attributes B, and they are indiscernible with respect to B. The equivalence classes of $\mathrm{IND}(B)$ are denoted $U/\mathrm{IND}(B)$ (or U/B) and can be calculated as follows:

$$U/\mathrm{IND}(B) = \otimes\{a \in B | U/\mathrm{IND}(\{a\})\},$$

where $A \otimes C = \{X \cap Y | \forall X \in A, \forall Y \in C, X \cap Y \neq \emptyset\}$

If $(x, y) \in \mathrm{IND}(B)$, then x and y are indiscernible by attributes from B. The equivalence classes of $\mathrm{IND}(B)$ are also called concepts of the knowledge B. The equivalence classes of the B-indiscernibility relation are denoted by $[x]_B$. Given any subset of attributes B, let any concept $X \subseteq U$ can be approximated using only the information contained within B by employing two exact sets called B-lower and B-upper approximations and can be defined as:

$$\underline{B}X = \left\{x | [x]_B \subseteq X\right\} \quad \text{and} \quad \bar{B}X = \left\{x | [x]_B \cap X \neq \emptyset\right\}$$

2.2 Neighborhood Rough Sets

Given arbitrary $x_i \in U$ and $B \subseteq C$, the neighborhood $\delta_B(x_i)$ of x_i in feature space B is defined as in [9, 10]:

$$\delta_B(x_i) = \left\{x_j | x_j \in U, \Delta^B\left(x_i, x_j\right) \leq \delta\right\},$$

where Δ is distance metric function.

$\delta_B(x_i)$ is the neighborhood information granule centered with sample x_i. The size of the neighborhood depends on threshold δ, by choosing the greater value of δ, more samples fall into the neighborhood of x_i. The shape of the neighborhoods depends on the norm used in the function. If $\delta = 0$, the neighborhood granule degrades to equivalent class. In this case, the neighborhood rough set model degenerates to Pawlak's rough set. Therefore, the neighborhood rough sets are

natural generalization of Pawlak rough set. A neighborhood information system is called a neighborhood decision system, denoted by NDT $= \langle U, A, N \rangle, A = C \cup D$, where C and D are the condition and decision attributes, and X_i is the object subsets with decisions, $i = 1, 2, \ldots, N$, $\delta_B(x_i)$ is the granules of neighborhood generated by attributes $B \subseteq C$, and the decision attribute D of lower and upper approximations with respect to attribute B is defined as:

$$\underline{N_B}D = \bigcup_{i=1}^{N} \underline{N_B}X_i, \overline{N_B}D = \bigcup_{i=1}^{N} \overline{N_B}X_i$$

where

$$\underline{N_B}X = \{x_i | \delta(x_i) \subseteq X, x_i \in U\}, \overline{N_B}X = \{x_i | \delta(x_i) \cap X \neq \phi, x_i \in U\}.$$

2.3 Exponential Kernel-based Fuzzy Rough Sets [11]

In this section, the exponential kernel is described in brief. Let U be a non empty finite set (universe of discourse) samples, x_i is contained in U and is described by a vector $x_{ij} \in R^n$, where $j = 1, 2, \ldots, n$. Thus, $U \subseteq R^n$. The exponential kernel [14] is defined as:

$$K(x_i, x_j) = \exp\left(-\frac{\left\|x_i - x_j\right\|}{\theta}\right),$$

where $\left\|x_i - x_j\right\|$ is the Euclidean distance between samples x_i and x_j; and (i) $K(x_i, x_j) \in [0, 1]$; (ii) $K(x_i, x_j) = K(x_j, x_i)$; and (iii) $x_i K(x_i, x_i) = 1$. Since the properties of reflexivity and symmetry are satisfied, exponential kernel induces the fuzzy relation and is denoted by R_E^n. Assume $x = (x_1, \ldots, x_n) \in R^n$, the exponential kernel $R_E^{(k)} = \exp\left(-\frac{\left\|x_i - x_j\right\|}{\theta}\right)$ is the similarity of samples and x_j with respect to attribute k, and θ is the kernel parameter. Exponential kernel functions can be expressed by a T-norm-based combination of reflexive functions. For example, let $x = (x_1, \ldots, x_n) \in R^n$ and $y = (y_1, \ldots, y_n) \in R^n$, exponential kernel $\exp\left(-\frac{\|x-y\|}{\theta}\right) = \prod_i^n \exp\left(-\frac{(x_i - y_i)}{\theta}\right)$, because its product is a T-norm.

Let $I = (U, A)$ be an information system, $A = C \cup D$ be the condition and decision attribute, R_E is fuzzy T-equivalence relation on U computed with exponential kernel in a sample space $B \subseteq C$. U is divided into $\{d_1, d_2, \ldots, d_l\}$ with the decision attribute. The fuzzy positive region D contains all objects of U that can be classified into classes of U/D using the information available in B is given by: $POS_B(D) = \bigcup_{x \in d_i} \underline{R_E} d_i, i = 1, 2, \ldots, l$.

2.4 Fuzzy Granulation

Granulation of an object is a collection of groups of data points i.e., granules that have very similar characteristics. Similar characteristics of granules may be of similarity, equality, and proximity between the data points. The concept of information granulation was described by Zadeh [15], it is considered perceptions bounded by fuzzy boundaries, and the values of perceptions may take indistinguishable granulated data points. The granulation structures are labeled with integer values representing the decision classes. These granulated structures are presented in a decision table and are used to determine the dependency factors of the conditional attributes using interval type-2 fuzzy sets (IT2 FSs).

In the next section, a rough fuzzy classification model is presented which is based on the integration of the merits of both class imbalance strategies and the theory of rough set extension-based feature selection methods. Neighborhood rough set (NRS)-based method and exponential kernel-based fuzzy rough set are used in the selection of most informative granulated features. In addition to the rough set extension-based feature selection methods, the Gaussian IT2 membership function is used for generating granulated feature.

3 The Proposed Model for Classification

The general steps for classification model are depicted in Fig. 1. The major steps are as follows:

1. Generate fuzzy granules using interval type-2 fuzzy membership functions.
2. Different rough set extension-based feature selection methods are employed for removing irrelevant features from the granulated input features.
3. After performing feature selection, the selected features are then evaluated by a classification learning algorithm.

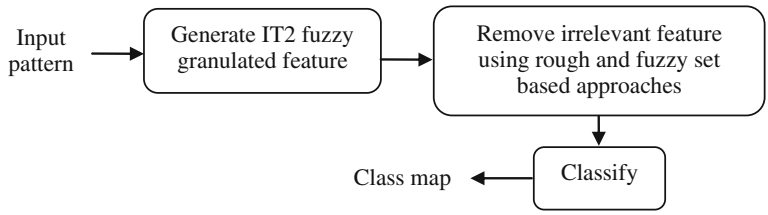

Fig. 1 General taxonomy of the proposed model for classification

3.1 IT2 Fuzzy Granulation

The membership function of fuzzy sets plays a prominent role for efficient handling of class overlapping. For IT2 fuzzy granulation, each input pattern vector of feature is described to its fuzzy membership values corresponding to total number of classes by using Gaussian IT2 MFs as proposed by Liang et al. in [16].

Let H_{ij}, $i = 1, \ldots, s$, $j = 1, \ldots, n$, be a given data set, and in all the S-patterns, consider $H_{j_{\text{lower}}}$ and $H_{j_{\text{upper}}}$ denote the lower and upper membership values along the jth feature. In real-life situations, many data contain outliers and noise, which can affect the parameters viz mean and standard deviation of membership function. This outliers and noise can be removed by taking an average of feature values of the S-patterns along the jth feature, F_j. Then, the average values of the patterns, having the label values in the ranges $[H_{j_{\text{lower}}}, H_{j_{\text{upper}}}]$, are defined in terms of interval of lower and upper membership functions $H_{j_{\text{lower}}}$ and $H_{j_{\text{upper}}}$, which is a type-1 fuzzy set in $[0, 1]$.

Pattern present in IT2 fuzzy set is three dimensional. For n-dimensional pattern, if H_{in} represents n feature of ith pattern H_i, then the IT2 fuzzy granule of the features is defined as $\overrightarrow{H_i} = [\mu_{\text{lower}}(\overrightarrow{H_i}), \mu_{\text{upper}}(\overrightarrow{H_i})]$, where μ indicates the value of the Gaussian IT2 MFs function along each feature axis [16] and the greater uncertainty will result in larger spread of the foot print of uncertainty.

In any decision system, D contains d-decision classes of a decision attribute. If for a given decision system that the n-dimensional pattern vectors M_{kj} and S_{kj}, $j = 1, \ldots, n$, are the mean and standard deviation, respectively, of the patterns belonging to the kth class, then the weighted membership G_{ik} of a pattern $\overrightarrow{H_i}$, $i = 1, \ldots, r$ from the kth decision class is defined as:

$$G_{ik} = \sqrt{\exp\left[-\frac{1}{2}\left(\frac{H_{ij} - M_{kj}}{S_{kj}}\right)^2\right]}$$

where H_{ij} is the value of the jth component of the ith pattern. The parameters defining the membership functions take a value which depends on the standard deviation of the attribute set.

3.2 Feature Selection and Data Classification

In the process of granulation, each feature value is represented with more than one membership value and thus the feature dimension increases. To alleviate problem of reducing the features dimension, different rough- and fuzzy set-based feature

selection methods are applied in the second step of the proposed model. After the features are selected, a classifier is built as in the third step to classify the input pattern based on the selected features. Selection of training and test instances for all classes has been made by splitting the data sets into two parts and repeating each of these splitting parts ten times and the final results are taken as an average.

4 Performance Evaluation

In order to investigate the performance of the different models, a comparative study of the learning strategies for class-imbalanced data is presented in this section. The data sets used for the present study are described next.

4.1 Data Sets

Ten UCI data sets [17] consisting of six two-class data sets viz. Ionosphere (Iono), Credit Card (CC), Wdbc, Wpbc, German and Sonar and four multi-class data sets viz Heart, Primary Tumor (Tumor), Wine and Lymphography (Lym) are used in the experimentations. The data sets are described in Table 1.

It can be seen from Table 1 that the class distribution of each data set is skewed and consequently, the imbalance ratios (IR) for the data sets of the majority class to the minority class in size range from 1.5 to 31.21.

Table 1 Data set descriptions with imbalance ratios

Data set	Instances	Attributes	Class	Class distribution	IR
Iono	351	34	2	126-225	1.78
CC	690	15	2	307-383	1.25
Heart	303	13	5	13-35-36-55-164	22.30
Tumor	339	17	22	84-20-9-14-39-1-14-6-2-28-16-7-24-2-1-10-29-6-2-1-24	1.5
Wdbc	569	31	2	212-357	1.69
Wpbc	198	33	2	47-151	31.21
Wine	178	13	3	48-59-71	2.7
Lym	148	18	4	2-4-61-81	23.69
German	1,000	24	2	300-700	2.3
Sonar	208	60	2	97-111	1.14

4.2 Performance Evaluation Metrics

Numerical evaluation of the classifiers produces a single number summarizing a classifiers performance. In most of the applications, imbalanced data sets mainly focus on two-class problem as multi-class problem can be designed to two-class problem. By convention, the class label of the minority class is represented as positive class, and the class label of the majority class is represented as negative. The performance of a classifier is evaluated based on the analysis of confusion matrix [18]. Accuracy is one of the most common traditional measures for predicting performance of a classifier. However, predictive accuracy might not be appropriate when the data are imbalanced or the class distribution is skewed for predicting classification performance measures. In order to evaluate the classification performance of an imbalanced data set, the traditional classification accuracy cannot be generally used because minority class has a minor impact on the accuracy when compared to the majority class. Therefore, complex numerical measures are employed to evaluate the classification performance of such an imbalance problem [19]. The widely used measures for the class imbalance problem viz *F*-measure [20] and the geometric mean (*G*-mean) [21] are used in the present work for the experimentations.

4.3 Comparison of Learning Strategies for Class Imbalanced Data

The three different strategies used for class imbalance learning are as follows: weighting, re-sampling, and filtering. Liu et al. [22] investigated that when the class distribution of a training data set is skewed, rough set-based method is usually biased to the majority class and has a poor prediction for the minority class as the priori knowledge of class distribution is not taken into account. Re-sampling training data set can be used in the traditional rough set-based method for performing class imbalance learning at the data level, but during the process of discretization, there may be some information loss of the majority class and it severely affects the learning process. In the present work, random re-sampling technique is used for balancing class distribution of a training data set, and neighborhood rough set and exponential kernel-based fuzzy rough set are used to perform learning. In order to evaluate the performance of each strategy, different models employed for this comparison are described next.

Model 1: *Under-sampling with neighborhood rough sets*—In this method, the *i*th class is randomly under-sampled until the size of the *i*th class is equal to the size of the minimum class, and then, neighborhood rough set is used to perform learning and KNN is used for classification. The neighborhood rough set model is an extension of classical rough set model.

Model 2: *Under-sampling with exponential kernel approximation*—In this method, the *i*th class is randomly under-sampled until the size of the *i*th class is equal to the size of the minimum class, and then, exponential kernel approximation is used to perform learning and KNN is used for classification. Exponential kernel approximation is the integration of exponential kernel with fuzzy rough sets.

Model 3: *Interval type-2 granulated under-sampling with neighborhood rough sets*—Model 3 is an extension of Model 1 where the Gaussian IT2 membership function is used for generating granulated feature and then, random under-sampling technique is employed.

Model 4: *Interval type-2 granulated under-sampling with exponential kernel approximation*—Model 4 is an extension of Model 2 where the Gaussian IT2 membership function is used for generating granulated feature and then, random under-sampling technique is employed.

5 Experimental Results and Discussion

This section presents the experimental results of the classification models over different benchmark data sets. In the present investigation, the performance of the different models with different combinations of rough- and fuzzy set-based strategies for imbalance learning is carried out. Four different combinations of classification models are considered for performance comparison, and obtained results are compared empirically with performance evaluation metrics.

The comparative experiments are carried out by tenfold cross validation. The data sets have been made by splitting the data sets as two parts for the selection of training and test instances for all classes. Each of these splitting sets is repeated ten times, and the average over splitting sets is considered.

The models based on under-sampling technique comprise strategy of neighborhood rough set (Model 1) and exponential kernel approximation (Model 2), and models based on interval type-2 granulated under-sampling technique comprise strategy of neighborhood rough set (Model 3) and exponential kernel approximation (Model 4). The performance evaluations metrics, *F*-measure and *G*-mean, values achieved by different models are tabulated in Table 2.

From Table 2, it is observed that performance metric *F*-measure produces better results for Model 2 when compared with Model 1 in all data sets except Sonar data set and when compared with granulated under-sampling methods, Model 3 is better for CC, Tumor, Wdbc, and Wpbc data sets, whereas Model 4 is better for Iono, Heart, Wine, Lym, German, and Sonar data sets.

From Table 2, it is found that *G*-mean achieves better results for Model 2 when compared with Model 1 for all data sets considered in the experimentation for performance metric *G*-mean except Sonar data set. Model 3 also performs better to the performance metric *G*-mean when compared with Model 4 for data sets (CC, Heart, Wpbc, Lym, and Sonar). Model 4 achieves better results for Iono, Tumor, Wdbc, Wine, and German data sets when compared with Model 3 for performance

Table 2 *F*-measure and *G*-mean achieved by different strategies

Data set	*F*-measure				*G*-mean			
	Model 1	Model 2	Model 3	Model 4	Model 1	Model 2	Model 3	Model 4
Iono	0.7825	**0.7855**	0.7948	**0.7995**	0.7007	**0.7065**	0.7266	**0.7686**
CC	0.7951	**0.8009**	**0.8760**	0.8034	0.6792	**0.7286**	**0.6671**	0.6496
Heart	0.7205	**0.7650**	0.7412	**0.7718**	0.6188	**0.6230**	**0.6110**	0.6076
Tumor	0.6290	**0.6519**	**0.6933**	0.6600	0.4524	**0.5197**	0.4823	**0.5123**
Wdbc	0.8548	**0.8607**	**0.8834**	0.8811	0.5443	**0.5607**	0.5272	**0.5758**
Wpbc	0.6852	**0.7110**	**0.7312**	0.7232	0.5221	**0.5316**	**0.6481**	0.5481
Wine	0.9221	**0.9267**	0.8963	**0.9804**	0.7990	**0.8189**	0.7938	**0.8042**
Lym	0.8650	**0.8909**	0.8666	**0.8923**	0.0016	**0.2316**	**0.3007**	0.2272
German	0.058	**0.7912**	0.9047	**0.9131**	0.0602	**0.0438**	0.8714	**0.8733**
Sonar	**0.9159**	0.8872	0.6443	**0.9020**	**0.9314**	0.9195	**0.9211**	0.8977

Optimal values are highlighted in bold

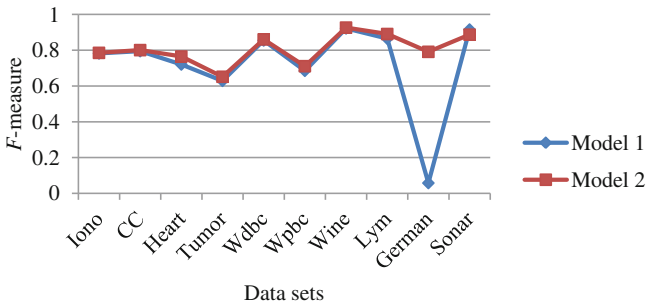

Fig. 2 *F*-measure of the two classification models

metric *G*-mean. Figures 2, 3, 4, and 5 show the plots of the performance of the classification models based on the complex numerical performance measures viz *F*-measure and *G*-mean.

From the graphical analysis, it is observed that Model 2 and Model 4 are performing better compared to Model 1 and Model 3 with respect to *F*-measure as depicted in Figs. 2 and 3. From Figs. 4 and 5, it is observed that Model 2 and Model 4 perform better as compared with models (Model 1 and Model 3) with respect to *G*-mean.

From the analysis of the experimental results with respect to *F*-measure and *G*-mean, it is observed that as a whole Model 2 (under-sampling with exponential kernel approximation) and Model 4 (Interval type-2 granulated under-sampling

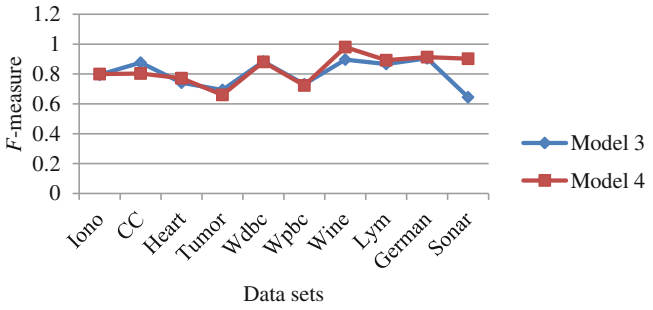

Fig. 3 *F*-measure of the two classification models

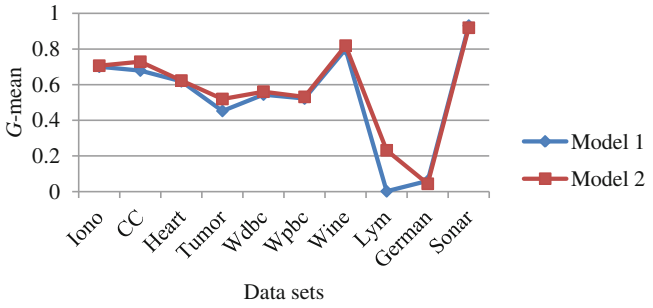

Fig. 4 *G*-mean of the two classification models

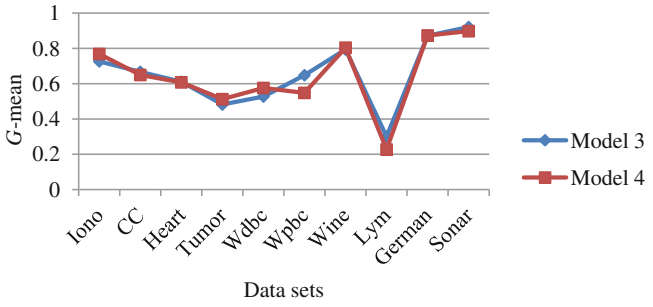

Fig. 5 *G*-mean of the two classification models

with exponential kernel approximation) perform better in comparison with Model 1 (under-sampling with neighborhood rough sets) and Model 3 (Interval type-2 granulated under-sampling with neighborhood rough sets) models for class imbalance learning, respectively.

6 Conclusion

In this paper, interval type-2 fuzzy granulation has been applied to the rough- and fuzzy set-based strategies for classification of imbalanced data and a model called rough fuzzy classification for class-imbalanced data is proposed. Superiority of the model is tested for appropriately determining the classification results, and it is seen from the experimental results that the proposed model outperforms the rough- and fuzzy set-based strategies for class imbalance learning for the considered UCI data sets. From the analysis of the experimental results, it is seen that under-sampling with exponential kernel approximation (Model 2) and Interval type-2 granulated under-sampling with exponential kernel approximation (Model 4) outperform the other models in terms of performance evaluation metrics for class imbalance learning.

Acknowledgment Author (RUM) gratefully acknowledges UGC for granting Maulana Azad National Fellowship for the research work.

References

1. Duda, R.O., Hart, P.E., Stork, D.G.: Pattern Classification, 2nd edn. Wiley, New York (2001)
2. García, V., Mollineda, R., Sánchez, J.: On the KNN performance in a challenging scenario of imbalance and overlapping. Pattern Anal. App. **11**, 269–280 (2008)
3. Chawla, N.V.: Data mining for imbalanced datasets: an overview. In: Data Mining and Knowledge Discovery Handbook, pp. 875–886 (2010)
4. Weiss, G.: Mining with rarity: a unifying framework. SIGKDD Explor. **6**(1), 7–19 (2004)
5. Drummond, C., Holte, R.C.: C4.5, class imbalance, and cost sensitivity: why under-sampling beats over-sampling. In: Chawla , N. et al. (eds.) Proceedings of ICML'03, Washington DC, USA (2003)
6. Pal, S.K., Skowron, A.: Rough-Fuzzy Hybridization: A New Trend in Decision Making. Springer, Singapore (1999)
7. Pal, S.K., Mitra, S.: Multilayer perceptron, fuzzy sets, and classification. IEEE Trans. Neural Netw. **3**, 683–697 (1992)
8. Pawlak, Z.: Rough sets. Int. J. Comput. Inf. Sci. **11**, 341–356 (1982)
9. Lin, T.Y.: Granulation and nearest neighborhoods: rough set approach. In: Pedrycz, W. (ed.) Granular Computing: An Emerging Paradigm, pp. 125–142. Physica-Verlag, Heidelberg (2001)
10. Hu, Q., Yu, D., Liu, J., Wu, C.: Neighborhood rough set based heterogeneous feature subset selection. Inf. Sci. **178**, 3577–3594 (2008)
11. Mazumder, R.U., Begum, S.A., Biswas, D.: An Exponential kernel based fuzzy rough sets model for feature selection. Int. J. Comput. Appl. (IJCA) **81**(6), 24–31 (2013)
12. Pawlak, Z.: Rough Sets: Theoretical Aspects of Reasoning about Data. Kluwer Academic Publishers, Dordrecht (1991)
13. Pawlak, Z., Skowron, A.: Rough sets: some extensions. Inf. Sci. **177**(1), 28–40 (2007)
14. Genton, M.: Classes of kernels for machine learning: a statistics perspective. J. Mach. Learn. Res. **22**, 99–312 (2001)
15. Zadeh, L.A.: Toward a theory of fuzzy information granulation and its centrality in human reasoning and fuzzy logic. Fuzzy Sets and Syst. **90**, 111–127 (1997)

16. Liang, Q., Mendel, J.M.: Interval type-2 fuzzy logic systems: theory and design. IEEE Trans. Fuzzy Syst. **8**(5), 535–550 (2000)
17. Blake, C., Merz, C., Hettich, S., Newman, D.J.: UCI repository of machine learning databases. University of California, School of Information and Computer Sciences, Irvine, CA (1998)
18. Chawla, N.V., Bowyer, K.W., Hall, L.O., Kegelmeyer, W.P.: SMOTE: synthetic minority oversampling technique. J. Artif. Intell. Res. **16**, 321–357 (2002)
19. Gu, Q., Zhu, L., Cai, Z.: Evaluation measures of the classification performance of imbalanced data sets. In: Cai, Z. et al. (eds.) Computational Intelligence and Intelligent Systems. Commun. Comput. Inf. Sci. **51**, 461–471 (2009)
20. Buckland, M., Gey, F.: The Relationship between recall and precision. J. Am. Soc. Inf. Sci. **45** (1), 12–19 (1994)
21. Kubat, M., Holte, R.C., Matwin, S.: Machine learning for the detection of oil spills in satellite radar images. Mach. Learn. **30**, 195–215 (1998)
22. Liu, J., Hu, Q., Yu, D.: A weighted rough set based method developed for class imbalance learning. Inf. Sci. **178**, 1235–1256 (2008)

Mind Reading by Face Recognition Using Security Enhancement Model

Vranda Vyas, Sameer Saxena and Deepshikha Bhargava

Abstract Face recognition has always been an area of interest for the researchers because it seems so fascinating in itself. As the time has passed, the evolution of human brain and social intelligence has enhanced the analysing power of a human brain for the displaying of face to infer the emotion accordingly. Face of a human being is considered to be the most common channel to read and infer the emotion in the case of mind reading. Theory of mind (ToM) is the inbuilt technique provided to every human being "as reported by Premack and Woodruff (Behav Brain Sci 1:515–523, 1991)". According to ToM, a person has the ability to read someone else' mind. Mind reading has a great amount of future advancement if worked upon with the different equipment and devices in the high-tech laboratories. The researchers have worked in this direction and have developed softwares. The aim of such software is to apply concept of security in face recognition but still there is a scope for improvement. This paper presents a comparative study between algorithms used for detecting the face as the key component in mind reading. Further, a model is proposed to enhance the security in face recognition. The proposed model also suggests interface that would help users to identify the people watching their pictures posted online.

Keywords SECJS · Socially intelligent interfaces · Emotional interfaces · Theory of mind · Facial feature analysis

V. Vyas (✉) · S. Saxena · D. Bhargava
Amity Institute of Information Technology,
Amity University Rajasthan, Jaipur, India
e-mail: vranda.vyas88@gmail.com

S. Saxena
e-mail: ssaxena1@jpr.amity.edu

D. Bhargava
e-mail: dbhargava1@jpr.amity.edu

K.N. Das et al. (eds.), *Proceedings of Fourth International Conference on Soft Computing for Problem Solving*, Advances in Intelligent Systems and Computing 335,
DOI 10.1007/978-81-322-2217-0_15

1 Introduction

Mind reading plays an important role in enhancing our ability to share our mental states. Building mind reading machines had a specific goal. It was to understand the mental and emotional state [2, 3] of a person and react accordingly with the help of computer-enabled technologies.

A person has the ability to read others' mind effortlessly. Theory of mind (ToF) [1, 4] gives it an intentional and goal-oriented framework. It represents the set of abilities of a person to read mind.

The most natural, powerful and versatile medium of communicating the wide range of mental states is human face. It involves both affective and intellectual component. With the increasing complexity of human–computer interaction, a new interaction paradigm is needed. The systems need to have socio-emotional intelligence. It would gather information autonomously about the user's state and to respond adaptively to it. Computer technology has yet no direct channel to infer the mental and emotional reaction. Also, it does not provide effective information about the cases of mind blindness. Facial and eye movements play an effective role in mind reading.

Earlier researches have left many areas to be worked on. This research paper discusses the comparison between algorithms being conducted to detect facial expressions. It also presents the idea about how the face recognition is interfering in our private life.

It is easy and essential to predict and perceive the behaviour of others in a crowd of people. But the ToF creates confusion in reading the mind of an animal and a human. Therefore, a different aspect is yet to be developed in human mind to solve the confusion [5, 6].

Considering some loopholes, the research model is also proposed in this paper. The paper is organized as follows: Sect. 2 elaborates about the literature review, Sect. 3 highlights the comparison of algorithms on the basis of static and dynamic images. In Sect. 4, further investigations and identification of the issues and the problems are discussed. In Section 5, a model is proposed named as security enhancement by collaborating Java and steganography (SECJS) to give a technical view to the problem. The conclusion and future work is also reported in Sect. 6.

2 Literature Review

The invention of EEG has made it possible to study the depth of the subject with the help of the computer and artificial intelligence. The emotions itself are the basis of a face. They have a huge impact on every human being. There is rationality that incorporates in a human being even in the presence of various machine–human interactions. This is the basis of the different error prone or unwanted outcomes that anyone would have experienced when a human and a machine interacts [7, 8].

The earlier researches also say that if we talk about figures, then we will come to know that the accuracy of the Cohn–Kanade database was dropped from 85 %(when

the users were already trained) to 60 % when the users were oblivious of the prototypes of the basic emotions. This is one of the bases of our comparison in this research.

Stephen Hawking, a physicist, who himself was surrounded by machines developed iBrain. It is a nearly black coloured head held band with a feather like device of the size of a matchbox. This simple looking device helps the person to communicate with others by merely thinking about it. It is the part of new generation of portable neural devices. It works on the concept of monitoring and diagnosing the conditions such as sleep, depression and autism [2, 9].

This invention was more emphasized on making the patients to go beyond the limit. Earlier they had to blink their eyes for communication. But with the invention of iBrain, communication became more easy and meaningful [10].

Also, at the University of Utah, the researchers use microelectrodes to decode the brain signals. This approach could ultimately help those who are 'locked in' (Lou Gehrig's disease) by disease and cannot communicate. But now, words can be read directly from patients' minds by attaching microelectrode grids to the surface of the brain. It helps them to learn about the signals generated. Later, they are converted to words. It can be an ultimate development for helping the patients who cannot speak. The patients know how to speak, but they cannot get signals from the brain. This ceases them to communicate correctly with their face and expressions [11].

3 Comparison Between Cohn–Kanade Algorithm in Static and Dynamic Environment

The comparison between general algorithm and Cohn–Kanade algorithms is shown in Figs. 1 and 2. The comparison was conducted with static images and dynamic images or videos, respectively. It analyses that the variations are seen much evident in the Cohn–Kanade algorithm.

The year 2000 was the time when Cohn–Kanade (CK) database was released for research purpose. It was useful for research in the automatic detection of facial expressions. Since that time, Cohn–Kanade database has been a widely used data test bed for the development of algorithms and their evaluation.

Following limitations were encountered during that period of time:

1. Validation of the action units exists but the same is not for the emotion labels.
2. Lack of common platform for evaluation of the algorithms.
3. The common database does not have any standard protocols.

Although the Cohn–Kanade database was used for the action units and emotion detection, it was lacking in:

The comparative study between various new algorithms and the existing benchmark algorithms.

As and when the data set is used with a random subset of the original database, it makes the analysis difficult.

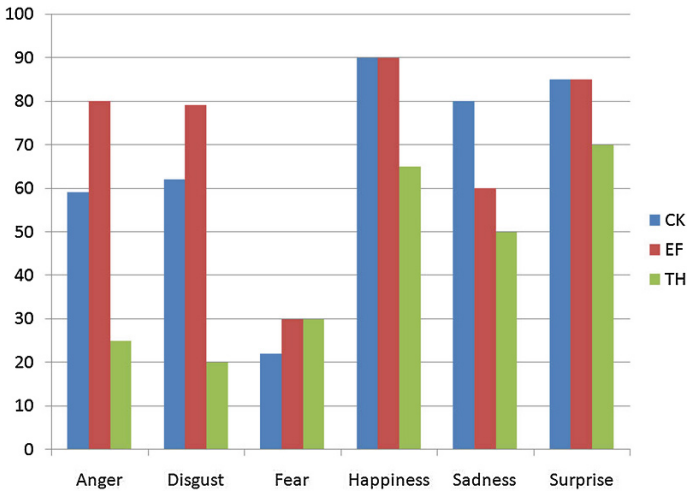

Fig. 1 The analysis of algorithms by showing dynamic images (videos)

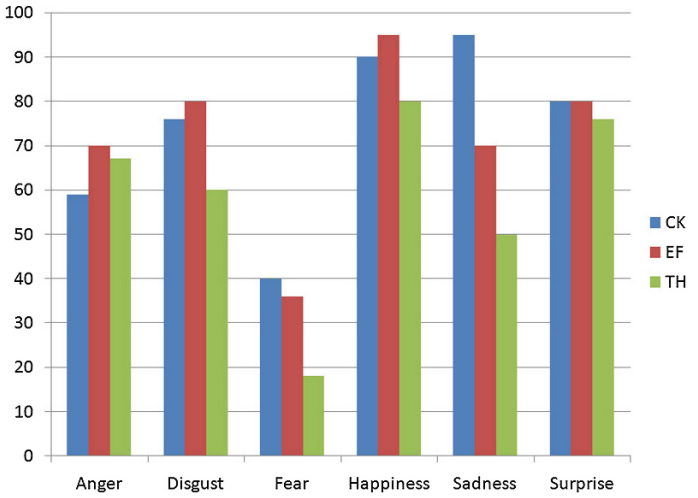

Fig. 2 The analysis of algorithms by showing static images

To work on the drawbacks discussed, an extended Cohn–Kanade (CK+) database was presented.

The results within the elevated database were as follows:

(a) In this new elevated database, the number of sequence was increased by 22 %.
(b) Number of subjects were also increased by 27 %.
(c) The expressions that are targeted were now much more revised. They were validated in terms of emotion labels and also fully coded by FACS.

4 Limitations

Earlier conducted researches have proved that the development of the technology of face recognition has its pros and cons. It has on the one hand created a varied advantage, but on the other hand, it is ceaselessly breaching into our private life. Various researchers say that we are on the verge of being virtually cloth less. We are uploading various images and other data online with our own interest and knowledge. What we do not know is the sensitive issues that can arise without our knowledge. The related researches have been conducted regarding the issue. As a result, 30 % of the random pictures clicked were identified by the face recognition software. By the data mining techniques, the social security numbers were also identified.

5 Proposed Model—Security Enhancement by Collaborating Java and Steganography (SECJS)

This paper proposes a model to enhance security in face recognition. The model also suggests an interface that would help the users identify the people watching their pictures posted online. The working of this model is explained as follows:

1. A user uploads an image through the interface suggested in the model.
2. When the image is downloaded or even visited, the information of the visitor is saved.
3. IP address, host name or even the location can be trapped in the form of information with the help of Java platform.

Further, the information attained is encrypted in the image itself with the help of image steganography. Later, the user can copy the URL of the particular image and paste it in the given interface. As the user clicks on the button named decrypt, all the visitors' list will appear in the given list box.

This will enhance the security up to a smaller level. For this, we need to have detailed knowledge of Java and also know the concepts of steganography. It is necessary because if we know them separately, then only we can collaborate them with the help of the proposed logical models (Fig. 3 and Fig. 4).

In the interfaces shown in Figs. 5 and 6, we have to track two type of events: click_event() and keyboard_event(). The click_event() will help us track the person trying to download the image. Whereas the keyboard_event() will work in the case of the use of print screen. Both the methods will help us track the IP and hostname and also the location of the connecting client if required.

The control points involved in it are as follows:

(a) Cyber ethics
(b) Proxy server
(c) Disconnection of JavaScript by the browser.

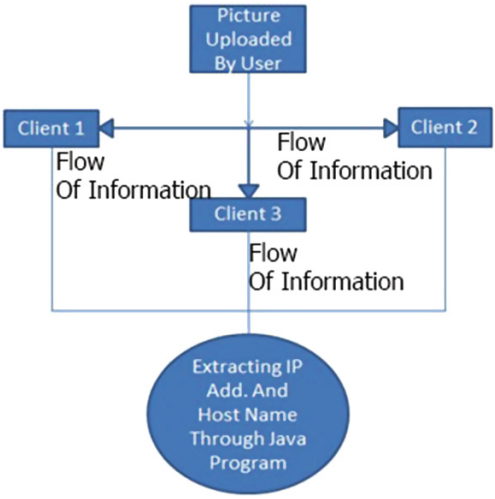

Fig. 3 IP address and host names extracted from the client through Java program

Fig. 4 Image steganography used to encrypt information within the image

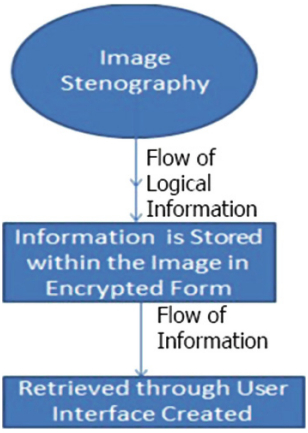

This research is an attempt towards enhancing the security through the proposed model and suggested interfaces; however, there is still lots of scope towards its future research.

6 Conclusion and Future Work

The principle contribution of this paper is the comparative study conducted on the two algorithms. The security issues that came forward in the work face recognition is also proposed through a model. This is an attempt to report promising research directions that include:

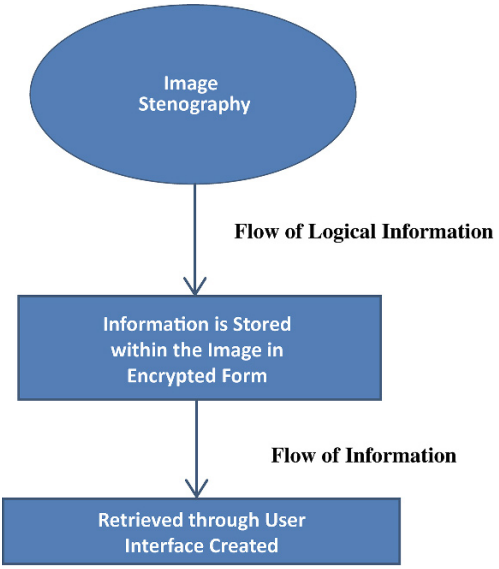

Fig. 5 The interface which will help the user to upload an image

Fig. 6 The interface through which every user can know the viewers of the image

1. Working on the data set given by the CK and CK+ databases so as to get a comparative result.
2. Trying to apply the interface and the model proposed on a smaller level to check its working structure.

By recognizing mental states beyond the basic emotions, the scope of applications can be extended in which facial analysis systems can be integrated. This paper

presents a multidisciplinary study on the how information posted online can be harmful. An evolutionary scenario is also proposed in which humans have evolved a ToM owing to the complexity of social relationships. We believe that the evolution of the recursion level in a ToM is crucial for the fundamental human traits. There must be a close relationship between the evolution of the recursive structure, and the origin of language, especially the evolution of grammar, which would be a significant issue to be considered. Hence, if the work continuously undertaken in this way, it can keep a check on who is breaching our privacy.

References

1. Premack, D., Woodruff, G.: Does the chimpanzee have a theory of mind? Behav. Brain Sci. **1**, 515–523 (1991)
2. Bhargava D., Saxena S.: RoHeMaSys: Medical Revolution with Design and Development of Humanoid for Supporting Healthcare. Advances in Intelligent Systems and Computing, Proceedings of the Third International Conference on Soft Computing for Problem Solving. Springer India, vol. **258** pp. 133-142 (2014)
3. Bhargava, D., Sinha, M.: Performance analysis of agent based IPSM. International Joint Conference on Computer Science and Software Engineering (JCSSE), pp. 253–258, IEEE (2012)
4. Masanori, T., Arita, T.: Asymmetry between even and odd levels of recursion in a theory of mind. In: Proceedings of ALIFE X, pp. 405–411 (2006)
5. Corballis, M.C.: Recursion as the key to the human mind. In: Sterelny, K., Fitness, J. (eds.) From Mating to Mentality: Evaluating Evolutionary Psychology, pp. 155–171. Psychology Press, New York (2003)
6. Dunbar, R. On the origin of the human mind. In: Carruthers, P., Chamberlain, A. (eds.) The Evolution of Mind, pp. 238–253. Cambridge University Press, Cambridge (2000)
7. El Kaliouby, R., Robinson, P.: Mind reading machines: automated inference of cognitive mental states from video. IEEE International Conference on Systems, Man and Cybernetics, vol. 1, IEEE (2004)
8. Petersen, M.K. et al.: Smartphones get emotional: mind reading images and reconstructing the neural sources. In: Affective Computing and Intelligent Interaction, pp. 578–587. Springer, Berlin (2011)
9. Golan, O., Baron-Cohen, S.: Systemizing empathy: teaching adults with Asperger syndrome or high-functioning autism to recognize complex emotions using interactive multimedia. Dev. Psychopathol. **18**(02), 591–617 (2006)
10. Fattouh, A., Odile, H., Guy, B.: Emotional BCI control of a smart wheelchair. Int. J. Comput. Sci. Issues (IJCSI) **10**, 3 (2013)
11. Barkow, J.H., Cosmides,L.E., Tooby, J.E.: The Adapted Mind: Evolutionary Psychology and the Generation of Culture. Oxford University Press, Oxford (1992)
12. Bhargava D., Sinha M.: Design and implementation of agent based inter process synchronization manager. Int.J. Comput. Appl. (IJCA) **46**, 21 (2012). doi: 10.5120/7065-9670

Enhancement of Power Transfer Capability of HVDC Transmission System Using Fuzzy Logic Controller

M. Ramesh and A. Jaya Laxmi

Abstract To handle bulk of power, the AC power transmission is not economical over long distance. High-voltage direct current (HVDC) transmission system is selected as the alternative not only in economic aspects but also in stability point of view. But the operation and control of HVDC links pose a challenge for the designers to choose the proper control strategy under various operating conditions. Traditionally, PI controllers are used for the rectifier current control of the HVDC system, but due to fixed proportional (P) and integral (I) gains, these controllers can perform well only over a limited operating range. However, in controlling a non-linear plant such as the firing angle of the rectifier side in HVDC system, the model controls such as fuzzy logic controllers show better performance to the dynamic disturbances than traditional PI controllers. The CIGRÉ model as one of the conventional methods has been studied and improves the stability HVDC system.

Keywords HVDC transmission · CIGRÉ benchmark model · Faults in HVDC system · Proportional integral (PI) controller · Fuzzy logic controller (FLC)

M. Ramesh (✉)
EEE Department, Medak College of Engineering and Technology,
Kondapak, Medak District, India
e-mail: marpuramesh223@gmail.com

M. Ramesh
EEE Department, JNTU, Anantapur 515002, Andhra Pradesh, India

A.J. Laxmi
Department of EEE, Jawaharlal Nehru Technological University,
College of Engineering, Kukatpally, Hyderabad 500085, Andhra Pradesh, India
e-mail: ajl1994@yahoo.co.in

K.N. Das et al. (eds.), *Proceedings of Fourth International Conference on Soft Computing for Problem Solving*, Advances in Intelligent Systems and Computing 335,
DOI 10.1007/978-81-322-2217-0_16

1 Introduction

High-voltage direct current (HVDC) power transmission system offers several advantages, one of which is to rapidly control the transmitted power. Therefore, they have a considerable impact on the stability of the AC systems. Moreover, HVDC link is effective for frequency control and improves the stability of the system. The importance of AC–DC power transmission systems regarding improvement of stability and the HVDC transmission link is highly controllable. It is possible to take benefit of this unique characteristic of the HVDC link to augment the stability of the AC systems. A proper design of the HVDC controls is essential to ensure satisfactory performance of overall AC/DC system [1, 2]. The main objective of DC link controllers at either end (rectifier and inverter) is to operate the link efficiently under normal and abnormal conditions. The control of an HVDC transmission system is greatly influenced by the AC/DC system strength. The AC/DC system strength is defined by the relative term "short circuit ratio (SCR)" [3]. The SCR can be expressed as follows:

$$\text{SCR} = \frac{\text{Short Circuit MVA of AC System}}{\text{DC Converter MW Rating}}$$

An SCR value of three or above indicates the strong AC system, and the SCRs of weak and very weak AC systems range between three and two and below two, respectively [4–8]. The output of fuzzy logic controller can be utilized to modulate the power order of the DC control, which in turn modulates the DC power. The stabilizing control is implemented through large signal modulation of power in response to a control signal derived from the AC system variables. The effectiveness of the control can be enhanced by increased overload rating of the converters which permit short-term overloads. In this paper, apart from PI controller, a fuzzy logic-based controller is developed to improve power transfer capability of HVDC system.

2 HVDC System Model

Figure 1 represents the HVDC test system. The system is modeled in MATLAB/Simulink simulation package and is connected to an AC system having a SCR of 2.5. In this model, two 6-pulse converters are connected in series (bipolar 6-pulse converter) instead of a 12-pulse converter. In a real system, 12-pulse converters are used but bipolar 6-pulse converter is used here for simplicity and ease of computation. The HVDC transmission test system is composed of three sub-systems, as given below:

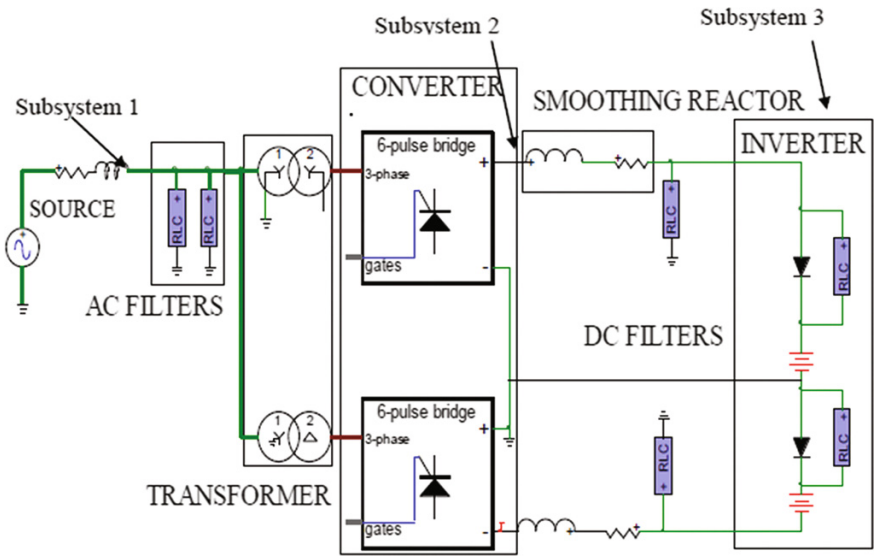

Fig. 1 Six-pulse bipolar HVDC system

1. *Sub-system 1*
   A fixed *R–L* impedance (R = 2,160 Ω and L = 150.8 mH) between the generation source and the converter bus is used in this model. In addition to this, AC filters are also used to provide reactive power required by the converter units as reactive power consumption of the converter changes with the change in load. Source voltage of 345 kV at 50 Hz is used for the AC side of the system.
2. *Sub-system 2*
   The DC side of the converter has a nominal voltage of 500 kV supplied by the inverter. The DC current is kept constant at 2,000 A with nominal DC power (P_d) of 1,000 MW. Two smoothing reactors located at the rectifier side (L_d = 597 mH) are used.
3. *Sub-system 3*

This sub-system refers to the inverter DC system. The inverter is only represented by fixed batteries of ±208.6 kV with a diode in series. The diode prevents any backflow during a DC fault as the diode is reverse biased to the current flow during DC fault. RC snubbers (R = 2,000 Ω and C = 0.1 μF) are also used in parallel with the diode. Here, the inverter-side representation is simplified as the study focus is on the rectifier side and its controller.

Error, no overshoot and load disturbances are rapidly rejected and variations of some of the motor parameters are fairly well dealt with become too high and will destabilize the system. To overcome this problem, we propose the use of a limiter ahead of the PI controller [10]. This limiter causes the speed error to be maintained within the saturation limits. Figure 4 shows the structure of PI controller.

3 Conventional CIGRÉ HVDC Benchmark System

The conventional CIGRÉ HVDC benchmark system shown in Fig. 2 was proposed in [10]. The system is a monopolar 500 kV, 1,000 MW HVDC link with 12-pulse converters on both the rectifier and inverter sides, connected to weak AC systems (short circuit ratio of 2.5 at a rated frequency of 50 Hz) that cause a considerable degree of difficulty for DC control. Damped filters and capacitive reactive compensation are also provided on both sides.

In the converter, the power circuit consists of the following sub-circuits.

(a) AC side
The AC side of the HVDC system consists of supply network, filters, and transformers on both sides of the converter. The AC supply network is referred by a Thevenin equivalent voltage source with equivalent source impedance. To absorb the harmonics produced by the converter as well as to supply reactive power to the converter, AC filters are used.

(b) DC side
The DC side of the converter consists of smoothing reactors for both the rectifier and inverter side. The DC transmission line is referred by an equivalent *T* network, which can be adjusted to fundamental frequency to provide a difficult resonant condition for the modeled system.

(c) Converter

The converter stations are represented by 12-pulse configuration with two six-pulse valves in series. The control model mainly consists of firing angle (α) and extinction angle (γ) measurements and generation of firing signals for both the rectifier and inverter. The rectifier control system uses constant current control

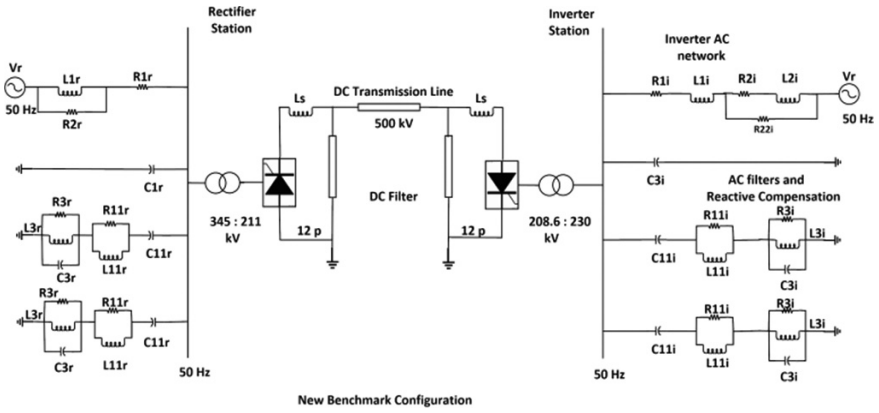

Fig. 2 Single-line diagram of the CIGRÉ benchmark HVDC system

(CCC) technique. DC current on the rectifier side is measured using proper transducers and passed through necessary filters before they are compared to produce the error signal. The error signal is passed then through a PI controller, which produces the required firing angle order [9]. The relationship between DC current I_d and delay angle α is obtained as follows:

The DC voltage at the rectifier is given by

$$V_{dr} = V_{dor} * \cos \alpha - X_{cr} * I_d \tag{1}$$

For constant I_d and small changes in angle α, we have

$$\frac{\Delta V_d}{\Delta \alpha} = -V_{do} * \sin \alpha \tag{2}$$

The relationship between DC current I_d and alpha is given by

$$I_d = \frac{V_{dor} * \cos \alpha - V_{doi} * \cos \gamma}{R_{cr} + X_{cr} - X_{ci}} \tag{3}$$

Equation (3) is only valid under steady-state conditions due to assumptions made in its derivation, and therefore, the plant dynamics are not indicated. If the inverter DC voltage is maintained constant by controlling gamma (CEA control), then the DC current is a function of cos α, i.e., a nonlinear relationship. This implies that the loop gain will be lowest for $\alpha = 90°$ resulting in no optimal dynamic properties for nominal values of $\alpha = 12°$ to $18°$.

(d) *Inverter Control*

The extinction angle control (γ) and current control have been implemented on the inverter side. The CCC with voltage-dependent current order limiter (VDCOL) has been used here through conventional (PI) controllers. For the current control, the reference limit is obtained through a comparison of the external reference and VDCOL output. The measured current is then subtracted from the reference limit to produce an error signal that is sent to the PI controller to produce the required alpha angle order. The extinction angle control (γ) uses another PI controller to produce gamma angle order for the inverter. Comparing the two angle orders, minimum is used to calculate the firing instant [8]. Figure 3 shows the simulated HVDC system with PI controller using MATLAB/Simulink.

PI controllers are commonly used in HVDC system in addition to AI controllers. A mathematical model of the real plant is required for the controller design with conventional methods. The difficulty of identifying the accurate parameters for a complex nonlinear and time-varying nature of real plants may render, in many cases, the fine tuning of parameters which is time consuming. Figure 4 shows the structure of PI controller.

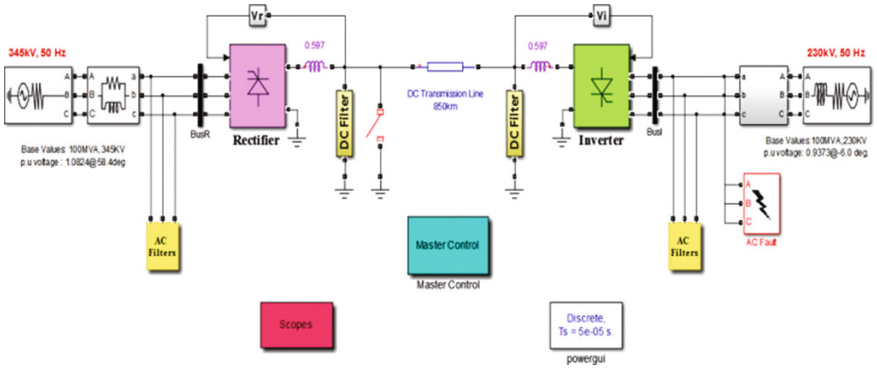

Fig. 3 HVDC system with PI controller

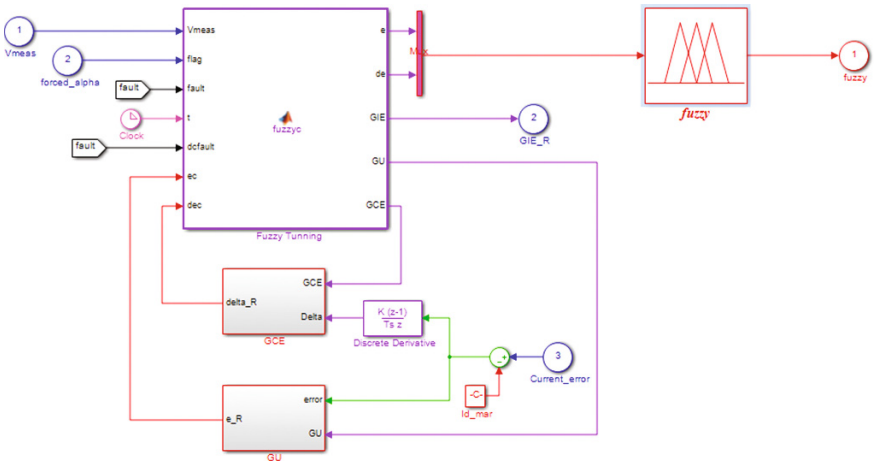

Fig. 4 Fuzzy controller design

4 Fuzzy Logic Controller

HVDC systems have the ability to rapidly control the transmitted power. Therefore, they have a considerable impact on the stability of the AC systems. Apart from conventional controllers (such as P, PI, and PID), numerous modern control techniques are reported in literature and already used in several AC–DC systems for deriving the necessary modulation signals to respective control schemes [4–7]. In this paper, apart from conventional PI controller, a fuzzy logic-based controller is developed to modulate the power order of the DC power. In this paper, defuzzifing of output signals is used for centre of gravity methods is used [6]. The fuzzy rules are summarized in Table 1. The rules show that using three-input membership functions (P, Z, N) and three-output membership functions (P, Z, N) will provide the necessary

Table 1 Fuzzy rules for fault clearing decision

		Error		
Error rate of change		*P*	*Z*	*N*
	P	*P*	*P*	*Z*
	Z	*P*	*Z*	*P*
	N	*Z*	*N*	*N*

functionality. The rules dictate that the results of each input membership function are combined using the AND operator, which corresponds to taking the minimum value. Fig. 4 shows the fuzzy controller design, respectively.

5 Simulation Results

The rectifier and the inverter are 12-pulse converters which are two universal bridge blocks connected in series. The rectifier and the inverter are interlinked through an 850-km line and 0.597 H smoothing reactors as shown in Fig. 3. The transformer tap position is rather at a fixed position determined by a multiplication factor applied to the primary nominal voltage of the converter transformers (1.01 on the rectifier side, 0.989 on the inverter side). The HVDC transmission link uses 12-pulse thyristor converters. Two sets of 6-pulse converters are needed for the implementation stage. The HVDC converters with thyristor valves will be assembled in a converter bridge of twelve-pulse configuration. This is accomplished by star–delta connection and star–star connection. Reduction of harmonic effects is another factor of investigation. Here, MATLAB/Simulink program is used as the simulation tool and two 6-pulse Graetz bridges are connected in series to form a 12-pulse converter. The two 6-pulse bridges are 345 kV, 50 Hz totally identical except there is an in-phase shift of 58.4° for the AC supply voltages. Some of the harmonic effects are cancelled out with the presence of 60° phase shift. The control of power can be achieved by two ways, i.e., by controlling the voltage or by controlling the current. It is crucial to maintain the voltage in the DC link constant and only adjust the current to minimize the power loss. The filters provide reactive power compensation for the rectifier consumption because of the firing angle.

1. *Without Fault*
   Figs. 5 and 6 show the system with no fault in voltage and current waveforms at rectifier and inverter side, respectively, using PI and fuzzy logic controller. From the simulation results, it is observed that DC voltage and current reach the reference value of 1.0 Pu at 0.4 s, i.e., about 0.1 s later after starting HVDC system. It is clear that for no fault, both the controllers perform well, but the fuzzy logic controller gives a better transient performance and quite a low overshoot as compared to the conventional PI controller. The complete HVDC system reaches stable state after 0.4 s.

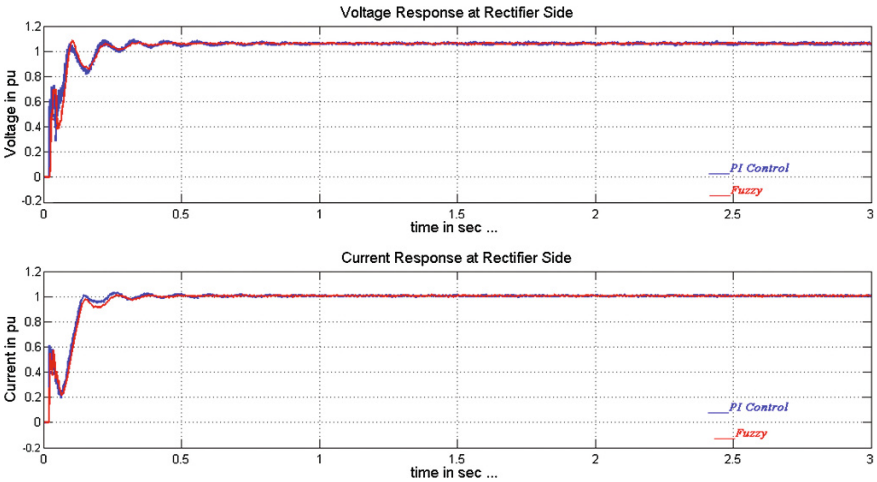

Fig. 5 Voltage and current on the DC side at rectifier

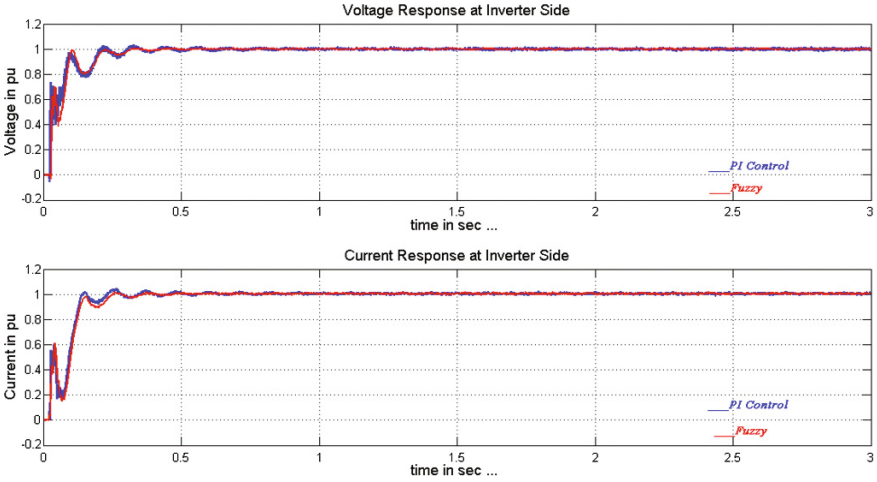

Fig. 6 Voltages and current at inverter

Figure 7 shows the change process of the active power of HVDC system without fault with PI controller and with fuzzy control. It is clear that for no fault, both the controllers perform well, but the fuzzy logic controller gives a better transient performance and quite a low overshoot as compared to the conventional PI controller.

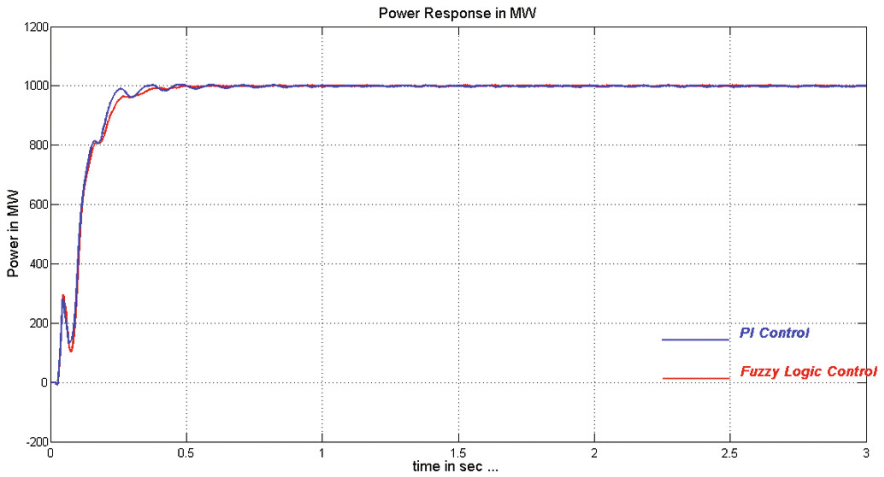

Fig. 7 Active powers at rectifier

2. *With Faults*
   In Figs. 8 and 9, it is observed that DC fault occurs at rectifier and inverter side of HVDC system, respectively. The PI controller and fuzzy logic controllers activate and clear the fault. Figures 8 and 9 show the waveforms after 0.6s DC fault occurrence at the rectifier and inverter. A large number of oscillations have been observed in DC link current and voltage magnitudes in case of a conventional controller. From the rectifier and inverter voltage plots, it is clear that in case of conventional controller, the rectifier and inverter valves undergo

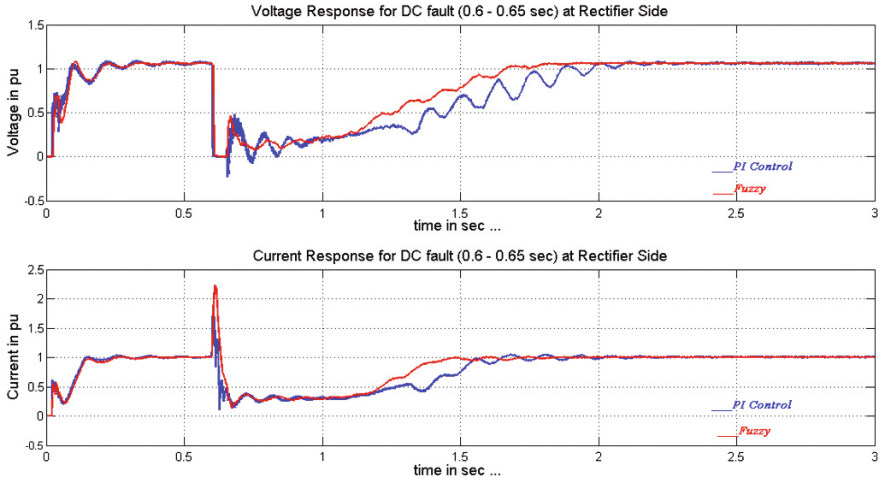

Fig. 8 When DC fault occurs at rectifier

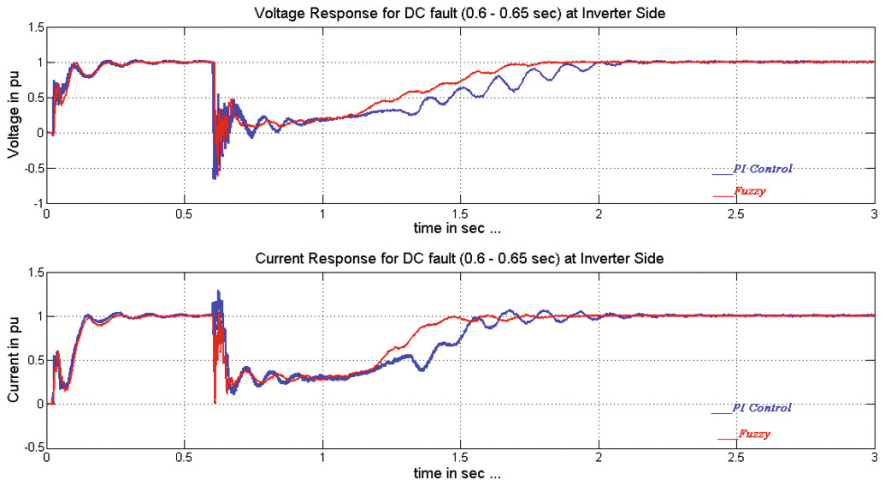

Fig. 9 When DC fault occurs on inverter

commutation failure several times as compared with fuzzy logic controller. Fuzzy logic controller reduces the recovery time by 1.7s after the disturbance.

Figure 10 shows the change process of the active power of HVDC system after a disturbance of a DC fault with PI controller and with fuzzy logic controller. It is clear that for DC fault, both the controllers perform well, but fuzzy logic controller gives a better transient performance and quite a low overshoot as compared to the conventional PI controller.

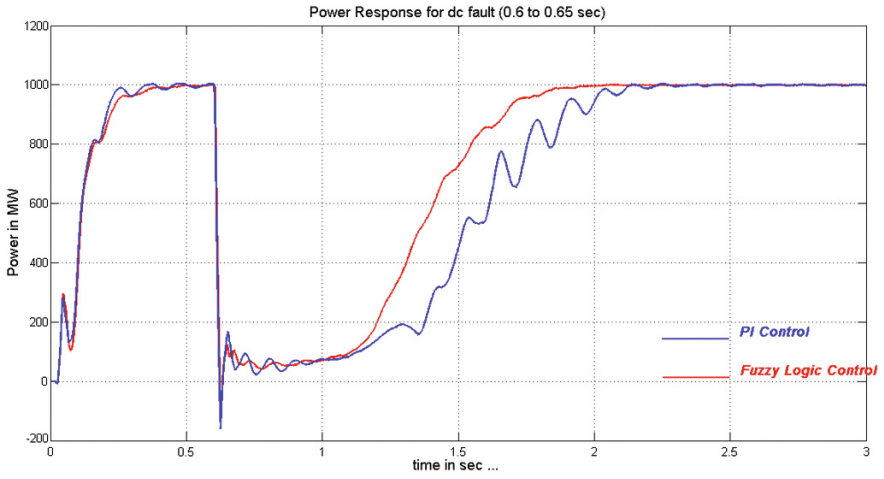

Fig. 10 Active power when DC fault occurs

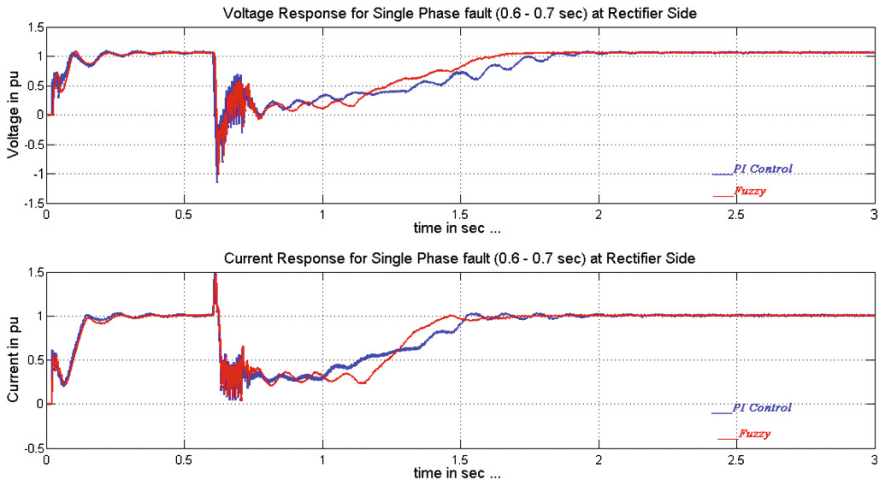

Fig. 11 When a line-to-ground fault occurs on rectifier side

In Figs. 11 and 12, it is observed that a line-to-ground fault occurs on rectifier and inverter side of HVDC system, respectively. The fuzzy logic controller activates and clears the fault. The fuzzy logic controller performs better than the fixed-gain PI controller. The fixed-gain PI controller takes longer time to recover after fault is cleared due to the narrow range of optimum controller gain parameters. On the other hand, the fuzzy logic controller has the ability to extend its optimum range of gain parameters depending on the system contingencies. Fuzzy logic controller reduces the recovery time by 1.6s after the disturbance.

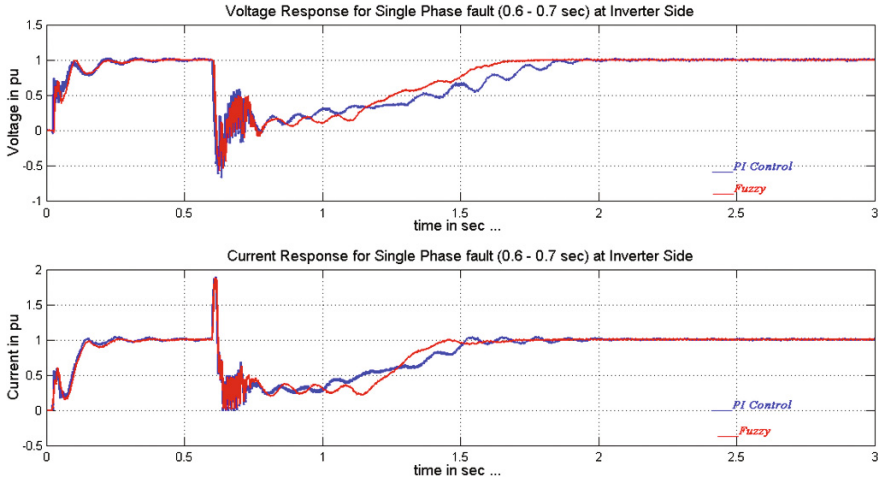

Fig. 12 When a line-to-ground fault occurs on inverter side

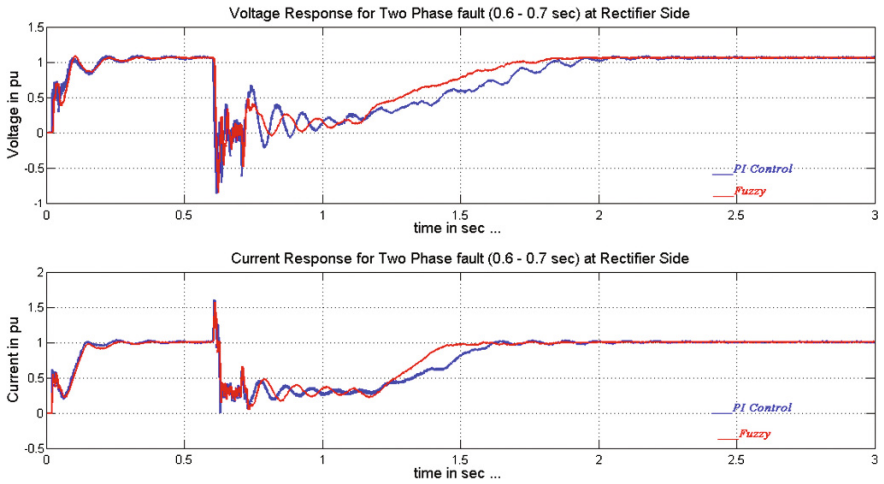

Fig. 13 When a line-to-line fault occurs on rectifier side

In Figs. 13 and 14, it is observed that a line-to-line fault occurs on rectifier and inverter side of HVDC system, respectively. The fuzzy logic controller activates and clears the fault. The fuzzy logic controller performs better than the fixed-gain PI controller. The fixed-gain PI controller takes longer time to recover after fault is cleared due to the narrow range of optimum controller gain parameters. On the other hand, the fuzzy logic controller has the ability to extend its optimum range of gain parameters depending on the system contingencies. Fuzzy logic controller reduces the recovery time by 1.6s after the disturbance.

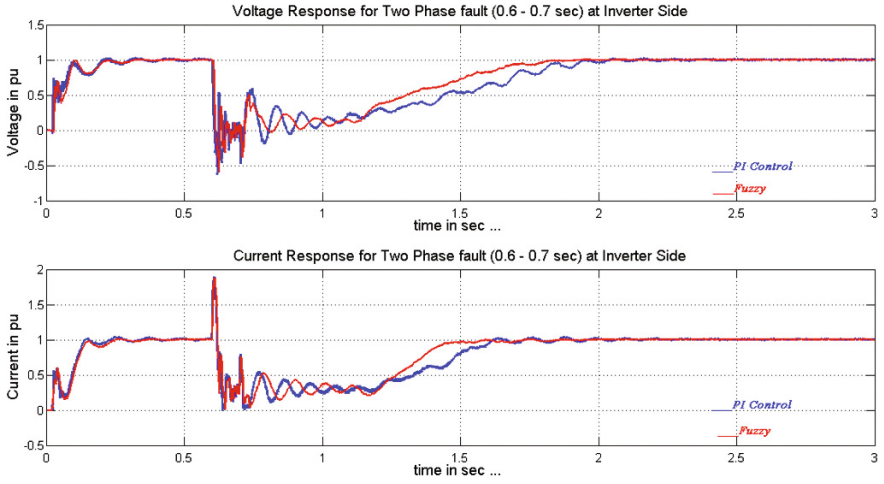

Fig. 14 When a line-to-line fault occurs on inverter side

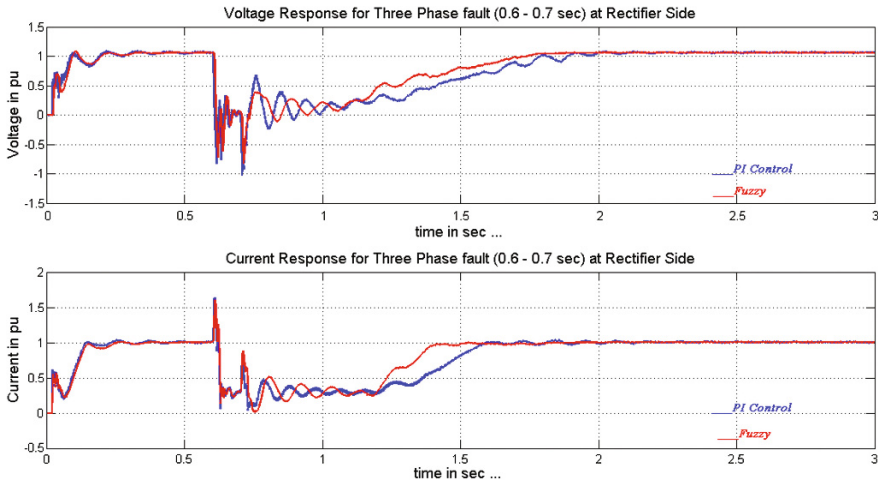

Fig. 15 When a three-phase fault occurs on rectifier side

In Figs. 15 and 16, it is observed that a three-phase fault occurs on rectifier and inverter side of HVDC system, respectively. The fuzzy logic controller activates and clears the fault. The fuzzy logic controller Performs better than the fixed-gain PI controller. The fixed-gain PI controller takes longer time to recover after fault is cleared due to the narrow range of optimum controller gain parameters. On the other hand, the fuzzy logic controller has the ability to extend its optimum range of gain parameters depending on the system contingencies. Fuzzy logic controller reduces the recovery time by 1.6s after the disturbance.

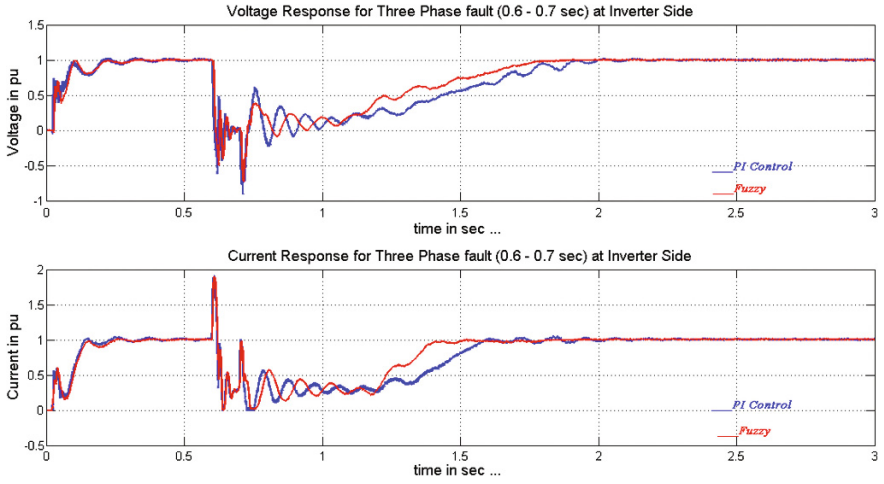

Fig. 16 When a three-phase fault occurs on inverter side

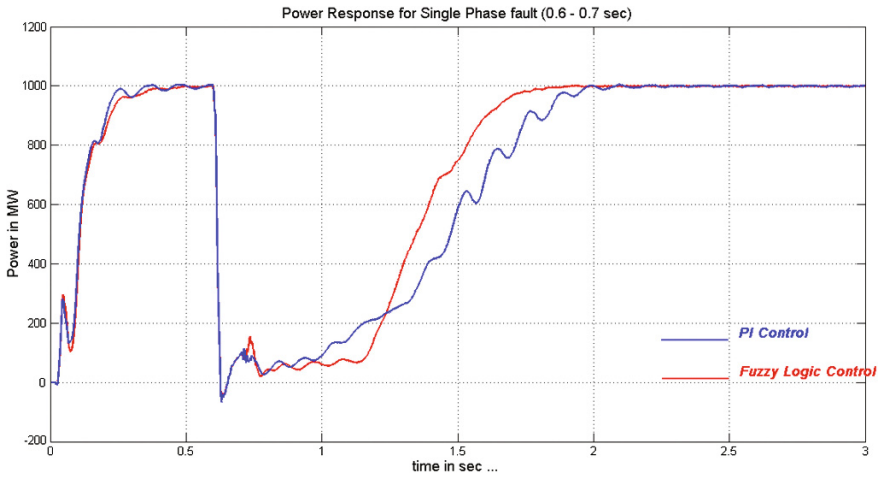

Fig. 17 Active power when a line-to-ground fault occurs

Figures 17, 18, and 19 shows the change process of the active power of HVDC system after a line-to-ground fault, line-to-ground fault and three-phase fault that occurs and how these faults are cleared using PI and the fuzzy logic controller. It is clear that both the controllers perform well but the fuzzy logic controller gives a better transient performance and quite a low overshoot as compared to the conventional PI controller.

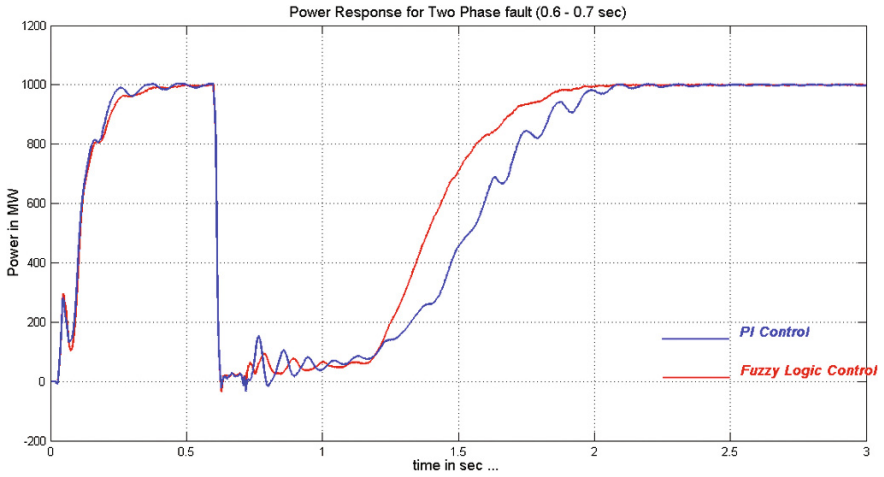

Fig. 18 Active power when a line-to-line fault occurs

Fig. 19 Active power when a three-phase fault occurs

6 Conclusion

For HVDC links where very large transient conditions are involved in the plant operation, it is more convenient to improve the PI control strategy rather than to work out complicated dynamic models which require sophisticated control strategies. The application of the linguistic rules is in fact simpler than sophisticated identification and optimization procedures. The implementation of fuzzy logic controller is also less complicated than that of optimization algorithms. In the system start-up process, the system controlled by fuzzy logic controller has much sharper reaction with the change and much smaller amplitude of starting and overshoot. Compared with the traditional PI controller, the fuzzy logic controller has higher accuracy and faster response to speed. This work shows the potential of the fuzzy logic controller scheme for a HVDC system. Fuzzy logic controller provides a more intelligent solution to the control of HVDC systems as compared to the conventional PI controller.

References

1. Kundur, P.: Power System Stability and Control. McGraw- Hill Inc., New York (1994)
2. Huang, G.M., Vikram, K.: HVDC Controls for Power System Stability, pp 597–602. IEEE Power Engineering Society (2002)
3. CIGRE WG 14.07.: Guide for planning DC lines terminating at AC systems locations having low short circuit capacities, Part I: AC-DC interaction phenomena (1992)
4. Hsu, Y.Y., Wang, L.: Damping of a parallel ac-dc power system using PID power system stabilisers and rectifier current regulators. IEEE Trans. Energy Convers. **3**(3), 540–547 (1988)

5. Emarah, A.S., Choudhry, M.A., Galanos, G.D.: Design of optimal modulation controllers for multi-area AC/DC systems using eigen value sensitivities. IEEE Trans. Power Syst. **PWRS-2** (3), pp. 522–528 (1987)
6. Dash, P.K., Liew, A.C., Routray, A.: High performance controllers for HVDC transmission links. IEE Proc. Gener. Transm. Distrib. **141**(5), 422–428 (1994)
7. To, K.W.V., David, A.K., Hammad, A.F.: A robust coordinated control scheme for HVDC transmission with parallel ac systems. IEEE Trans. Power Delivery **9**(3), 1710–1716 (1994)
8. Routray, A., Dash, P.K., Panda, S.K.: A fuzzy self-tuning pi controller for HVDC links. IEEE Trans. Power Electron. **11**(5), 669 (1996)
9. Rashid, M.H.: Power Electronics Handbook. Academic Press, New York (2001). ISBN 978-0125816502
10. Rao, S.: EHV-AC, HVDC, transmission and distribution engineering, 3rd edn. Khanna Publishers, New Delhi (1999)

Optimization of Clustering in SPIN-C and LEACH for Data Centric Wireless Sensor Networks

Ashutosh Tripathi, Narendra Yadav and Reena Dadhich

Abstract Routing the data in wireless sensor network (WSN) is a main issue in the guaranteed data transmission. Contextually, many algorithms consider the power and resource limitation, energy efficiency, scalability, attributes and location based with the assumption of homogeneous and heterogeneous distribution of nodes for data transferring. Therefore data dissemination is required to provide the effective data transmission from source node to sink node. This paper introduces the cluster head selection scheme used in SPIN to efficiently disseminate observations gathered by individual sensor nodes in the network. The paper proposes the cluster head selection scheme used in SPIN protocol and evaluated the performance of proposed protocol to prolong the time interval from the start of network operation till the death of the first node which is important reliable issues in wireless sensor networks for many feedback applications. The scheme is implemented and simulated with LEACH in NS2.34. Simulation shows proposed protocol exhibits significant performance gains over the LEACH for lifetime of network and guaranteed data transmission.

Keywords Wireless sensor networks · Clustering · Energy efficacy · SPIN · Data gathering · Routing protocol

A. Tripathi (✉)
Department of ECE, Amity University Rajasthan, Jaipur, India
e-mail: ashu20034@gmail.com

N. Yadav
Department of CSE, Sri Balaji Technical Campus, Jaipur, Rajasthan, India
e-mail: narensinghyadav@yahoo.com

R. Dadhich
Department of CSI, University of Kota, Kota, Rajasthan, India
e-mail: reena.dadhich@gmail.com

K.N. Das et al. (eds.), *Proceedings of Fourth International Conference on Soft Computing for Problem Solving*, Advances in Intelligent Systems and Computing 335,
DOI 10.1007/978-81-322-2217-0_17

1 Introduction

A wireless sensor network [1–3] consists of a large number of nodes with redundancy existing in data sensing from environment, data gathering from the nodes, aggregation of processed data, etc. The improvement in redundant capability of nodes is feasible by improving the assignments of roles and protocol level setting to nodes. Decisions concerning role assignment should be made based on node properties including location in the environment (absolute and relative to other nodes), sensing capabilities, energy supply, and processing capabilities.

In WSN, each node guarantees delivery of specific information to a destination node after specific and typical process. Any node in the network can easily transmit the data packet; if it may have enough battery power during the process of data delivery from the source to destination but during the transmission, the large amount of energy is required. After every intermediate transmission, the remaining energy of the node decreases because of decreasing energy of the node. Decreasing of energy may tend to exhaust leading to dead node. To overcome this problem, data should be routed in a manner such that energy expenditure during transmission among the nodes is less to reserve their energy, instead of routing the data to a path that maximizes energy expenditure. One of the factors which make sensor networks more fault-tolerant is energy backup. If the sensor node has sufficient energy, it would be able to remove itself from failure.

In this paper, C-SPIN (cluster version of SPIN protocol) scheme is proposed. This scheme guarantees the data delivery to base station. For transferring the data, this scheme does not send the data packet throughout the network but clustering algorithms used for same. In proposed scheme, total number of packet transmissions is less. Therefore, a significant amount of total energy can be saved. C-SPIN protocol is implemented using TCL/C++ programming language and evaluated using NS2.34 simulator.

The rest of the paper is organized as follows: In Sect. 2, related work of SPIN family of protocols is given. Section 3 describes the problem statement and proposed solution. Section 4 describes simulation results and performance analysis of C-SPIN protocol and comparison with LEACH protocol. Finally, in Sect. 5, The paper conclude with a discussion on some future work that we have planned for beyond and what is presented here.

2 Related Works

SPIN protocol as discussed in [4, 5] is used in data dissemination from individual sensor node to all sensor nodes in the network. It is a data centric routing protocol. Each sensor node has its own resource manager that keeps track of resource consumption. In SPIN, the way that data queries and forwarded to base station is important aspect and decides the lifetime of SPIN protocol. Due to single hop approach, many nodes deplete their energy soon. This protocol has replaced the classic flooding in

which source node sends its data to all its neighbors. Based on receiving packet of data, each node stores and then sends a copy of the data to all its neighbors. Approach of this protocol is overcome of implosion, overlap, and resources blinding.

In paper [4, 6], the authors proposed a scheme named modified SPIN (M-SPIN) and compared its performance with traditional SPIN protocol. The authors proposed that the energy consumption not only depends on sensing the data but also on processing the sensed data and transmitting or receiving them to or from its neighbor nodes. So if it is possible to control number of transmission and receipt of messages, a significant amount of energy can be saved. This paper has added new phase that is called distance discovery phase. This phase is used to find out the best path from source node to base station. Other phases are negotiation and data transmission. During the best route finding, it is possible that single route used several times for data transmission from source node to base station. Nodes involved in this path exhaust more energy than the other node (nodes not used several times). In negotiation phase of M-SPIN, node has to share the new data to all such nodes having the need to receive the actual data, and in data transmission phase, data are immediately sent to requested node. In distance discovery phase of M-SPIN, a path is decided in for all the nodes in term of hope distance to base station. A particular fix path is used several times and such nodes involved in such routine, energy exhaust earlier than the other sensor node and such node get destroyed earlier due to several times used than the other node. But M-SPIN does not guarantee about the nodes destroyed earlier due to several times used than the other node.

3 Problem Statements and Problem Solution

3.1 Problem Statement

SPIN protocol works in three stages such as ADV-REQ_DATA. Upon receiving an ADV, each node checks whether it has already received or requested the advertised data. If not, it waits for certain amount of predefined time and sends a REQ message out to the broadcast address specifying the original advertiser in the header of the message. On receiving a REQ message, only the original advertiser will respond and send the actual data to the requesting nodes. Then, negotiation mechanism ensures elimination of redundant data. But it does not establish any path for data transmission, and hence, data delivery is not guaranteed in SPIN. In this phase, if cluster head scheme is used, then not only a path is established, but also in guaranteed way, data can be transferred to base station. So it is possible to control number of data transmission with energy consumption. Fact is that energy consumption has a greatest portion during data transmitting or receiving to or from its neighbor nodes. This scheme does give the guarantee about the transmission of data to base station. So new scheme is required to manage the nodes get destroyed earlier in network due to several times used and have ability to gives guarantee of data transmission to base station with increasing the lifetime of network. All sensor

nodes are distributed equally and densely in a space for monitoring events with a assumption of large enough buffer size. Single base station located in the field. All sensor nodes have to send the data and rotation of clusterhead is changed only when their energy is less than threshold energy. An energy model for communication has been proposed [7–9]. The energy for transmitting m bit data over the a distance d is Etx(m,d) and the energy for receiving m bit data over e a distance d is Erx(m,d).

$$E_{\mathrm{Tx}}(m,d) = E_{\mathrm{Tx-elec}}(m) + E_{\mathrm{Tx-amp}}(m,d) \tag{1}$$

$$E_{\mathrm{Tx}}(m,d) = \left\{ \begin{matrix} mxE_{\mathrm{elec}} + E_{\mathrm{friss-amp}}xd2 \\ mxE_{\mathrm{elec}} + E_{\mathrm{friss-amp}}xd4 \end{matrix} \right\} \tag{2}$$

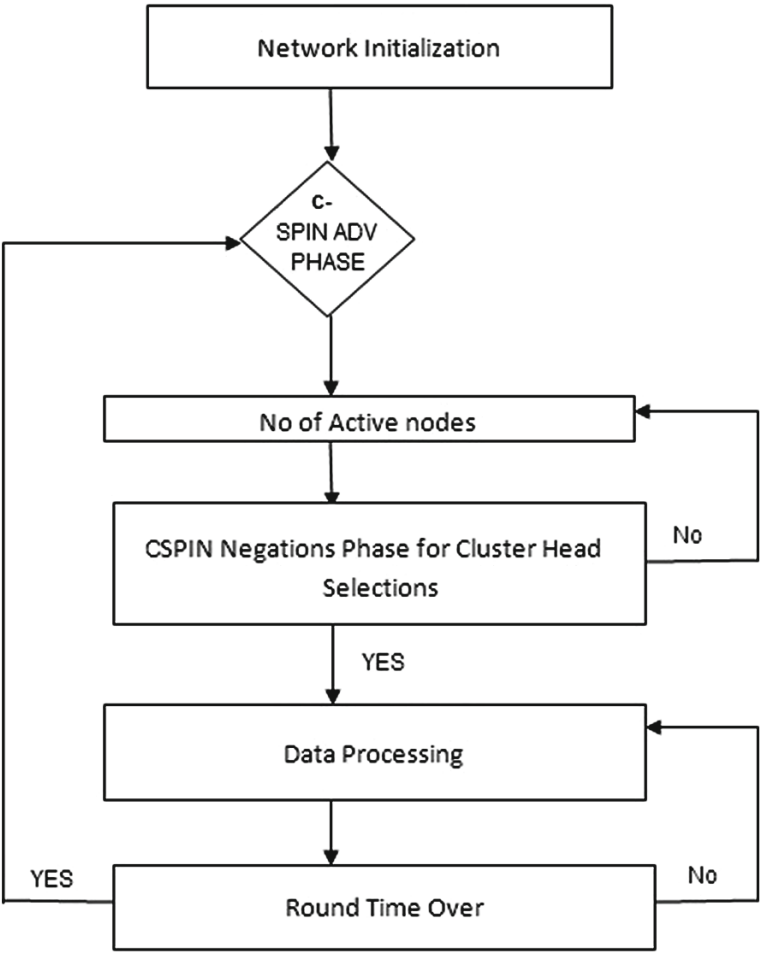

Fig. 1 Proposed SPIN-C scheme

$$E_{\mathrm{Rx}}(m, d) = mxE_{\mathrm{elec}} \tag{3}$$

Network model for proposed scheme assumes energy required for running the transmitter and receiver circuitry E_{elec} as 50 nJ/bit. The crossover distance d_0 is considered 50 m. Based on above Eqs. (1)–(3), shortest generic route can be calculated.

3.2 Proposed Solution

The work of this paper proposes an efficient cluster head selection scheme for SPIN Protocol. Aim of the proposed scheme is to reduce the intercommunications distance between the nodes and also distances between the clusterhead by means of route shorten method. Proposed scheme divided into the three phase. First phase introduces the process of cluster head generation among the sensor node within 50

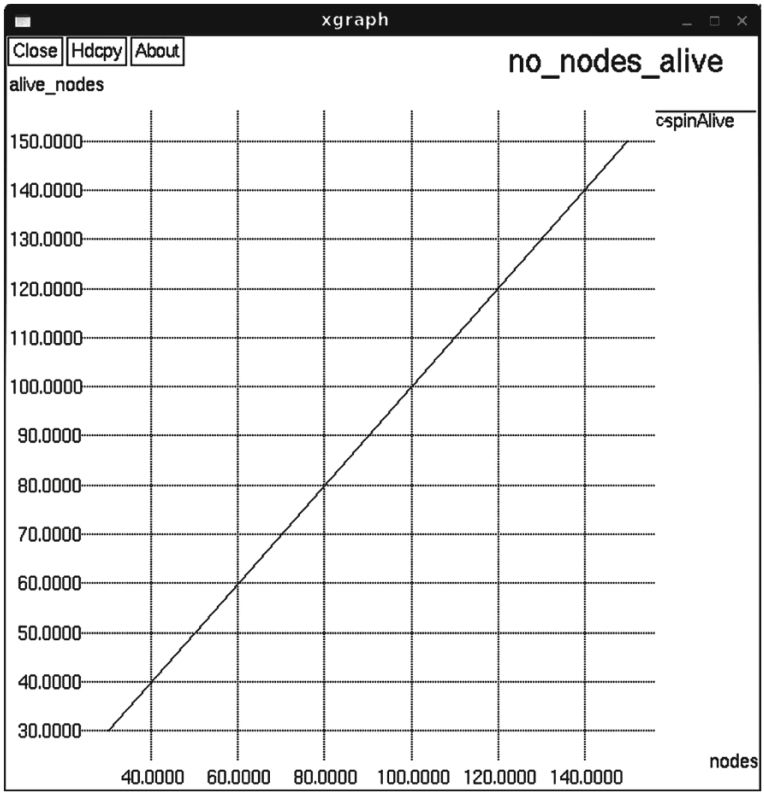

Fig. 2 Number of nodes alive after the implementation of C-SPIN protocol

m distance to find cluster head of each sensor node in the network. To generate the clusterhead, send the hello packet to all the nodes and select the clusterhead within the 50 m distance. Other phases are negotiation and data transmission. In proposed scheme, the role of negotiation phase is to decide the cluster head role rotation after every round of commutation [9]. Clusterhead consumes more energy as compared to other sensor node. So for increasing the lifetime of network and sensor node, role of clusterhead is rotated among the all sensor nodes in the cluster, and cluster head rotation is carried out on the basis of total energy of clusterhead and sensor node in a cluster. After every round of data transmission, cluster is decided based on energy. In last phase, data transferring from cluster to cluster and finally data received to base station. Assume that nodes are homogeneous, this means that all the nodes in the field have the same initial energy [9]. LEACH protocol guarantees that each and every node will become a cluster head exactly once every rounds. Nodes that are elected to be cluster heads in the current round and the non-elected nodes belong to the set in order to maintain a steady number of cluster heads per round. The decision is made at the beginning of each round by each node choosing a random

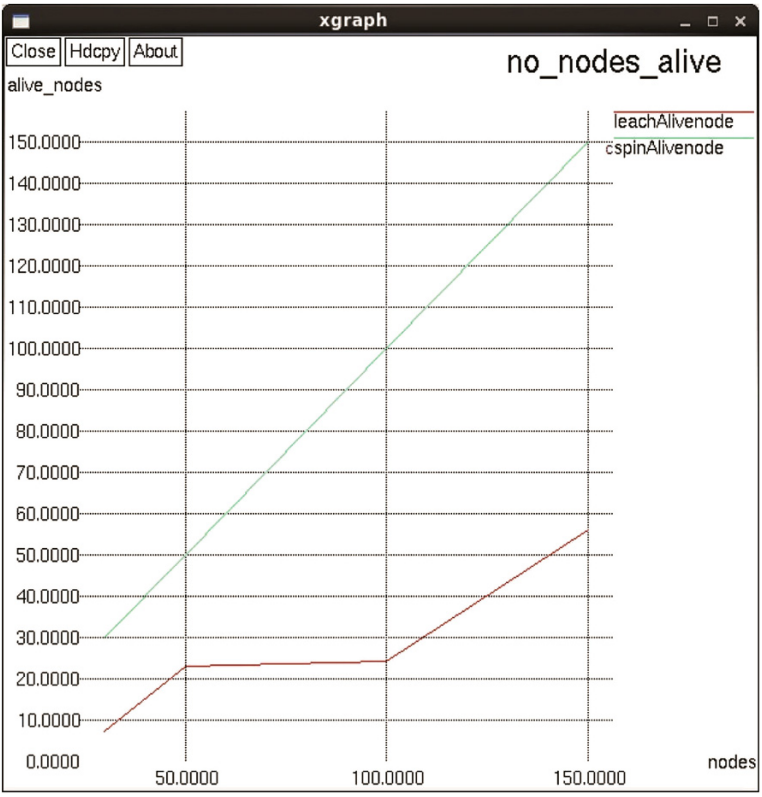

Fig. 3 Comparisons of C-SPIN and LEACH protocol for 150 nodes for number of nodes alive

number in [0, 1]. The nodes became a cluster head if generated valve, v, is less then T(n). The cluster head slection threshold is designed to ensure with high probality that a predefined fraction of, P, is elected cluster at each round. further, the threshold ensures that nodes which serves in the last 1/P round are not selected in the current round. The threshold is set as:

$$T(s) = \left\{ \frac{P_{\text{opt}}}{1 - P_{\text{opt}}(r \bmod \frac{1}{P_{\text{opt}}})} \right\} \quad \text{if } s \in G \tag{4}$$

where $T(s)$ r is the current round number (starting from round 0). The election probability of nodes to become cluster heads increases in each round and becomes equal to. Note that by round, we define a time interval where all cluster members have to transmit to their cluster head once.

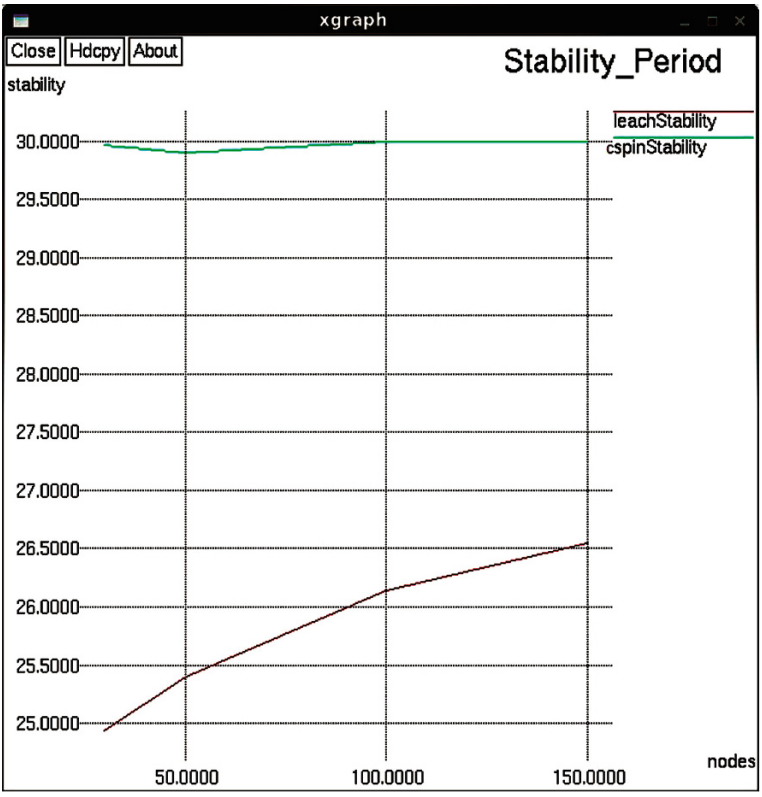

Fig. 4 Comparisons of C-SPIN and LEACH protocol for 150 nodes for stability period

4 Simulation Results

Evaluation of the performance analysis of the proposed scheme and LEACH is done by using network simulator NS-2 [10, 11] with incorporation of MIT uAMP [9] project (NS2Extension). Implementation of both protocols has been written in TCL and C++ programming language. Comparisons of LEACH and C-SPIN are used to measure the performance of C-SPIN. This unique feature of SPIN brings new routing design based on geographical and gives many solutions in geographical requirements.

5 Simulation Summaries

Simulation result of proposed SPIN-C protocol has been tested with network size 50, 100, and 150 nodes and packet size 100 Bytes with the flat node and dynamic node. Events generated to reach base station from different source nodes. Different matrices are used for the network performance. These result shows that diameter of source node is shorter than the minimum length of shortest path from source node

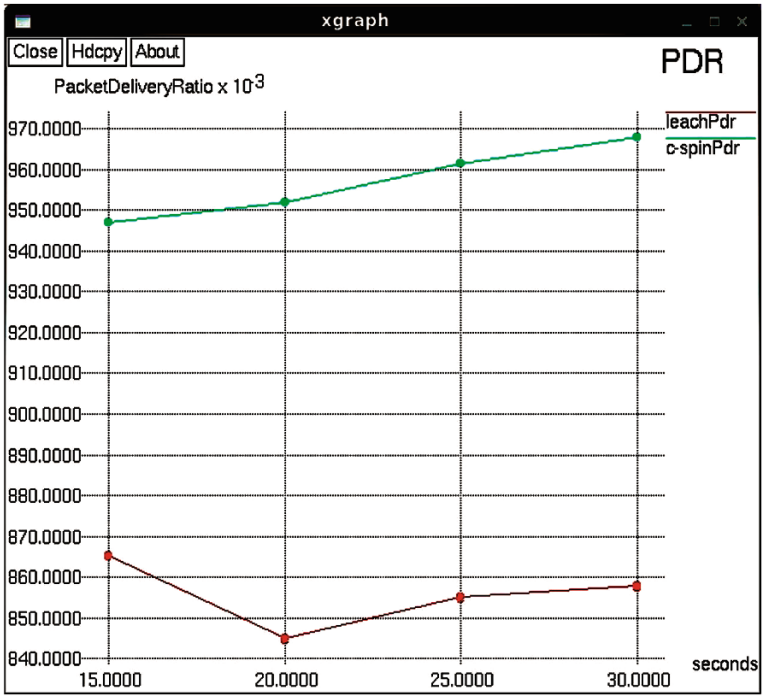

Fig. 5 Comparisons of C-SPIN and LEACH protocol for 150 nodes for PDR

to sink node then number of transmission under the data centric routing and it is more energy efficient. But if not, then it is more energy consumable. Figures 2, 3, and 4 show that the number of nodes alive when it takes to route a data packet from the source node to the base station and stability of networks. Figure 5 shows the percentage of data packets generated by source nodes and successfully delivered to the base station and expressed the efficient use of clustering in SPIN and significant performance gains over the LEACH for lifetime of network and stability and network alive.

6 Conclusion

In this paper, Cluster version of SPIN protocol proposed. Negotiation is done before and after the sending actual data. In future ,it may be possible to work on dynamic replacement of node and cluster head in network after the dead and provide the better solution.

References

1. Akyildiz, I., Su, W., Sankarasubramaniam, Y., Cayirci, E.: A survey on sensor networks. IEEE Commun. Mag. **40**(8), 102–114 (2002)
2. Tubaishat, M., Madria, S.: Sensor networks: an overview. IEEE Potential **22**, 20–23 (2003)
3. Estrin, D., Govindan, R.: Next century challenges: scalable coordination in sensor networks. MobiCom **1999**, 263–270 (1999)
4. Rehna, Z., Roy, S.: A modified spin for wireless sensor network. IEEE Comput. Commun. Networking Technol. **4**, 11–15 (2011)
5. Heinzelman, W.: Application—Specific Protocol Architectures for Wireless Networks. Ph.D Thesis, MIT (2000)
6. Rehna, Z., Kumar, K.: Spin implementation in Tinny OS environment using nesC. In: Proceedings of 1st IEEE Conference Computing Communication and Networking Technologies (2010)
7. Carle, J., Simplot-Ryl, D.: Energy-efficient area monitoring for sensor networks. Computer **37**, 40–46 (2004)
8. Anastasi, G., Conti, M., Francesco, M.D., Passarella, A.: Energy conservation in wireless sensor networks: a survey. Ad Hoc Netw. **7**, 537–568 (2009)
9. Heinzelman, W.R., Chandrakasan, A., Balakrishnan, H.: Energy efficient communication protocol for wireless microsensor networks. In: Proceedings of 33rd Hawai International Conference on Systems Science, Ser. HICSS'00, vol. 8, pp. 10–20. IEEE Computer Society, Washington, DC (2000)
10. F.K and V.K The network Simulator Ns-2. http://www.isi.edu/nsnam/ns
11. Chuang, P.J.: Efficient Data Gathering Scheme for Wireless Sensor Networks, pp. 370–379. Springer, Berlin (2005)
12. Karl, H., Willig, A.: Protocol and Architecture for Wireless Sensor Networks. Wiley, London (2005)

Application of Genetic Algorithm in Optimization of Hydrodynamic Bearings

L. Roy and S.K. Kakoty

Abstract This paper presents comparison of the optimum performance characteristics of four different bearing configurations. An attempt has been made to find out the effect of four different bearing configurations of hydrodynamic journal bearing by changing groove locations. Various groove angles that have been considered are 10°, 20°, and 30°. The Reynolds equation is solved numerically in a finite difference grid satisfying the appropriate boundary conditions. Four optimum performance parameters considered viz non-dimensional load carrying capacity, flow coefficient, friction variable, and mass parameter. Optimum configuration of bearings ensures best flow, load and stability, and least friction of the bearings. Genetic algorithm (GA) for multi-objective function has been used for optimum performance parameter comparison of the bearings. Flow coefficient value is found higher for elliptical bearing, and optimum value of non-dimensional load carrying capacity mass parameter found to be the highest for four-lobe bearing.

Keywords Bearing configurations · Hydrodynamic journal bearing · Optimum performance · Multi-objective genetic algorithm

1 Introduction

Journal bearings are used extensively in rotating machines because of their low wear and good damping characteristics. Fluid film journal bearings are available to support a rotating shaft in a turbomachinery system. A full bearing has a much simple configuration but exhibits instability at higher rotational speeds. It is relatively less expensive compared to the multi-lobe bearings. It is well known that

L. Roy (✉) · S.K. Kakoty
Indian Institute of Technology Guwahati, Guwahati 781309, India
e-mail: lintu@iitg.ernet.in

S.K. Kakoty
e-mail: sashin@iitg.ernet.in

K.N. Das et al. (eds.), *Proceedings of Fourth International Conference on Soft Computing for Problem Solving*, Advances in Intelligent Systems and Computing 335,
DOI 10.1007/978-81-322-2217-0_18

whirl instability occurs at high speed in oil journal bearing. Present-day bearings, at over increasing speeds and loads, confront the engineer with many new problems. Excessive power losses reduce the efficiency of the engine, and high bearing temperature poses a danger to material of the bearing as well as the lubricant. Instability arising mainly in the form of oil whip may ruin not only the bearing but also the machine itself. New bearing designs are sought to meet the new requirements. Pinkus [1] was the first to study elliptical bearing. His work was on finite two-lobe elliptical bearing with the numerical solution of Reynolds equation. In his work on elliptical bearing the nature of the oil flow, power loss was obtained for various L/D ratios, ellipticity, and various operating conditions. A journal bearing fed by two-axial grooves has wide practical application due to its good load carrying capacity and ability to operate when reversal of shaft rotation occurs [2]. The authors studied the effect of loading direction on the performance of a twin-axial groove cylindrical bore bearing. It was anticipated that, if the bearing was loaded into the groove, its load carrying ability would be diminished, but the effect on hydrodynamic lubricant flow and power loss was not so obvious. If the positions of the grooves were arranged for carrying a relatively higher load, then the likelihood of bearing instability reduced, since the journal will run more eccentrically. Again hydrodynamic leakage and friction are affected by the direction of loading. So a question arises where the position of the groove should lie so as to give the optimum load, flow, friction, and critical speed. Theoretical analysis of three-lobe bearing based on the solution of Reynolds equation for laminar as well as for turbulent region was presented by Malik et al. [3]. Both static and dynamic characteristics of three-lobe bearing were presented. Load support, frictional power loss, stiffness and damping coefficient, and stability margin in terms of critical mass parameter were presented in graphical form. As the dynamic performance is a prime consideration in the design and selection of bearings for modem high-speed machinery, it appears that some optimum bearing configurations from this point of view may be derived from more detailed studies of non-circular bearing configurations as indicated by Sinhasan et al. [4]. Among the previous work on two-axial groove oil journal bearing, Klit and Lund [5] used finite element method to find dynamic coefficients of plain circular, elliptical, three-lobe and four-lobe bearing with axial grooves. A new technique for optimizing hybrid journal bearings was presented by Rowe and Koshal [6]. The method involved the comparison of the bearings to be optimized with a reference bearing on the basis of load/total power, load/pumping power, and load/flow. Lin and Noah [7] used genetic algorithm (GA) to optimize the performance of a hydrodynamic journal bearing. Mathew et al. [8] covered the basic concepts and advantages of the canonical or traditional GA. Few illustrations were given in detail. A variety of applications were also mentioned. The transition scheme of the GA was probabilistic, whereas traditional methods used gradient information. Because of these features of GA, they were used as general-purpose optimization algorithm. The most striking difference between GAs and many traditional optimization methods was that GAs work with a population of points instead of a single point, and the expected GA solution might be a global solution. Another advantage with a population-based search algorithm was that the

multiple optimal solutions could be captured in the population easily, thereby reducing the effort to use the same algorithm many times. Hashimoto and Matsumoto [9] described the optimum design methodology for improving operating characteristics of hydrodynamic journal bearings. Hirani [10] formulated a problem to minimize temperature rise, power loss, and oil flow. An evolution-based optimization methodology for cylindrical journal bearings had been applied for journal bearings. McCall [11] presented genetic algorithms (GAs), a heuristic search and optimization technique inspired by natural evolution. GAs have been successfully applied to a wide range of real-world problems of significant complexity. When there are hundreds of publications on application of GAs, only couple of representative publications are cited here.

It has been observed that GAs have been successfully applied for optimizing bearing performance. However, performance of two-groove, elliptical, three-lobe, and four-lobe bearing has not been optimized pertaining to location of groove positions with multiple objectives. In view of this, an attempt has been made in this paper to compare the performance parameters of four different hydrodynamic journal bearings for maximum non-dimensional load, oil flow, and maximizing critical speed vis-à-vis mass parameter, a function of speed and minimization of friction variable.

To facilitate the optimum bearing design, a comparison of the non-dimensional value of mass parameters and flow coefficients for different configurations in groups are determined, and the optimum performance is determined on the basis of maximization of non-dimensional load carrying capacity, mass parameter, flow coefficients, and minimization of friction variable. An attempt can be made to obtain an optimum configuration of the groove position around the circumference of the four hydrodynamic journal bearings for maximum oil flow and maximum critical speed vis-à-vis mass parameter, a function of speed. The oil flow rate depends on several factors, such as the viscosity of the lubricant, the geometry (length, diameter, and radial clearance) of the bearing, operating eccentricity, the inlet oil pressure, and the arrangement of feeding sources as well as groove location of the bearing. The pressure developed in the film due to journal motion also contributes to the flow. An adequate oil flow takes away frictional heat and does not allow rapid rise in temperature. If the feeding groove (in which pressure is zero) falls in the load carrying film, this part of the bearing makes no contribution to the load carrying ability. GAs, a heuristic search and optimization technique inspired by natural evolution. GAs have been successfully applied to a wide range of real-world problems of significant complexity. However, the performance of two-groove, elliptical, three-lobe, and four-lobe journal bearing has not been optimized pertaining to location of groove positions with the multiple objectives. In view of this, an attempt has been made in this paper to obtain a comparison of optimum performance characteristics of four different hydrodynamic journal bearings for maximum non-dimensional load, flow, and mass parameter, a function of speed and minimization of friction variable.

2 Theory

The governing equation is the Reynolds equation in two dimensions for an incompressible fluid. It can be written in dimensionless form as in Eq. (1), and its perturb form for small amplitude of vibration can be written as Eqs. (1), (2), and (3)

$$\frac{\partial}{\partial\theta}\left(\bar{h}_0^3\frac{\partial\bar{p}_0}{\partial\theta}\right)+\left(\frac{D}{L}\right)^2\frac{\partial}{\partial\bar{z}}\left(\bar{h}_0^3\frac{\partial\bar{p}_0}{\partial\bar{z}}\right)=\frac{\partial\bar{h}_0}{\partial\theta} \tag{1}$$

$$\begin{aligned}\frac{\partial}{\partial\theta}\left(\bar{h}_0^3\frac{\partial\bar{p}_1}{\partial\theta}\right)+\left(\frac{D}{L}\right)^2\frac{\partial}{\partial\bar{z}}\left(\bar{h}_0^3\frac{\partial\bar{p}_1}{\partial\bar{z}}\right)+3\frac{\partial}{\partial\theta}\left(\bar{h}_0^2\frac{\partial\bar{p}_0}{\partial\theta}\cos\theta\right)\\+\left(\frac{D}{L}\right)^2\frac{\partial}{\partial\bar{z}}\left(\bar{h}_0^2\frac{\partial\bar{p}_0}{\partial\bar{z}}\cos\theta\right)=-\sin\theta+i2\lambda\cos\theta\end{aligned} \tag{2}$$

$$\begin{aligned}\frac{\partial}{\partial\theta}\left(\bar{h}_0^3\frac{\partial\bar{p}_2}{\partial\theta}\right)+\left(\frac{D}{L}\right)^2\frac{\partial}{\partial\bar{z}}\left(\bar{h}_0^3\frac{\partial\bar{p}_2}{\partial\bar{z}}\right)+3\frac{\partial}{\partial\theta}\left(\bar{h}_0^2\frac{\partial\bar{p}_0}{\partial\theta}\sin\theta\right)\\+\left(\frac{D}{L}\right)^2\frac{\partial}{\partial\bar{z}}\left(\bar{h}_0^2\frac{\partial\bar{p}_0}{\partial\bar{z}}\sin\theta\right)=-\cos\theta+i2\lambda\sin\theta\end{aligned} \tag{3}$$

Boundary conditions used for the steady-state pressure and dynamic pressure distribution are as follows:

$$\frac{\partial\bar{p}_i}{\partial\theta}=0 \quad \text{and} \quad \bar{p}_i=0 \quad \text{at} \quad \theta{=}\theta_{\mathrm{r}}$$
$$\bar{p}_i(\theta,\bar{z})=0 \quad \text{when} \quad \theta_{\mathrm{s}}\le\theta\le\theta_{\mathrm{e}}$$

where $\bar{p}_i=\bar{p}_0,\bar{p}_1,\bar{p}_2$ and

$\theta\mathrm{s}=$ starting angle of the groove w.r.t vertical axis
$\theta\mathrm{e}=$ angle at which the groove ends w.r.t vertical axis
$\theta\mathrm{r}=$ angle at which the film cavitates w.r.t vertical axis

The non-dimensional steady-state load components are given by

$$\overline{W}_{X_0}=\int_{\theta_1}^{\theta_2}\int_0^1\bar{p}_0\cos\theta\mathrm{d}\theta\mathrm{d}\bar{z} \tag{4}$$

$$\overline{W}_{Z_0}=\int_{\theta_1}^{\theta_2}\int_0^1\bar{p}_0\sin\theta\mathrm{d}\theta\mathrm{d}\bar{z} \tag{5}$$

$$\overline{W}_0 = \sqrt{\overline{W}_{X_0}^2 + \overline{W}_{Z_0}^2} \tag{6}$$

Equation (1) is solved for the steady-state pressure distribution $(\bar{p}_0)$, discretizing in a finite difference grid of size 88 × 14 and using Gauss–Seidel method with successive over-relaxation (SOR) technique satisfying the boundary conditions. The convergence criterion adopted for pressure calculation is $\left|1 - \frac{\Sigma \bar{p}_{\text{old}}}{\Sigma \bar{p}_{\text{new}}}\right| \leq 10^{-5}$. Chosen bearing eccentricity and arbitrary attitude angle picked at random results in magnitude of forces generated due to pressure wedge in the bearing. The attitude angle is changed till the horizontal force component $\left(\overline{W}_{Z_0}\right)$ in the pressure wedge becomes zero. This eventually locates the attitude angle. For this equilibrium position, the vertical force $(\overline{W}_{X_0})$ gives the load capacity $\overline{W}_0$. The Sommerfeld number is given by $\mathrm{S} = \frac{1}{\pi \bar{W}_0}$. The flow coefficient in the dimensionless form can be written as

$$\bar{q}_Z = \frac{1}{2}\left(\frac{D}{L}\right)^2 \int_0^{2\pi} \bar{h}^3 \frac{\partial \bar{p}_0}{\partial \bar{z}}|_{\bar{z}=\pm 1} \mathrm{d}\theta \tag{7}$$

The friction variable, $\bar{\mu} = (R/C)\mu = \frac{\bar{F}}{\bar{W}_0}$, is given by

$$\bar{\mu} = \mu(R/C) = \frac{\int_0^{2\pi} \left(3\bar{h}\frac{\partial \bar{p}_0}{\partial \theta} + \frac{1}{h}\right)\mathrm{d}\theta}{6\bar{W}} \tag{8}$$

Equations (2) and (3) for $\bar{p}_1$ and $\bar{p}_2$ are solved satisfying the boundary conditions and known values of $\bar{p}_0$ using the same procedure used for calculating steady-state pressure. Dynamic loads due to $\bar{p}_1$ and $\bar{p}_2$ are given by

$$\sum_{i=1}^{2} W_{Xi} = \sum_{i=1}^{2} \int_{\theta_1}^{\theta_2} \int_0^1 p_i \cos\theta \mathrm{d}\theta \mathrm{d}\bar{z} \quad \text{and} \quad \sum_{i=1}^{2} W_{Zi} = \int_{\theta_1}^{\theta_2} \int_0^1 p_i \sin\theta \mathrm{d}\theta \mathrm{d}\bar{z} \tag{9}$$

It is found that the fluid film, which supports the bearing, is equivalent to a spring mass damping system. Since the journal executes small harmonic oscillations about its steady-state position, the dynamic load carrying capacity can be expressed as a spring and a viscous damping force. The expressions for stiffness and damping coefficients, mass parameter, and whirl ratios are discussed [12].

3 Optimization Techniques

It has been found that the location of the groove has influence on non-dimensional load carrying capacity ($\bar{W}$), flow ($\bar{q}_Z$), friction variable ($\bar{\mu}$), and mass parameter ($\bar{M}$) as well as other variables. GA is the most popular stochastic method used to find the optimum solution for all kinds of problem. GAs perform a multiple directional search by maintaining a population of potential solutions. The population-to-population approach attempts to make the search escape from local optima [8]. GAs are very helpful when the developer does not have precise domain expertise, because GAs possess the ability to explore and learn from their domain. GA has been used in this work as GA, being a heuristic search and optimization technique inspired by natural evolution, has been successfully applied to a wide range of real-world problems of significant complexity. It has been suggested that heuristic optimization provides a robust and efficient approach for solving complex real-world problems [11].

3.1 Multi-objective Problem Formulation

The problem is framed with four objectives. The eccentricity ratio (ε), starting angle of first groove (θ_1), and starting angle of second groove (θ_2) are variables and act as chromosome for two-groove bearing, in addition a starting angle of third groove (θ_3) for three-lobe bearing and starting angle of fourth groove (θ_4) for four-lobe bearing, the groove angles being 10° in all the cases. It has been observed that the load carrying capacity is slightly higher with 10° groove angles in comparison with 20° and 30° groove angles. The objectives are combinations of the four objectives. The variable bounds for the bearings' groove location are shown in Table 1.

Objective function for the multivariable problem is given as

$$\begin{aligned}\text{Minimize}\quad f = {} & w_1[\bar{\mu}/(\bar{\mu}_{\max} - \bar{\mu}_{\min})] + w_2[1 - \bar{q}_z/(\bar{q}_{z\max} - \bar{q}_{z\min})] \\ & + w_3[1 - \overline{w}/(\overline{w}_{\max} - \overline{w}_{\min})] + w_4\left[1 - \overline{M}/\left(\overline{M}_{\max} - \overline{M}_{\min}\right)\right]\end{aligned} \tag{10}$$

$\bar{\mu} = \mu\left(\frac{R}{C}\right)$ = friction variable, $\bar{q}_z$ = flow coefficient, $\bar{w}$ = non-dimensional load capacity, $\bar{M} = \frac{MC\omega^2}{W}$ = mass parameter, and w_1, w_2, w_3, and w_4 are the associated weight. $\bar{\mu}_{\max}$, $\bar{\mu}_{\min}$ are the corresponding maximum value and minimum value and so on. Weighted sum method [9] is used to handle four objectives at a time. Four different weights, w_1, w_2, w_3, and w_4, are considered for the four objectives, respectively. Weights are selected in such a way that the nature of the performance parameter can be easily understood.

Table 1 Variable bounds for the bearing problem

Bearing configurations	Variable	Lower bound	Upper bound
For two-groove and elliptical bearing	ε	0.1	0.9
	Starting angle of first groove (θ_1)	0°	180°
	Starting angle of second groove (θ_2)	170°	350°
For three-lobe bearings	ε	0.05	0.441
	Starting angle of first groove	0°	180°
	Starting angle of second groove	100°	210°
	Starting angle of third groove	210°	350°
For four-lobe bearings	ε	0.05	0.375
	Starting angle of first groove (θ_1)	0°	80°
	Starting angle of second groove (θ_2)	90°	170°
	Starting angle of third groove (θ_3)	180°	260°
	Starting angle of fourth groove (θ_4)	270°	350°

4 Results and Discussion

A code has been developed to calculate the steady-state and dynamic characteristics for given values of L/D ratios and groove locations, which is subsequently used for obtaining optimum groove locations for different objective functions. An optimum groove location has been obtained depending on maximization of flow coefficient and mass parameter with the help of GA toolbox of MATLAB.

The generic algorithm convergence rate to true optima depends on the probability of crossover and mutation on one hand, and the maximum generation on the other hand. In order to preserve a few very good strings, and rejecting low-fitness strings, a high crossover probability is preferred. The mutation operator helps to retain the diversity in the population, but disrupts the progress toward a converged population and interferes with beneficial action of the selection and crossover. Therefore, a low probability, 0.001–0.1, is preferred. The GA updates its population on every generation, with a guarantee of better or equivalent fitness strings. For well-behaved functions, 30–40 generations are sufficient. For steep and irregular functions, 50–100 generations are preferred. Considering these factors, a population size of 50, mutation probability of 0.1, and a crossover probability of 0.8 have been selected. A convergence plots of four different bearing configurations are shown in Figs. 1 , 2, 3 and 4.

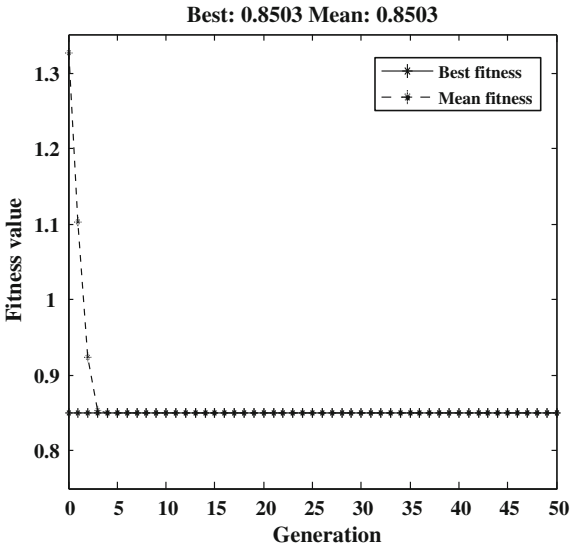

Fig. 1 Fitness value considering friction variable as objective function for two-groove bearing

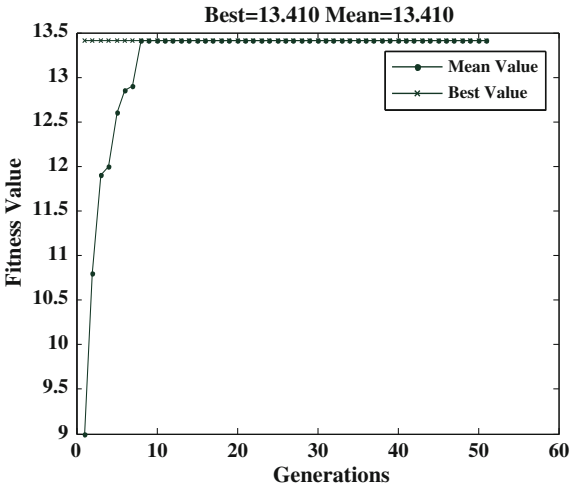

Fig. 2 Fitness value considering flow coefficient as objective function for elliptical bearing

A comparison of the various optimum parameters of four different bearing configurations is made as shown in various Fig. 5, 6, 7 and Fig. 8. From Fig. 5, it has been observed that the optimum value of friction is lowest for elliptical and four-lobe bearing, and it is higher for two-axial groove bearing. Flow coefficient value is higher for elliptical bearing than the other bearing configurations (Fig. 6). Optimum value of non-dimensional load carrying capacity is higher for four-lobe bearing than other bearing configurations (Fig. 7) and optimum value of mass parameter found to be the highest for four-lobe bearing (Fig. 8).

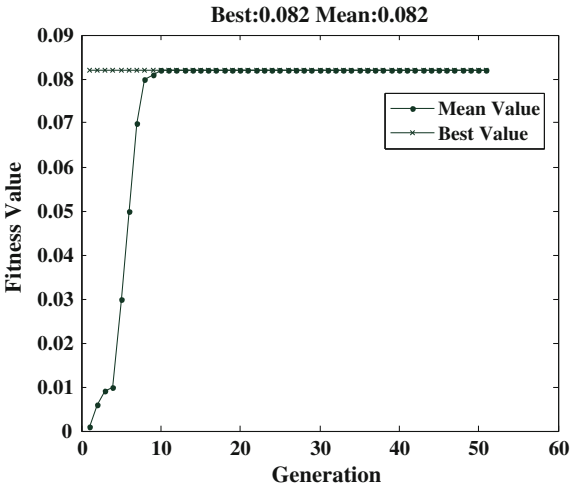

Fig. 3 Fitness value considering load as objective function for three-lobe bearing

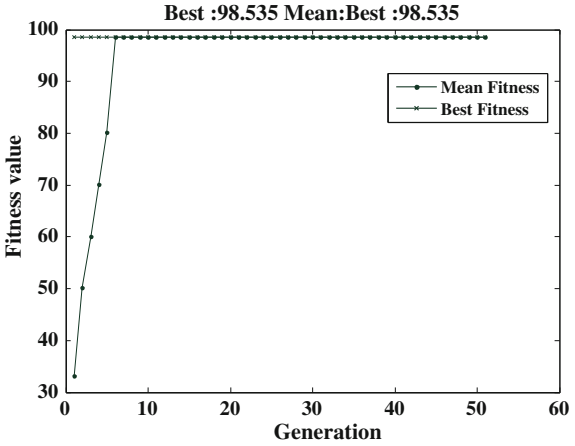

Fig. 4 Fitness value considering mass parameter as objective function for four-lobe bearing

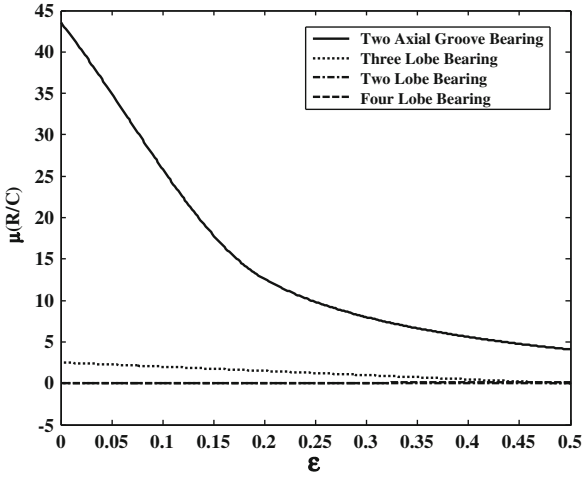

Fig. 5 Comparison of friction variable for four different bearing configurations

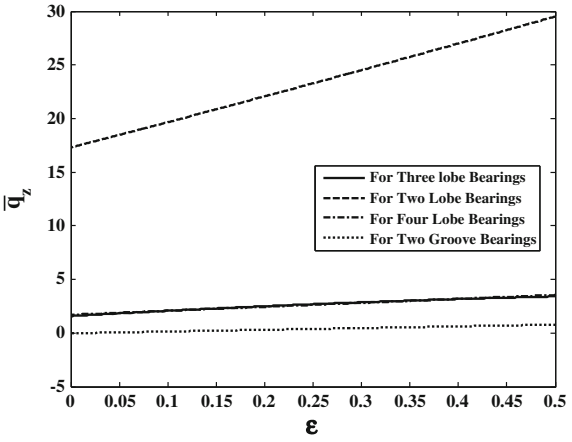

Fig. 6 Comparison of flow coefficient for four different bearing configurations

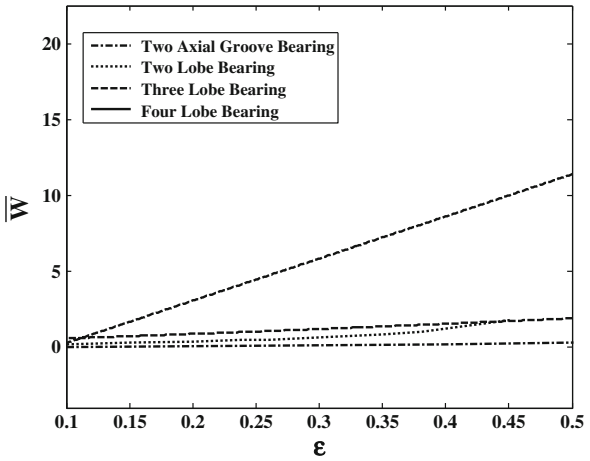

Fig. 7 Comparison of non-dimensional load for four different bearing configurations

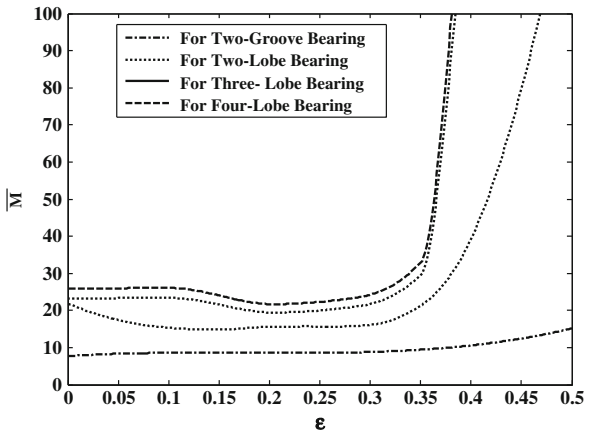

Fig. 8 Comparison of mass parameter for four different bearing configurations

5 Conclusion

From the obtained results using GA tool box of MATLAB, the following conclusions can be drawn

1. GA can be applied successfully by optimizing problems in a discrete nature.
2. Optimum friction variable value for two-groove bearing is found to be higher for two-axial groove bearing and is least for elliptical and four-lobe bearing.
3. Optimum flow coefficient value is found to be highest for elliptical bearing configuration and is least for two-groove bearing.
4. Optimum value of non-dimensional load carrying capacity mass parameter found to be the highest for four-lobe bearing.

References

1. Pinkus, O.: Analysis of elliptical bearing, transaction of ASME. J. Basic Eng. **78**, 965–973 (1956)
2. Gethin, D.T., El Deihi, M.K.I.: Effect of loading direction on the performance of a twin-axial groove cylindrical-bore bearing. Tribol. Int. **20**(4), 179–185 (1987)
3. Malik, M., Sinhasan, R., Chandra, M.: Design data for three-lobe bearings. Trans. ASLE **24** (3), 345–353 (1981)
4. Sinhasan, R., Malik, M., Chandra, M.: A comparative study of some three lobe bearing configurations. Wear **72**, 277–286 (1981)
5. Klit, P., Lund, J.W.: Calculation of the dynamic coefficients of a journal bearing, using a variational approach. J. Tribol. **108**(3), 421–425 (1986)
6. Rowe, W.B., Koshal, D.: A new basis for the optimization of hybrid journal bearings. Wear **64** (1), 115–131 (1980)
7. Lin, Y.J., Noah, S.T.: Using genetic algorithms for the optimal design of fluid journal bearing. In: Proceedings of the ASME Design Engineering Technical Conferences, pp. 12–15 (1999)
8. Mathew Tom, V., Beasley, D., Bull David R., Martin, R.R.: An overview of genetic algorithms: part 2, research topics. Univ. Comput. **15**(4), 170–181 (1993)
9. Hashimoto, H., Matsumoto, K.: Improvement of operating characteristics of high-speed hydrodynamic journal bearings by optimum design: part I-formulation of methodology and its application to elliptical bearing design. J. Tribol. **123**(2), 305–312 (2001)
10. Hirani, H.: Multiobjective optimization of a journal bearing using the Pareto optimality concept. Proc. Inst. Mech. Eng. Part J: J. Eng. Tribol. **218**(4), 323–336 (2004)
11. McCall, J.: Genetic algorithms for modelling and optimization. J. Comput. Appl. Math. **184** (1), 205–222 (2005)
12. Roy, L., Kakoty, S.K.: Optimum groove location of hydrodynamic journal bearing using genetic algorithm. Adv. Tribol. **2013**, 1–13 (2013)

Diversity-Based Dual-Population Genetic Algorithm (DPGA): A Review

A.J. Umbarkar, M.S. Joshi and P.D. Sheth

Abstract Maintaining population diversity is a challenge for the success of genetic algorithm. A numerous approaches have been proposed by researchers for adding diversity to the population. Dual-population genetic algorithm (DPGA) is one of them which is an effective optimization algorithm and provides diversity to the main population. Problems in GA such as premature convergence and population diversity is well addressed by DPGA. The aim of writing this review paper is to study how DPGA has been evolved. DPGA is inherently parallelizable, and hence, it can be port to parallel programming architecture for large-scale or large-dimension problems.

Keywords Dual-population genetic algorithm (DPGA) · Population diversity · Meta-heuristic algorithms · Premature convergence

1 Introduction

The genetic algorithms (GAs) are population-based search algorithms. Its population evolves by using genetic operators such as selection, crossover, and mutation. They are simpler than calculus-based, enumerative, random optimization techniques and dynamic programming (DP) in implementation [1]. It is used for solving problems

A.J. Umbarkar (✉) · P.D. Sheth
Department of Information Technology, Walchand College of Engineering, Sangli, Maharashtra, India
e-mail: anantumbarkar@rediffmail.com

P.D. Sheth
e-mail: pranalisheth@gmail.com

M.S. Joshi
Department of Computer Engineering, Jawaharlal Nehru Engineering College, Aurangabad, Maharashtra, India
e-mail: madhuris.joshi@gmail.com

K.N. Das et al. (eds.), *Proceedings of Fourth International Conference on Soft Computing for Problem Solving*, Advances in Intelligent Systems and Computing 335,
DOI 10.1007/978-81-322-2217-0_19

from a wide spectrum of problems from combinatorial optimization (scheduling, routing, assignment, etc.), time series prediction, data mining to game playing, or robot control. The problem associated with GAs is that as the populations evolve, they lose diversity and their individuals are trapped in local optima, especially when involving complex problems which have a lot of peaks in the fitness landscape [2]. Literature terms this problem premature convergence.

One of the proposed solutions for the above problem is Dual Population Genetic Algorithm (DPGA). DPGA uses a reserve population along with main population. This provides additional diversity to main population. The information exchange between populations takes place through interpopulation crossbreeding. This technique helps to solve the problem of premature convergence [2]. Hence, we have carried out a detailed survey of DPGA and studied how it evolves.

The paper provides a brief literature review of all versions of DPGA that have been published till date. Section 2 describes DPGA with implementation details such as fitness function for reserve population and evolutionary process. Section 3 explains literature review of DPGA. Finally, Sect. 4 discusses the findings of this review work and future scope.

2 Dual-Population Genetic Algorithm

The idea of reserve population with the objective as population diversity was introduced in 2006 by Park and Ruy [3]. DPGA can be said multi population GA in which it handles two or more main and reserve populations. DPGA can also be considered a memory-based algorithm because the additional (reserve) population can be used as a repository for maintaining diversity or additional information. DPGA does preserve additional information at the level of populations unlike other memory-based algorithms. The main population of a DPGA is implemented as that of ordinary GA. It evolves to find good solutions to the given problem. In contrast, the reserve population evolves only to provide diversity to the main population.

There must be provision to exchange information between main population and reserve population discussed above. Generally, MPGA generates new children from the same population. As MPGA populations have evolutionary objective/fitness function, good migrants are easily assimilated to the new population. Contrary as populations of DPGA have different evolutionary objective, individual of one population hardly to survive in the other. Therefore, to achieve information exchange, DPGA uses interpopulation crossbreeding. DPGA produces offspring by inbreeding between the individuals of the same population as well as by crossbreeding between individuals from different populations. Since the crossbred offspring contains genetic material from both populations, they often have suitable fitness and can be assimilated into one of the new populations more easily.

DPGA starts with two randomly generated populations. The individuals of each population are evaluated by its own fitness function. The evolution of each population is obtained by inbreeding between parents from the same population,

crossbreeding between parents from different populations, and survival selection among these offspring. In the following section, fitness function used for the reserve population and the procedure of reproduction, survival selections for both the populations are described.

2.1 Fitness Function for Reserve Population

The objective function of problem works as the fitness function of the main population. Fitness function for reserve population is defined in other way. An individual in the reserve population is given a high fitness value if its average distance to each of the individuals of the main population is large. Therefore, the reserve population can provide the main population with additional diversity.

(a) Fitness function using Hamming distance

Assuming a binary representation for the chromosomes and the Hamming distance as the distance measure, the fitness of a chromosome x of the reserve population is defined in Eq. (1) [4].

$$\text{fitness}_R(x) = \frac{1}{n}\sum_{i=1}^{n} \text{hd}(m_i, x) = \frac{1}{n}\sum_{i=1}^{n}\sum_{k=1}^{l} |m_{i,k} - x_k| \tag{1}$$

where

n	size of main population
m_i	ith chromosome of the main population
hd(m_i,x)	Hamming distance between m_i and x
l	length of chromosome
$m_{i,k}$	kth gene on chromosome m_i and x_k

(b) Fitness function using the given distance δ

In the following form of fitness function described in Eq. (2), each individual of the reserve population can maintain a given distance δ from the individuals of the main population [5].

$$fr_\delta(x) = 1 - |\delta - d(M, x)| \tag{2}$$

where

$d(M, x)$	average distance ($0 \le d(M, x) \le 1$) between the main population M and individual x of the reserve population
δ	desired distance ($0 \le \delta \le 1$) between two populations

$d(M, x)$ can be defined as either of the following two distances.

(i) The average distance between x and all the individuals of the main population M.
(ii) The distance between x and the best individual M of the main population.

Assuming that a binary representation for a chromosome $d(M, x)$ is calculated using Eq. (3) [2, 4, 5]

$$d(M,x) = \frac{1}{|M|}\sum_{m\in M} \mathrm{hd}(m,x) = \frac{1}{l}\sum_{k=1}^{l} |f_{M,k} - x_k| \tag{3}$$

where

n	size of main population
m_i	ith chromosome of the main population
$\mathrm{hd}(m_i, x)$	Hamming distance between two chromosome vectors m and x
l	length of chromosome
$m_{i,k}$	kth gene on chromosome m_i and x_k
$f_{M,k}$	frequency of the kth gene value '1' of the main population M
x_i	frequency of kth gene value '1' of the chromosome vector x and is identical to the kth gene value of the chromosome

The definitions of $d(M, x)$ and δ enable $fr_{\delta}^{(x)}$ to take a maximum value of 1 when the distance from x to the main population is δ and decreases linearly as $d(M, x)$ deviates from δ [2].

If δ is too small, the reserve population cannot provide enough diversity to the main population. If δ is too big, it becomes difficult for the crossbreeding to be successful in generating an offspring that can survive in the main population. In turn, this implies that the reserve population cannot provide useful diversity to the main population. Instead, the reserve population would disrupt the convergence of the main population by injecting different gene values. Hence, adjusting the value of δ a priori which produces good offspring and helps main population to converge to a good region is a research question. However, the best value of δ differs from problem to problem [2].

The value of δ can be adjusted dynamically as explained in [2, 6]. While the main population itself contains enough diversity, for example, during an early stage of the search, the reserve population plays its role well with a relatively large δ. However, as the main population converges and its average fitness gets higher, δ should be adjusted to smaller values because otherwise the crossbred offspring disturb the search as mentioned above.

One way of adjusting δ is to let it find its way gradually toward a reasonable value. We guess that a good target value for δ could be the distance between the parents involved in successful reproductions. A reproduction is considered successful if one of the following conditions is met [2].

1. Both the parents are selected from the main population, and an offspring is better than both of its parents.

2. One of the parents is selected from the main population, and an offspring is better than the parent from the main population.

A good value for δ is pursued by updating it after each generation using the Eq. (4).

$$\delta_{t+1} = \delta_t + \alpha \cdot \Delta_t \tag{4}$$

where α is the update rate. A more rapid change toward the target distance can be made by a greater α. Δ_t is the error term obtained as follows:

$$\Delta_t = \begin{cases} \frac{1}{|G_t|} \cdot \sum_{(p,p') \in G_t} & \text{dist}(p,p') - \delta_t, \\ & \text{if } |\text{Gt}| > 0 \\ 0, & \text{Otherwise} \end{cases} \tag{5}$$

where G_t is the set of parent pairs of successful reproductions at generation t. Equation (5) reveals that target distance for δ is the average distance between the pair of parents involved in successful reproductions.

2.2 DPGA Methodology

The algorithm selects four parents, two from main population and two from reserve population. The parent selection from main population depends on fitness value calculated by objective function, whereas parent selection from reserve population depends on fitness value calculated by Eq. (1) or by Eq. (2) [4, 5].

From four parents, the algorithm generates six offspring by two inbreeding and one crossbreeding process. Two offspring are generated by mating two parents selected from the main population; another two offspring are generated by mating two parents selected from the reserve population, and yet another two offspring are generated by mating one parent selected from the main population and one parent selected from the reserve population. The above procedure of generation of new population is represented in the diagrammatic form in Fig. 1 [2, 4].

A stepwise detail algorithm of DPGA [2, 4, 5] is described in Fig. 2. Naming convention is retained similar to Fig. 1.

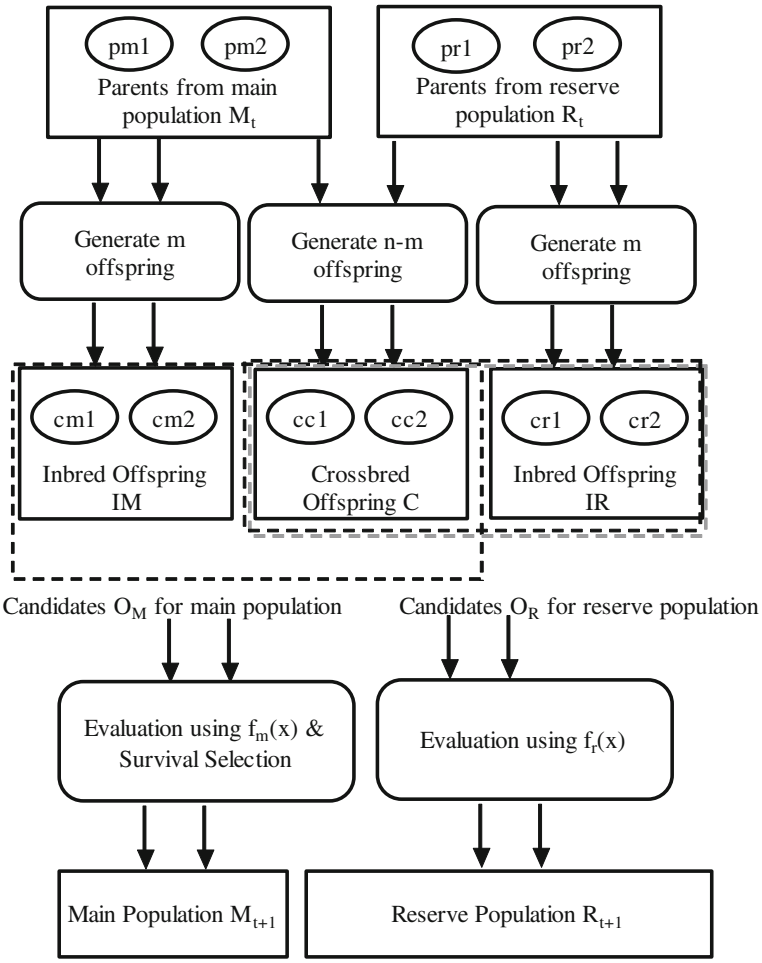

Fig. 1 Procedure for producing new populations

3 Literature Review

Diversity in the population is problem in EA, particularly in GA. DPGA literature survey shows that it is performing better than SGA and even all counter algorithms based on similar concept. The other population diversity-based works are improved fast EP (IFEP) [7], adaptive EP with Lévy mutation (ALEP) [8], island model GA (IMGA) [9], restricted truncation selection (RTS) [10], real-coded memetic algorithm (RCMA) with crossover hill climbing (XHC) [11], comprehensive learning particle swarm optimizer (CLPSO) [12], RCMA with adaptive local search (LSRCMA) [13], differential evolution with neighborhood search (NSDE) [14], covariance matrix adaptation evolution strategy (CMAES) [15], diversity-guided

Procedure DPGA
Begin
Initialize main population M_0 and R_0
Evaluate M_0 using $f_m(x)$
Evaluate R_0 using $f_r(x)$
t:= 0
Repeat
  Repeat
  Step I: Parent Selection:
    1. Select two parent p_{m1} and p_{m2} from M_t
    2. Select two parent p_{r1} and p_{r2} from R_t
  Step II: Offspring generation:
    1. (Inbreeding) Generate two offspring c_{m1} and c_{m2} by recombining p_{m1} and p_{m2}
    2. (Inbreeding) Generate two offspring c_{r1} and c_{r2} by recombining p_{r1} and p_{r2}
    3. (Crossbreeding) Generate two offspring c_{c1} and c_{c2} by recombining p_{m2} and p_{r1}
    4. Mutate all generated offspring
  Step III: Evaluation & Survival selection:
    1. Evaluate c_{m1}, c_{m2} c_{c1} and c_{c2} i.e.O_M using $f_m(x)$ and add the best two to M_{t+1}
    2. Evaluate c_{r1}, c_{r2}, c_{c1} and c_{c2} i.e.O_R using $f_r(x)$ and add the best two to R_{t+1}
  U**ntil**$|M_{t+1}|$ = = pop_size
  t:= t+ 1
Until terminated = **true** // e.g., $t > t_{max}$
End

Fig. 2 Pseudocode for DPGA

evolutionary programming (DGEP) [16], dynamic differential factor and population diversity [17], constrained multi-objective optimization algorithm with diversity enhanced differential evolution [18], and a particle swarm optimization with diversity-guided convergence acceleration and stagnation avoidance [19].

Park and Ruy [3] proposed novel evolutionary algorithm named DPGA. It has two distinct populations with different evolutionary objectives: the prospect population and the preserver population. The prospect population works like population of regular genetic algorithm. Although this local competition helps to find a local peak in a search space, it also causes the population to easily lose the diversity. The preserver population helps to maintain the diversity by preserving some of those chromosomes which are the losers of the local competition. They implemented one max problem, deceptive function, royal road function, and TSP using DPGA. Results show that DPGA outperforms traditional genetic algorithm.

Park and Ruy [4] introduced DPGA-ED that is an improved design DPGA. Unlike DPGA, reserve population of DPGA-ED evolves by itself. Previously, DPGA could not evolve on its own. It depends on genetic data of main population. Therefore, the content of reserve population ultimately becomes similar to main population, and thus, DPGA looses it aim of adding diversity. An individual in reserve population is assigned with high fitness value if its average distance to each of the individuals of the main population is large. In this way, diversity is provided to main population. DPGA-ED by allowing reserve population to evolve achieves a significant performance improvement by avoiding premature convergence of both the populations. Experiments on multimodal test functions showed that this algorithm performs better than ordinary GA as well as other evolutionary algorithms based on similar concepts.

Park and Ruy [5] proposed a new fitness function of the reserve population based on the distance to the main populations. The experimental results have shown that the performance of DPGA is highly related to the distance between the populations and that the best distance differs for each problem. Generally, it is difficult to decide the best distance between the populations without prior knowledge about the problem. Therefore, this paper also proposes a method to dynamically adjust the distance between the populations using the distance between good parents, i.e., the parents that generated good offspring.

Park and Ruy [4] proposed DPGA2 that uses two reserve populations. The reserve populations are at different distances from the main population. The information inflow from the reserve populations is controlled by survival selection. Experimental results show that DPGA2 shows a better performance than other evolutionary algorithms for non-stationary optimization problems without relying on prior knowledge about the problem.

Park and Ruy [2] experimented on various classes of problems using binary, real-valued, and order-based representations. Results showed that DPGA quite often outperforms not only the standard GAs but also other GAs having additional mechanisms of diversity preservation.

Sels and Vanhoucke [20] considered the problem of scheduling a number of jobs, each job having a release time, a processing time, and a due date, on a single machine with the objective of minimizing the maximum lateness. They developed a hybrid DPGA and compared its performance with alternative methods on a new diverse data set. Extensions from a single to a dual population by taking problem-specific characteristics into account can be seen as a stimulator to add diversity in the search process, which has a positive influence on the important balance between intensification and diversification. Based on a comprehensive literature study on GAs in single machine scheduling, a fair comparison of genetic operators was made.

Umbarkar and Joshi [21] compared DPGA with OpenMP GA for multimodal function optimization. Genetic algorithms (GAs) are useful for solving multimodal problems. It is quite difficult to search the search space of the multimodal problem with large dimensions. There is a challenge to use all the core of the system. The DPGA attempts to explore and exploit search space on the multimodal problems. Parallel GAs (PGAs) are better option to optimize multimodal problems. OpenMP

GA is parallel version of GA. The DPGA uses an extra population called reserve population to provide additional diversity to the main population through cross-breeding. DPGA and PGA both provide niching technique to find optimal solution. Paper presents the experimentation of DPGA, OpenMP GA, and SGA. The experimentation results show that the performance of the OpenMP GA is remarkably superior to that of the SGA in terms of execution time and speedup. OpenMP GA gives optimum solution in comparison with OpenMP GA and SGA for same parameter settings.

Umbarkar et al. [22] proposed the binary-encoded multithreaded parallel DPGA (MPDPGA) which solves the problems of population diversity and premature convergence on multicore system. Experiments show that the performance of MPDPGA is better than serial DPGA (SDPGA) and simple GA (SGA).

4 Discussion

Analyzing various papers on DPGA, we can deduce

- Although DPGAs are effective in solving many practical problems in science, engineering, and business domains, they may execute for a long time to find solutions for some huge problems, because several fitness evaluations must be performed. A promising approach to overcome this limitation is to parallelize these algorithms for parallel, distributed, and networked computers. Table 1 enlists the versions of DPGA evolved over time and problems solved.
  DPGAs can find optimal solution to non-deterministic polynomial (NP) hard problems in relatively less time if they run on parallel execution platforms such as graphic processing unit (GPU) and Intel Phi MIC.
- For solving highly computation-intensive problems (constrained optimization and multi-objective functions), DPGAs on GPGPU/OpenMP/MPI, etc., parallel programming platforms can be employed.
- The success of DPGA depends on the distance δ between the two populations. It is difficult to decide the value of δ without prior knowledge or intensive experiments on the given problem. Massively parallel many cores/multicores can be used at this juncture.
- The concept of diversity, i.e., pair of evolving populations, can be added to other meta-heuristic algorithms (TLBO, PSO, etc.) as niching technique to find optimal solution with minimum efforts.

Table 1 Versions of DPGA evolved over time and problems solved by them

S. No.	DPGA version	Novelty and problems solved	Year
1	DPGA	It has two distinct populations prospect population and preserver population with different evolutionary objectives to solve premature convergence problem of GA [3]	2006
		Proposed preserver function provides additional diversity to prospect population	
2	DPGA-ED	Unlike DPGA, reserve population of DPGA-ED evolves by itself and thus overcomes breach of diversity. Crossbreeding and survival selection are used newly for information exchange between main and reserve population. Various multimodal test functions are tested against DPGA-ED, but more diverse problem yet needs to be tested [4]	2007
3	DPGA-A	Uses new fitness function for reserve population that dynamically adjusts the distance between the populations which is important in maintaining diversity. Ten-dimension version of Rosenbrock, Griewangk, Rastrigin, and Schwefel function is solved using DPGA-A, but the best population differs in each problem [5]	2007
4	DPGA2	It has two reserve populations. One uses small value of δ for fitness function, and other uses large value of δ. Appropriate diversity provided, regardless of problem characteristics. Knapsack problem, royal road function, and deceptive functions are solved in [6]. DPGA2 provides solution for dynamic optimization problem without prior knowledge about the problem	2008
5	DPGA for all data	Implemented on various classes of problems, i.e., 23 benchmark test functions for binary, real-valued representations and four versions of TSP for order-based representation [2]	2010
6	Hybrid DPGA	Application-specific single machine maximum lateness problem [20]	2011
7	MPDPGA	Multithreaded parallel DPGA which solves premature convergence and diversity problems of GA [22]	2014

References

1. Tang, K., Mang, K., et al.: Genetic algorithm and their applications. IEEE Signal Process. Mag. **13**(6), 22–37 (1996). doi:10.1109/79.543973
2. Park, T., Ruy, K.: A dual-population genetic algorithm for adaptive diversity control. IEEE Trans. Evol. Comput. **14**(6), 865–883 (2010). doi:10.1109/TEVC.2010.2043362
3. Park, T., Ruy, K.: A Dual-Population Genetic Algorithm for Balance Exploration and Exploitation. Acta Press Computational Intelligence (2006)
4. Park, T., Ruy, K.: A dual population genetic algorithm with evolving diversity. In: Proceedings of IEEE Congress on Evolutionary Computing, pp. 3516–3522 (2007). doi:10.1109/CEC.2007.4424928

5. Park, T., Ruy, K.: Adjusting population distance for dual-population genetic algorithm. In: Proceedings of Australian Joint Conference on Artificial Intelligence, pp. 171–180 (2007). doi:10.1109/TEVC.2010.2043362
6. Park, T., Choe, R., Ruy, K.: Dual-population genetic algorithm for nonstationary optimization. In: Proceedings of GECCO'08 ACM, pp. 1025–1032 (2008). doi:10.1145/1389095.1389286
7. Yao, X., Liu, Y., Lin, G.: Evolutionary programming made faster. IEEE Trans. Evol. Comput., 82–102 (1999). doi:10.1109/4235.771163
8. Lee, C., Yao, X.: Evolutionary programming using mutations based on the Lévy probability distribution. IEEE Trans. Evol. Comput. **8**, 1–13 (2004). doi:10.1109/TEVC.2003.816583
9. Bäck, T., Fogel, D., Michalewicz, Z., et al.: Handbook on Evolutionary Computation. IOP Publishing Ltd./Oxford University Press, Oxford (1997)
10. Harick, G.: Finding multimodal solutions using restricted tournament selection. In: Proceedings of 6th International Conference on Genetic Algorithms (ICGA), pp. 24–31 (1995)
11. Lozano, M., Herrera, F., Krasnogor, N., Molina, D.: Real-coded memetic algorithms with crossover hill-climbing. Evol. Comput. **12**(3), 273–302 (2004). doi:10.1162/1063656041774983
12. Liang, J., Qin, A., Suganthan, P., Baskar, S.: Comprehensive learning particle swarm optimizer for global optimization of multimodal functions. IEEE Trans. Evol. Comput. **10**, 281–295 (2006). doi:10.1109/TEVC.2005.857610
13. Molina, D., Herrera, F., Lozano, M.: Adaptive local search parameters for real coded memetic algorithms. In: Proceedings of IEEE Congress Evolutionary Computation (CEC 2005), pp. 888–895 (2005). doi:10.1109/CEC.2005.1554777
14. Yang, Z., He, J., Yao, Z.: Making a difference to differential evolution. In: Michalewicz, Z., Siarry, P. (eds.) Advances in Metaheuristics for Hard Optimization, pp. 397–414, Springer (2007). doi:10.1007/978-3-540-72960-0_19
15. Hansen, N., Muller, S.D., Koumoutsakos, P.: Reducing the time complexity of the de-randomized evolution strategy with covariance matrix adaptation (CMAES). Evol. Comput. **11**, 1–18 (2003). doi:10.1162/106365603321828970
16. Alama, M.S., Islama, M.M., Yaob, X., Murased, K.: Diversity guided evolutionary programming: a novel approach for continuous optimization. Applied soft computing, 12, pp. 1693–1707 Elseiver, London (2012). doi:10.1016/j.asoc.2012.02.002
17. Cheng, J., Zhang, G.: Improved differential evolutions using a dynamic differential factor and population diversity. In: Proceedings of International Conference on Artificial Intelligence and Computational Intelligence, pp. 402–406 (2009). doi:10.1109/AICI.2009.151
18. Qu, B., Suganthan, P.: Constrained multi-objective optimization algorithm with diversity enhanced differential evolution. In: IEEE Conference on Evolutionary Computation (CEC 2010) (2010). doi:10.1109/CEC.2010.5585947
19. Worasucheep, C.: A particle swarm optimization with diversity-guided convergence acceleration and stagnation avoidance, In: Proceedings of 8th International Conference on Natural Computation (ICNC 2012), pp. 733–738 (2012). doi:10.1109/ICNC.2012.6234647
20. Sels, V., Vanhoucke, M.: A hybrid dual population genetic algorithm for the single machine maximum lateness problem. In: Evolutionary COP 2011, LNCS 6622, pp. 14–25 (2011). doi:10.1007/978-3-642-20364-0_2
21. Umbarkar, A., Joshi, M.: Dual population genetic algorithm (GA) versus OpenMP GA for multimodal function optimization. Inter. J. Comput. Appl. **64**(19), 29–36 (2013). doi:10.5120/10744-5516
22. Umbarkar, A., Joshi, M., Hong, W.: Multithreaded parallel dual population genetic algorithm (MPDPGA) for unconstrained function optimizations on multi-core system. Appl. Math. Comput. **243**, 936–949 (2014). doi:10.1016/j.amc.2014.06.033

Speed Control of Multilevel Inverter-Based Induction Motor Using V/F Method

Smrati Singh, Piyush Sharma, Arpit Varshney and Ankit Kumar

Abstract In this paper, the speed of a three-phase induction motor is controlled by using modified cascaded five-level inverter and we compared the total harmonic distortion of the modified cascaded five-level inverter with the conventional three-level inverter. To reduce the total harmonic distortion, multicarrier PWM is used. An open-loop speed control has been achieved by using V/f method. The simulation result gives that the modified cascaded five-level inverter effectively controls the motor speed and enhances the drive performance through reduction in total harmonic distortion (THD).

Keywords Modified cascaded five-level inverter (MCFLI) · Induction motor · Multicarrier PWM · THD · V/f control

1 Introduction

Adjustable speed drives (ASDs) are the essential and endless demand of the industries and researchers. They are widely used in the industries to control the speed of conveyor systems, blower speeds, machine tool speeds, and other applications. In many

S. Singh (✉) · A. Varshney
Electrical and Electronics Engineering Department, SRM University, NCR Campus, Modinagar, Uttar Pradesh, India
e-mail: smrati.friends@gmail.com

A. Varshney
e-mail: arpit291189@gmail.com

P. Sharma
Electrical Engineering Department, SS College of Engineering, Udaipur, Rajasthan, India
e-mail: piyushsharma034@gmail.com

A. Kumar
School of Electrical, Electronics and Communication Engineering, Subharti University, Meerut, India
e-mail: sunnytyagi2005@gmail.com

K.N. Das et al. (eds.), *Proceedings of Fourth International Conference on Soft Computing for Problem Solving*, Advances in Intelligent Systems and Computing 335,
DOI 10.1007/978-81-322-2217-0_20

industrial applications, traditionally, DC motors were the workhorses for the ASDs due to their tremendous speed and torque response. But, they have the inherent inconvenience of commutator and mechanical brushes, which undergo wear and tear with the passage of time. In most cases, AC motors are preferred to DC motors, in particular an induction motor due to its low cost, low maintenance, lower weight, higher efficiency, improved ruggedness, and reliability. All these features make the use of induction motors mandatory in many areas of industrial applications [1–5].

The advancement in power electronics and semiconductor technology has triggered the development of high-power and high-speed semiconductor devices in order to achieve a smooth, continuous, and step-less variation in motor speed. Applications of solid-state converters/inverters for adjustable speed induction motor drive are widespread in electromechanical systems for a large spectrum of industrial systems. Voltage or current converters, as they generate discrete output waveforms, force the use of machines with special isolation and in some applications large inductances connected in series with the respective load. Also, it is well known that distorted voltages and current waveforms produce harmonic contamination, additional power losses, and high-frequency noise that can affect not only the power load but also the associated controllers. All these unwanted operating characteristics associated with pulse-width modulation (PWM) converters could be overcome with multilevel converters. Nowadays, multilevel inverters are the promising alternative and cost-effective solution for high-voltage and high-power applications including power quality and motor drive problems. Multilevel structure allows raising the power-handling capability of the system in a powerful and systematic way.

In this paper, three-level and a modified cascaded five-level inverter Simulink models are developed for induction motor drives. A modified cascaded five-level inverter has less number of switches as compared to conventional five-level H-bridge inverter. THD of this inverter has been compared with the conventional three-level inverter and gives a reduced amount of THD. The simulation of three-level and modified cascaded five-level inverter-fed induction motor models is carried out in MATLAB. The FFT spectrums for the outputs are analyzed to study the reduction in the harmonics.

2 Multilevel Inverter

Multilevel voltage source converters are emerging as a new breed of power converter options for high-power applications. The multilevel voltage source converters typically synthesize the staircase voltage wave from several levels of dc voltages. There are some multilevel voltage source converters which are

1. Diode clamp
2. Flying capacitors
3. Cascaded inverters

Increasing the number of voltage levels in the inverter without requiring higher rating on individual devices can increase power rating. The unique structure of multilevel voltage source inverters allows them to reach high voltages with low harmonics without the use of transformers or series-connected synchronized switching devices. The harmonic content of the output voltage waveform decreases significantly. Ac loads require constant or adjustable voltages at their input terminals. When such loads are fed by inverters, it is essential that output voltage of the inverters is so controlled as to fulfill the requirements of AC loads. This involves coping with the variation of DC input voltage, for voltage regulation of inverters and for the constant volts/frequency control requirement. There are various techniques to vary the inverter gain. The most efficient method of controlling the gain (and output voltage) is to incorporate PWM control within the inverters. The carrier-based PWM schemes used for multilevel inverters are one of the most straightforward methods of describing voltage source modulation realized by the intersection of a modulating signal (duty cycle) with triangular carrier waveform [6, 7].

3 Modified Cascaded Five-Level Inverter

In modified cascaded five-level inverter, an auxiliary circuit is added in the simple H-bridge inverter. The output voltage of simple H-bridge inverter is the three-level voltage waveform, and to make it a five-level waveform, the auxiliary circuit is connected, which contains two back-to-back IGBT switches in series with the diodes. Figure 1 shows a single-phase modified cascaded five-level inverter.

For $+V_{dc}/2$, switches S_4 and S_6 are on, for $+V_{dc}$, switches S_1 and S_4 are on, for $-V_{dc}/2$, switches S_2 and S_3 are on, for $-V_{dc}$, switches S_2 and S_5 are on, and for zero, either switches S_4, S_1 or switches S_2, S_4 is conduct shows in Table 1. Therefore, five-level inverter output voltage is obtained. Multicarrier sinusoidal PWM law has been adopted to generate the gating pulses for modified cascaded five-level inverter.

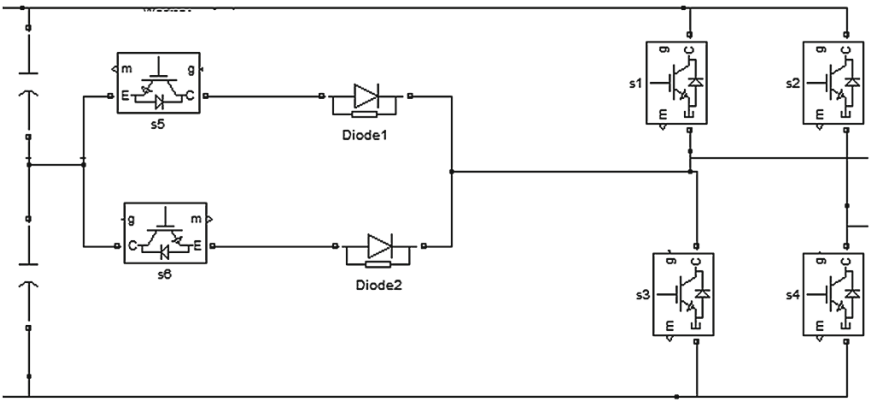

Fig. 1 Single-phase modified cascaded five-level inverter

Table 1 Switching states

On switching state	V_a	V_b	$V_{ab} = V_0$
S4, S1	V_{dc}	0	$+V_{dc}$
S4, S6	$V_{dc}/2$	0	$+V_{dc}/2$
S4, S3	0	0	0
S2, S1	$V_{dc}/2$	$V_{dc}/2$	0
S2, S5	0	V_{dc}	$-V_{dc}$
S2, S3	0	$V_{dc}/2$	$-V_{dc}/2$

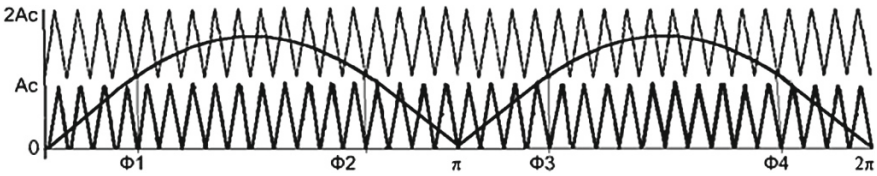

Fig. 2 Pulse width modulation for generating the gate pulses

4 Adopted Pulse Width Modulation

Figure 2 shows the pulse width modulation for generating gate pulses of single-phase MCFLI. To obtain the five-level PWM, reference sine wave is compared with two triangular carrier waves of high frequency (about 1.6–2 kHz). First, V_{ref} is compared with the carrier 1 as $V_{ref} > V_{c1}$ up to Φ1. After Φ2, V_{ref} is compared with V_{c2} and similar outputs received. If modulating index is $(M_a) > 0.5$, the output will be a five level. Modulating index is $M_a = A_m/2A_c$, where A_m is amplitude of modulating (reference) signal and A_c is the amplitude of carrier signal.

5 Speed Control of Induction Motor

It is very important to control the speed of induction motors in industrial and engineering applications. Efficient control strategies are used for reducing operation cost too. Speed control techniques of induction motors can be broadly classified into two types—scalar control and vector control. Scalar control involves controlling the magnitude of voltage or frequency of the induction motor (Fig. 3) [8–11].

Having known the torque–speed characteristic of the motor, its speed can be controlled in three ways:

(i) Changing the number of poles
(ii) Varying the input voltage at fixed frequency
(iii) Varying both the input voltage and frequency accordingly

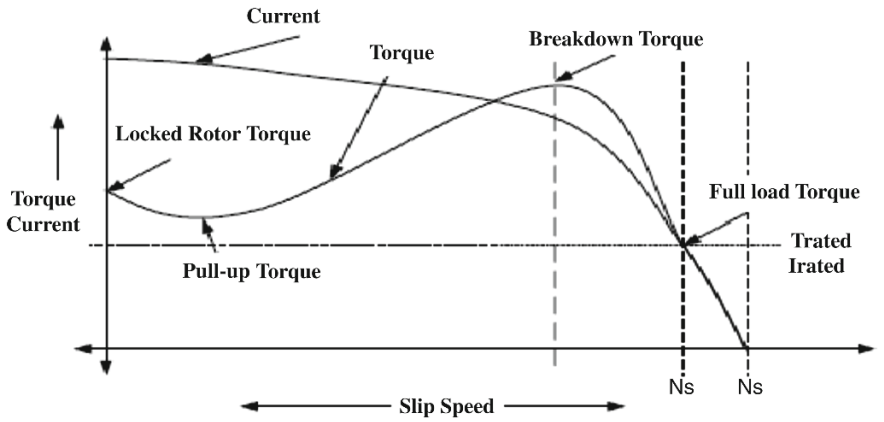

Fig. 3 Torque–speed characteristic of induction motor

To maintain the torque capability of the motor close to the rated torque at any frequency, the air gap flux, φ_{ag}, is maintained constant. Any reduction in the supply frequency without changing the supple voltage will increase the air gap flux, and the motor may go to saturation. This will increase the magnetizing current, distort the line current and voltage, and increase the core loss and copper loss, and it makes the system noisy.

The air gap voltage is related to φ_{ag} and the frequency f as

$$E_{ag} = K_1 \varphi_{ag} f \tag{1}$$

$$V_s \approx K_1 \varphi_{ag} f \tag{2}$$

or

$$\varphi_{ag} = \text{constant} \approx \frac{V_s}{f} \tag{3}$$

where K_1 is a constant.

6 V/F Control of Induction Motor

Figure 4 shows the block diagram of closed-loop V/f control of three-phase induction motor. The speed error is processed through a PI controller and slip speed regulator. The slip speed regulator sets the slip speed command ω_{sl}, whose maximum value is limited to limit the inverter current to a permissible value [12–15].

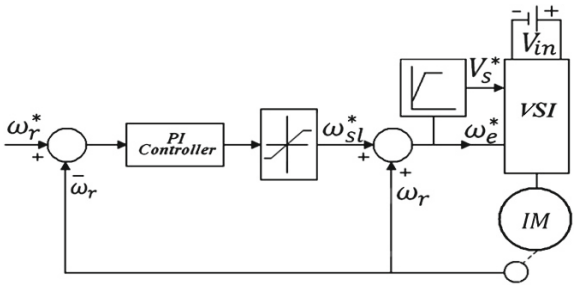

Fig. 4 Closed-loop volts/Hz control of induction motor

The synchronous speed, obtained by adding actual speed ω_r and slip speed ω_{sl}, determines the inverter frequency. The reference signals for the closed-loop control of the machine terminal voltage V_s^* are generated from frequency f using a function generator. It ensures nearly a constant flux operation up to the base speed and the operation at a constant terminal voltage above the base speed. A step increased in speed command ω_m^* produces a positive speed error. The slip speed command ω_{sl}^* is set at a maximum value. The drive accelerated at a maximum permissible inverter current and producing the maximum available torque until the speed error is reduced.

7 Simulation Results

Figure 5 shows the MATLAB/Simulink model of closed-loop V/f control of three-phase induction motor. It consists of DC source, three-phase inverter, and three-phase induction motor as open loop, and in addition to that, it has PI controller and limiter.

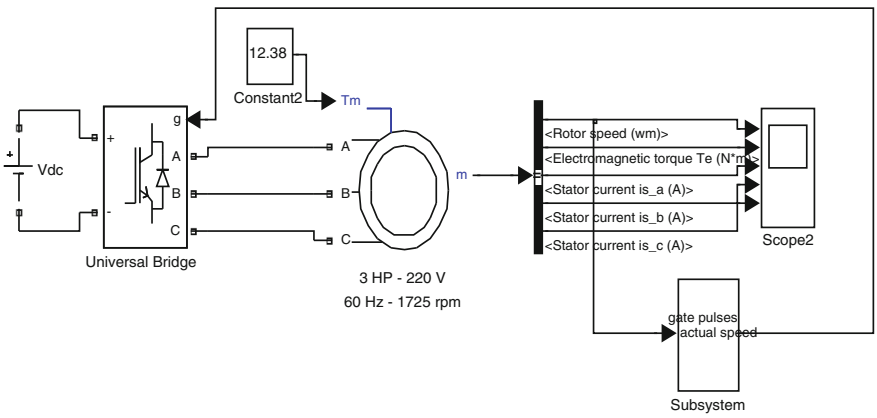

Fig. 5 MATLAB/Simulink model for closed-loop V/f control of induction motor

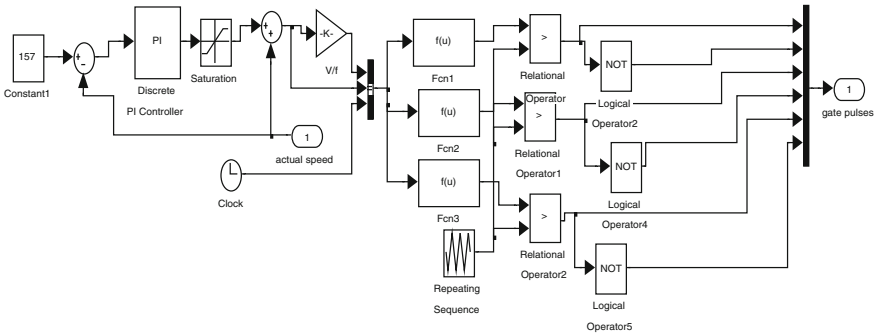

Fig. 6 MATLAB/Simulink model for pulse generation

Now, the simulation circuit is run with closed-loop control that shows speed of the induction motor. Here, a subsystem shows the generation of gate pulses, and a universal bridge is used as a three-phase inverter. Figure 6 shows the Simulink model for generating the pulses.

Figures 7, 8 and 9 show the motor speed, torque, and stator current of a three-phase inverter-fed induction motor. Reference speed is set at 157 rad/s. It reaches the steady state at 0.3 s.

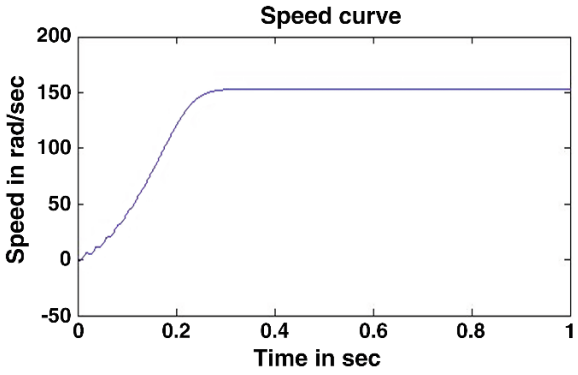

Fig. 7 Speed of three-level inverter-fed I/M

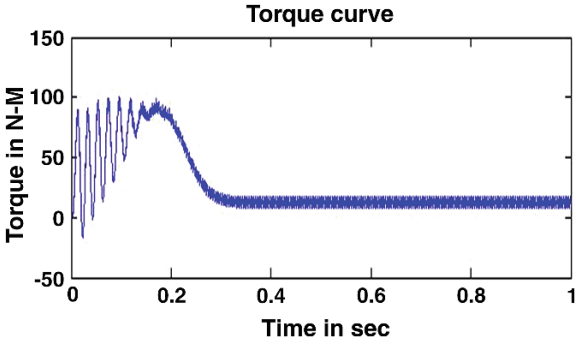

Fig. 8 Torque curve of three-level inverter-fed I/M

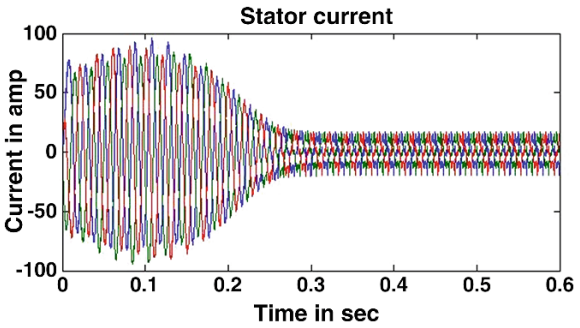

Fig. 9 Stator current of three-level inverter-fed I/M

Figure 10 shows the PWM generation for a modified cascaded five-level inverter for one phase. PWM generation is considered the more important in the inverter design, and several multicarrier techniques have been developed to reduce the distortion in multilevel inverters, based on the classical (SPWM) with triangular carriers.

The PWM pattern adopted in modified cascaded five-level inverter makes the inverter producing output voltage with three levels (zero and half supply dc voltage positive and negative, respectively) at modulation index ($M_a \leq 0.5$) and five levels (zero, half, and full supply voltage positive and negative, respectively) at modulation index ($M_a > 0.5$).

Figure 11 shows the modified cascaded five-level inverter for a single phase. Here, only six controlled switches are used to get five levels which reduced the complexity of the circuit and the total harmonic distortion as compared to conventional inverter.

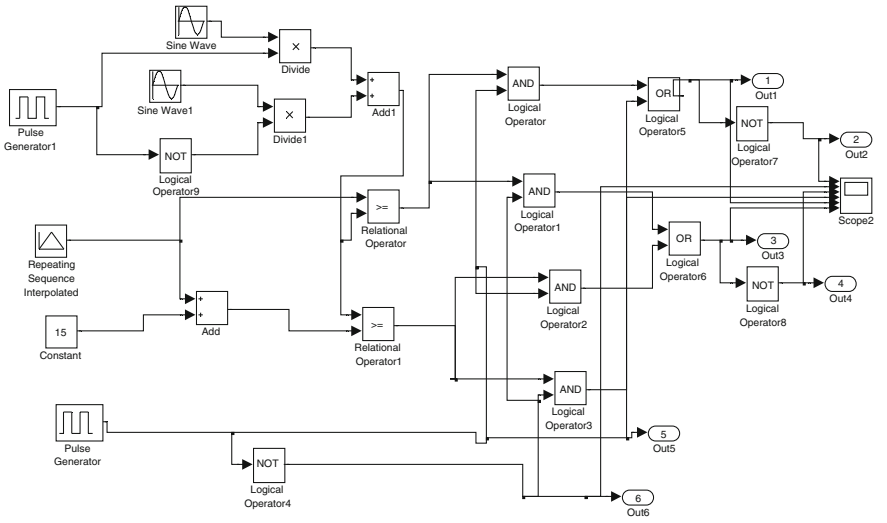

Fig. 10 MATLAB/Simulink model for pulse generation of MCFLI

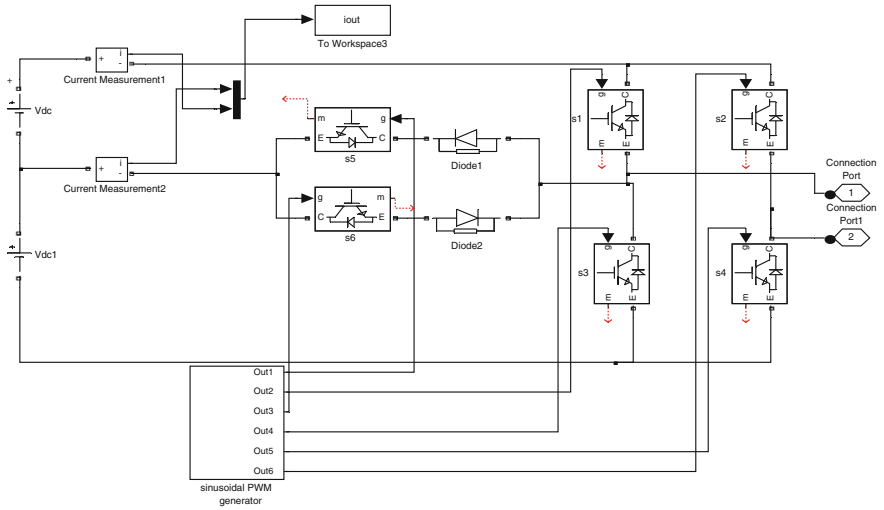

Fig. 11 MATLAB/Simulink model for modified cascaded five-level inverter

Figure 12 shows Simulink model for the open-loop V/f control of the modified cascaded five-level inverter-fed induction motor. Here, remaining two phases have been obtained by giving a 120° phase shift in modulating signal. The scope is connected through bus selector that shows speed, torque, and stator current of the induction motor.

Figures 13, 14, 15, 16, 17, 18 and 19 show the phase voltage, line voltage, motor speed, torque, stator current, and THD of a modified cascaded five-level inverter. By comparing the three-phase inverter and a modified cascaded five-level inverter, we can say that the distortion in five-level inverter voltage is less. The current

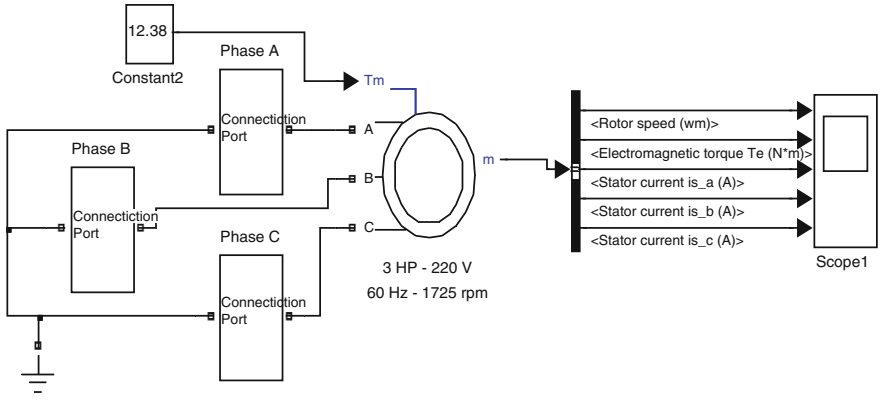

Fig. 12 MATLAB/Simulink model for modified cascaded five-level inverter-fed I/M

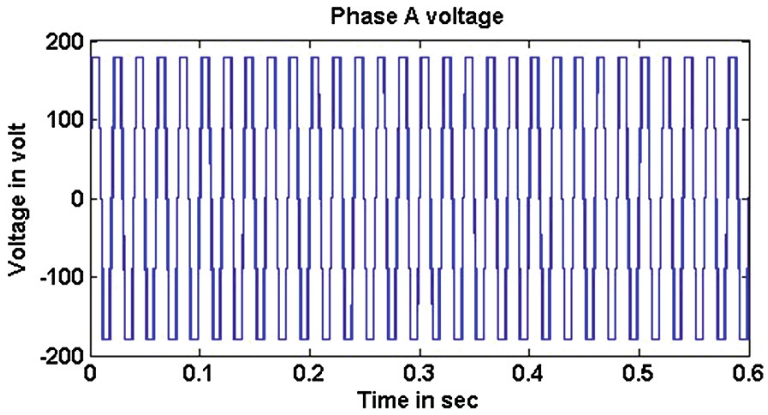

Fig. 13 Phase voltage of a modified cascaded five-level inverter

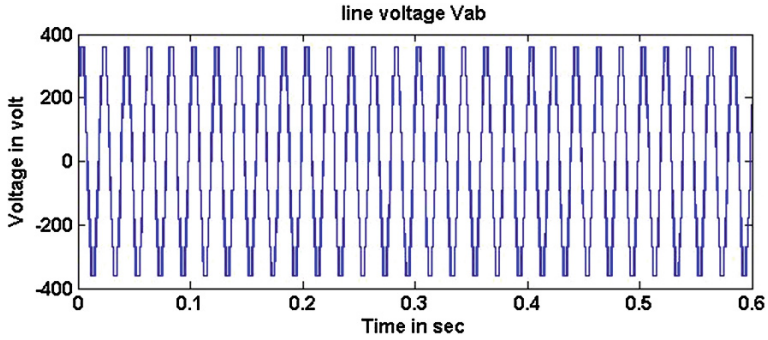

Fig. 14 Line voltage of a modified cascaded five-level inverter

waveforms are closed to sinusoidal. The speed and torque ripples are very less as compared to three-phase inverter. Dynamic response is also better for five-level inverter, which can be observed from the speed and torque waveforms. Figures 18 and 19 represent the harmonic spectrum analysis of a five-level inverter. In this case, the total harmonic distortion is 12.30 % in phase voltage and 1.55 % in line voltage. Table 2 shows the comparison of THD in three-level inverter and modified cascaded five-level inverter.

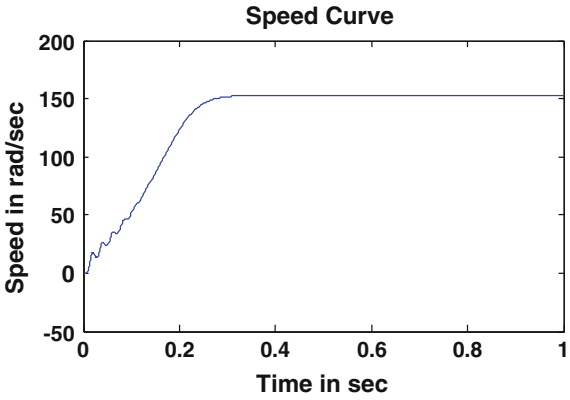

Fig. 15 Speed of a modified cascaded five-level inverter-fed I/M

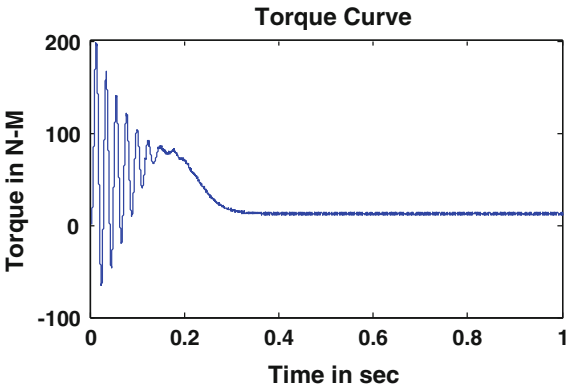

Fig. 16 Torque of a modified cascaded five-level inverter-fed I/M

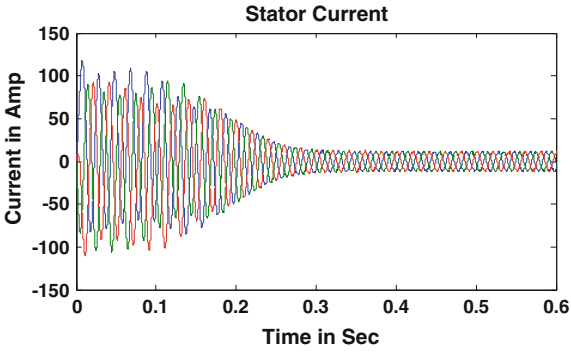

Fig. 17 Stator current of a modified cascaded five-level inverter-fed I/M

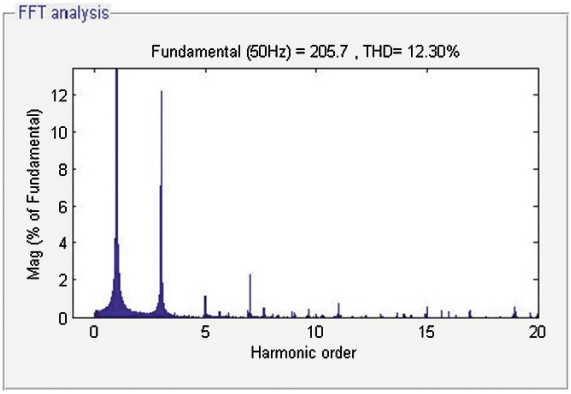

Fig. 18 Harmonic spectrum of phase voltage and voltage of modified cascaded five-level inverter

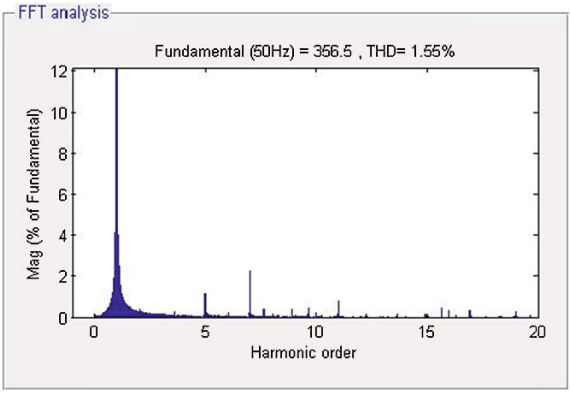

Fig. 19 Harmonic spectrum of line

Table 2 Comparison of THD

Parameter	THD (%) in three-level inverter	THD (%) in modified cascaded five-level inverter
Phase voltage	22.50	12.30
Line voltage	4.27	1.55

8 Conclusion

A three-level and a modified cascaded five-level inverters have been simulated. The following features of the system have been demonstrated in the simulation study. The less total harmonic distortion has been achieved in phase voltage and line voltage with modified cascaded five-level inverter. Speed of the induction motor has been controlled and achieved the steady-state response in 3 s in the case of three-level inverter and in 25 s in the case of modified five-level inverter.

Appendix

Parameter Values

Induction motor: R_S = 0.435 Ω, L_{lS} = 4e − 3H, $R'_r = 0.816\,\Omega$, $L'_{lr} = 2e - 3$ H, L_m = 69.31e3 H, p = 4, power = 3 hp, line–line voltage (rms) = 220 V.

PI controller: K_i = 50, K_p = 2.

References

1. Rashid, M.H.: Power Electronics: Circuits, Devices and Applications, 2nd edn. Prentice-Hall Inc., Englewood Cliffs (1993)
2. Bose, B.K.: Power Electronics and Motor Drives. Academic Press, an imprint of Elsevier, Massachusetts (2006)
3. Rodriguez, J., Lai, J.S., Peng, F.Z.: Multilevel inverters: survey of topologies, controls, and applications. IEEE Trans. Ind. Appl. **49**(4), 724–738 (2002)
4. Ogbuka, C.U., Agu, M.U.: A modified closed loop V/F controlled induction motor drive. Pac. J. Sci. Technol. **10**(1) (2009)
5. FloraViji Rose, S., Manikandan, B.V.: Simulation and implementation of multilevel inverter based induction motor drive. IEEE Trans. Ind. Appl. **IA-9**(3) (2009)
6. Tolbert, L.M., Peng, F.Z., Habetler, T.G.: Multilevel converters for large electric drives. IEEE Trans. Ind. Appl. **35**, 36–44 (1999)
7. Stemmler, H.: Power electronics in electric traction applications. In: IEEE Conference of Industrial Electronics, Control and Instrumentation, IECON'93, Vol. 2, No. 7, pp 07–713 (1993)
8. Selvaraj J., Rahim, N.A.: Multilevel inverter for grid-connected PV system. IEEE Trans. Ind. Electron. **56**(1) (2009)
9. Manasa, S., Balaji Ramakrishana, S., Madhura, S. Mohan, H.M.: Design and simulation of three phase five level and seven level inverter fed induction motor drive with two cascaded H-bridge configuration. Int. J. Electri. Electron. Eng. (IJEEE) **1**(4), 25–30 (2012)
10. Murugesan, M., Sivaranjani, S., Asokkumar, G., Sivakumar, R.: Seven level modified cascaded inverter for induction motor drive applications. J. Inf. Eng. Appl. **1**(1), 36–45 2011
11. Tembhekar, T.D.: Improvement and analysis of speed control of three phase induction motor drive including two methods. In: Second International Conference on Emerging Trends in Engineering and Technology, ICETET-09 (2009)
12. Holmes, D.G., McGrath, B.P.: Multicarrier PWM strategies for multilevel inverters. IEEE Trans. Ind. Electron. **49**(4), 858–867 (2002)
13. Sundararajan, K., Nachiappan, A., Veerapathiran, G.: Comparison of current controllers for a five-level cascaded H-bridge multilevel inverter. Int. J. Comput. Eng. Res. (ijceronline.com) **2** (6), 55–62 (2012)
14. Rose, S.F.V., Manikandan, B.V.: Simulation and implementation of multilevel inverter based induction motor drive. INCACEC **2009**, 1–8 (2009)
15. Pravin, S.E., Starbell, R.N.: Induction motor drive using seven level multilevel inverter for energy saving in variable torque load application. ICCET **2011**, 352–357 (2011)

Application of New Hybrid Harmony Search Algorithms Based on Cellular Automata Theory for Solving Magic Square Problems

Do Guen Yoo, Ali Sadollah, Joong Hoon Kim and Ho Min Lee

Abstract Magic square construction is a complex and hard permutation problem of recreational combinatorics with a long history. The complexity level enhances rapidly when the number of magic squares increases with the order of magic square. This paper proposes two hybrid metaheuristic algorithms, so-called cellular harmony search (CHS) and smallest-small-world cellular harmony search (SSWCHS) for solving magic square problems. The inspiration of the CHS is based on the cellular automata (CA) formation, while the SSWCHS is inspired by the structure of smallest-small-world network (SSWN) and CA using the concept of HS. Numerical optimization results obtained are compared with different optimizers in terms of statistical results and number of found feasible solutions. Computational results show that the proposed hybrid optimizers are computationally effective and highly efficient for tackling magic square problems.

Keywords Magic square · Harmony search · Metaheuristics · Feasibility problem · Combinatorial optimization

D. Guen Yoo (✉) · A. Sadollah · J.H. Kim · H.M. Lee
School of Civil, Environmental and Architectural Engineering, Korea University, Seoul 136-713, Republic of Korea
e-mail: godqhr425@korea.ac.kr

A. Sadollah
e-mail: sadollah@korea.ac.kr

J.H. Kim
e-mail: jaykim@korea.ac.kr

H.M. Lee
e-mail: dlgh86@korea.ac.kr

K.N. Das et al. (eds.), *Proceedings of Fourth International Conference on Soft Computing for Problem Solving*, Advances in Intelligent Systems and Computing 335,
DOI 10.1007/978-81-322-2217-0_21

1 Introduction

Magic squares have been a popular topic in recreational mathematics, papers, and books for generations. Magic squares have appeared in astrology, jewelry, paintings, carvings, and so forth. Magic squares have been investigated in an attempt to create them and better understanding of their interesting properties. A brief history of the magic square includes the earliest known example dating back to 650 BC in China [1].

In nineteenth century, mathematicians applied the magic squares in probability and analysis problems [2]. For instance, attractive patterns may be obtained by connecting consecutive numbers in some special classes of magic squares. Nowadays, magic squares are studied in relation to factor analysis, combinatorial mathematics, matrices, modular arithmetic, and geometry. In the times of information technology, magic squares have found many practical applications in artificial intelligence, graph theory, game theory, electronic circuits, and, etc., and probably will be extended to more innovated applications.

Kraitchik [3] developed several general deterministic techniques for constructing even and odd squares of order n. These deterministic methods cannot construct any other possible magic squares with additional properties [4, 5]. Essentially, differing from the deterministic methods, this paper investigated the application of stochastic optimization methods based on the concept of the cellular automata formation and the topological structure of smallest-small-world network.

Recently, metaheuristic optimization methods are widely used in problem solving era [6]. Among optimization methods, many researchers are interested in these stochastic approaches due to their simplicity and efficiency for tackling complex optimization problem such as combinatorial problems [7].

Im et al. [8] recently developed two hybrid methods that utilize the concepts of cellular automata formation along with the smallest-small-world theory, named as CHS and SSWCHS. The HS is inspired based on musical performance processes that occur when a musician searches for a better state of harmony [9].

The CHS and SSWCHS were successfully applied for continuous optimization problems [8]. This study compares the relative performance of the CHS and SSWCHS in combinatorial optimization problems of magic square problems. Furthermore, the efficiency of the proposed improved algorithms is compared with optimization results obtained by other existing optimizers.

The main goal of this paper is to generate possible solution of 3 by 3 and 4 by 4 magic squares using the CHS and SSWCHS. The remainder of this paper is organized as follows: The next section describes magic square problem formulation and its optimization model. In Sect. 3, the proposed CHS and SSWCHS approaches along with their processes are explained in brief. Section 4 compares statistical optimization results using the proposed hybrid methods with other optimization engines. Finally, conclusions are drawn in Sect. 5.

2 Magic Square Problems

A magic square is an arrangement of distinct and integer numbers (i.e., each number is used once), in a square grid, where the numbers in each row and in each column, and the numbers in the forward and backward main diagonals, all add up to the same number. Indeed, the magic square is a square matrix of order n.

Therefore, a magic square always contains n^2 numbers, and its size is defined as being "of order n" [10]. The constant that is the sum of every row, column, and diagonals (i.e., main and minor diagonals) is called the magic constant or magic sum, M. Every normal magic square has a unique constant determined solely by the value of n, which can be calculated using the following equation [11]:

$$M = \frac{n(n^2+1)}{2} \tag{1}$$

In optimization point of view, magic square problems classified as satisfiability problem, also called the feasibility problem, is just the problem of finding any feasible solution at all without regard to objective value. This can be regarded as the special case of mathematical optimization where the objective value is the same for every solution, and thus, any solution is optimal. Therefore, in order to solve magic square problems having n order, the following optimization model is suggested as follows [12]:

$$\begin{aligned}
&\forall i,j \in \{1,2,\ldots,N\} && \text{All different}\{x_{ij}\}\\
&\text{subject to:}\\
&g_1 : \sum_{i=1}^{N} x_{ij} = M && \forall j \in \{1,2,\ldots,N\}\\
&g_2 : \sum_{j=1}^{N} x_{ij} = M && \forall i \in \{1,2,\ldots,N\}\\
&g_3 : \sum_{i=1}^{N} x_{ii} = M\\
&g_4 : \sum_{i=1}^{N} x_{i(N-i+1)} = M
\end{aligned} \tag{2}$$

where g_1 and g_2 denote constraints of any violations in horizontal and vertical lines, respectively. g_3 and g_4 represent constraints of any violations in major and minor diagonals. In this study, we tackled the magic squares having order 3 and 4 (n = 3 and 4).

Further statistical analysis reveals that the number of magic squares increases exponentially with the order; therefore, the difficulty of searching a magic square also dramatically increases [13]. It is worth pointing out that there is no known deterministic algorithm for generating even-order normal magic squares. However, there are some methods for creating magic squares of specific even orders [14].

3 Proposed Hybrid Methods

In this section, we proposed two improved variations of HS that use the CA and topological structure concept (i.e., CHS) [8, 15, 16] and, in addition of having CA feature, has the shortest path of the smallest-small-world network (SSWN) (i.e., SSWCHS) [8, 17]. A population is just a group of certain number of arbitrary objects in the same harmony memory as for the harmony memory (HM) in the original HS. Meanwhile, these objects are not related to each other. In the configuration of these populations as a kind of random network, the characteristic path length (L) and clustering coefficient (C) are also very low. This is a characteristic of original HS.

In contrast, if the population only consists of a grid of cellular networks, the C is relatively high, however, the L is also high. Since high L makes the interactions of remote nodes difficult, therefore, we need to reduce the L. The SSWN models have advantages of both random and regular networks. They have low L for fast interaction between nodes, and also high C ensuring sufficient redundancy for high fault tolerance [17]. In this study, the population of the original HS [9] (i.e., HM) consists of a form of cellular networks (i.e., CHS). In addition, we can reduce the L and increase the C via the shortcuts concepts of the SSWN (i.e., SSWCHS).

3.1 Cellular Harmony Search

The operation process of the CHS is shown in Fig. 1. The CHS's main operation process is the same as the HS. However, the CHS's initial population uses a cellular form such as sub-population (i.e., 3×3 matrix as shown in Fig. 1). In this process, new harmony memory in the sub-network is produced and it is compared with the existing population. If the new solution is better than the lowest ranked object, they switch the position. After fitness comparison among grid cells, the object of the highest priority is located in the center of the sub-network. Finally, the centers of the sub-network nodes are compared, and the object of the entire population of the highest priority and the central node are just replaced in the new HM [8].

3.2 Smallest-Small-World Cellular Harmony Search

Talking about the SSWCHS, it performs by interactions among the center nodes using shortcuts in the CHS. In the SSWCHS, the center nodes are added in the calculation process as shown in Fig. 2. In this process, the SSWCHS is performed to obtain the final optimal solution through building one more population among best solutions of each sub-population.

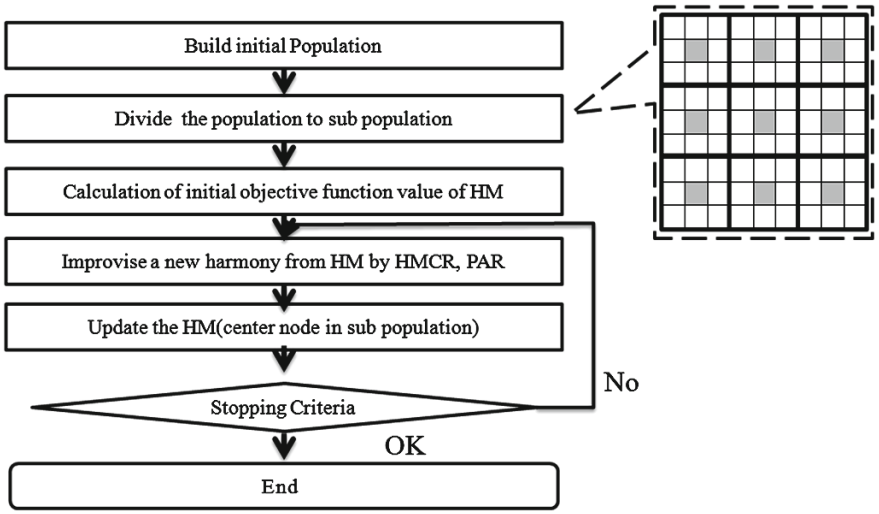

Fig. 1 Processes of the CHS [8]

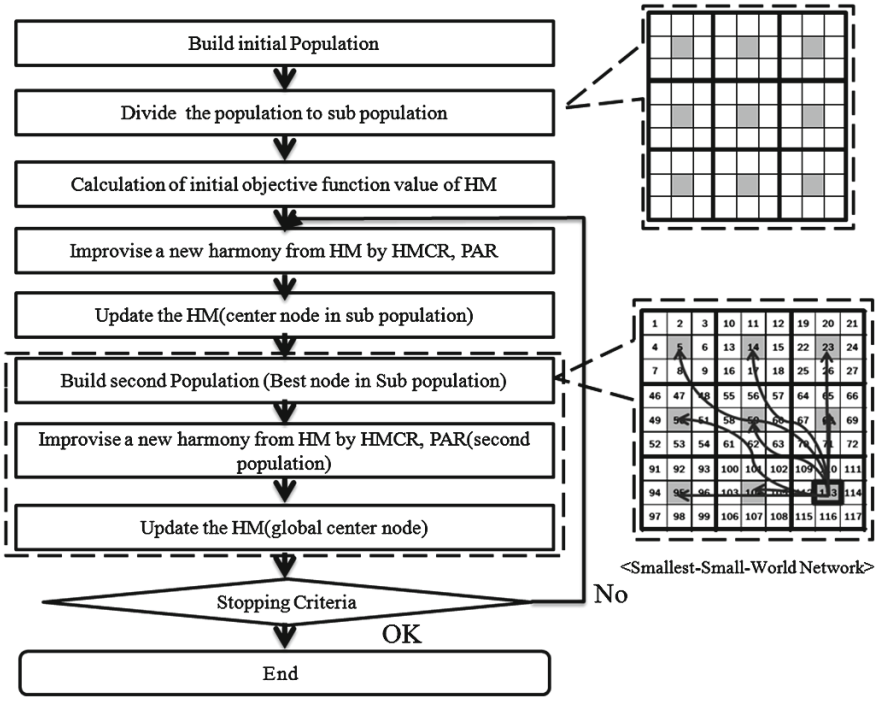

Fig. 2 Processes of the SSWCHS [8]

4 Optimization Results and Discussions

There are 9 and 16 integer numbers for magic squares with order 3 and 4, respectively, which have to be selected; hence, the problem search space consists of $9^9 = 3.9 \times 10^8$ and $16^{16} = 18.4 \times 10^{17}$ different configurations, considered as difficult solution space for finding a feasible solution satisfying all considered constraints. In light of dimension of search space for considered magic squares, the need of using metaheuristic approaches is understood.

As there were not adequate and comprehensive statistical results in literature, we implemented and launched different optimizers for having comparative study. Therefore, the genetic algorithm (GA) [18], the simulated annealing (SA) [19], the particle swarm optimization (PSO) [20], the ant system colony (ASC) [21], and the HS [9] were considered and coded in this research.

100 independent optimization runs were carried out for each test problem in order to have statistically significant results. The MATLAB programming software was used for coding and implementation purposes. The task of optimization was carried out on Pentium IV system 3,400 GHz CPU with 8 GB RAM. In order to have fair comparison with other optimizers, the maximum number of function evaluation (NFEs) (i.e., assumed as stopping condition) is set to 10,000 for all considered orders.

Table 1 Obtained optimization results for magic square with orders 3 and 4 using harmony-based algorithms

Method	HMS	FS[a]	Best NFEs[b]	Average NFEs	Worst NFEs	SD[c]	No. runs	Max. NFEs
3 × 3								
HS	30	87	36	411.49	2,035	247.41	100	10,000
	81	97	110	1,053.13	2,278	344.07	100	10,000
	225	100	287	3,089.22	6,630	1,101.02	100	10,000
CHS	81	100	90	748.98	3,582	500.96	100	10,000
	225	100	75	1,046.75	2,000	325.624	100	10,000
SSWCHS	81	100	90	722.10	3,150	409.71	100	10,000
	225	100	78	1,129.44	2,054	396.78	100	10,000
4 × 4								
HS	30	38	667	1,515.78	4,127	8,967.77	100	10,000
	81	46	2,602	4,394.84	8,947	1,403.78	100	10,000
	225	1	9,007	9,007	9,007	0	100	10,000
CHS	81	85	909	2,971.69	8,811	1,456.67	100	10,000
	225	96	2,275	5,348.70	9,750	1,683.59	100	10,000
SSWCHS	81	89	1,550	3,985.28	9,690	2,057.17	100	10,000
	225	96	1,742	5,795.02	9,984	1,759.23	100	10,000

[a] Number of detecting feasible solution
[b] Number of function evaluations
[c] Standard deviation

Table 2 Comparison of statistical optimization results among different optimizers for magic square with order 3

Method	Feasible solution	Best NFEs	Average NFEs	Worst NFEs	SD	No. runs	Max. NFEs
ASC	27	650	5,929.62	10,000	2,806.04	100	10,000
GA	39	160	678.97	8,245	1,351.16	100	10,000
PSO	84	100	273.81	1,100	195.81	100	10,000
SA	93	361	5,214.44	7,861	1,463.67	100	10,000
HS	100	287	3,089.22	6,630	1,101.02	100	10,000
CHS	100	75	1,046.75	2,000	325.624	100	10,000
SSWCHS	100	78	1,129.44	2,054	396.78	100	10,000

Table 1 shows comparison among harmony-based algorithms for two considered magic squares using different harmony memory sizes (HMS). The SSWCHS and CHS have outperformed the HS in terms of statistical results for NFEs and number of detected feasible solution. As can be seen in Table 1, the CHS and SSWCHS have very close competition for 3 by 3 magic square problem. It is worth to mention that these two optimizers are marginally different with each other.

Tables 2 and 3 represent the comparison among several metaheuristic methods for magic squares having 3 and 4 orders, respectively. Looking at Table 2, the HS, CHS, and SSWCHS found 100 feasible solutions out of 100 runs, while the CHS is outperformed against other reported methods in terms of statistical results for the NFEs. The ASC has the weakest performance among other reported optimization methods (see Table 2).

In Table 3, it can be concluded that only the CHS and SSWCHS have detected more feasible solutions than other methods. The only method which has been competed with the proposed hybrid methods is the HS. However, the HS found feasible solutions in less than 50 % of total number of runs. Similar to the 3 by 3 magic square, the ASC shows the weakest results, while the GA is ranked for the second worst method for finding possible feasible solutions. As it shows, when the

Table 3 Comparison of statistical optimization results among different optimizers for magic square with order 4

Method	Feasible solution	Best NFEs	Average NFEs	Worst NFEs	SD	No. runs	Max. NFEs
ASC	0	0 (12)[a]	0 (17.71)	0 (23)	0 (2.57)	100	10,000
GA	3	765	930	1,150	198.30	100	10,000
SA	32	5,941	7,931.62	9,671	875.27	100	10,000
PSO	36	350	2,183.33	9,700	2,183.30	100	10,000
HS	46	2,602	4,394.84	8,947	1,403.78	100	10,000
CHS	96	2,275	5,348.70	9,750	1,683.59	100	10,000
SSWCHS	96	1,742	5,795.02	9,984	1,759.23	100	10,000

[a] Values in parentheses stand for violation

order of magic square increases, the performance and efficiency of the CHS and SSWCHS are more observed.

5 Conclusions

Magic squares have been studied for at least three thousand years. In this paper, magic square problems, classified as combinatorial problems, were tackled using two new hybrid optimization methods, so-called CHS and SSWCHS. The concepts of the CHS are derived based on the CA formation, while the SSWCHS is inspired by adding the topological structure of smallest-small-world network to the CHS.

Using comparative study among different harmony-based algorithms and also other optimization methods, the proposed improved methods have shown their superiority over others in terms of number of found feasible solutions. Computational time [i.e., number of function evaluations (NFEs)] proves that the SSWCHS and CHS statistically surpassed other considered optimizers finding feasible solution in less NFEs. In this paper, the CHS and SSWCHS prove their efficiencies for solving magic square problems, while the CHS is slightly outperformed the SSWCHS.

Metaheuristic algorithms not only can stochastically construct conventional magic squares of high orders quite efficiently, possibly they also may be applied in constructing some special classes of magic squares with additional properties. Therefore, based on the results obtained from the proposed optimizers, they may be considered as suitable alternatives for efficient solving of magic square problems.

Acknowledgments This work was supported by the National Research Foundation of Korean (NRF) grant funded by the Korean government (MSIP) (NRF-2013R1A2A1A01013886).

References

1. Madachy, L.S.: Magic and antimagic squares. Chapter 4 in Madachy's Mathematical Recreations (1979)
2. Xie, T., Kang, L.: An evolutionary algorithm for magic squares. IEEE, 906–913 (2003)
3. Kraitchik M.: Magic squares. Chapter 7 in Mathematical Recreations, pp. 142–192. Norton, New York (1942)
4. Abe, G.: Unsolved problems on magic squares. Disc. Math. **127**, 3–13 (1994)
5. Monfroy, E., Castro, C., Crawford, B.: Using local search for guiding enumeration in constraint solving. In: Euzenat, J., Domingue, J. (eds.) AIMSA. Lecture notes in computer science, vol. 4183, pp. 56–65. Springer, Berlin (2006)
6. Blum, C., Andrea, R.: Metaheuristics in combinatorial optimization: overview and conceptual comparison. ACM Comput. Surv. **35**(3), 268–308 (2003)
7. Osman, I.H., Laporte, G.: Metaheuristics: a bibliography. Ann. Oper. Res. **63**, 513–623 (1996)
8. Im, S.S., Yoo, D.G., Kim, J.H.: Smallest-small-world cellular harmony search for optimization of unconstrained benchmark problems. J. Appl. Math (2013)

9. Geem, Z.W., Kim, J.H., Loganathan, G.V.: A new heuristic optimization algorithm: harmony search. Simulation **76**, 60–68 (2001)
10. Berlekamp, E.R., Convay, 1.H., Guy, R.K.: Winning ways for your mathematical plays, vol.2: Games in particular, pp. 778 783. Academic Press, London, pp. 85 113. Dover, New York 1979 (1982)
11. Pinn, K., Wieczerkowski, C.: Number of magic squares from parallel tempering monte carlo. Int. J. Mod. Phys. C **9**, 541–547 (1998)
12. Cadoli, M., Mancini, T., Patrizi. F.: Sat as an effective solving technology for constraint problems. In: Esposito, F., Ras, Z., Malerba, D., Semeraro, G., (eds.) ISMIS, Volume 4203 of Lecture Notes in Computer Science, pp. 540–549. Springer, Berlin (2006)
13. Smith, B. M., Sturdy P.: Value ordering for finding all solutions. In Kaelbling, L.P., Saffiotti, A., (eds.) IJCAI, pp. 311 316. Professional Book Center, Mumbai (2005)
14. Beck, C., Prosser, P., Wallace, R.: Toward understanding variable ordering heuristics for constraint satisfaction problems. In: Fourteenth Irish Artificial Intelligence And Cognitive Science Conference—AICS, 11–16 (2003)
15. Von Neumann, J.: Theory of Self-reproducing Automata. University of Illinois Press, Urbana and London (1966)
16. Wolfram, S.: Statistical mechanics of cellular automata. Rev. Mod. Phys. **55**(3), 601–644 (1983)
17. Nishikawa, T., Motter, A.E., Lai, Y.-C., Hoppensteadt, F.C.: Smallest small-world networks. Phys. Rev. E **66**, 046139 (2002)
18. Goldberg, D.E.: Genetic algorithms in search, optimization, and machine learning, reading, mass., Addison-Wesley Pub. Co, Reading (1989)
19. Kirkpatrick, S., Gellat, J.R.C.D., Vecchi, M.P.: Optimization by simulated annealing. Science **220**, 671–680 (1983)
20. Kennedy, J., Eberhart R.: Particle swarm optimization. In: IEEE IJCNN, Perth, Australia, 4, pp. 1942–1948 (1995)
21. Dorigo, M., Gambardella, J. M: Ant Colony System: a cooperative learning approach to the traveling salesman problem. IEEE Trans. Evol. Comput. 1(1), TR/IRIDIA/1996–5, Université Libre de Bruxelles, Belgium (1997)

A Survey on Imaging-based Breast Cancer Detection

Debalina Saha, Mrinal Kanti Bhowmik, Barin Kumar De and Debotosh Bhattacharjee

Abstract Breast cancer is undoubtedly a dreadful and life-threatening disease. It is fairly common in women and also the second deadliest cancer in the world. It is arguably the most frightening type of cancer because of its well-publicized nature and potential for lethality. If identified and properly treated in its early stage, the chance of cure increases. Different imaging techniques are there which plays a vital role in the detection of breast cancer. In recent days, mammography and thermography are the two main techniques accepted in the medical field to detect breast cancer followed by other screening methods. A literature survey is presented in this paper based on these two techniques followed by the analysis of their affordability, reliability, and outcomes.

Keywords Breast cancer · Mammography · Thermography · Infrared imaging

D. Saha (✉) · M.K. Bhowmik
Department of Computer Science and Engineering, Tripura University
(A Central University), Suryamaninagar, Agartala 799022, India
e-mail: debalinasaha1988@gmail.com

M.K. Bhowmik
e-mail: mkb_cse@yahoo.co.in

B.K. De
Department of Physics, Tripura University (A Central University),
Suryamaninagar, Agartala 799022, India
e-mail: barin_de@yahoo.com

D. Bhattacharjee
Department of Computer Science and Engineering, Jadavpur University,
Kolkata 700032, India
e-mail: debotosh@ieee.org

K.N. Das et al. (eds.), *Proceedings of Fourth International Conference on Soft Computing for Problem Solving*, Advances in Intelligent Systems and Computing 335,
DOI 10.1007/978-81-322-2217-0_22

1 Introduction

Breast cancer is a disease in which malignant (cancer) cells form in the tissue of the breast. It usually starts off in the inner lining of milk ducts or in the lobules that supply them with milk. A breast cancer that started off in the lobules is known as lobular carcinoma, while one that developed from the ducts is called ductal carcinoma. According to American Cancer Society's 2002 report on Cancer Facts and Figures [1], breast cancer is the most commonly diagnosed cancer in women and accounts 30 % of all cancers in women. As a cause of cancer death, it is next to lung cancer and also one of the common cancers in India. On the other hand, research [2] has shown that the breast cancer patient has 85 % chance of cure if detected earlier (tumor size less than 10 mm) as opposed to 10 % if detected lately. Usuki et al. [3] have reported that the rate of the growth of tumor is proportionate to its temperature. In the present days, mammography and thermography are the two most widely used methods for the detection of the breast cancer. Mammography is a specific type of imaging that uses a low-dose X-ray system to examine breasts. A mammography exam, called a mammogram, is used to aid in the early detection and diagnosis of breast diseases in women. It is also very useful method for the detection of masses and microcalcifications.

Thermography is a physiologic test that manifests heat patterns and strongly indicates the breast abnormality. Thermal infrared (TIR) imaging is noninvasive, non-ionizing, risk-free, patient-friendly, and the cost is considerably low. These features, together with its early detection capability, have enabled TIR imaging a strong candidate for complementary diagnostic tool to traditional mammography. This paper presents the literature survey of the two techniques—mammography and thermography—and also provides the information of its affordability, reliability, and its outcomes.

The rest of the paper is organized as follows: Sects. 2 and 3 describe the techniques mammography and thermography. Section 4 provides information about the databases presently available and used by the researchers. Section 5 and 6 present the extensive survey of mammography and thermography. The comparative studies between these two techniques are carried out based on different conditions in Sect. 7. And lastly, in Sect. 8, conclusion and future work of this work is discussed.

2 Mammography

Mammography is a special type of X-ray imaging of the breast to find the tumor present in the breast. It uses very low dose of ionizing radiation (usually around 30 kVp) [4, 5]. Early diagnosis of the patient is the successful treatment of breast cancer. Mammography plays a vital role in early detection of breast cancers. According to the US Food and Drug Administration (FDA) [18], mammography

can find 85–90 % of breast cancer in women those who are over 50 of age and also can detect a lump up to two years before it can be felt. Once a lump is detected, mammography can be a key in evaluating the lump to determine if it is cancerous or not. While screening, mammography can detect most breast cancer, but it can miss up to 15 % of cancers. These cancers may not be detected on a mammogram film, because of

- Low differentiation between the appearances of the cancerous tissue compared against the normal parenchymal tissue.
- Varied morphology of the findings, many of them not related to the cancer.
- Similarities between the morphologies of the findings.
- Possible deficiencies in the mammogram acquisition process.
- Visual fatigue of the radiologist.

3 Thermography

Thermography is a physiologic test that manifests heat patterns and strongly indicates the breast abnormality. The test can detect changes in the breast temperature that indicate breast diseases and abnormalities in the breast. In the last two decades, the breast thermography has achieved an average sensitivity and specificity around 90 % for breast tumor detection [6]. In addition, TIR imaging is a noninvasive, non-ionizing, risk-free, patient-friendly, and the cost is considerably low. These features together with its early detection capability have enabled TIR imaging a strong candidate for complementary diagnostic tool to traditional mammography. Thermography is very useful for detecting non-palpable breast cancer. It cannot be detected by other exams. Because of its non-radiation, non-contact, and low-cost, thermography has clearly manifested to be very valuable. In the field of medical, interest has increased in the application of thermography due to its low equipment cost and advance technologies in camera. As a breast cancer risk assessment tool in the USA, thermography has been approved by the FDA since 1982, as a screening tool for breast cancer. Thermography was first introduced in 1956 and was accepted widely by medical professionals at that time [7]. However, this acceptance rapidly ended in 1977 after a report written by Feig [8] tested the sensitivity of thermography compared to other methods of breast cancer detection. The main reason for the increase of temperature in breast cancer is due to nitric oxide (NO). The breast cancer cells produce this NO [9]. This NO interferes with the normal neuronal control of breast tissue blood vessel flow by causing regional vasodilatation in the early stages of cancerous cell growth and enhancing angiogenesis in later stages [10]. The subsequent increased blood flow in the area causes a temperature increase relative to the normal breast temperature, and even deep breast lesions seem to have the ability to induce changes in skin temperature [11]. Breast cancer metabolic processes may also contribute to the detectable increase in heat. These changes relate to physiological breast processes. It is believed that in

healthy individuals, generally, the temperature is symmetrical across the midline of the body [12]. Subjective interpretation of many diagnostic imaging modalities, including infrared thermographic images, relies on the underlying philosophy that normal contralateral images are relatively symmetrical and that small asymmetries may indicate a suspicious lesion [13]. Therefore, in breast cancer, infrared thermography detects disease by identifying areas of asymmetric temperature distribution on the breasts' surface.

4 Mammography and Thermography Databases

Several databases have commonly been used as test beds for the performance of the two imaging techniques—mammography and thermography—and to compare processing results with others for performance evaluations. Mammographic Image Analysis Society Digital Mammogram Database (MIAS) and Digital Database for Screening Mammography (DDSM) are examples of well-known and broadly used mammographic databases. MIAS database is in .png format with 8-bit images, DDSM database is in LJPEG format. Other examples of databases are computer-assisted library for mammography (CALMa) and Lawrence Livermore National Laboratory (LLNL)/UCSF database and LAPIMO. The images are in the TIFF default format with 12 bits of contrast images, and their spatial resolutions are either 0.085 or 0.150 mm.

The MIAS database contains 322 images with resolutions of 50 and 200 μm/pixel. Only 118 in the database contain some abnormality (66 are benign and 52 are malignant) and the other 204 are diagnosed as normal. The abnormalities found in these mammograms are microcalcifications circumscribed masses, speculated masses ill-defined masses, architectural distortions, and asymmetries. Since there are not many databases of thermography, only DMR is available online for accessing the database of thermogram of breast cancer. DMR or Mastology Research Database is an online platform that stores and manages mastological images for early detection of breast cancer (Table 1).

Table 1 List of databases

S. No	Name of the database	Total number of images	Image resolution	Format of images
1	Nijmegen database	40	2,048 × 2,048	Nil
2	Mammographic Image Analysis Society Digital Mammogram Database (MIAS)	322	50 and 200 μm/pixel	png
3	Digital Database for Screening Mammography (DDSM)	400	Nil	LJPEG
4	Lawrence Livermore National Laboratory (LLNL)	198	35 μm/pixel	gz
5	Laboratory of Analysis and Processing of Medical and Dental Images (LAPIMO)	Nil	0.085 mm	TIFF

5 Previous Works on Mammography

Different approaches have been obtained by different researchers to detect breast cancer through mammography. Some of the approaches have been discussed here. One approach followed is based on wavelet transform. The author Laine et al. [14] exploited the orientation and selectivity of the frequency of multiscale wavelet transforms to make mammographic features more obvious through localized contrast gain. This paper is divided into two parts. First part contains a mathematical foundation for an approach to accomplish image contrast enhancement by multiresolution representations of the dyadic wavelet transform. In the second part, an arbitrary region of interest (ROI) of a digital mammogram by Deslauriers–Dubuc interval wavelets is extracted. Image used for the experiment was a digital mammogram of size 400 × 512 and size 512 × 512 containing stellate lesions. Another author Yu and Guan [15] proposed a CAD system consists of two main steps using wavelet transform. In the first step, segmentation of potential of microcalcification is done by using the mixed features, received from the wavelet transform and gray-level statistical analysis. The resultant is labeled into single potential microcalcification objects. In the next step, based on the 31 features, these single potential microcalcification objects are assorted as true or false single microcalcification objects. By using GRNN via SFS ad SBS, the distinguishing power of these mentioned features is also analyzed. This method is used on Nijmegen database of 40 mammograms. The images of this database are digitized at a size of 2,048 × 2,048 by a 12-bit CCD camera (Eikonix 1412). For evaluating the performance, free-response operating characteristics curve (FROC) is used. It is seen that the proposed system gives a satisfactory detection performance after getting the resultant. In the first step when the mixed features are used, 90 % mean true positive detection rate is achieved at a cost of 0.5 false positive per image. In the second step, 15 features are selected by the sequential backward selection method. Next, author Andrew et al. [16] described a method to make an approach for mammographic feature enhancement through wavelet transform. It consists of the application of local and global nonlinear operators within levels of a redundant multiresolution representation. The resultant accents the significant features in mammography which also improved the breast pathology visualization. On the basis of three over complete multiscale representations, this method is described: (1) the dyadic wavelet transform (separable), (2) the -transform (non-separable, non-orthogonal), and (3) the hexagonal wavelet transforms (non-separable). In this study, digitization of the film radiographs of the breast was done by using a sampling distance of 200 μm on a Kodak laser film digitizer, with 10-bit quantization (contrast resolution). Before processing, each digital image was cropped to a matrix size of 512 × 512. Wang and Karanyiannis [17] have also presented an approach to detect microcalcifications in digital mammograms by using wavelet-based sub-band image decomposition. The microcalcification represents the high-frequency components of the image spectrum. Microcalcification is detected by decomposing the mammograms into different frequency sub-band. Then, the low-frequency sub-band is suppressed, and finally,

high-frequency containing mammograms from the sub-band are reconstructed. The original mammogram is decomposed into a set of orthogonal sub-band of different resolution and frequency content. The decomposition is based on wavelet analysis filtering and down sampling along the rows and columns of the image. By using statistical analysis alone and combining with Gaussian filter or only by using Gaussian, some work has also been done for the detection of microcalcification. Microcalcification plays an important role in breast cancer. The author Gurcan et al. [18] suggested a method in which the mammogram image is first processed by a sub-band decomposition filter bank. For the detection of microcalcification clusters, analysis of the resultant bandpass sub-image is done. Skewness and kurtosis have been used to locate the locations of microcalcification clusters. At first, the sub-images are divided into overlapping square regions in which the skewness and kurtosis are estimated. When any region has been seen having high positive skewness and kurtosis, then it is considered as a ROI. This method became successful in finding all the critical regions of the affected area. This method is applied over 40 different mammogram images of size 2,048 × 2,048, which constitute all the available images in the Nijmegen database. After using all these parameters in the experiments, all of the 105 microcalcification clusters in the database were detected. It gave an average of 3.3 false alarms for per mammogram image. Another author Hernandez-Cisneros et al. [19] also used the sequential difference of Gaussian filters (DoG) and three evolutionary artificial neural networks (EANNs) to classify the microcalcification clusters in mammograms. It is then compared against a feed-forward artificial neural network (ANN) trained with back propagation. The mammograms used in this project were provided by the Mammographic Image Analysis Society (MIAS). The MIAS database contains 322 images with resolutions of 50 and 200 μm/pixel. Only 118 in the database contain some abnormality (66 are benign and 52 are malignant) and the other 204 are diagnosed as normal. The abnormalities found in these mammograms are microcalcifications, circumscribed masses, speculated masses, ill-defined masses, architectural distortions (20 cases), and asymmetries (17 cases). Mudigonda et al. [20] proposed a method for the detection of masses in mammographic images that have used Gaussian smoothing and sub-sampling operations as preprocessing steps. Segmentation of the mass portion is done by grounding intensity links from the central portion of masses into the surrounding areas. This method is introduced to analyze oriented flow link textural information in mammogram. To classify the detected region as true mass region or false mass region, they proposed some features. These features are based on flow orientation in adaptive ribbons of pixels across the border of masses. The methods were tested with a total of 56 images (each of size 1,024 × 1,024 pixels at a resolution of 200 m) including 30 benign breast masses, 13 malignant, and 13 normal cases selected from the mini MIAS database. The overall detection accuracy is 74 % with a total of 43 cases. Some work has been on segmentation by using isocontour map and inclusion tree. The author Hong and Sohn [21] described a novel method for the segmentation of regions of interest in mammograms. The algorithm for this method describes the boundaries of the breast, the pectoral muscle, and dense regions that include candidate masses. The resulting representation constitutes an analysis of the

Table 2 Databases used by different researchers

Author	Database used	Total number of images	Image resolution	Database description
Laine et al. [14]	Nil	2	400 × 512 and 512 × 512	Nil
Yu and Guan [15]	Nijmegen database	40	2,048 × 2,048	105 clusters of microcalcifications
Andrew et al. [16]	Nil	Nil	512 × 512	Nil
Wang and Karayiannis [17]	Nil	Nil	512 × 512	Nil
Gurcan et al. [18]	Nijmegen database	40	2,048 × 2,048	105 clusters of microcalcifications
Hernandez-Cisneros et al. [19]	MIAS	322	50 and 200 μm/pixel	Images containing abnormality = 118
Mudigonda et al. [20]	Nil	56	1,024 × 1,024 with 200 μm/pixel	Benign = 30 Malignant = 13 Normal = 13
Hong et al. [21]	DDSM	400	Nil	Nil

global structure of the object in the mammogram. They proposed a topographic representation known as isocontour map, in which a salient region forms a dense quasi-concentric pattern of contours. The topological and geometrical structure of the image is analyzed by using an inclusion tree. The "saliency" of the region is measured topologically as the minimum nesting depth. Features at various scales are analyzed in multiscale isocontour maps and demonstrated the multiscale scheme, which provide an efficient way of achieving better delineations. Experimental results demonstrate that the proposed method has potential as the basis for a prompting system in mammogram mass detection. The segmentation algorithm has been applied to 400 mammograms with masses of varying size and subtlety obtained from the University of South Florida (USF) database. The algorithm achieved 100 % detection rate with 3.8 false positives per image and 90 % with 2.3, respectively (Tables 2 and 3).

6 Previous Works on Thermography

In thermography, also various approaches are followed to detect the breast cancer. Some of them are discussed here. An automated approach using asymmetry analysis is one of the methods followed for detection of breast cancer in thermography. Scales et al. [22] tried to outline the fully automated approach that is able to locate the breast regions in the analyzed images successfully. This consists of a sequence of

Table 3 Listing of different methods used for mammography

S. No.	Author	Method used	Database used	Purpose
1	Laine et al. [14]	Wavelet-based contrast enhancement	Nil	Feature analysis and contrast enhancement of mammogram for suspicious region
2	Yu and Guan [15]	Wavelet transform and gray-level statistical analysis	Nijmegen database	Potential microcalcification pixel segmentation
3	Andrew et al. [16]	Wavelet transform	Nil	Emphasizing significant features in mammography and improve the visualization of breast pathology
4	Wang and Karayiannis [17]	Wavelet-based sub-band image decomposition	Nil	Detection of microcalcifications in digital mammograms
5	Gurcan et al. [18]	Statistical analysis	Nijmegen database	Detection of microcalcifications in mammograms using higher order statistics
6	Hernandez-Cisneros et al. [19]	Gaussian filters and artificial neural network	MIAS	Classification of microcalcification in mammograms
7	Mudigonda et al. [20]	Gaussian smoothing and sub-sampling operations	Nil	Detection of masses in mammographic images and classification of masses
8	Hong and Sohn [21]	Isocontour mapping and inclusion tree	DDSM	Detection of the boundaries of the breast, the pectoral muscle, as well as dense regions that include candidate masses

canny edge detectors to determine the body boundaries and to isolate the most likely candidates for the bottom breast boundary. Three different strategies for identifying the bottom breast boundary are investigated: a variation of the Hough transform to identify the curved edges in the image, the algorithm used to detect the longest connected edges that are not part of the body boundary, and a third approach involving the density of detected edges in the breast region. The last two methods show great promise in successfully segmenting the breasts. Qi et al. [23] proposed an automatic approach to asymmetry analysis in thermograms including automatic segmentation and pattern classification. Hough transform is used to extract the four feature curves that can uniquely segment the left and right breasts. These feature curves include the left and the right body boundary curves and the two parabolic curves indicating the lower boundaries of the breasts. Upon segmentation, unsupervised learning technique is applied to classify each segmented pixel into a certain number of clusters. Asymmetric abnormalities have been identified based on pixel distribution within the same cluster. Another approach followed is based on fuzzy logic. Schaefer et al. [24] in their work have taken a different approach to arrive at a

compact and effective rule base and applied a genetic algorithm that optimizes the features and parameters of the fuzzy rules. The resulting classification system is more compact and hence faster while maintaining the same good classification performance as is proved by experimental results on a set of nearly 150 cases where they achieved a correct classification rate of about 80 %, which is comparable to other imaging modalities such as mammography. Moghbel and Mashohor [25] in their paper compared different approaches to detect breast cancer. It was based on neural networks and fuzzy systems which have been implemented in different CAD designs. The greatest improvement in CAD systems was achieved with a combination of fuzzy logic and ANN in the form of FALCON-AART complementary learning fuzzy neural network (CLFNN). With a CAD design based on FALCON-AART, it was possible to achieve an overall accuracy of nearly 90 %. Some other approaches are also followed like Qi et al. [26] focused on the discussion of using TIR imaging in early detection of breast cancer. They provided a new method for analyzing a thermal system based on an analogy to electrical circuit theory, referred to as thermal–electric analog. They demonstrated the use of analog to estimate the depth of the heat source and furthermore help to understand the metabolic activities undergoing within the human body. The method has been used in early breast cancer detection and has achieved high sensitivity. Vreugdenburg et al. [27] aimed systematically to identify and evaluate all the available evidence of safety, effectiveness, and diagnostic accuracy for three emerging classes of technology promoted for breast cancer screening and diagnosis: Digital infrared thermal imaging (DITI), electrical impedance scanning (EIS), and elastography. The principal outcome measures were safety, effectiveness, and diagnostic accuracy. Data were extracted using a standardized form and validated for accuracy by the secondary authors. No effectiveness studies were identified. Only one EIS screening accuracy study was identified, while all other studies involved symptomatic populations. Sensitivity and specificity varied greatly for DITI (Sens 0.25–0.97, Spec 0.12–0.85), EIS (Sens 0.26–0.98, Spec 0.08–0.81), and ultrasound elastography (Sens 0.35–1.00, Spec 0.21–0.99). Acharya et al. [28] tried to evaluate the feasibility of using thermal imaging as a potential tool for detecting breast cancer. In this work, they have used 50 IR breast images (25 normal and 25 cancerous). Texture features were extracted from co-occurrence matrix and run length matrix. For automatic classification of normal and malignant breast conditions, these features were fed to the support vector machine (SVM) classifier (Table 4).

7 Comparative Studies of Mammography and Thermography

Some breasts conditions are there which are not visible to the mammography test. Breast thermography can detect it at an early stage. Mammography X-rays use a low energy form of ionizing radiation (around 30 kVp) during screening, but

Table 4 Listing of different methods used for thermography

Sl. no	Author	Method used	Images used	Purpose
1	Scales et al. [22]	Asymmetry analysis	Nil	Segmentation of the breasts to detect breast cancer
2	Qi et al. [23]	Asymmetry analysis	Nil	Automatic segmentation and pattern classification
3	Schaefer et al. [24]	Hybrid fuzzy rule	150	Classification for diagnosis purpose
4	Moghbel and Mashohor [25]	Fuzzy logic and artificial neural network	Nil	Detection of breast cancer
5	Liu et al. [26]	Thermal texture maps	Nil	To understand the metabolic activities to detect breast early
6	Vreugdenburg et al. [27]	Nil	6,808	Identification and evaluation of all the available evidence for breast cancer screening and diagnosis
7	Acharya et al. [28]	Support vector machine (SVM)	50	Classification of normal and malignant breast

Table 5 Performance comparison of mammography and thermography

	Mammography	Thermography
Cost	More	Less
Radiation use	Yes	No
Early detection	No	Yes
Accuracy (%)	90 (or more)	89 (up to)
Size of the tumor (cm)	1.66	1.28
Screening age	After 40	After 20
Specificity (%)	80	85
Sensitivity (%)	73	88

thermography does not use any radiation. Mammography is not capable of detecting breast cancer early enough. Thermography detects cancer in its earlier stages 8–10 years before a mammogram. Thermography detects the tumor at the size of 1.28 cm, whereas mammography can detect it at a size of 1.66 cm. Mammography is less effective than thermography due the density of breast tissue. Thermography is consistently much effective in the detection of active breast disease. Mammography screening is recommended after the age of 40, whereas thermography can be done after the age of 20. Table 5 shows the comparative studies of mammography and thermography.

8 Conclusion

This paper has overviewed the different techniques and comparative studies based on mammography and thermography for the detection of breast cancer. Digital mammography is very widely used for early detection of breast cancer, but due to its use of ionizing radiation, thermography is more acceptable in the field of medical science. Thermography does not use any ionizing radiation and is an excellent management tool for screening purpose. In the future, the next approach will be to have an extensive survey on these techniques and proposing a new method.

Acknowledgments The first author would like to thank Biometrics Laboratory and Biomedical IR Imaging Laboratory, Department of Computer Science and Engineering of Tripura University (A central university) for providing the necessary infrastructure facilities to carry out the work. The research is supported by the grant no. BT/533/NE/TBP/2013 dated 03/03/2014 from Department of Biotechnology (NER Division), Ministry of Science and Technology, Government of India.

References

1. http://www.cancer.org/downloads/STT/CancerFacts&Figures2002TM.pdf (2002)
2. Ng, E.Y.K., Sudarshan, N.M.: Numerical computation as a tool to aid the thermographic interpretation. J. Med. Eng. Technol. **25**(2), 53–60 (2001)
3. Usuki, H., Onoda, Y., Kawasaki, S., Misumi, T., Murakami, M., Komatsubara, S., Teramoto, S.: Relationship between thermographic observations of breast tumors and the DNA indices obtained by flow cytometry. Biomed. Thermol. **10**(4), 282–285 (1990)
4. Ng, E.Y.K., Ung, L.N., Ng, F.C., Sim, L.S.J.: Statistical analysis of healthy and malignant breast thermography. J. Med. Eng. Technol. **25**(6), 253–263 (2001)
5. http://en.wikipedia.org/wiki/Mammography
6. Keyserlingk, J.R., Ahlgren, P.D., Yu, E., Belliveau, N., Yassa, M.: Functional infrared imaging of the breast. IEEE Eng. Med. Biol. 3M1 (2000)
7. Boyd, N.F., et al.: Mammographic density and breast cancer risk: current understanding and future prospects. Breast Cancer Res. **13**(6), 223 (2011)
8. Feig, S.A.: Role and evaluation of mammography and other imaging methods for breast cancer detection, diagnosis, and staging. In: Seminars in nuclear medicine, vol. 29, no. 1. WB Saunders, Philadelphia (1999)
9. Kerr, J.: Review of the effectiveness of infrared thermal imaging (thermography) for population screening and diagnostic testing of breast cancer. New Zealand Health Technology Assessment, Department of Public Health and General Practice, Christchurch School of Medicine and Health Sciences (2004)
10. Anbar, M.: Clinical thermal imaging today. Eng. Med. Biol. Mag. IEEE **17**(4), 25–33 (1998)
11. Snyder, R.L., et al.: Acute spiral ganglion lesions change the tuning and tonotopic organization of cat inferior colliculus neurons. Hear. Res. **147**(1), 200–220 (2000)
12. Ng, E.Y.-K., et al.: Computerized detection of breast cancer with artificial intelligence and thermograms. J. Med. Eng. Technol. **26**(4), 152–157 (2002)
13. Qi, H., Head, J.F.: Asymmetry analysis using automatic segmentation and classification for breast cancer detection in thermograms. Engineering in medicine and biology society, 2001. In: Proceedings of the 23rd Annual International Conference of the IEEE, vol. 3. IEEE (2001)
14. Laine, A., Jian, F., Wuhai, Y.: Wavelets for contrast enhancement of digital mammography. Eng. Med. Biol. Mag. IEEE **14**(5), 536–550 (1995)

15. Yu, S., Guan, L.: A CAD system for the automatic detection of clustered microcalcifications in digitized mammogram films. IEEE Trans. Med. Imaging **19**(2), 115–126 (2000)
16. Andrew, L., Fan, J., Yang, W.: Wavelets for contrast enhancement of digital mammography. Eng. Med. Biol. Mag. IEEE **14**(5), 536–550 (1995)
17. Wang, T.C., Karayiannis, N.B.: Detection of microcalcifications in digital mammograms using wavelets. IEEE Trans. Med. Imaging **17**(4), 498–509 (1998)
18. Gurcan, M.N., et al.: Detection of microcalcifications in mammograms using higher order statistics. Sig. Process. Lett. IEEE **4**(8), 213–216 (1997)
19. Hernández-Cisneros, R.R., Terashima-Marín, H., Conant-Pablos, S.E.: Detection and classification of microcalcification clusters in mammograms using evolutionary neural networks. In: Advanced Computational Intelligence Paradigms in Healthcare-3, pp. 151–180. Springer, Berlin (2008)
20. Mudigonda, N.R., Rangayyan, R.M., Leo Desautels, J.E.: Detection of breast masses in mammograms by density slicing and texture flow-field analysis. IEEE Trans. Med. Imaging **20** (12), 1215–1227 (2001)
21. Hong, B.-W., Sohn, B.-S.: Segmentation of regions of interest in mammograms in a topographic approach. IEEE Trans. Inf. Technol. Biomed. **14**(1), 129–139 (2010)
22. Scales, N., Herry, C., Frize, M.: Automated image segmentation for breast analysis using infrared images. In: Wang, T.C. (ed.) Proceedings of the 26th Annual International Conference of the IEEE EMBS, San Francisco
23. Qi, H., Kuruganti, P.T., Snyder, W.T.: Detecting breast cancer from thermal infrared images by asymmetry analysis. Med. Med. Res. **38** (1995)
24. Schaefer, G., Nakashima, T., Zavisek, M.: Analysis of breast thermograms based on statistical image features and hybrid fuzzy classification. In: Advances in visual computing, pp. 753–762. Springer, Berlin (2008)
25. Mehrdad, M., Mashohor, S.: A review of computer assisted detection/diagnosis (CAD) in breast thermography for breast cancer detection. Artif. Intell. Rev. **39**(4), 305–313 (2013)
26. Qi, H., Kuruganti, P.T, Liu, Z.: Early detection of breast cancer using thermal texture maps. In: Proceedings of IEEE International Symposium on Biomedical Imaging 2002. IEEE (2002)
27. Vreugdenburg, T.D., et al.: A systematic review of elastography, electrical impedance scanning and digital infrared thermography for breast cancer screening and diagnosis. Breast Cancer Res. Treat. **137**(3), 665–676 (2013)
28. Acharya, U.R., et al.: Thermography based breast cancer detection using texture features and support vector machine. J. Med. Syst. **36**(3), 1503–1510 (2012)

Automated Cervical Cancer Detection Using Pap Smear Images

Payel Rudra Paul, Mrinal Kanti Bhowmik and Debotosh Bhattacharjee

Abstract Cervical cancer is the most common cancer among the women. Pap smear screening is the most effective test for detecting the cervical precancerous. But this process requires a long time to complete and also may be an erroneous procedure. In this paper, an automated cervical cancer detection method is presented. This method introduces adaptive median filter to remove impulse noises from the Pap smear images and then uses bi-group enhancer to discriminate the nuclei pixels from other object pixels. Then, segmentation methodology is presented to separate the nucleus regions from the cervical smear images. Two clustering-based classifiers, minimum distance and K-nearest neighbor classifiers, have been used in the classification phase for verifying the performance. The technique was evaluated using 158 Pap smear images from DTU/HERLEV Pap smear benchmark database. The accuracy of the detection method is 92.37 and 98.31 % for minimum distance and K-nearest neighbor classifiers, respectively.

1 Introduction

Cervical cancer is the fourth most common cancer and also the fourth most frequent cause of cancer death (266,000 deaths in 2012) among women worldwide (International Agency for Research on Cancer, December, 2013) [1]. According to a

P.R. Paul (✉) · M.K. Bhowmik
Department of Computer Science and Engineering, Tripura University
(A Central University), Suryamaninagar, Agartala 799022, India
e-mail: payel.rudrapaul@gmail.com

M.K. Bhowmik
e-mail: mkb_cse@yahoo.co.in

D. Bhattacharjee
Department of Computer Science and Engineering, Jadavpur University,
Kolkata 700032, India
e-mail: debotosh@ieee.org

K.N. Das et al. (eds.), *Proceedings of Fourth International Conference on Soft Computing for Problem Solving*, Advances in Intelligent Systems and Computing 335,
DOI 10.1007/978-81-322-2217-0_23

report released on Friday by a USA-based research and advocacy group, India tops the world in cervical cancer deaths with nearly 73,000 a year [2]. Cervical cancer (cancer of the cervix) is a cancer of the entrance to the uterus (womb). It is a preventable disease, and regular screening and adequate treatment can prevent women from having cervical cancer [3]. Cervical precancerous screening is done using Pap smear, which is based on the staining of cervical cells, using the technique that was first introduced by George Papanicolaou in early 1940s [4]. The main purpose of the Pap smear is to detect the precancerous changes in the cervix. Different types of cells exist in the cervix. They are located in separate areas: squamous area and columnar area. Squamous epithelium consists of four layers: basal, parabasal, intermediate, and superficial layers containing cells with different morphological features. Cells of the basal and parabasal layers are small and round with a small nucleus and cytoplasm. Cells of intermediate and superficial layer have small nuclei and larger cytoplasm The columnar cells exist in a single layer—the basal layer has the characteristics of columnlike shape with a large nucleus at one end [5].

The interpretation of Pap smear images by skilled cytotechnicians and doctors relies on the visual recognition of changes in the nuclei of cells affected by disease. However, this process is a monotonous, erroneous task and takes a long time to complete [6]. In order to solve these problems, several automatic approaches have been introduced by many researchers for the classification of cervical cells in Pap smear images.

An automated detection of cell nuclei that can be applied directly in Pap smear images containing both isolated and clustered cells was presented in [6–9]. In [7], filters and morphological operators are applied in all three channels of a color image for the determination of the locations of nuclei in the image. Then, the nucleus boundary is determined by the snake deformation. In [6, 8, 9], Plissiti et al. use grayscale morphological reconstruction in combination with the detection of regional minima in the image for the detection of the locations of the candidate nuclei centroids in the image. In [6], distance-dependent rule using Euclidean distance and given threshold is applied for the determination of the final nuclei locations. Fuzzy c-means clustering algorithm is then used for the classification of the detected centroids in classes of interest. In [8], the boundaries of the nuclei are defined with the watershed transform in the morphological color gradient image. The clustering step is then performed using fuzzy c-means algorithm for the elimination of the detected regions that do not correspond to the actual nuclei locations. And in [9], a priori knowledge about the nucleus appearance is incorporated for the extraction of more accurate nuclei centroids. The elimination of the undesirable artifacts is achieved through two steps. In the first step, a distance-depended rule is applied for the reduction of false-positive occurrences. In the second step, an unsupervised (fuzzy c-means) and a supervised [support vector machine (SVM)] classification techniques are used in order to determine the final set of nuclei centroids. Some techniques are developed for the segmentation of the

nucleus and the cytoplasm from presegmented cervical cell images based on edge detection. Tsai et al. [10] develop a cytoplast and nucleus contour (CNC) detector. The CNC detector uses a median filter and a bi-group enhancer to remove noise and to make a precise separation of the pixels that lie between two objects. After that, k-means algorithm is used to discern between the pixels on a cytoplast and those on a background. And maximal color difference (MCD) method is used to identify the contour of nucleus. In [11], Yang-Mao et al. (2008) proposed an edge enhancement nucleus and cytoplast contour (ENNCC) detector. They use trim-meaning filter and a bi-group enhancer to remove noise and to make a clear-cut separation of the pixels that lie between two objects. After that, a mean vector difference (MVD) enhancer is used to suppress the gradient of noise and to enhance the gradient of object contour. The ENNCC detector uses Otsu's method and the hit-and-miss transform-based skeletonization (HMTS) algorithm to draw the contours of the nucleus and cytoplast. Pai et al. [12] present a nucleus and cytoplast contour detector (NCC detector) to detect the CNC of a cell in a cervical smear image. They also used MVD enhancer for the same purpose as [10]. After that, the adaptable threshold decision (ATD) method and then the maximal gray-level-gradient-difference (MGLGD) method are used to extract the nucleus from the cell. In the domain of Pap smear classification, many approaches have been proposed, and they concern techniques such as neuro fuzzy systems [13], nearest-neighbor-based classifiers [13, 14], supervised and unsupervised hard and fuzzy c-means techniques [15], Gustafson–Kessel clustering [15], and SVM [16].

This paper presents an automated method for the detection of cervical cancer using Pap smear images and also evaluates the performance of the method in terms of sensitivity, specificity, and accuracy. In this paper, adaptive median filter is introduced to remove the impulse noises from the cervical smear images. Then, segmentation methodology is presented to segment the nucleus regions. The organization of this paper is as follows: Discussion about used database is given in Sects. 2, and 3 briefly describes the proposed method for automated cervical cancer detection, and experimental results and discussion are given in Sect. 4. Finally, conclusion and future work are given in Sect. 5.

2 Data Collection

In this paper, DTU/HERLEV Pap smear benchmark database developed by Jantzen and Dounias is used for experimental purpose [17]. The database consists of 917 samples distributed unevenly on seven classes and was collected by the Department of Pathology at Herlev University Hospital and the Department of Automation at Technical University of Denmark. The first three classes correspond to normal cells, and the last four classes correspond to abnormal cells [18]. The cell distribution of the database is depicted in Table 1.

Table 1 Description of the Pap Smear Benchmark database

Type	#Cells
Normal	
1. Superficial squamous epithelial	74
2. Intermediate squamous epithelial	70
3. Columnar epithelial	98
Total	242
Abnormal	
4. Mild squamous non-keratinizing dysplasia	182
5. Moderate squamous non-keratinizing dysplasia	146
6. Severe squamous non-keratinizing dysplasia	197
7. Squamous cell carcinoma in situ intermediate	150
Total	675

3 Cervical Cancer Detection Method

The paper presents a method for automated cervical cancer detection using Pap smear images. This method covers mainly four steps: bi-group enhancement, segmentation, feature extraction, and classification. This paper also presents the performance evaluation of the proposed method in terms of sensitivity, specificity, and accuracy. The method is summarized in Fig. 1.

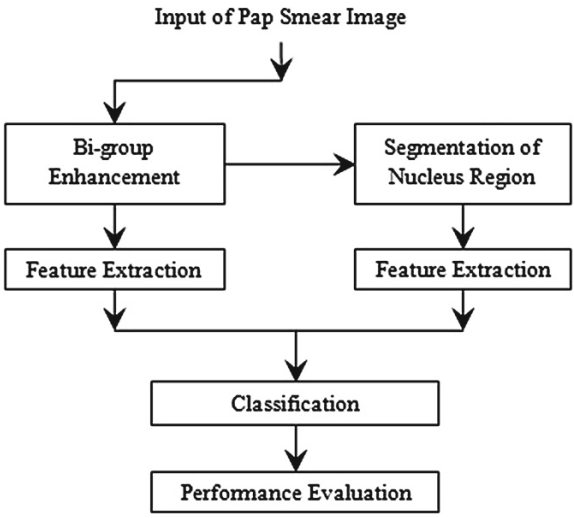

Fig. 1 Schematic of the method

3.1 Bi-group Enhancement

Segmentation of the image directly depends on the quality of the image. It is very difficult to generate an accurate edge map when the images are corrupted by noises. Several denoising techniques such as mean filter [19], median filter [19], and Gaussian filter [19] have been presented in the past studies. Generally, median filter has been used to improve the image quality and also denoise the images [10]. But standard median filter causes unnecessary loss of details due to the replacement of every pixel in the image by the median of the corresponding neighborhood. To reduce the distortion of the images, this paper adopts the adaptive median filter [19] to remove the impulse noise from the cervical cell images. Let I be the input cervical smear image and I_0 be the grayscale image of I. After denoising, the gray image, $I_{0,}$ becomes I_t.

Tsai et al. [10] proposed bi-group enhancer to discriminate the object pixels from other object pixels. Here, bi-group enhancer is applied to sharpen the contour of the nucleus from other objects before extracting the nucleus area by improving the contrast between the nucleus and the cytoplasm boundary based on the pixel intensities of cervical cell image.

Let p_{ij} be the pixel located at location (i, j) in I_t and w_{ij} be the corresponding window of p_{ij} of size $n \times n$, where p_{ij} is the central pixel of w_{ij}. The pixels of w_{ij} are sorted in ascending order based on the pixel intensity levels, where $c_{ij} = \{c_1, c_2, \ldots, c_{n^2}\}$ are assumed to be the pixel intensity values on w_{ij}. For mid $= \frac{n^2+1}{2}$, with n considered to be an odd number, calculate mean values from c_1 to c_{mid} as well as from $c_{\text{mid}+1}$ to c_{n^2} as c_{lower} and c_{upper}, respectively, where

$$c_{\text{lower}} = \frac{1}{\text{mid}} \sum_{i=1}^{\text{mid}} c_i \tag{1}$$

$$c_{\text{upper}} = \frac{1}{\text{mid} + 1} \sum_{i=\text{mid}+1}^{n^2} c_i \tag{2}$$

Hence, the bi-group enhancer replaces each c with c', where c' is defined as follows:

$$c = \begin{cases} c_{\text{lower}}, & \text{if} \quad c_{\text{lower}} \le c \le c_{\text{mid}} \\ c_{\text{upper}}, & \text{if} \quad c_{\text{mid}+1} \le c \le c_{n^2} \\ c, & \text{otherwise} \end{cases} \tag{3}$$

If c is in the indefinite intervals, this approach replaces c with the mean value c_{lower} of the first half of c_{ij}'s or with the mean value c_{upper} of the later half of c_{ij}'s. The original input images and their corresponding grayscale images are shown in Fig. 2a–d, e–h, respectively. Figure 3a–d, e–h shows the resulted filtered and enhanced images, respectively.

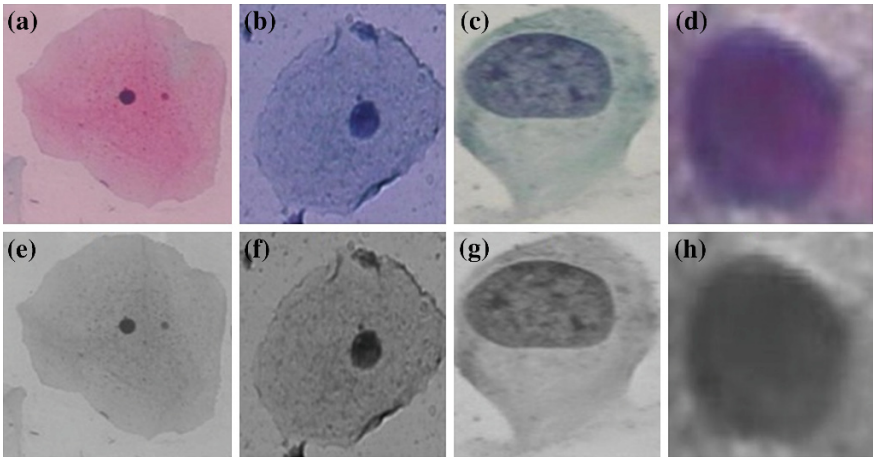

Fig. 2 **a–d** Original input images, **e–f** grayscale images

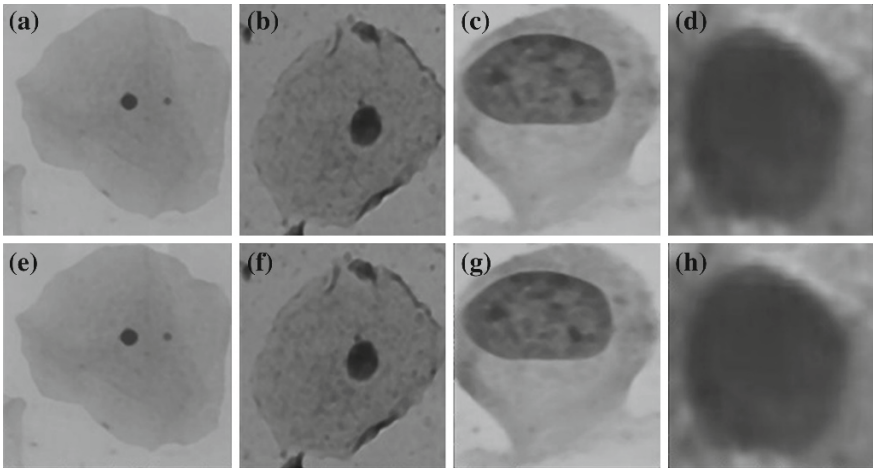

Fig. 3 **a–d** Filtered images, **e–h** enhanced images

3.2 Segmentation of Nucleus Region

The aim of this step is to segment the nucleus regions from the cervical smear images. In this paper, the algorithm of k-means clustering followed by morphological operations is used to segment the nucleus regions. Here, k-means is used to cluster the objects into two clusters using the Euclidean distance metric [20]. In k-means algorithm, K initial cluster centers are chosen for K clusters. Datasets are partitioned into K clusters based on the closeness of each data points with cluster

centers. For each data points, calculate the distance between data points and each cluster centers and assign it to the closest cluster. Here, closeness is measured in terms of Euclidean distance metric. After all the data points are distributed into K clusters, find the K new cluster centers by taking the mean of all the data points of K clusters, respectively. The process is repeated until there are no changes in cluster centers. Various steps of k-means algorithm are outlined below:

1. Calculate the histogram of the intensities.
2. Initialize K cluster centers with K random intensities for K clusters.
3. Repeat the following steps until there is no change in cluster centers.
4. For each pixel, find the distance from its intensity to each cluster centers and assign it to the closest cluster.

$$c_i^{(t)} = \arg\min_i \left\| x_j - \mu_i^{(t)} \right\|^2 \tag{4}$$

where c denotes the cluster and t be the iterations of the process. i and j iterate over all the cluster centers and intensities, respectively.

5. Calculate the new cluster centers by calculating the mean of all members of each cluster.

$$\mu_i^{(t+1)} = \frac{1}{\left| c_i^{(t)} \right|} \sum_{x_j \in c_i^{(t)}} x_j \tag{5}$$

The result of the k-means algorithm is the segmentation of nucleus area from the cervical cell image. After that, morphological operations are applied to the output of the k-means algorithm; erosion and morphological reconstruction are used to correctly segment the nucleus region. Figure 4a–d, e–h show the segmented nucleus regions after applying k-means clustering and morphological operations, respectively.

3.3 Feature Extraction

Feature extraction is the process of extracting the features for classification purpose. It is a challenging task to extract good feature sets for more accurate classification. Here, three features are calculated: two from enhanced images and one from segmented images. Following are the features that are extracted from the cervical cell images:

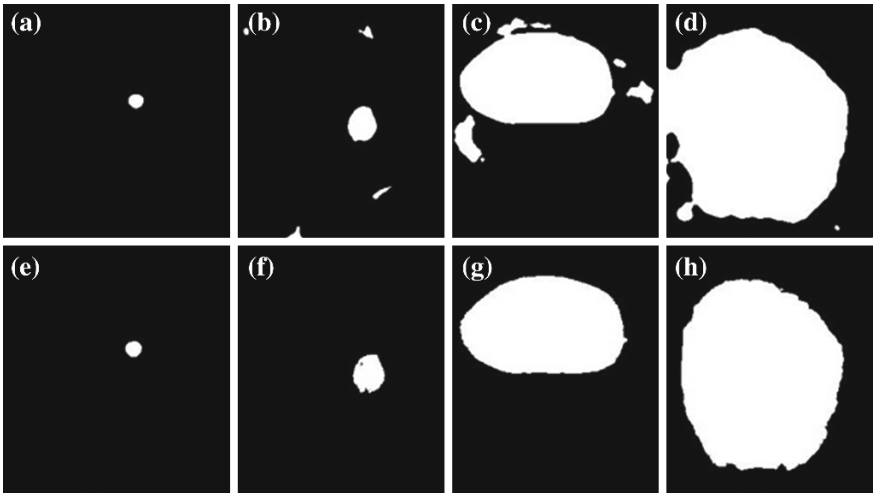

Fig. 4 Segmented nucleus regions **a–d** after applying k-means clustering, **e–h** after applying morphological operations

3.3.1 Feature Extraction from Enhanced Images

Mean. The first feature used to classify normal and abnormal cells is mean of the cell image which is calculated from the output image of step 1. Abnormal cell has lower mean value compared to normal cell. Mean is calculated by taking the average of all the intensities of the image. Equation 6 shows the calculation of the mean:

$$M = \frac{1}{N}\sum_{i=1}^{N} x_i \tag{6}$$

where N is the size of the image and x_i is the individual pixels of the image.

Standard Deviation. Standard deviation is commonly used for measuring the spread of the image. Abnormal cells have spreaded nucleus compared to normal cells. So, the value of standard deviation is higher for abnormal cells. Standard deviation is calculated using Eq. 7.

$$\text{standard deviation} = \sqrt{\frac{1}{N}\sum_{i=1}^{N}(x_i - M)^2} \tag{7}$$

3.3.2 Feature Extraction from Segmented Images

Nucleus Area. To classify the normal and abnormal cells, nucleus area is the most important feature. Normal cells have small nucleus area, whereas abnormal cells

Table 2 Classification results

Classifier	TP	TN	FP	FN	Sensitivity (%)	Specificity (%)	Accuracy (%)
Minimum distance classifier	75	34	0	9	89.29	100	92.37
K-nearest neighbor classifier	82	34	0	2	97.62	100	98.31

have increased nucleus area. The area of the nucleus is the total number of pixels in nucleus region. Table 2 represents the feature values of normal and abnormal cells.

3.4 Classification

Classification is necessary to classify the cells into normal and cancerous based on the extracted feature values. Here, two different clustering-based classifiers are used in the classification phase of proposed approach: minimum distance classifier and K-nearest neighbor classifier.

3.4.1 Minimum Distance Classifier

To classify a feature vector X, measure the distance from each X to each of the class centers μ_i in the training set and assign X to the class of the nearest center, where center is defined by the mean value of that class. Mean is calculated by the following Eq. 8 [19]:

$$\mu_i = \frac{1}{n}\sum_{x \in C_i} x \tag{8}$$

where n is the total number of feature vectors in class C_i of the training set and x is the feature vector of class C_i of the training set; i iterate over all the classes in the training set.

Here, Euclidean distance rule is used to measure the distances from each X to each of the class centers and is defined by the following Eq. 9 [19]:

$$d(X, \mu_i) = \sqrt{\sum_{x \in X} (x - \mu_i)^2} \tag{9}$$

3.4.2 K-Nearest Neighbor Classifier

To classify the unknown feature vector X, K-nearest neighbor classifier searches the K training feature vectors that are closest to the X. These K training feature vectors are the 'K-nearest neighbors' of the unknown feature vector. The unknown feature vector is assigned as the most common class among its K-nearest neighbors.

Here, closeness is defined in terms of distance metric, such as Euclidean distance. The Euclidean distance between two feature vectors, say X_1 and X_2, is defined by Eq. 10 [19]:

$$d(X_1, X_2) = \sqrt{\sum_{i=1}^{n} (x_{1i} - x_{2i})^2} \tag{10}$$

where x_{1i} and x_{2i} are the features from X_1 and X_2, respectively, for all $i = 1, 2, \ldots, n$.

3.5 Performance Evaluation

The basic measures to quantify the medical diagnostic accuracy of the test include sensitivity and specificity. The sensitivity (true positive rate) of a medical test gives the probability of giving 'positive' result when the patient is ill [21]. This can be written as follows:

$$\text{Sensitivity} = \frac{\text{TP}}{\text{TP} + \text{FN}} \times 100\,\% \tag{11}$$

The specificity (sometimes called the true negative rate) is the probability of getting a 'negative' result when the patient is well [21]. This can be written as follows:

$$\text{Specificity} = \frac{\text{TN}}{\text{TN} + \text{FP}} \times 100\,\% \tag{12}$$

The accuracy of the test is defined by,

$$\text{Accuracy} = \frac{\text{TP} + \text{TN}}{\text{TP} + \text{TN} + \text{FP} + \text{FN}} \times 100\,\% \tag{13}$$

True positive (TP)	Abnormal cells correctly identified as abnormal
True negative (TN)	Normal cells correctly identified as normal
False positive (FP)	Normal cells incorrectly identified as abnormal
False negative (FN)	Abnormal cells incorrectly identified as normal.

4 Results and Discussion

The method has been applied in 158 cervical Pap smear images, in which 54 normal cell and 104 abnormal cell images are there. To fully explore the system performance, training and testing has been conducted. For training purpose, 40 cell images are used, which include 20 normal cell and 20 abnormal cell images. For testing purpose, 118 cell images are used, which includes 34 normal cell and 84 abnormal cell images. The results of the classification are given in Table 2.

As we can see from Table 2, within 84 abnormal cells, 75 cells and 82 cells were correctly classified using minimum distance classifier and K-nearest neighbor classifier, respectively, and within 34 normal cells, all cells were correctly classified using both of the classifier. The classification accuracy of our method using minimum distance classifier in differentiating the cancerous and normal cells is 92.37 % with sensitivity 89.29 % and specificity 100 %. On the other hand, K-nearest neighbor gives impressive accuracy of 98.31 % with sensitivity 97.62 % and specificity 100 %.

5 Conclusion and Future Work

An automated cervical cancer detection method given in this paper shows good accuracy. A group of strategies combined in one set to develop this detection method. Removal of the impulse noises has been done by adaptive median filter, and bi-group enhancer has been used to improve the contrast between nucleus and cytoplasm boundary based on the pixel intensity. Then, segmentation methodology is introduced to segment the nucleus regions. Minimum distance classifier and K-nearest neighbor classifier have been used in the classification phase of the method to classify the Pap smear cervical cell images into normal and abnormal cells. The classification accuracy of the minimum distance classifier in differentiating the normal and abnormal cells is 92.37 %. On the other hand, K-nearest neighbor gives impressive accuracy of 98.31 %. The future scope of this work includes effort to improve the classification performance with the selection of more features from the nucleus and also from the cytoplasm and to classify the abnormal cells in stage wise.

Acknowledgments The work presented here is being conducted in the Biomedical Infrared Imaging Laboratory of Tripura University (A Central University). The first author is thankful to the Biometrics Laboratory of Computer Science Engineering Department, Tripura University (A Central University) for providing necessary infrastructural facility to carry out the work.

References

1. http://www.iarc.fr
2. http://www.deccanherald.com/content/331636/039india-tops-cervical-cancer-deaths039.html
3. http://www.cancer.org/cancer/cervicalcancer/detailedguide/cervical-cancer-what-is-cervical-cancer
4. Papanicolaou, G.N.: A new procedure for staining vaginal smears. Science **95**(2469), 438–439 (1942)
5. Norup: Classification of pap-smear data by transductive Neuro-fuzzy methods. Master thesis, Technical University of Denmark, Oersted-DTU, Automation (2005)
6. Plissiti, M.E., Tripoliti, E.E., Charchanti, A., Krikoni, O., Fotiadis, D.I.: Automated detection of cell nuclei in PAP stained cervical smear images using fuzzy clustering. Springer, Berlin (2009)
7. Plissiti, M.E., Charchanti, A., Krikoni, O., Fotiadis, D.I.: Automated segmentation of cell nuclei in PAP smear images. In: Proceedings of IEEE International Special Topic Conference on Information Technology in Biomedicine, pp. 26–28 (2006)
8. Plissiti, M.E., Nikou, C., Charchanti, A.: Watershed-based segmentation of cell nuclei boundaries in Pap smear images. In: Proceeding of Information Technology and Applications in Biomedicine (ITAB), 10th IEEE International Conference on 01/2010 (2010)
9. Plissiti, M.E., Nikou, C., Charchanti, A.: Automated detection of cell nuclei in Pap smear images using morphological reconstruction and clustering. In: IEEE Transaction on Information Technology in Biomedicine, vol. 15, no. 2, March 2011
10. Tsai, M.H., Chan, Y.K., Lin, Z.Z., Yang-Mao, S.F., Huang, P.-C.: Nucleus and cytoplast contour detector of cervical smear image. Pattern Recogn. Lett. **29**, 1441–1453 (2008)
11. Yang-Mao, S.F., Chan, Y.K., Chu, Y.P.: Edge enhancement nucleus and cytoplast contour detector of cervical smear images. IEEE Trans. Syst. Man Cybern. Part B **38**(2), 353–366 (2008)
12. Pai, P.-Y., Chang, C.-C., Chan, Y.-K.: Nucleus and cytoplast contour detector from a cervical smear image. Expert Syst. Appl. **39**, 154–161 (2012)
13. Byriel, J.: Neuro-fuzzy classification of cells in cervical smears. MSc thesis, Technical University of Denmark, Dept. of Automation (1999)
14. Marinakis, Y., Dounias, G.: Pap smear diagnosis using a hybrid intelligent scheme focusing on genetic algorithm based feature selection and nearest neighbor classification. In: Proceedings of NiSIS 2006, Tenerife, Spain. Nature inspired Smart Information Systems (NiSIS), EU co-ordination action, NiSIS (2006). http://www.nisis.de
15. Erik, M.: Pap-smear classification. MSc thesis, Technical University of Denmark, Oersted-DTU, Automation (2003)
16. Chen, Y.-U., Huang, P.-C. Lin, K.-C., Lin, H.-H., Wang, L.-E., Cheng, C.-C., Chen, T.-P., Chan, Y.-K., Chiang, J.Y.: Semiautomatic segmentation and classification of Pap smear cells. IEEE J. Biomed. Health Inf., vol. 0–0, no. 0–0 (2013)
17. The Pap-Smear Benchmark Database. http://fuzzy.iau.dtu.dk/smear/download.html
18. Jantzen, J., Dounias, G.: Analysis of Pap-smear image data. In: Mexican International Conference on Artificial Intelligence—MICAI, pp. 258–267 (2009)
19. Gonzalez, R.C., Woods, R.E.: Digital image processing, 3rd edn. Pearson education inc. (2008)
20. Kanungo, T., Mount, D.M., Netanyahu, N.S., Piatko, C.D., Silverman, R., Wu, A.Y.: An efficient k-Means clustering algorithm: analysis and implementation. In: IEEE Transactions on Pattern Analysis and Machine Intelligence, vol. 24, no. 7, July 2002
21. http://en.wikipedia.org/wiki/Sensitivity_and_specificity

Background Subtraction Algorithm for Moving Object Detection Using SAMEER-TU Dataset

Kakali Das, Mrinal Kanti Bhowmik, Barin Kumar De and Debotosh Bhattacharjee

Abstract Identifying moving objects plays an important role in video-based applications. In this paper, a background subtraction approach for object detection technique is proposed, which is an improvised version of an existing background subtraction algorithm called visual background extractor (ViBe). Here, the performance of the existing technique has been modified by a median filter. This technique is implemented on different existing databases and also on newly created Society of Applied Microwave Electronics Engineering and Research-Tripura University (SAMEER-TU) dataset. The detection accuracy of the technique is also measured, and a comparison is also carried out between existing and proposed technique, and results are reported in experimental results, in terms of detection accuracy for color video sequence.

Keywords ViBe · SAMEER-TU · Background subtraction

K. Das (✉) · M.K. Bhowmik
Department of Computer Science and Engineering, Tripura University,
Suryamaninagar, Agartala 799022, India
e-mail: kakalids54@gmail.com

M.K. Bhowmik
e-mail: mkb_cse@yahoo.co.in

B.K. De
Department of Physics, Tripura University,
Suryamaninagar, Agartala 799022, India
e-mail: barin_de@yahoo.co.in

D. Bhattacharjee
Department of Computer Science and Engineering, Jadavpur University,
Kolkata 7000032, India
e-mail: debotosh@indiatimes.com

K.N. Das et al. (eds.), *Proceedings of Fourth International Conference on Soft Computing for Problem Solving*, Advances in Intelligent Systems and Computing 335,
DOI 10.1007/978-81-322-2217-0_24

1 Introduction

Detection of moving objects in video images is one of the most influential and fundamental technologies to developing a computer vision systems for real-world application, such as video monitoring system, intelligent-highway system, and intrusion monitoring. Traditionally, the most vital task of monitoring safety is based on human visual observation, which requires a hard-working watchman. Therefore, the automatic detection of moving objects in the monitoring system can help a human operator, even if it cannot totally replace the person's presence. An efficient algorithm is required to facilitate a monitoring system required for detecting moving objects in video. For monitoring system, moving object detection is a basic step of different complex processes such as automated navigation, activity analysis, and event recognition [1].

One commonly used approach to moving object detection is through background subtraction, which consists an up-to-date model for background and detecting moving objects that differ from the design. In this paper, the technique described for moving object detection from a video sequence operates on each pixel independently. This is called pixel-based background subtraction technique. There are many simple background subtraction techniques for static background such as running average [2], first-order low-pass filtering [3], temporal median filtering, [4] and modeling of each pixel with a Gaussian [5]. But they are not suitable for complex background. Complex backgrounds are those which include as follows:

- **Light changes** Gradual variations of the lighting conditions in the scene
- **Moving background** Small movements of background objects, such as swaying tree branches, and bushes blowing in the wind, such as waving trees
- **Cast shadows** The background model may include the shadow cast by moving objects that obviously behaves like an another moving object
- **Bootstrapping** The background model may not be complete and static (free of moving objects)
- **Camouflage** Moving objects may have similar color and structure as background [1].

W4 [6] model is a simple and effective model for handling the complex background. In this method, each pixel is represented by its minimum and maximum intensity levels and the maximum intensity difference between consecutive frames of the training sequence. Using this property of pixel, here background modeling has been done. This model gives satisfactory results in controlled environments, but this model is not suitable for handling all types of complex background.

For the handle complex backgrounds, Stuffer and Grimson [7] described a technique, which is most popular technique. In this technique named Gaussian mixture model, the background model is created by modeling each pixel observed over time by a weighted mixture of Gaussian [7].

There is another method named codebook algorithm. In the codebook method described by Wu and Peng, [8] each pixel is represented by codebook and

codebook of each pixel consists of spatial and temporal context of that pixel. Codebooks are able to capture background motion over a long period of time with a limited amount of memory. But if structural change occurs in the background, the background updation mechanism cannot handle it properly.

This paper presents an improvised background subtraction algorithm for moving object detection, which presented by Olivier Barnich and Marc Van Droogenbroeck [9]. This paper also presents an analysis of the algorithm on different databases which include perception database and a newly created database, namely SAMEER-TU database, to evaluate the robustness of the method.

The rest of the paper is organized as follows: Section 2 describes the creation of the database; Sect. 3 describes the improvised technique for object detection, and Sect. 4 deals with experimental results and discussion along with qualitative assessment of the technique. Finally, Sect. 5 concludes the work.

2 SAMEER-TU Database Creation

2.1 Design of SAMEER-TU Database

This section describes some attributes of the SAMEER-TU database. The SAMEER-TU database contains visual and its corresponding thermal images of natural scenes and human face images in outdoor uncontrolled condition and also visual and thermal videos for moving object detection. And this database is being created in the Biometrics Laboratory of Department of Computer Science and Engineering of Tripura University (TU), India. Visual images and videos are captured by visual camera NIKON D5100, and thermal images and videos are captured by FLIR 60 thermal camera. This database contains 5,640 visual images of natural scenes and face images in outdoor uncontrolled condition. It includes 5 thermal videos and 3 visual videos.

The main concern of the paper is to detect moving object in visual videos. So, only the 3 visual videos are used for this paper purpose. The database does not provide any ground truth for the videos, so in this work, using the proposed algorithm is used to create the ground truth for the videos taken from the SAMEER-TU database (Figs. 1, 2, 3, and 4).

2.2 Design of Visual Videos Database

Equipment Used for Video Capturing Nikon D5100n cameras with Nikon 18–55 mm lens, shutter speed 1/125–1/200, apertures f/5.6–f/8 are used for capturing the videos. The video sequences depict the problem of dynamic background. These videos are captured in the month of April of the year 2014.

Fig. 1 Natural scene images in foggy days from SAMEER-TU database

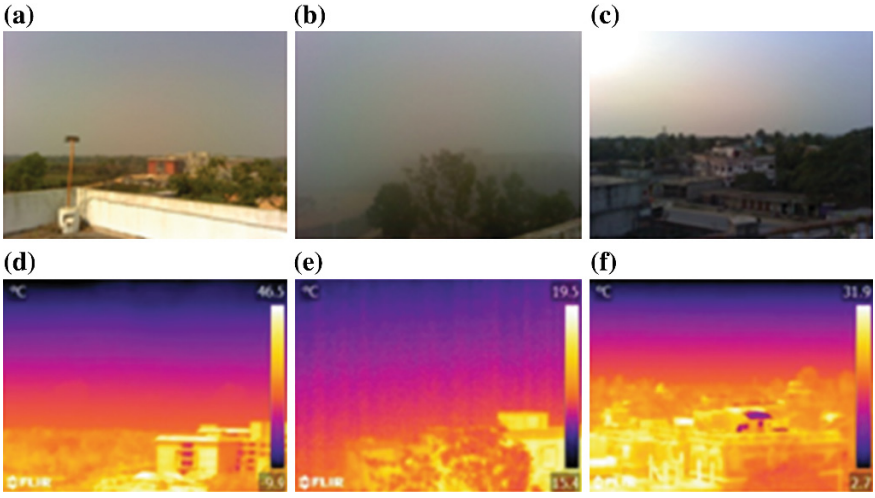

Fig. 2 Natural scene images and their corresponding thermal images from SAMEER-TU database

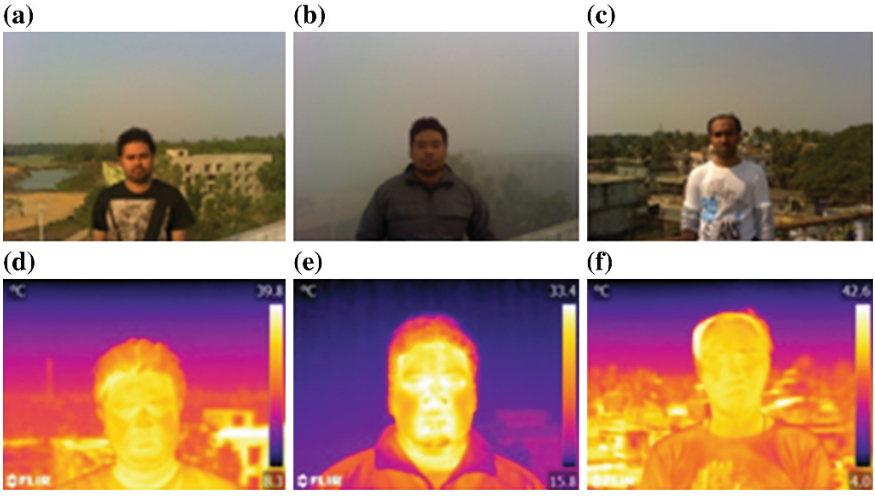

Fig. 3 Face images and their corresponding thermal images

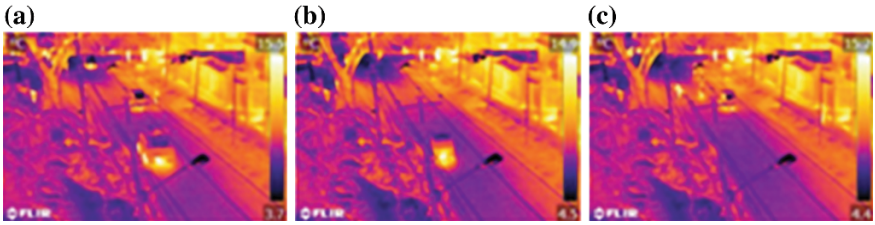

Fig. 4 Frames of thermal video sequence from SAMEER-TU database

Description of Videos These three videos are captured in outdoor condition. The 3 videos include 162, 3,232, 1,700 frames, respectively, of 640 × 424 resolutions and acquired at 25 frame per second (FPS). Among these videos, 2 videos contain a swaying tree as a background. Means it depicted the dynamic background problem. And the other is a simple video with moving pedestrians and vehicles.

Video 1 This video mainly depicts the problem of dynamic background where it contains a swaying a tree at the background. And a vehicle passes in front of it. It contains 162 frames of 640 × 424 resolutions.

Video 2 The background is same as in the Video 1 just the focus is changed here. Now the background contains swaying trees and buildings. And vehicles and pedestrians are passes in front of them. It includes 3,232 frames of 640 × 424 resolutions.

Video 3 This video depicts a simple video for moving object detection. It contains buildings in background and pedestrians and vehicles passes in front of it. It includes 3,232 frames of same resolutions.

Perspective of the Datasets In this paper, these datasets are used to determine the performance of the algorithms on the new dataset. As the ground truths are not available, so the ground truths for each of the frame of the datasets are created by this algorithm in this work.

3 Moving Object Detection

3.1 Step 1: Create Background Models

Many popular techniques for background subtraction required a large number of frames of a video sequence to initialize their background models, and this is also necessary to determine the temporal distribution of the background pixels. In this work, the background model is initialized from a single frame.

In this way, it provides a reliable segmentation of foreground in the first frame, which is more useful for video surveillance with a short sequence. But there is no temporal information in the first frame. But, here, the concept is that neighboring pixels share a similar temporal distribution. That is why in this paper, the pixel

models are populated with values found in the spatial neighborhood of each pixel. More precisely, it fills the background pixel model with the neighborhood values of that pixel in the first frame. In this paper, samples are selected randomly in the 8-connected neighborhood of each pixel [9].

So, the background model can be obtained from the Eq. (1).

$$M(X) = \{V_1, V_2, V_3, \ldots, V_N\} \tag{1}$$

where, $M(X)$ is the model of the pixel 'X,' V_1, V_2 are the neighborhood's pixel's value (Figs. 5, 6, and 7).

Fig. 5 Frames from the video 1 sequence

Fig. 6 Frames from the video 2 sequence

Fig. 7 Frames from video 3 sequence

3.2 Step 2: Classify a New Pixel

In this paper, the problem of background subtraction considers as a classification problem; here, a new pixel value is classified with respect to its immediate neighborhood in the chosen color space, and it will avoid the effect of any outliers. That is why each background pixel is modeled with a collection of samples not with an explicit model of pixel. There is no need of pdf estimation of the background pixel. The new pixel value is compared to its closest samples of its corresponding pixel model. This is a fundamental difference of this algorithm with existing algorithms. A new value is compared to its corresponding background samples and should be close to some of the sample values instead of the majority of all values [9].

To classify a pixel value $V(X)$ according to its corresponding model $M(X)$, here, it will compare with the set of samples defined by a sphere of radius R centered on $V(X)$. The pixel value $V(X)$ is then classified as background if the cardinality, denoted #, of the set intersection of this sphere, and the collection of model samples $M(X)$ is larger than or equal to a given threshold $\#_{\min}$. More formally, compare $\#_{\min}$ to.

$$\#\{SR(V(X)) \cap \{V_1, V_2, V_3, \ldots V_N\}\} \tag{2}$$

The comparison of one pixel of the new frame with the pixels of its corresponding model is based on Euclidean distance. Here, Euclidean distance is the measurement of the similarity of the new pixel with its corresponding background pixel. In this paper, the considered minimum distance is 10. If the current pixel value had the Euclidean distance less than or equal to 10 with any two pixel reside in the corresponding model, then it will be a background pixel other than it is classify as a foreground pixel [9].

3.3 Step 3: Updation of Background Pixel Model

This step is concerned about the updation of the background model to deal with the illumination change, to get the appropriate result over time, and to handle new object in the scene. In this paper, the update process incorporates three important components: (1) a memoryless update policy, which ensures a smooth decaying life span for the samples stored in the background pixel models, (2) a random time subsampling to extend the time windows covered by the background pixel models, and (3) a mechanism that propagates background pixel samples spatially to ensure spatial consistency and to allow the adaptation of the background pixel models that are masked by the foreground [9].

The process offers an exponential monotonic decay for the remaining life span of the samples. The method improves the time relevance of the estimation by allowing a few old samples to remain in the pixel model. Here, the old samples are selected randomly, and this sample is replaced by the new pixel. In other words, the past has no effect on the future. This property called the memoryless property.

But it is also unnecessary to update each background pixel model for each new frame. By making the background update less frequent, here, the expected life span of the background samples is artificially extended. And for that, a random sub-sampling policy is used where. When a pixel value has been classified as belonging to the background, a random process determines whether this value is used to update the corresponding pixel model or not. To achieve this, here, the approach is employed where background pixel value has one chance in 16 of being selected to update its pixel model.

As the underlying idea of this technique is neighboring pixels share a similar temporal distribution [9], that is why, here, a new background sample of a pixel not only updates its corresponding background model should also update the models of neighboring pixels. And the neighboring pixel model which will be updated is also selected randomly.

Applying this background subtraction algorithm on the one frame taken from the "campus" and "Bunglow" sequence of CDW 2012 dataset and on the another frame taken from the "Video 1" sequence of SAMEER-TU dataset, the results shown in Fig. 8.

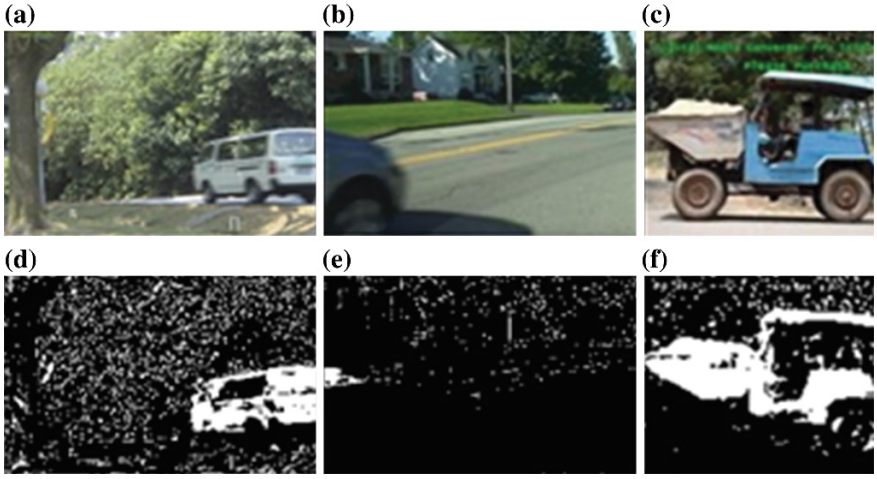

Fig. 8 **a** Input image from "campus" sequence of CDW 2012 dataset. **b** Input image of "Bunglows" sequence from Perception dataset. **c** Input image of "video 1" sequence from SAMEER-TU dataset output after applying the present technique on. **d–f** Output after applying the present technique on (**a–c**)

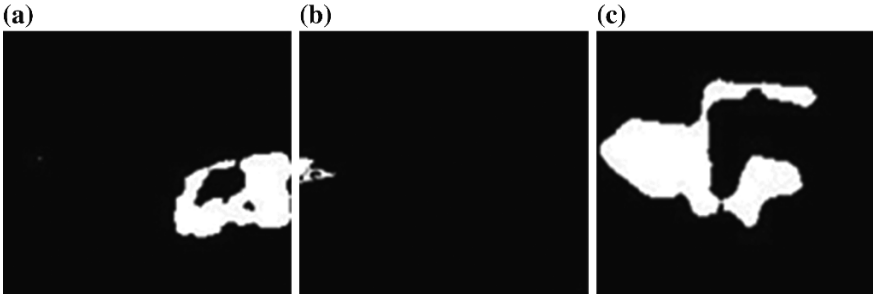

Fig. 9 Output after postprocessing: **a** output image for Fig. 7a **b** output image for Fig. 7b **c** output image for Fig. 7c

3.4 Postprocessing

From the result shown in Fig. 8, this can be seen that postprocessing is now played a crucial step in this technique to obtain a better result. This technique is motivated from the algorithm presented by Barnich and Van Droogenbroeck [9]; in their work, they are not mentioned any postprocessing for the result. This paper uses median filter as postprocessing process, and this is the best-known order-statistics filter. The median filter replaces the value of a pixel by the median of the gray levels in the neighborhood of that pixel [10]. The result after applying the median filter on Fig. 8 shown in Fig. 9.

4 Experimental Results

To fully explore the system performance, the testing has been conducted with different database. The particulars of the databases relevant to this study are given below:

4.1 Data and Qualitative Results

Experimental results for moving object detection for several image sequences using the proposed algorithm have been produced. This paper describes four different sequences, which represent typical situations critical for video surveillance systems and other video analysis systems and present qualitative results obtained with the proposed method.

A detailed discussion about the algorithm parameters selection should be made.

- The number of samples consists in each background model will be 20, $N = 20$
- The radius of the sphere, R, which is used to compare a new pixel with the samples of the model. Here, $R = 20$, which corresponds to a perceptible difference in color (see Eq. 2).
- And the number of close pixel samples needed to classify a new pixel value as background, $\#_{min} = 2$, (see Eq. 2).
- And the time sub-sampling factor used for update the pixel model, $\Phi = 16$

And a detailed description of the sequences used in this paper.

Sequence Campus Dataset Sequence campus is an outdoor sequence consisting 1,438 frames of 160 × 128 spatial resolutions, made publicly available in the downloaded section of http://perception.i2r.astar.edu.sg/bk_model/bk_index.html. The scene consists of a road with waving tree branches in the strong wind, where vehicles and pedestrians are passing through that road and sometimes multiple objects are there on the road. It represents an example of frequently moving background.

In Fig. 10a, c we report one of the sequence frame and the corresponding moving object detection mask computed by the presented algorithm with $N = 20$, $R = 10$, #min = 2, $\Phi = 16$. The detection mask shows that the moving vehicle is perfectly detected instead of moving background and the shadow casts created by the moving object, and the moving tree branches are not included in the result.

Sequence Boats Dataset Sequence boats belong to a set of sequences that represent dynamic background problem for background subtraction. Here, the scene consists of shimmering water, and boats are passing through it. This sequence contains 8,000 frames of 360 × 240 spatial resolutions. This sequence is collected from the database CDW 2012, which is publicly available in this download link http://www.changedetection.net/.

The test image and its corresponding ground truth image are reported in the Fig. 11a, b respectively. Comparing the ground truth with the moving object detection mask computed by the proposed algorithm with $N = 20$, $R = 10$, #min = 2, $\Phi = 16$ reported in Fig. 6c, we can observe that that detection accuracy is quite appreciable.

Sequence From SAMEER-TU Dataset. These are taken from the newly created SAMEER-TU database. And the Video 1 and Video 2 sequences consist of 162 frames and 3,000 frames of 640 × 424 spatial resolution, respectively, acquired

Fig. 10 Segmentation of sequence campus **a** Input image. **b** Ground truth. **c** result

Fig. 11 Segmentation of sequence boats **a** Input image. **b** Ground truth. **c** Result

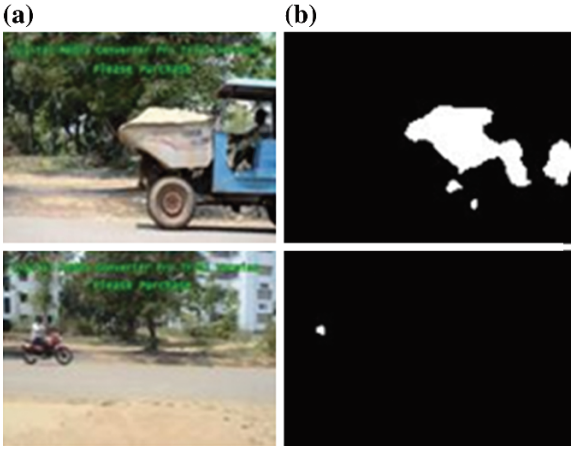

Fig. 12 Segmentation of sequence SAMEER-TU dataset. **a** Input image. **b** Ground truth

at 25 fps. Both the scene consists of a road, where a car passes through this road. These are easy sequences, but they had the difficulty of dynamic background as there is a swaying tree.

Figure 12a shows one frame from this sequence, and its corresponding results are shown in Fig. 12b. Here, the car is detected correctly. And the noise for swaying tree is also removed successfully.

4.2 Qualitative Evaluation

To get a systematic evaluation of proposed method, the performance of the proposed method was evaluated quantitatively on randomly selected samples from first four sequences.

In the previous work [11], the results were evaluated quantitatively from the comparison with the "ground truths" in terms of the following:

- The number of true positives (TP), which accounts for the number of correctly detected foreground pixels.
- The number of false positives (FP), which accounts for the number of background pixels incorrectly classified as foreground.
- The number of true negatives (TN), which accounts for the number of correctly classified background pixels.
- The number of false negatives (FN), which counts r the number of foreground pixels incorrectly classified as background.
- Based on the above-mentioned quantities, Elhabian [11] described three methods for quantifying a classifier's performance.

The Percentage of Correct Classification:

$$\mathrm{PCC} = \frac{\mathrm{TP} + \mathrm{TN}}{\mathrm{TP} + \mathrm{TN} + \mathrm{FP} + \mathrm{FN}} \tag{3}$$

If the PCC percentage is high, then, there is less error in detection and vice versa. Here, for all the selected samples for evaluation, the PCC is calculated, and the result is tabulated in Table 1.

4.3 Accuracy Results

After applying the algorithm without postprocessing step on "campus" sequence, it is obtained that the calculated PCC for the frames whose ground truths are given in the database is in the range 80–85 %.

And as the CDW 2012 database provides ground truths for all the frames of one sequence, so we calculate average PCC for the whole sequence. And the PCC calculated for the sequence Bungalows is 82.2 % and for "Boats" is 83 %. And the PCC is calculated before applying the postprocessing.

After doing the postprocessing step, calculated PCC for "campus" is in the range 94–95 %. And calculated PCC for the "Bunglows" and "boats" are 94.80 and 94.40 %, respectively.

5 Conclusion and Future Work

An object detection framework has been proposed for surveillance and navigation applications, which combines four crucial steps. Firstly, a background pixel model, which can be initialized from a single frame. Secondly, a pixel classification process which classifies a pixel according to its corresponding model. Thirdly, an update mechanism which ignores insertion time of a pixel in the pixel model and replaces values randomly. This update mechanism also ensures spatial consistency of the

background model by allowing samples to diffuse between neighboring pixel models. And lastly, a filtering process which gives more accurate results. Furthermore, the accuracy of the system is also measured, and a comparison is also carried out between the results that are obtained by implemented this technique on different datasets and a new dataset which is created for this purpose. And this is observed that the accuracy of the system increases from 80 to 95 % after using the filtering process for each dataset.

Future scope in this work is to implement an object tracking system using this object detection technique.

Acknowledgments First author is thankful to the Society for Applied Microwave Electronics Engineering and Research (SAMEER), R&D Lab of Department of Electronics and Information Technology (DeitY), Ministry of Communications and Information Technology, Government of India. The database is presented here is being created in the Biometrics Laboratory of Computer Science Engineering Department of Tripura University (A Central University), India under the project entitled "Development of Thermography Infrastructure facility for Security and Navigation System-Phase-1", grant no SMR/PD(R)/NER/2012–13/Thermography, Dated: 22nd March 2013 from the Society for Applied Microwave Electronics Engineering and Research (SAMEER), IIT Bombay Campus, Powai, Mumbai 400076.

References

1. Maddalena, L., Petrosino, A.: A self-organizing approach to background subtraction for visual surveillance applications. IEEE Trans. Image Process. **17**(7), 1168–1177 (2008)
2. Cavallaro, A., Ebrahimi, T.: Video object extraction based on adaptive background and statistical change detection. In: Proceedings of SPIE on visual communications and image processing, vol. 4310, pp. 465–475. SPIE, Jan 2001
3. El Maadi, A., Maldague, X.: Outdoor infrared video surveillance: a novel dynamic technique for the subtraction of a changing background of IR images. Infrared Phys. Technol. **49**, 261–265 (2007)
4. Abbott, R., Williams, L.: Multiple target tracking with lazy background subtraction and connected components analysis. Mach. Vis. Appl. **20**, 93–101 (2009)
5. Wren, C., Azarbayejani, A., Darrell, T., Pentland, A.: Pfinder: realtime tracking of the human body. IEEE Trans. Pattern Anal. Mach. Intell. **19**, 780–785 (1997)
6. Haritaoglu, I., Harwood, D., Davis, L.: W4: real-time surveillance of people and their activities. IEEE Trans. Pattern Anal. Mach. Intell. **22**, 809–830 (2000)
7. Stauffer, C., Grimson, E.: Learning patterns of activity using realtime tracking. IEEE Trans. Pattern Anal. Mach. Intell. **22**, 747–757 (2000)
8. Wu, M., Peng, X.: Spatio-temporal context for codebook-based dynamic background subtraction. Int. J. Electron. Commun. **64**(8), 739–747 (2010)
9. Barnich, O., Van Droogenbroeck, M.: ViBe: a powerful random technique to estimate the background in video sequences. IEEE Trans. Image Process. **20**(6), 1709–1724 (2011)
10. Gonzalez, R.C., Woods, R.E., Eddins, S.L.: Digital image processing using MATLAB, 2nd edn. McGraw Hill, New York (2012)
11. Elhabian, S., El-Sayed, K., Ahmed, S.: Moving object detection in the spatial domain using background removal techniques—state-of-art. Recent Pat. Comput. Sci. **1**, 32–54 (2008)

Internet of Things: Route Search Optimization Applying Ant Colony Algorithm and Theory of Computation

Tushar Bhardwaj and S.C. Sharma

Abstract Internet of Things (IoT) possesses a dynamic network where the network nodes (mobile devices) are added and removed constantly and randomly; hence, the traffic distribution in the network is quite variable and irregular. The basic but very important part in any network is route searching. We have many conventional route searching algorithms such as link-state and distance vector algorithms, but they are restricted to the static point-to-point network topology. In this paper, we proposed a hypothetical but feasible model that uses the ant colony optimization (ACO) algorithm for route searching. ACO is dynamic in nature and has a positive feedback mechanism that conforms to the route searching. In addition, we have embedded the concept of deterministic finite automata (DFA) minimization to minimize the number of iterations done by ACO in finding the optimal path from source to sink. Analysis and proof show that ACO gives the shortest optimal path from the source to the destination node, and DFA minimization reduces the broadcasting storm effectively.

Keywords Route searching · Ant colony algorithm · DFA minimization · IoT

1 Introduction

The Internet of Things (IoT) is an emerging concept coined by Kevin Ashton in the year 1999 [1]; according to him, the world is a network of many objects forming a IoT. From the day of its inception, the meaning of *things* has been changed as

T. Bhardwaj (✉)
IIT Roorkee, Saharanpur Campus, Saharanpur 247001, India
e-mail: tushariitr1@gmail.com

S.C. Sharma
Wireless and Computer Lab, IIT Roorkee, Saharanpur Campus,
Saharanpur 247001, India
e-mail: scs60fpt@gmail.com

K.N. Das et al. (eds.), *Proceedings of Fourth International Conference on Soft Computing for Problem Solving*, Advances in Intelligent Systems and Computing 335,
DOI 10.1007/978-81-322-2217-0_25

technology evolved. In last ten years or so, IoT has covered a large range of applications such as health care, transport, and utilities [2]. The very indispensable point of interest is that information and communication system are invisibly injected in the environment around us. The outcome of such system is generation of the huge amount of data that has to be processed, transferred, analyzed, etc. Zhou [3] have mentioned in his work about the four pillars of IoT: wireless sensor network (WSN), radio frequency identification (RFID), machine-to-machine (M2M), and supervisory control and data acquisition (SCADA). All the four pillars are directly or indirectly referring to some sensor nodes that are attached to the devices for communication.

For communication among sensors, there should be a path or route to communicate. The shorter the route, the less time for communication. We have many conventional route searching algorithms such as link-state and distance vector algorithms, but they are restricted to the static point-to-point network topology, whereas in IoT, the network is of dynamic nature. Therefore, the routing algorithm must fit the dynamisms of the sensor network in IoT.

This paper presents a hypothetical but feasible model that finds the shortest optimal route between the source and destination node in an IoT network and hence improves the searching time of the network by minimizing the iterations required by optimizing tool to find the shortest path. The authors have used ant colony optimization (ACO) for creating the shortest path between the source and sink nodes. To minimize the iterations of ACO, authors have embedded the concept of deterministic finite automata (DFA) minimization to reduce the searching time by eliminating the useless nodes which are not leading to the destination node.

This paper is divided into following sections: Sect. 2 is about the motivation for the proposed model. Section 3 lays emphasis on the related work and literature review. Section 4 describes the analogy of ACO to real world. Section 5 contains the proposed model and its working in detail. Section 6 contains the proofs and results for comparison. Section 7 concludes our work and future work to be done. Chapter ends with the references.

2 Motivation

The root to most of the route searching techniques ties a knot with travelling salesman problem (TSP). The basic idea is to find the minimum shortest path (in terms of cost) in the given network.

Most of the conventional algorithms such as Dijkshtra and Prims are used to find the shortest path but for a static network. Figure 1 illustrates MATLAB implementation of Dijkstra's algorithm of finding the shortest path between node 1 and node 15 in a network of 50 nodes.

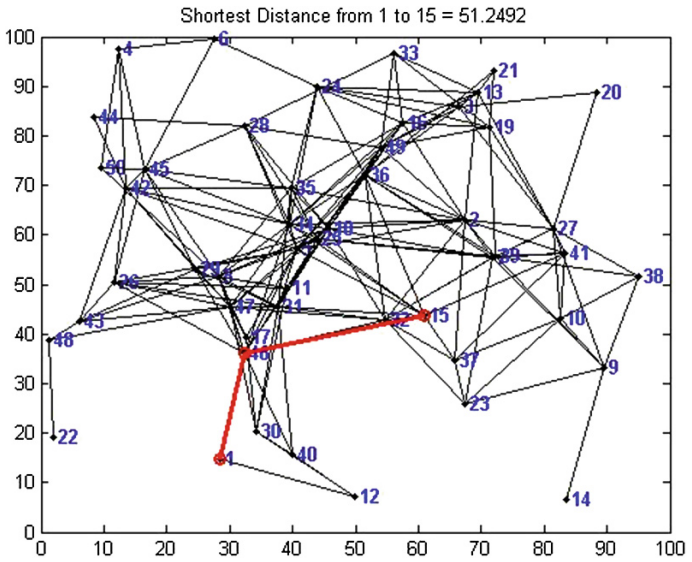

Fig. 1 Dijkstra's algorithm

Here, number of nodes is fixed and the network is static, whereas in IoT, both these entities are variable. Therefore, the conventional route searching algorithms fail to cope up with the dynamic nature of IoT network.

When implementing ACO, it takes many iterations to generate a path from source to sink. This is the major drawback of ACO algorithm when compared with Dijkstra's and A* algorithms [4]. If the number of iterations can be reduced, then the time taken in path creation can be minimized. The plot of number of path versus iterations is given in Fig. 2. But the main question arises that how to reduce the iterations? The authors have proposed a model that answers the question by eliminating the nodes of the network which are useless*.

*A useless node may be due to anyone of the two reasons mentioned below:

1. **Unreachable Nodes**: These are the nodes that are not reachable from the source node due to following reasons:
   - Dead nodes (inactive node).
   - Dumb nodes (nodes sensing but not participating in communication).
2. **Non-distinguishable Nodes**: These are the states that cannot be distinguished from one another for any given source and sink route. Elimination here does not meant to remove those nodes from the network, but to neglect those nodes in next following iterations. If we are able to neglect those nodes, then the convergence rate will increase and hence the search time decreases.

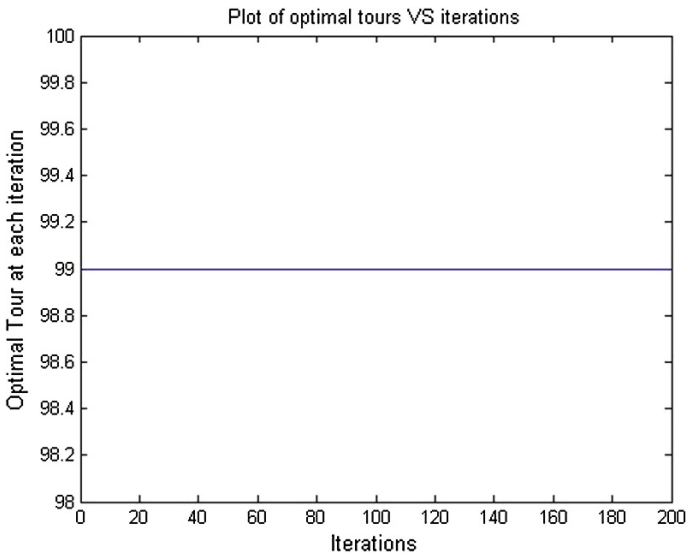

Fig. 2 Plot of optimal tours versus iterations implementation

3 Literature Review

Woungang et al. [5] have used ACO and design a model to detect and control congestion is the sensor nodes, which leads to packet loss and excessive energy consumption. Misra et al. [6] have laid emphasis on the existence of dumb nodes in stationary wireless sensor networks (WSN). They have defined a dumb node as a node that senses, but does not communicate due to any environmental disturbance. As a result of this temporary behavior, a node may get isolated from the network. Okdem et al. [7] introduce ACO algorithm to get a dynamic and reliable routing protocol for WSN. In an another similar work by Hui et al. [8] showcases the usage of ACO in calculating the path delay and frequency, a node is acting as a router to achieve a dynamic and adaptive routing.

4 Analogy

We have heard a lot about ants moving forward and backward and leaving pheromone at the nodes. But what exactly is happening in the real world of computer networking? In this section, authors have laid emphasis on how the ACO algorithm reflects in the real world. Just for data communication give it a look.

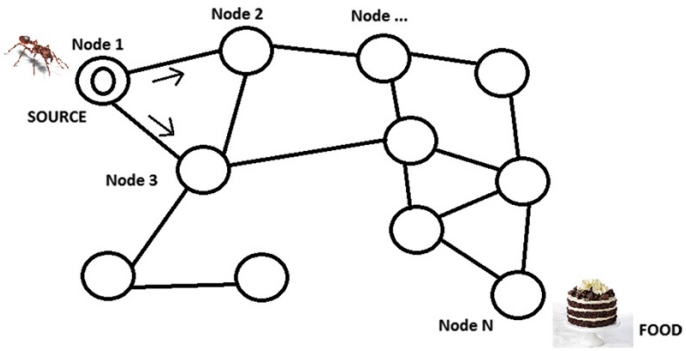

Fig. 3 Illustration of ACO

4.1 ACO Concept

Ants wander randomly in the search for foods. On finding it, they return to the ant colony. As an ant walks back to its colony, it leaves a trail of pheromone. Other ants smell these pheromones and follow the path created by the original ant rather creating a new and random path/paths as shown in Fig. 3. These ants also leave their own pheromone. Over the time, most official trails get reinforced. The rest of the trails evaporate.

One way is to stimulate ant colony. We can create software agents which represent the real ants and give them a goal, i.e., food. If we do it right, then ant will find the goal without our help.

4.2 Data Communication in ACO

To establish a routing network in a real computing world, let any node transmits a searching signal (ants) from source to sink node. To understand the working procedure of forward and backward ants, there are two phases which encompass the whole routing scenario as shown in Fig. 4.

4.2.1 Solution Construction

- At a standard interval T from every node S, a forward ant F_{s-d} (searching signal) is launched toward a destination node D.
- Forward ants share the same data queues as data packets, so they face the same traffic complexity.
- If F_{sd} is a unit (in bits) of the data flow s to d, then the probability of creating at node s a forward ant with node d as destination is

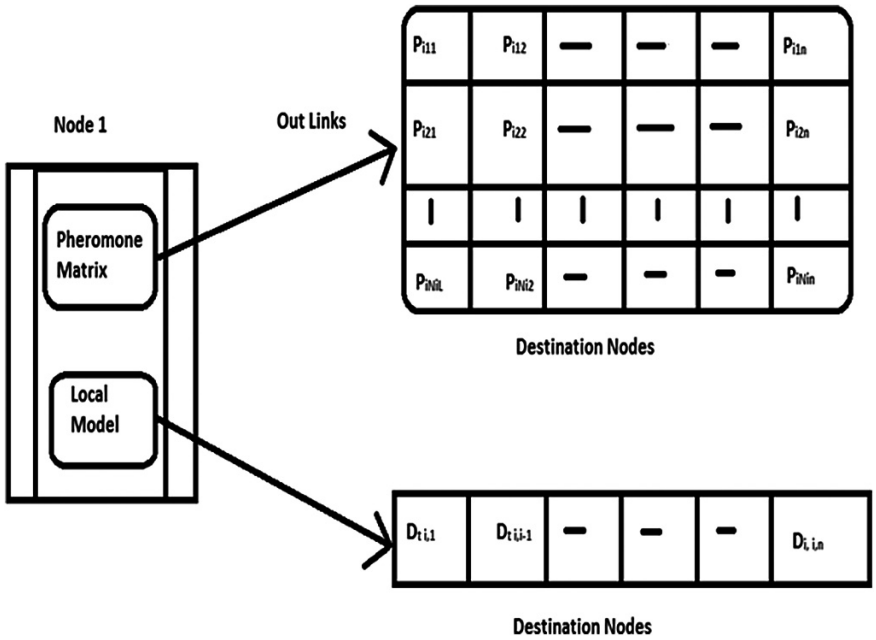

Fig. 4 Solution construction and data structure update

$$Q_{sd} = \frac{F_{sd}}{\sum F_s}$$

- When the forward ants move from the source to the destination node, they keep the memory of the traffic condition and paths.

4.2.2 Data Structure Update

- When an ant arrives at a destination node (j), then the backward ant updates the two basic data structures of the node, the local model of the traffic M and the pheromone matrix T for all the entries corresponding to the forward/destination node (d).

5 Proposed Model

In this section, authors have discussed the proposed model for the route searching optimization in detail. Keeping in mind the dynamism of wireless sensor communication, we have used ACO algorithm to find a path between source and sink node. As the artificial ants move from one node to another, the route is being

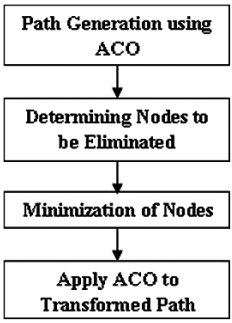

Fig. 5 Proposed model

generated and leads to a final destination. In this model, we have tried to minimize the iterations used by ACO in finding the route. The proposed model illustrated in Fig. 5 is bifurcated into three phases: (1) path generation using ACO, (2) determining nodes to be eliminated, and (3) minimization of nodes. The working of each of the phase is mentioned below in detail.

5.1 Phase 1: Path Generation Using ACO

In this section, we have laid emphasis on the ACO algorithm working and implementation.

5.1.1 Working of ACO

At regular intervals concurrently and asynchronously, from each node, artificial ants are triggered and launched toward destination node [9]. These ants act concurrently and independently and communicate in an indirect way. The mode of communication is the amount of pheromones and heuristic value (Sect. 5.1.2) by which they read and write locally on the nodes. The main task of each artificial ant is to find the shortest cost path between source and destination nodes. Ants apply a greedy policy at every intermediate node to choose the next node. During the path, the ants take the information about the time limit, congestion status, and the node identifiers of the path. Once the ants find the required or desired destination, they revert back to the same path in the opposite direction. During the revert path, the information stored at the local nodes and the value of pheromone stored there are updates (Sect. 5.1.3). Once the artificial ants reached the source node, they are removed from the network. A complete flowchart is given in Fig. 6.

Note We will apply ant colony algorithm to a given graph. After applying ACO, a virtual path will be in the form of connected nodes. The given nodes in the graph can be transformed into the states, and the system can be defined as DFA.

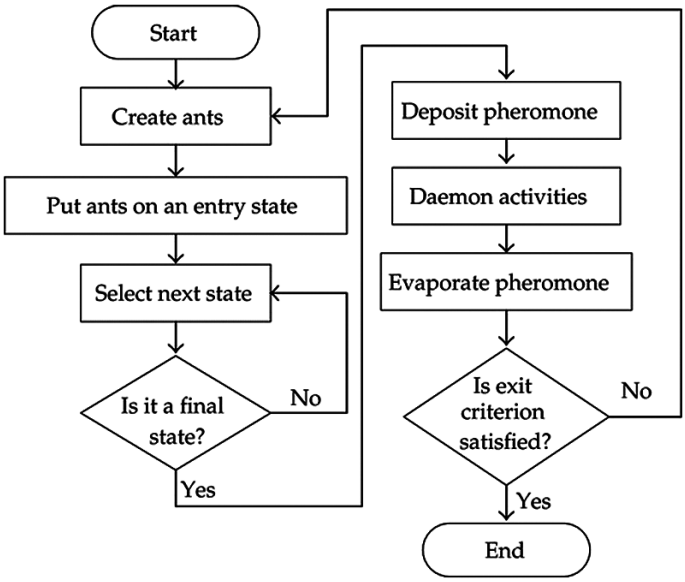

Fig. 6 Ant colony optimization flowchart. *Image source* http://www.hindawi.com/journals/mpe/2012/246978

5.1.2 Transition Rule

- $T(i, j)$ is the amount of pheromone currently on the path that goes directly from node i to node j.
- $H(i, j)$ is the heuristic value of this link—in the classic TSP application, this is chosen to be 1/distance (i, j)—i.e., the shorter the distance, the higher the heuristic value.
- $p_k(i,j)$ is the probability that ant k will choose the link that goes from i to j.
- β is a parameter that we can call the *heuristic strength.*

The rule is as follows:

$$p_k(i,j) = \frac{T(i,j) \cdot H(i,j)^{\beta}}{\sum_{\text{unvisitedcities } c} T(i,c) \cdot H(i,c)^{\beta}}$$

where our ant is at node i, and j is a node as yet unvisited on its tour, and the summation is over all of k's unvisited cities.

5.1.3 Global Pheromone Update

- $A_k(i, j)$ is amount of pheromone added to the (i, j) link by ant k.
- m is the number of ants.

- ρ is a parameter called the pheromone decay rate.
- L_k is the length of the tour completed by ant k.

$T(i, j)$ at the next iteration becomes

$$\rho \cdot T(i,j) + \sum_{k=1}^{m} A_k(i,j)$$

5.2 Phase 2: Determining Nodes to Be Eliminated

As discussed in the previous section, ant decides where to go from a node to another, based on probabilities calculated from pheromone strengths and next-hop distances.

Therefore, at the end of first iteration of ACO, there will be distinct paths from source to sink with a probability constraints (pheromone strength and next-hop distance) attached to every path, Fig. 7a. We will sort the paths w.r.t. the probability and determine the nodes having much distance to cover. For example, in Fig. 7a, node 1(D = 1.0) and node 4(D = 1.3) are much far as compared to nodes 2 and 3 from source node s. Therefore, in the given graph, nodes 1 and 4 can be marked for elimination and get extracted from the graph.

5.3 Phase 3: Minimization of Nodes

In this section, we have detailed the working of DFA minimization to remove those marked nodes (we get from the previous section). DFA minimization is a concept from the subject of theory of computer science [10, 11], in which the cyclic nodes and nodes that are not reaching to the particular destinations are neglected from the network to give a better performance in terms of route searching. To eliminate any node from a given graph, we have assumed the marked node as useless node. After minimization, the graph will look like Fig. 7b. It is clearly visible from the figure that during second iteration, the ants have to only go to nodes 2 and 3. Therefore, the ant's workload has been reduced to a great extent. Hence, the number of iterations will also get minimized.

5.3.1 DFA Minimization Algorithm

Step 1: We have an DFA $M = (Q, \sum, \partial, q_0, F)$.

Q = Total number of internal states/nodes
$\sum$ = Input Alphabets

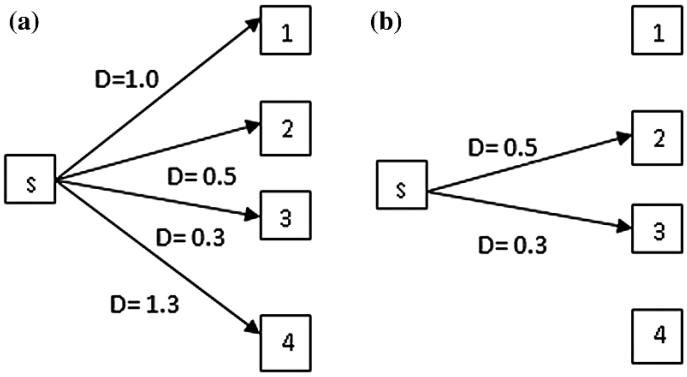

Fig. 7 **a** Distances from source node *s* to nearby nodes, **b** minimized nodes

∂ = Transition Function
q_0 = Initial State
F = Final State

Step 2: There are two states r and s, and they are distinct if

- r in F and s not in F or vice versa, or
- for some α, $\partial(r, \alpha)$, and $\partial(s, \alpha)$ are distinct

Step 3: By applying the inductive definition, we can find that the states are different.

Step 4: Design a lower triangular table distinct, initially blank.

Step 5: For each pair of states (r, s):

- if r is final and s is not, or vice versa
  - DISTINCT $(r, s) = €$

Step 6: Iteration will go on until no change:

- For each pair of states (r, s) and each symbol α
  - If DISTINCT (r, s) is blank and
    DISTINCT $(\partial (r, \alpha), \partial (s, \alpha))$ is not blank

    DISTINCT $(r, s) = \alpha$

Step 7: Join all the states that are not distinct.

Note Again ACO is applied to the transformed graph, and the cycle continues till the best optimal path is being found.

6 Results

In this section, authors have proved the above-proposed model in terms of the number of iterations used by ACO algorithm.

Attiratanasunthron [12] have proved that the polynomial running time bounds for an ACO algorithm for the single-destination shortest path problem on directed acyclic graph. They have shown that the expected number of iterations required for an ACO algorithm with n ants is $O(1@rn^{\wedge}2m \log n)$ for graph with n nodes and m edges, where $@r$ is an evaporation rate.

Keeping in mind the above results, we have proved that the number of iterations can be minimized by ACO algorithm, with minimizing the number of nodes.

6.1 Proof

Given:
For an ACO algorithm with n ants for graphs with n nodes and m edges,

The number of iterations is given by,

$$I : O(1@rn^{\wedge}2m \log n) \tag{1}$$

It meant that the time complexity of number of iteration varies with the three parameters, i.e., number of ants, number of nodes, and number of edges.

Assumptions:
In our research work, we have fixed few parameters such as

- $A_k(i, j)$ is amount of pheromone added to the (i, j) link by ant k.
- m is the number of ants.
- ρ is a parameter called the pheromone decay rate.
- L_k is the length of the tour completed by ant k.

Let the total number of nodes be n and number of edges be m. In Sects. 5.2 and 5.3, authors have shown that how can we minimize the number of nodes from a given graph.

Suppose the number of nodes get minimized is x and hence consequently the number of edges be y.

Therefore, the new values of number of nodes and edges will be

- New number of nodes n': $[n - x]$
- New number of edges m': $[m - y]$

Putting the values of n' and m' in Eq. (1), we get the new complexity given below:

The new number of iterations is

$$I' : O(1@rn^{\wedge}2m' \log n') \tag{2}$$

On comparing Eqs. (1) and (2), we get

$$I > I'$$

Hence, it has been proved that if the number of nodes is minimized, it directly effects the number of iterations required to find a optimal route from a source to sink. Therefore, the proposed model can be implemented to minimize the number of iterations required by ACO algorithm and hence improves the performance exponentially.

7 Conclusion

The proposed model states that the route is being generated by the ant colony algorithm and hence reduced to a more effective and optimal route with the help of DFA minimization. It has been clearly found that the reduction in the number of nodes leads to a more cost-effective path to the destination node. The model reduces the ambiguity in the path and minimizes the cyclic nodes, which leads to the time elapsed during the journey of the ant. The proof in the result section has shown that how complexity can be reduced by this model. Hence, this model can be implemented for better results in ACO algorithm.

References

1. Ashton, K.: That 'Internet of Things' thing. RFiD J. **22**, 97–114 (2009)
2. Sundmaekar, H., Guillemin, P., Friess, P., Woelffle, S.: Vision and challenges for realising the Internet of Things. Cluster of European Research Projects on the Internet of Things–CERP IoT (2010)
3. Zhou, H.: The Internet of Things in the Cloud: A Middleware Perspective. CRC Press, Taylor & Francis Group, Boca Raton, London (2013)
4. Rapant, L.: Application of dynamic graphs for the fastest route search in a transport network. Diploma thesis (2011)
5. Dhurandher, S.K., Misra, S., Mittal, H., Agarwal, A., Woungang, I.: Ant Colony Optimization-Based Congestion Control in Ad-hoc Wireless Sensor Networks (2009)
6. Misra, S., Kar, P., Roy, A., Obaidat, M.S.: Existence of dumb nodes in stationary wireless sensor networks. J. Syst. Softw. **91**, 135–146 (2014)
7. Okdem, S., Karaboga, D.: Routing in Wireless Sensor Networks using Ant Colony Optimization (2009)
8. Hui, X., Zhi-gang, Z., Xue- guang, Z.: A Novel Routing Protocol in Wireless Sensor Networks based on Ant Colony Optimization (2009)
9. Working of Ant Colony Algorithm, link: https://www.macs.hw.ac.uk/∼dwcorne/Teaching/bic10_ants.ppt
10. people.cs.clemson.edu/∼goddard/texts/theoryOfComputation/3a.pdf
11. www.cse.chalmers.se/∼coquand/AUTOMATA/o2.pdf
12. Attiratanasunthron, N., Fakcharoenphol, J.: A running time analysis of an ant colony optimization algorithm for the shortest paths in directed acyclic graphs. J. Inf. Process. Lett. **105**(3), 88–92 (2008)

Multi-objective Optimization of Knitted Fabric Comfort and Ultraviolet Radiation Protection by Evolutionary Algorithm

Anindya Ghosh, Prithwiraj Mal, Abhijit Majumdar and Debamalya Banerjee

Abstract The present work does a simultaneous maximization of air permeability and ultraviolet radiation protection of single jersey cotton knitted fabrics. As these two objectives are conflicting in nature, i.e., not a single combination of knitting parameters does exist which produce concurrent maximum air permeability as well as maximum ultraviolet radiation protection. Therefore, it has several optimal solutions from which a trade-off is needed depending upon the requirement of user. In this work, the optimal solutions are obtained with an elitist multi-objective evolutionary algorithm based on Non-dominated Sorting Genetic Algorithm II (NSGA-II). These optimum solutions may lead to the efficient exploitation of knitting parameters to produce fabrics with optimum protection from ultraviolet radiation and comfort.

Keywords Air permeability · Genetic algorithm · Fabric comfort · NSGA-II · Pareto optimal solutions · Ultraviolet protection factor

1 Introduction

Of late, the concept of mass production in textile industry is changing rapidly toward engineered production. This has been empowered mainly due to the advent of various machine learning techniques such as ANN, genetic algorithm (GA).

A. Ghosh (✉)
Government College of Engineering and Textile Technology Berhampore, Baharampur, West Bengal, India
e-mail: anindya.textile@gmail.com

P. Mal
National Institute of Fashion Technology, Madhapur, Hyderabad, India

A. Majumdar
Department of Textile Technology, Indian Institute of Technology Delhi, New Delhi, Delhi, India

D. Banerjee
Department of Production Engineering, Jadavpur University, Kolkata, India

K.N. Das et al. (eds.), *Proceedings of Fourth International Conference on Soft Computing for Problem Solving*, Advances in Intelligent Systems and Computing 335,
DOI 10.1007/978-81-322-2217-0_26

Apparel textiles protect our skin from the solar ultraviolet (UV) radiation. The UV protection ability of a textile fabric is expressed by the ultraviolet protection factor (UPF). Heavy cotton fabrics can provide good protection against UV radiation. However, during summer season heavy fabrics are not good from a comfort point of view as the air permeability is very low. The simultaneous maximization of fabric air permeability as well as UPF is conflicting in nature. For these two conflicting objectives, each of them corresponds to a different optimal solution. A single solution which is the best with respect to both the objectives may not exist. Rather, we can visualize a set of optimal solutions where a gain in UPF calls for a sacrifice in air permeability.

In single objective optimization, there is only one optimal solution, but in multi-objective optimization, there are multiple optimal solutions termed as Pareto optimal solutions or non-dominated solutions in which all solutions are equally important. For clarity, these solutions are joined with a curve. The curve formed by joining these points is termed as Pareto optimal front [1]. Depending upon the requirement of the user, any one solution from the Pareto optimal front can be selected. There have been few researches on application of multi-objective optimization in textile field. Settle and Langenhove [2] studied the multi-objective optimization to maximize yarn tensile strength at minimum cost. Skordos et al. [3] studied multi-objective optimization problem to optimize shear and drape behavior of woven fabric. Ghost et al. [4] developed Non-dominated Sorting Genetic Algorithm II (NSGA-II) technique of multi-objective optimization to maximize cotton strength at minimum raw material quality.

In this work, an attempt has been made for simultaneous maximization of two conflicting objectives viz. air permeability and UPF of single jersey cotton knitted fabrics. Since evolutionary algorithm finds multiple optimal solutions in one single simulation run, it becomes a unique technique in solving multi-objective optimization problems. Here, NSGA-II developed by Deb [1] is used to solve the proposed multi-objective optimization problem. The following sections present experimental, multi-objective optimization by NSGA-II, results and discussion, and conclusion. The "experimental" section contains the details of variables and their levels that affect the air permeability and UPF of a single jersey fabric. The design of experiment, experimental details, and the results are shown in this section. In the "multi-objective optimization by NSGA-II" section, the development of NSGA-II algorithm for multi-objective optimization of two conflicting objects, i.e., air permeability and UPF is discussed. In the section "results and discussion," the Pareto optimal solutions of air permeability and UPF are shown and discussed.

2 Experimental

Four variables such as loop length, carriage speed, input tension, and yarn count were considered for the preparation of knitted fabric samples. Each variable was considered at three levels. The coded levels of variables and their corresponding

actual values are given in Table 1. Altogether, 36 single jersey fabric samples were prepared using Shima Seiki knitting machine according to the Box and Bhenken orthogonal design of experiments as shown in Table 2. The Box and Bhenken design [5] is a response surface design that is used to optimize various process parameters of a process. This method is often employed after identification of controllable factors and to find the factor levels that optimize the response. In orthogonal Box and Bhenken design, the design can be blocked orthogonally. A 4-factor 3-level orthogonal Box and Bhenken design is shown below:

$$\begin{bmatrix} \pm1 & \pm1 & \pm1 & 0 \\ \pm1 & \pm1 & 0 & \pm1 \\ \pm1 & 0 & \pm1 & \pm1 \\ 0 & \pm1 & \pm1 & \pm1 \end{bmatrix}$$

Air permeability Tester (FX 3300, TEXTEST AG) was used to measure the air permeability at 100 Pa air pressure according to ASTM D737.

The UPF of fabric specimen was determined by the in vitro method, according to the AATCC 183:2004 standard. In this method, the measurement of basic properties of the fabric viz. fabric density, yarn diameter, and open area portion is determined with photo analysis. The values of UV transmission were then calculated using a spectrophotometer. The transmission values obtained were then used to calculate the in vitro UPF [6].

The UV transmittance analyzer (Labsphere 2000F) was used for measuring the UPF of fabric samples. The UV transmittance was measured in a step of 1 nm wavelength by passing UV rays through the fabric. The UPF of fabric was calculated by using Eq. (1). For each experimental run, 10 samples were tested for UPF and the average value was taken.

$$\mathrm{UPF} = \frac{\sum_{\lambda=290}^{\lambda=400} E(\lambda)S(\lambda)\Delta(\lambda)}{\sum_{\lambda=290}^{\lambda=400} E(\lambda)S(\lambda)T(\lambda)\Delta(\lambda)} \tag{1}$$

where $E(\lambda)$ is relative erythemal spectral effectiveness, $S(\lambda)$ is solar spectral irradiance ($\mathrm{Wm}^{-2}\ \mathrm{nm}^{-1}$), $\Delta\lambda$ = measured wavelength interval (nm), and $T(\lambda)$ = average spectral transmittance of the sample.

Air permeability and UPF values of the fabric samples corresponding to different experimental runs are given in Table 2. The regression coefficients were determined

Table 1 Actual values of the variables corresponding to coded levels

Variables	Coded level		
	−1	0	+1
Loop length (X_1), mm	6.6	7.0	7.41
Carriage speed (X_2), m/s	0.25	0.6	0.95
Input tension (X_3), gf	6	8	10
Yarn count (X_4), Ne	5	7.5	10

Table 2 Orthogonal Block Box Bhenken design for 4 variables

Experimental No.	Level of variables				Air permeability ($cm^3/cm^2/s$)	UPF
	X_1	X_2	X_3	X_4		
1	−1	−1	−1	0	116.6	11.65
2	−1	−1	+1	0	116	11.25
3	−1	+1	−1	0	110.07	11.47
4	−1	+1	+1	0	113	11.69
5	+1	−1	−1	0	162	8.42
6	+1	−1	+1	0	160	8.66
7	+1	+1	−1	0	161.6	8.73
8	+1	+1	+1	0	174.6	8.22
9	0	0	0	0	138.1	9.33
10	−1	−1	0	−1	42.16	22
11	−1	−1	0	+1	226.4	5.37
12	−1	+1	0	−1	41	25.1
13	−1	+1	0	+1	235.7	5.21
14	+1	−1	0	−1	62.43	17.5
15	+1	−1	0	+1	278	4.2
16	+1	+1	0	−1	62.59	16.98
17	+1	+1	0	+1	290.2	4.05
18	0	0	0	0	121.9	10.49
19	−1	0	−1	−1	44.5	19.58
20	−1	0	−1	+1	240.7	5.06
21	−1	0	+1	−1	42.37	23.41
22	−1	0	+1	+1	259.2	4.18
23	+1	0	−1	−1	65.67	16.32
24	+1	0	−1	+1	316.9	3.95
25	+1	0	+1	−1	68.67	14.53
26	+1	0	+1	+1	319.9	3.93
27	0	0	0	0	144	10.16
28	0	−1	−1	−1	53.5	17.48
29	0	−1	−1	+1	289.8	4.06
30	0	−1	+1	−1	46.66	22.26
31	0	−1	+1	+1	260	4.3
32	0	+1	−1	−1	49.24	21.84
33	0	+1	−1	+1	297.2	4.24
34	0	+1	+1	−1	45.45	20.12
35	0	+1	+1	+1	286	4.09
36	0	0	0	0	133	10.23

based on the experimental results. The coefficients were tested for significance at the 95 % confidence level. Only significant terms were taken into consideration for a further investigation of the results. The response surface equation for air permeability and UPF is given in Table 3 along with the R^2 values and mean accuracies. The R^2 denotes the co-efficient of determination that indicates how well data fit to a statistical model.

It is evident from the Table 3 that air permeability of the knitted fabric is the function of variables X_1, X_3, and X_4, whereas UPF is a function of variables X_1 and X_4 only. Hence, the variable X_2 has no influence on air permeability and the variables X_2 and X_3 have no effect on UPF.

3 Multi-objective Optimization by NSGA-II

3.1 Objective Functions

Both the objective functions, which correspond to air permeability and UPF, respectively, as given in Eq. (2), are subjected to maximization.

$$\left.\begin{array}{l}\text{Objective 1 : Maximize } \; 134.25 + 22.29X_1 + 111.49X_4 + 9.60X_1X_4 + 10.36X_3^2 + 25.9X_4^2 \\ \text{Objective2 : Maximize } \; 10.05 - 1.69X_1 - 7.69X_4 + 1.32X_1X_4 + 2.05X_4^2\end{array}\right\} \tag{2}$$

The above multi-objective optimization problem is solved using NSGA-II.

3.2 Development of NSGA-II for Multi-objective Optimization

The goal of the NSGA-II algorithm is to find a set of solutions, which is as close as possible to the Pareto optimal front and as diverse as possible simultaneously. Except for the fitness assignment method, the basic structure of NSGA-II is similar to that of GA [2]. The steps involved in this algorithm are briefly explained [3, 4, 7–9].

Table 3 Response surface equations for various parameters

Parameter	Response surface equation	Co-efficient of determination (R^2)	Mean accuracy (%)
Air permeability	$134.25 + 22.29X_1 + 111.49X_4 + 9.60X_1X_4 + 10.36X_3^2 + 25.94X_4^2$	0.991	92.80
UPF	$10.0 - 1.69X_1 - 7.69X_4 + 1.32X_1X_4 + 2.05X_4^2$	0.974	94.58

Step 1: Initialization of random binary population
A binary coded population of size N is randomly generated. Each individual of the population represents 3 parameters or inputs. In this work, 8 bits are chosen for each parameter, thereby making a total string length of an individual equal to 24. The binary coded parameters are then converted into real value by a linear mapping using the following expression:

$$x_i = x_i^L + \frac{\left(x_i^U - x_i^L\right)}{\left(2^{\mathrm{ls}_i} - 1\right)} \times x_i^D \tag{3}$$

where x_i is the real value of the ith input parameter, x_i^L and x_i^U are the lower and upper limits of the ith input parameters, respectively, ls_i is the string length of the ith input parameter, and x_i^D is the decoded value of the ith parameter. This real valued population consists of a set of 3 parameters is used in making solutions of the two objective functions viz. air permeability and UPF.

Step 2: Fast non-dominated sorting
The population is sorted based on their non-domination levels. In this technique, two entities are calculated, first one is the domination count (n_i) that represents the number of solutions, which dominates the solution i, and the second one is S_i that represents the number of solutions which are dominated by the solution i. This is accomplished by comparing each solution with every other solution and checked whether the solution under consideration satisfies the rules given below

$$\left.\begin{array}{l} Objective1_i > Objective1_j \ \ and \ Objective2_i \geq Objective2_j \ or \\ Objective1_i \geq Objective1_j \ \ and \ Objective2_i > Objective2_j \end{array}\right\} \tag{4}$$

where $\mathrm{Objective1}_i$ and $\mathrm{Objective1}_j$ are the fitness values of 1st objective for the ith and jth solutions, respectively. Similarly, $\mathrm{Objective2}_i$ and $\mathrm{Objective2}_j$ are the fitness values of 2nd objective for the ith and jth solutions, respectively. If the rules are satisfied; then, the solution j is dominated else non-dominated. Thus, the whole population is divided into different ranks. Ranks are defined as the several fronts generated from the fast non-dominated sorting technique such that Rank-1 solutions are better than the Rank-2 solutions and so on.

Step 3: Crowded tournament selection
Once the populations are sorted, crowding distance is assigned to each individual belonging to each rank. This is because the individuals of the next generation are selected based on the rank and the crowding distance. This crowding distance ensures a better spread among the solutions.

A better spread means a better diversity among the solutions. In order to calculate crowding distance, fitness of the objective functions for the solutions belonging to a particular rank is sorted in descending order with respect to each objective. An infinite distance is assigned to the boundary solutions, i.e., for the first and nth solutions, if n number of solutions belong to a particular rank. This ensures that the individuals in the boundary will always be selected and hence result in better spread among the solutions [5]. For other solutions belonging to that rank, the crowding distances are initially assigned to zero. For $r = 2$ to $n - 1$ solutions, this is calculated by the following formula:

$$I(r)m = I(r)m + \frac{f_m(r-1) - f_m(r+1)}{f_m^{\max} - f_m^{\min}} \tag{5}$$

where $I(r)m$ is the crowding distance of the rth individual for mth objective, $m = 1$ and 2, $f_m(r - 1)$ is the value of the mth objective for $(r - 1)$th individual, and $f_m^{\max}$ and $f_m^{\min}$ are the maximum and minimum values of the mth objective, respectively.

Step 4: Crowded tournament selection

A crowded comparison operator compares two solutions and returns the winner of the tournament. A solution i wins a tournament with another solution j if any of the following conditions are true:

(i) If solution i has a better rank than j
(ii) If they have the same rank but solution i has larger crowding distance than solution j

Step 5: Recombination and Selection

The offspring and current population are combined, and selection is done in order to obtain the population of the next generation. The offspring are generated by 2-point crossover with a probability of 0.9 and bitwise mutation with a probability of 0.1. The elitism is ensured, as the best population from the offspring and parent solutions are selected for the next generation. The $2N$ solutions are then sorted based on their non-domination, and crowding distances are calculated for all the individuals belonging to a rank. In order to form the population of the current generation, the individuals are taken from the fronts subsequently unless it reaches to the desired population number (N). The filling starts with the best non-dominated front (Rank 1 solutions), with the solutions of the second non-dominated front, followed by the third non-dominated front, and so on. If by adding all individuals in a front, the population exceeds N, and then individuals are selected based on their crowding distance. The steps are repeated until maximum generation number is reached.

4 Results and Discussion

NSGA-II starts with randomly generated 200 initial populations (N), and it ranks the individuals based on the dominance. The fast non-dominated sorting procedure finds out the non-domination frontiers (ranks) where individuals of the frontier set are non-dominated by any solution. By using this procedure, the scattered initial solutions make four frontiers after 12 generations. Hence, the whole initial scattered solutions are now grouped into four ranks. After finding the frontiers, the crowding distance is calculated for each individual by applying Eq. 5. The crowding distance selection operator helps NSGA-II in distributing the solution uniformly to the frontier rather than bunching up at several good points. Subsequently, step 1 to step 5 of NSGA-II are repeated and the solutions of four frontiers are converged into a single Pareto front at the end of 103 generations leading to the final set of solutions.

The Pareto optimal front for air permeability and UPF of the single jersey knitted fabrics is illustrated in Fig. 1, which contains 140 non-dominated solutions. As none of the solutions in the Pareto front are better than other, any one of them is an acceptable solution. The choice of one solution over other exclusively depends upon the requirement of the end user. Table 4 depicts only few selected Pareto optimal non-dominated solutions. If better fabric comfort at high level of UPF is required, a suitable combination of X_1, X_3, and X_4 could be selected from the Pareto optimal solution.

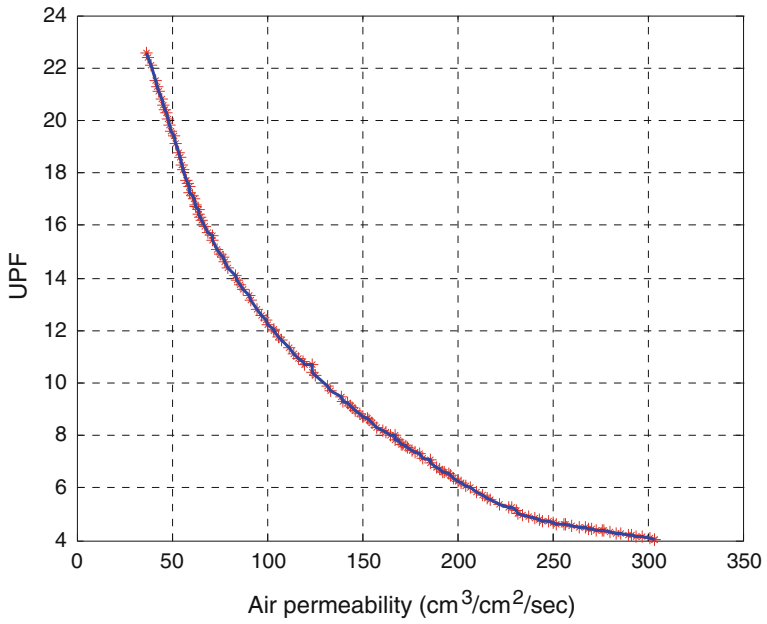

Fig. 1 Pareto optimal front for air permeability and UPF

Table 4 Some selected Pareto optimal solutions

X_1	X_3	X_4	Air permeability ($cm^3/cm^2/s$)	UPF
7.35	8.01	7.95	176.3	7.46
6.63	8.05	9.04	186.79	6.9
6.61	8.04	9.35	202.2	6.18
7.36	8.02	7.84	171.57	7.66
7.33	8.04	7.58	156.38	8.46
7.02	8.04	8.16	167.28	8.07
6.7	8.03	9.14	197.32	6.5
6.63	8.02	8.6	163.9	8.09
7.38	8.01	7.43	151.98	8.63
6.61	8.04	9.37	203.5	6.13

5 Conclusions

The NSGA-II technique of multi-objective optimization has been developed with an aim to maximize simultaneously air permeability and UPF of single jersey cotton knitted fabric. NSGA-II is capable of finding the Pareto optimal solutions for production of fabrics with optimal comfort and UPF. These optimum solutions may lead to the efficient utilization of knitting parameters to produce desired quality of fabrics.

References

1. Deb, K.: Multiobjective Optimization Using Evolutionary Algorithms. Wiley, Chichester (2001)
2. Sette, S., Lengenhove, L.V.: Optimization the fibre-to-yarn production process: finding a blend of fibre qualities to create an optimal price/quality yarn. Autex Res. J. **2**, 57 (2002)
3. Skordes, A., Sutdiffe, M.P.F., Klintworth, J.W., Adofsson, P.: In Proceedings of the 27th Conference SAME EUROPE, Paris (2002)
4. Ghosh, A., Das, S., Banerjee, D.: Multi objective optimization of yarn quality and fibre quality using evolutionary algorithm. J. Inst. Eng. (India) Ser. E **94**, 15–21 (2013)
5. Box, G.E.P., Behnken, D.W.: Some new three level design for the study of quantitative variables. Technometrics **2**, 455–476 (1960)
6. Urbas, R., Sluga, F., Miljkovic, J., Bertenjev, I.: Comparison of in vitro and in vivo ultraviolet protective properties of PET textile samples. Acta Dermatovenerol. APA **21**, 11–14 (2012)
7. Goldberg, D.E.: Genetic Algorithms in Search, Optimization and Machine Learning Reading. Addison-Wesley, Boston (1989)
8. Srinvas, N., Deb, K.: Multi-objective function optimization using non-dominated sorting genetic algorithm. Evol. Comp. J. **2**, 221–248 (1994)
9. Deb, K., Pratap, A., Agarwal, S., Meyarivan, T.: A fast and elitist multi-objective genetic algorithm: NSGA-II. IEEE Trans. Evol. Comput. **6**, 182–197 (2002)

Optimal Product Design of Textile Spinning Industry Using Simulated Annealing

Subhasis Das, Anindya Ghosh and Bapi Saha

Abstract In this paper, we have tried to manufacture cotton yarns with requisite strength by choice of suitable raw material and process parameters. In an attempt to achieve a yarn having optimal strength, a constrained optimization problem is formulated with the relation between raw material and yarn properties. Frydrych's theoretical model of yarn strength is used as objective function of the optimization problem. The simulated annealing (SA) method has been used to solve the optimization problem by searching the best combination of raw material and process parameters that can translate into reality a yarn with the desired strength. The results show that SA is capable of identifying the set of parameters that gives optimum yarn strength.

Keywords Cotton fibre properties · Simulated annealing · Frydrych model · Yarn strength · Yarn engineering

1 Introduction

Nowadays, engineered product manufacturing has assumed a pre-eminent role in every domain of technology. Textile technology thus cannot remain unaffected by this trend which has already etched even greater footprints in some other

S. Das (✉) · A. Ghosh
Department of Textile Technology, Government College of Engineering and Textile Technology, Berhampore 742 101, India
e-mail: subhasis.tex@gmail.com

A. Ghosh
e-mail: anindya.textile@gmail.com

B. Saha
Department of Mathematics, Government College of Engineering and Textile Technology, Berhampore 742 101, India
e-mail: bapi.math@gmail.com

K.N. Das et al. (eds.), *Proceedings of Fourth International Conference on Soft Computing for Problem Solving*, Advances in Intelligent Systems and Computing 335,
DOI 10.1007/978-81-322-2217-0_27

engineering disciplines. Many works have been reported on yarn engineering in recent years [1–9]. Yarns as basic stuff of garments, therefore, call for much greater attention where the principle of engineered product manufacturing can be most deservedly applied. The manufacturing of yarns in textile spinning mills with optimum quality parameters, especially yarn strength by selecting the appropriate raw materials and process parameters, is referred to yarn engineering. The decision of raw material and process parameter selection for attaining the optimum yarn properties is a very complex one. In most of the textile spinning industries, this decision is taken by operations manager based on the mental models which suffers from vagueness and bounded rationality. Cotton fibres have large number of measurable quality attributes, and each of them plays some role on the yarn properties. Therefore, a scientific system should encompass a technique for predicting the yarn properties from the fibre properties and an optimization algorithm for finding the best suited set of fibre properties to attain optimum yarn properties.

The cotton yarn quality is largely governed by the fibre properties. The relationship between the fibre and yarn properties is highly nonlinear. Frydrych's mechanistic model [10] with high degree of predictive accuracy has emerged out as the potent and convincing approach in establishing fibre-yarn esoteric interrelationship. Although the Frydrych's mechanistic model for yarn strength prediction was developed way back in eighties decade, its applications have been limited due to the mathematical rigours involved in the computational works. But with the advent of very high computational speed and non-traditional optimization techniques, it has now become possible to optimize yarn strength derived from this model. In this paper, an attempt has been made to maximize yarn strength obtained from the Frydrych's model using simulated annealing (SA).

2 Mechanistic Model for Yarn Strength Prediction

The model used by Frydrych [10] to predict the strength of cotton yarns incorporates the migrating property of a fibre. The relevant equations for evaluating the fibre length, fibre stress and strain generated in it were developed in accordance with the yarn structure described by Zurek [11]. Many equations described by Frydrych [10] owe their origin to previous works by Zurek [11] and Zurek et al. [12]. In this paper, the mechanistic model for yarn strength prediction developed by Frydrych discussed stepwise:

The metric twist factor is

$$\alpha_{\mathrm{m}} = t\sqrt{\frac{Tt_{\mathrm{y}}}{1000}} \tag{1}$$

where t = twist per metre (m^{-1}) and Tt_{y} = yarn linear density (mg/m).

The density of yarn according to Barella [13] is

$$\rho_y = 560 + 2.8\alpha_m \tag{2}$$

The nominal twist parameter is

$$g = 2\pi RT = \sqrt{\frac{125.7}{\rho_y}}\left(\frac{\alpha_m}{100}\right) \tag{3}$$

The equivalent fibre diameter is

$$d_f = \sqrt{\frac{4Tt_f}{\pi\rho_f}} \tag{4}$$

where Tt_f is linear density of fibre (mg/m), and ρ_f is the fibre density (kg/m^3).

The yarn diameter (in mm) is

$$d_y = \sqrt{\frac{4Tt_y}{\pi\rho_y}} \tag{5}$$

The reduced twist parameter [14] is

$$g_c = 2\pi\left(R - \frac{d_f}{4}\right)T = g\left(1 - \frac{1}{2}\frac{d_f}{d_y}\right) \tag{6}$$

The contraction factor is

$$s = \frac{\ln\sqrt{1 + g_c^2}}{\sqrt{1 + g_c^2} - 1} \tag{7}$$

The coefficient of the yarn diameter contraction can be calculated according to the following formula:

$$u = 1.13 - \frac{0.0265}{g_c} - 0.12\sqrt[4]{100a_h} \tag{8}$$

Since a_h is unknown, it is first assumed that $a_h = a_f$, and the value of u is calculated. Knowing the approximated value of u, the strain of the breaking zone of the yarn is found from the relationship

$$a_h = \sqrt{\left(\frac{1 + a_h}{s}\right)^2 - u^2 g_c^2 - 1} \tag{9}$$

Then, a new value of u is calculated, and again a new value of a_h is found. This process is continued until the calculated values of u do not change.

The parameter of change of the fibre axis shape is

$$k = \frac{1 + a_h}{u} \tag{10}$$

The critical value of the twist parameter is

$$g_r = \frac{g}{k}\left(1 - \frac{2}{u}\frac{d_f}{d_y}\right) \tag{11}$$

The radius of the fibre axis curvature in the external layer of yarn is

$$P = (Ru - d_f)\frac{1 + g_r^2}{g_r^2} \tag{12}$$

The z is a parameter which represents the change in yarn strength because the fibres are constrained from moving freely in the yarn, and the numerical value z can be calculated from the formula as follows:

$$f(z) = \frac{4P}{\mu(c\eta l_f - \lambda)} = \frac{1 - z}{(2z + 1)\ln\left(1 + \frac{1}{2z}\right) - 1} \tag{13}$$

where μ is the coefficient of friction between fibres, c is a coefficient depending on the spinning system, 1.0 for carded yarn and 1.1 for combed yarn, η is the length of fibre ends outside of the yarn; l_f is the mean length of fibres, λ is the length of fibre ends outside the yarn.

The fracture zone length is

$$l_h = \frac{2P}{\mu}\ln\left(1 + \frac{1}{2z}\right) \tag{14}$$

The ratio of the specimen length to the length of fracture zone is

$$q = \frac{y}{l_h} \tag{15}$$

The parameter C depends on twist and the change in fibre axis shape, while the yarn was being strained

$$C = \frac{2k}{g^2}\ln\frac{[1.0253g^2 + 1]^{0.5} + [1.0253g^2 + k^2]^{0.5}}{[0.0253g^2 + 1]^{0.5} + [0.0253g^2 + k^2]^{0.5}} \tag{16}$$

The parameter v_{Fh} is dependent on the coefficient of variation of yarn strength, the actual mass variation of the yarn, Martindale's limit mass variation [15], fibre linear density and yarn count. The coefficient of irregularity of yarn linear density for a combed spinning system (β = 1.35) is determined according to the relationship:

$$v_{\mathrm{Fh}} = \beta\sqrt{\frac{Tt_{\mathrm{y}}}{Tt_{\mathrm{f}}}} \tag{17}$$

where Tt_{f} and Tt_{y} is the fibre and yarn linear density (mg/m), respectively.

The yarn stress at zero gauge length Q_{h} was calculated from the equation

$$Q_{\mathrm{h}} = z\,Q(\varepsilon)C \tag{18}$$

where $Q(\varepsilon)$ is the breaking stress of fibre,

The strength of a 'y' mm long yarn sample (Q_{y}) was obtained by using the modified Peirce's equation [10]

$$Q_{\mathrm{y}} = Q_{\mathrm{h}}\left[1 - 3.64v_{\mathrm{Fh}}\left(1 - q^{-\frac{1}{7}}\right)\right] \tag{19}$$

where Q_{h} is the yarn stress at zero gauge length, v_{Fh} is the variation coefficient of the breaking force in the length of the fracture zone.

3 An Overview of Simulated Annealing

SA was first put forward by Metropolis et al. [16] and successfully applied to the optimization problems by Kirkpatrick et al. [17]. It emulates the cooling process of molten metals through annealing with the concept of Metropolis algorithm. At any instant, if the current point is $x^{(t)}$ and the function value at that point is $E(t) = f(x^{(t)})$, Metropolis algorithm suggests that the probability of the next point being at $x^{(t+1)}$ depends on the difference in the function values at these two points or on $\Delta E = E(t + 1) - E(t)$ and is calculated using the Boltzmann probability distribution:

$$P(E(t+1)) = \min[1, \exp(-\Delta E/kT)] \tag{20}$$

where T is the temperature, and k is the Boltzmann constant. In the context of function minimization, if $\Delta E \leq 0$, according to the above expression, the probability is one and the point $x^{(t+1)}$ is always accepted. Nonetheless, if $\Delta E > 0$, which implies that the function value at $x^{(t+1)}$ is worse than that at $x^{(t)}$, according to the Metropolis algorithm, there is also some finite probability of selecting the point $x^{(t+1)}$. If the

parameter T is large, this probability is more or less high for points with largely disparate function values; therefore, any point is almost acceptable. In contrast, if the parameter T is small, the probability of accepting an arbitrary point is small; therefore, the points with only small deviation in function value are accepted.

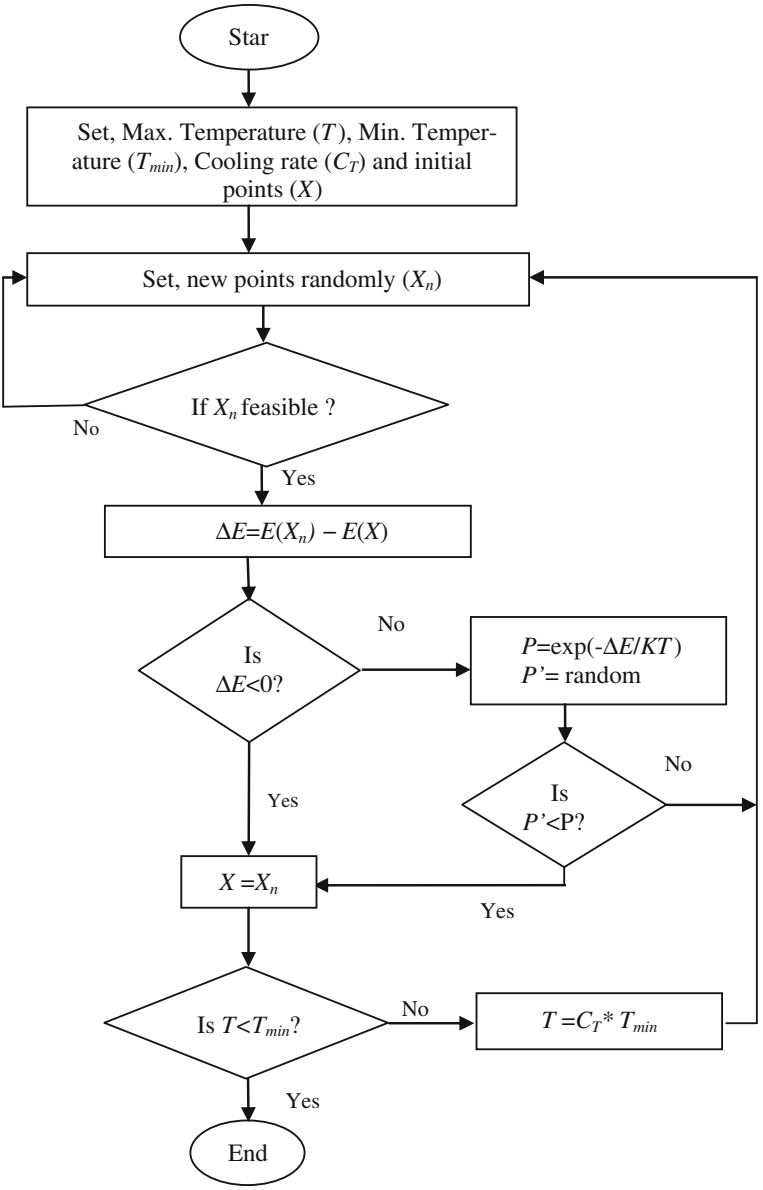

Fig. 1 Flow chart of SA

SA is a point-by-point search method. The algorithm begins with an arbitrary point in the search space and a high initial temperature T. A second point is created at random in the vicinity of the initial point, and the difference in the function values (ΔE) at these two points is calculated. If the second point has a smaller function value, the point is accepted; otherwise, the point is accepted with a probability exp ($-\Delta E/kT$). This completes one iteration of the SA procedure. In the next iteration, another point is created at random in the neighbourhood of the current point, and the Metropolis algorithm is used to accept or reject the point. In order to simulate the thermal equilibrium at every temperature, a number of points are usually tested at a particular temperature, before reducing the temperature at a fixed cooling rate. The algorithm is terminated when a sufficiently small temperature ($T_{\min}$) is obtained or a small enough change in function values is found. The flow chart of the SA algorithm is depicted in Fig. 1.

4 Formulation of Optimization Model

The 20 tex (1 m yarns weight is 20 mg) yarn made from cotton fibre in ring spinning system is considered in this study. The mechanistic model of yarn strength prediction developed by Frydrych [10] has been used for formulation of optimization problem. The maximization of yarn strength is done using SA. The following optimization problem is developed to select the process parameter such as twist per metre (t) and raw material parameters such as cotton fibre liner density (Tt_{f}), breaking strain (a_{f}), breaking stress ($Q(\varepsilon)$) *and* mean length (l_{f}) for the production of cotton yarn with maximum strength.

Maximize:

$$Q_{\mathrm{y}} = Q_{\mathrm{h}}\left[1 - 3.64 v_{\mathrm{Fh}}\left(1 - q^{-\frac{1}{7}}\right)\right].$$

Subject to inequality constraints:

$$\left.\begin{aligned} & t^{L} \le t \le t^{U} \\ & Tt_{\mathrm{f}}^{L} \le Tt_{\mathrm{f}} \le Tt_{\mathrm{f}}^{U} \\ & a_{\mathrm{f}}^{L} \le a_{\mathrm{f}} \le a_{\mathrm{f}}^{U} \\ & Q(\varepsilon)^{L} \le Q(\varepsilon) \le Q(\varepsilon)^{U} \\ & l_{\mathrm{f}}^{L} \le l_{\mathrm{f}} \le l_{\mathrm{f}}^{U} \end{aligned}\right\} \quad (21)$$

where the superscripts L and U refer to the values of lower and upper bounds, respectively.

Table 1 Optimized value of constraints

Controlling parameters	Optimized values
Twist/metre	681.46
Fibre fineness (tex)	0.13478
Fibre breaking strain	0.067481
Average fibre length	32.733
Fibre breaking strength (g/tex)	34.317

Table 2 Boundary of constraints

Controlling parameters	Lower boundary	Upper boundary
Twist/metre (m^{-1})	650	700
Fibre linear density (tex)	0.120	0.150
Fibre breaking strain (%)	6.0	7.0
Average fibre length (mm)	25	33
Fibre breaking stress (g/tex)	28	35

5 Results and Discussion

Figure 1 depicts the flow chart of the SA method for maximization of cotton yarn strength by selecting the appropriate raw material and process parameters which govern the strength of yarn. The optimization problem of Eq. (21) was solved using SA algorithm with MATLAB (version 7.7) coding on a 2.6 GHz, PC. Maximum number of iteration was set to 1,000. The values of T, $T_{\min}$, cooling rate and number of iteration at each temperature for SA were set as 1,000, 0.9, 10 % and 30, respectively.

Table 1 shows the lower and upper bounds of inequality constraints. Table 2 gives the optimum combination of fibre properties and twist/metre that can translate into reality a yarn of maximum strength. The obtained value of yarn strength with the optimized parameters is 19.845 g/tex.

6 Conclusion

SA is an efficient technique for engineering design of textile product since it can easily be implemented and it is computationally inexpensive as fewer parameters are involved. The SA is used to search the best combination of parameters that can translate into reality a yarn with requisite quality by solving the constrained optimization problem deriving from the Frydrych's yarn strength equations mapping the input–output relation between fibre-yarn properties. The model is capable of identifying the set of parameters that gives maximum yarn strength. For references, follow the given guidelines.

References

1. Ramesh, M.C., Rajamanickam, R., Jayaraman, S.: The prediction of yarn tensile properties by using artificial neural networks. J. Text. Inst. **86**(3), 459–569 (1995)
2. Cheng, L., Adams, D.L.: Yarn strength prediction using neural networks, part i: fibre properties and yarn strength relationship. Text. Res. J. **65**(9), 495–500 (1995)
3. Pynckels, F., Kiekens, P., Sette, S., Langenhove, L.V., Impe, K.: The use of neural nets to simulate the spinning process. J. Text. Inst. **88**(4), 440–448 (1997)
4. Sette, S., Boullart, L., Langenhove, V.L., Kiekens, P.: Optimizing the fibre-to-yarn production process with a neural network/genetic algorithm approach. Text. Res. J. **67**(2), 84–92 (1997)
5. Shanmugam, S., Chattopadhyay, S.K., Vivekanandan, M.V., Sreenivasamurthy, H.V.: Prediction of micro-spun yarn lea CSP using artificial neural networks. Indian J. Fibre Text. Res. **26**(4), 372–377 (2001)
6. Guha, A., Chattopadhyay, R., Jayadeva.: Predicting yarn tenacity: a comparison of mechanistic, statistical and neural network models. J. Text. Inst. 92(2), 139–145 (2001)
7. Rajamanickam, R., Hansen, S.M., Jayaraman, S.: Analysis of the modelling methodologies for predicting the strength of air-jet spun yarns. Text. Res. J. **67**(1), 39–44 (1997)
8. Majumdar, A., Ghosh, A.: Yarn strength modelling using fuzzy expert system. J. Eng. Fibers Fabr. **3**, 61–68 (2008)
9. Das, S., Ghosh, A., Majumdar, A., Banerjee, D.: Yarn engineering using hybrid artificial neural network-genetic algorithm model. Fibers Polym. **14**, 1220–1226 (2013)
10. Frydrych, I.: A new approach for predicting strength properties of yarn. Text. Res. J. **62**(6), 340–348 (1992)
11. Zurek, W.: The Structure of Yarn. Foreign Scientific Publications Department of the National Center for Scientific, Technical and Economic Information, Warsaw (1975)
12. Zurek, W., Frydrych, I., Zakrzewski, S.: A method of predicting the strength and breaking strain of cotton yarn. Text. Res. J. **57**, 439–444 (1987)
13. Barella, A.: Law of critical yarn diameter and twist influence on yam characteristics. Text. Res. J. **20**, 249–253 (1950)
14. Zurek, W., Gluza, J., Miskiewicz, J.: The yarn contraction coefficient. Prz. Wlok **23**, 523–525 (1969)
15. Martindale, J.G.: A new method of measuring the irregularity of yarns with some observations on the origin of irregularities in worsted slivers and yarns. J. Text. Inst. **36**, T35–T47 (1945)
16. Metropolis, N., Rosenbluth, A., Rosenbluth, M., Teller, A., Teller, E.: Equation of state calculations by fast computing machines. J. Chem. Phys. **21**, 1087–1092 (1953)
17. Kirkpatrick, S., Gelatt, C.D., Vecchi, M.P.: Science **220**, 671–680 (1983)

Contrast Restoration of Fog-Degraded Image Sequences

Tannistha Pal, Mrinal Kanti Bhowmik and Anjan Kumar Ghosh

Abstract Poor visibility in the presence of fog is a major problem for many applications of computer vision. Still image and video systems are typically of limited use in poor visibility condition as the degraded images/frames lack visual vividness and offer low visibility of the scene contents. This paper investigates the defogging effects on images and frames by using a fast defogging method on our own newly developed database, namely Society of Applied Microwave Electronics Engineering and Research-Tripura University (SAMEER-TU) database which consists of 5,390 color images and 10 videos captured in foggy as well as in clear condition. The first step of the method ensures contrast enhancement yielding better global visibility, but the images/frames containing very dense fog still suffer from low visibility. In that case, Luminance and chromatic weight map have been used. Finally for verifying the robustness of the method, qualitative assessment evaluation in respect of peak-signal-to-noise ratio (PSNR) and root-mean-square error (RMSE) is introduced as a contributory step in this paper.

Keywords SAMEER-TU database · Defogging of images and frames · Contrast enhancement · Luminance weight map · Chromatic weight map · Qualitative assessment evaluation

T. Pal (✉)
Department of Computer Science and Engineering, National Institute of Technology, Agartala, Barjala, Jirania 799055, India
e-mail: tannisthapaul@gmail.com

M.K. Bhowmik · A.K. Ghosh
Department of Computer Science and Engineering, Tripura University (A Central University), Suryamaninagar, Agartala 799130, India
e-mail: mkb_cse@yahoo.co.in

A.K. Ghosh
e-mail: anjn@ieee.org

K.N. Das et al. (eds.), *Proceedings of Fourth International Conference on Soft Computing for Problem Solving*, Advances in Intelligent Systems and Computing 335,
DOI 10.1007/978-81-322-2217-0_28

1 Introduction

Poor visibility in bad weather condition is the main challenge of computer vision applications, mainly caused by atmospheric aerosols, such as fog, haze, and rain. Most computer vision applications such as video surveillance, remote sensing, and intelligent vehicles assume that the input images/frames should have clear visibility. However, due to bad weather condition, images and video lose the contrast and color fidelity, and those reduce the effectiveness of human visual system. Generally, the effect of computer vision applications is limited by heavy fog that degrades the contrast information of the scene and significantly reduces the visibility of the image/frame [1, 2], and therefore, improving visibility is an inevitable task. However, standard filtering does not restore these low contrast images/frames [3].

Many research works have been done using contrast enhancement techniques to restore contrast of weather-degraded images/frames [1, 3, 4], which do not need any scene depth information and avoid complicated atmospheric scattering model. He et al. [5] proposed a simple but effective image dark channel prior to remove haze from a single image. Tarel and Hautiere [6] developed a contrast enhancement assessment method which is based on computing the ratio between the gradients of the visible edges in the image before and after visibility enhancement. Tan [7] presented an algorithm for restoring contrast from a single input image by maximizing the contrast of the direct transmission while assuming a smooth layer of air light. Zhu et al. [1] proposed an image clearness technique for fog by using a moving mask-based sub-block overlapped histogram equalization method. In a very recent work, Ancuti and Ancuti [8] proposed an effective method to remove the effects of fog from a single image using a fusion-based strategy based on a single degraded image. This method performs in a per-pixel fashion, which is straightforward to implement.

This paper presents a newly created database, namely Society of Applied Microwave Electronics Engineering and Research-Tripura University (SAMEER–TU) database in an outdoor environment containing natural scene images and videos captured by both NIKON D5100 Visual Camera and FLIR E60 Thermal Camera. Total of 5,640 visual images have been captured by Nikon D5100 in foggy, poor illumination, and normal conditions, and 120 images of visual and its corresponding thermal images have been captured by FLIR E60 in the same conditions. Based on the visibility parameter and other ground truth information obtained per hour from the meteorological department [9, 10], the weather condition is categorized as foggy, poor illumination and normal conditions. Total of 5 thermal videos are taken where the duration of the video is 90 min, and 10 visual videos are taken whose duration is 179 min 50 s. This paper also describes a method for enhancing the visibility of visual degraded images and videos in dense foggy condition by using contrast enhancement operation, luminance weight map, and chromatic weight map followed by multiscale fusion. In order to verify the robustness of the method, qualitative assessment evaluation is introduced as a contributory step of this paper. In this paper, only foggy

images and the same images captured in normal condition have been taken from SAMEER-TU database for implementation purpose and for qualitative assessment evaluation.

The rest of this paper is organized as follows. Section 2 presents the creation of our own developed SAMEER-TU database, Sect. 3 describes a method for enhancing the visibility of fog-degraded images/videos, Sect. 4 deals with Experimental Results and Discussion along with Qualitative Assessment Evaluation, and Sect. 5 concludes this work.

2 Creation of SAMEER-TU Database

2.1 Design and Development of SAMEER-TU Database

This paper briefs the creation of a database consisting of natural scenes in outdoor uncontrolled condition, which is being created in the Biometrics Laboratory of Department of Computer Science and Engineering of Tripura University (TU), India. In this database, total 5,640 visual images and 10 videos are captured by visual camera NIKON D5100. Out of 5,640 images, 1,020 images are captured in foggy condition, 250 images in poor illumination condition, and 4,370 images in normal condition. Sometimes images captured in dense fog in poor illumination condition by visual camera lose the total contrast and color fidelity, and it is very difficult to improve the visibility of the image. So a database is also being created consisting of visual and its corresponding thermal images, captured by thermal camera, i.e., FLIR E60 to fuse both thermal and its corresponding visual images/frames to enhance the visibility of the fog-degraded images. Some sample images of natural scenes captured by NIKON D5100 visual camera and FLIR E60 thermal camera are shown in Figs. 1 and 2, respectively.

This paper mainly focuses on contrast enhancement method for improving the visibility of visual fog-degraded images and frames. So only foggy images and the same images captured in normal condition have been used from SAMEER-TU database to test the algorithm and for qualitative assessment purpose, respectively.

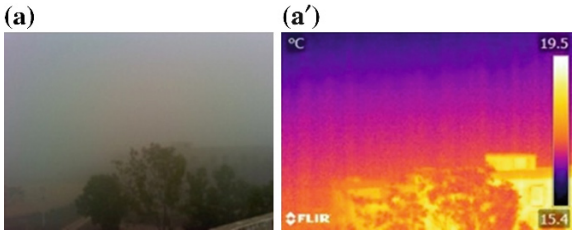

Fig. 1 **a** Foggy visual image. **a′** Corresponding thermal image

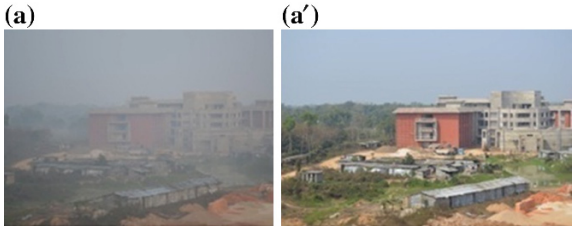

Fig. 2 **a** Foggy visual image. **a′** Corresponding clear/normal visual image

2.2 Designing of Natural Scene Database in Foggy Weather Condition

The SAMEER-TU database consists of 5,390 natural scene visual images captured in foggy and normal/clear conditions which can be useful for the researchers for the development and testing of new algorithms and also for comparative evaluations of different systems.

Equipment Setup for Image Capturing Nikon D5100 cameras with Nikon 18–55-mm lens, shutter speed 1/125–1/200, apertures f/5.6–f/8 are used for capturing the images. All natural scene images and videos are captured in an outdoor environment in foggy and normal conditions from the month of January to March of the year 2014.

Image Capturing Conditions Images in an outdoor environment are mainly influenced by weather effects such as fog, haze, and rain which results in poor visibility of the image. In this database, images have been captured in foggy and normal conditions. Foggy condition usually occurs when the difference between normal temperature and dew point is less than 2.5 °C, relative humidity remains nearly 100 % and visibility remains less than 1 km [11, 12]. Clear condition is generally considered when the visibility remains 3 km [13]. While capturing those images, the temperature normally ranges from 5 to 20 °C, humidity ranges from 95 to 100 %, dew point ranges from 5 to 15 °C, wind speed ranges from 1 to 3.5 mph, and visibility ranges from 0 to 3 km [9, 10]. Each image is attached with useful ground truth information such as visibility, temperature, humidity, wind speed, and dew point temperature.

Naming Convention The SAMEER-TU database contains high-quality color visual images (3,696 × 2,448 pixels, 24 bits per pixel) of outdoor natural scenes captured after every 15 min from 6 a.m. to 6 p.m. After capturing, all the images have been renamed for ease of understanding. To make the naming convention meaningful, different codes have been used for different natural scenes in different days. The naming code of the image is as follows: Day Number_Natural Scene Number_Outdoor Condition, for example, image name D1_NS1_OD[6.00a.m]_I(1).jpg indicates that the image is taken in Day 1 (6.02.14) of Natural Scene 1 which have been captured in an outdoor environment at 6.00 a.m. with image sequence no. 1.

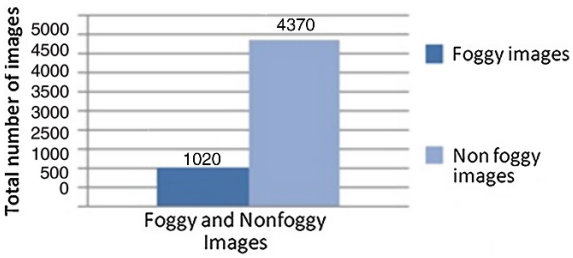

Fig. 3 Distribution of foggy and nonfoggy images

Statistical Analysis of Natural Scenes in Foggy and Nonfoggy Conditions Based on visibility parameter obtained per hour from meteorological department [9, 10], images have been classified as foggy and nonfoggy images. Foggy images or videos are considered when the visibility remains less than 1 km [11, 12], while the clear image is normally considered when visibility remains 3 km [13]. These foggy and nonfoggy images or videos are useful to verify the robustness of the algorithm used in this paper. The distribution of foggy and nonfoggy images is shown in Fig. 3.

3 Enhancement of the Fog-Degraded Image Sequences in Poor Visibility Condition

This paper implements a technique for enhancing the fog-degraded visual image and frames of video [8] along with qualitative assessment evaluation. Figure 4 presents the system flow of the technique.

3.1 Step 1: Derived Input to Improve the Contrast in Fog-Degraded Image/Frame

Color cast due to the air light influence and lack of visibility into distant regions due to scattering and attenuation phenomena are the main obstacles for degradation of the image/frame. The derived input from the foggy frame deals with the contrast enhancement that yields a better visibility mainly in the degraded region [8].

The derived input is obtained from the below equation

$$I_2(x) = \gamma(I(x) - \overline{I}) \tag{1}$$

where
$I_2(x)$ is the derived input image/frame
$I(x)$ is the foggy image/frame

$\bar{I}$ is the average luminance value of the foggy image/frame that is found out by averaging the RGB color channels

γ is a factor whose default value is 2.5, and x is the pixel value of the image/frame.

Experimental result of Step 1 is shown in Fig. 6.

Experiments conducted in each step have been performed in MATLAB using graphical user interface (GUI). The experimental result of Step 1 is shown in Fig. 5.

The contrast enhancement operation mentioned in Step 1 increases the contrast of the foggy image/frame. But its limitation lies when images/frames contain dense

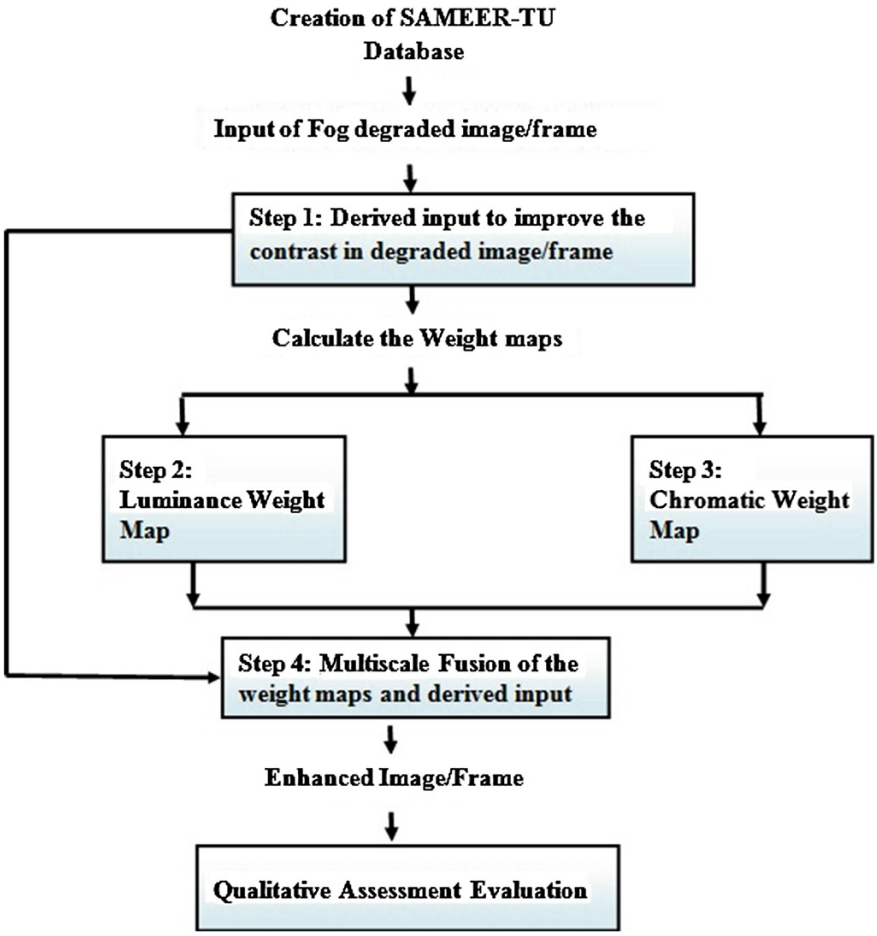

Fig. 4 System flow of the technique

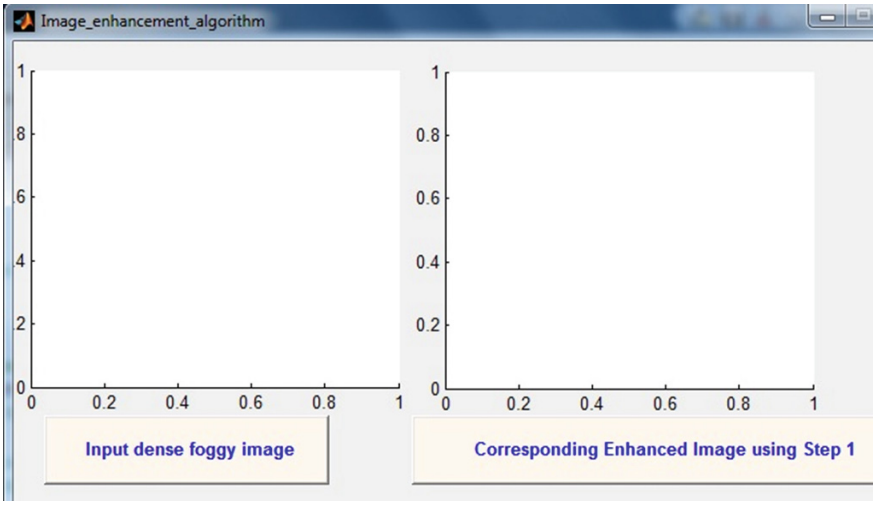

Fig. 5 Load input dense foggy image/frame and its corresponding enhanced image/frame using graphical user interface

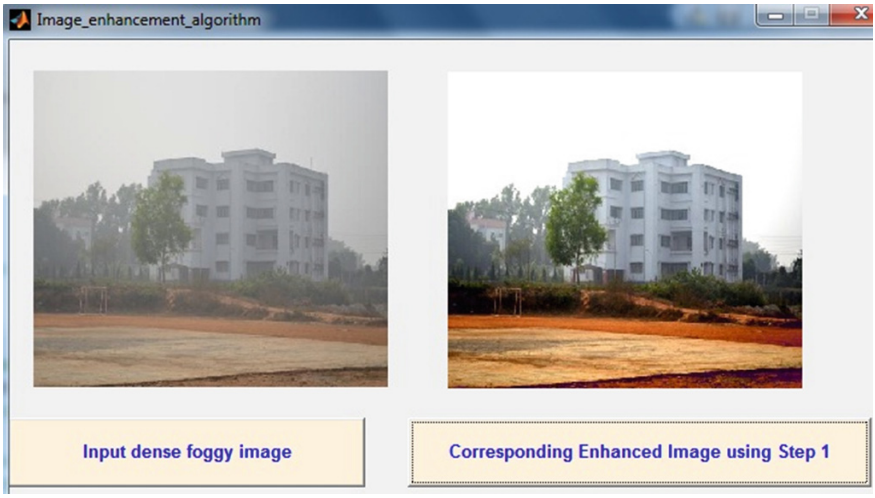

Fig. 6 Corresponding enhanced image/frame of the real-time dense foggy image/frame by using Step 1

fog and suffer from low visibility. For this, luminance weight map and chromatic weight map have been used. Luminance weight map measures the luminance gain of the derived input image/frame and adds brightness to the image/frame while chromatic weight map measures the saturation gain and adds colorfulness to the image/frame.

3.2 Step 2: Luminance Weight Map

The luminance weight map measures the luminance gain of the derived input image/frame. This weight is processed based on the RGB color channel information [8]. The luminance weight map is obtained from the below equation

$$W_L^K = \sqrt{\frac{1}{3}\left[(R^k - L^k)^2 + (G^k - L^k)^2 + (B^k - L^k)^2\right]} \tag{2}$$

where L represents luminance computed by averaging the RGB channels and k indexes the derived input.

Experimental result of Step 2 is shown in Fig. 7.

3.3 Step 3: Chromatic Weight Map

The chromatic weight map controls the saturation gain in the derived input image/frame. This weight map is used because in general images characterized by a high level of saturation are preferable [8]. The chromatic weight map is obtained from the below equation

$$W_c^k(x) = \exp\left(-\frac{(S^k(x) - S_{\max}^k)^2}{2\sigma^2}\right) \tag{3}$$

$S_k(x)$ is the saturation value given by the equation

$$S_k(x) = 1 - \frac{3}{(R+G+B)}[\min(R,G,B)] \tag{4}$$

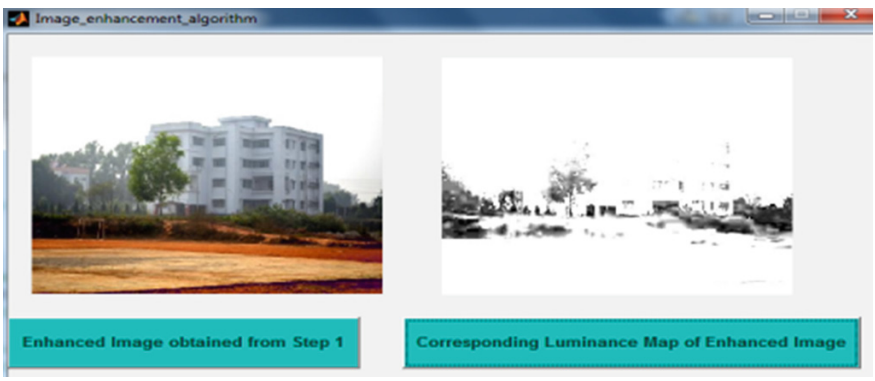

Fig. 7 Corresponding luminance map of enhanced image/frame by using Step 2

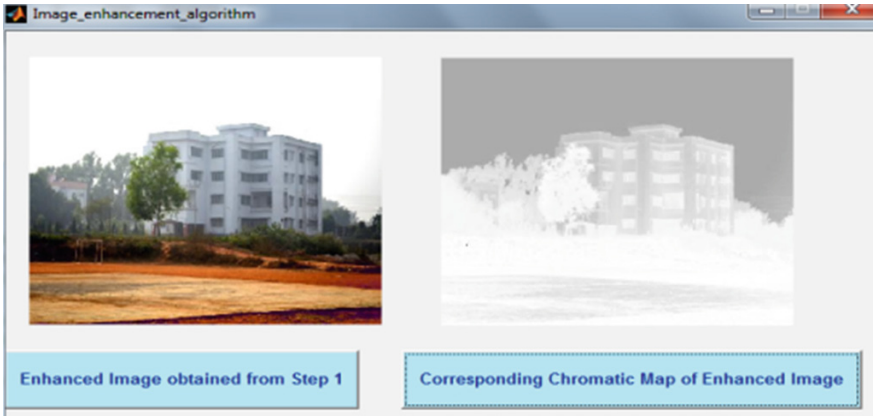

Fig. 8 Corresponding chromatic map of enhanced image/frame by using Step 3

where k indexes the derived input.

$S_{\max}$ is a constant and it depends by the color space employed (for HSI color space $S_{\max} = 1$) and the default value of standard deviation is $\sigma = 0.3$.

Result of Step 3 is shown in Fig. 8.

3.4 Step 4: Multiscale Fusion

In the fusion process, specific weight maps are used in order to conserve the most significant detected features. The resultant weight W_k is obtained by multiplying the luminance weight map and chromatic weight map. To yield a consistent result, normalization of the resultant weight map is done. Each pixel x of the output image F is calculated by summing the inputs I_k weighted by corresponding normalized weight maps $\overline{W}^k$ [8]. The multiscale fusion is obtained from the below equation

$$F(x) = \sum_k \overline{W}^k(x) I_k(x) \tag{5}$$

where I_k symbolizes the input (k is the index of the input) that is weighted by the normalized weight maps. Result of Step 4 is shown in Fig. 9.

4 Results and Discussion

Experiments have been conducted on 120 outdoor real natural scene images taken in dense foggy condition. Due to the scattering of aerosol particles in foggy condition, the scene loses the contrast and color fidelity and thereby reducing the

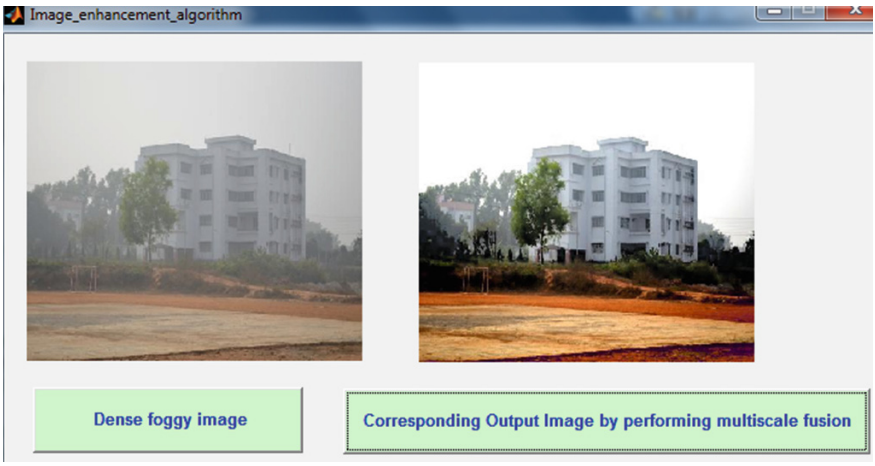

Fig. 9 Fog-free output image/frame by performing multiscale fusion

visibility [14]. Therefore, image enhancement algorithm described previously on Sect. 3 is applied on the dense foggy static images from SAMEER-TU database to restore the contrast. It is observed that by using the first step of contrast enhancement operation of the proposed method, the contrast gets increased in the foggy images and thereby increasing the visibility of the images. But the images containing dense fog still suffer from low visibility. To overcome this limitation, luminance weight map and chromatic weight map are used in a per-pixel fashion to enhance the visibility of the dense foggy images. Luminance weight map measures the luminance gain of the input image and adds brightness to the image while chromatic weight map measures the saturation gain and adds colorfulness to the image. Finally, a multiscale fusion is carried out with contrast enhancement operation and weight maps to enhance the visibility of the image in dense fog. Experimental result reveals that the proposed technique works well on dense foggy static images which have been shown in Fig. 9.

The same technique is also been implemented on the frames of 5 foggy videos from SAMEER-TU database. Experimental result reveals that the technique mentioned in Sect. 3 achieves good defogging effect on large number of dense foggy videos by increasing the visibility. Results of experiments on fog-degraded frames and videos are shown in Table 1 and Fig. 10, respectively.

The next phase of the experiment illustrates a qualitative assessment evaluation on the dense foggy images or frames to test the robustness of our method. The qualitative assessment evaluation is performed based on peak-signal-to-noise ratio (PSNR) and root-mean-square error (RMSE).

Table 1 Experimental result on fog-degraded frames

Total 3 no of sample frames are shown (Each frames are selected from each 10 frames)	**Camera**: Nikon D5100		**Date of Creation**: 2/18/2014
	Time from: 06.43 AM		**Video Content**: Natural Scene
	Dimension: 1920 X 1080		**Duration of Video**: 30 sec
	Frame rate: 10frame/sec		**Total no of Frames**: 300
	10 sec	15 sec	30 sec
Fog degraded frames			
Enhanced frames using proposed method			

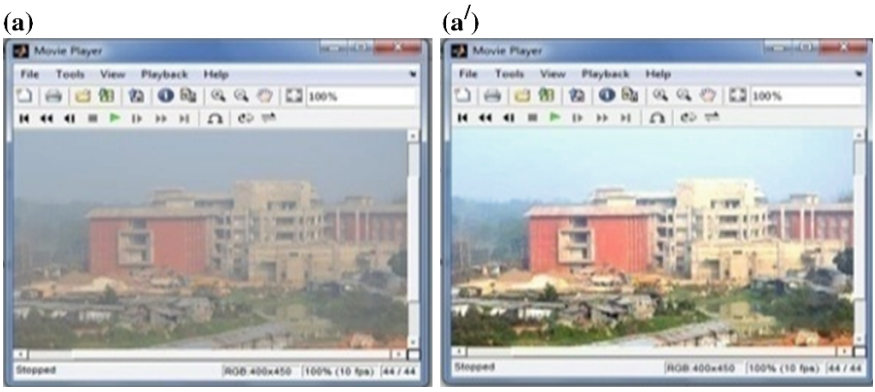

Fig. 10 **a** Represents real-time dense foggy video. **a′** Represents corresponding enhanced video by using our method

4.1 Qualitative Assessment Evaluation

One of the common, reliable methods to measure the accuracy in the image processing field is the PSNR and RMSE [15]. These methods are commonly used as a measure for quality reconstruction of an image/frame.

Peak Signal To Noise Ratio (PSNR) The most popular distortion measure between the original image and the restored image is the PSNR. The PSNR is used for quality reconstruction of an image/frame. High value of PSNR indicates the

high quality of the image/frame. PSNR is used to identify whether a particular algorithm produces better results [15].

PSNR is computed using the following equation:

$$\mathrm{PSNR} = \mathrm{MN}\max_{m,n} I_{m,n}^2 / \sum_{m,n} (I_{m.n} - \overline{I_{m,n}})^2 \tag{6}$$

$I_{m,\ n}$ represents a pixel whose coordinates are $(m,\ n)$ in the original image/frame
$\overline{I_{m,n}}$ represents a pixel whose coordinates are $(m,\ n)$ in the restored image/frame
MN is the total number of rows and columns, i.e., the total number of pixels in an image/frame.

Here, max is maximum pixel value of image/frame when pixel is represented by using eight bits per sample. This is 255 bar color image with three RGB values per pixel.

Root Mean Square Error (RMSE) The RMSE is used as a measure for quality reconstruction of an image/frame. Low value of RMSE indicates the high quality of the image/frame. RMSE is used to identify whether a particular algorithm produces better results [15].

RMSE is computed using the following equation:

$$\mathrm{RMSE} = \sqrt{\frac{1}{\mathrm{MN}} \sum_{(m.n)} (I_{m,n} - \overline{I_{m,n}})^2} \tag{7}$$

$I_{\ m,\ n}$ represents a pixel whose coordinates are $(m,\ n)$ in the original image/frame
$\overline{I_{m,n}}$ represents a pixel whose coordinates are $(m,\ n)$ in the restored image/frame
MN is the total number of rows and columns, i.e., the total number of pixels in an image/frame

Table 2 describes the qualitative assessment of frames of some videos from SAMEER-TU database in respect of PSNR and RMSE values. In Table 2, PSNR1 and RMSE1 represent PSNR and RMSE values of the image/frame captured in a clear day with the frame captured in the foggy day, while PSNR2 and RMSE2 represent PSNR and RMSE values of the frame captured in a clear day with the enhanced frame using our technique. The higher PSNR value means the frame has a better quality, while low value of RMSE indicates high quality of the frame [16, 17].

Table 2a, b, and c represents images/frames captured in a clear day; a′, b′, and c′ represent corresponding images/frames captured in dense foggy day; a″, b″, and c″ represent restoration of the dense foggy images/frames to its enhanced form using our technique.

Table 2 Qualitative assessment evaluation of some images/frames

Image/Frame captured in a Clear Day	Image/Frame captured in a Dense Foggy Day	Restoration of the Foggy Image/Frame to its clear form using a Technique	PSNR1 & RMSE1	PSNR2 & RMSE2
 a	 a′	 a′	PSNR=16.0722 RMSE=40.2376	PSNR=19.2941 RMSE=37.2222
 b	 b′	 b′	PSNR=14.1510 RMSE=50.1982	PSNR=17.4288 RMSE=48.6183
 c	 c′	 c″	PSNR=14.7710 RMSE=46.7403	PSNR=18.1903 RMSE=42.0452

From Table 2, it is observed that PSNR2 value is higher than PSNR1, while the value of RMSE2 is lower than RMSE1 which reflect that the video quality of the enhanced frames using our method is better than the real-time dense foggy frames, i.e., restoration of the real-time dense foggy frames to its clear form is accomplished as far as possible.

5 Conclusion

This paper briefs the creation of SAMEER-TU database of 5,390 natural scene images and 10 videos in outdoor uncontrolled environment in foggy and normal conditions. The paper also describes a technique for enhancing the visibility of visual degraded images or videos in the presence of dense fog. Experimental results reveal that the implemented method performs well for dense fog-degraded visual images or frames, but the limitation of the algorithm is observed when images or frames are captured in a dense fog with very low illumination condition. In the future work, the research team will focus on implementing a fusion method to fuse visual degraded foggy image/frames and its corresponding thermal image/frames to acquire better visibility of the highly dense foggy image/frames in a very low illumination condition.

Acknowledgments The first author is thankful to the Society of Applied Microwave Electronics Engineering and Research (SAMEER), R&D Lab of Department of Electronics and Information Technology (DeitY), Government of India. The database presented here is being created in the Biometrics Laboratory of Department of Computer Science and Engineering of Tripura University (A Central University), India, under the project entitled "Development of Thermography Infrastructure facility for Security and Navigation System-Phase-1" supported by the Grant No. SMR/PD(R)/NER/2012–13/Thermography, dated 22/03/2013 from the Society of Applied Microwave Electronics Engineering and Research (SAMEER), IIT Bombay campus, Powai, Mumbai 400076.

References

1. Zhu, P., Zhu, H., Qian, X., Li, H.: An image clearness method for fog. Int. J. Image Graph. **9** (3), 124–127 (2004)
2. Ramya, C., Rani, S.: A novel method for the contrast enhancement of fog degraded video sequences. Int. J. Comput. Appl. **54**(13), 1–5 (2012)
3. Yingxin, L.: Poor contrast foggy image enhancement algorithm research. Tianjin University (2003)
4. Li, P.: Method of removing fog effect from images. Nanjing University of Technology (2005)
5. He, K., Sun, J., Tang, X.: Single image haze removal using dark channel prior. In: Proceedings of IEEE conference on computer vision and pattern recognition, pp. 1956–1963, June 2009
6. Tarel J.-P., Hautiere, N. Fast visibility restoration from a single color or gray level image. In: Proceedings of IEEE international conference on computer vision, pp. 2201–2208, Sept–Oct 2009
7. Tan, R.T.: Visibility in bad weather from a single image. In: Proceedings of IEEE Conference on Computer Vision and Pattern Recognition, pp. 1–8, June 2008
8. Ancuti, C.O., Ancuti, C.: Single image dehazing by multi-scale fusion. IEEE Trans. Image Process. **22**(8), 3271–3282 (2013)
9. www.imdaws.com
10. www.weatherspark.com
11. http://geoworld.wikia.com/wiki/FOG,HAIL,MIST_AND_DEW
12. http://www.metoffice.gov.uk/learning/fog
13. http://www.livescience.com/33895-human-eye.html
14. Narasimhan, S., Nayar, S.: Vision in bad weather. In: Proceedings of IEEE Conference on Computer Vision, pp. 820–827, Sept 1999
15. Kutter, M., Petitcolas, F.A.P.: A fair benchmark for image watermarking systems. In: Wong and Delp [106], pp. 226–239. ISBN 0-8194-3128-1
16. Xu, Z., Liu, X.: Bilinear interpolation dynamic histogram equalization for fog-degraded image enhancement. Int. J. Inf. Comput. Sci. **7**(8), 1727–1732 (2010)
17. Kaushik, P., Sharma Y.: Comparison of different image enhancement techniques based upon Psnr and Mse. Int. J. Appl. Eng. Res. **7**(11), 2012 (2012)
18. Narasimhan, S., Nayar, S.: Contrast restoration of weather degraded Images. IEEE Trans. Pattern Anal. Mach. Intell. **25**(6), 713–724 (2003)

Optimization of Primary Loop Pump Power of a Loop-type Liquid Metal Fast Breeder Reactor with Annular Fuel Using Genetic Algorithm

Shubhajit Karmakar, Swarnendu Sen and Sanjib Kumar Acharyya

Abstract The present study focuses on the optimum design based on primary loop of a liquid metal fast breeder reactor (LMFBR). Inside the core annular fuel, rods are used for better heat transfer to the liquid sodium coolant. Value of the outlet temperature of the coolant from the core, surface temperature of the fuel pin, and pumping power at different volume flow rates are studied, and genetic algorithm (GA) is used to minimize pumping power required to maintain flow in the primary loop for an optimal design parameters.

Keywords Genetic algorithm · LMFBR · Head loss · Annular fuel · Pump power

1 Introduction

The practice of nuclear engineering focuses on the design and operation principles of commercial nuclear plant. For an effective design of any engineering system, techniques of optimization are applied to find the best operating condition. Liquid metal fast breeder reactor (LMFBR) is a type of reactor in which neutrons are given off by fission reactions can breed more fuel from otherwise non-fissionable isotopes. The cooling and the heat transfer are done by liquid sodium. Because of its property of low melting point (371 K), high boiling point (1,165 K), and high heat capacity, it can cope up with the high volumetric power density encountered in LMFBR [1]. Annular fuel pellet are used for better heat transfer to the coolant

S. Karmakar
School of Nuclear Studies and Application, Jadavpur University, Kolkata 700032, India
e-mail: kshubha.ee@gmail.com

S. Sen (✉) · S.K. Acharyya
Department of Mechanical Engineering, Jadavpur University, Kolkata 700032, India
e-mail: sen.swarnendu@gmail.com

S.K. Acharyya
e-mail: sanjibacharyya24@gmail.com

K.N. Das et al. (eds.), *Proceedings of Fourth International Conference on Soft Computing for Problem Solving*, Advances in Intelligent Systems and Computing 335,
DOI 10.1007/978-81-322-2217-0_29

because annular design increases coolant surface area and reduces conduction thickness. Pellets are stacked on top of one another to form fuel rods, which is surrounded by stainless steel clad. The melting point of clad material (1,700 K) is avoided to reach during operation of the reactor. There are three stages of heat transfer in LMFBR: inside the core the heat transfer is from fuel to primary liquid sodium coolant, primary liquid sodium coolant to secondary liquid sodium coolant in intermediate heat exchanger (IHX), and between this secondary coolant and evaporating water in steam generator [2]. This somewhat complex system ensures that the primary coolant stays in the primary vessel and that any radioactive substances in the primary vessel are not transferred to the steam generator, where the potential exists for chemical interaction between the sodium and the water due to minute leakages.

Over the years, a number of attempts have been made to develop more systemic procedure of optimization and design of LMFBR components to obtain optimal set of design parameters. Lv et al. [3] carried used colony complex algorithm and gradient crossover genetic algorithm for design of weight of reactor coolant pump and optimization of pump inner motor. Their result shows that the optimized weight is 12.482 % less than the prototype used by them. Kobayashi et al. [4] applied sequential unconstrained minimization technique for optimization of core design, and power balance method is applied for burn up calculations in LMFBR core. Sathiyasheela and Mohanakrishnan [5] analyze temperature drop across the fuel clad in annular fuel and found that the temperature drop is pronounced in transients of higher step and ramp reactivity insertions and lump model is justified. Heat transfer with lumped model annular pellet matches good with numerical schemes such as Crank–Nicolson method.

Our attention is only on the primary loop of a loop-type LMFBR, containing Core, IHX, and a pump. The behavior of coolant temperature, fuel surface temperature of the fuel pin, and the pumping power due to the variations of a design variable are studied, and genetic algorithm (GA) is used to find the minimum pumping power required to maintain flow in the primary loop under given range of design variables and output power. The GA is a search techniques based on the methods of natural selection and natural genetics-reproduction, crossover, and mutation. MATLAB software is used to develop GA for our analysis of LMFBR.

2 Formulations

2.1 Mathematical Formulation

Complexity in the real LMFBR makes unsuitable for direct use in optimization. In this section, simplified models for primary loop components relevant to minimization of pumping power are developed.

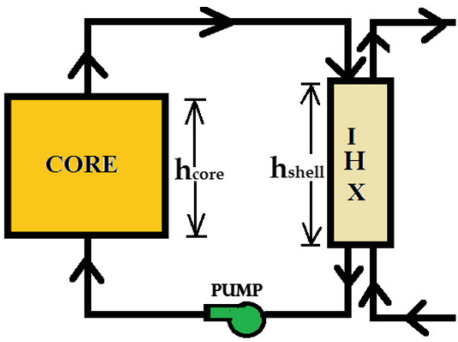

Fig. 1 Primary loop components of LMFBR

The following assumptions are made:

(a) The thickness of the cladding is neglected.
(b) Height of the core is same as that of the height of a fuel pin.
(c) Lumped temperature in radial direction of a fuel rod.
(d) Heat flow within the solid fuel is normal to the coolant stream, i.e., there is no heat conduction along the fuel rod parallel to the coolant channel.
(e) Core is cylindrical in shape and the fuel rods are uniformly arranged inside it.
(f) Minor head losses are neglected.

The primary loop components are shown in Fig. 1.

2.1.1 Temperature of the Coolant

As the coolant flows through the core of the reactor, consisting of uniform arrangement of fuel rods, the coolant carries away the heat generated from the fuel rods. Assuming no radial heat flux variation and sinusoidal heat generation along fuel axis, an energy balance in the coolant gives:

$$wC_p(T_{\text{outlet}} - T_{\text{inlet}}) = \int_{Z_{\text{inlet}}}^{Z_{\text{outlet}}} q'(z)\mathrm{d}z = \int_{Z_{\text{inlet}}}^{Z_{\text{outlet}}} q'_0 \sin\left(\frac{\pi z}{H_{\text{core}}}\right)\mathrm{d}z \qquad (1)$$

where $w, C_p, q'(z), q'_0, H_{\text{core}}, T_{\text{outlet}}$ and T_{inlet} are mass flow rate (m^3/s) associated with a single rod in a core, specific heat of the coolant (J/Kg-K), power rating at any position along the fuel axis (kW/m), linear heat generation rate at the centerline of the core, height of the core (kW/m), temperature of the coolant (K) at Z_{outlet}, i.e., outlet temperature of the coolant and temperature of the coolant (K) at Z_{inlet}, i.e., inlet temperature of the coolant, respectively.

After integration, assuming $Z_{\text{inlet}} = 0$, temperature at any position inside the core, along fuel axis can be found out as:

$$T(z) = T_{\text{inlet}} + \frac{q_0' H_{\text{core}}}{\pi w C_P}\left[1 - \cos\left(\frac{\pi z}{H_{\text{core}}}\right)\right] \tag{2}$$

Outlet temperature of the liquid sodium coolant coming out from the core is found out by substituting $z = H_{\text{core}}$ in Eq. 2 is given below:

$$T_{\text{outlet}} = T_{\text{inlet}} + 2\frac{q_0' H_{\text{core}}}{\pi w C_P} \tag{3}$$

During the operation of the reactor, the outlet temperature of the coolant should be restricted below a prescribed value to avoid any boiling of coolant inside the core.

2.1.2 Surface Temperature of the Fuel Pin

For calculation of an annular fuel surface temperature, considering the heat generation due to fission will be dissipated to the coolant flowing over inner and outer surface of the fuel, and there is no temperature variation of the fuel pin in radial direction under steady state, one can write

$$A_c q'(z)\mathrm{d}z = h_{\text{in}}[T_s(z) - T_{\text{in}}(z)]P_{\text{in}}\mathrm{d}z + h_{\text{out}}[T_s(z) - T_{\text{out}}(z)]P_{\text{out}}\mathrm{d}z \tag{4}$$

where A_c, h_{in}, h_{out}, P_{in}, P_{out}, $T_s(z)$, $T_{\text{in}}(z)$, and $T_{\text{out}}(z)$ are cross-sectional area of a fuel (m^3), heat transfer coefficient associated with an inner diameter of a fuel pin (W/m^2-K), heat transfer coefficient associated with hydraulic diameter of the core (W/m^2-K), inner perimeter of the fuel (m), outer perimeter of the fuel (m), surface temperature of the fuel rod along axis of the fuel (K), temperature of the coolant flowing inside a fuel rod (K), and temperature of the coolant flowing around the fuel rod (K), respectively.

Following assumption b and c, we can write $T_{\text{in}}(z) = T_{\text{out}}(z) = T(z)$ (say) and $H_{\text{core}} = L$, respectively, and substituting the sinusoidal variation of heat generation, the surface temperature of the fuel pin varies along the axial length of the fuel and is shown:

$$T_s(z) = \frac{q_0' \sin\left(\frac{\pi z}{H_{\text{core}}}\right)(d_{\text{out}}^2 - d_{\text{in}}^2)}{4(h_{\text{in}} d_{\text{in}} + h_{\text{out}} d_{\text{out}})} + \left\{T_{\text{inlet}} + \frac{q_0' L\left(1 - \cos\left(\frac{\pi z}{L}\right)\right)}{\pi\left(\frac{\rho Q}{N_{\text{rods}}}\right)c_p}\right\} \tag{5}$$

where L, N_{rods}, Q, d_{out}, d_{in} are length of a fuel rod (m), number of rod in core, volume flow rate (m^3/s), outer diameter of the fuel rod (m), and inner diameter of the fuel rod (m), respectively.

From Eq. 5, it is seen that the surface temperature of a fuel pin is a function of position along the axial direction of the fuel pin, i.e., z. Maximum surface temperature of the fuel pin occur at the midpoint of the fuel rod, i.e., $z = \frac{L}{2}$. During the

operation of the reactor, the maximum surface temperature should be maintained below a prescribed value so as to avoid melting of cladding material (stainless steel) and the interaction of radioactive fuel with liquid sodium coolant in the primary loop.

2.1.3 Head Loss in Core

Inside the core, there are (N_{rods} + 1) parallel paths formed by inner circular channel of N_{rods} number of annular fuel rods and a non-circular channel formed by the space left inside the core after insertion of N_{rods} annular fuel rods. A non-circular channel such as flow region between fuel rods or an annular space can be imagine as an circular channel with good approximation of diameter equivalent to an circular pipe diameter is known as hydraulic diameter D_e. It is defined as follows:

$$D_e = 4\frac{\text{Cross-section of the coolant}}{\text{Wetted perimeter of duct}} \tag{6}$$

$$D_e = \frac{D - N_{rods}\{d_{out}^2 - d_{in}^2\}}{D + N_{rods}\{d_{out} + d_{in}\}} \tag{7}$$

For parallel paths, discharge is shared by parallel paths and head loss is equal in any path. Equating the major head loss of coolant through the channel with diameter D_e equals to the major head loss of the coolant through the inner diameter d_{in} fuel rod and by using Darcy and Weisbach equation [6], the volume flow rate Q_{ext} of the coolant flowing through the circular pipe with the hydraulic diameter D_e can be shown as:

$$Q_{ext} = \frac{Q}{\left[1 + N_{rods}\sqrt{\frac{f}{f_c}\frac{d_{in}^5}{D_e^5}}\right]} \tag{8}$$

The major head loss inside the core is equal to the head loss in any of the parallel paths. So, equating the major head loss in core is equal to the head loss in the channel with hydraulic diameter D_e. Using Darcy and Weisbach equation [6], Eqs. 7 and 8, the core major head loss can be shown as given below:

$$h_{core} = \frac{\dfrac{fLQ^2}{\left\{1+N_{rods}\sqrt{\frac{f}{f_c}\frac{d_{in}^5}{D_e^5}}\right\}^2}}{3\left[\frac{D^2 - N_{rods}\left\{d_{out}^2 - d_{in}^2\right\}}{D + N_{rods}(d_{out}+d_{in})}\right]^5} \tag{9}$$

D and D_e represent the diameter (m) and hydraulic diameter (m) of the core, respectively. f represents Darcy coefficient of friction associated with annular fuel rod with inner diameter d_{in} and length L and f_c Darcy coefficient of friction

associated with hydraulic diameter D_e of the core and length equal to the length of a fuel rod or height of the core.

2.1.4 Head Loss in IHX

IHX is a vertical, counter flow (CF), shell and tube heat exchanger that transfers heat from active primary sodium to inactive secondary sodium. Primary sodium flows on the shell side. Head loss in shell side of IHX [7] is given as follows:

$$h_{\text{shell}} = \frac{2f_s G_s^2 D_s (N_B + 1)}{\rho^2 D_{\text{es}} \left(\frac{\mu}{\mu_w}\right)^{0.14}} \tag{10}$$

where f_s is the fanning friction factor for flow on the shell side, G_s is the mass velocity on the shell side. D_s the shell inner diameter, D_{es} is the equivalent diameter of the shell, N_B is the number of baffle, μ and μ_e are the viscosities of the liquid sodium at bulk temperature and wall temperature, respectively.

2.1.5 Pump Power

Pump power to maintain flow in primary loop of LMFBR is given as:

$$P_T = \rho g h_{\text{core}} + \rho g h_{\text{shell}} \tag{11}$$

where ρ and g are the density of liquid sodium and acceleration due to gravity respectively.

2.2 Optimization

From the above discussion, it is apparent that the power of the pump is critical to enhance the coolant performance and the efficiency of heat transport in the primary loop is governed by the pump power. Hence, it is advantageous at this stage to design the system to ensure the minimization of pump power. Hence, in this work, it is attempted to find out optimum values of outer diameter d_{out} and inner diameter d_{in} of the fuel and the volume flow_rate_Q.

$$\text{Design Variables } X = [d_{\text{out}}, d_{\text{in}}, Q] \tag{12}$$

$$\text{With an objective to minimize the pump power } f(\text{X}) = P_{\text{T}} \tag{13}$$

For satisfaction of the other requirements mentioned above, constraints in Eqs. (14–18) are considered as mentioned below and a constrained optimization algorithm is used including penalty parameters.

Subjected to constraints:

$$g1 = T_s - 1,700 < 0 \tag{14}$$

$$g2 = T_{\text{outlet}} - 900 < 0 \tag{15}$$

$$g3 = d_{\text{out}} - d_{\text{in}} > 0 \tag{16}$$

$$g4 = d_{\text{out}} - P < 0 \tag{17}$$

$$h1 = \left(\frac{\pi}{4} d_{\text{out}} - \frac{\pi}{4} d_{\text{in}}\right) - \text{(volume of a fuel rod)} \tag{18}$$

Four inequality constraints are imposed to the problem. The first constraint "$g1$" in Eq. 14 imposes restriction on the maximum surface temperature of the fuel rod which must be below 1,700 K to avoid melting of stainless steel clad. The second constraint "$g2$" in Eq. 15 takes care of the fact that the temperature of the coolant coming from the core should not be greater than 900 to avoid verge of boiling of coolant. The third constraint "$g3$" in Eq. 16 takes care of the fact that the outer diameter of the fuel rod should always be greater than inner diameter of the annular fuel rod. The fourth constraint "$g4$" in Eq. 17 imposes a restriction that the outer diameter of the fuel rod should be less than pitch of the fuel, so that there should be some minimum gap between the two adjacent fuel rods to maintain coolant flow around it and to transfer heat energy from fuel rod to the coolant. Only one equality constraint "$h1$" in Eq. 18 is imposed, which restrict the volume of a fuel rod. Since the volume of the fuel rod is constant, so that the total input power in the form of fuel rod is considered to be constant.

A nonlinear constrained problem is reduced to unconstrained by penalty method.

$$\text{Penalty function } P(X) = f(X) + \beta_1 (g1)^2 + \beta_2 (g2)^2 + \beta_3 (g3)^2 + \beta_4 (g4)^2 + (h1)^2 \tag{19}$$

$\beta_1, \beta_2, \beta_3$, and β_4 take a high value if constrains are not satisfied, otherwise zero.

For minimization problem, Fitness Value

$$F(X) = \frac{1}{1 + f(X)} \tag{20}$$

is maximized

Binary-coded GA is used for the optimization problem. GA has an advantage of easy implementation in computer, not problem specific and does not require any auxiliary information except the objective function values. It works with population

of points instead of a single point. It is a guided search with definite strategies. Although randomized, GA is not random search as they exploit prior information to direct the search into a region of better performance with in a search space [8]. GA captures multiple optimal solutions in a population, thereby reducing the effort of same algorithm many times.

Three genetic operations are performed for minimization of $f(X)$ which are as follows:

A. *Selection or Reproduction* It the first operator operated on random generated binary population matrix. It is an operator that makes more copies of better string in a new population in every new generation. Roulette-Wheel Selection methods with "Elitist Strategy" are used.
B. *Crossover* It is a second operation on the population that recombines new strings to get better string in next generation. Simple crossover with probability P_c is used. Between two consecutive strings known as parent strings, simple single-point crossover is performed in each binary-coded design variables separately and the resulting strings are known as child strings.
C. *Mutation* is the third operator. It is a bitwise operator, change a single bit in a string. Bit inversion mutation process is applied here. With mutation probability P_m, a string is selected among the population. At random position or positions of that string, the bit is altered.

Crossover operator is mainly responsible for the search of new strings, even though a mutation operator is used for this purpose sparingly. With the completion of the three genetic operators, a generation or iteration of GA is completed. In each generation, the best solution is identified and stored forcibly in next generation. This is repeated till convergence or stopping criterion of maximum number of generations or iterations is satisfied. Due to the probabilistic development of the solution, GA does not guarantee optimality even when it may be reached. However, they are likely to be close to the global optimum. This probabilistic nature of the solution is also the reason they are not contained by local optimal.

3 Result and Discussion

A run of GA with design variable range d_{out} = 0.01–0.025 m, d_{in} = 0.001–0.01 m, and Q = 10–20 m^3/s is shown in Fig. 2. Figure 2 shows that as the generation number increases, the fitness value converges so as to achieve the objective of minimum pumps power.

String length = 10; Population Size, Pop = 10; Crossover probability, P_c = 0.8; and Mutation probability, P_m = 0.05.

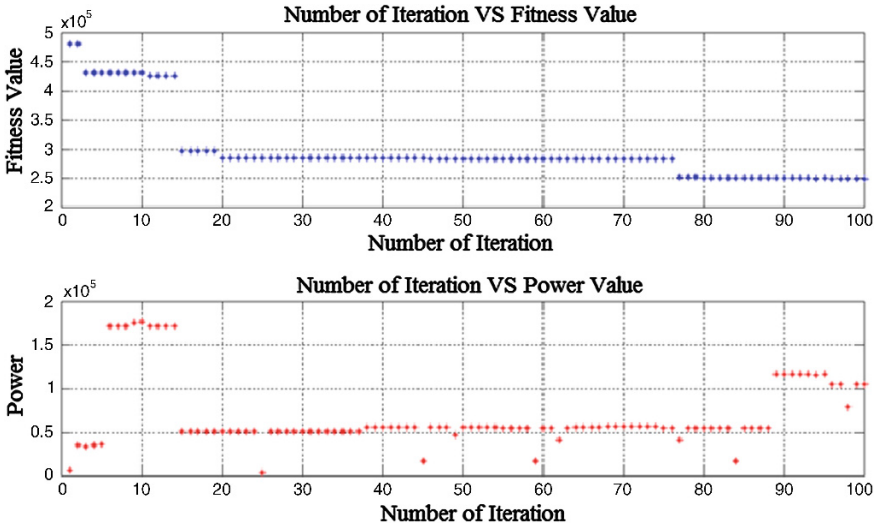

Fig. 2 Plot for converging of fitness value function and minimization of pump power during program running

3.1 Search for Feasible Range of Volume Flow Rate

For different values of volume flow rate range, optimum values of volume flow rate are taken within the given range and is plotted with different core parameters to find the permissible or feasible range of volume flow rate of the reactor under given fixed core and IHX parameters shown in Tables 1 and 2. The curves are shown in Figs. 3, 4, and 5.

Boiling point of sodium is 1,165 K. To avoid any verge of boiling, the outlet temperature of sodium is kept below 900 K. Inlet temperature of the sodium is 670 K. A temperature difference of 150–200 K is necessary between inlet and outlet of sodium inside the core for effective operation of the reactor. Figure 3 shows that the outlet temperature increases with decrease in volume flow rate and vice versa. So, flow rate is bounded by upper and lower limits. Fuel surface temperature increases as the volume flow rate decreases and vice versa as shown in Fig. 4. Fuel surface temperature depends on the volume flow rate. And the temperature of the fuel should not exceed the melting point of the clad (1,700 K). This imposes upper restriction to volume flow rate. Figure 4 shows that with in volume flow rate of 4–25 m^3/s, the constraints imposed in Eq. 14 is not violated and fuel surface temperature much below the clad melting point. The pumping power increases with volume flow rate as shown in Fig. 5. For the design problem, the volume flow rate is chosen to be restricted between 0.001 and 30 m^3/s. For a fixed volume flow rate, the pumping power increases as the ratio of inner to outer diameter of the fuel pin increases as shown in Fig. 6. This phenomenon is obvious because of increase in

Table 1 Core-fixed parameters

Linear power density	35 kW/m
Number of fuel rods	10,000
Diameter of the core	6 m
Height of the core	4 m
Length of a fuel rod	4 m
Pitch of the fuel rods	25 mm
Volume of a fuel rod	552,920.307 mm^3
Inlet temperature of the core	670 K

Table 2 IHX-fixed parameters

Type	Shell and tube
Shell internal diameter	3 m
Tube length	12 m
Tube outer diameter	21.7 mm
Baffle spacing	1.5 m
Number of baffles	8
Pitch (square array)	40 mm

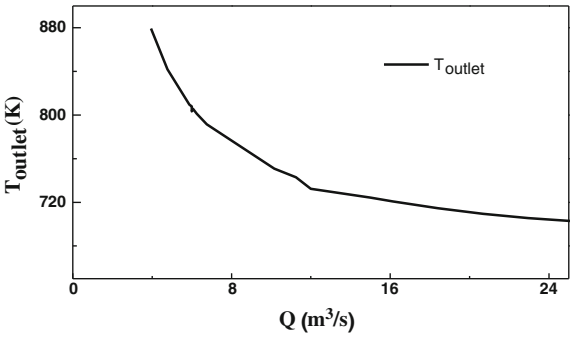

Fig. 3 Variation of fuel surface temperature with volume flow rate

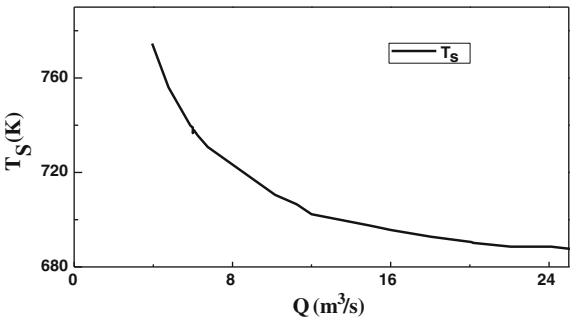

Fig. 4 Variation of coolant outlet temperature with volume flow rate

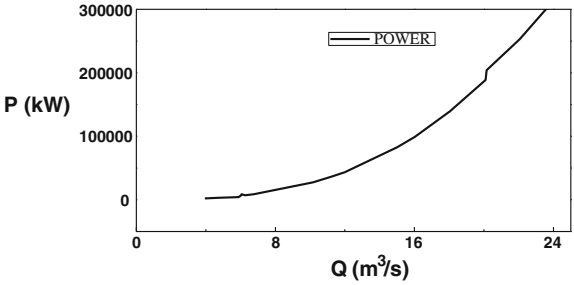

Fig. 5 Variation of pumping power with volume flow rate

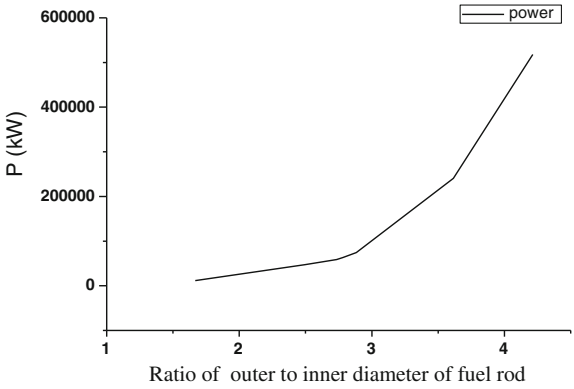

Fig. 6 Variation of pumping power with the ratio of outer to inner diameter of a fuel pin for an approximate $Q = 7.5$ m^3/s

ratio of inner to outer diameter reduces hydraulic diameter, and to maintain same flow rate, the pump has to pump with more power.

The program is repeatedly run with the ranges of design variable shown in Table 3 and with GA parameters: String length = 10; Population size, Pop = 10; Crossover probability, $P_c = 0.8$; and Mutation probability, $P_m = 0.05$ to find the minimum number of generation after which the objective function converges to give optimal solution. The observations are in Table 4.

Table 4 shows that after 4 different input generations or iteration number, the convergence of $f(X)$ is always before 300 generations. So, the maximum number of generation is chosen to be 300.

Table 3 Design parameters

Design parameters	Range of operation for optimization
d_{in}	1–10 mm
d_{out}	10–25 mm
Q	0.001–30 m^3/s

Table 4 Result for minimum number generation number

Input generation or iterations number	$f(x)$ Converges at generation number
200	140
300	255
400	292
500	80

3.2 Optimization Results

Optimization results correspond to GA parameters of string length 10; Population size, Pop = 10; Crossover probability, P_c = 0.8; and Mutation probability, P_m = 0.05, and design parameter range as on Table 3 is shown in Table 5. Stopping criterion = 300 generations.

3.3 Optimal Condition

From Table 5, it is observed that for the given condition of the reactor-fixed parameters and design parameter range, the minimum of pumping power is 1,519.51545 kW. The values of pumping power after each generations or iterations and convergence of fitness value function are shown in Fig. 7.

Table 5 Optimization data

d_{out} (mm)	d_{in} (mm)	d_{out}/d_{in}	Q (m^3/s)	T_{outlet} (K)	T_s (K)	Power (kW)
16.56	9.93	1.667673	7.5080811	779.363	724.695	11,533.3385
13.739	5.504398	2.496	7.5080811	779.363	724.70	47,189.7232
14.23753	5.20527	2.73521	7.5148289	779.26	724.65	58,621.20
14.20821	5.10850	2.781288	7.5080811	779.363	724.701	63,250.7954
14.2228	4.93255	2.883457	7.5374	778.937	724.48	74,342.074
13.739	3.80	3.615526	7.5080811	779.3627	724.70	240,513.707
13.66568	3.2434	4.213381	7.5080811	778.515	724.28	517879.699
16.02	8.917	1.796568	3.5492688	901.345	785.688	1,519.51545
15.3958	7.7478	1.987119	3.5492688	901.345	785.688	1,878.0269
15.3666	7.765395	1.978852	3.76241	888.239	779.136	2,212.2242
14.69208	6.32258	2.3237	3.75454	888.696	777.367	3,686.89936
14.3695	5.530791	2.598	3.527	902.74	786.39	4,896.9257
14.07624	4.72140	2.993	3.4906197	907.226	788.634	9,094.09911
13.72434	3.507331	3.913044	3.762414	888.23	779.143	44,909.764
14.208	5.258	2.702	15.015162	724.68	697.36	438,981.590

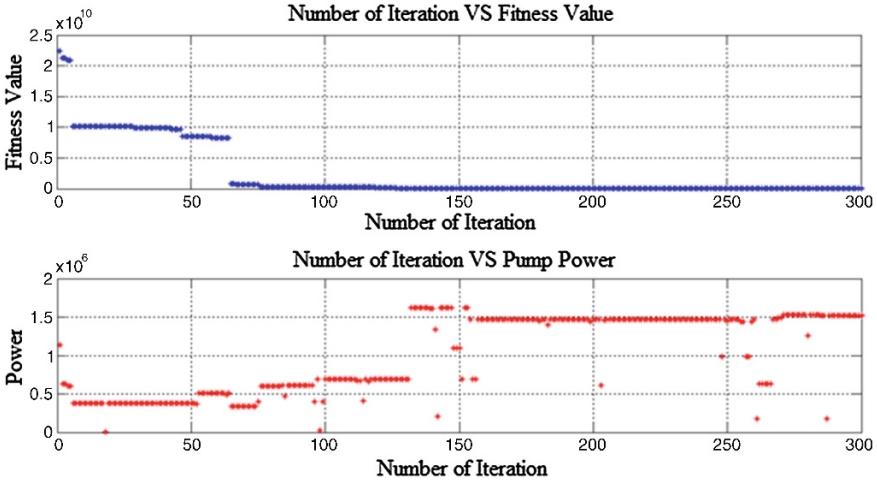

Fig. 7 Plot for converging of fitness value function and search for minimum pump power in every iteration during running of GA

$$\text{Minimum pump power } f(X) = P_{\mathrm{T}} = 1,519.51545 \text{ kW}$$

$$\text{Design variable } X = [d_{\text{out}},\, d_{\text{in}},\, Q] = \left[16.02 \text{ mm},\ 8.917 \text{ mm},\ 3.5492688 \text{ m}^3/\text{s}\right]$$

Corresponding to the minimum value of pump power, the surface temperature of the fuel and coolant outlet temperature are 785.688 and 901.345 K, respectively. Coolant outlet temperature of 901.345 K violates the constraints imposed in Eq. 15. This violation is very small of 1.345 K which may be allowable.

4 Conclusions

Three design parameters play an important role in power requirement to maintain flow in primary loop of LMFBR. The effect of each parameter on pumping power is as follows:

1. Pumping power increases with increase in flow.
2. With the increase in flow, both the surface temperature of the fuel rod and outlet temperature of the coolant decreases.
3. Pumping power increases with the increasing ratio of outer to inner diameter of the fuel rod.

In the next stage, the optimal values of the design parameters are obtained which satisfies the objective of minimization of pump power under given circumstances of specific power output. The optimal solution obtained by GA may not be a global optimum, because it is a non-exhaustive search without any specific direction for optimization. It may only be a local optimum.

References

1. Liquid metal coolants for fast reactor coolant by sodium, lead and lead bismuth eutectic, IAEA nuclear energy series no NP-T-16 (2012)
2. Collier, G.J., Hewitt, G.F.: Introduction to Nuclear Power. Hemisphere Publishing Corporation, New York (1987)
3. Lv, X., Yan, C., Li, J., Wang, J.: Optimization design of the weight of reactor coolant pump. In: IEEE Conference on Power and Energy Engineering, pp. 1–6 (2012)
4. Kobayashi, Y., Kondo, S., Togo, Y.: Application of sequential unconstrained minimization technique to LMFBR core design optimization problem. J Nucl. Sci. Technol. **11**(11), 471–479 (1974)
5. Sathiyasheela, T., Mohanakrishnan, P.: Annular fuel pin heat transfer and lumped model correction. Prog. Nucl. Energy **52**, 487–490 (2009)
6. Cengel, Y.A., Ghajar, A.J.: Heat and mass transfer, 2nd edn. McGraw-Hill, New York (2011)
7. Peters, M.S., Timmerhaus, K.D., West, R.E.: Plant design and economics for chemical engineers. McGraw-Hill, New York (2003)
8. Tabassum, M., Mathew, K.: A genetic algorithm analysis towards optimization solutions. Int. J. Digit. Inf. Wireless Commun. **4**(1), 124–142 (2014)

Recent Advances on Erythrocyte Image Segmentation for Biomedical Applications

Salam Shuleenda Devi, Ram Kumar and R.H. Laskar

Abstract Image segmentation is the process of partitioning an image into multiple segments and it is one of the most important steps for automatic cell analysis, because the result of final classification depends mainly on the correct image segmentation. In this paper, some general segmentation methods have reviewed which is mainly used in biomedical image processing especially in erythrocyte image. The main goal of biomedical image segmentation was to extract the foreground which contains the useful information from complicated background for the medical diagnosis.

Keywords Image processing · Image segmentation · Blood segmentation · Blood cells and erythrocytes (red blood cells)

1 Introduction

During the past few years, several researchers have focused on the development of automatic systems that can analyze and detect different types of diseases using medical images. Medical images have become one of the major tools and techniques used for several medical diagnosis and clinical trials. The main goals of medical image segmentation were to extract the useful information which can be used for biomedical diagnosis of various diseases from the complicated background. There are several medical imaging techniques such as microscopic imag-

S.S. Devi (✉) · R. Kumar · R.H. Laskar
ECE Department, National Institute of Technology,
Silchar, Silchar 788010, Assam, India
e-mail: shuleenda26@gmail.com

R. Kumar
e-mail: ramkumar.purnea@gmail.com

R.H. Laskar
e-mail: rhlaskar@ece.nits.ac.in

K.N. Das et al. (eds.), *Proceedings of Fourth International Conference on Soft Computing for Problem Solving*, Advances in Intelligent Systems and Computing 335,
DOI 10.1007/978-81-322-2217-0_30

ing, X-ray imaging, magnetic resonance imaging, and ultrasound imaging [1]. In this paper, different segmentation techniques used for erythrocyte (RBC) segmentation have review which is used for detection of various diseases such as malaria and leukemia. Erythrocytes segmentation is the analysis of microscopic erythrocytes (RBCs) images which is used to study the deformability of the cells due to several diseases.

2 Blood Cells Morphology

Blood is a bodily fluid normally found in mammals which is used to deliver nutrients and oxygen to the cells and transports metabolic waste products away from those same cells. A blood cell is a cell found in blood which is of different categories such as red blood cell (erythrocytes), white blood cell (leukocytes), platelets (thrombocytes), and plasma. Total 45 % of the blood tissue by volume consists of three kinds of blood cells, and remaining 55 % of the volume is plasma. Red blood cells carry oxygen and collect carbon dioxide through the use of hemoglobin and have a life span of 120 days. White blood cells help to defend the body against both infectious disease and foreign materials. There are different types of white blood cell exist such as granulocytes (composed by neutrophil, basophil, and eosinophil) and agranulocytes (lymphocyte and monocyte) (Fig. 1).

Blood cell analysis for diagnosis of several diseases is done using microscopic images. In microscopic blood images, number of red cells is much more than white blood cells. Differentiation of three types of blood cells can be done using features such as texture, color, size, and morphology of nucleus and cytoplasm [2]. When several infections such as malaria, leukemia, and hemolytic anemia occur, the characteristics of WBC and RBC change. In malaria, erythrocytes are infected by

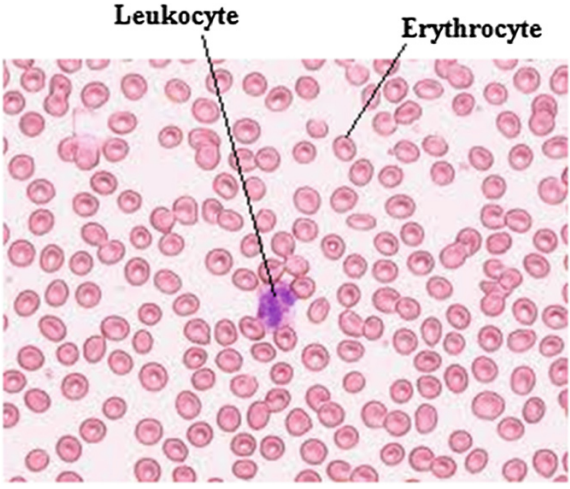

Fig. 1 Microscopic blood cells image

malaria parasite and due to this, the shape, size, and color of the erythrocytes changes. In hemolytic anemia, there will be deformation of erythrocytes characteristics such as shape, size, texture, and color. When leukemia occurs, there will be abnormal increase of immature white blood cells called blasts. Blood cells counting were performed manually by medical technologists by using the blood smear images of the patients which is obtained under microscope. A manual count may give correct information about cell counting which is used for the analysis of the diseases, but the accuracy of cell analysis depends on the practice of the expert and it is one of the time-consuming task. So automatic segmentation for the analysis of the diseases is strongly needed, and in recent few years, several automatic segmentation algorithms have been designed.

3 Image Segmentation

Image segmentation is elaborated as partitioning of an image into multiple segments for the analysis of the object. Several segmentation algorithms have been proposed in these recent years for the analysis of the images with better accuracy. Some of the practical applications of image segmentation are medical imaging (locate tumors and other pathologies, measure tissue volumes), finger print recognition, face recognition, etc. Based on different technologies, image segmentation approaches are divided into different categories such as edge detection, thresholding, region-based segmentation, segmentation based on partial differential equation, clustering. Biomedical image analysis is one of the applications of image segmentation. The main aim of medical image analysis is to diagnose the diseases [3]. There is several medical image segmentation techniques mainly used for blood cell analysis. Blood cell analysis is done using microscopic images. Segmentation can be categorized as supervised or unsupervised learning/classification [4, 5].

There are several segmentation techniques using threshold method such as mean method, P-tile method, histogram-dependent technique (HDT), edge maximization technique (EMT), and visual technique [6].

In this paper, the issue of automatic selection for multi-level thresholding is overcome and improves the efficiency of Otsu's method for image segmentation based on evolutionary approaches [7]. Several meta-heuristics are being applied for improving the accuracy and computational efficiency of minimum cross entropy thresholding (MCET) method. Mean structural similarity index measurement (SSIM) and universal image quality index (UIQI) are also being used for performance evaluation [8].

A new automatic seeded region growing algorithm called ASRG-IB1 using color image segmentation and multispectral images has been proposed. In this method, seeds are automatically generated using histogram analysis. In order to obtain intervals of representative pixel value, the histogram of each band is analyzed. An image pixel is considered a seed if its gray values for each band fall in some representative interval [9].

Chen et al. [10] applied 8-connection chain codes technique for an automatic segmentation and classification of abnormal erythrocytes in blood smears. The preprocessing phase includes three steps for image analysis and segmentation. First, Otsu's method is used for image binarization which is a high-speed and effective thresholding approach. It is mainly applied to separate the background from objects on a gray level histogram. Mathematical morphology is used to remove noises of small objects and smooth the edges of the object. Both overlapping and isolated erythrocytes are segmented with an automatic threshold. With the different magnification ratios of thin blood smears, the automatic threshold can be used to recognize erythrocytes as either overlapping or isolated. Here, mean and standard deviation of object areas are calculated and then set the threshold as mean plus standard deviation in that the standard deviation expresses the differences in the number of degree from the object areas. In this technique, three major issues have been overcome. First, overlapping erythrocytes in blood smears are split by using a procedure based on 8-connection chain codes. Second, normal and abnormal erythrocytes are recognized using directional information from chain codes. Finally, hemolytic anemia is classified into its four subtypes by incorporating three novel types of features including differential value of chain codes, irregularity of erythrocytes, and variation of eight directions.

Wang et al. [11] proposed a new method for cell detection that use both shape information and intensity of cell for obtaining better segmentation result. Segmentation and online learning algorithms in acquiring, tracking, and analyzing cell-cycle behaviors of a population of cell generated by time-lapse microscopy have been presented. Cell segmentation is the basis of cell phase identification and tracking, and by considering that cells may cluster or overlap with each other, the cell detection prior to segmentation is far trivial. The proposed method consists of 3-step detection algorithm. First, cell shape information is obtained with binarization process. Second, both intensity and shape information is used for local maxima generation. Finally, the pixels of nuclei are allowed to move inside the gradient vector field, and the pixels will ultimately converge at these local maxima, and the detected cells are then segmented via seeded watershed algorithm. The proposed algorithm has lesser over-segmentation.

How et al. [12] carry out comparisons between nine image segmentation techniques which are gray level thresholding, morphological operators, filtering operators, gradient-in method, edge detection operators, RGB color thresholding, color matching and hue, saturation, lightness (HSL), color thresholding technique, and pattern matching on erythrocytes microscopic image, and finally, it has been concluded that there is no single method that can give better result for erythrocytes segmentation.

Yu et al. [13] proposed a method for recognition and analysis of cell nuclear phases for high-content screening based on morphological features such as gray feature, shape recognition, geometrical features, and prior information of normal cellular cycle. Otsu's method is used to binarize the image. Image contours play an important role for the shape analysis and recognition of images for accurate description. Line segment, critical points, and their convexity and concavity are

features which are used to analyze the shape of the image contour. The proposed method gives not only the phases of cell nuclei but also the dynamic tracing results of cell nuclei can be found. The identification rate of cell phases is 94.68 % for all nuclei of the database.

Sharif et al. [14] discussed about an approach for red blood cell segmentation which is used to perform automated counting for erythrocytes (RBC). The proposed methods involve are YCbCr color conversion, masking, morphological operators, and watershed algorithm. The combination method of YCbCr color conversion and morphological operator produces segmented white blood cell (WBC) nucleus, and it is used to remove WBC from blood cell microscopic image. Morphological operators involve binary erosion diminish small object like platelet. After separation of background and foreground, only erythrocytes are left as foreground. The resulted erythrocytes are passed through marker controlled watershed algorithm in order to overcome occlusion of erythrocytes cell.

Vromen and McCane [15] present a model for automatic segmentation of scanning electron microscope image of red blood cells (erythrocytes) which is based on contour tracing approach. In this paper, second order polynomial model and a simple Bayesian approach to ensure smooth boundaries, and a post-processed ellipse fitting procedure to reduce noise contours.

Wang et al. [16] approached a RBC (erythrocytes) image segmentation method through shape feature extraction. 3D shape surface feature has been used to obtain acceptable performance, the classification and recognition based on the real shape of RBC's. 3D shape of red blood cell from gray tone images using scanned electronic microscope based on shape-from-shading technique, as well combined with linear approximation is reconstructed.

In this paper, a novel method is proposed to detect the RBCs in a thin blood film image without using any segmentation techniques or non uniform illumination correction methods. The morphological operations and further processing are performed directly on the grayscales image and not on the negative. This technique employs the information of size of the cells obtained from the granulometric process and the intensity values. It locates its position in the image and counts the total number of RBCs with an accuracy of 98 %. Annular ring ratio (ARR) transform is the main approach which detects peaks of intensity at the center of each RBC. A concentric ring for dilation and a disk for erosion are used to remove the platelets, parasites, and other artefacts in the image [17].

Berge et al. [18] proposed an algorithm that identifies and counts red blood cells in microscope images of thin blood smears. Iterative analysis is used to improve the segmentation performance. In preprocessing step, RGB image is converted to gray scale image and 5 × 5 median filters, and morphologically closed using a disk-shaped structuring element of radius 2 pixels to smooth image and remove pixel noise, respectively. Granulometry has been used in various studies for RBC size estimation. Various techniques such as boundary extraction, curvature calculation, and points of maximum curvature are used for RBC clump splitting.

RBC (erythrocytes) image segmentation is performed using shape reconstruction and multi-scale surface fitting. Guided contour tracing is used to find the boundary

of red blood cells in a scanned electron microscope image automatically. Shape from shading is used to recover the 3D shape of a surface from a gray level monochrome image. It is used to reconstruct the 3D shape of red blood cell from gray tone images using scanned electronic microscope based on shape from shading technique, as well combined with linear approximation. In automatic malaria diagnosis through microscopy imaging technique, infected erythrocytes are segmented from complicated background using a new algorithm. This new algorithm consists of hole filling, separating isolated and compound cell, segmenting compound cells, detection of the contours of erythrocytes. In this paper, RGB image is converted to gray scale image by using only green channel of the RGB image and is filtered for illumination correction by using median filter. Several features such as shapes features, intensity features, and texture features have been used to get better accuracy for malaria parasite segmentation. In malaria-infected blood cell segmentation, different stages of malaria can be detected [19, 20].

Blood cell segmentation is one of the important steps for medical image analysis. There is no single segmentation technique that can be considered good for blood cell segmentation. Blood cell segmentation consists of different techniques to have better accuracy [21, 22].

4 Conclusion

This paper gives an outline of different techniques used for erythrocyte blood cells image segmentation for diagnosis of various diseases. Different algorithms can be developed to segment region of interest which will give the exact accuracy to diagnose the diseases. The main goal of the erythrocyte segmentation was to extract the erythrocyte cells from complicated background using different methods. Using blood image segmentation algorithms, various diseases such as malaria, leukemia and hemolytic anemia, can be diagnosed. In malaria blood cell analysis, one can detect not only the cell components in the blood image but also parasites with four different stages such as *plasmodium falciparum* ring form parasites, ring form *plasmodium vivax*, mature *plasmodium vivax trophozoite*, and immature *plasmodium vivax* can be segmented and the ratio of the infected cells to normal cells can be calculated. There is no individual segmentation method which can be considered good for blood cell segmentation.

References

1. Costrarido, L.: Medical image analysis methods. Medical-image processing and analysis for CAD systems, pp. 51–86. Taylor and Francis, New York (2005)
2. Blood cell morphology. http://www.cellavision.com/cellatlas

3. Gonzalez, R.C., Woods, R.E.: Digital image processing, 3rd edn. Prentice Hall, Upper Saddle River (2002)
4. Dass, R., Priyanka, Devi, S.: Image segmentation techniques. Int. J. Electron. Commun. Technol. **3**(1), 66–70 (2012)
5. Adollah, R., Mashor, M.Y., Mohd Nasir, N.F., Rosline, H., Mahsin, H., Adillah, H.: Blood cell image segmentation: a review. Biomed. Proc. **21**, 141–144 (2008)
6. Saleh Al-amri, S., Kalyankar, N.V., Khamitkar, D.: Image segmentation by using threshold techniques. J. Comput. **2**(5), 83–86 (2010)
7. Truong, Q.B., Lee, B.R.: Automatic multi-thresholds selection for image segmentation based on evolutionary approach. Int. J. Control Autom. Syst. **11**, 834–844 (2013)
8. Sarkar, S., Patra, G.R., Das, S.: A differential evolution based approach for multilevel image segmentation using minimum cross entropy thresholding. SEMCCO, pp. 51–58. Springer, Berlin (2011)
9. Gomez, O., Gonzalez, J.A., Morales, E.F.: Image segmentation using automatic seeded region growing and instance-based learning, pp. 192–201. Springer, Berlin (2007)
10. Chen, H.-M., Tsao, Y.-T., Tsai, S.-N.: Automatic image segmentation and classification based on direction texton technique for hemolytic anemia in thin blood smears. Mach. Vis. Appl. **25**, 501–510 (2013)
11. Wang, M., Zhou, X., Li, F., Huckins, J., King, R.W., Wong, S.T.C.: Novel cell segmentation and online learning algorithms for cell phase identification in automated time-lapse microscopy. In: IEEE International Symposium, pp 65–68 (2007)
12. How K.B., Bin, A.S.K., Siong, N.T., Soo, K.K.: Red blood cell segmentation utilizing various image segmentation techniques. In: Proceeding of International Conference on Man-Machine Systems (2006)
13. Yu, D., Pham, T.D., Zhou, X., Wong, S.T.C.: Recognition and Analysis of Cell Nuclear Phases for High-Content Screening Based on Morphological Feature Pattern Recognition, pp. 498–508(2009)
14. Sharif, J.M., Miswan, M.F., Ngadi, M.A., Salam, M.S.H., Jamil, M.M.A.: Red blood cell segmentation using masking and watershed algorithm: a preliminary study. In: International Conference on Biomedical Engineering, pp. 258–262 (2012)
15. Vromen, J. McCane, B.: Red blood cell segmentation from SEM images. In: 24th International Conference Image and Vision Computing, New Zealand (2009)
16. Yi, F., Chen, P., Li L.: White blood cell image segmentation using on-line trained neural network. In: IEEE Engineering in Medicine and Biology 27th Annual Conference (2005)
17. Wang, R., Fang, B.: A combined approach on RBC image segmentation through shape feature extraction. Math. Probl. Eng. **2012**(194953), (2012)
18. Kareem, S., Morling, R.C.S, Kale, I.: A novel method to count the red blood cells in thin blood films. In: Proceedings of IEEE, pp. 1021–1024 (2011)
19. Vromen, J., McCane, B.: Red blood cell segmentation using guided contour tracing. In: 18th annual colloquium of the spatial information research centre university of Otago. Dunedin. New Zealand
20. Berge, H., Taylor, D., Krishnan1, S., Douglas, T.S.: Improved red blood cell counting in thin blood smears, pp. 204–207. IEEE
21. Wang, R., MacCan, B., Fang, B.: RBC image segmentation based on shape reconstruction and multi-scale surface fitting. In: 3rd international symposium on information science and engineering, pp. 586–589. IEEE (2010)
22. Springl, V.: Automatic malaria diagnosis through microscopic imaging, Thesis, Faculty of electrical engineering. Prague (2009)

Optimization Models for Solid Waste Management in Indian Cities: A Study

Dipti Singh and Ajay Satija

Abstract India is a developing country. India's population is over 1.27 billion people (2014) which are approximated as one-sixth of the world's population. Such population growth may leave behind the world's most heavily populated nation China by 2025 (US Census Bureau 2011). Solid waste management is an important environmental issue of all developed and developing countries. The growth of solid waste is basically due to population explosion, urbanization, and mismanagement of municipal corporation. Limitations of Indian Municipality Corporation are waste gathering inefficiency, lack of financial funds, poor planning, and lack of technical knowledge on changing complication of waste materials. In this paper, few important optimization models/techniques proposed by different researchers are studied that may be beneficial for ongoing project work in Municipal solid waste management (MSWM) in different metropolitan cities at various states in India. Much work has not been done in this direction. On the basis of extensive study of literature, it is suggested that the Indian municipal corporation must adopt 4R principles involving reduce, reuse, recycle, and recover to minimize solid waste.

Keywords Municipal solid waste management · Landfill · Optimization

1 Introduction

Municipal solid waste (MSW) is garbage or refused material discarded by the society. This garbage may be in any form in our home as dust, polythene bags, waste plastic as mugs, bottles, used news papers, cardboards wrapping of new electronic

D. Singh (✉)
Department of Applied Sciences, Gautam Buddha University, Greater Noida, India
e-mail: diptipma@rediffmail.com

A. Satija
Department of Mathematics, Inderprastha Engineering College, Ghaziabad, India
e-mail: aajaysatija@rediffmail.com

K.N. Das et al. (eds.), *Proceedings of Fourth International Conference on Soft Computing for Problem Solving*, Advances in Intelligent Systems and Computing 335,
DOI 10.1007/978-81-322-2217-0_31

appliances, used electronic wastes as fused wires, switches, damaged appliances as mixer, grinder, cancergeneous broken TV/computer CRTs, used invertors batteries, mosquito killing spray cans, used toilet/floor cleaner toxic chemicals bottles/cans, i.e., domestic commodities waste as well as hospital, clinical waste, building construction material waste as broken bricks, dried concrete, etc. Some of above are biodegradable, partially biodegradable, and non-biodegradable [1].

Main reason of MSW is due to increased population, urbanization, industrialization, financial issues, illiteracy, lack of public awareness for cleanness and resulting diseases, improper landfilling, improper application of 4R principles involving reduce, reuse, recycle, and recover to minimize the solid waste, per capita income, urban–rural lifestyle differences, variation in solid waste characteristics, lack of related law policies, etc. The municipal solid waste corporation (MSWC) is responsible for administrating and providing services regarding neat and clean environment to the society. The main objective of MSWC is not only to reduce MSW but also managing the solid waste via recycling, waste processing, and waste transformation. MSW is not same from one territory to another territory. Various optimization models for different metropolitan cities are proposed in literature in different cities of various countries. In this paper, few of them are studied, and their methodologies and conclusions are summarized relative to Indian subcontinent's highly populated metropolitan cities. Further importance of 4R principles is suggested, and without following such principles, solid waste cannot be reduced in our society. The future scope of optimization techniques paves a direction of minimizing various costs, decision support system, future predictions, etc.

2 Literature Review

In this section, various optimization models for solid waste management have been discussed. These models are proposed to minimize the cost of solid waste management in India only. For this country, only few models are available for different sites.

2.1 Integrated Linear Model (ILM)

Gerlagh et al. [2] have proposed a linear programming model which minimizes the total cost regarding solid waste in society. This model has been implemented on metropolitan city Bangalore. The proposed model has three components: (1) waste generating sector [home, office, and industry (say factors)] as input; (2) waste processing sector (rag pickers, waste purchasers shops, and waste treatment plants); and (3) extracts (greenhouse gases). Here, generated waste is processed by waste processing sector, and final waste extract after recycling is converted to new reusable products and transferred to society. The authors have characterized the

waste–good by pair of waste generated and responsible factors. Further, profit and loss have been evaluated by means of recyclable and non-recyclable waste. The economical law used is demand price = supply price + constraint/hidden price. The simulation result shows that about 1.8 billion rupees are used to process 1.3 million tones of solid waste. Unemployment gets reduced by 58 %. 31 % uses of area of dumping sites get minimized. Recycled waste price gets reduced by 50 %. Hence, global warming issue, environmental hazardous elements, urban land wastage, etc., all factors get minimized [2].

2.2 Advanced Locality Model (ALM)

Sarika [3] has proposed an optimization linear model for integrated municipal solid waste management (MSWM) in Mumbai, India. The author have discussed MSWM services and related expenditure budget. As population increased, MSW gets increased. Similarly, Municipal Corporation Greater Mumbai (MCGM) has been failed to manage financial and managerial issues within period 1991–2001. Data are obtained from MCGM, Stree Mukti Sangathan, Exel industry and Bhawalkar, Ecology Research Institute for this model. Within this period, waste generation was increased with rate of 0.45–0.53 kg per day per capita. The waste generated was 6,256 tons in 2000–2001 and 6,500 tons in 2001–2002, and corresponding money spent was increased 52,456 to 61,435 million Rs. (source MCGM 2001–2002). The proposed linear model is applied to two plants and related landfill areas. First plant is community compost plant: Here, the proposed model is called advanced locality model 'ALM' in which ward (subdivision of Mumbai) people, MCGM, and NGOs work together to resolve the problems of SWM in greater Mumbai. Second plant is mechanical aerobic composite plant in which Indian largest agrocompany 'Excel' Industry converts organic component of MSW into manure, and cost of collection is more than Rs. 1,400 per ton of waste. Third, MCGM follows sanitary landfilling approach because land cost is very high in Mumbai. Three disposal sites, 801 decision variables, 53 constraints, 24 generation nodes, three aerobic compositing plants, and three sanitary landfills are considered in this model. The objective function is defined as minimized (CT–BT). CT is the cost related with integrated solid waste management system (ISWM). BT is the benefit related with ISWM, where $CT = \Sigma CA_a + \Sigma CV_v + \Sigma COD_o$ = the overall waste processing cost at aerobic composting plant a and community compost plant v along with waste disposal cost at sanitary landfill o, where $BT = \Sigma BA_a + \Sigma BV_v + \Sigma BCOD_o$ = the overall waste processing benefits at aerobic composting plant a and community compost plant v along with waste disposal benefits of waste management at sanitary landfill o. The constraints are as follows: (1) The generated waste at particular node is to be transported to either community compost plant v or to an aerobic compost plant a or to landfill a., i.e., $G_i = \Sigma W_{iv} + \Sigma W_{ia} + \Sigma W_{io}$. (2) The planned capacity of solid waste to aerobic plant a ($\sum W_{ia}$) and compost plant v ($\sum W_{iv}$) should be less

than maximum capacity of solid waste to aerobic plant a ($Cap_{max,\ a}$) and compost plant v ($Cap_{max,\ v}$), i.e., $\Sigma W_{ia} \leq \left(Cap_{max,a}\right)$ and $\Sigma W_{iv} \leq \left(Cap_{max,v}\right)$. The optimization model is solved by using BDMPL solver [3].

2.3 Mixed Integer Goal Programming (MIGP) Linear Model

Pati et al. [4] proposed a mixed integer goal programming model for paper recycling system. The three objectives of the model are as follows: (1) Reverse logistics cost (C): Budget expanses regarding recycling of wastepaper should be feasible; (2) Non-relevant wastepaper target (N): Collected wastepaper quality should be better at vendor level; and (3) Wastepaper recovery target (W): Wastepaper collection should be maximized. The MIGP linear model is summarized as:

The objective function is to minimize $\{d_c^+, d_q^+, d_e^-\}$, where d_c^+ is positive reverse logistic activities deviation; d_q^+ is positive non-relevant paper (lower grade) target deviation; and d_e^- is negative deviation from minimum waste collection, i.e., wastepaper collection should be maximize.

Following are the essential constraints:

1. Reverse logistics cost constraint
   $(RL)c + d_c^- d_c^+ = T_{RLC}$ = reverse logistic cost + negative reverse logistic activities deviation—positive reverse logistic activities deviation = total reverse logistic cost.
2. Non-relevant wastepaper target (W_A)

$$\Sigma\Sigma\Sigma Qgdv I - \Sigma\Sigma\Sigma QMsgp + d_q^- d_q^+ = W_A$$

   where $Qgdv I$ = the amount of unsegregated wastepaper (I), and the transfer root is vendor customer v through dealer d to godown owner g
   and $QMsgp$ = the amount of segregated wastepaper (p), and p is transferred via root of godown owner to supplier s to manufacturer M.
3. Wastepaper recovery target (C_T)

$$\Sigma\Sigma\Sigma Qgdv I + d_e^- d_e^+ = C_T$$

The simulation results are applied on Indian paper recycling companies. LINDO-32 software has been used for simulation result of model. The observations are as follows: The minimum limit of paper-waste collection (CT) is 150,000 tones (T), and the maximum limit of non-relevant wastepaper in reverse network is 15,000 tones (T). If reverse logistics cost (C) is optimized to 60 %, then all above three goals would be fulfilled in CNW priority. As C is increased, both wastepaper recovery and non-relevant waste coincide. The optimized results have been observed better for decision making for paper recycling industry [4].

2.4 Integer Programming Model (IPM)

Gupta and Sharma [5] have proposed an integer programming model for integrated planning of solid waste management in Jaipur. In Jaipur, there are 77 wards and eight different zones. They discussed the problems of MSWM in the city due to high population and their waste disposal in dumping sites as drains, lanes, and storm water drainage sites without any recycling or reuse processes. Authors have suggested the solutions of such problem by constructing compost plant, recycling plant, mechanical compost plant, RDF plant, vermicular compost plant, and formation of landfill sites nearby such plant for reducing transportation cost. In proposed model, the waste material would be collected at various collection sites in the city and choosing optimum roots to transfer such garbage to specific segregation sites where after separation, waste has been transferred to particular treatment plant by dumpers. For example, biomedical wastes from various hospitals are transferred to biomedical treatment plants. The objective function F to be minimized is $F = F_1 + F_2 + F_3 - B$. Here, F is overall cost, F_1 represents total transportation cost, F_2 represents investment and handling expense, F_3 represents dumpers cost, and B represents profit at plants regarding production. Mass balance constraints are as follows: The total solid waste moved within collection nodes ≤ total amount of waste within that points. The total solid waste moved within plants and corresponding landfills collection nodes ≤ total amount of waste within that points. The total solid waste moved within biomedical nodes ≤ total amount of waste within that points. All variables should be positive integers. Capacity constraints are as : Total waste at different plants ≤ plant capacities [5].

2.5 Adaptive Neuro-Fuzzy Inference System (ANFIS)-Based Model

Tiwari et al. [6] have proposed an optimized model based on adaptive neuro-fuzzy inference system model (ANFIS model) for highly populated Durg district of Chhattisgarh state (India). Durg is famous for agriculture. Bhilai is a town of Durg district having famous industrial steel plant. It is observed that if at present valid data of industrial solid waste (ISW) is not available, then ISW future cannot be predicted. Basically, ANN models are used in various disciplines of research areas. But there are some limitations to use such models: (1) ANN models unable to interpret the output results in various research disciplines; (2) ANN models lack to explain the complex relationship between system components, and hence, user gets unable to understand the external view of system; and (3) ANN models fail to explain such systems in which output is given but input is to be evaluated. If ANN models are used with fuzzy inference system, then the user can better understand the system. Jang and Sun have used the combine approach named as adaptive neuro-fuzzy inference system to overcome such problems. ANFIS has two

components: One is antecedent and another is conclusion. Generalized bell-shaped function along with two Sugeno fuzzy model rules has been used here. Reasonable fuzzy rule size and proper membership functions depending upon population size and situation of problem have been used here. Only ANN technique cannot be used here due to its drawback of problem of improving exact information to the user; hence, fuzzy inference system is used along with here. ANFIS architecture has five layers:

Layer 1: There are adaptive nodes along with node functions

$$O_{1,i} = \mu_{Ai}(x) \quad \text{for} \quad i = 1, 2$$

Or

$$O_{1,i} = \mu_{Bi-2}(y) \quad \text{for} \quad i = 3, 4$$

Here, x and y are input values to node I; A, B are fuzzy sets; $O_{1,i}$ is membership function of fuzzy set A or B; and $\mu_{Ai}(x)$ is bell-shaped membership function.

Layer 2: In second layer, there are outputs of inputs initiated from first layer

$$O_{2,i} = w_i = \mu_{Ai}(x) * \mu_{Bi}(y) \quad i = 1, 2, \ldots, n$$

Layer 3: The outputs of this layer get normalized with node function $O_{3,i}$ (denoted by N)

$$O_{3,i} = w_i/(w_1 + w_2) \quad i = 1, 2$$

Layer 4: Each node in this layer is associated with node function $O_{4,i}$

$$O_{4,i} = (w_i/(w_1 + w_2)) * (p_i x + q_i y + r_i) \quad i = 1, 2$$

(p_i, q_i, r_i) is parameter set of ith node

Layer 5: This layer contains the total output of all incoming input signals from Layer 4

$$O_{5,i} = (\Sigma w_i z_i)/(\Sigma w_i)$$

Using above model, the simulation results are observed as: The authors have predicted 88,980 MT of ISW would be generated within time 2001–2026 on the basis of data 1961–2001 and 2009 for Durg–Bhilai. To predict this, see MATLAB version 7.8.0.347. Root-mean-square error formula evaluating (comparison of efficiency of models) and average relative error expresses travel time in future. For high-populated data, ANFIS gives better result than ANN model. In the MATLAB simulation result, approximately 40,190.29984 MT ISW would be produced in

Durg–Bhilai cities up to 2026. Further, the authors have compared the results of uncertainty up to 95 % confidence interval within ANN model and ANFIS model. ANFIS model is proved much reliable [6].

2.6 Municipal Solid Waste for Power Generation (MSWFPG) Linear Model

Karajgi et al. [7] proposed a mathematical model in which various linear mass balance equations (regarding mass of waste (tons/day) collected from different sources) have been simplified under constrains and related cost has been reduced. Distinct waste flows paths have been observed. Collection, separation, and final disposal processes comprise of various activities of flow of waste to incineration process. Overall cost plays role of objective function here. During incineration process, generated heat is evaluated. Heat generated is the sum of product of heat generated in each activity multiplied with corresponding weight. Only domestic waste generated has been considered in this model. The objective function for MSWFPG linear model is cost function U and is defined by cost $U = \Sigma\, \alpha_{u,k} x_{u,k}$. Here $\alpha_{u,k}$ is the cost coefficient for processing waste item k at unit process u in Rs./ton., and $x_{u,k}$ is the mass of waste item k processed by unit process u tons/year.

That is, cost $U = \Sigma\Sigma\alpha_{ij} x(A_i, E_{ij})$ for $i = 1, j = 1, \ldots, 4$, where α_{ij} is the cost coefficient for processing the waste in path E_{ij} (basically, α_{ij} includes cost of labors for various processes); A_1 is the amount of waste to incineration; The various paths E_{ij} be (1) waste to incineration,(2) waste to recycle plant,(3) waste to compost yard, and (4) waste to dump yard. The constraints are

$$x(A_1, E_{11}) + x(A_1, E_{12}) + x(A_1, E_{13}) + x(A_1, E_{14}) \geq B_0;$$
$$x(A_1, E_{11}) \geq B_1; \quad x(A_1, E_{12}) \geq B_2; \quad x(A_1, E_{13}) \geq B_3; \quad x(A_1, E_{14}) \geq B_4.$$

B_0, B_1, B_2, B_3, and B_4 represent the average amount of waste in all processes, average amount of waste to incineration, average amount of waste to recycle plant, average amount of waste to compost yard, and average amount of waste to dump yard, respectively. Finally, the amount of heat is HV = $\sum w_i\, h_i$; w_i is the mass of dry waste of ith component; h_i be the heat value of ith component; and N is number of components of MSW. Here, domestic waste is considered but industrial as well as biomedical waste/hospital waste is not considered here. The simulated results are applied on Dharwad city (Karnataka state) having area 200.23 km^2 (22 municipal wards) and population about 2.5 lakhs. The six months waste collection has been considered. Daily, 140 tons waste has been collected from different sources. Heat generated during incineration process is 3,632 kWh/ton, and corresponding 68,390 kWh energy is generated per day. Calculated value of cost function is Rs. 18, 34,445/day. The cost of electrical energy is observed Rs. 26.81/kWh [7].

2.7 Empirical and Artificial Neural Network (ANN) Model Approach

Patel and Meka [8] have proposed an approach to combine empirical models to predict the population of 98 different cities of Gujarat state with ANN model. ANN model estimates the approximate production of solid waste. Further, the simulation results have validated. The ANN model has two main components: (1) The first component named as dynamic component which is used for population prediction and is stated as: The four empirical models used for population prediction for first component are as follows: (1) arithmetic projection (predicts future population on the basis of past data) mathematically $P_n = P_o(1 + r * t)$; (2) geometric projection (predicts that population increases with geometric fix rate) mathematically $P_n = P_o(1 + r\text{^}t)$; (3) incremental increase method (predicts incremental population growth per unit time) mathematically $P_n = P_o + nX + 0.5 * (n * (n + 1))Y$; and (4) population growth reduced rate (predicts future population decrease growth rate) $P_n = P_o[1 + (r + r1)t]$, where P_n = population in nth decade; P_o = population in base year; r = population growth rate; $r1$ = average decrease in percentage increase of population; t = number of decades from base year; X = average growth in Population; and Y = incremental population growth. (2) The second component is the ANN component which is used to forecast the amount of MSW. This model has been used for solid waste generation. The ANN model assumes raw data for six inputs (say input neurons): (1) MSW generation in current year, (2) population of cities, (3) social aspect, (4) economic aspect, (5) longitude of cities, and (6) latitude of cities (helps in prediction of solid waste) and one output representing solid waste generation for next year. There are two functions named as linear transfer function and tansigmoidal function are used. Linear transfer function is used to explain a linear input output relation, whereas tansigmoidal function is used for nonlinear relationship, i.e., tansigmoidal functions are used for input and intermediate neurons. Each neuron is associated with weight and bias. Such weights and bias have been identified with Lavenbur-Marquate algorithm and MATLAB simulation.

The corresponding two algorithms used in this model are as follows:

1. The first algorithm for linear transfer function is as follows:

$$a = \text{purelin}(n) = n$$

2. The second algorithm for tansigmoidal function is as follows:

$$a = \text{tansig}(n) = 2/\left(1 + \text{e}^{-2*n}\right) - 1$$

Here, a and n are neuron output and input, respectively.

ANN model validation has been done with the help of data set of population and solid waste of 98 cities of Gujarat. Simulation results show that percentage prediction errors are less than 2 %, and hence, data get validated [8].

3 Basic Solutions (Suggested Remedial Actions) to MSWM

4R principles: reduce; reuse, recycle, and recover are basic components of 4R principles.

3.1 Reduce

If people reduce their needs and related consumption, then related waste products will be decreased. In office, documents may be sent via emails by scanning. Save paper by using paper while printing both sides, biodegradable paper bags should be used. In industry, always better quality machines, tools, etc., should be used so that transportation, processing cost, etc., would be reduced. In home, people should make sufficient food for their family (Fig. 1).

3.2 Reuse

The people may reuse items by donating them to needy people, e.g., donating old books to libraries, used cloths and toys to poor children, electrical and electronic appliances as TV, refrigerators, coolers, furniture to poor people, or some NGOs related to charity groups. In home, people should use refillable items as refillable gas cylinders, gas lighters, rechargeable cells/batteries, refillable oil advent candles, refillable ink cartridges, and use better quality of electrical and electronic appliances, etc.

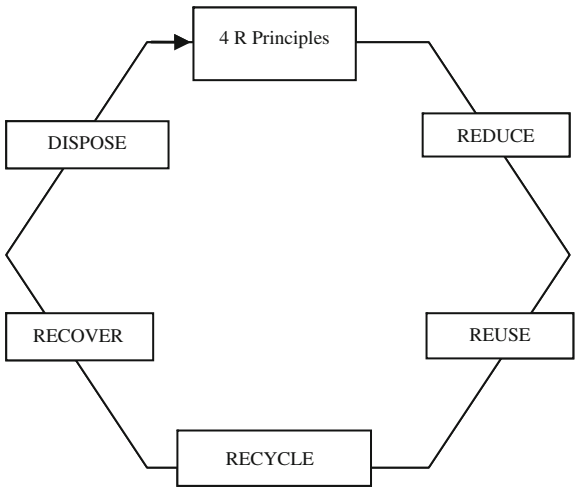

Fig. 1 The hierarchy of 4R principles

3.3 Recycle

In this process, first waste products are collected and get separated/segregated, and then, those waste products are processed in their related recycle plants, and after all, new reusable products are produced for public usage. The major benefits of recycling process are that less energy is used to recycle waste product as compared to energy used to produce new product. The air, land, and water pollution get reduced. Various temperature enhancing greenhouse gases as water vapors (H_2O), carbon dioxide (CO_2), methane (CH_4) get reduced. Recycled materials are papers, newspapers, metallic plastic and glass containers, cans, or bottles. Using US economic bureau report (Nathan), per year $2.4 billion of plastic get recycled, 12,471 jobs for people get created, and $529.2 million of benefit will be availed on recycling plastics in recycling plants.

3.4 Recovery

Energy can be recovered from biodegradable waste material, for example, plant waste as wood, leaves, etc., eatable waste as used bread, rice, vegetables, and fruits get collected and composed into container. Due to biodegradable processes under high pressure and heating such waste materials to high temperature, the waste material gets converted into solid, liquid, and gaseous state. The refined solid waste products can be converted into flammable synthetic gases (CO and H_2) by using gasification. Such gas can be further used to produce electricity. Hence, in such manner, energy gets recovered [9].

4 Future Scope of Related Work

In this paper, seven different SWM approaches are analyzed in form of different optimized models. It is observed that such approaches may be useful in finding and solving the limitations of each other up to some extent. It is found via Central Electricity Authority (CEA) prediction out of the 100 power plants that the CEA supervises, 38 will be closed with only 7 days and 20 plants would be closed with only 0–4 days due to shortage of coal. Tamil Nadu, Andhra Pradesh, Maharashtra, Gujarat, Chhattisgarh, Uttar Pradesh, and some NTPC plants would be affected [10]. To resolve such issue, the following approach can be used: MSWFPG linear model [7] along with Eempirical and ANN model approach [8] can be combined for finding the solution of SWM in Gujarat state. There are 63 rivers in Gujarat state. Hence, the problem of availability of water gets reduced. Using incineration process, the heat from organic waste (either from segregated biodegradable or non-biodegradable waste) can be produced. Through this heat, steam can be generated

and turbines can be run with river water. Hence, there are two benefits are being seen: first is SWM and second is the generation of electricity. Similarly, in another case, there are six rivers in Mumbai. In ALM model [3], the organic/non-organic waste is being sent to dump site and no further its arrangement is shown in model. This waste in ALM model along with incineration process in MSWFPG linear model can be combined to find the solution of electricity, and hence, landfilling problem can be reduced in Mumbai. As Mumbai is highly populous metro city, the ANN model approach can be used where survey of SWM is typical. Such approach may be useful for finding the solution of electricity and optimizing solid waste management in Indian cities.

References

1. Welsh Assembly Mechanical Biological Treatment. Environment Countryside and Planning Website, Welsh Assembly (2005)
2. Gerlagh, R., Beukering, P.V., Verma, M., Yadav, P.P.: Integrated modeling of solid waste in India. CREED working paper series 26, Amsterdam (1999)
3. Sarika, R.: Optimization model for integrated municipal solid waste management in Mumbai, India. Environ. Dev. Econ. **12**, 105–121 (2007). doi:10.1017/s1355770X0600341-x
4. Pati, R.K., Vrat, P., Kumar, P.: A goal programming model for paper recycling system. Sci. Direct Omega **36**, 405–417 (2008)
5. Gupta, A., Sharma, D.C.: Integer programming model for integrated planning of solid waste management in Jaipur. Int. J. Sci. Eng. Res. **2**, 1–10 (2011). ISSN 2229-5518
6. Tiwari, M.K., Bajpai, S., Dewangan, U.K.: Prediction of industrial solid waste with ANFIS model and its comparison with ANN model—a case study of Durg-Bhilai Twin city India. Int. J. Eng. Innovative Technol. **2**, 192–201 (2012). ISSN: 2277-3754
7. Karajgi, S.B., Kumar, U., Kamalapur, G.D.: Modeling of power generation using municipal solid waste in India. Int. J. Electr. Comput. Eng. **2**, 197–202 (2012). ISSN: 2088-8708
8. Patel, V., Meka, S.R.: Forecasting of municipal solid waste generation for medium scale towns located in the state of Gujarat, India. Int. J. Innovative Res. Sci. Eng. Technol. **2**, 4707–4716 (2013). ISSN: 2319-8753
9. ENVIS Urban Municipal Waste Management Newsletter (Sponsored by: Ministry of Environment and Forests, Government of India, New Delhi). National Solid Waste Association of India, Reg No. BOM.13//1996 GBBSD (June 2008). http://www.nswai.com/images/newsletters/june2008.pdf
10. Coal shortage may leave nation in dark in a week. http://indiatoday.intoday.in/story/india-black-out-coal-shortage-ntpc-central-electricity-authority/1/366533.html (2014)

Hybridization of Self Organizing Migrating Algorithm with Quadratic Approximation and Non Uniform Mutation for Function Optimization

Dipti Singh and Seema Agrawal

Abstract Self-organizing migrating algorithm (SOMA) is relatively a new population-based stochastic search technique for solving nonlinear global optimization problems. There has been done very less work on hybridization of SOMA with other methodologies in order to improve its performance. This paper presents hybridization of self-organizing migrating algorithm with quadratic approximation or interpolation (SOMAQI) and non-uniform mutation. This hybridization (M-SOMAQI) uses the quadratic interpolation (QI) and non-uniform mutation for creating a new solution vector in the search space. To validate the efficiency of this algorithm, it is tested on 15 benchmark test problems taken from the literature, and the obtained results are compared with SOMA and the SOMAQI. The numerical and graphical results conclude that the presented algorithm shows better performance in terms of population size, efficiency, reliability, and accuracy.

Keywords Self-organizing migrating algorithm · Quadratic interpolation · Non-uniform mutation · Function optimization

1 Introduction

Hybrid strategy is regarded as an effective method of improving the performance of population-based algorithms. Performing local search on population-based algorithms can maintain diversity and be capable to find the local optima with high accuracy. There are a number of population-based algorithms for solving global optimization problems such as genetic algorithms (GA), differential evolution (DE),

D. Singh (✉)
Department of Applied Sciences, Gautam Buddha University, Greater Noida, India
e-mail: diptipma@rediffmail.com

S. Agrawal
Department of Mathematics, S.S.V. College, Hapur, India
e-mail: seemagrwl7@gmail.com

K.N. Das et al. (eds.), *Proceedings of Fourth International Conference on Soft Computing for Problem Solving*, Advances in Intelligent Systems and Computing 335,
DOI 10.1007/978-81-322-2217-0_32

particle swarm optimization (PSO), and self-organizing migrating algorithms (SOMA) Among the above-mentioned algorithms, SOMA is relatively a new population-based stochastic search technique which is based on the social behavior of a group of individuals. This algorithm was developed by Zelinka and Lampinen in 2000 [1].

Many attempts have been made in literature to hybridize population-based algorithms with other existing approaches. Mohan and Shankar [2] developed random search technique for global optimization based on quadratic approximation. Deep and Dipti [3] developed a new hybrid algorithm SOMGA for function optimization. Millie et al. [4] presented a variant of quantum behaved PSO (Q-QPSO) for solving global optimization problems. Deep and Thakur [5] proposed a new mutation operator for real coded genetic algorithm. Deep and Bansal [6] presented the hybridization of PSO with quadratic approximation operator (QA). Xing et al. [7] developed a novel mutation operator based on the immunity operation. Deep and Das [8] proposed a quadratic approximation-based hybrid genetic algorithm for function optimization. Deep and Katiyar [9] proposed a new mutation operator for real coded GA, and its performance is compared with real coded power mutation operator. Esmin and Matwin [10] established a hybrid HPSOM algorithm. Recently, Singh et al. [11] developed a novel variant (SOMAQI) of SOMA, in which quadratic interpolation has been combined with SOMA to improve its efficiency for finding the solution of global optimization problems. In this paper, an improved version (M-SOMAQI) of SOMAQI has been proposed. In proposed variant, SOMAQI is combined with non-uniform mutation for better efficiency. To validate the claim, a set of 15 well-known test problem has been used to evaluate the performance of M-SOMAQI, and results are compared with the results obtained by SOMA and SOMAQI. On the basis of results, we can say that the proposed algorithm can achieve the global optimal solution with a small population size in less number of function evaluations and in less time. This paper is organized as follows. In Sect. 2, preliminaries: methodologies of SOMAQI and non-uniform mutation are given. In Sect. 3, the proposed algorithm M-SOMAQI is presented. In Sect. 4, the numerical results are discussed. Finally, the paper concludes with Sect. 5 drawing the conclusions of the present study.

2 Preliminaries

2.1 Self-organizing Migrating Algorithm with Quadratic Interpolation (SOMAQI)

The methodology of this algorithm is given as follows:

First, the individuals are generated randomly. At each generation, the individual with highest fitness value is selected as leader and the worst one as active individual. Now, the active individual moves toward leader in n steps of defined length. The movement of this individual is given by

$$x_{i,j}^{\mathrm{MLnew}} = x_{i,j,\mathrm{start}}^{\mathrm{ML}} + (x_{L,j}^{\mathrm{ML}} - x_{i,j,\mathrm{start}}^{\mathrm{ML}}) t\mathrm{PRTVector}_j \quad (1)$$

where

t	ϵ (0, by step to, path length)
ML	is actual migration loop
$x_{i,j}^{\mathrm{MLnew}}$	is the new positions of an individual
$x_{i,j,\mathrm{start}}^{\mathrm{ML}}$	is the positions of active individual
$x_{L,j}^{\mathrm{ML}}$	is the positions of leader.

PRT is a vector is created before an individual proceeds toward leader. It is defined in the range (0, 1).

Then, we again select the best and worst individual from the population. A new point x' is created using quadratic interpolation at the end of each generation using equation

$$x' = \frac{1}{2} \frac{\left[\left(R_{2\_}^2 R_3^2\right) * f(R_1) + \left(R_{3\_}^2 R_1^2\right) * f(R_2) + \left(R_{1\_}^2 R_2^2\right) * f(R_3)\right]}{\left[(R_2 - R_3) * f(R_1) + (R_3 - R_1) * f(R_2) + (R_1 - R_2) * f(R_3)\right]} \quad (2)$$

For this, we choose three distinct particles R_1, $R_{2,}$ and R_3, where R_1 is the leader, and R_2 and R_3 are randomly chosen particles from the remaining population. This new point is accepted only if it is better than active individual and is replaced with active individual.

2.2 Non-uniform Mutation Operator

This randomly selects one solution x_{ij} and sets its value according to the following rule:

$$x_{ij}^0 = \begin{cases} x_{ij} + \left(\mathrm{ub}_j - x_{ij}\right).\tau(t) & \text{if} \quad a_1 < 0.5 \\ x_{ij} - \left(x_{ij} + \mathrm{lb}_j\right).\tau(t) & \text{if} \quad a_1 \geq 0.5 \end{cases} \quad (3)$$

where $\tau(t) = \left(a_2\left(1 - \frac{t}{t_{\max}}\right)\right)^b$ and $x_{ij}\epsilon\left(\mathrm{lb}_j, \mathrm{ub}_j\right)$ with a_1 and a_2 two random numbers in [0,1], b and a constant parameters, t the time or generation number, and $t_{\max}$ the maximum number of generations any algorithm is allowed to run. The bounds (lower bound lb_j and upper bound ub_j) are taken equal to the bounds of the parameters of the problem to be optimized.

3 Proposed Hybrid M-SOMAQI Algorithm

In this section, a variant of SOMA, M-SOMAQI, has been presented which uses the quadratic interpolation and mutation for creating the new solution member in the search space.

3.1 Methodology

First, the individuals are generated randomly, and the optimal solution is obtained using SOMA. Now, a new point is created using quadratic interpolation, for this, we choose three particles R_1, R_2, and R_3, where R_1 is the leader, and R_2 and R_3 are randomly chosen particles from the remaining population. This new point is accepted only if it is better than earlier obtained optimal solution. Now, a new point is created using non-uniform mutation at the end of each generation using Eq. (3). This new point is accepted only if it is better than earlier obtained optimal solution. The process is continued until some termination criterion is satisfied. The computational steps of M-SOMAQI are given in Appendix 1.

4 Numerical Results

The proposed algorithm is coded in C++ and run on a Presario V2000 1.50-GHz computer. The numerical results of the 15 problems given in Appendix 2 are obtained. All the problems are of minimization and have the minimum value as 0. Since M-SOMAQI is probabilistic technique and relies heavily on the generation of random numbers; therefore, 100 trials of each are carried out, each time using a different seed for the generation of random numbers. A run is considered to be a success if the optimum solution obtained falls within 1 % accuracy of the known global optimal solution. The stopping criterion is either a run is a success or a fixed number of function calls (150,000) are performed. The comparative performance of M-SOMAQI, SOMAQI, and SOMA is measured in terms of three criteria, namely accuracy, efficiency, and reliability. They are described as follows:

(i) *Accuracy*, which is based on average function values,
(ii) *Efficiency*, which is based on *r* average number of function calls, and
(iii) *Reliability,* which is based on the success rate of the algorithms.

Trials for the 15 problems are performed for dimension $n = 30$, 50, and 100. The value of parameters after fine-tuning related to M-SOMAQI, namely population size, has been taken as 10. PRT varies from 0.3 to 1, step size has been taken as 0.31, and path length has been set as 3.0.

Table 1 shows the number of successful runs of a total of 100 runs, corresponding to M-SOMAQI, SOMA, and SOMAQI. Results show that the ranking of all the algorithms is SOMA<SOMAQI<M-SOMAQI. M-SOMAQI is the best in all the 15 problems. Hence, M-SOMAQI is *most reliable.*

Table 2 shows the average number of function calls corresponding to M-SOMAQI, SOMA, and SOMAQI. Results show that the ranking of all the algorithms is SOMA<SOMAQI<M-SOMAQI. M-SOMAQI is the best in 13 problems. Hence, M-SOMAQI is *most efficient.*

Table 3 shows the mean objective function value corresponding to M-SOMAQI, SOMA, and SOMAQI. Results show that the ranking of all the algorithms is SOMA SOMAQI<M-SOMAQI. M-SOMAQI is the best in 13 problems. Hence, M-SOMAQI is *most accurate.*

In order to reconfirm our results, we compare the relative performance of all the algorithms simultaneously. We use a performance index (PI). The relative performance of an algorithm using this modified PI is calculated in the following manner.

$$\mathrm{PI} = \frac{1}{N_p}\sum_{i=1}^{N_p}\left(k_1\alpha_1^i + k_2\alpha_2^i + k_3\alpha_3^i\right) \tag{4}$$

where

$$\alpha_1^i = \frac{\mathrm{Sr}^i}{\mathrm{Tr}^i},$$

$$\alpha_2^i = \begin{cases} \dfrac{\mathrm{Mo}^i}{\mathrm{Ao}^i}, & \text{if } \mathrm{Sr}^i > 0 \\ 0, & \text{if } \mathrm{Sr}^i = 0 \end{cases} \text{ and}$$

$$\alpha_3^i = \begin{cases} \dfrac{\mathrm{Mt}^i}{\mathrm{At}^i}, & \text{if } \mathrm{Sr}^i > 0 \\ 0, & \text{if } \mathrm{Sr}^i = 0 \end{cases} \text{ and}$$

where Sr^i = number of successful runs of ith problem, Tr^i = total number of runs of ith problem, Ao^i = mean objective function value obtained by an algorithm of ith problem, Mo^i = minimum of mean objective function value obtained by all algorithms of ith problem, At^i = average number of function evaluations of successful runs taken by an algorithm in obtaining the solution of ith problem, Mt^i = minimum of mean execution time of successful runs taken by all algorithms in obtaining the solution of ith problem, and N_p = Total number of problems analyzed. k_1,k_2 and k_3($k_1 + k_2 + k_3 = 1$ and $0 \le k_1, k_2, k_3 \le 1$) are the weights assigned to percentage of success, mean objective function value, and average number of function evaluations of successful runs, respectively.

From the above definition, it is clear that modified PI is a function of k_1,k_2 and k_3 since $k_1 + k_2 + k_3 = 1$, one of k_i, $i = 1, 2, 3$ could be eliminated to reduce the number of variables from the expression of PI. But it is still difficult to analyze the behavior of this PI, because the surface of PI for all the algorithms is

Table 1 Percentage of success of M-SOMAQI, SOMAQI, and SOMA for Dim. 30, 50, and 100

P. No	Dimension	Number of successful runs out of 100		
		SOMA	SOMAQI	M-SOMAQI
1	30	10	100	**100**
	50	0	100	**100**
	100	0	100	**100**
2	30	60	100	**100**
	50	0	100	**100**
	100	0	100	**100**
3	30	100	100	**100**
	50	100	100	**100**
	100	100	100	**100**
4	30	10	100	**100**
	50	23	100	**100**
	100	17	100	**100**
5	30	0	97	**100**
	50	0	100	**100**
	100	0	100	**100**
6	30	07	0	**39**
	50	0	0	**31**
	100	0	0	**39**
7	30	100	100	**100**
	50	100	100	**100**
	100	90	100	**100**
8	30	100	100	**100**
	50	100	100	**100**
	100	100	100	**100**
9	30	0	100	**100**
	50	0	99	**100**
	100	0	99	**100**
10	30	100	100	**100**
	50	100	100	**100**
	100	0	100	**100**
11	30	0	88	**97**
	50	0	96	**98**
	100	0	67	**95**
12	30	0	100	**100**
	50	0	100	**100**
	100	0	100	**100**
13	30	0	100	**100**
	50	0	100	**100**
	100	0	100	**100**

(continued)

Table 1 (continued)

P. No	Dimension	Number of successful runs out of 100		
		SOMA	SOMAQI	M-SOMAQI
14	30	0	100	**100**
	50	0	100	**100**
	100	0	100	**100**
15	30	0	100	**100**
	50	0	100	**100**
	100	0	99	**100**

Table 2 Average number of function evaluations of M-SOMAQI, SOMAQI, and SOMA for Dim. 30, 50, and 100

P. No	Dimension	Average number of function evaluations of successful runs		
		SOMA	SOMAQI	M-SOMAQI
1	30	47,818	1,297	**1,100**
	50	150,000	1,376	**1,235**
	100	150,000	1,392	**1,244**
2	30	20,023	786	**742**
	50	150,000	921	**790**
	100	150,000	1,410	**888**
3	30	13,702	669	**587**
	50	27,044	934	**629**
	100	84,144	1,192	**709**
4	30	43,534	1,534	**1,295**
	50	72,521	2,110	**1,258**
	100	95,521	2,062	**1,309**
5	30	150,000	2,300	**982**
	50	150,000	1,240	**957**
	100	150,000	1,347	**1,104**
6	30	150,000	150,000	**100,010**
	50	150,000	150,000	**100,010**
	100	150,000	150,000	**100,010**
7	30	22,924	966	**767**
	50	44,712	1,075	**813**
	100	123,908	1,557	**1,108**
8	30	26,786	1,173	**944**
	50	57,088	1,337	**1,120**
	100	141,010	1,864	**1,080**
9	30	150,000	3,041	**1,477**
	50	150,000	2,649	**2,508**
	100	150,000	4,687	**4,236**

(continued)

Table 2 (continued)

P. No	Dimension	Average number of function evaluations of successful runs		
		SOMA	SOMAQI	M-SOMAQI
10	30	35,712	332	**85**
	50	78,148	178	**166**
	100	150,000	162	**118**
11	30	150,000	**2,463**	3,111
	50	150,000	**3,082**	4,489
	100	150,000	7,709	**4,870**
12	30	150,000	2,666	**2,307**
	50	150,000	2,789	**2,629**
	100	150,000	**3,413**	4,273
13	30	150,000	2,582	**1,090**
	50	150,000	3,159	**1,402**
	100	150,000	4,932	**2,214**
14	30	36,372	3,497	1,607
	50	70,822	5,531	**1,152**
	100	150,000	5,323	**1,473**
15	30	150,000	6,676	**5,767**
	50	150,000	5,967	**5,407**
	100	150,000	7,993	**6,735**

overlapping and it is difficult to visualize them. Hence, equal weights are assigned to two terms at a time in the PI expression. This way PI becomes a function of one variable. The resultant cases are as follows:

(i)

$$k_1 = w, \quad k_2 = k_3 = \frac{1-w}{2}, \quad 0 \leq w \leq 1$$

(ii)

$$k_2 = w, \quad k_1 = k_3 = \frac{1-w}{2}, \quad 0 \leq w \leq 1$$

(iii)

$$k_3 = w, \quad k_1 = k_2 = \frac{1-w}{2}, \quad 0 \leq w \leq 1$$

The graphs corresponding to each of case (i), (ii), and (iii) are shown in following figures. The horizontal axis represents the weight *w,* and the vertical axis represents the PI.

Table 3 Mean objective function value of M-SOMAQI, SOMAQI, and SOMA for Dim. 30, 50, and 100

P. No	Dimension	Mean of objective function value of successful runs		
		SOMA	SOMAQI	M-SOMAQI
1	30	0.00905	0.00656	**0.00577**
	50	3.413	0.00744	**0.00710**
	100	9.06	0.00741	**0.00622**
2	30	0.00817	0.00536	**0.00340**
	50	0.5119	0.00397	**0.00332**
	100	2.336	0.00539	**0.00469**
3	30	0.00810	0.00743	**0.00430**
	50	0.00940	0.0049	**0.0039**
	100	0.00810	0.00754	**0.00614**
4	30	0.00758	0.00555	**0.00295**
	50	0.00895	0.00523	**0.00512**
	100	0.00940	0.00593	**0.00359**
5	30	17.32	0.00687	**0.00541**
	50	35.06	0.00739	**0.00674**
	100	118.156	0.00722	**0.00479**
6	30	**0.033**	27.3108	0.0527
	50	276.092	47.9958	**0.04550**
	100	1,284.4	98.125	**0.05267**
7	30	0.00815	0.00750	**0.00547**
	50	0.00884	0.00308	**0.00214**
	100	0.00771	0.00655	**0.00408**
8	30	0.00807	0.00280	**0.00142**
	50	0.00807	0.00581	**0.00368**
	100	0.00921	0.00673	**0.00450**
9	30	14.0672	0.00869	**0.00815**
	50	57.0017	0.00797	**0.00513**
	100	363.09	0.00658	**0.00331**
10	30	0.00832	0.00147	**0.00146**
	50	0.00995	0.00149	**0.00137**
	100	1.078	0.00816	**0.00021**
11	30	9.17935	0.00781	**0.00441**
	50	13.0147	0.00991	**0.00302**
	100	20.8049	0.00945	**0.00337**
12	30	0.49723	0.00954	**0.00952**
	50	0.499441	0.00946	**0.00915**
	100	0.49998	0.00932	**0.00931**
13	30	1,343.16	0.00735	**0.00559**
	50	9,521.35	0.00763	**0.00600**
	100	53,198.5	0.00755	**0.00400**

(continued)

Table 3 (continued)

P. No	Dimension	Mean of objective function value of successful runs		
		SOMA	SOMAQI	M-SOMAQI
14	30	0.00811	0.00698	**0.00427**
	50	0.00882	0.00623	**0.00622**
	100	0.0488	0.00733	**0.00573**
15	30	24.4029	0.00885	**0.00815**
	50	12.9596	0.00863	**0.00823**
	100	454.84	0.019408	**0.01913**

In case (i), the mean objective function value and average number of function evaluations of successful runs are given equal weights. PI's of M-SOMAQI, SOMAQI, and SOMA for all dimensions 30, 50, and 100 are superimposed in the Figs. 1, 4 and 7. It is observed that the value of PI for M-SOMAQI is more than SOMA and SOMAQI.

In case (ii), equal weights are assigned to the numbers of successful runs and mean objective function value of successful runs. From Figs. 2, 5 and 8, it is clear that M-SOMAQI has the highest PI.

In case (iii), equal weights are assigned to average number of function evaluations of successful runs and average number of successful runs. From Figs. 3, 6 and 9, it is clear that M-SOMAQI has the highest PI.

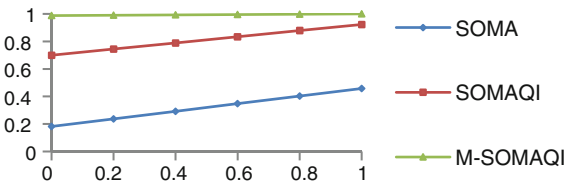

Fig. 1 PI for combination of SOMA, SOMAQI, and M-SOMAQI for Dim. 30 case 1

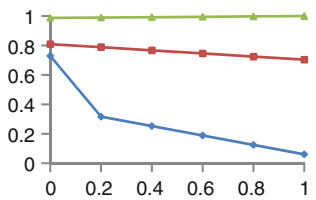

Fig. 2 PI for combination of SOMA, SOMAQI, and M-SOMAQI for Dim. 30 for case 2

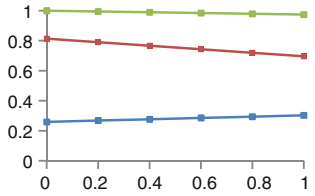

Fig. 3 PI for combination of SOMA, SOMAQI, and M-SOMAQI for Dim. 30 for case 3

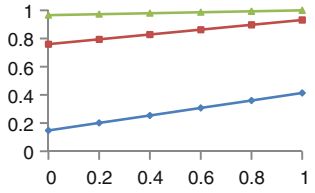

Fig. 4 PI for combination of SOMA, SOMAQI, and M-SOMAQI for Dim. 50 for case 1

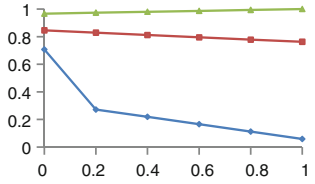

Fig. 5 PI for combination of SOMA, SOMAQI, and M-SOMAQI for Dim. 50 for case 2

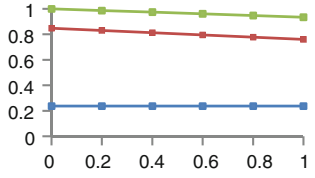

Fig. 6 PI for combination of SOMA, SOMAQI, and M-SOMAQI for Dim. 50 for case 3

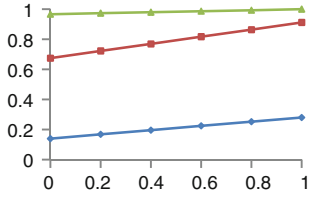

Fig. 7 PI for combination of SOMA, SOMAQI, and M-SOMAQI for Dim. 100 for case 1

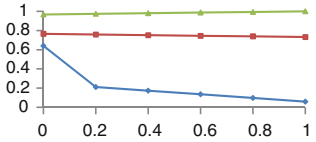

Fig. 8 PI for combination of SOMA, SOMAQI, and M-SOMAQI for Dim. 100 for case 2

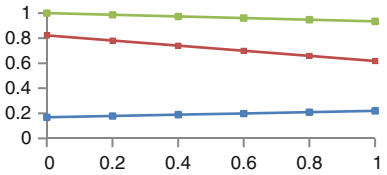

Fig. 9 PI for combination of SOMA, SOMAQI, and M-SOMAQI for Dim. 100 for case 3

5 Conclusions

In this paper, a variant of SOMA with quadratic interpolation and non-uniform mutation (M-SOMAQI) is proposed. The proposed algorithm is tested on 15 unconstrained benchmark problems and compared with the results of SOMA and SOMAQI. The results are obtained using population size 10 only. On the basis of the results, it can be concluded that the presented algorithm outperforms SOMA and SOMAQI in terms of efficiency, reliability, and accuracy.

Appendix 1

The computational steps of M-SOMAQI are given as follows:

Step 1: generate initial population and evaluate all individuals in the population;
Step 2: generate PRT vector for all individuals and sort all the individuals;
Step 3: select the best fitness individual as leader and worst as active;
Step 4: for active individual, new positions are created using Eq. (1). Then, the best position is selected and replaces the active individual by the new one;
Step 5: create new point by quadratic interpolation from using Eq. (2);
Step 6: if new point is better than active, replace active with the new one;
Step 7: sort all of them and select the best fitness individual as leader and worst as active;
Step 8: create new point by non-uniform mutation using Eq. (3);

Step 9: if new point is better than active, replace active with the new one;
Step 10: if termination criterion is satisfied, stop else go to step 2;
Step 11: report the best individual as the optimal solution;

Appendix 2

Problem 1 Ackley function

$$\min f(x) = -20\exp\left(-0.02\sqrt{\frac{1}{n}\sum_{i=1}^{n} x_i^2}\right) - \exp\left(\frac{1}{n}\sum_{i=1}^{n}\cos(2\pi x_i)\right) + 20 + e,$$
$$\text{for } x_i \in [-30, 30]$$

Problem 2 Cosine mixture

$$\min f(x) = 0.1n + \sum_{i=1}^{n} x_i^2 - 0.1\sum_{i=1}^{n}\cos(5\pi x_i), \quad \text{for } x_i \in [-1, 1]$$

Problem 3 Exponential

$$\min f(x) = 1 - \exp\left(-0.5\sum_{i=1}^{n} \mathrm{x}_i^2\right), \quad \text{for } x_i \in [-1, 1]$$

Problem 4 Griewank

$$\min\ f(x) = 1 + \frac{1}{4,000}\sum_{i=1}^{n} x_i^2 - \prod_{i=1}^{n}\cos\left(\frac{x_i}{\sqrt{\mathrm{i}}}\right), \quad \text{for } x_i \in [-600, 600]$$

Problem 5 Rastrigin

$$\min f(x) = 10n + \sum_{i=1}^{n}\left[x_i^2 - 10\cos(2\pi x_i)\right], \quad \text{for } x_i \in [-5.12, 5.12]$$

Problem 6 Rosenbrock

$$\min f(x) = \sum_{i=1}^{n-1}\left[100(x_{i+1} - x_i^2)^2 + (x_i - 1)^2\right], \quad \text{for } x_i \in [-30, 30]$$

Problem 7 Sphere

$$\min f(x) = \sum_{i=1}^{n} x_i^2, \quad \text{for } x_i \in [-5.12, 5.12]$$

Problem 8 Axis parallel hyper-ellipsoid

$$\min f(x) = \sum_{i=1}^{n} i x_i^2, \quad \text{for } x_i \in [-5.12, 5.12]$$

Problem 9 Zakharov

$$\min f(x) = \sum_{i=1}^{n} x_i^2 + \left(\sum_{i=1}^{n} \frac{i}{2} x_i\right)^2 + \left(\sum_{i=1}^{n} \frac{i}{2} x_i\right)^4, \quad \text{for } x_i \in [-5.12, 5.12]$$

Problem 10 Schwefel 3

$$\min f(x) = \sum_{i=1}^{n} |x_i| + \prod_{i=1}^{n} |x_i|, \quad \text{for } x_i \in [-10, 10]$$

Problem 11 Saloman

$$\min f(x) = 1 - \cos(2\pi ||x_i||) + 0.1||x_i||, \quad ||x_i|| = \sqrt{\sum_{i=1}^{n} x_i^2},$$
$$\text{for } x_i \in [-100, 100]$$

Problem 12 Schaffer 1

$$\min f(x) = 0.5 + \frac{\left(\left(\sin\sqrt{\sum_{i=1}^{n} x_i^2}\right)^2 - 0.5\right)}{\left(1 + 0.001\left(\sum_{i=1}^{n} x_i^2\right)\right)^2}, \quad \text{for } x_i \in [-100, 100]$$

Problem 13 Schwefel double sum

$$\min f(x) = \sum_{i=0}^{n-1} \left(\sum_{j=0}^{i} x_i\right)^2, \quad \text{for } x_i \in [-100, 100]$$

Problem 14 De Jong's function with noise

$$\min f(x) = \sum_{i=0}^{n-1} (i+1)x_i^4 + \text{rand}(0,1), \quad \text{for } x_i \in [-1.28, 1.28]$$

Problem 15 Dixon and Price Function

$$\min f(x) = (x_1 - 1)^2 + \sum_{i=2}^{n} i\left(2x_i^2 - x_{i-1}\right)^2, \quad \text{for } x_i \in [-10, 10]$$

References

1. Zelinka, I., Lampinen, J.: SOMA—self organizing migrating algorithm. In: Proceedings of the 6th International Mendel Conference on Soft Computing, pp. 177–187, Brno (2000)
2. Mohan, C., Shankar, K.: Random search technique for global optimization. Asia Pac. J. Oper. Res. **11**, 93–101 (1994)
3. Deep, K., Dipti: A new hybrid self organizing migrating genetic algorithm for function optimization. IEEE Congress on Evolutionary Computation, pp. 2796–2803 (2007)
4. Pant, M., Thangaraj, R., Abraham, A.: A new pso algorithm with crossover operator for global optimization problems. In: Corchado, E., et al. (eds.) Second International Symposium On Hybrid Artificial Intelligent Systems (HAIS'07). Soft computing Series. Innovations in Hybrid Intelligent Systems, vol. 44, pp. 215–222. Springer, Berlin (2007)
5. Deep, K., Thakur, M.: A new mutation operator for real coded genetic algrithms. Appl. Math. Comput. **193**, 229–247 (2007)
6. Deep, K., Bansal, J.C.: Hybridization of particle swarm optimization with quadratic approximation, vol. 46, pp. 3–24, Opsearch. Springer, Berlin (2009)
7. Xing, L.N., Chen, Y.W., Yang, K.W.: A novel mutation operator base on immunity operation. Eur. J. Oper. Res. **197**, 830–833 (2009)
8. Deep, K., Das, K.N.: Performance improvement of real coded genetic algorithm with Quadratic approximation based hybridization. Int. J. Intell Defence Support Syst. **2**, 319–334 (2010)
9. Deep, K.S., Katiyar, V.K.: A new real coded genetic algorithm operator: log logistic mutation. In: Proceedings of The International Conference on Soft Computing for Problem Solving. Advances in intelligent and soft computing, vol. 130, pp. 193–200 (2012)
10. Esmin, A.A.A., Matwin, S.: A hybrid particle swarm optimization algorithm with genetic mutation. Int. J. Innovative Comput. Inf. Control **9**, 1919–1934 (2013)
11. Singh, D., Agrawal, S., Singh, N.: A novel variant of self organizing migrating algorithm for function optimization. In: Proceedings of the 3rd International Conference on Soft Computing for Problem Solving. Advances in intelligent and soft computing, vol. 258, pp. 225–234 (2013)

Identification of Single and Double Jersey Fabrics Using Proximal Support Vector Machine

Abul Hasnat, Anindya Ghosh, Subhasis Das and Santanu Halder

Abstract Single and double jersey knitted fabrics are different in many aspects, but it is difficult to identify them in open eye, and in textile industry, it is essential to identify them automatically. So far, no hands-on state-of-the-art technology has been adopted for identification of single and double jersey fabrics. This novel work endeavors to recognize these two kind of knitted fabrics by means of proximal support vector machine (PSVM) using the features extracted from gray level images of both fabrics. A *k*-fold cross-validation technique has been applied to assess the accuracy. The robustness, speed of execution, proven accuracy coupled with simplicity in algorithm holds the PSVM as a foremost classifier to recognize single and double jersey fabrics.

Keywords Single jersey · Double jersey · Image processing · Pattern classification · Proximal support vector machine · *K*-fold cross-validation

1 Introduction

Off late, fabric defect identification from images [1–8] is becoming progressively more significant since it may be able to automate the inspection of fabric defects during weaving. Sometimes identification in open eye of different fabric types is also

A. Hasnat (✉) · A. Ghosh · S. Das
Government College of Engineering and Textile Technology, Berhampore, West Bengal, India
e-mail: abulhasnat.007@gmail.com

A. Ghosh
e-mail: anindya.textile@gmail.com

S. Das
e-mail: subhasis.tex@gmail.com

S. Halder
Kalyani Government Engineering College, Kolkata, West Bengal, India
e-mail: sant.halder@gmail.com

K.N. Das et al. (eds.), *Proceedings of Fourth International Conference on Soft Computing for Problem Solving*, Advances in Intelligent Systems and Computing 335,
DOI 10.1007/978-81-322-2217-0_33

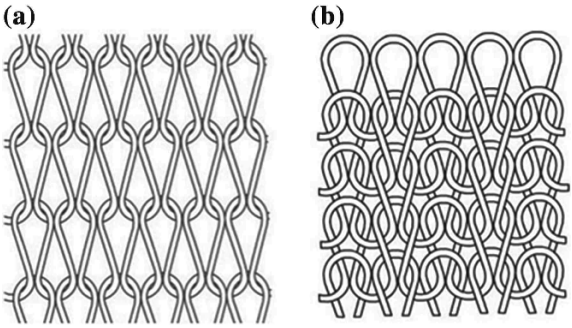

Fig. 1 Snapshots of weft-knitted fabrics, **a** single jersey, **b** double jersey

difficult. Knitted fabrics are produced commercially for apparel, household, and technical products, and they are used for an extremely large array of products, ranging from stockings and tights to imitation furs and rugs. In this paper, two different structures of weft-knitted fabrics are considered such as single jersey fabric and double jersey fabric for pattern identification using proximal support vector machine (PSVM). Single jersey fabric is made on one set of needles. Whereas double jersey fabric is made on two set of needles arranged perpendicular to each other. Figure 1 shows schematic images of single jersey and double jersey knitted fabrics.

This paper is organized as follows: Sect. 2 presents brief discussion on the proposed method. Section 3 explains in details about the capturing the images. Section 4 explains the construction of GLCM from captured images. Section 5 discusses the features extraction process from the captured images. Section 6 shows an outline of PSVM and the knitted fabric classification process. Section 7 shows experimental results and discussion, and finally Sect. 8 concludes and remarks about some of the aspects analyzed in this paper.

2 Proposed Methodology

A pattern recognition system for classifying single and double jersey fabrics can be partitioned into a numbers of components as illustrated in Fig. 1. At first, a digital camera captures the single and double jersey fabrics. Next, the camera's signals are processed to simplify subsequent operations without losing relevant information. The information from each fabric image is then sent to a feature extractor, whose purpose is to reduce the data by measuring certain features or attributes. PSVM use these features to evaluate the evidence presented and make a final decision as to the fabric type.

The proposed system works in four steps: (A) capturing the images of single and double jersey fabrics using Leica digital microscope; (B) image processing where median filter is applied first and gray level co-occurrence matrix (GLCM) is constructed; (C) feature extraction from the constructed GLCM matrix; (D) classification of the fabrics by PSVM using the extracted features. Figure 2 shows the flowchart of the proposed system.

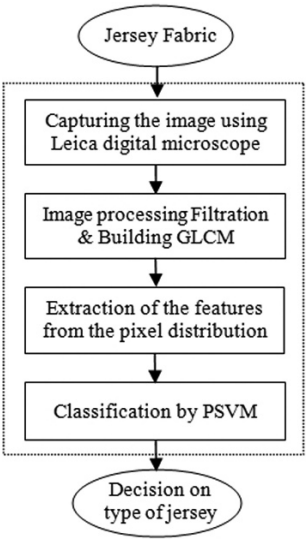

Fig. 2 Flowchart of the proposed system

3 Capturing the Fabric Images

Fabric images were captured using a LEICA camera (Model EZ-4D) with a magnification of 16X. Samples were illuminated by three halogen lights positioned approximately 20 cm above directly and to the right and left of the sample to supply illumination in diagonal directions of 45°. Figure 3 depicts the typical images of single and double jersey fabrics. Altogether, 80 images were captured for the experimentation and 40 from each category. The digitized images were constituted of 2,048 × 1,536 pixels [8] with subsequent conversion into gray level of 0–255 and stored as a two-dimensional gray matrix [5, 6]. Once converted into gray level, each image was enhanced by median filter which eliminates undesirable noise. Figure 3 shows sample of the captured images.

It is evident from the Fig. 3 that though both fabrics made from same material and design, but there exist structural difference in two different classes of fabrics.

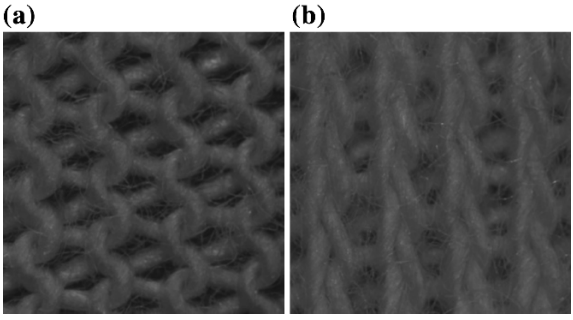

Fig. 3 Images of knitted fabrics, **a** single jersey, **b** double jersey

4 Construction of Gray Level Co-occurrence Matrix

After capturing the fabric images, the camera's signals are processed to simplify subsequent operations without losing relevant information. The digitized images were constituted of 2,048 × 1,536 pixels with subsequent conversion into gray level of 0–255 and stored as a two-dimensional gray matrix. Once converted into gray level, each image was enhanced by a median filter which eliminates undesirable noise. In next step, GLCM (G) is constructed along 0° keeping the spatial displacement $d = 1$ [1, 6]. Figure 4 illustrates an example of constructing matrix G with the specified rule defined as 'one pixel to the immediate right'. In Fig. 4, we take a representation of a very small image in array form and its co-occurrence matrix G. One can find that element (1, 2) of G is 2 because the number occurrence of a pixel having value 1 with its neighbor (immediately to the right) with pixel value 2 is twice. Thus, following the pre-defined rule, all other elements of the matrix G are calculated. Number of possible intensity levels in the image limits the size of G. It assumes a size of 256 × 256 for a gray image having 256 possible levels. This size, if not a large one, can be cumbersome when sequential operations are performed. In order to limit the size of G so that computational stress remains bearable we can group the whole intensity levels in bands of 32 each. As a result of such quantization 256 intensity levels get reduced to only eight which makes the size of G is 8 × 8 matrix.

In this way, 80 G matrixes are constructed from 80 images (40 from each category) which are used in next section for feature extraction.

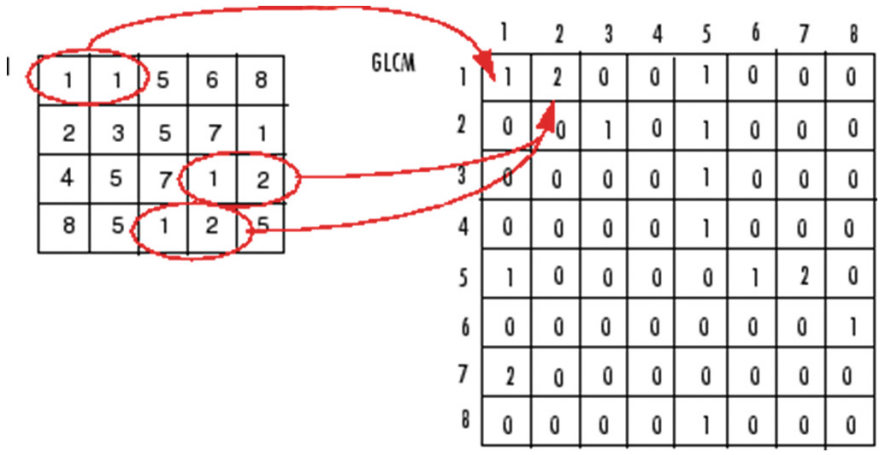

Fig. 4 Formation of 8 × 8 GLCM

5 Feature Extraction

In this step, features are extracted from GLCM constructed from each of the images. The eight features extracted are dissimilarity, contrast, energy, homogeneity, correlation, entropy, maximum probability, and variance.

When each element of the matrix G of size $g \times g$ is divided by the sum total value of all its elements, we have an estimate of the probability $p_{i,j}$ (that a pair of points satisfying our defining rule have the desired intensity). We can formally write the formalization as under:

$$p_{i,j} = e_{i,j}/n \tag{1}$$

where n is the sum of the elements of G and $e_{i,j}$ is the each element of G. And probability is in the range of [0, 1] and making a sum always 1, so that we can write

$$\sum_{i=1}^{g}\sum_{j=1}^{g} p_{i,j} = 1 \tag{2}$$

where $g \times g$ is the dimension of the matrix. Some of the descriptors or features as derived from G are explained below.

(a) **Dissimilarity**: It measures the dissimilar features of images and defined as

$$\text{Dissimilarity} = \sum_{i=1}^{g}\sum_{j=1}^{g} ((i-1) \times (p - \frac{i}{2}) + (j-1)) \tag{3}$$

(b) **Contrast**: It measures the contrast of intensity between two neighboring pixels over the entire matrix; mathematical expression being

$$\text{Contrast} = \sum_{i=1}^{g}\sum_{j=1}^{g} (i-j)^2 p_{i,j} \tag{4}$$

(c) **Energy**: It is a measure of uniformity of the image portion under consideration with values in the range 0 and 1. When image is of constant energy or uniformity, it assumes a value of 1; mathematical formulation being

$$\text{Energy} = \sum_{i=1}^{g}\sum_{j=1}^{g} (p_{i,j}^2) \tag{5}$$

(d) **Homogeneity**: It measures the spatial closeness of the distribution of elements in normalized G to the diagonal and its expression is given by

$$\text{Homogeneity} = \sum_{i=1}^{g}\sum_{j=1}^{g}\frac{p_{i,j}}{1+|i-j|} \tag{6}$$

(e) **Correlation**: This measures the extent of correlation of a pixel with its neighbor considering the entire matrix which is expressed as:

$$\text{Correlation} = \sum_{i=1}^{g}\sum_{j=1}^{g}\frac{(i-\mu_i)(j-\mu_j)p_{i,j}}{\sigma_i\sigma_j}, \quad \sigma_i \neq 0;\ \sigma_j \neq 0 \tag{7}$$

where μ_i, μ_j are the means and σ_i, σ_j are the standard deviations of ith row and jth column of the normalized G.

(f) **Entropy:** It measures the randomness of the elements of G. The entropy is 0 when all $p_{i,j}$'s are 0 and is maximum when all $p_{i,j}$'s are equal. The maximum value is $2\log_2 g$.

$$\text{Entropy} = -\sum_{i=1}^{g}\sum_{j=1}^{g}p_{i,j}\log_2 p_{i,j} \tag{8}$$

(g) **Maximum probability**: Measures the strongest response of G. The range of values is [0, 1].

$$\text{Max Pr} = \text{MAX}_{ij}(p_{i,j}) \tag{9}$$

(h) **Variance**: The variance is a measure of spread out of the distribution of pixels.

$$\text{Variance} = \sum_{i=1}^{g}\sum_{j=1}^{g}(i-\mu)^2 p_{i,j} \tag{10}$$

Thus eight features $f_1, f_2, f_3, f_4, f_5, f_6, f_7, f_8$ representing dissimilarity, contrast, energy, homogeneity, correlation, entropy, maximum probability, and variance, respectively, are extracted from each of the 80 G matrix and stored along with the type of the jersey. Table 1 shows the extracted data.

6 An Outline of Proximal Support Vector Machine

Consider the problem of separating the set of training vectors belonging to two separate classes, (x, y); $x \in \Re^n$; $y \in \{-1, +1\}$; i = 1, 2, …, m. Theoretically, infinity number of hyper planes in $\Re^n$ which are parameterized by w and b can be conceived that can separate the data into two classes. Our objective is to find a hyper plane that correctly classifies the data. To visualize it as a classification

Table 1 Extracted features from the images

S. No.	f_1	f_2	f_3	f_4	f_5	f_6	f_7	f_8	Type
01	0.03818	0.03961	0.45043	0.98111	0.95090	1.10950	0.62927	15.684	1
02	0.04202	0.04407	0.33801	0.97926	0.96266	1.28930	0.40421	18.375	1
03	0.04113	0.04292	0.37426	0.97967	0.95699	1.22490	0.53216	16.874	1
04	0.03900	0.04048	0.41137	0.98070	0.95493	1.16930	0.58609	16.085	1
05	0.02922	0.03017	0.46596	0.98555	0.95656	0.97018	0.58242	12.930	1
06	0.02908	0.02979	0.46710	0.98558	0.95700	0.96945	0.58509	12.954	1
07	0.03122	0.03228	0.48185	0.98455	0.95661	1.01890	0.63325	13.637	1
08	0.03352	0.03481	0.49609	0.98342	0.95167	1.02090	0.65933	14.260	1
09	0.03984	0.04064	0.35667	0.98022	0.96381	1.25300	0.43447	19.090	1
10	0.04326	0.04411	0.36481	0.97851	0.96599	1.32590	0.52660	20.947	1
11	0.03884	0.03997	0.38052	0.98077	0.96405	1.22020	0.50738	19.945	1
12	0.03839	0.03924	0.38117	0.98095	0.95956	1.19960	0.53127	17.366	1
13	0.03108	0.03177	0.50637	0.98457	0.95409	0.99416	0.66872	14.297	1
14	0.03749	0.03818	0.35218	0.98137	0.96459	1.25110	0.49348	16.813	1
15	0.04012	0.04108	0.37559	0.98010	0.96150	1.21570	0.47806	19.658	1
16	0.04246	0.04374	0.40492	0.97899	0.96269	1.27270	0.59277	24.021	1
17	0.03377	0.03434	0.48290	0.98321	0.95390	1.05070	0.65139	14.581	1
18	0.03850	0.03915	0.37466	0.98086	0.96055	1.20830	0.50942	17.763	1
19	0.03812	0.03877	0.36382	0.98105	0.96282	1.21650	0.44838	18.527	1
20	0.02997	0.03031	0.51598	0.98507	0.95596	0.98897	0.68365	14.680	1
21	0.02669	0.02698	0.50528	0.98670	0.95773	0.91586	0.64524	13.462	1
22	0.04006	0.04071	0.37172	0.98008	0.95917	1.19920	0.46264	18.559	1
23	0.03810	0.03875	0.39426	0.98106	0.95944	1.20370	0.56497	15.944	1
24	0.03885	0.03966	0.35344	0.98071	0.96273	1.24300	0.48750	17.230	1
25	0.03997	0.04085	0.38467	0.98016	0.96346	1.22360	0.52109	20.146	1
26	0.04182	0.04277	0.36127	0.97925	0.96289	1.26150	0.47192	19.541	1
27	0.03650	0.03727	0.42988	0.98188	0.95653	1.13880	0.60766	16.020	1
28	0.03376	0.03426	0.48071	0.98320	0.95386	1.05290	0.65706	15.367	1
29	0.03303	0.03350	0.49025	0.98357	0.95387	1.03720	0.66639	15.378	1
30	0.04084	0.04200	0.40465	0.97978	0.96268	1.22890	0.56735	21.118	1
31	0.03833	0.03952	0.38771	0.98103	0.96083	1.17130	0.48610	19.690	1
32	0.03824	0.03904	0.39931	0.98101	0.95777	1.17720	0.56242	17.110	1
33	0.04019	0.04085	0.34889	0.98002	0.96383	1.25930	0.40836	18.623	1
34	0.04069	0.04148	0.33222	0.97979	0.96536	1.29290	0.40484	18.086	1
35	0.03952	0.04054	0.38198	0.98041	0.96555	1.24660	0.52945	20.325	1
36	0.03791	0.03853	0.37333	0.98115	0.96486	1.21790	0.47966	19.598	1
37	0.03756	0.03819	0.38724	0.98133	0.96053	1.20530	0.55431	16.286	1
38	0.03643	0.03709	0.45139	0.98190	0.95335	1.09730	0.63034	15.893	1
39	0.03095	0.03132	0.50658	0.98459	0.95529	1.00500	0.67466	14.666	1
40	0.03736	0.03798	0.40436	0.98143	0.95840	1.17560	0.57635	15.933	1
41	0.03711	0.03973	0.44095	0.98178	0.94535	0.99729	0.49952	19.701	-1
42	0.03106	0.03222	0.70310	0.98465	0.91951	0.69814	0.83337	16.013	-1

(continued)

Table 1 (continued)

S. No.	f_1	f_2	f_3	f_4	f_5	f_6	f_7	f_8	Type
43	0.03603	0.03899	0.47665	0.98236	0.94398	0.94250	0.59375	21.243	-1
44	0.03694	0.03994	0.44333	0.98190	0.94571	0.99534	0.50387	20.356	-1
45	0.03585	0.03877	0.43973	0.98244	0.94737	0.99917	0.48751	19.792	-1
46	0.03062	0.03187	0.65618	0.98488	0.93115	0.77096	0.80155	16.221	-1
47	0.02044	0.02133	0.68421	0.98993	0.94654	0.64711	0.81337	14.771	-1
48	0.03017	0.03236	0.68928	0.98521	0.92292	0.71736	0.82413	16.092	-1
49	0.03637	0.03844	0.46180	0.98209	0.94654	0.97166	0.56577	20.986	-1
50	0.02160	0.02285	0.72456	0.98939	0.93711	0.60951	0.84343	15.089	-1
51	0.03722	0.03943	0.55611	0.98168	0.93078	0.87997	0.71291	17.635	-1
52	0.03825	0.04118	0.44856	0.98124	0.94401	0.99516	0.53539	20.669	-1
53	0.03630	0.03855	0.50520	0.98215	0.94062	0.95236	0.65949	17.985	-1
54	0.03956	0.04193	0.44984	0.98052	0.94215	1.01910	0.56840	18.871	-1
55	0.03560	0.03831	0.57463	0.98254	0.93248	0.88600	0.73701	17.005	-1
56	0.01958	0.02042	0.73251	0.99035	0.94150	0.58154	0.84790	15.035	-1
57	0.03631	0.03800	0.47775	0.98208	0.94532	0.99204	0.62485	18.220	-1
58	0.03857	0.04151	0.43693	0.98108	0.94385	1.01170	0.48882	19.760	-1
59	0.03453	0.03712	0.58139	0.98307	0.94289	0.88937	0.74071	23.356	-1
60	0.03955	0.04203	0.55088	0.98055	0.92762	0.90299	0.71070	17.543	-1
61	0.04038	0.04294	0.45354	0.98014	0.94010	1.01520	0.57743	18.775	-1
62	0.03785	0.03970	0.56522	0.98133	0.92951	0.88147	0.72419	17.423	-1
63	0.03984	0.04275	0.44033	0.98045	0.94137	0.99964	0.49040	20.223	-1
64	0.03764	0.04031	0.46510	0.98152	0.94254	0.95787	0.56942	21.025	-1
65	0.03840	0.04129	0.44364	0.98117	0.94275	1.00070	0.52603	19.425	-1
66	0.03933	0.04221	0.44816	0.98070	0.93916	0.97363	0.51517	19.676	-1
67	0.02388	0.02473	0.72176	0.98820	0.93269	0.63055	0.84278	15.243	-1
68	0.03768	0.03958	0.45853	0.98142	0.94351	0.98841	0.57431	18.943	-1
69	0.02787	0.02992	0.71371	0.98634	0.92277	0.67292	0.83983	15.741	-1
70	0.02070	0.02206	0.72650	0.98986	0.93781	0.59407	0.84405	15.031	-1
71	0.04013	0.04251	0.43707	0.98024	0.94254	1.02460	0.51780	19.429	-1
72	0.03824	0.04066	0.49715	0.98119	0.94323	0.96615	0.64172	21.819	-1
73	0.02251	0.02410	0.70655	0.98897	0.93724	0.64688	0.83205	15.158	-1
74	0.03825	0.04033	0.49000	0.98115	0.93941	0.97134	0.63893	18.199	-1
75	0.03796	0.03998	0.46402	0.98129	0.94126	0.97017	0.57877	18.995	-1
76	0.03622	0.03829	0.55245	0.98216	0.93456	0.89801	0.71250	17.474	-1
77	0.03256	0.03487	0.48555	0.98402	0.95022	0.93168	0.60948	21.361	-1
78	0.02436	0.02532	0.74479	0.98798	0.92731	0.60966	0.85900	15.609	-1
79	0.03231	0.03439	0.66136	0.98413	0.92417	0.76037	0.80459	16.424	-1
80	0.03669	0.03935	0.45655	0.98199	0.94216	0.95431	0.53882	19.499	-1

1 represents single jersey, *−1* represents double jersey

problem of m points in n dimensions (or attributes) of real space $\Re^n$ with their belongingness to either class +1 or −1, let us consider a standard soft margin support vector machine (SVM) [9–16] whose mathematical formalization with linear kernel may be represented by a quadratic problem

$$\begin{array}{ll} \text{Minimize}_{\xi,w,b} & \frac{1}{2}\|w\|^2+\frac{c}{2}\|\xi\| \\ \text{subjected to} & y(\langle x\cdot w\rangle - eb)+\xi \geq e \quad \text{and} \quad \xi \geq 0 \end{array} \tag{11}$$

Here, c is the penalty term and the parameter ξ is called the error variable, e is a vector of ones, w geometrically represents normal to the hyper planes effecting the separation of data. Two planes are defined as:

$$\left.\begin{array}{l} (x'w-b)=+1 \\ (x'w-b)=-1 \end{array}\right\} \tag{12}$$

where b is a constant measuring distance of the hyper planes from the origin. We can therefore draw the conclusion that the plane that is situated in the mid region is as follows:

$$x'w = b \tag{13}$$

It can be shown that distance of separation between the planes is $\frac{2}{\|w\|}$ and maximizing this distance will definitely improve the generalization capability of SVM [9–16]. If first norm of the error variable ξ is minimized with c in Eq. 11, then we get an approximate plane as in Eq. 13 such that:

$$\left.\begin{array}{l} (x'w-b)>0, \quad \text{then} \quad y\in+1 \\ (x'w-b)<0, \quad \text{then} \quad y\in-1, \\ (x'w-b)=0, \quad \text{then} \quad y\in+1 \text{ or } -1 \end{array}\right\} \tag{14}$$

At this juncture, problem of optimization can be modified as under:

$$\begin{array}{ll} \text{Minimize}_{\xi,w,b} & \frac{1}{2}\left\|\begin{matrix} w \\ b \end{matrix}\right\|^2+\frac{c}{2}\|\xi\|^2 \\ \text{Subjected to} & y(\langle x.w\rangle - eb)+\xi \geq e \end{array} \tag{15}$$

Here, no explicit non-negativity constraint is needed on ξ, and second norm of the error vector ξ is minimized instead of first one and margin between the hyper planes also maximized with respect to w and b. This new formulation adds advantages of strong convexity of objective function without upsetting any other aspects of the standard formulations in Eq. 11.

We are now in a position to introduce PSVM [9–16] by completely replacing inequality constraint by equality one which though simple is very significant as it admits of explicit exact solutions of it in terms of available data; however, in case of equations with inequality constraints, this was impossible as their interdependence

was too involved. From the perspective of geometry, we can visualize PSVM as a classifier that does its task by judging the proximity of the test points to one of the twin hyper planes that are widened apart to the utmost. Mathematically, the distance between these twin planes are denoted by $\frac{1}{2}\left\|\begin{matrix} w \\ b \end{matrix}\right\|^2$, which is also the reciprocal of the second norm distance squared (Fig. 5). Therefore, mathematically PSVM is an optimization problem with objective function

$$\begin{aligned} &\text{Minimize}_{\xi,w,b} \quad \tfrac{1}{2}\left\|\begin{bmatrix} w \\ b \end{bmatrix}\right\|^2 + \tfrac{C}{2}\xi^2 \\ &\text{subjected to} \quad y(\langle x.w\rangle - eb) + \xi = e \quad \text{and} \quad \xi \geq 0 \end{aligned} \tag{16}$$

Standard SVM's mathematical characterization can be explained by linear programming perturbation theory which yields a least 2-norm approximate solution to the system of linear inequalities, the same is applicable for PSVM. But a regularized least squares of a system of linear equations $y(\langle x.w\rangle - eb) + \xi = e$, yields an approximate solution of (w, b) with least 2-norm. Figure 5 shows the PSVM classifier in $(\underline{w}, b)$ space.

Now applying Karush–Kuhn–Tucker (KKT) conditions for optimality in our equality constraints, we can write the following Lagrangian:

$$L(w, b, \xi, \lambda) = C\frac{1}{2}\xi^2 + \frac{1}{2}\left\|\begin{bmatrix} w \\ b \end{bmatrix}\right\|^2 - \lambda(y(w.x - b) + \xi - e \tag{17}$$

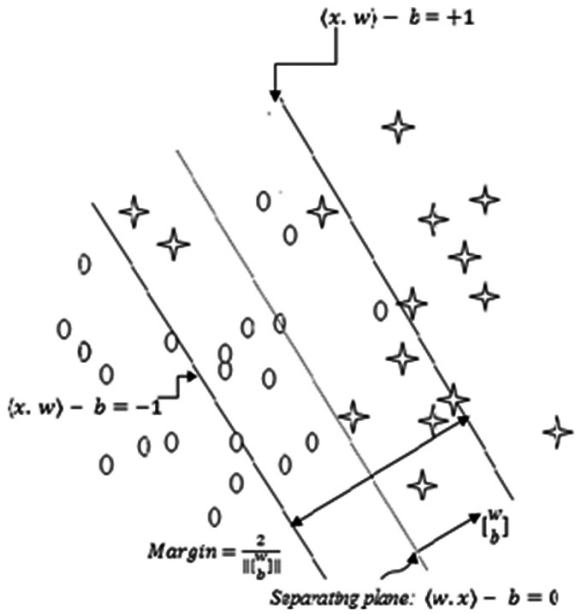

Fig. 5 PSVM classifier in (w, b) space

where $\lambda \in R^m$ is called Lagrange multiplier. Differentiating $L(w, b, \xi, \lambda)$ with respect to each variable and equating each of them to zero, we get:

$$\begin{aligned} \frac{\partial L}{\partial w} &= w - xy\lambda = 0 \\ \frac{\partial L}{\partial b} &= b + e'y\lambda = 0 \\ \frac{\partial L}{\partial \xi} &= C\xi - \lambda = 0 \\ \frac{\partial L}{\partial \lambda} &= y(w \cdot x - b) + \xi - e = 0 \end{aligned} \tag{18}$$

Thus, we get

$$w = xy\lambda, \quad b = -e'y\lambda, \quad \xi = \frac{\lambda}{C} \tag{19}$$

Substituting these in the last equality of Eq. (18), we get a clear expression of λ in terms of problem variables x and y as given below:

$$\lambda = \left(\frac{I}{C} + y(x \cdot x' + ee')y\right)^{-1} e = \left(\frac{I}{C} + HH'\right)^{-1} e \tag{20}$$

where H is defined as:

$$H = y[x - e] \tag{21}$$

To avoid the inversion of matrix which is as massive as $m \times m$ in Eq. (20), we can circumvent this by using Sherman–Morrison–Woodbury formula giving following expression for λ as:

$$\lambda = C\left(I - H\left(\frac{I}{C} - HH'\right)^{-1} H'\right)e \tag{22}$$

where I is an identity matrix.

7 Results and Discussion

A k-fold cross-validation was applied to assess the performance of the PSVM classifier for classifying single and double jersey fabrics. In k-fold cross-validation, the initial dataset is randomly partitioned into k mutually exclusive subsets or folds

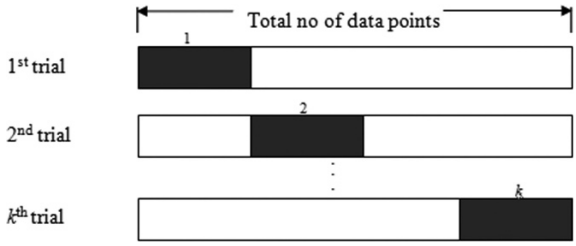

Fig. 6 Schematic representation of *k*-fold cross-validation

D_1, D_2, …, D_k, each of approximately equal size. The training and testing are performed k times. In iteration i, partition D_i is reserved as the test set and the remaining partition are collectively used to train the model. In this method, each data point is used the same number of times for training and once for testing. Therefore, the validation of the model becomes more accurate and unbiased. The *k*-fold cross-validation method is schematically depicted in Fig. 6, where 1, 2, … k represent the fold corresponding to testing data.

The classifier was trained using 9 of the folds and tested on the sample fold left out for each cycle; therefore, the training and testing were performed for 10 cycles. The expected generalization accuracies referring to training as well as testing were estimated as $\mu \pm \sigma$, where μ and σ are the mean and standard deviation of the accuracies over 10 trials. Several values of the penalty term (C) were tried out, and the best performance was obtained with $C = 500$. The training accuracy was expectedly higher than the testing accuracy because latter is done on the unseen data. The average grand accuracies of training and testing dataset for PSVM are 99.375 % ± 0.6709 and 98.75 % ± 3.9528, respectively. The results shows that the fabric classification accomplished by means of image recognition through PSVM agrees eminently well with only very little room for an error. It holds immense potentiality even when large scale exercise is required for classification of single and double jersey fabrics. Nevertheless, the time required for execution of PSVM algorithm is fantastically small in comparison with that of standard SVM [9–16]. This is ascribed to the fact that PSVM reduces the quadratic optimization problem in standard SVM to as simple as a system of linear equations.

8 Conclusions

Application of soft computation in the field of textile engineering is becoming very important during the last decade, and the present study holds the key of effective checking mechanism to differentiate single and double jersey fabrics. Although single and double jersey fabrics are difficult to identify in open eye and but a machine makes the process of identification of single and double jersey easy.

PSVM is a potential and efficient classifier to distinguish the single and double jersey fabrics. The time required for execution of PSVM algorithm is awfully small. While classifying single and double jersey fabric images, the performance rating of PSVM adjudged in terms of training and testing accuracies is reasonably well. Moreover, PSVM is much less vulnerable to over fitting.

References

1. Ghosh, A., Guha, T., Bhar, R.B., Das, S.: Pattern classification of fabric defects using support vector machines. Int. J. Cloth. Sci. Tech. **23**, 142–151 (2011)
2. Salem, Y.B., Nasri, S.: Automatic classification of woven fabrics using multi-class support vector machine. Res. J. Text. Apparel **13**, 28–36 (2009)
3. Orjuela, V.S.A., Vansteenkiste, E., Rooms, F., Philips, W., de Keyser, R., de Meuleneester, S.: Carpet wear classification using co-occurrence matrices and support vector machines. Text. Res. J. **80**, 2132–2143 (2010)
4. Bu, H.G., Huang, X.B., Wang, J., Chen, X.: Detection of fabric defects by auto regressive spectral analysis and support vector data description. Text. Res. J. **80**, 579–589 (2010)
5. Tsai, S., Lin, C.H., Lin, J.J.: Applying an artificial neural network to pattern recognition in fabric defects. Text. Res. J. **65**(3), 123–130 (1995)
6. Sobus, J., Pourdeyhimi, B., Gerde, J., Uclay, Y.: Assessing changes in texture periodicity due to appearance loss in carpets: gray level co-occurrence analysis. Text. Res. J. (1991). doi:10.1177/004051759106101001
7. Ghosh, A., Hasnat, A., Guha, T.: Pattern classification of fabric defects using probabilistic neural network. In: Proceedings of 2nd National Conference on Emerging Trends in Textile, Fibre and Apparel Engineering, pp. 236–242 (2013)
8. Gonzalez, R.C., Woods, R.E.: Digital Image Processing, 3rd edn. Prentice Hall, New Jersey (2009)
9. Fung, G., Mangasarian, O.L.: Proximal support vector machine classifier. In: Proceedings of the International Conference on Knowledge Discovery and Data Mining, pp. 77–86 (2001)
10. Fung, G., Mangasarian, O.L.: Multi-category proximal support vector machine classifiers. Mach. Learn. **59**, 77–97 (2005)
11. Vapnik, V.: The Nature of Statistical Learning Theory, 2nd edn. Springer, New York (1999)
12. Cristianini, N., Shawe-Taylor, J.: An Introduction to Support Vector Machines and Other Kernel Based Learning Methods. Cambridge University Press, Cambridge (2000)
13. Suykens, J.A.K., Vandewalle, J.: Least-square support vector machine classifiers. Neural Process. Lett. **9**, 293–300 (1999)
14. Suykens, J.A.K., Van Gestel, T., De Brabanter, J., De Moor, J., Vandewalle, J.: Least Squares Support Vector Machines. World Scientific Publishing Co., Singapore (2002)
15. Johnson, R.A., Wichern, D.M.: Applied Multivariate Statistical Analysis, 6th edn. Prentice Hall, New Jersey (2007)
16. Han, J., Kamber, M.: Data Mining Concepts and Techniques, 2nd edn. Morgan Kaufmann Publishers, San Francisco (2006)

Dynamic Modelling & Simulation of Induction Motor Drives

P.M. Menghal and A. Jaya Laxmi

Abstract Induction motors (IMs) have many applications in the industries, because of the low maintenance and robustness. The speed control of IM is more important to achieve maximum torque and efficiency. The rapid development of power electronic devices and converter technologies in the past few decades, however, has made possible efficient speed control by varying the supply frequency and voltage, giving rise to various forms of adjustable-speed IM drives. In about the same period, there were also advances in control methods and artificial intelligent (AI) techniques, including expert system, fuzzy logic, neural networks, and genetic algorithm. Researchers soon realized that the performance of IM drives can be enhanced by adopting artificial intelligent-based methods. This paper presents dynamic modeling and simulation of IM using AI controller. The integrated environment allows users to compare simulation results between classical and AI controllers. The fuzzy logic controller and artificial neural network controllers (NNCs) are also introduced to the system for keeping the motor speed to be constant when the load varies. The performance of fuzzy logic and artificial neural network (ANN)-based controllers is compared with that of the conventional proportional integral controller. The performance of the IM drive has been analyzed for constant, variable loads, and induction generator mode.

Keywords Dynamic modeling · Proportional integrator (PI) controller · Fuzzy logic controller (FLC) · Neuro-network (NN) · Intelligent controller · Adaptive neuro-fuzzy inference system (ANFIS)

P.M. Menghal (✉)
Faculty of Degree Engineering, Military College of Electronics and Mechanical Engineering, Secunderabad 500 015, India
e-mail: prashant_menghal@yahoo.co.in

P.M. Menghal
Department of EEE, JNTU, Anantapur 515002, Andhra Pradesh, India

A. Jaya Laxmi
College of Engineering, Jawaharlal Nehru Technological University, Kukatpally, Hyderabad 500085, Andhra Pradesh, India
e-mail: ajl1994@yahoo.co.in

K.N. Das et al. (eds.), *Proceedings of Fourth International Conference on Soft Computing for Problem Solving*, Advances in Intelligent Systems and Computing 335,
DOI 10.1007/978-81-322-2217-0_34

1 Introduction

Induction motors (IMs) have been used as the workhorse in industry for a long time due to their easy build, high robustness, and generally satisfactory efficiency [1]. In recent years, scientists and researchers have acquired significant development on various sorts of control theories and methods. Among these control technologies, intelligent control methods, which are generally regarded as the aggregation of fuzzy logic control, neural network control, genetic algorithm, and expert system, have exhibited particular superiorities. Therefore, control strategy must be adaptive and robust. As a result, several control strategies have been developed for IM drives with in last two decades. This paper presents the speed control scheme of scalar-controlled IM drive in open-loop and closed-loop modes and involves decoupling of the speed and ref speed into torque and flux producing components. Fuzzy logic, ANN, and adaptive neuro fuzzy inference system (ANFIS)-based control scheme has been simulated. The performance of fuzzy logic-, ANN-, and ANFIS-based controllers is compared with that of the conventional proportional integral controller in open loop and closed loop. The dynamic modeling of IM is done, and the performance of the IM drive has been analyzed for constant, variable loads, and induction generator mode. Figure 1 shows proposed control scheme for an IM in open loop and closed loop [2–5].

2 Dynamic Modeling and Simulation of Induction Motor Drive

The IMs' dynamic behavior can be expressed by voltage and torque which are time varying. The differential equations that belong to dynamic analysis of IM are so sophisticated. Then with the change of variables, the complexity of these equations

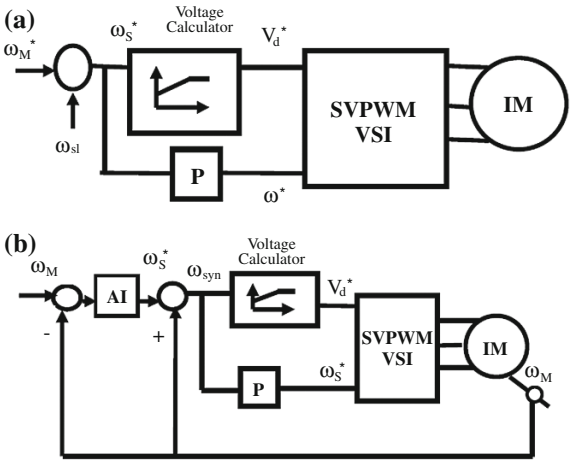

Fig. 1 Basic v/v control of induction motor. **a** Open loop v/f control. **b** Closed v/f control

decreases through movement from poly-phase winding to two-phase winding (q–d). In other words, the stator and rotor variables such as voltage, current, and flux linkages of an induction machine are transferred to another reference model which remains stationary [1, 6–10].

In Fig. 2, stator inductance is the sum of the stator leakage inductance and magnetizing inductance ($L_{ls} = L_s + L_m$), and the rotor inductance is the sum of the rotor leakage inductance and magnetizing inductance ($L_{lr} = L_r + L_m$). From the equivalent circuit of the IM in d–q frame, the model equations are derived. The flux linkages can be achieved as:

$$\frac{1}{\omega_b}\frac{d\psi_{qs}}{dt} = v_{qs} - \frac{\omega_e}{\omega_b}\psi_{ds} - R_s i_{qs} \tag{1}$$

$$\frac{1}{\omega_b}\frac{d\psi_{ds}}{dt} = v_{ds} - \frac{\omega_e}{\omega_b}\psi_{qs} - R_s i_{ds} \tag{2}$$

$$\frac{1}{\omega_b}\frac{d\psi_{qr}}{dt} = v_{qr} - \frac{(\omega_e - \omega_r)}{\omega_b}\psi_{dr} - R_s i_{qr} \tag{3}$$

$$\frac{1}{\omega_b}\frac{d\psi_{dr}}{dt} = v_{dr} + \frac{(\omega_e - \omega_r)}{\omega_b}\psi_{qr} - R_s i_{dr} \tag{4}$$

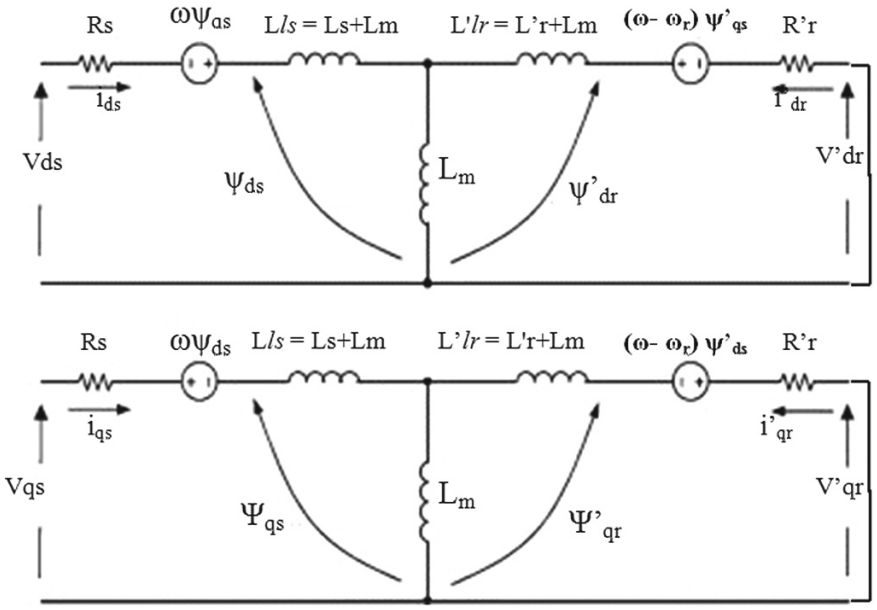

Fig. 2 d–q Model of induction motor

By substituting the values of flux linkages in the above equations, the following current equations are obtained as follows:

$$i_{\mathrm{qs}} = \frac{\left(\psi_{\mathrm{qs}} - \psi_{\mathrm{mq}}\right)}{X_{\mathrm{ls}}} \tag{5}$$

$$i_{\mathrm{ds}} = \frac{(\psi_{\mathrm{ds}} - \psi_{\mathrm{md}})}{X_{\mathrm{ls}}} \tag{6}$$

$$i_{\mathrm{qr}} = \frac{\left(\psi_{\mathrm{qr}} - \psi_{\mathrm{mq}}\right)}{X_{\mathrm{ls}}} \tag{7}$$

$$i_{\mathrm{dr}} = \frac{(\psi_{\mathrm{dr}} - \psi_{\mathrm{md}})}{X_{\mathrm{ls}}} \tag{8}$$

where ψ_{mq} and ψ_{md} are the flux linkages over L_{m} in the q and d axes, respectively. The flux equations are written as follows:

$$\psi_{\mathrm{mq}} = X_{\mathrm{ml}}\left(\frac{\psi_{\mathrm{qs}}}{X_{\mathrm{ls}}} + \frac{\psi_{\mathrm{qr}}}{X_{\mathrm{lr}}}\right) \tag{9}$$

$$\psi_{\mathrm{md}} = X_{\mathrm{ml}}\left(\frac{\psi_{\mathrm{ds}}}{X_{\mathrm{ls}}} + \frac{\psi_{\mathrm{dr}}}{X_{\mathrm{lr}}}\right) \tag{10}$$

$$X_{\mathrm{ml}} = \frac{1}{\frac{1}{X_m} + \frac{1}{X_{\mathrm{ls}}} + \frac{1}{X_{\mathrm{lr}}}} \tag{11}$$

In the above equations, the speed ω_r is related to the torque by the following mechanical dynamic equation as follows:

$$T_e = T_{\mathrm{load}} + \mathrm{J}\frac{\mathrm{d}\omega_{\mathrm{m}}}{\mathrm{d}t} = T_{\mathrm{load}} + \frac{J2}{p}\frac{\mathrm{d}\omega_r}{\mathrm{d}t} \tag{12}$$

then ω_r is achievable from above equation, where

p number of poles

J moment of inertia (kg/m^2)

In the previous section, dynamic model of an IM is expressed. The model constructed according to the equations has been simulated by using MATLAB/SIMULINK as shown in Fig. 3 in open-loop and closed-loop modes with PI controller of operation of IM. A 3 phase source is applied to conventional model of an IM and the equations are given by

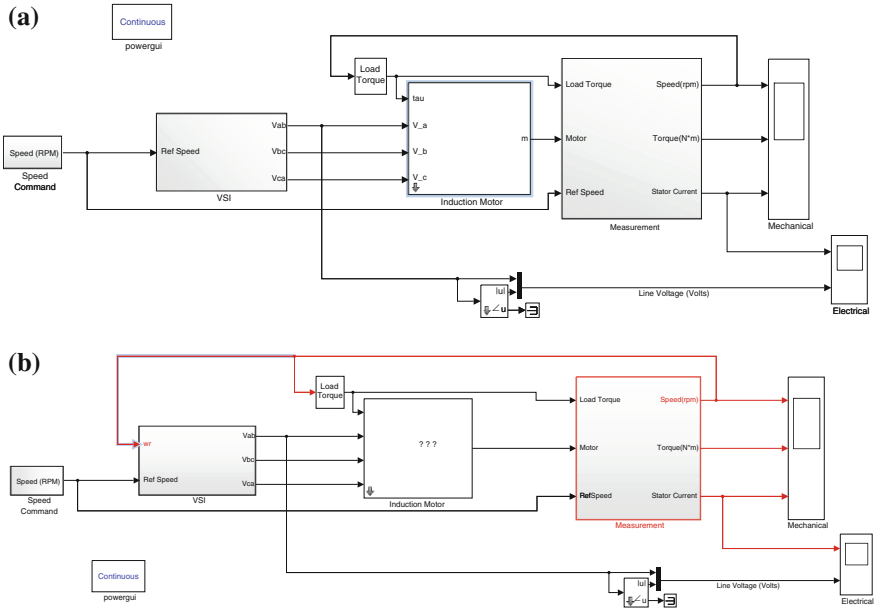

Fig. 3 Simulated induction motor model with PI controller. **a** Open-loop control. **b** Closed-loop control

$$V_a = \sqrt{2}V_{\text{rms}} \sin(\omega t) \tag{13}$$

$$V_b = \sqrt{2}V_{\text{rms}} \sin\left(\omega t - \frac{2\pi}{3}\right) \tag{14}$$

$$V_c = \sqrt{2}V_{\text{rms}} \sin\left(\omega t + \frac{2\pi}{3}\right) \tag{15}$$

By using Parks transformation, voltages are transformed to two phases in the d–q axes and are applied to IM. In order to obtain the stator and rotor currents of IM in two phases, inverse Park transformation is applied in the last stage [1, 6–10].

PI controllers are varied much sensitive to parameter variations inherent in real plant operations. The gain equation for the PI controller is given by

$$T = K_p e + K_{texti} \int e \, \mathrm{d}t$$

The output of the PI controller is updated by varying the PI controller gains (K_p and K_i) based on the control law in the presence of parameter variation and drive nonlinearity. The use of PI controllers for speed control of induction machine drives is characterized by an overshoot during tracking mode and a poor load

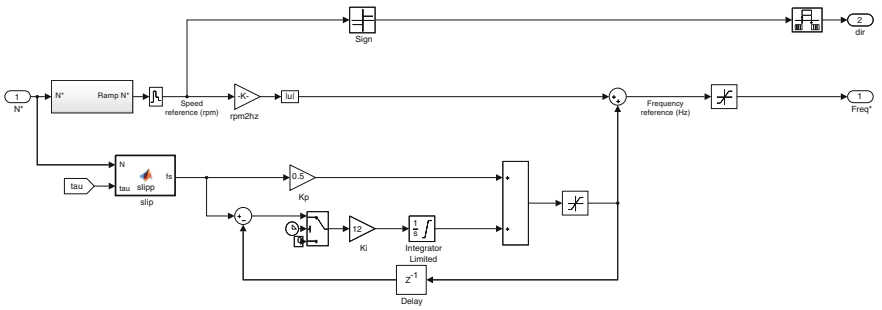

Fig. 4 PI controller

disturbance rejection. This is mainly caused by the fact that the complexity of the system does not allow the gains of the PI controller to exceed a certain low value.

If the gains of the controller exceed a certain value, the variations in the command torque controller gains are very high. The motor reaches the reference speed rapidly without overshoot, as step commands are tracked with almost zero steady state error, as load disturbances are rapidly rejected and variations of some of the motor parameters are fairly well dealt with become too high and will be destabilize the system. To overcome this problem, we propose the use of a limiter ahead of the PI controller [4]. This limiter causes the speed error to be maintained within the saturation limits. Figure 4 shows the structure of PI controller.

3 Artificial Intelligent Controller

Despite the great efforts devoted to IM control, many of the theoretical results cannot be directly applied to practical systems. Intelligent control techniques are generally classified as expert system control, fuzzy logic control, neural network control, and genetic algorithm. Various AI controllers are as follows

(a) *Fuzzy Logic Controller*: The speed of IM is adjusted by the fuzzy controller. In Table 1, the fuzzy rules' decision implemented into the controller is given. The conventional simulated IM model as shown in Fig. 3 is modified by adding

Table 1 Modified fuzzy rule decision

		Δ_e				
		NB	NS	ZZ	PS	PB
e	PB	ZZ	NS	NS	NB	NB
	PS	PS	ZZ	NS	NS	NB
	ZZ	PS	PS	ZZ	NS	NS
	NS	PB	PS	PS	ZZ	NS
	NB	PB	PB	PS	PS	ZZ

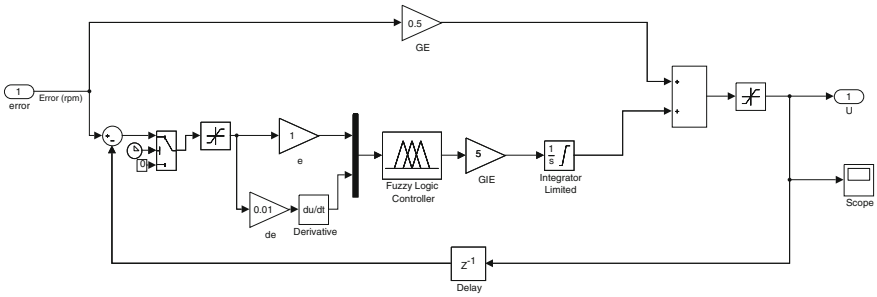

Fig. 5 Fuzzy controller

fuzzy controller and is shown in Fig. 5. Speed output terminal of IM is applied as an input to fuzzy controller, and in the initial start of IM, the error is maximum, so according to fuzzy rules, FC produces a crisp value. Then, this value will change the frequency of sine wave in the speed controller. The sine wave is then compared with triangular waveform to generate the firing signals of IGBTs in the PWM inverters. The frequency of these firing signals also gradually changes, thus increasing the frequency of applied voltage to IM [5, 11]. As discussed earlier, the crisp value obtained from fuzzy logic controller is used to change the frequency of gating signals of PWM inverter. Thus, the output AC signals obtained will be variable frequency sine waves. The sine wave is generated with amplitude, phase, and frequency which are supplied through a GUI. Then, the clock signal which is sampling time of simulation is divided by crisp value which is obtained from FLC. So by placing three sine waves with different phases, one can compare them with triangular waveform and generate necessary gating signals of PWM inverter. So at the first sampling point, the speed is zero and error is maximum. Then, whatever the speed rises, the error will decrease, and the crisp value obtained from FLC will increase. So the frequency of sine wave will decrease which will cause IGBTs switched ON and OFF faster. It will increase the AC supply frequency, and the motor will speed up. The inputs to these blocks are the gating signals which are produced in speed controller block. The firing signals are applied to IGBT gates that will turn ON and OFF the IGBTs.

(b) *Artificial Neural Network* (*ANN*): The ANN can be trained by a learning algorithm which performs the adaptation of weights of the network iteratively until the error between target vectors and the output of the ANN is less than a predefined threshold. The most popular supervised learning algorithm is back propagation, which consists of a forward and backward action. The objective of this NNC is to develop a back propagation algorithm such that the output of the neural network speed observer can track the target one. Figure 6 depicts the network structure of the NNC, which indicates that the neural network has

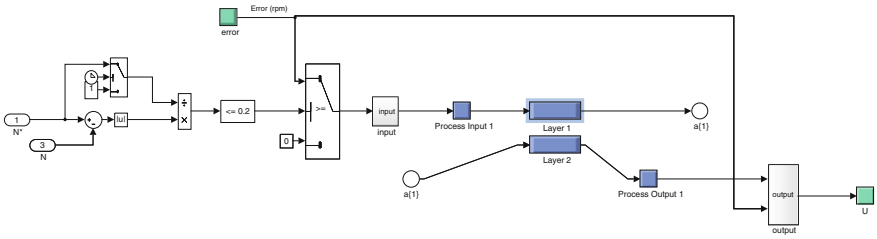

Fig. 6 Neural network controller

three layered network structure. It can be seen that the d-axis and q-axis voltage equations are coupled by the terms d_E and q_E. These terms are considered as disturbances and are canceled by using the proposed decoupling method. If the decoupling method is implemented, the flux component equations become

$$\Phi_{\mathrm{dr}} = G(s)v_{\mathrm{ds}}$$
$$\Phi_{\mathrm{qr}} = G(s)v_{\mathrm{qs}}$$

Large values of η may accelerate the ANN learning and consequently fast convergence but may cause oscillations in the network output, whereas low values will cause slow convergence. Therefore, the value of η has to be chosen carefully to avoid instability. The proposed NNC is shown in Fig. 6 [11, 12].

(c) *Adaptive Neuro Fuzzy Inference System* (*ANFIS*): With the advent of AI techniques, these drawbacks can be mitigated. One such technique is the use of fuzzy logic in the design of controller either independently or in hybrid with PI controller. Adaptive ANFIS replaces the drawbacks of fuzzy logic control and ANN. Adaptive neuro-fuzzy combines the learning power of neural network with knowledge representation of fuzzy logic. Neuro-fuzzy techniques have emerged from the fusion of artificial neural networks (ANNs) and fuzzy inference systems (FIS) and have become popular for solving the real-world problems. A neuro-fuzzy system is based on a fuzzy system which is trained by a learning algorithm derived from neural network theory. There are several methods to integrate ANN and FIS, and very often, the choice depends on the applications. In this paper, the inputs will be $e(k)$ and $\Delta_e(k)$ [5]. Figure 7 shows the overall structure of adaptive neuro-fuzzy model.

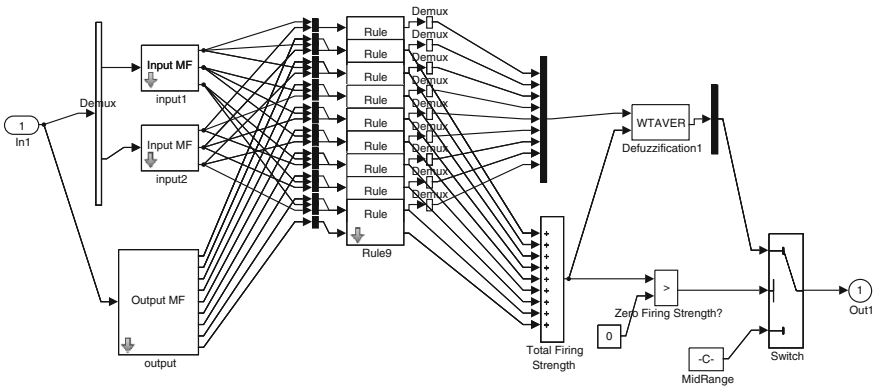

Fig. 7 Adaptive neuro-fuzzy model

4 Performance Assessment of Artificial Intelligent Controller-Based Induction Motor Drive

A complete simulation model for scalar v/f-controlled IM drive incorporating PI, fuzzy logic controller, NNC, and ANFIS is developed in open-loop and closed-loop modes. The performance of the AI-based IM drive is investigated at different operating conditions. In order to prove the superiority of the ANFIS, a comparison is made with the response of conventional PI, FLC, and neural network-based IM drive. The parameters of the IM considered in this study are summarized in Appendix. The performances of the scalar-controlled IM with all intelligent controllers are presented at constant load and variable load in open- and closed-loop modes. The dynamic behaviors of the PI controller, FLC controller, NNC, and ANFIS are shown in Figs. 8, 9, 10, 11, 12, and 13 at constant load, variable load conditions, and induction generator mode.

1. *At constant load conditions*: A drive with PI controller has a peak overshoot, but in case of fuzzy controller, NNC and ANFIS, it is eliminated as shown in Figs. 10 and 13. The PI controller is tuned at rated conditions in order to make a fair comparison. Figures 8, 9, 10, 11, 12, and 13 shows the simulated starting performance of the drive with conventional PI, FLC, neural network, and ANFIS-based drive systems, in open loop and closed loop, respectively. Although the PI controller is tuned by trial and error to give an optimum response at this rated condition, the ANFIS controller yields better performance in terms of faster response time and lower starting current. It is worth mentioning here that the performance obtained by the proposed AI controller is faster than the PI controller, i.e., it achieves the steady-state condition faster than the PI controller.
2. *At variable load conditions*: Drive with PI controller speed response has small peak at 0.6 s, but in case of fuzzy controller, neural network, and ANFIS controller speed response, it is quick and smooth response which is shown in Fig. 10.

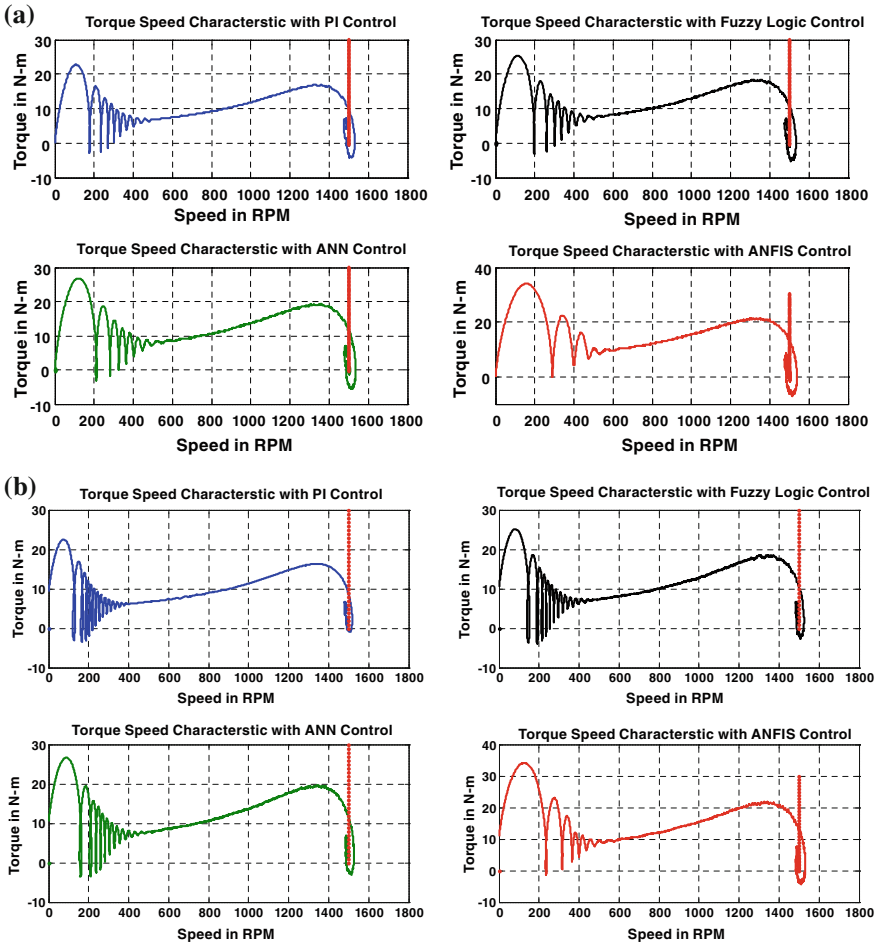

Fig. 8 Torque–speed characteristics: AI controller. **a** Constant load. **b** Variable load

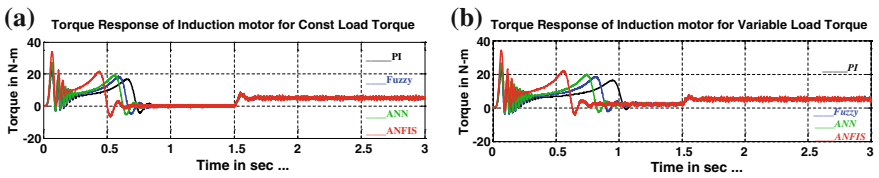

Fig. 9 Torque responses: AI controller. **a** Constant load. **b** Variable load

Figures 8, 9 and 10 show the waveforms of speed, torque, and torque–speed characteristics with four controllers. Figure 10 shows the speed response for step change in the load torque using the PI, fuzzy, neural network, and ANFIS

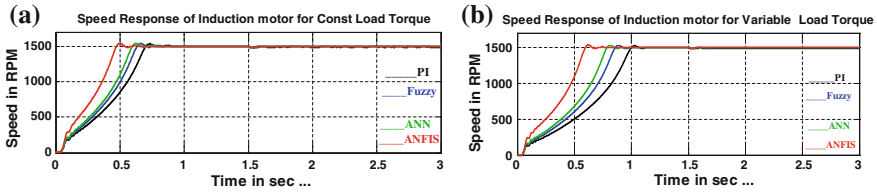

Fig. 10 Speed responses: AI controller. **a** Constant load. **b** Variable load

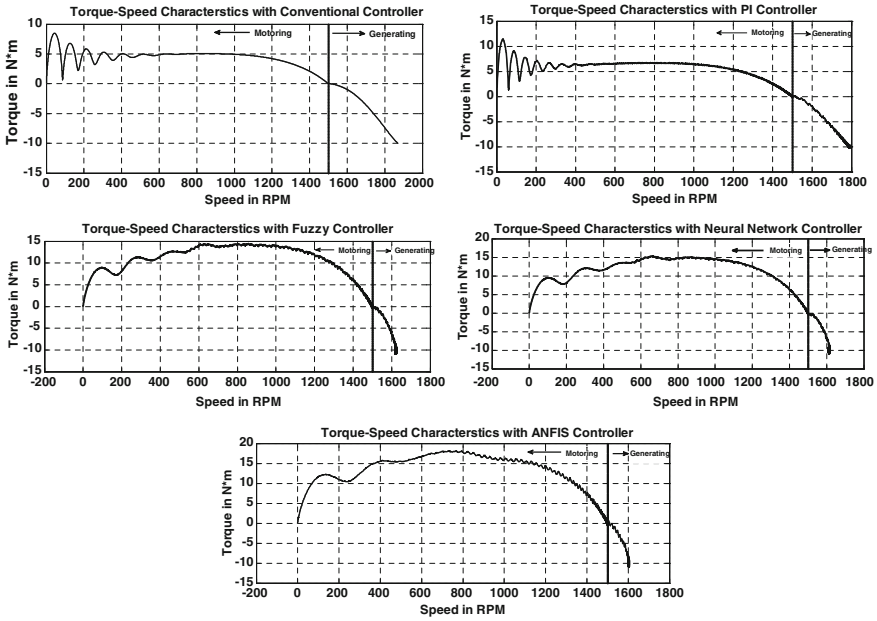

Fig. 11 Torque–speed characteristics: AI controller in motoring and generation mode

controllers, respectively. The motor starts from standstill at load torque = 5 Nms and at $t = 0.6$ s, a sudden full load of 15 Nms is applied to the system; then, it is controlled by fuzzy, neural network, and ANFIS controller. Since the time taken by the PI-controlled system to achieve steady state is much higher than fuzzy, neural network, and ANFIS-controlled system, the step change in load torque is applied at $t = 3$ s. The motor speed follows its reference with zero steady-state error and a fast response using a fuzzy controller, neural network, and ANFIS. On the other hand, the PI controller shows steady-state error with a high starting current. It is to be noted that the speed response is affected by the load conditions. This is the drawback of a PI controller with varying operating conditions. It is to be noted that the neuro-controller and ANFIS give better responses in terms of overshoot, steady-state error and fast response when compared with PI and fuzzy.

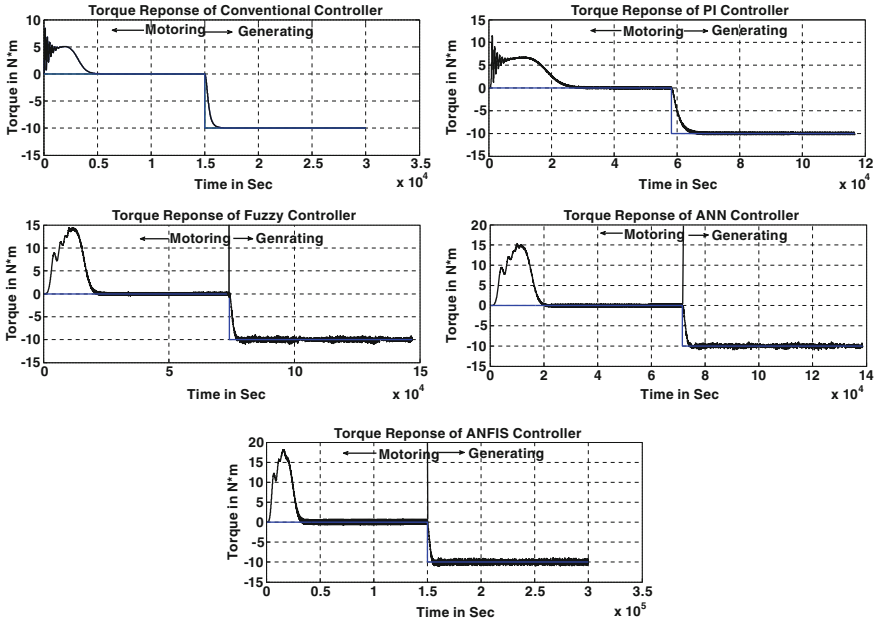

Fig. 12 Torque characteristics: AI controller in motoring and generation mode

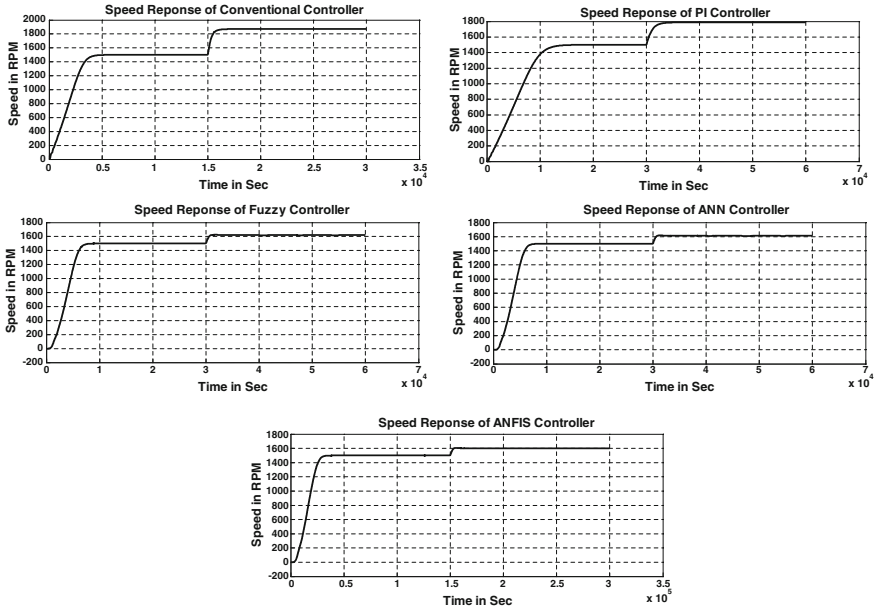

Fig. 13 Speed characteristics: AI controller in motoring and generation mode

These figures also show that the neuro-and ANFIS controller-based drive system can handle the sudden increase in command speed quickly without overshoot, under-shoot, and steady-state error, whereas the PI and fuzzy controller-based drive system has steady-state error and the response is not as fast as compared to neural network and ANFIS. Thus, the proposed ANFIS-based drive has been found superior to the conventional PI controller, FLC, and ANFIS-based system. Recently, because of the increasing importance of distributed energy resources such as wind turbines and micro turbines, there is renewed attention to induction generators. The model described in this paper can also be used to model an induction generator. The only change, compared with motoring operation, is that an external mover rotates the motor at a speed higher than the synchronous speed. This change can be implemented in SIMULINK by using a negative load torque instead of a positive one used for motoring. Figure 11 shows the torque–speed curve of the induction machine in both motoring and generating regions. The machine accelerates freely to almost the synchronous speed initially and then a large negative torque is applied so that the machine works as generator.

5 Conclusion

It is apparent that by adding learning algorithm to the control system will decrease the rising time more than expectation and it proves ANFIS controller has better dynamic performance as compared to NN, FLC, and conventional PI controller. The comparative results prove that the performance of scalar v/f-controlled drive transient and dynamic response of induction machine, with ANFIS controller is superior to that with conventional PI, fuzzy, and NNC. For variable loads, when there is a sudden change in load, the ANFIS controller reaches its steady-state value faster and there are no overshoots as compared to the PI, Fuzzy and NN controller. This proves the robustness of ANFIS controller.

Finally, the operation of the model to simulate both IMs and generators has been shown with AI controllers so that there is no need for different models for different applications.

6 Appendix

The following parameters of the induction motor are chosen for the simulation studies:

Three phase star connected squirrel cage IM kW = 0.5 HP, 0.147 kW, rated stator voltage = 230 V, frequency = 50 Hz, rated current = 2A, N = 4, speed = 1,500 rpm $J = 0.001$ kg m^2, $f = 0.000124$ $R_s = 14.6$ Ω/phase, $R_r = 12.76$ Ω/phase, $L_m = 0.2963$ H, $L_s = 0.0222$H, $L_r = 0.058$.

References

1. Chan, T.F, Shi, K.: Applied Intelligent Control of Induction Motor Drives. IEEE Willey Press New Jersey (2011)
2. Jordan, H.E.: Analysis of induction machines in dynamic systems. IEEE Trans. Power Apparatus Syst. **Pas-84**(11), 1080–1088 (1965). doi: 10.1109/TPAS.1965.4766139
3. Menghal, P., Jaya Laxmi, A.: Neural network based dynamic performance of induction motor. In: Springer Proceeding Advances in Intelligent Systems and Computing (AISC) vol. 259, pp. 539–552 (2014). doi:10.1007/978-81-322-1768-8_48
4. Shi, K.L, Chan, T.F., Wong, Y.K., HO S.L.: Modeling and simulation of the three phase induction motor using SIMULINK. Int. J. Elect. Eng. Educ. **36**, 163–172 (1999)
5. Dandil, B., Gokbulut, M,. Ata, F.: A pi type fuzzy –neural controller for induction motor drives. J Appl. Sci. (2005). doi:10.3923/jas.2005.1286.1291
6. Menghal, P.M., Jaya Laxmi, A.: Neural network based dynamic simulation of induction motor drives. IEEE International Conference on Power, Energy and Control (2013). doi:10.1109/ICPEC.2013.6527722
7. Menghal, P.M., Jaya Laxmi A.: Adaptive neuro fuzzy interference (ANFIS) based simulation of induction motor drive. Int Rev Model Simul (IRMOS). **5**(5),2007–2016 (2012)
8. Uddin, M.N., Hafeez, M.: FLC-Based DTC scheme to improve the dynamic performance of an IM drive. IEEE Trans. Ind. Appl. (2012). doi:10.1109/TIA.2011.2181287
9. Uddin, M.N.: Hao wen: development of a self-tuned neuro-fuzzy controller for induction motor drives. IEEE Trans. Ind. Appl. (2007). doi:10.1109/TIA.2007.900472
10. Krause, P.C.: Analysis of Electrical Machinery and Drives System. IEEE Willey Press, New Jersey (2000)
11. Menghal, P.M., Jaya Laxmi, A.: Adaptive neuro fuzzy based dynamic simulation of induction motor drives. IEEE International Conference on Fuzzy Systems, pp. 1–8(2013). doi:10.1109/FUZZ-IEEE.2013.6622452
12. Uddin, M.N., Radwan T.S., Rahman, A.: Performance of fuzzy logic based indirect vector control for induction motor drive. IEEE Trans. Ind. Appl. (2002). doi:10.1109/TIA.2002.802990

Design of PID and FOPID Controllers Tuned by Firefly Algorithm for Magnetic Levitation System

Lalbahadur Majhi, Prasanta Roy and Binoy Krishna Roy

Abstract This paper concerns design and implementation of PID and fractional-order PID (FOPID) controllers to control position of an electromagnetically suspended ferromagnetic ball in a magnetic levitation (Maglev) system in real time. The Maglev system, manufactured by Feedback Instruments (Model No 33-210) is used as a platform to test the performance of proposed controllers. Parameters of PID and FOPID controllers are tuned by firefly algorithm (FA). FA is a meta-heuristic algorithm based on movement of fireflies toward more attractive and brighter ones. PID and FOPID controllers are implemented in MATLAB and SIMULINK environment inside PC using fractional-order modeling and control toolbox. Controller in the SIMULINK environment inside PC is connected to the Maglev system through Advantech card. Effectiveness of proposed controllers is tested by checking the ability of the suspended ball to track a reference signal. Step change, sine wave, and square wave are used as reference signals. Real-time results have revealed satisfactory transient and steady-state responses over the contemporary existing controllers. FOPID controller showed better results compared to PID.

Keywords Magnetic levitation · PID · FOPID · Firefly algorithm

L. Majhi (✉) · P. Roy · B.K. Roy
Department of Electrical Engineering, National Institute of Technology, Silchar, Silchar, India
e-mail: lbmajhi@gmail.com

P. Roy
e-mail: proylinux@gmail.com

B.K. Roy
e-mail: bkrnits@gmail.com

K.N. Das et al. (eds.), *Proceedings of Fourth International Conference on Soft Computing for Problem Solving*, Advances in Intelligent Systems and Computing 335,
DOI 10.1007/978-81-322-2217-0_35

1 Introduction

1.1 Basic Principle of Magnetic Levitation System

In a Maglev system, a ferromagnetic object is levitated against gravity and its position is controlled using electromagnetic force of attraction [1]. Due to the absence of mechanical contact frictional forces get eliminated. Hence, system efficiency get enhanced. Magnetic levitation technology is used in various engineering applications such as high-speed trains, levitation of wind turbine, and personal rapid transit. Actual position of the levitated object is measured by a sensor. Based on the difference between desired and actual position of the suspended object, a controller can inject suitable current to electromagnetic coil which generates required force on the ferromagnetic object to control its position and make it able to track a reference signal [1, 2]. Without the presence of a controller, Maglev system is inherently unstable. The relation between force, current, and position is also nonlinear.

1.2 Literature Review

In [3], a FOPID controller is designed for a magnetic levitation system by minimizing various performance indices such as ISE, ITSE, IAE, and ITAE using classical optimization technique. A fuzzy controller and a neural adaptive controller has been used in [4, 5], respectively, for Maglev system. Advanced control strategies such as feedback linearization [6], sliding mode control [7], $H\infty$ control [8], and quantitate feedback theory [9] etc. are also used in Maglev system. However, the survey is not an exhaustive one. Moreover, comparisons of results have been done with only those papers which have hardware implemented results. Review of literatures indicates that fractional-order controllers are relatively less explored for such systems. This paper focuses on designing a FOPID controller for such systems by optimizing ISE using FA.

1.3 PID and FOPID Controller

As discussed in Sect. 1.1, the presence of a controller in Maglev system is mandatory; otherwise, system is inherently unstable. PID controller is simple to design and implement as well as cost-effective. It also shows acceptable robustness. Therefore, in spite of availability of sophisticated and advanced controllers, PID controller has been chosen in this paper. Many researchers have shown in recent past that FOPID controller has greater potential over PID due to its extra two

degrees of freedom in terms of its non-integer order of derivative and integration. One of such literatures is given in [10]. Therefore, FOPID controller has been chosen as another controller for this system. The transfer function of PID and FOPID controllers is given in Eqs. (1) and (2), respectively, with usual notations. The parameters λ and μ stand for the order of integration and derivative, respectively.

$$\frac{U(s)}{E(s)} = \left(K_{\mathrm{P}} + \frac{K_I}{s} + K_{\mathrm{D}}s\right) \tag{1}$$

$$\frac{U(s)}{E(s)} = \left(K_{\mathrm{P}} + \frac{K_I}{s^{\lambda}} + K_{\mathrm{D}}s^{\mu}\right) \tag{2}$$

1.4 What Is Firefly Algorithm (FA) and Why to Tune PID and FOPID by FA?

Firefly algorithm (FA) is based on social behavior of fireflies flying in the tropical summer sky. They communicate with each other, search for mates, and prey using bioluminescence with varied flashing patterns. Mimicking the characteristics of their movement, an optimization algorithm is developed in [11, 12]. Details of the algorithm have been discussed in Sect. 4.2. In [13], FA has been successfully used to tune the PID parameters for a set of test plants.

Fractional-order controller dynamics is governed by fractional-order differential equation. Fractional-order differential equation is very complex to analyze mathematically. Hence, finding out FOPID parameters by classical mathematics is a challenging task. Metaheuristic algorithm like FA does not require to analyze or solve the internal dynamics of the controller. Rather, it does a methodical search to find suitable values of PID parameters K_{P}, K_{I}, and K_{D}, and FOPID parameters K_{P}, K_{I}, K_{D}, μ, and λ for which a performance index (PI) is minimized. The PI is a measure of controller performance. It is generally a function of error signal.

2 Description of Magnetic Levitation System Model Used Here

As shown in Fig. 1, the Maglev unit, manufactured by Feedback Instruments (Model No 33-210) consists of a connection interface panel with a mechanical unit on which an electromagnetic actuator coil is mounted. A ferromagnetic ball is used as levitated object. An infrared (IR) sensor is attached at the middle of the unit. A desktop computer is connected with the mechanical unit through Advantech card.

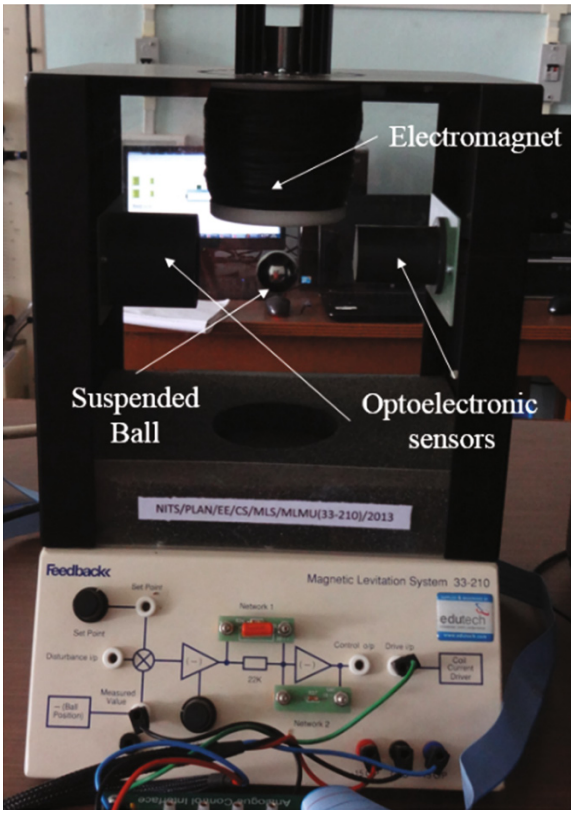

Fig. 1 Magnetic levitation system (feedback 33-210)

MATLAB–SIMULINK environment inside the computer serves as main control unit [2]. Infrared sensor measures vertical position of the ball and passes this information to the controller inside the digital computer through an ADC interface. Controller compares measured position of the ball with reference input position and adjusts the current through the electromagnetic actuator to control the required force so that the levitated ball position is stable and it can follow a reference trajectory. Manufacturer of the Maglev system (Model No 33-210) has also provided an inbuilt PID controller [2].

3 Modeling of Maglev System by System Identification

As discussed in Sect. 1.1, Maglev system is an open-loop unstable system. So, open-loop identification is not possible. However, it can be identified by closed-loop identification. Identification is carried out following the steps given in [2, 14].

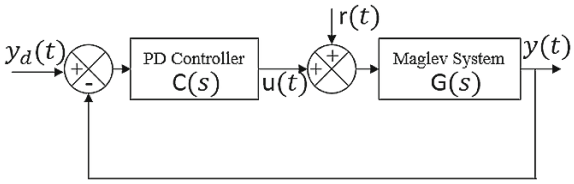

Fig. 2 System with PD controller

In [2, 14] a PD controller is used to make the system stable as shown in Fig. 2. Excitation signal $r(t)$ in Fig. 2 was chosen to be a random binary sequence. Using offline real-time input and output data in MATLAB CONTSID Toolbox, a transfer function is obtained between $r(t)$ and $y(t)$. From the block diagram of Fig. 2, transfer function has been calculated as given in Eq. (3) can be written as below.

$$T(s) = \left(\frac{Y(s)}{R(s)}\right)_{y_d=0} = \frac{G(s)}{1 + C(s)G(s)} \tag{3}$$

The PD controller has a transfer function

$$C(s) = (4 + 0.2s) \tag{4}$$

From Eqs. (4) and (5), $G(s)$ is calculated and shown in Eq. (3).

$$G(s) = \frac{0.00296s^3 + 0.7351s^2 + 87.08s + 4581}{s^3 + 83.86s^2 + 2158s + 1352} \tag{5}$$

4 Controller Design

4.1 Selection of Performance Index (PI)

Performance index (PI) of a controller is generally a function of error signal $e(t)$. It is a quantitative measure to evaluate the performance of a controller. For a feedback control system, integral square error (ISE) is one of the obvious choices as PI. Therefore, ISE has been chosen as PI for optimization. Mathematical description of ISE is given in Eq. (6).

$$J = \text{ISE} = \int_0^\infty e^2(t)\mathrm{d}t; \tag{6}$$

4.2 Tuning of Controller Parameters Using Firefly Algorithm (FA)

Firefly algorithm (FA) is a nature-inspired algorithm based on the movement and flashing characteristics of fireflies. It consists of three particular idealized rules which are based in major flashing characteristics of fireflies [11, 12]. These are as follows:

- All fireflies are unisex, so that one firefly will be attracted to all other fireflies regardless of their sex [11, 12].
- Attractiveness is proportional to their brightness. Thus, between any two fireflies, the less brighter one will move toward brighter one. The degree of attractiveness is proportional to the brightness which decreases as their distance increases. If there is no brighter one than a particular firefly, then it will move randomly [11, 12].
- Brightness of fireflies is determined by the landscape of the objective function or PI [11, 12].

For an optimization problem, the brightness is associated with the fitness function in order to obtain efficient optimal solutions. In this algorithm, when searching for solutions, two main procedures are followed: (i) attractiveness and (ii) movement, which are defined as follows:

Attractiveness
The form of attractiveness function of a firefly is the following monotonically decreasing function [11, 12].

$$\beta(r) = \beta_0 e^{(-\gamma r^m)}\ ; \quad m \geq 1 \tag{7}$$

In Eq. (7), r is the distance between any two fireflies, β_0 is the initial attractiveness at $r = 0$, and γ is the absorption parameter which controls the decrease of light intensity. The distance r_{ij} between ith and jth fireflies, at position X_i and X_j respectively, is governed by Eq. (8) [11, 12].

$$r_{ij} = \left\| X_i - X_j \right\| = \sqrt{\sum_{k=1}^{d} \left(x_{ik} - x_{jk} \right)^2} \tag{8}$$

where x_{ik} is the kth component of the spatial coordinate of the ith firefly (X_i) and d is the dimension number.

Movement
Movement of ith firefly which is attracted by a brighter jth firefly is governed by Eq. (9) [11, 12].

$$X_i^{n+1} = X_i^n + \beta_0 e^{\left(-\gamma r_{ij}^2\right)}\left(X_j^n - X_i^n\right) + \alpha\left(\text{rand}() - \frac{1}{2}\right) \tag{9}$$

X_i^n and X_i^{n+1} are the present and future position of a firefly, respectively. The second term in Eq. (9) is used for considering a firefly's attractiveness to light intensity seen by adjacent fireflies. The third term in Eq. (9) is used for the random movement of a firefly in case there are not any brighter ones. The coefficient α is a randomization parameter determined by the problem of interest, while rand () generates is a vector of uniformly distributed random number in d dimensional space. Whole optimization process can be summarized in a flowchart given in Fig. 3 [11–13]. A pseudocode representation of FA is given below [11–13].

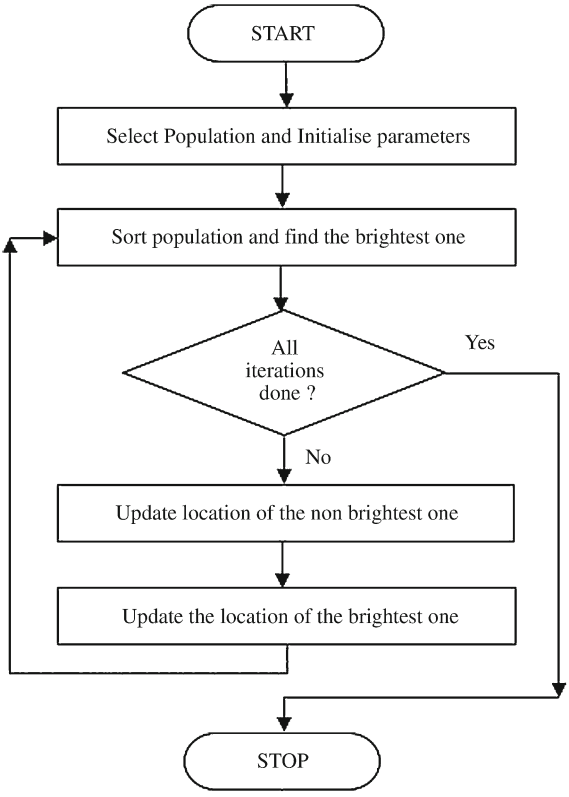

Fig. 3 Flowchart of Firefly Algorithm

```
Begin
Initialize algorithm parameters
Define the objective function of f(x), where
x=(x1,……..xd)'
Generate the initial population of fireflies of
xi (i=1, 2, …n)
Determine the light intensity of Ii at xi via
f(xi)
While (t<MaxGen)
       For i=1 to n (all n fireflies)
          For j=1 to n (n fireflies)
             If (Ij>Ii),move firefly i towards j;
             end if
      Attractiveness varies with distance r via
exp(-γr2);
      Evaluate the new solutions and update light
intensity;
       End for j loop;
   End for I loop;
Sort and rank the fireflies and find the current
best one;
End while;
Post process results and visualization;
End procedure
```

For PID and FOPID tuning purpose, initializing parameters chosen for FA are shown in Table 1.

The optimization process is continued until there is no significant changes found in the value of PI for 100 consecutive iterations or when all the generations are completed. Optimized controller parameters are shown in Table 2. Simulated step responses of the system using PID and FOPID tuned by FA are shown in Fig. 4.

Table 1 Initializing parameters for firefly algorithm

Number of fireflies $(n) = 40$	Absorption coefficient$(\gamma) = 1$
Randomness $(\alpha) = 0.5$	Initial attractiveness, $(\beta_0) = 0.2$
Generation number$(N_g) = 500$	Index of r $(m) = 2$

Table 2 Optimized controller parameters found by FA

Controller	K_P	K_I	K_D	λ	μ
PID	3.6947	1.7276	0.45143	–	–
FOPID	4.06893	1.8281	0.12244	0.4356	0.1707

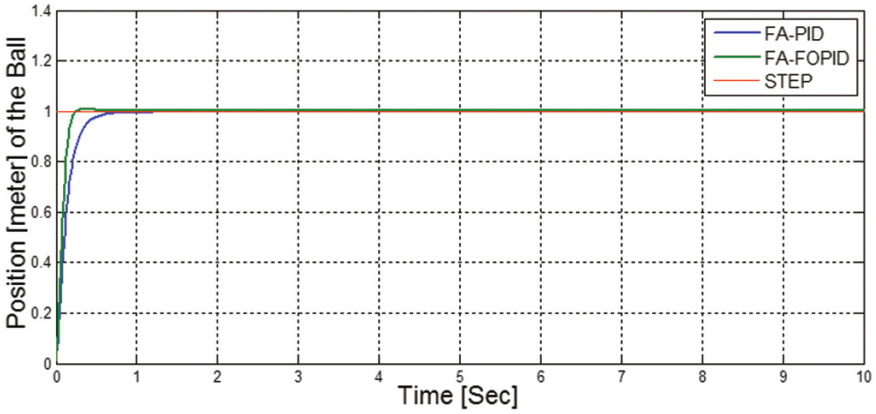

Fig. 4 Simulated step responses using PID and FOPID controllers tuned by firefly algorithm

4.3 Implementation PID and FOPID Controllers for Maglev System

Designed PID and FOPID controllers in Sect. 4.3 are implemented in real time using MATLAB and SIMULINK environment inside digital computer which is connected to the Maglev mechanical unit through Advantech card. An additional MATLAB toolbox, fractional-order modeling and control (FOMCON) is installed inside SIMULINK environment to generate fractional-order transfer function of FOPID controller [15]. Due to large initial error, integral action at initial stage may increase the control signal to a very high value. It can cause a high overshoot and can also make the system unstable. Even it can push the ball beyond the sensor operating region. Hence, in the first 15 s, only PD controller is used to stabilize the ball. After 15 s, integral action is turned on to reduce steady-state error.

5 Results and Discussions

In the simulated step responses in Fig. 4, FOPID controller tuned by FA shows better result (overshoot 0.528 % and settling time 0.327 s) than that of PID (overshoot 0 % and settling time 0.783 s). Although in terms of overshoot, PID is better but 0.582 % overshoot is negligible in case of FOPID. Moreover, due to very short settling time, tracking of a reference signal will be better in case of FOPID. Real-time results in Figs. 5, 6, 7, 8, 9, and 10 clearly indicate that FOPID controller tuned by FA is working much better than PID controller in terms of tracking of a reference signal.

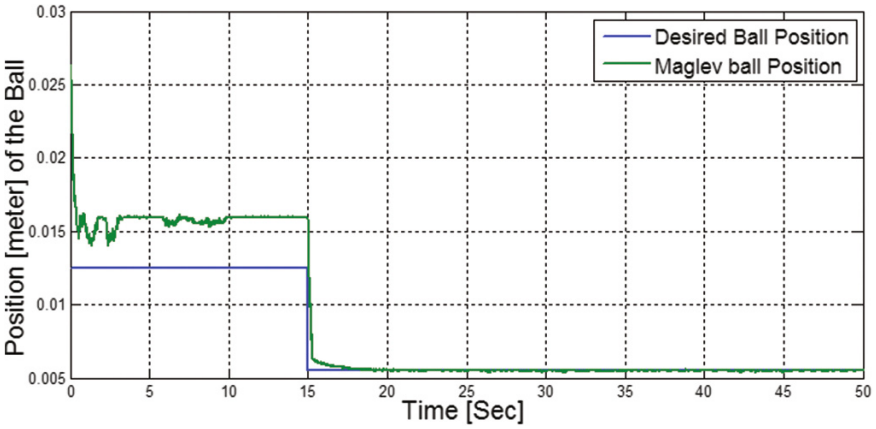

Fig. 5 Real-time response using PID controller tuned by FA with step change as reference input (only PD controller is applied for first 15 s.)

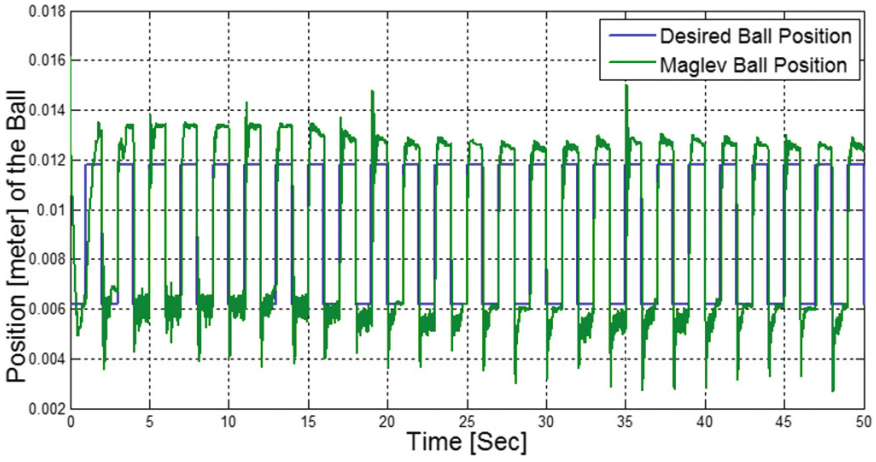

Fig. 6 Real-time response using PID controller tuned by FA with square wave signal as reference input (only PD controller is applied for first 15 s.)

The Maglev model used in this paper is relatively new. Hence, little research work has been done on it. Hence, comparisons have been done mostly with similar contemporary set ups. Literatures with only simulation results have not been compared. Results in this paper clearly show better performance system inbuilt PID controller [2] in terms of tracking of a reference signal. In [3], classical optimization method is applied to design fractional-order PID controller by minimizing ISE, IAE, ITSE, MCE, etc. But results in [3] show higher overshoot (10–15 % in different cases) and higher settling time (8–10 s. in different cases) than this paper.

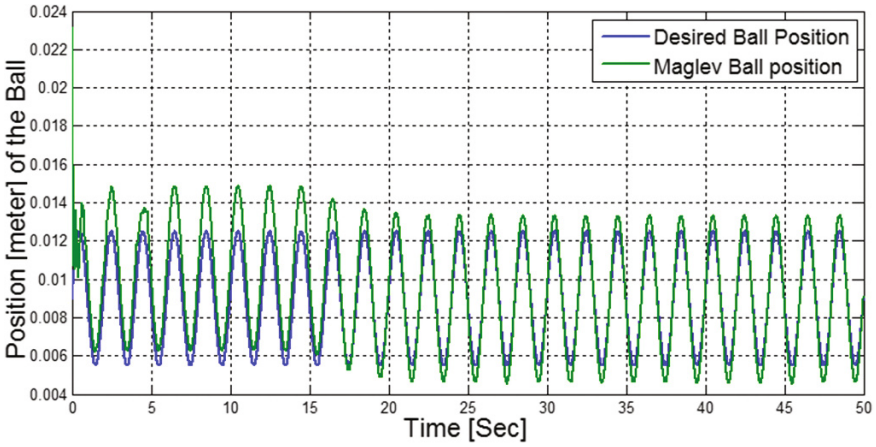

Fig. 7 Real-time response of the system using PID controller tuned by FA with sine wave signal as reference input (only PD is applied for first 15 s.)

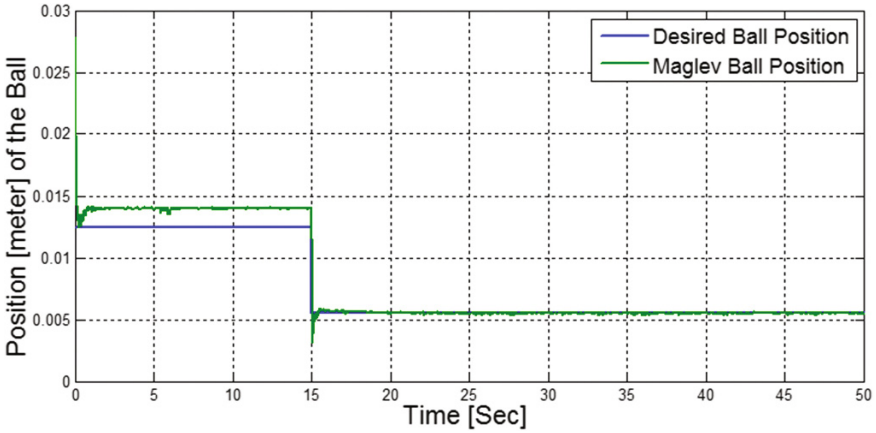

Fig. 8 Real-time response of the system using FOPID controller tuned by FA with step change signal as reference input (only FOPD is applied for first 15 s.)

Results in [4] and [5] are limited to simulation studies only hence it has not been compared. Controller in Naz et al. [6] gives similar transient and steady-state behaviors of this paper but response in Naz et al. [6] contains undesirable phenomenon of chattering initially. Robust H∞ controller in Wei et al. [8] provides less settling time but higher overshoot (4 %) than this paper. Response in [8] also contains significant steady-state error. QFT-based controller in Nataraj and Patil [9] obtains higher settling time (1 s) than this paper.

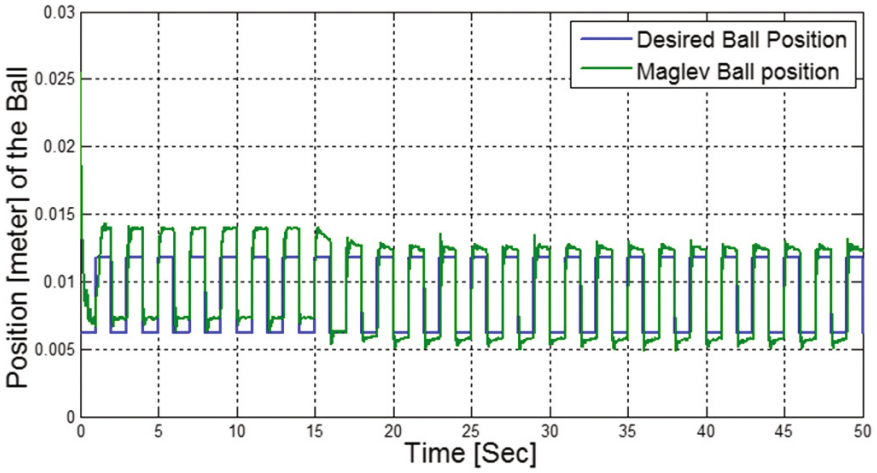

Fig. 9 Real-time response using FOPID controller tuned by FA with square wave signal as reference input (only FOPD is applied for first 15 s.)

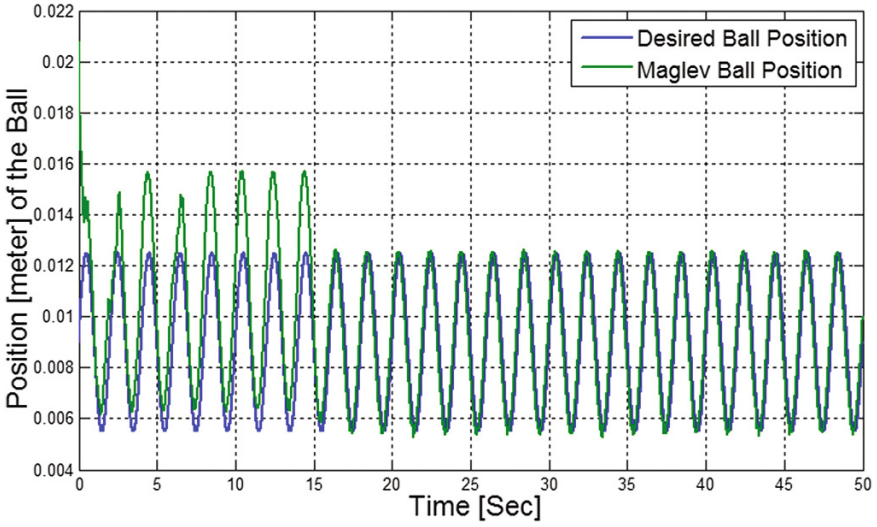

Fig. 10 Real-time response using FOPID controller tuned by FA with sine wave signal as reference input (only FOPD applied for first 15 s.)

6 Conclusions and Future Scope

Comparisons with other reported literature justify that FA is a suitable and reasonably simple tool to tune PID and FOPID controller's parameters. Although several tuning procedures are available for PID controller, most of them are

applicable for linear systems only. However, number of techniques to find FOPID controller parameter is very limited till date, due to its complex fractional-order dynamics. It is also concluded from the results that proposed FOPID controller works better than PID controller due to its extra two degrees of freedom in terms of non-integer order of derivative and integration. Comparisons with literatures also justify that FOPID controllers tuned by FA works better than several existing controllers. Step change, square wave, and sine wave are used as reference signals in this paper. A more complex reference signal like random signal will be used in future. The robustness of the controller due to variation of system parameters and external disturbances is not tested which may be taken into account in future.

References

1. Ahmad, I., Javaid, M.A.: Nonlinear model and controller design for magnetic levitation system. In: 9th WSEAS International Conference on Signal Processing, Robotics and Automation, Cambridge, UK (2010)
2. Manual of Maglev system Model No 33-210. http://www.feedback-instruments.com/products/education/control_instrumentation/magnetic_levitation_system
3. Gole, H., Harshit, P., Barve, A., Kesarkar, A., Selvaganesan, N.: Investigation of fractional control performance for magnetic levitation experimental set-up. International Conference on Emerging Trends in Science, Engineering and Technology (INCOSET), Tiruchirappalli, India (2012)
4. Gholami, M., Aliyari, S., Shoorehdeli, M., Dashti, Z.A.S., Teshnehlab, M.: Design of fuzzy parallel distributed compensation controller for magnetic levitation system. Fuzzy Systems (IFSC), 2013 13th Iranian Conference, Qazvin, Iran (2013)
5. Dashti, Z.A.S, Gholami, M., Jafari, M., Shoorehdeli, M.A., Hajimani, M.: Neural adaptive controller for magnetic levitation system. Iranian Conference on Intelligent Systems, Bam, Iran (2014)
6. Naz, N., Malik, M.B., Salman, M.: Real time implementation of feedback linearizing controllers for magnetic levitation system. IEEE Conference on Systems, Process and Control (ICSPC), Kuala Lumpur, Malaysia, (2013)
7. Lin, F.J., Chen, S.Y.: Intelligent integral back stepping sliding mode control using recurrent neural network for magnetic levitation system. Neural Networks (IJCNN), The 2010 International Joint Conference, Barcelona, Spain (2010)
8. Wei, G.. Guo, Y., Huang, F., Wu, Y.: Experimental studies on H∞ control for magnetic levitation system with friction compensation. Modelling, Identification and Control (ICMIC), 2012 Proceedings of International Conference, Wuhan, Hubei, China (2012)
9. Nataraj, P.S.V.: Patil, M.D.: Nonlinear control of a magnetic levitation system using quantitative feedback theory (QFT). Reliability, Safety and Hazard (ICRESH), 2010 2nd International Conference, Mumbai, India (2010)
10. Podlubny, I., Dorcak, L., Kostial, I.: On fractional derivatives, fractional-order dynamic systems and $PI^{\lambda}D^{\mu}$ controllers. In: 36th IEEE Conference on Decision and Control, 1997, San Diego, US (1997)
11. Yang, X.S.: "Firefly Algorithm" in Nature Inspired Metaheuristic Algorithm. 2nd edn, UK Luniver Press, 2010, chapter 10, pp. 81–89
12. Gandomi, A.H., Yang, Xin-She, Alavi, A.H.: Mixed variable structural optimization using Firefly Algorithm. Computers and Structures, ELSEVIER **89**, 2325–2336 (2011)

13. Bendjeghaba, O, Boushaki S.I., Zemmour N.: Firefly algorithm for optimal tuning of PID controller parameters. Fourth International Conference on Power Engineering, Energy and Electrical Drives, 2013, Istanbul, Turkey (2013)
14. Majhi, L., Borah, M., Roy, P.: Fractional order system identification of maglev model from real-time data. IEEE International Conference on Advanced Communication Control and Computing Technologies, 2014, Ramanathapuram, India (2014)
15. Tepljakov, A., Petlenkov, E., Belikov, J.: A flexible MATLAB tool for optimal fractional-order PID controller design subject to specifications. In: Proceedings of the 31st Chinese Control Conference, Hefei, pp. 4698–4703 (2012)

Distance-Based Analysis for Base Vector Selection in Mutation Operation of Differential Evolution Algorithm

A.R. Khaparde, M.M. Raghuwanshi and L.G. Malik

Abstract There is a remarkable performance of differential evolution (DE) algorithm on continuous space problem. Mutation plays a very vital role in success of DE but in traditional DE all the vectors are selected in random manner. Sometimes, it gives a random exploration in search space. Here, the distance-based analysis for mutation vector selection is carried out and distance-based criteria for base vector (reference point) selection have proposed. Experimentation is conducted on eight standard uni-model and multi-model functions. Later, the results have compared with standard DE and other variant of DE. Experiments show that the proposed strategy has a very steady and stable exploration of search space.

Keywords Differential evolution algorithm · Analysis

1 Introduction

The differential evolution (DE) algorithm is a simple and efficient evolutionary algorithm. It is used to solve nonlinear and non-differentiable continuous space problems. DE has very fast convergence speed as compared to other evolutionary

A.R. Khaparde (✉)
Information Technology, G.H. Raisoni College of Engineering,
Rajiv Gandhi College of Engineering and Research, Nagpur, India
e-mail: khaparde.amit@gmail.com

M.M. Raghuwanshi
Computer Technology, Yeshwantrao Chavan College of Engineering,
Nagpur, Maharashtra, India
e-mail: m_raghuwanshi@rediffmail.com

L.G. Malik
G. H.Raisoni College of Engineering, Nagpur, India
e-mail: latesh.malik@raisoni.net

K.N. Das et al. (eds.), *Proceedings of Fourth International Conference on Soft Computing for Problem Solving*, Advances in Intelligent Systems and Computing 335,
DOI 10.1007/978-81-322-2217-0_36

algorithms. It requires very few control parameters to solve any problem. It is robust and easy to use. It lends itself very well to parallel computation [1–3]. But apart from this, DE has some problems such as premature convergence and stagnation [4, 5].

The performance of DE is depended upon the values of control parameters [6], strategies used for mutation [7], and type of crossover [8, 9] used to solve the problem. Mutation strategy selection is an important issue while solving any problem using DE. The past experimental results give a significant theoretical understanding of DE which allows mapping of mutation strategies with particular type of problems [7, 10], which helps researchers to solve the real-life problems [11, 12] and give improve variants of DE [13–16].

Selection of individuals in DE is carrying out at two different stages: First is at the level of mutation, i.e., selection of individual for the mutation process, and second is selection of individuals for the next generation. Selection of individual for next generation is greedy in nature. Selection of individual for mutation is randomizing in nature which may cause random exploration in search space.

Selecting the suitable individuals for mutation at particular generation can gradually increase the performance of DE [16–19]. Here, we have analyzed most distance-dependent possibilities with respect to target vector. Base vector in mutation operator acts as a reference point to form the cluster in search space, and this cluster leads to give a global optimum. Here, we have proposed the distance-dependent criteria with respect to target vector to select base vector (reference point) which has shown the smooth and steady exploration in search space.

2 Differential Evolution Algorithm

DE is novel parallel direct search method. It has three performance deciding parameters. It has the cycle of four stages. Generation, mutation, crossover, and selection are the four stages of DE. It starts with randomly initialize *NP* number of population vectors which can be describe by following function

$$X_{i,j} = X_{i\_\min} + \text{rand}\,[0, 1]\,(X_{i\_\max} - X_{i\_\min}) \tag{1}$$

where $X_{i\_\max}$, *and* $X_{i\_\min}$ are upper bound and lower bound of decision variables, respectively. Each vector can be represented as follows: $X_{i,j} = X_{1i,j}, X_{2i,j}$, $X_{3i,j} \ldots X_{Di,j}$, where $i = 1, 2 \ldots NP$. D is the number of variables in jth generation. Once the initial population created, it gets evaluated by using given fitness function. After evaluation of newly created population, mutation is next step. Mutation is used to create a new vector (mutant vector). The mutant vectors are created for each and every vector in population. Mutation can be represented as follows:

$$M_{i,j} = X_{r1,i} + F(X_{r2,j} - X_{r3,j}) \tag{2}$$

where $r1$, $r2$, $r3 \in 1 \ldots NP$ are mutually different integers and $F > 0 \in [0,2]$ known as scaling factor. There are two different ways suggested in [1–3] to choose $r1$. Either it can be randomly selected or it can be the best vector of given generation. In order to add diversity in the population, the recombination (crossover) is used. The trial vector is generated by recombination of mutant vector and target vector. Each member of population gets a chance to become a target vector. Crossover can be represented as follows:

$$V_{i,j} = \begin{cases} M_{i,j}, & \text{if } (\text{rand}(i) \leq \text{Cr or } i = \text{rand}_i(j)) \\ X_{i,j}, & \text{otherwise} \end{cases} \tag{3}$$

where rand(i) is random number between (0,1], Cr is crossover probability between (0,1], and $\text{rand}_i(j)$ is randomly chosen index between (1,D] which ensure that $V_{i,j}$ will have at least one parameter from $M_{i,j}$. There are two types of crossover given in traditional DE, first is binomial crossover and other is exponential crossover. The above one is binomial crossover.

The last step is selection; DE follows a greedy approach for selection. There is a tournament selection between trial vector and target vector, and the fittest one is selected for next generation. This can be represented as follows:

$$X_{i,j+1} = \begin{cases} V_{i,j}, & \text{if } (f(M_{i,j} \leq f(X_{i,j}) \\ X_{i,j}, & \text{otherwise} \end{cases} \tag{4}$$

DE has various variants on the basis of type of vector mutated (X), number of vector used for perturbation (Y), and type of crossover (Z). This can be represented as DE/X/Y/Z. Here, DE/rand/1/bin is used in experimentation.

Pseudo code of DE

Step 1: Initialization of initial population…… by using (1)

Until stopping criteria does not satisfied

Step 2: Mutation ……by using (2)

Step 3: Crossover …...by using (3)

Step 4: Selection …….by using (4)

Repeat

3 Distance-Based Selection of Mutation Operators

In DE, mutation plays a very vital role to solve any problem. As per (2), mutation is addition of scaled difference of two vectors with the base vector. The scaled difference provides the direction, whereas the base vector provides the reference point in search space. The information carried by this reference point is used in cluster formation, which further leads to the solution. Hence, the choice of proper base vector is very crucial in DE. The standard DE offers two choices to select the base vector: First is best vector and other is any random vector. In [7–14], the best/*/* is good choice to solve any uni-model problem, but it has lower performance in multi-model problem as compared to other strategies. rand/*/* has good performance in multi-model problem, it but has lower performance in uni-model problem as compared to best/*/*. Best/*/* formed the clusters near the best vector of the given generation [18]. Hence, there might be a case that the search gets stuck to local minima, whereas rand/*/* may cause the loss of useful information of cluster formation, which can cause high convergence speed, premature convergence, or sometime stagnation.

All individuals in standard DE get a chance to participate in crossover, because all individuals become a target vectors. Here, the distance of the target vector with respect to the others vectors has been used to make the decision of selection of vectors for the mutation. The experimentation is carried out in two different stages.

1. Distance-based selection of all three vectors with respect to target vector.
2. Base vector (reference point) selection with respect to target vector.

Further, the distance-based selection of all three vectors with respect to target vector is carry out in following ways:

1. First three nearest vectors from target vector (Method_1).
2. First three longest vectors from target vector (Method_2).
3. First vector is nearer to target vector and rest of two are longest from target vector (Method_3).
4. Best one of Method_3 will be base vector rest of two will be other two vectors.

And base vector (reference point) with respect to target vector is carry out in following ways:

1. A vector closer to the target vector (**C**).
2. A vector which is far away from the target vector (**L**).

Here, the Euclidian distance is considered as a distance between the two vectors. There is change only in mutation stage because mutation vector selected with respect to target vector, and other stages are same as standard DE.

Pseudo code of Method$_1$, Method$_2$, Method$_3$, Method$_4$

Step 1: Calculate the Euclidian matrix **M**, {such that each element $M_{i,j}$ represent the distance between vector$_i$ and vector$_j$ }

Step 2: for all methods are as follows :

Method$_1$: Consider the first three minimum values of each row of M as r_1, r_2, r_3.

Method$_2$: Consider the first three maximum values of each row of M as r_1,r_2,r_3 .

Method$_3$: Consider the minimum value and first two maximum values of each row of M as r_1,r_2,r_3, respectively.

Method$_4$: Consider the minimum value and first two maximum values of each row of M . Calculate the fitness value of each element say fr_1, fr_2, fr_3 respectively. Sort fr_1, fr_2, fr_3 in ascending order. Then consider first value individual as r_1 and second value individual as r_2 and third is r_3.

Step 3: Mutation using (2)

Pseudo code of C and L

Step 1: Calculate the Euclidian matrix **M**, {such that each element $M_{i,j}$ represent the distance between vector$_i$ and vector$_j$ }

Step 2: for C and L is as follows :

Consider the first minimum value of each row of M as r_1 whereas r2,r3 are selected randomly

Consider the first maximum value of each row of M as r_1 whereas r2,r3 are selected randomly

Step 3: Mutation using (2)

4 Experimental Study

Our main aim is to check the effect of distance-based vector selection in mutation operator of DE algorithm. Hence, the first eight uni- and multi-model functions from CEC 2006 are used for experimentation. The standard differential evolution algorithm (SDE) and other advance variants of DE, such as EPSDE and CoDE, are used for comparison. The value of control parameters is set as $NP = 10 * n$, $F = 0.5$,

Table 1 Benchmark problems with properties

S. No.	Problem name	S. No.	Problem name
F1	Shifted sphere function	F5	Schwefel's function with global optimum on bounds
F2	Shifted Schwefel's function	F6	Shifted Rosenbrock's function
F3	Shifted rotated high conditioned elliptic function	F7	Shifted rotated Griewank's function without bounds
F4	Shifted Schwefel's function with noise in fitness	F8	Shifted rotated Ackley's function with global optimum on bounds

Cr = 0.7 and maximum function evaluation = n * 10,000, whereas n = number of variables in objective function. Throughout the experimentation, the value of F and Cr is fixed. The performance of the each method is evaluated on following criteria:

1. **Success rate** = Number of successful runs/total number of runs
2. **Success Performance** = Average of max function evaluation of successful runs/success rate
3. **Minimum value of function**
4. **Max function evaluated for min value** (Tables 1, 2, 3, 4, and 5).

The scale-up study in first phase is not performed because of the main aim to give distance-based criteria for base vector selection. Table 2 shows neither Method_1 nor Method_2 is able to reach nearer to the solution. But Method_3 and Method_4 are somewhere nearer to the solutions. That shows the importance of base vector in the search space.

The scale-up study for base vector selection is carried out. The bold values show the better performance. Here, it can be said that C has better performance on L in all problems. The number of function evaluations of C is comparatively very less as compared to L, and success rate is also on higher side. That shows that most of the time, the DE with **C** converges toward the global optima at very high speed as compared to DE with **L**.

The above scale-up study shows that all of the above algorithms are able to solve most of the problems. But CoDE and EPSDE have very higher convergence rate. Here, DE with C has less maximum function evaluation as compared to other that shows that convergence to global optimum at higher speed as compared to other and the smooth exploration of search space.

Table 2 Comparison of proposed mutation vector selection methods

Fun No.	Parameters	$N = 5$			
		$Method_1$	$Method_2$	$Method_3$	$Method_4$
1	Min value	1.910827	14.3045	0.000575	**7.86E−07**
	Max functions evaluated	50,000	50,000	50,000	**206**
	Success rate	0	0	0	0.2
	Success performance	–		–	200,206
2	Min value	928.6117	228.483	**1.225942**	14.43496
	Max functions evaluated	50,000	50,000	50,000	50,000
	Success rate	0	0	0	0
	Success performance	–	–	–	–
3	Min value	403,666.5	220.5497	353.524	**199.7271**
	Max functions evaluated	50,000	50,000	50,000	50,000
	Success rate	0	0	0	0
	Success performance	–	–	–	–
4	Min value	521.1522	13.37092	**0.000174**	0.471594
	Max functions evaluated	50,000	50,000	50,000	50,000
	Success rate	0	0	0	0
	Success performance	–	–	–	–
5	Min value	1,310.217	972.8841	**58.38124**	60.95971
	Max functions evaluated	50,000	50,000	50,000	50,000
	Success rate	0	0	0	0
	Success performance	–	–	–	–
6	Min value	239.3783	**107.5929**	638.6175	1,441.788
	Max functions evaluated	50,000	50,000	50,000	50,000
	Success rate	0	0	0	0
	Success performance	–	–	–	–
7	Min value	1.079792	0.326317	**0.208578**	0.37285
	Max functions evaluated	50,000	50,000	50,000	50,000
	Success rate	0	0	0	0
	Success performance	–	–	–	–
8	Min value	20.07596	20.11086	20.0891	20.08026
	Max functions evaluated	50,000	50,000	50,000	50,000
	Success rate	0	0	0	0
	Success performance	–	–	–	–

Table 3 Comparison of base vector selection

Fun no.	Parameters	$N = 5$		$N = 10$	
		L	*C*	*L*	*C*
1	Min value	**6.92E−07**	8.55E−07	7.75E−07	**3.18E−07**
	Max functions evaluated	356	**181**	727	**372**
	Success rate	1	1	1	**1**
	Success performance	342.6	**187.4**	734.2	**374.6**
2	Min value	4E−07	4.09E−07	6.54E−07	**7.33E−07**
	Max functions evaluated	1,105	**286**	6,161	**810**
	Success rate	1	1	1	**1**
	Success performance	1,120	**283.2**	6,475	**827.4**
3	Min value	0.002667	**6.19E−07**	1,565.078	**4.72E−07**
	Max functions evaluated	50,001	**829**	100,001	**9,884**
	Success rate	0	**1**	0	**1**
	Min value	–	**828.2**	–	9,765.8
4	Max functions evaluated	**2.99E−07**	4.17E−07	6.1E−07	**6.93E−07**
	Success rate	1,258	**310**	8,794	**967**
	Success rate	1	1	1	**1**
	Success performance	1,274.8	**308**	8,812.6	**994.4**
5	Min value	8.36E−07	**6.17E−07**	54.12033	**8.67E−07**
	Max functions evaluated	3,824	**877**	100,001	**9,062**
	Success rate	0.8	**1**	0	**1**
	Success performance	16,292.5	**869.4**	–	**9,382.4**
6	Min value	**0.005178**	0.007152	0.008164	**0.0036**
	Max functions evaluated	3,547	**1,063**	16,295	**8,944**
	Success rate	1	**1**	1	1
	Success performance	**3,228.8**	4,388.4	16,004.2	6,152.6
7	Min value	0.032021	**0.006852**	0.073766	0.008817
	Max functions evaluated	50,001	**4,556**	100,001	**17,295**
	Success rate	0	**0.8**	0	**0.6**
	Success performance	–	**16,653.75**	–	**77,642.67**
8	Min value	20	**7.21378**	20.09819	20.10443
	Max functions evaluated	50,001	50,001	100,001	100,001
	Success rate	0	0	0	0
	Success performance	–	–	–	–

Table 4 Comparison of method *C* with other variants of DE when $n = 5$

Fun no.	Parameters	DE with *C*	EPSDE	CODE	DE
1	Min value	8.55E−07	2E−09	2E−09	3E−09
	Max functions evaluated	**181**	6,450	14,300	**186**
	Success rate	1	1	1	1
	Success performance	**187.4**	6,354	15,380	**185.48**
2	Min value	4.09E−07	3E−09	9E−09	2E−09
	Max functions evaluated	**286**	7,350	149,120	**332**
	Success rate	1	1	1	1
	Success performance	**283.2**	8,366	148,923.2	**339.68**
3	Min value	6.19E−07	3E−09	2E−09	2E−09
	Max functions evaluated	**829**	10,150	38,750	**1,631**
	Success rate	1	1	1	1
	Success performance	**828.2**	10,772	37,358	**1,621.16**
4	Min value	4.17E−07	3E−09	3E−09	2E−09
	Max functions evaluated	**310**	9,750	24,050	**365**
	Success rate	1	1	1	1
	Success performance	**308**	8,904	24,320	**362.6**
5	Min value	6.17E−07	5E−09	5E−09	5E−09
	Max functions evaluated	877	15,600	29,450	938
	Success rate	1	1	1	1
	Success performance	**869.4**	16,742	29,300	915.04
6	Min value	0.007152	3E−09	1E−09	3E−09
	Max functions evaluated	**1,063**	16,050	36,350	**1,072**
	Success rate	**1**	0.92	1	**0.84**
	Success performance	**4,388.4**	22,419.57	36,260	**6,710.57**
7	Min value	0.006852	0.126499	28.65308	8E−09
	Max functions evaluated	**4,556**	30,000	300,050	**10,538**
	Success rate	**0.8**	0	0	**0.08**
	Success performance	**16,653.75**	–	–	**354,854.5**
8	Min value	7.21378	16.67609	**2E−09**	**9E−09**
	Max functions evaluated	50,001	30,000	**14,300**	**16,924**
	Success rate	0	0	**1**	**0.04**
	Success performance	–	–	**15,380**	**736,948**

Table 5 Comparison of method *C* with other variants of DE when $n = 10$

Fun no.	Parameters	Near	EPSDE	CoDE	DE
1	Min value	3.18E−07	5E−09	5.86E−07	6E−09
	Max functions evaluated	**372**	20,000	65,500	**375**
	Success rate	**1**	1	1	**1**
	Success performance	**374.6**	21,904	66,640	**376.2**
2	Min value	7.33E−07	4E−09	0.000545	4E−09
	Max functions evaluated	**810**	28,700	100,000	**1,368**
	Success rate	**1**	1	0	**1**
	Success performance	**827.4**	27,208	–	**1,399.04**
3	Min value	4.72E−07	5E−09	31.95944	3E−09
	Max functions evaluated	**9,884**	41,100	100,000	**46,297**
	Success rate	**1**	1	0	**1**
	Success performance	**9,765.8**	45,432	–	**47,541.2**
4	Min value	6.93E−07	5.54E−07	0.004002	5E−09
	Max functions evaluated	**967**	25,000	100,000	**1,640**
	Success rate	**1**	1	0	**1**
	Success performance	**994.4**	25,296	–	**1,583.88**
5	Min value	8.67E−07	6.57E−07	0.001799	5E−09
	Max functions evaluated	**9,062**	43,800	100,000	25,521
	Success rate	**1**	1	0	1
	Success performance	**9,382.4**	49,732	–	25,397.08
6	Min value	0.0036	0.004723	0.817596	0.00806
	Max functions evaluated	**8,944**	93,000	100,000	**1,687**
	Success rate	**1**	0.92	0	**1**
	Success performance	**6,152.6**	62,486.96	–	**5,370.92**
7	Min value	0.008817	0.192059	1,267.046	0.009426
	Max functions evaluated	**17,295**	100,000	100,000	**29,284**
	Success rate	**0.6**	0	0	**0.24**
	Success performance	**77,642.67**	–	–	**360,156.7**
8	Min value	20.10443	20.18238	20.22638	20.06809
	Max functions evaluated	100,001	100,000	100,000	100,001
	Success rate	0	0	0	0
	Success performance	–	–	–	–

5 Conclusion

Based on the above result, neither longest distance from base vector, i.e. (Method_1), nor shortest distance from base vector, i.e. (Method_2), are promising methods for selection of vectors for mutation. The methods Method_3 and Method_4 show that the first vector, i.e., base vector acts as reference point in mutant vector calculation, whereas rest of the two vectors provide the direction. If the reference point does not

choose properly, then there might be case that the search gets stuck to local minima. None of any method be able to solve any problem within the constraint except Method_4 for problem $f1$, but they show the importance of base vector.

Method *C* performs better with respect to *L* in multi-model problems. In Method *L,* the longest distance vector always selected as reference point, and it causes the delay in useful cluster formation while searching; hence, the convergence speed is relatively high as compared to *C*. Method *C* uses the closer vector as reference point and causes quick formation of cluster in search space which causes efficient searching and fast convergence as compared to Method *L*. Both Method *C* and Method *L* explore the search space, but there is very smooth exploration by Method *C* as compared to Method *L*. As per the results as concern, Method *C* is giving better results, but Method *L* can be useful in that cases where the initial population is not uniform. Hence, on the bases of the above results, we can say that the base vector should be near to base vector (Euclidian space).

The performance of DE with *C* and SDE is same in uni-model problem, but convergence speed of SDE is higher as compared to DE with *C*. The success rate of new method is better than SDE in multi-model problems, and the new method has outperformed EPSDE and CODE algorithms. More parameters' tuning is required for new method.

6 Future Scope

Here, we have checked the methods on low-dimensional problems. These methods have to be checked on higher-dimensional problems. The scale-up study in terms of other parameter such as *NP*, Cr, and *F* has to be carried out. Definitely, these studies will give a more significant theoretical understanding of distance-based vector selection for mutation.

References

1. Storn, R., Price, K.: Differential evolution—a simple and efficient heuristic for global optimization over continuous spaces. J. Global Optim. **11**, 341–359 (1997)
2. Storn, R., Price, K.: Differential evolution—a simple and efficient adaptive scheme for global optimization over continuous spaces. TR-95-012, March 1995
3. Karabo, D., Okdem, S.: A simple and global optimization algorithm for engineering problems: differential evolution algorithm. Turk. J. Electr. Eng. **12**(1) (2004)
4. Lampinen, O., Zelinka, I.: "On Stagnation of the Differential Evolution Algorithm". In: Ošmera, P. (ed.) Proceedings of MENDEL 2000, 6th International Mendel Conference on Soft Computing, Brno, Czech Republic, 7–9 June 2000
5. Gamperle, R., Muller, S.: A parameter study for differential evolution. In: Proceeding WSEAS international conference on advances in intelligent Systems,fuzzysystems, evolutionary computation, pp. 293–298, 2002
6. Zaharie, D.: Differential evolution: From theoretical analysis to practical insights

7. Montes, E., Coello, C.C.: A comparative study of differential evolution variants for global optimization, Seattle, Washington, USA, GECCO'06, 8–12 July 2006
8. Zaharie, D.: A comparative analysis of crossover variants in differential evolution. In: Proceedings of pp. 171–181, ISSN 1896-7094 c 2007 PIPS
9. Zaharie, D.: Influence of Crossover on Behavior of Differential Evolution. Elsevier, Amsterdam (2009)
10. Ao, Y., Chi, H.: Experimental Study on Differential Evolution Strategies Global Congress on Intelligent Systems, 2009, IEEE
11. Wenyin, G., Zhihua, C.: An empirical study on differential evolution for optimal power allocation in WSNs. In: 8th International Conference on Natural Computation (2012)
12. Chattopadhyay, S., Sanyal, S., Chandra, A.: Comparison of various mutation schemes of differential evolution algorithm for the design of low pass FIR filter, (SEISCON 2011)
13. Zhou, R., Hao, J., Cao, H., Fan, H.: An Empirical Study on Differential Evolution Algorithm and its Several Variants (ICEMEAI 2011)
14. Epitropakis, M.G., Plagianakos, V.P., Vrahatis, M.N.: Balancing the Exploration and Exploitation Capabilities of the Differential Evolution Algorithm, 2008, IEEE
15. Lou, Y., Li, J., Shi, Y.: A Differential Evolution Based on Individual-Sorting and Individual-Sampling Strategies, 2011, IEEE
16. Price, K.V., Rönkkönen, J.: Comparing the Uni-Modal Scaling Performance of Global and Local Selection in a Mutation-Only Differential Evolution Algorithm CEC, Canada 16–21 July 2006
17. Bhowmik, P.I., Das, S., Konar, A., Das, S., Nagar, A.K.: A new differential evolution with improved mutation strategy. IEEE Congr. Evol. Comput. 1–8, (2010)
18. Epitropakis, M.G., Tasoulis, D.K., Pavlidis, N.G.: Enhancing differential evolution utilizing proximity-based mutation operators. IEEE TEC **15**(1), 99–119 (2011)
19. Das, S., Suganthan, P.N.: Differential evolution: a survey of the state-of-the-art. IEEE Tran. Evol. Comput. **15**(1), 4–31 (2011)

A Novel Chemo-inspired Genetic Algorithm for Economic Load Dispatch with Valve Point Loading Effect

Rajashree Mishra and Kedar Nath Das

Abstract The inherent drawback of the popular evolutionary algorithm as such genetic algorithm (GA) and also bio-inspired algorithm bacterial foraging optimization (BFO) lies in the fact that they very often suffer from the problem of being trapped into the local optimum. In recent past, various popular hybridized techniques of GA and BFO came out through different thought processes of the researches and have been implemented in the algorithm. Inspired by those ideas, in this paper, a novel approach has been opted for the hybridization of GA with BFO by incorporating chemotactic step as a local search operator at the end of the entire GA cycle; thus, the algorithm is named as chemo-inspired genetic algorithm (CGA) and it has also been extended for constrained optimization, and further it is named as CGAC, where "C" stands for being capable of handling constraints. At the outset, experiments are made to validate the superiority of CGAC over another hybrid method, namely LX-PM-C and H-LX-PM-C taking a set of 8 typical benchmark problems of various difficulty labels from the literature. Later, it has been applied to real-life application problem, where economic load dispatch (ELD) problem having 40 generators has been considered with valve point loading effect.

Keywords Benchmark functions · Economic load dispatch · Valve point loading effect · Chemo-inspired genetic algorithm

R. Mishra (✉)
KIIT University, Bhubaneswar, Orissa, India
e-mail: rajashreemishra011@gmail.com

K.N. Das
NIT Silchar, Silchar, Assam, India
e-mail: kedar.iitr@gmail.com

K.N. Das et al. (eds.), *Proceedings of Fourth International Conference on Soft Computing for Problem Solving*, Advances in Intelligent Systems and Computing 335,
DOI 10.1007/978-81-322-2217-0_37

1 Introduction

In the present day scenario problems concerning the load dispatch of small, medium, and large-scale power systems are a robust optimization problem in modern power systems generally known as economic load dispatch (ELD) problems. The core objective of the problem is determination of the least cost power generation from a set of online generating units under all physical constraints and also taking into account all the operational constraints. Many deterministic optimization approaches are available in the literature for solving ELD problems. The major drawback of such methods is that they are inappropriate to handle higher order nonlinearities and discontinuities in real input–output characteristics of the generation cost function. They have the inherent drawback of being trapped into the local minima instead of global ones and also require enormous computational efforts to handle large-scale ELD problem. In order to tackle such deficiencies of the deterministic approaches, several evolutionary computing methods came into existence such as GA [1], particle swarm optimization (PSO) [2], interactive honey bee mating optimization (IHBMO) [3], iteration particle swarm optimization (IPSO) [4], firefly algorithm [5]. In recent past, many popular hybrid methods were developed to tackle medium and large-scale ELD problems with various operational constraints. To list a few, DHS algorithm which is the hybridization of DE and harmony search algorithm [6], shuffled differential algorithm (SDE), the hybridization of differential evolution (DE) and shuffled frog leap algorithm [7], Hybrid Differential Evolution (HDE), the hybridization of biogeography-based optimization (BBO) and DE [8], DEPSO algorithm, the hybridization of DE and PSO [9], HPSO-GSA algorithm [10], where PSO is hybridized with the gravitational search algorithm (GSA), and many other algorithms.

Inspired by several hybridized techniques to solve the ELD problem, in this paper, a novel hybrid algorithm is proposed which is the hybridization of GA and bacterial foraging optimization (BFO). Here, the chemotactic step of BFO has been inserted at the end of the GA cycle and the algorithm thus named as chemo-inspired genetic algorithm (CGA). It has been further extended for handling the constrained problems, thus renamed as chemo-inspired genetic algorithm for constrained optimization (CGAC). Initially, the algorithm is applied on 8 benchmarking problems taken from the literature and is being compared with H-LX-PM-C where hybridization of quadratic approximation (QA) with LX-PM-C is later named as H-LX-PM-C [11]. In H-LX-PM-C, the real-coded GA uses Laplace crossover and Power mutation. Later to test the efficiency and robustness of the algorithm, it has been applied on real-life problems where 40 generator power system with valve point loading effect has been considered.

The rest of the paper is organized as follows. Strategies for handling constraints in the proposed algorithm CGAC, brief outline of GA and BFO, the proposed method CGAC is explained in different subsections of Sect. 2. The experimental setup of benchmark functions and results and discussions are presented in Sect. 3.

Section 4 describes problem definition of ELD problem with valve point loading effect and the corresponding result analysis for them. The final conclusion of this paper is drawn in Sect. 5.

2 Strategies for Handling Constraints in the Proposed Algorithm CGAC

The following strategies (shown in steps) are being adopted for handing constrained optimization problems.

Step 1: *Evaluation of Fitness*

The fitness of an individual in the population is calculated by

$$\text{Fit\_Fun} = \begin{cases} F\left(x^{(t)}, R^{(t)}\right), & \text{for Minimization function} \\ 1/\left(1 + F\left(x^{(t)}, R^{(t)}\right)\right), & \text{for Maximization function} \end{cases} \tag{1}$$

where $F\left(X^{(t)}, R^{(t)}\right)$ called the penalty function defined in Eq. (2).

$$F\left(x^{(t)}, R^{(t)}\right) = f\left(x^{(t)}\right) + \Omega\left(R^{(t)}, g^{(t)}, h^{(t)}\right) \tag{2}$$

Here, f stands for the objective function, t for generation number, g for inequality constraints, h for equality constraints, and Ω for penalty term which is given by

$$\Omega = R\langle(g(x))\rangle^2, \tag{3}$$

where

$$\langle\alpha\rangle = \begin{cases} 0, & \text{if } \alpha \geq 0 \\ \alpha, & \text{if } \alpha < 0 \end{cases} \tag{4}$$

and R is the penalty parameter as defined in (5). It is worth here to note that each equality constraint in (2) is being equivalently expressed in two inequality terms with ≤ and ≥.

Step 2: *Penalty parameter*

The penalty parameter $R^{(t)}$ for a particular generation 't' is proposed as follows.

$$R^{(t)} = 1.2^{\left\lfloor \frac{t}{22} \right\rfloor} \tag{5}$$

where $\lfloor . \rfloor$ indicates the floor function.

For the constraint-handling technique, an exterior penalty term has been used, where the bracket operator assigns a positive value to the infeasible points. The algorithm starts with a small initial value of $R^{(t)}$, and it increases step-wise with t. This way, the quality of the solution improves gradually by forcing the infeasible points toward the feasibility and finally approaches to a near optimal solution. The value of R in (5) is so fixed because it is suitable for the entire constrained problem considered, which is experimentally verified.

Step 3: *Selection of Individuals*

The CGAC uses the tournament selection according to Deb's rule [12], where two candidates in the population are compared by applying the following criteria.

(i) Feasible solution is preferred over an infeasible solution.
(ii) Between two feasible solutions, the one having better objective function value is preferred.
(iii) Between two infeasible solutions, the one having smaller constraint violation is preferred.

The idea of tournament selection is illustrated in Fig. 1, through three different instances.

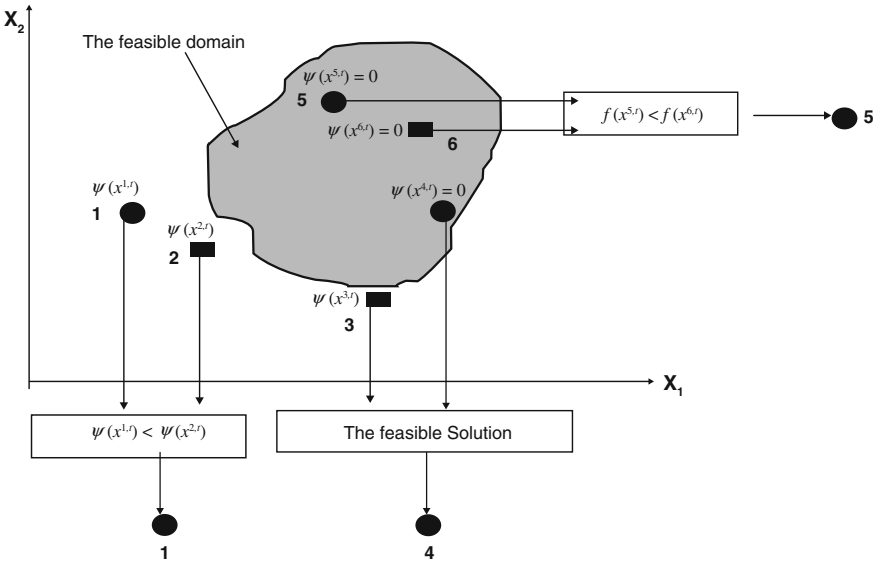

Fig. 1 The idea of the constraint tournament method

2.1 Brief on GA and BFO

This paper deals with the hybridization of some operators of GA and BFO. Although, both GA and BFO are well-known optimizers, it is still essential to present a brief outline of them. GA is a population-based method consisting of 4 major steps namely selection, crossover, mutation, and elitism. Based on the Darwin's principle of survival of fittest, GA selects the better individuals in the population with letting the worse die-off. Similarly, BFO also works with a population of individuals through its major operators like chemotaxis, reproduction, and elimination-dispersal steps. The detailed mechanisms of both GA and BFO are presented in our latest paper [13, 14]. Collectively, the objectives of both the mechanism are the same as to explore the search space and coming up with a near optimal solution. Each of them has some pitfalls in their inherent mechanism. Researchers [15, 16] tried to overcome them by the process of hybridization to solve unconstrained optimization problems. However, this paper presents a different type of hybridization of GA and BFO that is extended for being capable of handling constrained optimization problems later. The motivation and proposition of the method is presented in the next section.

2.2 The Proposed Chemo-inspired GA for Constrained Optimization (CGAC)

2.2.1 Motivation

The method of hybridization makes a mechanism more effective. Recently, researcher tried to hybridize GA and BFO [15]. However, visualizing both GA and BFO at a time, the following observations are noted.

(a) Selection, Crossover, Mutation, and Elitism are the four major operators in GA where as chemotaxis, reproduction, and elimination-dispersal are three principal mechanisms in BFO. In fact, *Selection* mechanism in GA is based on principle of retaining multiple copies of the best strings in the population which is similar in case of *Reproduction* step observed in classical BFO, where the least healthy bacteria dies and the healthier bacterium reproduce asexually.
(b) *Elitism* first combines the populations before and after the GA cycle and then eliminates the worse half in order to select the better half for the next generation. This mechanism is almost as similar as in elimination-dispersal step (in classical BFO), where elimination of strings and simultaneous insertion of new strings takes place with a very small probability at the end of BFO cycle.

From the above observations, it is realized that while hybridizing to BFO with GA, probably the *reproduction* and *elimination-dispersal steps* of BFO become inefficient as it is just like a repetition of few of the existing operators in GA. Hence,

only the c*hemotaxis* step of BFO that plays a major role has been picked up from BFO to hybridize in GA cycle as an additional operator. The proposed mechanism is now discussed in the next section. Clearly, CGAC has 5 major steps viz. Selection, crossover, mutation, elitism, and chemotaxis. To improve the solution quality further, three productive properties namely *Adaptive step size* [13, 16], *Squeezed search space* [13, 16], *Fitness function criterion* [13, 16] *and Modified Chemo tactic step size* [13] have been employed in the mechanism as illustrated in the improved BFO [16].

Pseudo code for CGAC:

The stepwise proposed algorithm CGAC is given below.

[Step 0] Parameter consideration

P : Dimension of the variable.

S : Number of bacteria.

N_c : Number of chemo tactic steps.

N_S : Swim steps.

C_{step}: Step size of the bacterium.

X^i : Initial position of the i^{th}bacterium.

$X^i(j)$: Position of the i^{th} bacterium at $\mathrm{j}^{\mathrm{th}}$the chemo tactic step.

F_{best}: The best fitness value of the bacteria swarm.

X_{best}: The corresponding position of the F_{best} .

$Min(j), Max(j)$: Search scope of the bacteria.

i : Index of bacteria number, $i = 1,2,.....S$.

j : Index of chemo tactic step, $j = 1,2,.....N_c$.

m : Index of the swimming steps, $m = 1,2,.....N_S$.

[Step 1] **Begin**: Initialize the population. Calculate the fitness function by (1).

While *(termination criterion is not satisfied)* ***do***

[Step 2] Apply binary tournament selection.

[Step 3] Apply crossover operator.

[Step 4] Apply mutation operator.

[Step 5] Use Elitism Operator.

[Step 6] Chemo taxis loop:

The detailed steps are

[Sub step a] **Re initialization of the search space as in [13]:**

For $j = 1 : N_c$

For $i = 1 : S\,1$

Compute the fitness function $fit\left(X^i(j)\right)$.

Update F_{best} and X_{best}

Squeeze the search space.

[Sub step b] **Tumble and Move:**

Calculate the new position: $X^i(j+1) = X^i(j) + C_{step}\frac{\Delta(i)}{\sqrt{\Delta(i)\Delta^T(i)}}$ (6)

where $\Delta(i) \in R^p$ with each element $\Delta_m(i), m = 1,2...P,$ a random number on [-1, 1]. (This results in a step size C_{step} in the direction of the tumble for bacterium i).

Calculate the C_{step} according to adaptive or chemo tactic step size as applicable.

[Sub step c] **Swim Step:**

Let $m = 0$ (counter for swim length).

While $m < N_S$ (If have not climbed down too long) **do**

Let $m = m + 1$.

If $fit(X^i(j+1)) < F_{best}$

Update F_{best} and X_{best} and calculate the new position as follows.

$$X^i(j+1) = X^i(j+1) + C_{step}\frac{\Delta(i)}{\sqrt{\Delta(i)\Delta^T(i)}} \quad (7)$$

Then compute the $fit(X^i(j+1))$ again. Else keep the bacterium stay still.

$X^i(j+1) = X^i(j)$. Calculate the fitness value of $X^i(j+1)$, let $m = N_S$.

End **While**

End for $(i = 1:S)$

End for $(j = 1: N_c)$

End **While**

End **begin**

3 Experimental Set Up

A set of 8 well-known benchmark functions (listed in Appendix [11]) have been picked up for numerical simulation to testify the performances of CGAC. The comparison is made with LX-PM-C and H-LX-PM-C [11]. LX-PM is a real-coded GA that uses Laplace crossover and Power Mutation, and its hybridization with QA Operator is named as H-LX-PM-C. Here, the last '*C*' denotes that the algorithm is being capable of handling constraints. The proposed CGAC is designed in C++, and the experiment is carried out on a P-IV, 2.8 GHz machine with 512 MB RAM under WINXP platform.

After a series of hand-tuning experiments, the values of the parameters are recommended as follows. Probability of crossover (P_c = 0.9), probability of mutation (P_m = 0.05), bit length (l = 20), maximum step size (C_{max} = 0.1), minimum step size (C_{min} = 0.008). For problems 5 and 7, the minimum and maximum step sizes are kept to be to 0.001 and 10^{-7}, respectively. A total of 40 chemotactic steps are considered for each problem. However, for problem 5, chemotactic steps are considered to be 90. The population size is fixed at 40. Out of 40 individuals, only 4 individuals/bacteria are allowed to go for the completion of chemotactic loop. The chemotactic loop is reinitialized after 10 generations for problems 5 and 7, respectively. But for the rest, the chemotactic loop is reinitialized after 100 generations. The stopping criteria are either a maximum of 2,000 generations is

attained or no improvement is found in the best objective function value achieved so far in a consecutive 100 generations. A run is said to be success if the objective function value obtained by the algorithm is within 1 % accuracy of the known optimal solution.

3.1 Analysis of Result

With the above experimental set up, each of 8 benchmark problems undergoes a total of 100 independent runs. The success rates are reported in Table 1. For the successful runs, the average function evaluations are reported in Table 2. The computational time is reported in Table 3. The mean function value and the standard deviation (S.D) are presented in Table 4. In Tables 1, 2, 3 and 4, the best values are highlighted with bold faced letters.

Looking at Table 1, CGAC nowhere achieves less success rate than LX-PM-C and H-LX-PM-C [11] in all 8 problems. Again, the last part of Table 4 bears the S.D of all the methods. Though CGAC takes more number of function evaluations and time, in return, it yields better objective function values, S.D, and more success rate. Therefore, CGAC is more accurate and more stable as compared with LX-PM-C and H-LX-PM-C.

Table 1 Percentage of success for 100 runs

Pb. No.	CGAC	H-LX-PM-C	LX-PM-C
1	**100**	**100**	**100**
2	**100**	98	99
3	**100**	5	3
4	**100**	**100**	98
5	**13**	5	5
6	**100**	12	11
7	**46**	22	15
8	**58**	52	34

Table 2 Average no of function evaluation

Pb. No.	CGAC	H-LX-PM-C	LX-PM-C
1	**9,671**	25,439	25,649
2	72,893	**30,472**	30,768
3	438,459	**10,204**	10,586
4	708,050	**49,209**	52,504
5	62,844	**31,428**	32,520
6	708,050	**10,273**	10,405
7	115,471	**10,153**	10,246
8	**12,611**	31,259	30,829

Table 3 Average no of computational time in (s)

Pb. No.	CGAC	H-LX-PM-C	LX-PM-C
1	**0.062**	0.5116	0.1203
2	0.31543	0.7176	**0.2195**
3	1.87665	0.1904	**0.0620**
4	8.23954	1.4472	**0.7026**
5	0.5903	0.7908	**0.3188**
6	3.723	0.2163	**0.0712**
7	0.414717	0.1945	**0.0627**
8	**0.1205**	0.6169	0.2983

Table 4 Mean objective function value and S.D

Pb. No.	Mean function values			S.D		
	CGAC	H-LX-PM-C	LX-PM-C	CGAC	H-LX-PM-C	LX-PM-C
1	**−320.000**	**−320.000**	**−320.000**	**0.0000**	**0.0000**	**0.0000**
2	−310.000	**−313.000**	**−313.000**	**0.0000**	**0.0000**	**0.00000**
3	**13.5909**	13.641	13.644	**1.49e−05**	0.0451	0.0223
4	**680.732**	682.282	682.433	**0.08851**	0.8681	1.3023
5	**−12.5672**	−11.951	−11.976	0.45374	**0.0693**	0.0726
6	**−5.50801**	−5.475	−5.475	**8.36e−14**	0.0125	0.0125
7	−16.7069	**−16.745**	−16.742	**0.03887**	0.1072	0.0999
8	5,136.99	**5,134.106**	5,139.564	**10.7796**	18.7828	16.0353

4 Problem Definitions of Economic Load Dispatch Problems with Valve Point Loading Effect

The objective of the ELD analysis with valve point loading effect is determination of the optimal combination of power generations by minimizing the total generation cost satisfying the generational constraints viz. (i) Power balance constraint, (ii) Generator capacity constraint. The overall problem can then be formulated as a constrained optimization problem as follows defined by Eq. (8).

$$\text{Min } F = \sum_{i=1}^{n} F_i(P_i) \tag{8}$$

where F is the objective function describing the total generation cost. P_i is the power output of the ith unit. $F_i(P_i)$ is the generation cost for the generator of unit i to produce power output P_i having quadratic cost function defined by Eq. (9). n is the number of committed units.

$$F_i = a_i P_i^2 + b_i P_i + c_i \tag{9}$$

where a_i, b_i and c_i are the coefficients of generator i. The generating units based on multi valve steam turbines are characterized by complex nonlinear fuel cost function. Such characteristics are happening due to the ripples induced during the valve point loading. The simulation of such phenomenon is done by super imposing the sinusoidal component on the quadratic heat rate curve. So, if the valve point loading effect is taken into, the sinusoidal terms are added to the quadratic cost function and modified generation cost is defined as follows by Eq. (10)

$$F_i = a_i P_i^2 + b_i P_i + c_i + \left| e_i \sin\left(f_i\left(P_i^{\min} - P_i\right)\right)\right| \tag{10}$$

The fuel cost $F_i(P_i)$ is the sum of the quadratic function and the sinusoidal function. Where a_i, b_i, and c_i are the coefficients of generator i. e_i, and f_i are the coefficients of unit i reflecting the valve point effects. Here, P_i is the power output of the ith generator. $P_i^{\min}$ is the minimum power output of the ith generator.

Subject to the following generator constraints:

(I) **Generator capacity constraints**

The power output P_i of the ith unit should vary within its minimum and maximum limits which is defined as Eq. (11)

$$P_i^{\min} \le P_i \le P_i^{\max} \tag{11}$$

where $P_i^{\min}$ and $P_i^{\max}$ are the minimum and maximum power output of the unit i.

(II) **Power balance constraint defined in Eq. (12)**

The power output P_i of the ith unit defined as Eq. (11) is subject to the following power balance constraint as defined in Eq. (12)

$$\sum_{i=1}^{n} P_i = P_D + P_L, \tag{12}$$

where P_D is load demand and P_L is the total transmission network losses of the system. The power loss P_L is calculated using the B-coefficients matrix, which can be expressed as the quadratic function of unit, s power output defined as Eq. (13).

$$P_L = \sum_{i=1}^{n}\sum_{j=1}^{n} P_i B_{ij} P_j + \sum_{i=1}^{n} B_{0i} P_i + B_{00} \tag{13}$$

where, B_{ij} is the ijth element of loss co-efficient square matrix of size n.

4.1 Experimental Setup

In this section, a power system having 40 generators has been considered with valve point loading effect. The expected power demand to be met by all the 40 generating units is 10,500 MW. The system data can be found from [17, 18]. The results have been compared with Hybrid Chaotic Particle Swarm Optimization and Sequential Quadratic Programming (CPSO-SQP), Evolutionary Programming (EP), Evolutionary Programming and Sequential Quadratic Programming (EP-SQP), PSO, Particle Swarm Optimization and Sequential Quadratic Programming (PSO-SQP), Chaotic Particle Swarm Optimization (CPSO) and many other popular algorithms in terms of mean cost, best cost, and CPU time. Again the results have been compared in terms of best, average, worst function value, S.D, total no of function evaluation with firefly algorithm and many other algorithms with whom it is being compared. For each problem, 100 independent runs are performed by keeping the following basic parameters fixed.

(I) Population size = 40
(II) Number of Bacteria reinitialized in chemotactic loop = 4
(III) The Probability of cross over (P_c) = 0.9
(IV) Probability of mutation (P_m) = 0.001
(V) Bit length (l) = 20
(VI) The stopping criteria are either a maximum of 500 generations is attained, or no improvement is observed in the best objective function value in consecutive 200 generations
(VII) The chemotactic loop is allowed after 700 generations
(VIII) Number of chemotactic steps = 40
(IX) Number of swim steps = 4.

Table 5 Comparison of the total generation cost in 40 unit generator [17]

Method	Mean time (s)	Best cost ($/h)	Mean cost ($/h)
EP	1,167.35	122,624.35	123,382.00
EP-SQP	997.73	122,323.97	122,379.63
PSO	933.39	123,930.45	124,154.49
PSO-SQP	733.97	122,094.67	122,245.25
GA-PS-SQP	46.98	121,458	122,039
CPSO	114.65	121,865.23	122,100.87
CPSO-SQP	98.49	121,458.54	122,028.16
GA-BFO	**25.1906**	121,598	121,869
CGAC	51.5447	**120,816.413**	**121,309**

Table 6 The best, average, and worst results of different ED solution in terms of function evaluation for the 40 unit test system [5]

Methods	Generation cost ($/h)				
	Best	Average	Worst	S.D	No. of function evaluation
HGPSO	124,797.13	126,855.70	NA	1,160.91	NA
SPSO	124,350.40	126,074.40	NA	1,153.11	NA
PSO	123,930.45	124,154.49	NA	NA	10,000
CEP	123,488.29	124,793.48	126,902.89	NA	NA
HGAPSO	122,780.00	124,575.70	NA	906.04	NA
FEP	122,679.71	124,119.37	127,245.59	NA	NA
MFEP	122,647.57	123,489.74	124,356.47	NA	NA
IFEP	122,624.35	123,382.00	125,740.63	NA	NA
TM	122,477.78	123,078.21	124,693.81	NA	4,050
EP-SQP	122,323.97	122,379.63	NA	NA	10,000
MPSO	122,252.26	NA	NA	NA	NA
ESO	122,122.16	122,558.45	123,143.07	NA	75,000
HPSOM	122,112.40	124,350.87	NA	978.75	NA
PSO-SQP	122,094.67	122,245.25	NA	NA	10,000
PSO-LRS	122,035.79	122,558.45	123,461.67	NA	20,000
Improved GA	121,915.93	122,811.41	123,334.00	NA	100,000
HPSOWM	121,915.30	122,844.40	NA	497.44	NA
IGAMU	121,819.25	NA	NA	NA	NA
HDE	121,813.26	122,705.66	NA	NA	100
DEC (2) SQP (1)	121,741.97	122,295.12	122,839.29	386.181	18,000
PSO	121,735.47	122,513.91	123,467.40	NA	20,000
APSO (i)	121,704.73	122,221.36	122,995.09	NA	20,000
ST-HDE	121,698.51	122,304.30	NA	NA	100
NPSO-LRS	121,664.43	122,209.31	122,981.59	NA	20,000
APSO (ii)	121,663.52	122,153.67	122,912.39	NA	20,000
SOHPSO	121,501.14	121,853.57	122,446.30	NA	62,500
BBO	121,479.50	121,512.06	121,688.66	NA	50,000
BF	121,423.63	121,814.94	NA	124.876	10,000
GA-PS-SQP	121,458.00	122,039.00	NA	NA	1,000
PS	121,415.14	122,332.65	125,486.29	NA	1,000
FA	121,415.05	121,416.57	121,424.56	1.784	25,000
GA-BFO	121,598	121,869	122,077	156.148	31,600
CGAC	**120,816.413**	**121,309**	**121,810.14929**	109.675	73,292

4.2 Result and Discussion

The comparison of the result for 40 generators power system in terms of mean cost, best cost, and mean CPU time are reported in Table 5. The best, average, worst function values, standard deviation, total no of function evaluation for 40 generators are mentioned in Table 6. The output of power generators in the best result of the proposed CGAC for the forty generators is shown in the Table 7 (for 500 generation) and Table 8 (for 1,500 generation). In all the tables, the bold face letters indicate the best result obtained by the corresponding mechanism/algorithm. The success rate (S.R), best, average, and worst function values, standard deviation, time, and total no of function evaluation varying the population size and keeping the generation (500 fixed) and (1,500 fixed) for forty generator are reported in Tables 9

Table 7 Output power of generators in the best result of the proposed CGAC for the 40 unit test system in 500 iterations

Unit	Power (MW)	Unit	Power (MW)
1	112.46837851377	21	523.606366735946
2	113.566474501022	22	524.281599313305
3	98.394564051022	23	523.906438737975
4	180.584211906587	24	526.356979710112
5	89.035333667093	25	523.232899887901
6	139.514815821588	26	523.745252366672
7	259.959707221718	27	523.4602245906172
8	284.3024390244	28	10.4602245906172
9	286.928402832608	29	10.1574136326231
10	130.502586843842	30	13.6266552228141
11	168.8178327735	31	92.0685454068619
12	167.890880480523	32	188.8835800967
13	214.575495314926	33	189.888543976299
14	395.423431799857	34	187.452132656415
15	303.693226522	35	166.56018882789
16	393.992561333057	36	165.295253081601
17	491.341849653355	37	91.573301862035
18	489.335393272222	38	108.825811220009
19	512.989771832746	39	109.851169444215
20	511.68853920777	40	510.70645685818
Total generation (MW)	10,500		
Generation cost ($/h)	120,624.035031642		

Table 8 Output power of generators in the best result of the proposed CGAC for the 40 unit test system (1,500 iterations)

Unit	Power (MW)	Unit	Power (MW)
1	111.85647378586	21	523.240803948258
2	110.412182247319	22	522.012851727391
3	97.1868106716195	23	524.276800419658
4	179.588460529772	24	524.729590158034
5	95.4948143909586	25	523.159787330412
6	139.870429869112	26	524.273977540929
7	299.673843072759	27	10.6575590682335
8	285.023446105388	28	11.5427604129404
9	284.569000786797	29	10.8503540519636
10	130.085115513935	30	90.8971938106398
11	94.1699010562	31	189.430570059367
12	94.392326729	32	189.742498152249
13	215.2131464129	33	188.626450182418
14	395.33760103	34	167.966850249125
15	394.416350761	35	164.536795174409
16	394.2911808883	36	170.227222659323
17	491.393386262251	37	109.818258112
18	489.307889278247	38	109.848089073256
19	510.838185156057	39	108.112543213407
20	511.141316548713	40	511.787183558548
Total generation (MW)	10,500		
Generation cost ($/h)	120,549.105519167		

and 10, respectively. It can be visualized from the Tables 5 and 6 that CGAC achieves better result in terms of best cost, mean cost, and mean time and all other parameters mentioned in those Tables in comparison with other algorithms mentioned though it takes more number of function evaluations. It can be observed from Table 9, as the population size increases keeping the generation 500 fixed, CGAC achieves the best, mean, worst objective function value, less standard deviation in 800 generations. Similarly, it achieves the best, worst, function value in 200 generations keeping the generation (1,500 fixed) visible from Table 10.

Table 9 Comparison of best, mean worst function value in terms of time and function evaluation varying population size in CGAC for 40 generator (Max gen = 500)

Pop. size	S.R	Best value	Mean	Worst	S.D	Time (s)	Function evaluation	Max iteration
200	100	120,816.413507	121,309	121,810.14929	109.675	51.5447	73,292	500
400	100	121,009.72185	121,201	121,514.646044	103.07	143.83	107,320	500
800	100	**120,624.03503164**	**121,104**	**121,252.8774668**	**94.7445**	698.917	253,489	500

Table 10 Comparison of best, mean worst function value in terms of time, and function evaluation varying population size in CGAC for 40 generator (Max gen = 1,500)

Pop. size	S.R	Best value	Mean	Worst	S.D	Time (s)	Function evaluation	Max iteration
40	100	120,681.156509	120,900	121,505	167.007	32.9503	420,040	1,500
80	100	120,610.526189	120,864	120,997.330109	131.339	42.2012	480,080	1,500
100	100	1,20,575.950677	120,823	120,999.9266	107.121	59.4816	510,100	1,500
150	100	120,549.105519	120,761	121,212.105519	180.527	119.076	585,150	1,500
200	100	**1,20,550.944596**	**120,727**	**120,937.44237**	136.779	190.334	647,983	1,500

5 Conclusion

In this paper, an attempt is made to hybridize the chemotactic step of BFO within the GA cycle and name it as chemo-inspired GA. It is further developed to handle constraints by using bracket penalty parameter. The algorithm thus generated for constrained optimization problems is abbreviated as CGAC. The validation of better performance of CGAC is investigated through a set of 8 constrained benchmark problems of different taste. From the results and discussion, it is concluded that though CGAC takes more number of function evaluations and computational time in comparison with LX-PM-C and H-LX-PM-C, still it provides more success rate, yields better objective function values and standard deviation (S. D) in most of the cases as compared to the real-coded GA that uses Laplace crossover and Power mutation. Further, one test case of ELD problem has been solved in which the parallel result is achieved with a conclusion that CGAC performs similar or better than hybrid CPSO-SQP algorithm, EP, EP-SQP, PSO, PSO-SQP, CPSO, firefly algorithm, GA-BFO and other popular and continuous methods available in the literature.

References

1. Chiang, C.L.: Genetic based algorithm for power economic load dispatch. IEEE Proc. Gener. Transm. Distrib. **1**(2), 261–269 (2007)
2. Chaturvedi, K.T., Pandit, M., Srivastava, L.: Particle swarm optimization with crazy particles for non-convex economic dispatch. Appl. Soft. Comput. **9**, 962–969 (2009)
3. Ghasemi, A.: A fuzzified multi objective interactive honey bee mating optimization for environmental/economic power dispatch with valve point effect. Electr. Power Syst. Res. **49**, 308–321 (2013)
4. Safari, A., Shayeghi, H.: Iteration particle swarm optimization procedure for economic load dispatch with generator constraints. Expert Syst. Appl. **38**, 6043–6048 (2011)
5. Yang, X.S., Hosseini, S.S.S., Gandomi, A.H.: Firefly algorithm for solving non-convex economic dispatch problems with valve loading effect. Appl. Soft Comput. **12**, 1180–1186 (2012)
6. Wang, L., Li, L.P.: An effective differential harmony search algorithm for the solving non-convex economic load dispatch problems. Electr. Power Syst. Res. **44**, 832–843 (2013)
7. Reddy, A.S., Vaisakh, K.: Shuffled differential evolution for large scale economic dispatch. Electr. Power Syst. Res. **96**, 237–245 (2013)
8. Bhattacharya, A., Chattopadhyay, P.K.: Hybrid differential evolution with biogeography based optimization for solution of economic load dispatch. IEEE Trans. Power Syst. **25**(4), 1955–1964 (2010)
9. Sayah, S., Hamouda, A.: A hybrid differential evolution algorithm based on particle swarm optimization for non convex economic dispatch problems. Appl. Soft Comput. **13**, 1608–1619 (2013)
10. Jiang, S., Ji, Z., Shen, Y.: A novel hybrid particle swarm optimization and gravitational search algorithm for solving economic emission load dispatch problems with various practical constraints. Electr. Power Syst. Res. **55**, 628–644 (2014)
11. Deep, K., Das, K.N.: A novel hybrid genetic algorithm for constrained optimization. Int. J. Syst. Assur. Eng. Manage. **4**(1), 86–93 (2013)

12. Deb, K.: An efficient constraint handling method for genetic algorithms. Comp. Methods Appl. Mech. Eng. **186**(2–4), 311–338 (2000)
13. Das, K.N., Mishra, R.: Chemo-inspired genetic algorithm for function optimization. AMC **220**, 394–404 (2013)
14. Das, K.N., Mishra, R.: A performance study of chemo-inspired genetic algorithm on Benchmark functions. In: Proceedings of 7th International Conference on Bio-inspired Computing: Theories and Applications (BICTA-2012). Advances Intelligent System and Computing, vol. 202, pp. 489–501. Springer, Berlin (2013)
15. Kim, D.H., Abraham, A., Cho, J.H.: A hybrid genetic algorithm and bacterial foraging approach for global optimization. Inf. Sci. **177**(18), 3918–3937 (2007)
16. Chen, Y., Lin, W.: An improved bacterial foraging optimization. In: Proceedings of the IEEE International Conference on Robotics and Biomimetics, 19–23 Dec 2009, Guilin, China (2009)
17. Cai, J., Li, Q., Li, L., Peng, H., Yang, Y.: A hybrid CPSO-SQP method for economic dispatch considering the valve-point effects. Energy Convers. Manage. **53**, 175–181 (2012)
18. Chaturvedi, K.T., Pandit, M., Srivastava, L.: Self-organizing hierarchical particle swarm optimization for non-convex economic dispatch. IEEE Trans. Power Syst. **23**(3), 1079–1087 (2008)

Engineering Design Optimization Using Hybrid (DE-PSO-DE) Algorithm

Kedar Nath Das and Raghav Prasad Parouha

Abstract In this paper, a novel hybrid intelligent algorithm, integrating with differential evolution (DE) and particle swarm optimization (PSO), is proposed. Initially, all individual in the population are divided into three groups (in increasing order of function value): inferior group, mid-group, and superior group. DE is employed in the inferior and superior groups, whereas PSO is used in the mid-group. The proposed method uses DE-PSO-DE, then it is denoted by DPD. At present, many mutation strategies of DE are reported. Every mutation strategy has its own pros and cons, so which one of them should be selected is critical for DE. Therefore, over 8 mutation strategies, the best one is investigated for both DEs used in DPD. Moreover, two strategies, namely *elitism* (to retain the best obtained values so far) and *Non-redundant search* (to improve the solution quality), have been employed in DPD cycle. Combination of 8 mutation strategies generated 64 different variants of DPD. Top 4 DPDs are investigated through solving a set of constrained benchmark functions. Based on the 'performance,' best DPD is reported and further used in solving engineering design problem.

Keywords Differential evolution · Particle swarm optimization · Non-redundant search · Elitism · IEEE CEC2006 function · Engineering design problem

1 Introduction

Engineering optimization problems are normally adopted to judge the performance of any optimization algorithm. These problems normally include mixed, continuous and discrete design variables, nonlinear objective functions, and nonlinear constraints.

K.N. Das (✉) · R.P. Parouha
NIT Silchar, Silchar, Assam, India
e-mail: kedar.iitr@gmail.com

R.P. Parouha
e-mail: rparouha@gmail.com

K.N. Das et al. (eds.), *Proceedings of Fourth International Conference on Soft Computing for Problem Solving*, Advances in Intelligent Systems and Computing 335,
DOI 10.1007/978-81-322-2217-0_38

Usually, these problems are also called constrained optimization problems. In recent decades, many optimization algorithms have been developed to solve various engineering design problems. Among them, differential evolution (DE) [1] and particle swarm optimization (PSO) [2] are successfully and widely applied in scientific and engineering research. Each of these algorithms has some advantages and disadvantages which may make them work well in some problems and not work well in some others. With hybridizing these algorithms, they may be able to cover each other's weaknesses and have a better performance. Hence, researchers started working on the hybridization techniques between DE and PSO in order to maintain a proper balance between exploration and exploitation.

Many numerous hybrids of DE and PSO [3–11] have been developed with diverse design ideas from many researchers. These approaches move around the enhancement of capabilities of DE and PSO in various aspects. Recently, parallel employment of DE/PSO [12–20] is preferred over the sequential one. Here, parallel in the sense, DE and PSO are used simultaneously on different part of the same population. These new variety hybridization of DE and PSO provided the better performance in the different field of optimization.

Keeping in view the earlier work, a further study is being carried out in this paper to improve the solution quality of the hybridization of DE and PSO in a different fashion. In this study, the process of hybridization is being emphasized with a tri-breakup of the population. The novel hybrid algorithm thus proposed is named as DE-PSO-DE (DPD) for solving engineering design problems.

The remaining contents are organized as follows. Section 2 provides a brief review of DE and PSO. Section 3 presents constrained handling technique used in this present study. In Sect. 4, the hybrid DPD strategy is proposed and explained in detail. Section 5 contains comparison of proposed algorithm with latest evolutionary algorithm for engineering design problem. The conclusion and future works are drawn at the last Sect. 6.

2 Brief on DE and PSO

2.1 Differential Evolution (DE)

The three main operators of DE are mutation, crossover, and selection.

(a) Mutation: There are many mutation strategies in DE, and some well-known mutation strategies [21, 22] are listed as follows:

M_1.	'DE/rand/1/bin'	$v_i = x_{r_1} + F \times (x_{r_2} - x_{r_3})$
M_2.	'DE/rand/2/bin'	$v_i = x_{r_1} + F \times (x_{r_2} - x_{r_3}) + F \times (x_{r_4} - x_{r_5})$
M_3.	'DE/best/1/bin'	$v_i = x_{\text{best}} + F \times (x_{r_2} - x_{r_3})$
M_4.	'DE/best/2/bin'	$v_i = x_{\text{best}} + F \times (x_{r_2} - x_{r_3}) + F \times (x_{r_4} - x_{r_5})$

(continued)

(continued)

M_5.	'DE/rand-to-best/1/bin'	$v_i = x_{r_1} + F \times (x_{\text{best}} - x_{r_2}) + F \times (x_{r_3} - x_{r_4})$
M_6.	'DE/current-to-best/1/bin'	$v_i = x_i + F \times (x_{\text{best}} - x_i) + F \times (x_{r_2} - x_{r_3})$
M_7.	'DE/rand-to-best/2/bin'	$v_i = x_{r_1} + F \times (x_{\text{best}} - x_{r_2}) + F \times (x_{r_3} - x_{r_4}) + F \times (x_{r_5} - x_{r_6})$
M_8.	'DE/current-to-best/2/bin'	$v_i = x_i + F \times (x_{\text{best}} - x_i) + F \times (x_{r_2} - x_{r_3}) + F \times (x_{r_4} - x_{r_5})$

where $F \in [0, 1]$ is the mutation coefficient, x_{best} represents the best individual in the current generation, $i \neq r_1 \neq r_2 \neq r_3 \neq r_4 \neq r_5 \neq r_6, \quad i, r_1, r_2, r_3, r_4, r_5, r_6 \in \{1, \ldots, N_p\}$, x_i is referred to the *target* vector; v_i is the *mutant* vector.

(b) Crossover: $U_{j,i,G+1} = \begin{cases} V_{j,i,G+1}; & \text{if} \quad (\text{rand}_j \leq CR) \text{or} (j = j_{\text{rand}}) \\ X_{j,i,G}; & \text{if} \quad (\text{rand}_j > CR) \text{or} (j \neq j_{\text{rand}}) \end{cases}$
where $j = 1, 2, \ldots, D$; $rand_j \in [0, 1]$; CR is the crossover constant takes values in the range [0, 1]; and $j_{rand} \in (1,2,\ldots,D)$ is the randomly chosen index.

(c) Selection: $x_{i,G+1} = \begin{cases} U_{i,G+1}; & \text{if} \quad f(U_{i,G+1}) \leq f(X_{i,G}) \\ X_{i,G}; & \text{otherwise} \end{cases}$

2.2 Particle Swarm Optimization (PSO)

PSO is a robust stochastic optimization technique based on the swarm intelligence. PSO also starts with an initial population with a fixed population size for an N dimensional problem. Let the *i*th particle $x_i(G) = (x_{i1}(G), x_{i2}(G), \ldots, x_{iN}(G))$ has velocity $v_i(G) = (v_{i1}(G), v_{i2}(G), \ldots, v_{iN}(G))$ at any generation '*G*'. During the simulation, each particle flies to its previous best position *pBest* and the global best position *gBest*. Thus, a particle's velocity and position are updated by the following equations:

$$v_i(G+1) = \underbrace{wv_i(G)}_{\text{Inertia component}} + \underbrace{c_1 r_1(G)(\text{pBest}_i(G) - x_i(G))}_{\text{Cognitive Component}} + \underbrace{c_2 r_2(G)(\text{gBest}(G) - x_i(G))}_{\text{Social Component}} \tag{1}$$

$$x_i(G+1) = x_i(G) + v_i(G+1) \tag{2}$$

where c_1 and c_2 are positive constants, called 'acceleration coefficients,' r_1 and r_2 are random numbers that are uniformly distributed in [0, 1], and w is called the 'inertia weight' that controls the impact of the previous velocity of the particle on its current one. The population of particles is then allowed to move by using (1) and (2) and tends to cluster together, approaching from different directions.

3 Constraints Handling

One important issue in constrained optimization is the method used to handle the constraints. The method must guide the optimization to feasible regions and be able to reach the bounds of the search space. Transformation method is one of the simplest and popular methods to handle constraints [23]. In this method, the constrained problem transfers to an unconstrained one just by adding penalty term to the objective function for each of the constraint violation, as follows.

$$F(x,R) = f(x) + \Omega\,(R,g,h)$$

where F: penalty function, f: objective function, Ω: penalty term, R: penalty parameter, $g(x)$: inequality constraint, $h(x)$: equality constraint.

The above transformation method is also known as penalty method. As pointed out by Michalewicz [24], penalty method is widely used to solve constrained optimization problem. But the difficult task is to fine-tune the parameter. In spite of that many penalty methods such as parabolic penalty, infinite barrier penalty, log penalty, inverse penalty, and bracket operator penalty are available in the literature. In general, these penalty methods are categorized into 3 types as follows.

i. Exterior penalty method (where only infeasible points are penalized)
ii. Interior penalty method (where only the feasible points are penalized)
iii. Mixed penalty method (where both infeasible and feasible points are penalized)

While solving the constrained optimization problems with evolutionary optimization algorithms, the mixed penalty method is that much efficient over the rest two. However, the exterior penalty method is preferred over the interior penalty method for a simple reason that inserting more infeasible strings in the population is rather easier than that of feasible points. Moreover, among all exterior penalty methods, 'bracket operator penalty' is the simplest and efficient one to use [23], which is given as follows.

$$\Omega = R\langle g(x)\rangle^2 \quad \text{where} \quad \langle\alpha\rangle = \begin{cases} 0, & \text{if } \alpha \geq 0 \\ \alpha, & \text{if } \alpha < 0 \end{cases}$$

It is worth to note here that the equality constrained needs to be converted to inequalities before applying bracket operator penalty method. Because of its efficiency, this method is considered to use in the present study.

4 Proposed Method DPD and the Selection of DE-Mutation-Strategies for DPD

The main aim of this research is to develop a new optimization approach for solving complex optimization problems in design and manufacturing area.

4.1 Proposed Method

Inspiration/Motivation:
Hybridization has turned out to be an effective and efficient approach to design high-performance optimizers, which is witnessed by the rapid evolution of diverse hybridization techniques in the past decades. The motivation behind the hybridization is parallel employment of DE/PSO (Sect. 1) with breakup initial population. Moreover, population breakup technology [12–20] uses with different heuristics exhibits—(i) accelerate the convergence rate and maintains better diversity, especially in the early stage of evolution, (ii) enhance the capability of local search and balance between exploration and exploitation, and (iii) obtain the global optimal solutions with higher likelihood. Also this kind of hybridization gets more importance, when solving complex constrained optimization problems.

Due to the robust behavior of mutation operators, DE has the ability to balance exploration and exploitation, over search space. As reported in [12–14, 18–20], DE works better at two or more different situations where the local search or the global search is essential. However, inherent shortcomings of DE, sometimes, stacking in some local minimal or choosing the path to premature convergence is unavoidable. Hence, many a time the diversity in the population needs to be maintained. Therefore, introduction of another mechanism becomes essential in the group based hybridization methods. It is also observed that the behavior of PSO is to wildly seek the potential solution. It diversifies the candidate solutions in a better way and probably also helps in avoiding some shortcomings of DE, in the hybrid system. All in all hybridization of DE and PSO is to take advantage of both algorithms for providing better solution, simultaneously.

Idea of the hybridization:
Keeping in view the above observations, a tri-breakup-population based mechanism is proposed. It initiates with a random population. Then strings are then sorted according to the increasing order of their function value. Now, the population is being allowed to break into three different groups A, B, and C, namely inferior group (first 1/3rd part of the population), mid-group (middle 1/3rd part of the population), and superior group (last 1/3rd part of the population), respectively. Of course, the population size is kept fixed to a multiple of 3 to favor the tri-breakup mechanism. According to the local and global searching behavior of DE (as observed above), it is allowed to being employed in both the inferior and superior

groups (i.e., to A and C). At the same time, PSO is used in the mid-group (i.e., to B) to overcome the shortcomings of DE. After this, combining the resultant population comes out from group A, B, and C. As it uses DE-PSO-DE, then it is renamed as DPD. Further two strategies, namely elitism and non-redundant search applied in DPD cycle, which works as follows:

Elitism:

Elitism works with the following two steps, in each generation.

(a) Merging together the initial population and the combining population left from group A, B, and C.
(b) Sorting them and allow the best half individuals to be selected for the next population in order to continue the simulation process.

Hence, by the process of elitism, the less-fit individual's die off and discard from the current population. Moreover, few of the best-fit individuals those are left out in the initial population get again a chance to participate in the next round.

NRS (Non-Redundant Search):

In DPD algorithm, NRS is used as a local search. The NRS works as follows

(a) Deleting all repeated individuals in the current population, except keeping only one copy.
(b) Filling the vacant position by randomly selected individuals.

Subsequently, NRS helps to avoid the individuals to cluster together at one place.

However, the key steps are as follows:

i. Random initialization of population.
ii. Fitness evaluation and sorting of individuals in the increasing order of fitness.
iii. Population breakup (into 3 parts, namely A, B, and C as described earlier).
iv. Employment of PSO and DE on Group A, B, and C, respectively.
v. Combine the resultant sub-populations to create a new population.
vi. Apply 'elitism' using two different populations given below.
    (a) Population before starting of the generation.
    (b) New population obtained at the end of the generation.
vii. Apply NRS.
viii. If the stopping criterion is satisfied, go to step ii. Else go to step ix.
ix. Report the optimal solution obtained and stop.

4.2 Selection of DE-Mutation-Strategies in DPD

In the previous section, it is decided to use DE-PSO-DE on the tri-breakup concept of population. In case of PSO, there is no much parameter to be fine-tuned. However, the kernel operator 'mutation' in DE has many variants. The selection of a suitable mutation operator in DE helps to explore the search space efficiently. In

order to select the best mutation operators, a total of 8 popular mutation [21, 22], as listed in subsection 2.1, are picked to participate in the present study. For a particular variant of DPD, the DE used on A and the DE used on C may have different mutation variants out of M_1–M_8, whereas the PSO is kept fixed for each variant. Therefore, a total of 64 variants of DPD are generated as follows:

DE (with 8 different strategies of mutation on A) + PSO on B (fixed) + DE (with 8 different strategies of mutation on C) = DPD (64 different variants)

More clearly, a particular mutation operator M_1 in the first DE can produce 64 variants of DPD, by employing M_1−M_8 in last DE of DPD, by keeping PSO fixed in each DPD. Therefore, there are $8 \times 8 = 64$ combinations of mutation operators are possible and hence a total of 64 variants of DPD are being produced. The pictorial representation of this concept is also presented in Fig. 1.

Out of these 64 variants of DPD, it is important to investigate the best DPD for solving optimization problems. For this purpose, a test bed of 22 constrained benchmark problems includes various types (linear, nonlinear, and quadratic) of objective functions with different number of decision variables and a range of types (linear inequalities, nonlinear equalities, and nonlinear inequalities), and number of constraints are picked from [25].

Experimental Setup: Each of the 22 problems is solved by all 64 DPD variants. Simulations were conducted on Intel(*R*) Core-i3, 2.20 GHz computer, 2 GB of RAM, in the C-Free Standard 4.0 Environment.

Through an extensive experimental fine tuning, the following parameters are recommended to best suit the proposed algorithm.

- The mutation factor F for group A, i.e., $F_A = 0.5$ and for group C, i.e., $F_C = 0.8$
- The crossover weight CR for group A, i.e., $CR_A = 0.9$ and for group C, i.e., $CR_C = 0.9$

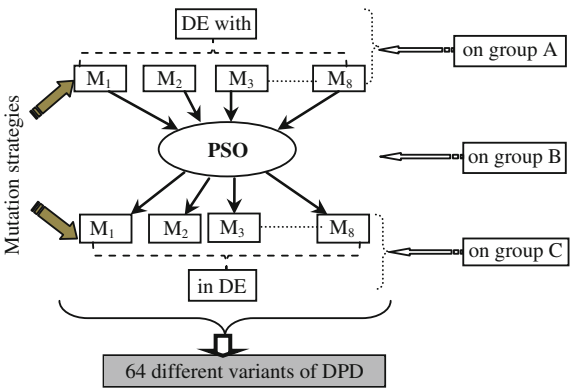

Fig. 1 Schematics view of establishment 64 variants of DPD

- For PSO, the acceleration constants C_1 and C_2 are both set to 2.0, and the inertia weights (w) is fixed at 0.7298
- The penalty parameter R is fixed at 1,000 to the objective function
- The population size is set to 99, multiple of 3 to favor the tri-population system for all the problems and dimensions under consideration.

Under the above experimental setup, two types of evaluation criteria are considered to estimate the top DPDs. First is based on only one parameter called 'objective function values' achieved, whereas second is bases on three parameters, namely success rate, objective function value, and required function evaluations. Both of them are discussed below.

Type-I: By *'top 20 scenarios'*

20 independent runs with 200 iterations are fixed to start the simulation. The average function value of 20 runs for each function is recorded by each of 64 DPDs. For a fixed function, the top 20 DPDs (in terms of better optimal solution) are collected as **'top 20 scenario.'** This is named as **'top 20 scenario.'** In this top 20 scenario, the numbers of functions solved by each of the variants of DPD are reported in Table 1.

Clearly, from Table 1, it is worth noting that the resulting number of function that could be solved by (2, 3) and (2, 6) is 0. Hence, mutation combination of (2, 3) and (2, 6) may here be concluded as the **worst variant of DPD**. The numerical values exists throughout in each order pair represents the serial number of the mutation operator as per the list reported in Sect. 2.1. For example, (3, 7) stands for (M_3, M_7). On the other hand, the **top four DPDs** are those using the mutation combinations **(3, 3), (3, 7), (3, 5), and (3, 1).** It is because they solved maximum number of benchmark problems, which is shown in bold face figures in Table 1. On the other hand, the **top four DPDs** are those using the mutation combinations **(3, 3), (3, 7), (3, 5), and (3, 1).** Hence, they are being renamed as **DPD-1, DPD-2, DPD-3, and DPD-4**, respectively. However, it will carry a lot of error to declare the best DPD out of them as the algorithms are probabilistic in nature. Therefore, the best DPD may differ when other parameters such as *number of function evaluations and success rate* are taken under consideration. Hence, a further analysis on the investigation of the best DPD out of these four is essential and is discussed below.

Type-II: By *'Performance'*

A major stick of comparison of algorithm called 'performance index' is being reported in [26]. A new concept, namely 'performance' is proposed here, with a slight modification to 'performance index' where $K_1 = K_2 = K_3$, as defined below. It signifies that equal importance has been given to the parameters based on multi criteria limited to (i) number of successful runs, (ii) minimum objective function value, and (iii) average number of function evaluations

Table 1 64 variants of DPD and their performance (in terms of number of functions solved as 'top 20 scenario')

Mutation combination	No. of functions solved	Mutation combination	No.of functions solved	Mutation combination	No. of functions solved	Mutation combination	No. of functions solved
(1,1)	06	(3,1)	19	(5,1)	01	(7,1)	14
(1,2)	09	(3,2)	18	(5,2)	01	(7,2)	10
(1,3)	06	(3,3)	22	(5,3)	01	(7,3)	16
(1,4)	08	(3,4)	18	(5,4)	03	(7,4)	15
(1,5)	08	(3,5)	19	(5,5)	02	(7,5)	11
(1,6)	05	(3,6)	18	(5,6)	01	(7,6)	11
(1,7)	08	(3,7)	21	(5,7)	02	(7,7)	14
(1,8)	05	(3,8)	18	(5,8)	02	(7,8)	10
(2,1)	02	(4,1)	16	(6,1)	10	(8,1)	09
(2,2)	01	(4,2)	15	(6,2)	09	(8,2)	06
(2,3)	00	(4,3)	16	(6,3)	08	(8,3)	08
(2,4)	01	(4,4)	15	(6,4)	10	(8,4)	06
(2,5)	02	(4,5)	16	(6,5)	09	(8,5)	07
(2,6)	00	(4,6)	15	(6,6)	10	(8,6)	10
(2,7)	03	(4,7)	15	(6,7)	10	(8,7)	09
(2,8)	03	(4,8)	16	(6,8)	10	(8,8)	07

$$\text{Performance} = \frac{1}{N_p}\sum_{i=1}^{N_p}\left(K_1\alpha_1^i + K_2\alpha_2^i + K_3\alpha_3^i\right)$$

$$\text{subject } to\ K_1 + K_2 + K_3 = 1 \text{ and } K_1 = K_2 = K_3$$

$$\text{where } \alpha_1^i = \frac{Sr^i}{Tr^i};\quad \alpha_2^i = \begin{cases} \frac{Mo^i}{Ao^i}, & if\ Sr^i > 0 \\ 0, & if\ Sr^i = 0 \end{cases} \quad \text{and} \quad \alpha_3^i = \begin{cases} \frac{Mf^i}{Af^i}, & \text{if } Sr^i > 0 \\ 0, & \text{if } Sr^i = 0 \end{cases}$$

$$for \quad i = 1, 2, \ldots, N_p$$

Sr^i Number of successful runs for ith problem
Tr^i Total number of runs for ith problem
Mo^i Mean optimal objective function value obtained by an algorithm for ith problem
Ao^i Minimum of mean optimal objective function value obtained by top 4 DPDs for ith problem
Mf^i Average number of function evaluations of successful runs required by an algorithm in obtaining the solution for ith problem
Af^i Minimum of average number of function evaluations of successful runs required by top 4 DPDs for ith problem
N_p Total number of problems considered

The evaluation of 'performance' for top 4 DPDs is being carried out over the same set 22 test functions [25] and over a set of four engineering design problem (reported in [13]). A total of 30 independent runs with 10,000 function evaluations for a run are fixed (rest parameters of DPD are same as presented earlier). The performance for test functions is reported in Fig. 2a and that for engineering design problem is reported in Fig. 2b. From the figures, it is concluded that DPD-1 performs the best. Hence, DPD-1 is considered for further study and usually renamed simply as DPD.

5 Comparison of DPD with Latest Existing Algorithm for Engineering Design Problem

In order to show the effectiveness and superiority of DPD, it is compared with latest existing evolutionary algorithm for four well-known constrained engineering design problems (taken from [13]). These problems are as follows:

E01 *Welded Beam design problem*
E02 *Pressure Vessel design problem*
E03 *Spring design problem*
E04 *Speed reducer design problem*

For each problem, 30 independent runs are performed. All parameters remain the same for DE and PSO (used in DPD) as discussed in Sect. 4.2. Better values are

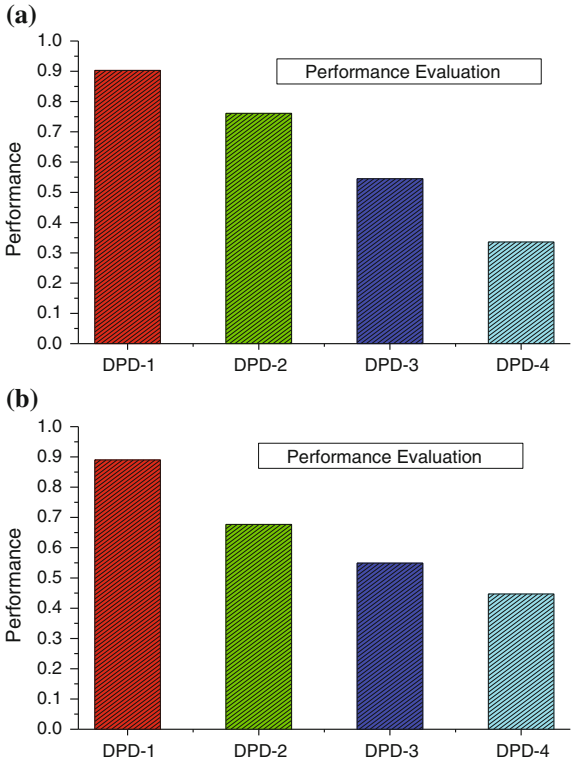

Fig. 2 **a** Performance evaluation for top 4 DPDs (under 22 constrained benchmark problems). **b** Performance evaluation for top 4 DPDs (under 4 constrained engineering design problems)

highlighted by bold face against each problem. The statistical results of DPD compared with PSO-DE, DETPS, $(\mu + \lambda)$-ES, UPSO, CPSO, CoDE, ABCA, and TLBO are presented in Table 2. All compared results are taken from DETPS [13] and PSO-DE [18]. It include best, mean, worst, std. (standard deviation), and number of function evaluation (NFEs).

The best feasible solution found by DPD for welded beam, pressure vessel, tension/compression spring design, and speed reducer is f(0.205729, 3.470488, 9.036623, 0.205729) = 1.724846; f(0.7781, 0.38464, 0.3196, 200.00) = 5884.689986; f(3.5, 0.7, 17.0, 7.3, 7.8, 3.343364, 5.285351) = 2993.758872 and f (0.051432, 0.351062, 11.609791) = 0.012638, respectively. DPD minimizes all 4 problems without violating any constraints. Ultimately, DPD outperforms others in all problems, in terms of best, mean, worst, and standard deviation. Moreover, it is also observed that (from Table 2 and Fig. 3a), the number of function evaluations by DPD is very less. It confirms the fast convergence speed and the extreme robustness. The average computation time (Fig. 3b) of the DPD for engineering design problems is extremely reasonable.

Finally, based on the above analysis, results, and comparisons, the proposed DPD algorithm is of better searching quality, efficiency, and robustness for solving engineering design problems.

Table 2 Simulation results produced by DPD and compared with others for engineering design problems (*NA* results are not available)

E. P.	Algorithm	Best	Mean	Worst	Std.	*NFEs*
E01	DPD	1.724846	1.724846	1.724846	0.00E + 00	6,500
	DETPS	1.724852	1.724852	1.724853	2.1E − 7	10,000
	PSO-DE	1.724852309	1.724852309	1.724852309	6.7E-16	66,600
	$(\mu + \lambda) - ES$	1.724852	1.777692	2.074562	8.8E − 2	30,000
	UPSO	1.92199	2.83721	4.88360	6.8E − 1	100,000
	CPSO	1.728024	1.748831	1.782143	1.3E − 2	200,000
	CoDE	1.733462	1.768158	1.824105	2.2E − 2	240,000
	ABCA	1.724852	1.741913	NA	3.1E − 2	30,000
	TLBO	1.724852	1.728447	NA	NA	10,000
E02	DPD	5884.689986	5884.689986	5884.689986	0.00E + 00	8,050
	DETPS	5885.3336	5887.3161	5942.3234	1.0E + 01	10,000
	PSO-DE	6059.714335	6059.714335	6059.714335	1.0E-10	42,100
	$(\mu + \lambda) - ES$	6059.7016	6379.9380	6820.3975	2.1E + 2	30,000
	UPSO	6544.27	9032.55	11,638.20	9.9E + 2	100,000
	CPSO	6061.0777	6147.1332	6363.8041	8.6E + 1	200,000
	CoDE	6059.7340	6085.2303	6371.0455	4.3E + 1	240,000
	ABCA	6059.7147	6245.3081	NA	2.1E + 2	30,000
	TLBO	6059.7143	6059.7143	NA	NA	10,000
E03	DPD	2993.758872	2993.758872	2993.758872	0.00E + 00	10,000
	DETPS	2996.348	2996.348	2996.348	5.2E-05	10,000
	PSO-DE	2996.348165	2996.348165	2996.348166	1.0E-07	70,100
	$(\mu + \lambda) - ES$	2996.348	2996.348	2996.348	0.0	30,000
	UPSO	NA	NA	NA	NA	NA
	CPSO	NA	NA	NA	NA	NA

(continued)

Table 2 (continued)

E. P.	Algorithm	Best	Mean	Worst	Std.	*NFEs*
	CoDE	NA	NA	NA	NA	NA
	ABCA	2997.058	2997.058	NA	0.0	30,000
	TLBO	2996.348	2996.348	NA	NA	10,000
E04	DPD	0.012638	0.012638	0.012638	4.350272E-015	7,140
	DETPS	0.012665	0.012680	0.012769	2.7E − 5	10,000
	PSO-DE	0.012665233	0.012665233	0.012665233	4.9E-12	42,100
	$(\mu + \lambda) - ES$	0.012689	0.013165	0.014078	3.9E − 4	30,000
	UPSO	0.013120	0.022948	0.050365	7.2E − 3	100,000
	CPSO	0.012675	0.012730	0.012924	5.2E − 5	200,000
	CoDE	0.012670	0.012703	0.012790	2.7E − 5	240,000
	ABCA	0.012665	0.012709	NA	1.3E − 2	30,000
	TLBO	0.012665	0.012666	NA	NA	10,000

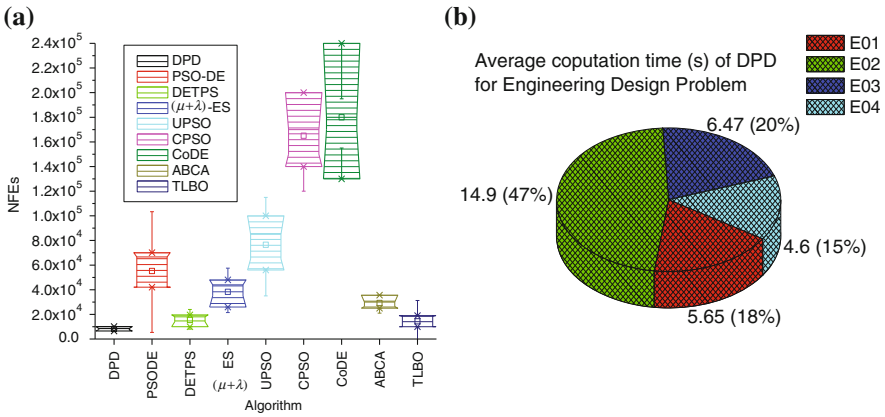

Fig. 3 Average (**a**) number of function evaluations (NEEs) of DPD and others, (**b**) computation time (s) of DPD, for engineering design problems

6 Conclusion

In this paper, the intrinsic relationship between PSO and DE is discovered. In order to demonstrate the effectiveness of the proposed method, it is applied to solve four constrained engineering design problems. Simulation results and comparisons show that the proposed DPD has higher accuracy and better robustness. In general, it is very effective for solving constrained engineering optimization problems. Also, it is simple, robust, converges fast, and able to find the optimum solution in almost every run. Therefore, tri-beakup technology for the population really makes the DE-PSO-DE faster and robust. Further, research effort focuses on different fashion of hybridization of DE and PSO algorithms for solving complex constrained engineering problems.

References

1. Storn, R., Price, K.: Differential evolution—a simple and efficient heuristic for global optimization over continuous spaces. J. Global Optim. **11**(4), 341–359 (1997)
2. Kennedy, J., Eberhart, R.C.: Particle swarm optimization. In: Proceeding of IEEE International Conference on Neural Networks. pp. 1942–1948 (1995)
3. Hendtlass, T.: A combined swarm differential evolution algorithm for optimization problems. Lect. Notes. Comput. Sci. **2070**, 11–18 (2001)
4. Pant, M., Thangaraj, R.: DE-PSO: a new hybrid meta-heuristic for solving global optimization problems. New. Math. Nat. Comput. **7**(3), 363–381 (2011)
5. Das, S., Abraham, A., Konar, A.: Particle swarm optimization and differential evolution algorithms: technical analysis, applications and hybridization perspectives. Advances of Computational Intelligence in Industrial Systems, Studies in Computational Intelligence, pp. 1–38. Springer, Germany (2008)

6. El Dor, A., Clerc, M., Siarry, P.: Hybridization of differential evolution and particle swarm optimization in a new algorithm: DEPSO-2S. Swarm. Evol. Comput. Lect. Notes. Comput. Sci. **7269**, 57–65 (2012)
8. Nwankwor, E., Nagar, A., Reid, D.: Hybrid differential evolution and particle swarm optimization for optimal well placement. Comput. Geosci. 1–20 (2012)
9. Ali, M., Siarry, P., Pant, M.: An efficient differential evolution based algorithm for solving multi-objective optimization problems. Eur. J. Oper. Res. **217**(2), 404–416 (2012)
10. Wang, Z., Hu, X., He, X.: New hybrid optimization based on differential evolution and particle swarm optimization. Jisuanji Gongcheng yu Yingyong (Comput. Eng. Appl.) **48**(6), 46–48 (2012)
11. Xin, B., Chen, J., Zhang, J., Fang, H., Peng, Z.: Hybridizing differential evolution and particle swarm optimization to design powerful optimizers: a review and tax-onomy. IEEE Trans. Syst. Man Cybern. Part C Appl. Rev. **42**(5), 744–767 (2012)
12. Kordestani, J.K., Rezvanian, A., Meybodi, M.R.: CDEPSO: a bi-population hybrid approach for dynamic optimization problems. Applied Intelligence. pp. 1–13 (2014)
13. Zhang, G., Cheng, J., Gheorghe, M., Meng, Q.: A hybrid approach based on differential evolution and tissue membrane systems for solving constrained manufacturing parameter optimization problems. Appl. Soft Comput. **13**, 1528–1542 (2013)
14. Han, M.F., Liao, S.H., Chang, J.Y., Lin, C.T.: Dynamic group-based differential evolution using a self-adaptive strategy for global optimization problems. Appl. Intell. **39**(1), 41–56 (2013)
15. Yadav, A., Deep, K.: An efficient co-swarm particle swarm optimization for non-linear constrained optimization. J. Comput. Sci. http://dx.doi.org/10.1016/j.jocs.2013.05.011, (2013)
16. Cagnina, L., Esquivel, S., Coello Coello, C.A.: A bi-population PSO with a shake-mechanism for solving constrained numerical optimization. IEEE Congress on Evolutionary Computation (CEC'2007), pp. 670–676. IEEE Press, Singapore (2007)
17. Cagnina, L.C., Esquivel, S.C.: Coello Coello, C.A.: solving constrained optimization problems with a hybrid particle swarm optimization algorithm. Eng. Optim. **43**(8), 843–866 (2011)
18. Liu, H., Cai, Z., Wang, Y.: Hybridizing particle swarm optimization with differential evolution for constrained numerical and engineering optimization. Appl. Soft. Comput. **10**(2), 629–640 (2010)
19. Wang, X., Yang, Q., Zhao, Y.: Research on hybrid PSODE with triple populations based on multiple differential evolutionary models. In: Proceedings International Conference Electrical Control Engineering Wuhan China. pp. 1692–1696 (2010)
20. Elsayed, S.M., Sarker, R.A., Essam, D.L.: Multi-operator based evolutionary algorithms for solving constrained optimization problems. Comput. Oper. Res. **38**, 1877–1896 (2011)
21. Ali, M., Pant, M., Abraham, A.: Simplex Differential Evolution. Acta. Polytechnica. Hungarica. **6**(5), 95–115 (2009)
22. Gong, W., Cai, Z.: Differential evolution with ranking based mutation operators. IEEE Trans. Syst. Man Cybern. Part C Appl. Rev. **43**(6), 2066–2081 (2013)
23. Deb, K.: Optimization for Engineering Design: Algorithms and Examples. Prentice-Hall of India, New Delhi (1995)
24. Michalewicz, Z.: A survey of constraint handling techniques in evolutionary computation methods. In Proceedings of the 4th Annual Conference on Evolutionary Programming, pp. 135–155, MIT Press, Cambridge (1995)
25. Liang, J.J., Runarsson, T., Mezura-Montes, E., Clerc, M., Suganthan, P., et al.: Problem Definitions and Evaluation Criteria for the CEC2006 Special Session on Constrained Real-Parameter Optimization. Technical Report, Nanyang Technological University, Singapore, December (2005)
26. Deep, K., Das, K.N.: Performance improvement of real coded genetic algorithm with Quadratic Approximation based hybridization. Int. J. Intell. Defence Support Syst. **2**(4), 319–334 (2009)

Predicting the Risk of Extinction of Species: Impact of Negative Growth Rate and Allee Effect

Bapi Saha

Abstract Predicting the risk of extinction of species is an important aspect in conservation biology. Mathematical models describing the density dependent per capita growth rates play a predominating role in quantifying the risk of extinction. We used population time series data from global population dynamics database (GPDD) to predict the threat status of the species using three commonly used growth models, allowing demographic disturbances. The best fitted model from a set of candidate models is used to evaluate the extinction measures. We observed that there are instances where the intrinsic growth rate is negative, which has not been reported earlier. We show that, in such cases, the extinction probability is high, but the species may adopt some strategy that saves them from extinction. The mathematical implications are described in light of ecological concepts.

Keywords Intrinsic growth rate · Allee effect · Extinction probability · Global population dynamics database · Per capita growth rate

1 Introduction

Soft computing technique has gradually become indispensable of the modern age. Among the various fields of application of soft computing, mathematical biology is one of them. The soft computing finds its application in different situation such as numerical solution of differential equations, drawing a bifurcation diagram, etc. Apart from that, conservation management is an important area of research in mathematical biology. Common measures like expected time to extinction and probability of extinction, given some initial population size or density, are used by conservation biologists for long-term management of threatened species [1, 2]. The

B. Saha (✉)
Government College of Engineering and Textile Technology,
Berhampore 742101, West Bengal, India
e-mail: bapi.math@gmail.com

K.N. Das et al. (eds.), *Proceedings of Fourth International Conference on Soft Computing for Problem Solving*, Advances in Intelligent Systems and Computing 335,
DOI 10.1007/978-81-322-2217-0_39

first step in the conservation management of a species is to identify the true growth law of the species. After identification of growth law, one needs to estimate the model parameters from the data. After obtaining the estimates of parameters, we can evaluate different extinction measures.

Growth curve models play an important role in population ecology in describing the population dynamics of some species. It is one of the central tools in modern ecological theory, particularly in conservation management. In population dynamics, the most widely used growth curve is the logistic growth model, whereas the population increases, the per capita growth rate (henceforth, PGR) decreases linearly and stabilize in carrying capacity of the environment. But Sibly et al. [3] showed that such density-dependent population growth curve seems to be concave in most animal populations and follows the theta-logistic equation. In logistic model, the fitness of the population (PGR) reaches maximum at the minimum population size, and the fitness decreases as population size increases due to intraspecies competition. In some cases, it may happen that the per capita growth rate of species is low and monotonically increasing when the population size is low. This type of growth mechanism is called Allee effect named after ecologist W.C. Allee [5–7]. The harmful effects of inbreeding depression, mate limitation, predator satiation, etc. reduce the fitness of the species as the population size decreases. These types of incidence correspond to mechanisms leading to Allee effects. In recent decades, due to the increasing number of threatened and endangered species, Allee effect has received much attention from conservation biologists.

The intrinsic growth rate is one of the primary indicators of species health, and its estimation from the time series data is an important aspect for any conservation biologist. The intrinsic growth rate (often denoted by, r) is generally taken to be positive in order to retain its physical interpretation [4]. However, when dealing with real data, there may be possible to obtain negative estimates of r. We have explored the global population dynamics database (GPDD) to study the growth profile of the species. GPDD is a database of various species around the world containing records of population counts over different years maintained by Imperial College London and can be downloaded as an access database from http://www.sw.ic.ac.uk/cpb/cpb/gpdd.html. This is a vast database containing more than 5,000 entries of different populations with varying taxonomic groups.

In this manuscript, we have used GPDD to estimate the PGR profile of the species using three commonly used growth rate models. We have extensively used MATLAB and database techniques to estimate the growth trend for each time series in GPDD. In this paper, we found two species for which the estimated 'r' is negative. We have shown that proper model selection is important in order to make better conservation management policies for different species. The detailed has been discussed in the result and conclusion section. In the following, we first describe the models that we have used to fit with time series data.

2 The Model

The general form of a deterministic single species model is $\frac{dx(t)}{dt} = \mu(x)$ where $x(t)$ the population size at time t and is a bounded, continuous function representing the density-dependant growth process. Different types of growth mechanism, such as negative-density dependent (e.g., logistic), density independent (exponential), and positive density-dependent (Allee effect) are demonstrated by different forms of $\mu(x)$.

In population dynamics, the most widely used model is logistic model and it takes the form

$$\frac{dx}{dt} = rx\left(1 - \frac{x}{K}\right)$$

whereas the θ-logistic model takes the form

$$\frac{dx}{dt} = rx\left(1 - \left(\frac{x}{K}\right)^{\theta}\right)$$

In both of the cases, r is the intrinsic growth rate, K is the carrying capacity, and θ is the density regulation around carrying capacity. $\theta > 1$ implies the convex relationship which means that per capita growth rate varies little until population size is near carrying capacity, then drops rapidly. Concave nature of the growth curve is represented by $\theta < 1$, which means that per capita growth rate is initially relatively high, and so small populations grow quickly, but then declines rapidly as population size increases (see Fig. 1). Large values of θ correspond to strong density dependence above K, but small values of θ allow larger fluctuations above K. So in the θ-logistic model, the per capita growth rate is a monotonically decreasing function of population size. This can be justified in this way that as the population size increases, intra-specific competition increases, per capita growth rate decreases and vanishes at carrying capacity. But when the population size is low, the Allee effect may be prevalent and there may exist a critical population size below which the per capita growth rate becomes negative. If this critical depensation level exists, the population becomes more vulnerable to extinction. It is observed that schooling fishes, in particular, are more vulnerable to critical depensation levels due to overfishing [8]. Sometimes over harvesting in dense schools causes the population to decline, so rapidly that it may not recover. The depleted school is also more vulnerable to predators that may lead to the ecological and economic collapse of the fishery [9]. So the strength of density dependence should be taken under serious consideration as it may play an important role and can have potential implications for the preservation of animal populations.

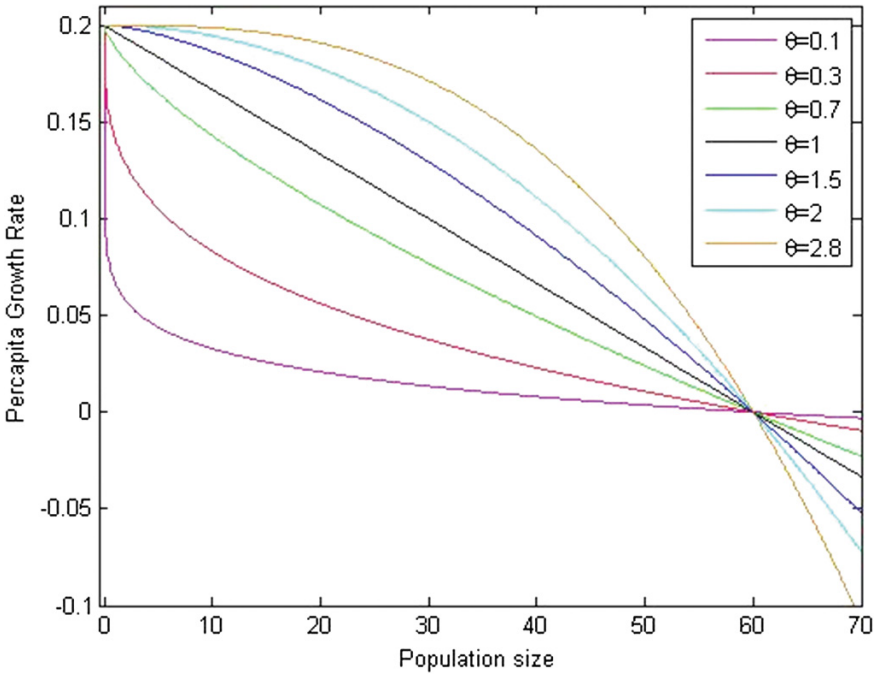

Fig. 1 Illustration of different types of curve that are generated from theta-logistic model for varying θ. PGR is maximum at small density and decrease to zero either linearly, convex, or concave way

In this paper, we take the well-known [8] Allee model

$$\frac{\mathrm{d}x}{\mathrm{d}t} = rx\left(1 - \frac{x}{K}\right)\left(\frac{x}{K} - \frac{A}{K}\right) \tag{1}$$

where r is the intrinsic growth rate, K is the carrying capacity, and A is the Allee threshold. If $A \leq 0$, the positive density dependence still persists, but there is no critical depensation. This situation is called a weak Allee effect. When there is a critical depensation in the population that is if $A > 0$, the situation is called a strong Allee effect. It can be shown that the equilibrium points 0 and K are stable equilibrium when $\theta > 0$ and K is unstable. If the population size falls bellow A then it will be attracted toward the stable equilibrium 0 and if the population size lies above A then it will be attracted to carrying capacity K. This is depicted in Fig. 2a, b.

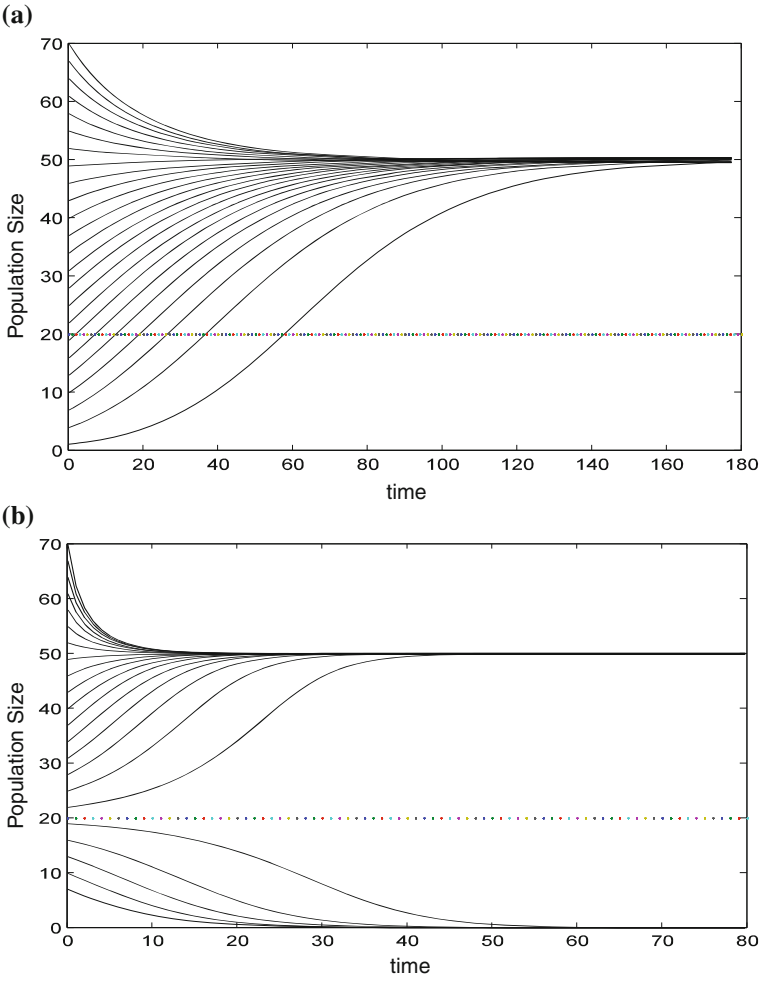

Fig. 2 **a** *Solid lines* numerical solutions of the θ- logistic model, for different initial population sizes. Parameters are $r = 0.06$, $K = 50$, $\theta = 0.7$. *Dashed lines* local unstable and stable equilibrium at $x = A$ and $x = K$. Any initial population size x_0 starting above 0 converges to carrying capacity, stable equilibrium. **b** *Solid lines* numerical solutions of the logistic model modified to incorporate an Allee effect, for different initial population sizes. Parameters are $r = 0.009$, $A = 20$, $K = 50$. *Dashed lines* local unstable and stable equilibria at $x = A$ (*dotted line*) and $x = K$. Any initial population size x_0 starting above the critical threshold A converges to carrying capacity, stable equilibria, whereas when x_0 is below critical threshold A, then it converges to zero

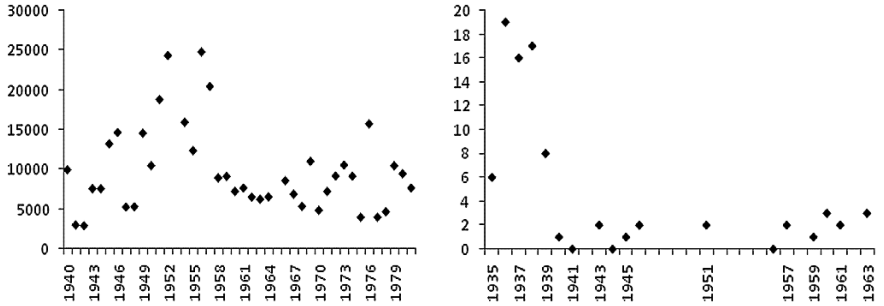

Fig. 3 The *first panel* is the time series plot of Mustela vison (GPDD ID 478) and the *second panel* is that of Lynx Canadensis (GPDD ID 420)

3 Stochastic Model

The variation between individual survival and reproduction leads to demographic stochasticity. The population process may be perturbed by random environmental changes, but at low population density, demographic stochasticity is more prevailing [10]. Thus, the extinction process of a given population cannot be properly analyzed unless we include the demographic disturbances [11, 12]. Stochastic models of population growth can be approximated by a diffusion process (including a discrete time birth–death process). This generally takes the form $\mathrm{d}x(t) = \mu(x(t))\mathrm{d}t + \sqrt{v(x(t))}\mathrm{d}W(t)$. In this case, $\mathrm{d}x(t)$ is the approximate population size change in time interval $\mathrm{d}t$, and $\mathrm{d}W(t)$ has a normal distribution with zero mean and variance $\mathrm{d}t$. $\mu(x(t))$ is called the infinitesimal mean and it specifies the underlying deterministic trend, while the infinitesimal variance v (x(t)) corresponds to stochastic fluctuations. The relevant expressions for demographic stochasticity and environmental stochasticity are given by Engen et al. [13], and they showed that $\sigma_d^2 x$ corresponds to demographic stochasticity and $\sigma_e^2 x^2$ corresponds to environmental stochasticity. These equations have become vital tools in modeling populations in stochastic environments.

At low population level, the species in question are more vulnerable to extinction. In this paper, we consider demographic stochasticity only, since at low population size, the effect of environmental stochasticity is negligible [1]. Incorporating demographic stochasticity in logistic, θ-logistic, and Allee model, we have

$$\frac{\mathrm{d}x}{\mathrm{d}t} = rx\left(1 - \frac{x}{K}\right) + \sigma_d\sqrt{x}\mathrm{d}W(t) \tag{1}$$

$$\frac{\mathrm{d}x}{\mathrm{d}t} = rx\left(1 - \left(\frac{x}{K}\right)^{\theta}\right) + \sigma_d\sqrt{x} \tag{2}$$

and

$$\frac{\mathrm{d}x}{\mathrm{d}t} = rx\left(1 - \frac{x}{K}\right)\left(\frac{x}{K} - \frac{A}{K}\right) + \sigma_d\sqrt{x} \tag{3}$$

3.1 Probability of Extinction

In case of a stochastic population, the first passage probability (i.e., the probability of attaining a large population size before attaining a small one) and the mean time to extinction are commonly used to evaluate population viability [14]. We are interested in evaluating the probability of extinction given some initial population size. Let $\xi(n; a, b)$ be the probability that the population reaches a before reaching an upper size b, starting at n, where $0 < a \leq n < b$. A standard formula gives,

$$\xi(n; a, b) = \frac{\int_n^b \exp[-\phi(x)]\mathrm{d}x}{\int_a^b \exp[-\phi(x)]\mathrm{d}x} \quad \text{where} \quad \phi(u) = 2\int \frac{m(u)}{v(u)}\mathrm{d}u \tag{4}$$

In the above expression, the (exponentiated) constant of integration cancels in the numerator and denominator. $\xi(n; a, b)$ is equal to 1 when $n = a$, and it is strictly monotone decreasing in the interval (a, b) and is equal to 0 when $n = b$. The probability of extinction starting from population size n under this model is found from (4) by letting $a \to 0$ and $b \to \infty$. An explicit analytical form for the probability of extinction is not available due to the complicated form of the chosen models. So we use numerical method to find the probability of extinction.

4 Statistical Analysis

We follow the usual convention in denoting the vector-valued parameter $\beta = (r, A, K)$ for model (1) and $\beta = (r, \theta, K)$ for model (2) in the space Θ of all admissible parameter values. Let $\{N_t\}_{t=1}^n$ be the given time series data and model the fluctuations in the data on a log-transformed scale. We have estimated per capita growth rate by $\log\left(\frac{N_{t+1}}{N_t}\right)$ in the interval $(t, t+1)$ and consider it as a response variable, say Y_t. The regression of Y on N is represented by$E(Y|N) = \mu(N, \beta)$, where $\mu(N, \beta) = rN\left(1 - \frac{N}{K}\right)$ for logistic, $rN\left(1 - \left(\frac{N}{K}\right)^{\theta}\right)$ for θ-logistic, and $rN\left(1 - \frac{N}{K}\right)\left(\frac{N}{K} - \frac{A}{K}\right)$ for Allee model. The distribution of Y_t conditional on N_t is assumed to be normally distributed with mean $\mu(N_t, \beta)$ and variance $\sigma_t^2 = \left[\frac{b(N_t)+d(N_t)}{N_t^2}\right]\sigma_d^2$ where $b(N_t)$ and $d(N_t)$ are the birth rate and death rate of the species.

Together with the assumption that observations are independent, this defines a nonlinear regression model with fixed regressor and known functional relationship

$$Y_t = \mu(N_t, \beta) + \varepsilon(t)(t = 1, 2, \ldots, n)$$

where $\varepsilon(t)$'s are independently normally distributed with mean zero and variance σ_t^2. The true value β^* of β is known to belong to θ, a subset of $\mathbb{R}^3$. The least squares estimate of β^*, denoted by $\hat{\beta}$, minimizes the residual sum of squares

$$S(\beta) = \sum_{t=1}^{n} \left[\frac{Y_t - \mu(N_t, \beta)}{\sigma_t}\right]^2$$

over $\beta \in$. We have used MATLAB nonlinear regression routine 'nlinfit' to estimate the model parameters, and the variance is computed from the residual sum of squares.

5 Result and Conclusion

Predicting the probability of extinction is important and challenging. Selection of best model is equally important as because a wrongly chosen model could lead to overestimation or underestimation of the extinction probability which can have severe consequences particularly for threatened species. In general, the growth process of different species revolves around logistic, θ-logistic, and Allee. In any of these models, the intrinsic growth rate is assumed to be positive. But after a vast data analysis, we found that in some of the cases, the intrinsic growth rate 'r' may be negative (see Fig. 4). In that case, the probability of extinction may be much higher than what is expected (Fig. 3).

If the intrinsic growth rate of a population is negative, it means that the death rate is greater than the birth rate and extinction is inevitable. From our model fitting results, we observed that the estimate of r is negative, which is an undesirable scenario in population dynamics [4]. In addition, from the stability analysis of the equilibrium points, we observe that the carrying capacity (K) and the origin are unstable, whereas the threshold population level A is stable. In this case, the PGR profile of the species is concave upward, unlike the concave downward profile of the model demonstrating Allee effect.

For the species (Mustela vison, GPDD ID 478, Lynx Canadensis, GPDD ID 420), the population usually maintains a low abundance, and in few time points only, it reaches higher abundance around the point (K). The basic dynamics demonstrated in the figure can be explained as: when the population falls at a low density and they could not recover to reach at higher density. Although, in such a scenario, the risk of extinction is high, but it may happen that the population adapts some strategy to adapt themselves to the environment. The strategy could be the

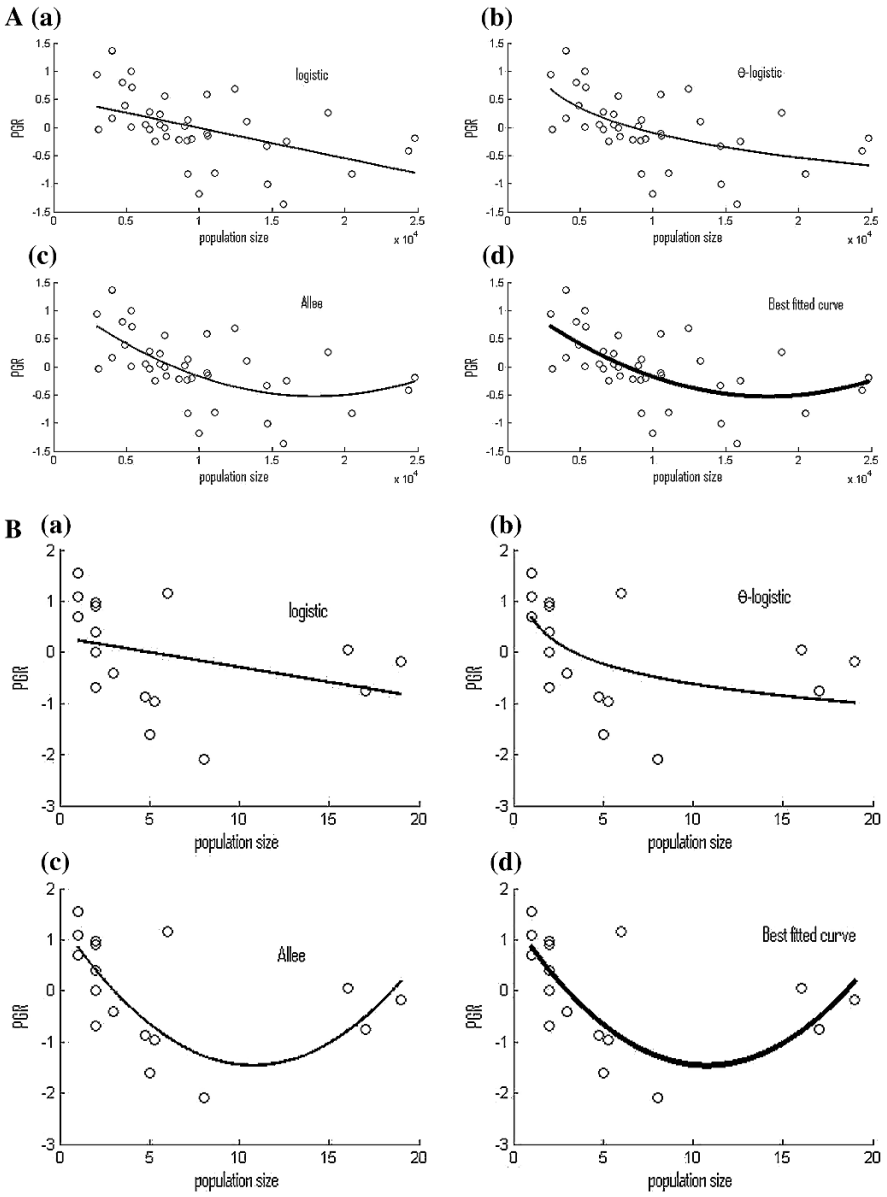

Fig. 4 Plot of population size versus PGR. **a** Mustela vison (GPDD ID 478). **b** Lynx Canadensis (GPDD ID 420). Three models are fitted to the PGR profile (*a*) logistic, (*b*) θ-logistic, and (*c*) Allee effect model. The best fitted model is given with *bold line* in sub-figure (*d*)

exchange of stability of the point A. For positive intrinsic growth rate, A is the extinction threshold, whereas for negative r, to save from extinction, the population maintain themselves at low density. The equilibrium point A plays the role similar to carrying capacity, so that the population's stable region gets confined in the interval $(0, A)$. It can also be mathematically shown that if the population is able to stabilize them in the interval, the resulting dynamics would be logistic. For $N \ll K, 1 - \frac{N}{K} \cong 1$, so that,

$$\frac{\mathrm{d}N}{\mathrm{d}t} = rN\left(1 - \frac{N}{K}\right)\left(\frac{K}{K} - \frac{A}{K}\right) \approx rN\left(\frac{K}{K} - \frac{A}{K}\right) = \left(-\frac{rA}{K}\right)N\left(1 - \frac{N}{K}\right)$$

Now, $\left(r_1 = -\frac{rA}{K}\right)$ is the new intrinsic growth rate, which is positive as $r < 0$. The above simple observation proves the result. With this renewed dynamics, the population is able to sustain at low density with a positive growth rate.

In this paper, we did a vast data analysis using the population size data given in GPDD. We used all the three models (logistic, θ-logistic, and Allee) to fit the data and consider the model which fitted the data best in terms of mean square error. In some cases, the best fitted model is Allee. Among those Allee model in some cases, the intrinsic growth rates are found to be negative. We calculate the probability of extinction using (4) for the species Mustela vison with GPDD id 478 and Lynx Canadensis with GPDD id 420. For the Mustela vison species, the estimated parameter values are $r = 350.5, K = 8,582.5, \theta = 0.001$ if θ-logistic model is fitted. The corresponding extinction probability is found to be 4.0433×10^{-217} which is very small. The best fitted model for this species is Allee model and the corresponding parameter values are $r = -4.2624$, $K = 27{,}597.8236$, $A = 8{,}233.0059$. The extinction probability is found to be 0.96. The estimation procedure does not converge for logistic curve (Table 1).

And for the species Lynx Canadensis, the estimated parameter values are $r = 250.61$, $K = 7,596.72$ for logistic model. $r = 3.5$, $K = 6.5$, $\theta = 0.023$ if θ-logistic model is fitted. The corresponding extinction probabilities are found to be 3.78×10^{-190} and 6.134×10^{-187}, respectively which are also very small. The best fitted model for this species is Allee model and the corresponding parameter values are $r = -0.2185$, $K = 18.5132$, $A = 3.0023$. The extinction probability is found to be 0.92.

In this paper, we have considered only two cases where we found the estimated value of 'r' to be negative. In both cases, the underlying model is Allee model. However, 'r' may be negative in case of θ-logistic model also [3]. From the above result, we observe that the chance of extinction is underestimated if we incorrectly choose the logistic or θ-logistic growth curve. So if we fit logistic or θ-logistic model to a species which is actually followed by Allee model, the species may seem to be less vulnerable than the actual. We may face the same problem if we take r positive when the actual value of it is negative. This is very harmful, particularly for endangered species. So proper model selection is very essential and we should not ignore the case where the intrinsic growth rate r is negative.

Table 1 The probability of extinction for the two species is described in the table with associated risk of extinction

Species name	Prob. of extinction (logistic)	Prob. of extinction (θ-logistic)	Prob. of extinction (Allee)
Mustela vison	*	4.0433×10^{-217}	0.96
Lynx Canadines	3.78×10^{-190}	6.134×10^{-187}	0.92

*means the nonlinear regression routine does not converge for logistic growth model

Acknowledgments Author is thankful to Amiya Ranjan Bhowmick for valuable discussions and editing help in the final version of the manuscript. The author is also thankful to Prof. Joydev Chattopadhay and Dr. Sabyasachi Bhattacharya, Indian Statistical Institute, Kolkata for giving valuable insights of the ecological and mathematical context of the problem.

References

1. Saha, B., Bhowmick, A.R., Chattopadhyay, J., Bhattacharya, S.: On the evidence of an Allee effect in herring populations and consequences for population survival: a model-based study. Ecol. Model. **250**, 72–80 (2013)
2. Saha, B., Bhowmick, A.R.: Predicting the extinction vulnerability of species: stochastic approach to deterministic population dynamic models. Bull. Cal. Math. Soc. **105**(3), 191–210 (2013)
3. Sibly, R.M., Barker, D., Denham, M.C., Hone, J., Pagel, M.: On the regulation of populations of mammals, birds, fish, and insects. Science **309**, 607–610 (2005)
4. Ross, J.V.: Comment on "on the regulation of populations of mammals, birds, fish and insects" II. Science **311**, 1100b (2006)
5. Allee, W.C., Emerson, A., Park, O., Park, T., Schmidt, K.: Principles of Animal Ecology. W. B. Saunders Co., Philadelphia (1949)
6. Dennis, B.: Allee effects: population growth, critical density, and the chance of extinction. Nat. Resour. Model. **3**, 481–538 (1989)
7. Fowler, C.W., Baker, J.D.: A review of animal populations dynamics at extremely reduced population levels. Ann. Rep. Int. Whaling Comm. **41**, 545–554 (1991)
8. Courchamp, F., Berce, L., Gascoigne, J.: Allee Effects in Ecology and Conservation. Oxford University Press, Oxford (2008)
9. Hilborn, R., Walters, C.: Quantitative Fisheries Stock Assessment: Choice, Dynamics and Uncertainty. Chapman and Hall, New York (1992)
10. Lande, R.: Demographic stochasticity and Allee effect on a scale with isotropic noise. Oikos **85**, 353–358 (1998)
11. Dennis, B.: Allee effects in stochastic populations. Oikos **96**, 389–401 (2002)
12. Courchamp, F., Clutton-Brock, T.H., Grenfell, B.T.: Inverse density dependence and the Allee effect. Trends Ecol. Evol. **14**, 405–410 (1999)
13. Engen, S., Bakke, O., Islam, A.: Demographic and environmental stochasticity—concepts and definitions. Biometrics **54**, 39–45 (1998)
14. Drake, J.M., Lodge, D.M.: Allee effects, propagule pressure and the probability of establishment: risk analysis for biological invasions. Biol. Invasions **8**(2), 365–375 (2006)

Demonstration of Improved Performance of a 4-Level DSEP to Enhance the Efficiency in Heterogeneous Wireless Sensor Networks

Gagandeep Singh

Abstract Multiple layer hierarchical routing protocols require energy management and power output optimization as the individual nodes in these networks tend to be small low-power devices. The superiority of multilayer hierarchical networks containing three layers over a two-layer implementation in terms of stability period, network lifetime, and throughput has already been demonstrated. In this paper, the improvement in these performance parameters brought about by the addition of a fourth layer has been elaborated.

Keywords WSN · Hierarchical networks · DSEP

1 Introduction

Wireless sensor network (WSN), an important application of adhoc networks, is fast emerging as a global technology and employs the concept of sensing, processing, and radio waves. WSN found their way into a broad variety of applications including industrial automation, highway surveillance, habitat observation, military applications, environmental applications, and at the bottom, commercial applications such as personal medical diagnostics, automated grocery checkout, and remote-controlled heating and lighting. Recent advances in communications and sensor design made these applications possible and the design of cheap low-power nodes using micro-electromechanical systems (MEMS) help envision all potential applications. Many routing, power management, and data dissemination protocols have been specifically designed focusing on scalability, geographic range, infrastructure, cost, heterogeneity, mobility, etc. Since network lifetime and energy consumption is also one of the major design issues in developing routing protocols for WSNs, a lot of researches

G. Singh (✉)
Department of Electronics and Communication Engineering,
Quantum School of Technology, Roorkee, India
e-mail: er.gagan89@gmail.com

K.N. Das et al. (eds.), *Proceedings of Fourth International Conference on Soft Computing for Problem Solving*, Advances in Intelligent Systems and Computing 335,
DOI 10.1007/978-81-322-2217-0_40

have been focused on it. Analysis of existing research indicates hierarchical routing to be a promising approach for efficient routing in WSN. A study of implementation of the hierarchical routing approach in homogenous and heterogeneous WSNs indicates that heterogeneous WSNs are comparatively more efficient. Further, a comparative study of different routing protocols for heterogeneous WSNs, viz. deterministic stable election protocol (DSEP), threshold sensitive stable election protocol (TSEP), and stable election protocol (SEP) up to the three levels in terms of network lifetime, stability period, and data transmission to base station shows that the 3-level DSEP is comparatively most efficient [1]. In 2-level heterogeneous WSNs, two types of nodes known as normal nodes and advanced nodes are used. Whereas in 3-level heterogeneous WSNs, there are three types of nodes known as normal nodes, intermediate, and advanced nodes, respectively. In this paper, an improvement in the 3-level DSEP by considering 4-level heterogeneity in the type of nodes such as "super node" between intermediate and advanced node was implemented.

2 Simulation of 4-Level DSEP

SEP and TSEP schemes for the heterogeneous WSNs prolong the stable region of the clustering hierarchy process when different initial energy nodes are considered as a characteristic parameters of heterogeneity [2, 3].

The analysis of the literature survey about the above-mentioned protocols, such as SEP and TSEP, they extend battery lifetime but cannot be applied to the multilevel heterogeneous WSNs. Another protocol DSEP, proposed [1, 4] after SEP and TSEP, was based on 3-level heterogeneity with modified threshold equation to determine the weighted probabilities to elect the cluster head which resulted in prolonged stability period, network lifetime, and throughput. An enhancement to 3-level DSEP is performed, where 4-level heterogeneity is considered by using the same threshold value.

Network model used for the simulation of 4-level DSEP consists 100 nodes in 100 × 100 network field. The base station is located at the center point (50 × 50). The packet size that the nodes send to their cluster heads as well as the combined packet size that a cluster head sends to the sink is set to 4,000 bits. In the four-level heterogeneity model, one more node such as super node is considered in between the intermediate node and advanced node on the basis of their energy.

The weighed election probability of four-level heterogeneity nodes known as normal node, advanced node, intermediate node, and super node are measured on the basis of their initial energy as shown in Fig. 1.

At the same time, the reference value of "p_i" is different for nodes. The probabilities of normal node, advanced node, intermediate node, and super node are as follows:

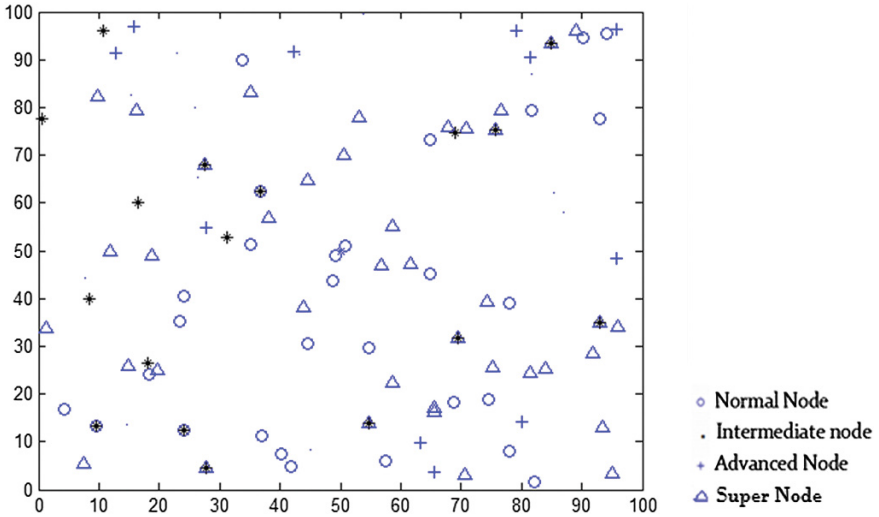

Fig. 1 Four-level heterogeneous wireless sensor network

$$p_i = \{p_{\text{nrm}}, p_{\text{in}}, p_{\text{sup}}, p_{\text{adv}}\} \tag{1}$$

where

$$p_{\text{nrm}} = \frac{p * E_{\text{residual}}}{\{(1 + mA + mxn + mc\lambda) * E_{\text{average}}\}} \tag{2}$$

$$p_{in} = \frac{p(1+\mu) * E_{\text{residual}}}{\{(1 + mA + mxn + mc\lambda) * E_{\text{average}}\}} \tag{3}$$

$$p_{\text{sup}} = \frac{p(1+\lambda) * E_{\text{residual}}}{\{(1 + mA + mxn + mc\lambda) * E_{\text{average}}\}} \tag{4}$$

$$p_{\text{adv}} = \frac{p(1+\text{A}) * E_{\text{residual}}}{\{(1 + mA + mxn + mc\lambda) * E_{\text{average}}\}} \tag{5}$$

Now, the threshold level is also taken under consideration to ensure the clusters heads selection and the threshold level for all types of nodes is calculated as [4]:

$$T(S_i) = \left\{ \frac{p_i}{1 - \left(p_i * \left(\text{r mod} \frac{1}{p_i}\right)\right)} \right\} * \{E_{\text{residual}} + \left(r_s \,\text{div} \frac{1}{p_i}\right) * (1 - E_{\text{residual}}) \tag{6}$$

3 Results and Discussions

The following cases had been taken into consideration for the comparative analysis of 3-level DSEP and 4-level DSEP.

3.1 Case 1: m = 0.4, A = 1.5, μ = 1, x = 0.2, λ = 0.5, y = 0.1 Over 7,000 Rounds

3.1.1 Stability Period

Figure 2 demonstrates that for existing 3-level DSEP, the first sensor node dies after 1,496 rounds, whereas in case of 4-level DSEP, the first sensor node dies at around 1,605 rounds which shows that stability period in 4-level DSEP is more as compared to 3-level DSEP.

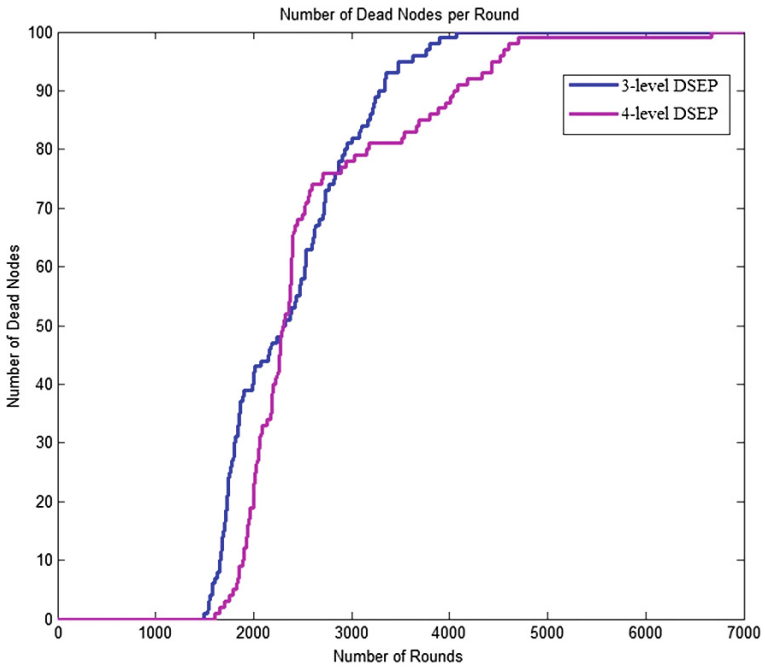

Fig. 2 Number of dead nodes

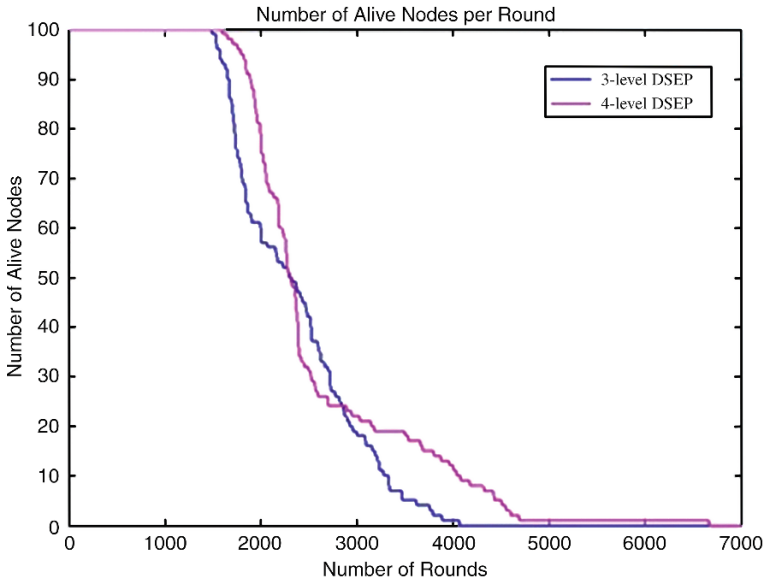

Fig. 3 Lifetime of the sensor network

3.1.2 Network Lifetime

Figure 3 illustrates the lifetime of the sensor network, and it is observed that for the 3-level DSEP protocol, the last sensor node dies at 4,076, whereas for 4-level DSEP, the last sensor node dies at around 6,672 over 7,000 rounds. Hence, network lifetime is greater in 4-level DSEP compared to 3-level DSEP.

3.1.3 Throughput of the Network

Figure 4 demonstrates the throughput in terms of data transmission from cluster head to the base station. It is observed that for the existing 3-level DSEP protocol, the throughput is stable enough up to around 3,300 rounds, whereas for the 4-level DSEP protocol, the throughput is stable enough up to 4,450 rounds which is higher than the existing 3-level DSEP.

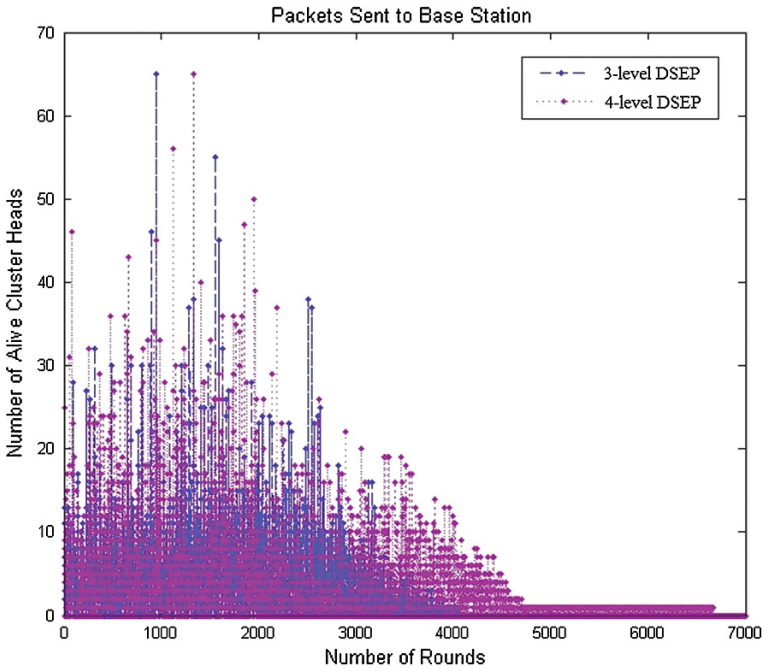

Fig. 4 Throughput of the sensor network

3.2 Case 2: m = 0.6, A = 2, μ = 1, x = 0.2, λ = 0.5, y = 0.05 Over 15,000 Rounds

3.2.1 Stability Period

Further, it is observed from the Fig. 5 that for the case of existing 3-level DSEP, the first sensor node dies at the 1,692 rounds, whereas the first sensor node dies for 4-level DSEP protocol is at 1,950 rounds which is again more than 3-level DSEP. So it results that in 4-level DSEP, stability period is greater than 3-level DSEP.

3.2.2 Network Lifetime

Figure 6 indicates that for 3-level DSEP, the last sensor node dies after 8,360 rounds and the last sensor node dies for 4-level DSEP is at 13,439 rounds which is again more than 3-level DSEP. So it shows that the lifetime of network for 4-level DSEP is better as compared to 3-level DSEP.

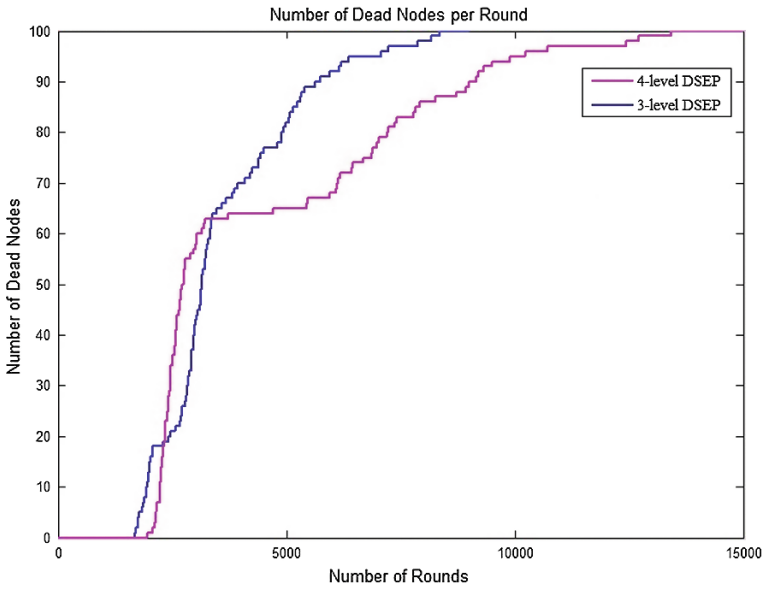

Fig. 5 Number of dead nodes

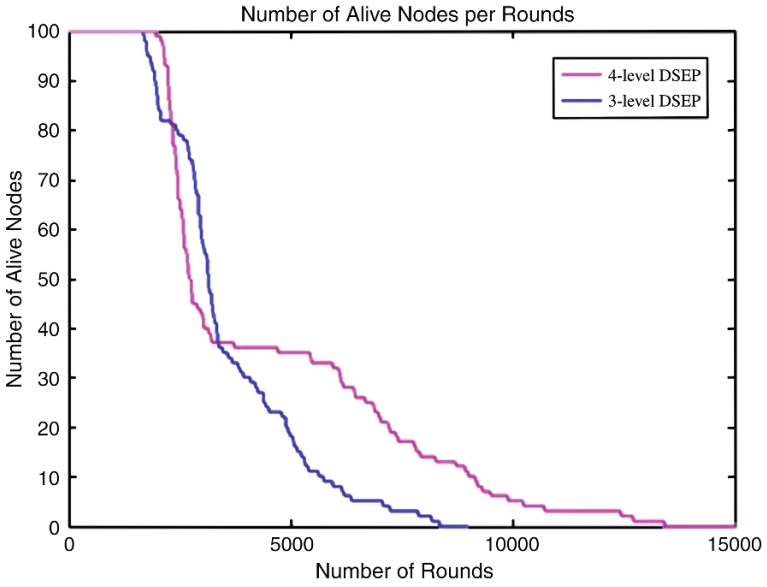

Fig. 6 Lifetime of the sensor network

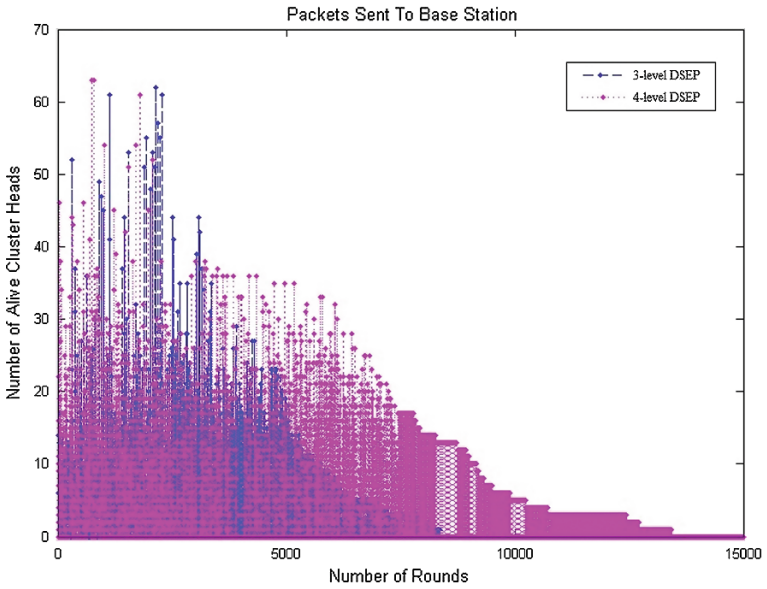

Fig. 7 Throughput of the sensor network

3.2.3 Throughput of the Network

Figure 7 illustrates that for the existing 3-level DSEP, the throughput is stable up to 5,500 rounds. Moreover, for the 4-level DSEP, the throughput is stable enough up to 9,500 rounds. So it shows that the data transmission from cluster head to base station is higher in case of 4-level DSEP as compared to 3-level DSEP.

4 Conclusion

The transmission energy increases with the increase in the distance between cluster head and base station. Thus, an advancement in the existing 3-level DSEP has been performed and a new 4-level hierarchical routing DSEP protocol has been presented. This protocol uses four levels of heterogeneity which consists of normal, intermediate, super, and advanced nodes, and cluster heads choice is same as in the case of 3-level DSEP. The simulation results confirmed that the 4-level approach results in a longer network lifetime, stability period, and throughput as compared to the existing 3-level DSEP protocols. Therefore, it is concluded that more the energy level of the network, more stable it is and more is the lifetime. Future work in this area can comprise of:

1. Increase in the heterogeneity based on the energy of nodes, which may improve the stability period and network lifetime.
2. Modification in threshold value for the different kinds of nodes to become a cluster head can be implemented as advancement.

References

1. Gagandeep, S., Singh, H.P., Anurag, S.: Comparative analysis of energy efficient protocols for prolonged life of wireless sensor network. In: Proceedings of the 3rd International Conference on Soft Computing for Problem Solving, 26–28 Dec, 2013, GNEC, IIT Roorkee, India, Advances in Intelligent Systems and Computing, vol. 259, pp. 75–82. Springer, Berlin (2014)
2. Smaragdakis, G., Matta, I., Bestavros, A.: SEP: a stable election protocol for clustered heterogeneous wireless sensor networks. In: Second International Workshop on Sensor and Actor Network Protocols and Applications (SANPA 2004) (2004)
3. Kashaf, A., Javaid, N., Khan, Z.A., Khan, I.A.: TSEP: threshold-sensitive stable election protocol for WSNs. In: Proceedings of 10th International Conference on Frontiers of Information Technology, pp. 164–168 (2012)
4. Bala, Manju, Awasthi, Lalit: Proficient D-SEP protocol with heterogeneity for maximizing the lifetime of wireless sensor networks. Int. J. Intell. Syst. Appl. **7**, 1–15 (2012)
5. Younis, O., Krunz, M., Ramasubramanian, S.: Node clustering in wireless sensor networks: recent developments and deployment challenges. IEEE Netw. **20**, 20–25 (2006)
6. Yu, L., Wang, N., Zhang, W.: Deploying a heterogeneous wireless sensor network. In: Proceedings of International Conference on WiCom, Singapore, pp. 2588–2591 (2007)
7. Gagandeep, S., Anurag, S., Harjitpal, S.: A comparative analysis of hierarchical routing protocols in wireless sensor networks. Int. J. Eng. Res. Technol. **2**(10), 3098–3102 (2014)

Control of Two-link 2-DOF Robot Manipulator Using Fuzzy Logic Techniques: A Review

Kshetrimayum Lochan and B.K. Roy

Abstract This paper reviews the literature on control of 2-DOF robot manipulator using fuzzy logic control (FLC). Different schemes of FLC laws are considered here. These are PID control, sliding mode control (SMC), and adaptive control. Importance of each control techniques with its advantages and disadvantages is discussed here. It is highlighted that the robustness of the system has improved considerably by using FLC than classical controller. A total of 65 papers were surveyed in this research area, covering contribution on each control technique for the 2-DOF robot manipulator for the time span of 1983–2014.

1 Introduction

Industrial robots were introduced in the 1950s and 1960s for human replacement in hazardous tasks, increasing in productivity and in quality improvement. Some of the common tasks of robots which are designed include the following: welding, transportation and material handling, painting, assembly, and manufacturing [1].

Initially, automated robot concept was developed by J.K. Devol in an era of 1950s called Unimate [2], which was installed at Ford Co. in 1961. Lots of research has been done since then that imitates human movements [3], robots for social purpose present in shopping malls [4], etc. After the 1980s, it has been observed that there has been a tremendous increase in industrial automation and also attention

K. Lochan (✉) · B.K. Roy
Department of Electrical Engineering, NIT Silchar, Assam 788010, India
e-mail: kshetrimayumlochan@gmail.com

B.K. Roy
e-mail: bkrnits@gmail.com

K.N. Das et al. (eds.), *Proceedings of Fourth International Conference on Soft Computing for Problem Solving*, Advances in Intelligent Systems and Computing 335,
DOI 10.1007/978-81-322-2217-0_41

for automatic control of dynamic systems. Various control techniques have been developed during this decade for robot control such as robust control [5], optimal control [6], adaptive control [7], PID control [8], and intelligent control [9, 10].

Intelligent control techniques have been applied as an alternative to classical control techniques which consist of three basic approaches [11]: knowledge-based expert system, FLC and control based on neural networks. In control system application, fuzzy logic incorporates human thinking as described in [12]. Human operator experiences are largely used in the design of fuzzy logic controllers. Such controllers are then implemented in computers to achieve better performances of the plant as compared to the human operator.

Mathematical modeling of process is not required in fuzzy control technique, but it requires modeling of the action from the knowledge based on the specialist or expert using linguistic terms, i.e., verbal description. Fuzzy control techniques are also used for handling linear and nonlinear systems, to control complex multivariable systems, and decision making for handling complexities in various types of plants. Hence, classical control techniques are applied directly on plant mathematical modeling, but fuzzy logic control acts in different approaches as discussed in [13].

In this paper, a survey is reported on the use of different variations in fuzzy logic controller to control a 2-DOF robot manipulator. Various fuzzy control schemes considered in this paper include the following: PD, PID, sliding mode and adaptive control. A comparison between classical PID controllers and intelligent fuzzy controllers is also presented in this survey. Literature review suggests that such exhaustive surveys on the use of a particular control approach to control robot manipulators are hardly available.

Organization of the paper is as follows: Sect. 2 describes the 2-DOF robot manipulator dynamics, and control of the robot manipulator using FLC is presented in Sects. 3 and 4 describes the fuzzy PID control, Sect. 5 presents the use of fuzzy SMC for control of the robot manipulator, Sect. 6 gives the use of FLC with adaptive control for manipulator, and finally, the paper ends with conclusions in Sect. 7.

2 Robot Manipulator Dynamics

Modeling of robot is associated with internal forces. Internal forces include inertia force, Coriolis force and friction force. The external forces include the gravitational forces and external load. Without considering the friction and the disturbances, a two-link rigid robot manipulator can be described as follows [14]:

$$\tau = M(q)\ddot{q} + v(q, \dot{q}) + g(q) \tag{1}$$

where, $v(q, \dot{q}) = c(q)[\dot{q}^2] + B(q)[\dot{q}\dot{q}]$, $q \in R^2$ is a vector of generalized coordinates. $M(q)$ is the 2×2 inertia matrix due to its mass of motion, $C(q)[\dot{q}^2]$ is the 2-vector

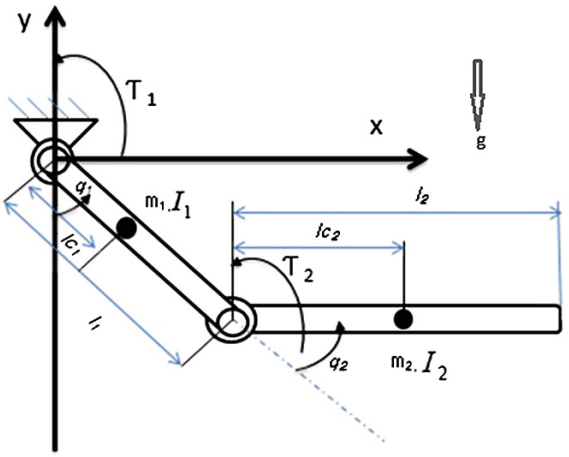

Fig. 1 A 2-DOF robot arm

of centrifugal force and $B(q)[\dot{q}\dot{q}]$ is the coriolis forces, $g(q)$ is the gravitational force vector, τ is the control torque vector, q is the angular displacement, and $\dot{q}$ is the angular velocity.

Consider a 2-DOF robot arm with two links as shown in Fig. 1. Taking into account, the symbols listed in Table 1, the robot dynamics, are represented as [14]:

$$\begin{bmatrix} M_{11} & M_{12} \\ M_{21} & M_{22} \end{bmatrix} \begin{bmatrix} \ddot{q}_1 \\ \ddot{q}_2 \end{bmatrix} + \begin{bmatrix} C_{11} & C_{12} \\ C_{21} & C_{22} \end{bmatrix} \begin{bmatrix} \dot{q}_1 \\ \dot{q}_2 \end{bmatrix} + \begin{bmatrix} g_1 \\ g_2 \end{bmatrix} + \begin{bmatrix} b_1\dot{q}_1 + f_{c1\,\mathrm{sgn}(\dot{q}_1)} \\ b_2\dot{q}_2 + f_{c2sgn(\dot{q}_2)} \end{bmatrix} = \begin{bmatrix} \tau_1 \\ \tau_2 \end{bmatrix} \tag{2}$$

The elements $M_{ij}(q)(i,j=1,2)$ of the inertia matrix $M(q)$ are as follows [14]:

$$\begin{aligned} M_{11} &= m_1 l_{c1}^2 + m_2(l_1^2 + l_{c2}^2 + 2l_1 l_2 \cos q_2) + I_1 + I_2 \\ M_{12} &= M_{21} = m_2 l_{c2}^2 + m_2 l_1 l_{c2} \cos(q_2) + I_2, \quad M_{22} = m_2 l_{c2}^2 + I_2 \end{aligned} \tag{3}$$

The elements $C_{ij}(q,\dot{q})(i,j=1,2)$ are derived from the centrifugal and Coriolis matrix $C(q,\dot{q})$ are as:

Table 1 Parameters and definition of the manipulators

Parameter	Symbol	Unit
Link 1 length	l_1	m
Link 2 length	l_2	m
Link 1 mass	m_1	kg
Link 2 mass	m_2	kg
Link 1 inertia	I_1	kg m^2
Link 2 inertia	I_2	kg m^2
Gravity acceleration	g	ms^{-2}

$$C_{11} = -m_2 l_1 l_{c2} \sin q_2 \dot{q}_2,\ C_{12} = -m_2 l_1 l_{c2} \sin q_2 (\dot{q}_1 + \dot{q}_2),$$
$$C_{21} = -m_2 l_1 l_{c2} \sin q_2 \dot{q}_1,\ C_{22} = 0 \tag{4}$$

The entries of the gravitational torque vector $G(q)$ are given by:

$$g_1 = m_1 l_{c1g} \sin q_1 + m_2 g[l_{c2} \sin (q_1 + q_2) + l_1 \sin q_1]$$
$$g_2 = m_2 l_{c2g} \sin (q_1 + q_2) \tag{5}$$

3 Fuzzy Logic Control (FLC) of Robot Manipulator

There are practical challenges to formulate an accurate mathematical model of real physical system. So, human experts incorporate linguistic information using FLC in order to reduce the problems. Initially, in [15, 16], novel spherical motor capable of 3-D motion in a single joint is designed for manipulators. These intelligent control techniques (fuzzy logic) are used for the purpose of dexterous actuations. Also, the proposed control structure supports the execution of a series of complex tasks in an uncertain or hostile environment. General steps in any FLC system are presented in Fig. 2. They are 1. fuzzifier, 2. fuzzy inference engine, 3. fuzzy rule base, and 4. defuzzifier.

For trajectory control of robot, input variables in FLC are error, i.e., e (deg) and error derivative, i.e., $\dot{e}$ (deg/s) of joint position. The joint control input u (torque) is the output variable of fuzzy controller.

Advantage of FLC includes robustness since they are not very sensitive to the changes in the environment. It is also an alternative, when precise mathematical formulation is not possible [17]. In [18], and use of FLC in robotics is presented for demonstrating the benefits which can be gained by using the FLC law. Design of a fuzzy (FC) based on pole assignment is shown in [19] to obtain the desired axes positions under variations in the robot parameters and payload variations. In [20], for the first time, use of FLC strategy for two-joint two-link manipulator is shown which incorporates a proportional plus integral controller (PI).

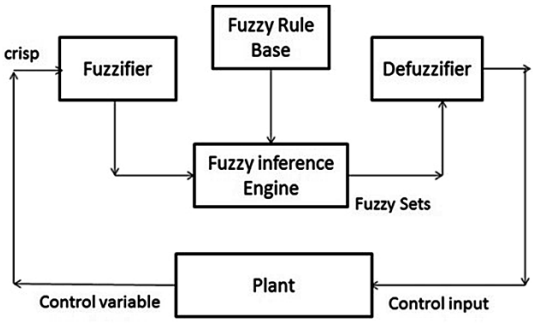

Fig. 2 Basic steps of fuzzy system

The implementation of hierarchical control on a robot manipulator using fuzzy logic is shown in [21], including the implementation of fuzzy PD controller in a Rhino robot. It also includes the comparison of performance with PD controller. In [22], initially, different issues involving the control of the robotic manipulators such as the effect of external disturbances and parameter variations on the control of trajectory tracking are identified. Later, it shows the comparative study on different intelligent control strategies such as PID control, model reference adaptive control (MRAC), and application of servomotor-driven 2-DOF SCARA arm. Comparison among controller is also shown using the performance measure in terms of tracking errors, steady state errors, and robustness of the system.

Four broad levels of applications of robot control system includes the following: identified-task design, system monitoring (including self-tuning and self-organization), information filtering and pre-processing, and in-loop direct control are presented in [23]. The issues on design and rule base size reduction concept are presented in [24]. The automatic regeneration method of fuzzy rule base is shown including the large-scale rule base size reduction.

In [25], a new approach combing computed torque control and FLC is developed for the trajectory tracking problems of 2-link robotic manipulators with structured uncertainty and/or unstructured uncertainty. Only use of fuzzy logic for controlling the robot manipulator is discussed till now, and next Sects. 4–6 present the use of FLC with robust controller to enhance the performance.

4 Fuzzy PID Control of Robot Manipulators

Manipulators are constructed from open-chain link mechanism and nonlinear coupled system, which are difficult to control. PID controls are being used for their simplicity and satisfactory performance for the tracking of slow-varying robot trajectories. Use of PID control for controlling 2-DOF robot arm is explained in [26]. PID control of the robot manipulator for the purpose of industrial application is described in [27].

When mass and inertia of the robot manipulators are not known accurately or if they vary in different operating condition, a conventional PID control may not work satisfactorily. However, operator can control these complexities based on their experiences. It is therefore necessary to design a control which can work on the experience of human operator, i.e., use of fuzzy control [28, 29]. Saturation of nonlinear PID regulator for industrial robot manipulators is discussed in [29]. However, PID control is also effective in controlling a highly nonlinear system with small tracking error given in [30–32]. In [33], for the first time, it has shown the concept to overcome the difficulty with the conventional PID controller, i.e., the use of fuzzy PID controller.

In [34], a new hybrid control scheme (fuzzy + PID) is introduced to control inertial parameter changes for a direct drive 2-link manipulator. Scharf and Mandic [35] shows the motion control of the robot manipulator using the application of the fuzzy + PD logic control system. It is also shown that fuzzy logic systems play the

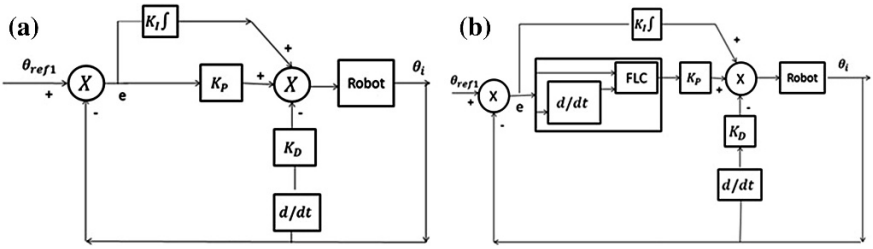

Fig. 3 **a** PID control structure. **b** PID control with fuzzy [35]

role of tuner for robot control gains. Control law used in PID control strategy is described as:

$$\tau_{PID} = K_D e + K_p e + K_I \int e dt \tag{6}$$

where K_D, K_I, and K_P are the controller gain matrices, and τ_{PID} is the vector of joint torque.

Block diagram of PID control of the robot manipulator with fuzzy logic is shown in Fig. 3.

The fuzzy PID control algorithm designed in paper [36] achieved the ideal control effect in the actual control. Conventional controllers include the following: simple PID, computed torque control, and feed forward inverse dynamics control, and intelligent control includes the following: fuzzy control, neural control, and neuro-fuzzy control.

In [37], fuzzy controller is combined with a conventional PID controller, to enhance the robustness of the PD-type controller. Fuzzy self-tuning algorithm is presented in [38] to select P, I and D gains of the PID controller with respect to the actual state of the robot manipulator. Comparisons between PID and fuzzy-PID are also discussed which are shown in Fig. 4. Next section highlighted the importance of FLC with SMC for the robot manipulator.

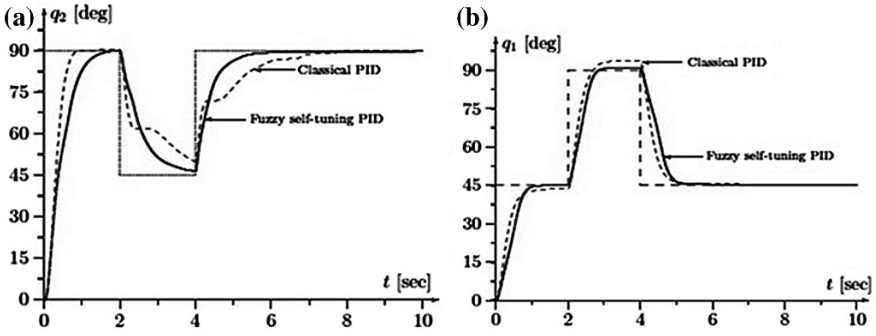

Fig. 4 Desired and actual positions 1 in (**a**) and for position 2 in (**b**) the fuzzy self-tuning PID control and classical PID [38]

5 Fuzzy Sliding Mode Control for Robot Manipulator

SMC is developed on the methodology of feedback control to achieve surface tracking for disturbance and parameter variation in a class of nonlinear, time-varying system. Designing of the sliding mode involves two major steps.

First step includes the design of the sliding surface to maintain the system trajectory on the surface, and second step involves the design of control law, which brings the system representative point (RP) to the sliding surface [39]. SMC is a nonlinear control method that depicts the dynamics of a nonlinear system by the application of discontinuous control signal. Approach of SMC design helps us to maintain stability and consistent performance for model uncertainty [39].

Some inherent advantages of SMC are easy realization, fast response, good transient performances, and insensitivity to parameter variation [39] that helps to control the robot manipulator. SMC scheme was first used in [40, 41] to control a two-link manipulator for handling variable load in a flexible manufacturing system environment. SMC is applied in various ways for controlling the robot manipulator [42].

In [43], SMC scheme based on fuzzy model is discussed for controlling the robot manipulator. SMC with fuzzy model is also used to overcome modeling errors and unknown disturbances [44] for enhancing the sliding mode controller performance. SMC with FLC for SCARA robot manipulator trajectory control is discussed in [45] to reduce chattering. SMC with fuzzy and PID is often absorbed in many papers [42, 46, 47].

The aim for designing a tracking control law is to obtain a suitable input torque τ such that the error between position vector q and desired trajectory q_d is zero. So, tracking error vector (5) is written as:

$$e = q_{\mathrm{d}} - q \tag{7}$$

First step of SMC is to design the sliding surface which is described as:

$$s = \dot{e} + \int_0^{\tau} \{ae_1 + k_2 e_2\}\mathrm{d}\tau \tag{8}$$

Equation (8) is a PID sliding surface, designed with function of error vector λ_i, a diagonal positive matrix. For the existence of stable sliding surface, $s = 0$ must satisfy and $e \rightarrow 0$ as $t \rightarrow \infty$ [47]. Based on the sliding surface, the robot dynamic equation is written as:

$$M\dot{s} = cs + f + \tau_D - \tau \tag{9}$$

where,

$$f = M(\ddot{q}_{\mathrm{d}} + \lambda_1 \dot{e} + \lambda_2 e) + c\left(\dot{e} + \lambda_1 e + \lambda_2 \int_0^{\tau} e\mathrm{d}\tau\right) + G \tag{10}$$

Second step of SMC is to design the control input which is described as:

$$\tau = \hat{f} + K_v s - \psi \,\mathrm{sgn}(s) \tag{11}$$

where,

$$\hat{f} = \hat{M}(\ddot{q}_\mathrm{d} + \lambda_1 \dot{e} + \lambda_2 e) + \hat{c}\left(\dot{e} + \lambda_1 e + \lambda_2 \int_0^\tau e \mathrm{d}\tau\right) + \hat{G} \tag{12}$$

A fuzzy tuneable gain is used to design the good response characteristics for PID and for the robustness property of SMC [48]. The system is done for two-link manipulator having model uncertainty and external disturbances. PID sliding surface is also designed in terms of robot dynamics equation. Hence, fuzzy tuning system is designed for adjusting both controller gain and PID coefficient in order to decrease the reaching time on the sliding surface, chattering, and oscillation in the response. Increasing the gain (K_v) of PID control can cause oscillation in the input torque around the sliding surfaces.

In order to control the oscillation, gain should be increased when the state trajectory is far from the sliding surface. It should also decrease when the state trajectory is nearer to the surface. Adaptive FLC with SMC can be used for tuning the gain. In this case, fuzzy system is designed with two inputs s and $\dot{s}$, i.e., distance of the state trajectory to the sliding surface and its derivative along one output [49]. In [50], robustness property of SMC and good response characteristics of PID are combined with fuzzy tuning gain approach to achieve more acceptable performance for the two-link robot manipulator. This includes model uncertainty and external disturbances. Comparison for the performances of SMC and fuzzy SMC is shown in Fig. 5 [50].

Use of adaptive control and also sliding mode together is discussed in the next section for controlling the robot manipulator dynamics.

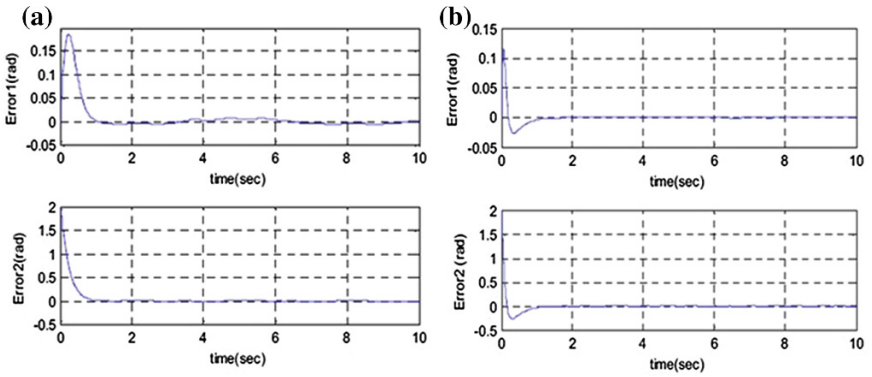

Fig. 5 The tracking errors in the case of using conventional SMC in (**a**), and the tracking errors in the case of using fuzzy SMC-PID in (**b**) [50]

6 Adaptive Fuzzy Control for Robot Manipulator

Robot dynamics contain many uncertainties such as payload parameter, friction, and disturbances. It is difficult to obtain the desired control performances when the control algorithm is based only on the robot dynamics model. So, more robust control is required to compensate the uncertainty and parameter variation. Hence, adaptive control is the best suited one [51].

Use of adaptive control for the robot manipulator was first introduced in [52]. Adaptive control for N-link manipulator with unknown load is also discussed in [53]. Control of the robot manipulator using adaptive control based on speed gradient and for rigid manipulator is shown, respectively, in [54, 55]. The robot dynamics uncertainty is overcome by using an adaptive control scheme, which utilizes an FLC system as a compensator for any uncertainty as discussed in [56]. To design a hybrid adaptive fuzzy control with a continuous switched supervisory controller, direct and indirect adaptive fuzzy control is used for SEIKOTT-3000 SCARA robot in [57].

Adaptive control, SMC, and PID control are used together with FLC for controlling the robot manipulator to improve the robustness and efficiency as presented in [58–62]. Block diagram of adaptive fuzzy SMC is shown in Fig. 6. In [63], adaptive fuzzy sliding mode controller is applied for the two-link robotic manipulators. Tracing errors e_1 and e_2 for joint position 1 and 2, respectively, using SMC and adaptive fuzzy sliding mode control (ADFSMC) are shown in Fig. 7.

A delayed output feedback control scheme for a class of unknown nonlinear system is presented in [64]. This scheme is used to achieve satisfactory H^{∞} tracking performance in the presence of external disturbances, time delays, and uncertainty for the control of a two-link robot manipulator system.

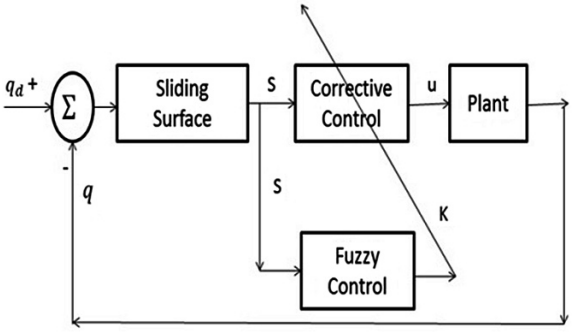

Fig. 6 AFSMC system

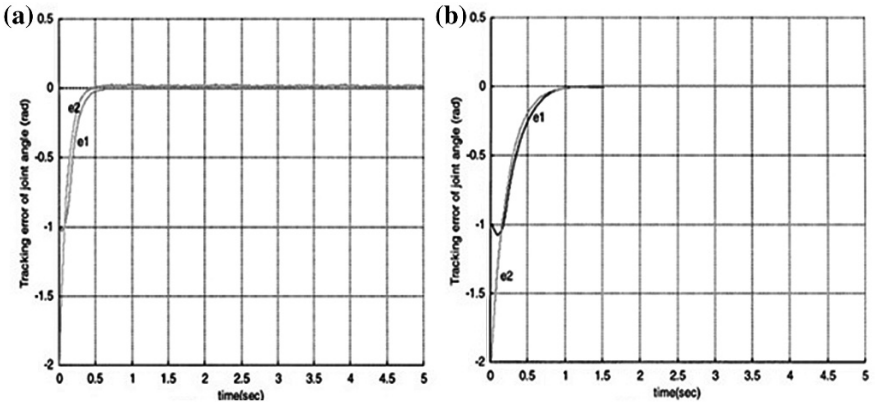

Fig. 7 Tracking errors e_1 and e_2 using SMC in (**a**) and using AFSMC in (**b**) for set point control [63]

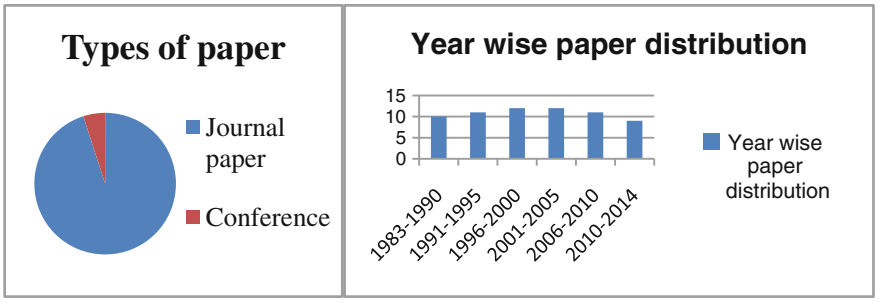

Fig. 8 Types of papers and their year wise distributions

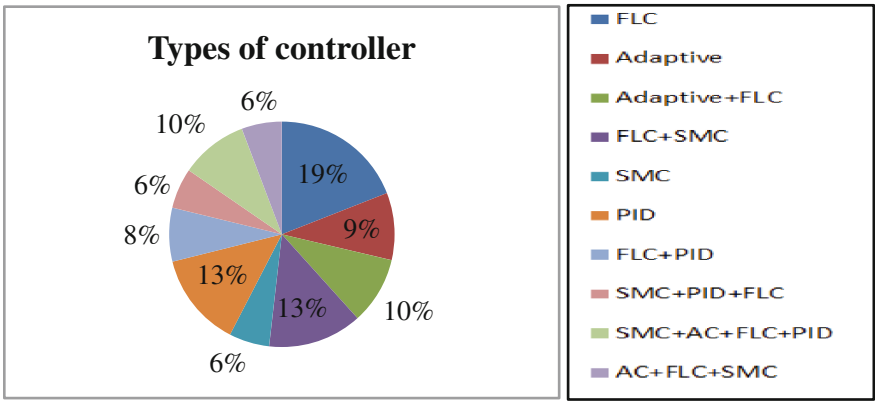

Fig. 9 Types of controller uses and their percentage in paper

7 Conclusions

A total of 65 papers were surveyed in this paper, covering sufficient depth of study for controlling the 2-DOF robot manipulators during the time span of 1983–2014 using FLC. FLC with classical control techniques such as PID control, SMC, and adaptive control together with FLC was introduced, and a range of contribution of such methods for control of robot manipulators is highlighted here. Only FLC of soft computing technique is taken here to show its importance. The review of recent literature shows that classical control is not efficient and robust for the control of robot manipulator under different uncertainties such as model uncertainty, varying payload, and parameter variation. It is absorbed from the literature that use of FLC with classical control techniques improves the robustness and efficiency of the system. Figures 8 and 9 show the types of papers used in this paper and their yearwise contributions with their types of controllers used, respectively.

References

1. Edwards, M.: Robots in industry: an overview. Appl. Ergon. **15**(1), 45–53 (1984)
2. Giralt, G.: Bibliotec Basic de Ciencia e Cultura. Instituto Piaget, Lisboa-Portugal (1997)
3. Lourens, T., Berkel, R.V., Barakova, E.: Communicating emotions and mental states to robots in a real time parallel framework using Laban movement analysis. Robot. Auton. Syst. **58**, 1256–1265 (2010)
4. Kirby, R., Forlizzi, J., Simmons, R.: Affective social robots. Robot. Auton. Syst. **58**, 322–332 (2010)
5. Soltanpour, M.R., Jafaar, K., Soltani, M.: Robust nonlinear control of robot manipulator with uncertainties in kinematics, dynamics and actuator models. Int. J. Innovative Comput. Inf. Control **8**, 5487–5498 (2012)
6. Mark, L., Nagurka Vincent, Y.: Optimal Design of Robotic Manipulator Trajectories: a Nonlinear Programming Approach. Carnegie Mellon University, Pittsburgh (1987)
7. Sabri, T.L.: Adaptive Control of Robotic Manipulators, PhD Thesis, University of Florida (1986)
8. Dieulot, J.-Y., Frederic, C.: Robust PID control of a linear mechanical axis: a case study. Mechatronics **19**, 269–273 (2009)
9. Rasit, K., Abdullah, F.: Model based intelligent control of a 3-joint robotic manipulator: a simulation study using artificial neural networks. ISCIS, pp. 31–40. Springer, Berlin (2004)
10. Prabhu, S.M., Garg, D.P.: Design of a fuzzy logic based robotic admittance controller. Intell. Autom. Soft Comput. **4**(2), 175–190 (1998)
11. Paraskevopoulos, P.N.: Digital Control Systems, 1st edition. Editora Prentice Hall, USA (1995)
12. Lee, C.C.: Fuzzy logic in control systems: fuzzy logic controller—part I & part II. IEEE Trans. Syst. Man Cybern. **20**(2), 404–435 (1990)
13. Keigo, W., Kiyotaka, I., Takaaki, O.: A nonlinear robust control using a fuzzy reasoning and its application to a robot manipulator. J. Intell. Robot. Syst. **20**, 275–294 (1997)
14. Herbert, T.: Modeling and control of robot manipulators, Lorenzo Sciavicco and Bruno Siciliano. J. Intell. Robot. Syst. **21**(1), 99–100 (1998)
15. Kelly, R., Haber, R., Haber-Guerra, R.E., Reyes, F.: Lyapunov stable control of robot manipulators a fuzzy self-tuning procedure. Intell. Autom. Soft Comput. **5**(4), 313–326 (1999)

16. Slotine, J.E., Sastry, S.S.: Tracking control of nonlinear systems using sliding surfaces, with application to robot manipulators. Int. J. Contr. **38**(2), 465–492 (1983)
17. Llama, M.A., Rafael, K., Santibaez, V.: A stable motion control system for manipulators via fuzzy self-tuning. Fuzzy Sets Syst. **124**, 133–154 (2001)
18. Wakileh, B.A.M., Gill, K.F.: Use of fuzzy logic in robotics. Comput. Ind. **10**, 35–46 (1988)
19. Basil, M., Al-Hadithi, Matıa, F., Jimenez, A.: Fuzzy Controller for Robot Manipulators, pp. 688–697. Springer, Berlin (2007)
20. Lim, C.M., Hiyama, T.: Application of fuzzy logic control to a manipulator. IEEE Trans. Robot. Autom. **1**(5), 688–691 (1991)
21. Kishan, K.K., Jamshidi, M.: Control of Robotic Manipulator Using Fuzzy Logic. In: Proceedings of the Third IEEE Conference on Fuzzy Systems and Computational Intelligence, 1, 518–523 (1994)
22. Nagrath, I.J., Chand, P.: Development and Implementation of Intelligent Control Strategy For Robotic Manipulator. In: IEEE/IAS International Conference on Industrial Automation and Control (I A & C'95), 215–220 (1995)
23. Clarence, W.D.S.: Applications of fuzzy logic in the control of robotic manipulators. Fuzzy Sets Syst. **70**, 223–234 (1995)
24. Hala, B.N.D., Adel, M.A.: Fuzzy control of robot manipulators: some issues on design and rule base size reduction. Eng. Appl. Artif. Intell. **15**, 401–416 (2002)
25. Song, Z., Yi, J., Zhao, D., Li, X.: A computed torque controller for uncertain robotic manipulator systems: Fuzzy approach. Fuzzy Sets Syst. **154**, 208–226 (2006)
26. David, I., Robles, G.: PID Control Dynamics of a Robotic Arm Manipulator with two Degrees of Freedom, Control de Procesos y Robotica, 1–7 August 17 (2012)
27. Rocco, P.: Stability of PID control for industrial robot arms. IEEE Trans. Robot. Automat. **12**, 606–614 (1996)
28. Hwang, G.C., Lin, S.C.: A stability approach to fuzzy control design for nonlinear systems. Fuzzy Sets Syst. **48**, 279–287 (1992)
29. Santibañez, V., Camarillo, K., Javier, M.V., Campa, R.: A practical PID regulator with bounded torques for robot manipulators. Int. J. Control Autom. Syst. **8**(3), 544–555 (2010)
30. Arimoto, S., Miyazaki, F.: Stability and Robustness of PID Feedback Control for Robot Manipulators of Sensory Capability. In: Brady, M., Paul R.P. (eds.) Robotics Research: First International Symposium, the MIT Press, Cambridge, MA, pp. 783–789 (1984)
31. Kelly, R.: A tuning procedure for stable PID control of robot manipulators. Robotica **13**, 141–148 (1995)
32. Cervantesa, I., Jose, A.: On the PID tracking control of robot manipulators. Syst. Control Lett. **42**, 37–46 (2001)
33. Bekit, B.W., Seneviratne, L.D., Whidborne, J.F., Althoefer, K.: Fuzzy PID Tuning for Robot Manipulators. In: Proceedings of the 24th Annual Conference of the IEEE Industrial Electronics Society, 1998, IECON '98, vol. 4: pp. 2452–2457 (1998)
34. Lia, W., Changa, X.G., Wahlb, F.M., Tsoc, S.K.: Hybrid fuzzy P+ID control of manipulators under uncertainty. Mechatronics **9**, 301–315 (1999)
35. Scharf, E.M., Mandic, N.J.: The application of a fuzzy controller to the control of a multi-degree of freedom robot arm. In: Industrial Application of Fuzzy Control, pp. 41–61 (1985)
36. Zhu, C., Zhang, H.: Parallel Robotics Control Strategy Study Based on Fuzzy-PID, pp. 664–669. Springer, Berlin (2011)
37. Huang, S.J., Lee, J.S.: A stable self-organizing fuzzy controller for robotic motion control. IEEE Trans. Ind. Electro. **47**(2), 421–428 (2000)
38. Meza, J.L., Santibanez, V., Soto, R., Llama, M.A.: Fuzzy self-tuning PID semiglobal regulator for robot manipulators. IEEE Trans. Ind. Electron. **59**(6), 2709–2717 (2012)
39. Slotine, J.E., Li, W.: Applied Nonlinear Control, Prentice Hall, New Jersey, 40–97, 276–289 (1991)
40. Young, K.K.D.: A variable structure model following control design for robotics applications. IEEE J. Robot. Autom. **4**(5), 556–561 (1988)

41. Su, C.Y., Leung, T.P.: A sliding mode controller with bound estimation for robot manipulators. IEEE Trans. Robot. Autom. **9**(2), 208–214 (1993)
42. Ha, Q.P., Rye, D.C., Durrant-Whyte, H.F.: Fuzzy moving sliding mode control with application to robotic manipulators. Automatica **35**, 607–616 (1999)
43. Ngo, H.Q.T., Shin, J.H., Kim, W.H.: Fuzzy sliding mode control for a robot manipulator. Artif. Life Robot. **13**, 124–128 (2008)
44. Abdelhameed, M.M.: Enhancement of sliding mode controller by fuzzy logic with application to robotic manipulators. Mechatronics **15**, 439–458 (2005)
45. Seok, J.G., Lee, M.C.: Design of a fuzzy-sliding mode controller for a scara robot to reduce chattering. KSME Int. J. **15**(3), 339–350 (2001)
46. Liu, J., Wang, X.: Sliding Mode Control for Robot. Springer, Berlin (2011)
47. Kang, C.G.: Variable structure fuzzy control using three input variables for reducing motion tracking errors. J. Mech. Sci. Technol. **23**, 1354–1364 (2009)
48. Javaheri, H., Vossoughi, G.R.: Sliding Mode Control with Online Fuzzy Tuning: application to a Robot Manipulator. In: IEEE International Conference on Mechatronics and Automation, pp. 1357–1362 (2005)
49. Dhaval, V., Ohri, J., Ankit, P.: Comparison of Conventional & Fuzzy based Sliding Mode PID Controller for Robot Manipulator. In: IEEE International Conference on Individual and Collective Behaviors in Robotics, pp. 115–119 (2013)
50. Mohammad, A., Ehsan, S.S.: Sliding Mode PID-Controller Design for Robot Manipulators by Using Fuzzy Tuning Approach. In: Proceedings of the 27th Chinese Control Conference, Kunming, Yunnan, China, 16–18 July, pp. 170–174 (2008)
51. Esogbue, A.O., Murrell, J.A.: Advances in fuzzy adaptive control. Comput. Math. Appl. **27**(9/10), 29–35 (1994)
52. Slotine, J.E., Li, W.: On the adaptive control of robot manipulators. Int. J. Robot. Res. **6**(3), 49–59 (1987)
53. Han, J.Y., Hemami, H., Yurkovich, S.: Nonlinear adaptive control of an N-link robot with unknown load. Int. J. Robot. Res. **6**(3), 71–86 (1987)
54. Woonchul, H.: Adaptive control based on explicit model of robot manipulators. IEEE Trans. Automat. Control **38**, 654–658 (1993)
55. Yan, R., Tee, K.P., Li, H.: Nonlinear Control of a Robot Manipulator with Time-Varying Uncertainties, pp. 202–211. Springer, Berlin (2010)
56. Yang, Y., Zhou, C., Du, J.: Adaptive robust fuzzy tracking control for pole balancing robots using small gain design. Intell. Autom. Soft Comput. **11**(2), 97–109 (2005)
57. Byung, K.Y., Woon, C.H.: Adaptive control of robot manipulator using fuzzy compensator. IEEE Trans. Fuzzy Syst. **8**(2), 186–199 (2000)
58. Liu, J., Sun, F.: Chattering free adaptive fuzzy terminal sliding mode control for second order nonlinear system. J. Control Theory Appl. **4**, 385–391 (2006)
59. Mehmet, O.: Fractional fuzzy adaptive sliding-mode control of a 2-DOF direct-drive robot arm. IEEE Trans. Syst. Man Cybern. Part B Cybern. **38**(6), 1561–1570 (2008)
60. Kim, Y.T.: Independent joint adaptive fuzzy control of robot manipulator. Intell. Autom. Soft Comput. **11**(1), 21–32 (2005)
61. Wang, J., Rad, A.B., Chan, P.T.: Indirect adaptive fuzzy sliding mode control: part I: fuzzy switching. Fuzzy Sets Syst. **122**(1), 21–30 (2001)
62. Sharkawy, A.B., Salman, S.A.: An adaptive fuzzy sliding mode control scheme for robotic systems. Intell. Control Autom. **2**, 299–309 (2011)
63. Guo, Y., Woo, P.Y.: An adaptive fuzzy sliding mode controller for robotic manipulators. IEEE Trans. Syst. Man Cybern. Part A Syst. Hum. **33**(2), 149–159 (2003)
64. Yu, W.S., Karkoub, M., Wu, T.S., Her, M.G.: Delayed output feedback control for nonlinear systems with two-layer interval fuzzy observers. IEEE Trans. Fuzzy Syst. **22**(3), 611–630 (2014)

Selection of Material Under Conflicting Situation Using Simple Ratio Optimization Technique

Rajnish Kumar and Amitava Ray

Abstract Optimal selection of material for engineering design from a set of materials is more complex due to availability of huge amount of material. An improper selection of material makes adverse effect on successful engineering design, productivity, quality, customer satisfaction, etc. Since the selection of material involves multiple criteria, therefore, the material selection problem is a multi-criteria decision making problem. A systematic and efficient approach toward the material selection is necessary in order to select the best material. In this paper, an integrated approach comprising of entropy and multiple objective on the basis of simple ratio analysis (MOOSRA) method is used to solve material selection problem. A case study on exhaust manifold has been taken for the analysis. The result shows that the carburized steel is the nest material while cast alloy is the worst material.

Keywords Material selection · Simple ratio analysis tool · Decision making

1 Introduction

Material selection plays critical role in engineering design. Material selection is one of the most challenging issues in the design and development of industrial products. It is also affect the success, competitive quality, customer satisfaction, and productivity of the products. The large amount of availability of materials makes very difficult and time consuming to decide specific material for optimal design [1–5]. It is estimated that more than forty thousand useful metallic alloys and probably close to that number of nonmetallic engineering materials like as plastics, ceramics,

R. Kumar (✉) · A. Ray
Department of Mechanical Engineering, National Institute of Technology, Silchar 788010, India
e-mail: rajnish12nits@gmail.com

A. Ray
e-mail: amitavaray.siliguri@gmail.com

K.N. Das et al. (eds.), *Proceedings of Fourth International Conference on Soft Computing for Problem Solving*, Advances in Intelligent Systems and Computing 335,
DOI 10.1007/978-81-322-2217-0_42

and glasses, composite materials, semiconductors, functionally graded materials, smart materials to be present [6]. An improper selection of material adversely affects productivity, profitability, and reputation of manufacturers [7]. The purpose and attributes in material selection procedure are observed to be often in conflicts and it involves trade-offs between significant factors, such as preferred properties working environment, manufacture method, product performance, and cost [8–11]. Thus, the material selection process is a multiple attribute decision making problem.

Multiple criteria decision making problem solve by various techniques such as Analytical Hierarchy Process [12], Multiple objective on the basis of Ratio analysis [4, 5], Technique for order preference by simulation of Ideal Solution [13], Data Envelope Analysis etc. are available for measuring performance in decision making. Kumar et al. [14], Kumar and Jagadish [15] used TOPSIS method to select cutting tool materials. Kumar and Jagadish [16] used MOORA method to find best material for gear design. Chang et al. [10] used Fuzzy Dematel Method for Developing Supplier Selection Criteria. Rao and Patel [17] used fuzzy to compute subjective weight of criteria and used to apply to selection of material problem for high speed navel craft. Chatterjee et al. [11], Chatterjee and Chakraborty [18] used to estimate optimal material for gear selection problem from Extended PROMETHEE II, COPRAS-G, and ORESTE. In next section discuss about proposed methodology, validation of methodology taking a case study, result, and discussion to find out optimal material.

2 Proposed Methodology

Multi-criteria decision making methods use when two or more alternatives are present in the decision matrix. In this case study, seven alternative materials and six criteria are taken in the decision matrix. Table 3 shows decision matrix of problem of material selection for exhaust manifold is a MCDM problem. To solve this problem proposed a methodology to solve this multiple attribute decision making problem.

Step 1: Decide the Decision matrix

$$A = \begin{array}{c} \\ A_1 \\ A_2 \\ \vdots \\ A_3 \end{array} \begin{array}{c} \begin{array}{cccc} \mathrm{X_1} & \mathrm{X_2} & \ldots & \mathrm{X_n} \end{array} \\ \begin{bmatrix} X_{11} & X_{12} & \ldots & X_{1n} \\ X_{21} & X_{22} & \ldots & X_{2n} \\ \vdots & \vdots & \ddots & \vdots \\ X_{m1} & X_{m2} & \ldots & X_{mn} \end{bmatrix} \end{array} \tag{1}$$

X_{ij} ($i = 1, 2, \ldots, m; j = 1, 2, \ldots, n$) is the performance value of ith alternative to the jth criteria.

Step 2: Normalize the decision matrix

$$Q_{ij} = \frac{X_{ij}}{\sqrt{\sum_{i=1}^{m} X^2}} \tag{2}$$

Step 3: Entropy value E_j of jth criteria obtained as follows:

$$E_j = -K \sum_{i=1}^{m} Q_{ij} \ln\left(Q_{ij}\right) \quad j = 1, 2, \ldots, n \tag{3}$$

where $k = 1/\ln m$ is a constant the guarantees $0 \leq E_j \leq 1$ and m is the number of alternatives.

Step 4: The degree of divergence (D_j) of the average information contained by each criterion can be obtained from Eq. (4)

$$D_j = \left|1 - E_j\right| \tag{4}$$

Step 5: Weight of Entropy of jth criterion can be defined as follows:

$$B_j = D_j / \sum_{j=1}^{n} D_j \tag{5}$$

Step 6: Determination of performance score of the alternatives

The performance score (P_i) of alternative is computed as the simple ratio of weighted sum of beneficial criteria to the weighted sum of non-beneficial criteria. This is shown in following equation.

$$P_i = \frac{\sum_{j=1}^{g} X_{ij}}{\sum_{j=g+1}^{n} X_{ij}} \tag{6}$$

where $j = 1, 2, \ldots, g$ indicate the beneficial criteria, and $j = g + 1, g + 2 \ldots n$ indicate the non-beneficial criteria. B_j = Associated weighted weight of the jth criteria.

3 Validation of the Proposed Methodology

In this section, a case study is used to demonstrate the proposed methodology. In this study, an exhaust manifold has been taken as a case study. The Criteria of the materials are as follows (Table 1): surface hardness (SH), core hardness (CH), surface

fatigue limit (SFL), bending fatigue limit (BFL), ultimate tensile strength (UTS), and cost (C). Alternative materials (Table 2) are ductile iron, cast iron, cast alloy steel, hardened alloy steel, surface hardened alloy steel, carburized steel, and nitrided steels. The decision matrix of the exhaust manifold has been shown in Table 3.

Step 1: The decision matrix of the exhaust manifold is shown in Table 3. There are seven materials and six criteria have been considered in this decision matrix.

Step 2: Normalized (Q_{ij}) the decision matrix using Eq. (2) and result is shown in Table 4.

Step 3: Calculate the Entropy value (E_j) using Eq. (3).

Table 1 Attribute of materials

Criteria	Unit
Surface hardness (SH)	Bhn
Core hardness (CH)	Bhn
Surface fatigue limit (SFL)	N/mm^2
Bending fatigue limit (BFL)	N/mm^2
Ultimate tensile strength (UTS)	N/mm^2
Cost (C)	USC/lb

Table 2 List of alternative material

S. No.	Material
1	Ductile iron
2	Cast iron
3	Cast alloy steel
4	Hardened alloy steel
5	Surface hardened alloy steel
6	Carburized steels
7	Nitrided steels

Table 3 Decision matrix of material

S. No.	SH	CH	SFL	BFL	UTS	C
1	220	220	460	360	880	0.342
2	200	200	330	100	380	0.171
3	270	270	630	435	590	0.119
4	270	270	670	540	1,190	1.283
5	585	240	1,160	680	1,580	3.128
6	700	315	1,500	920	2,300	2.315
7	750	315	1,250	760	1,250	4.732

Table 4 Normalized matrix

S. No.	SH	CH	SFL	BFL	UTS	C
1	0.17237	0.31421	0.18291	0.22737	0.2537	0.05453
2	0.1567	0.28564	0.13122	0.06316	0.10955	0.02726
3	0.21155	0.38562	0.25051	0.27474	0.17009	0.01897
4	0.21155	0.38562	0.26642	0.34106	0.34307	0.20455
5	0.45836	0.34277	0.46126	0.42948	0.4555	0.4987
6	0.54846	0.44989	0.59646	0.58107	0.66307	0.36908
7	0.58764	0.44989	0.49705	0.48001	0.36037	0.75443

Table 5 Criteria weighting by entropy method

S. No.	SH	CH	SFL	BFL	UTS	C
B_j	0.20134	0.39475	0.22708	0.21041	0.2059	0.23949

Table 6 Performance score of alternatives

S. No.	SH	CH	SFL	BFL	UTS	Cost	P	Rank
1	0.034706	0.124033	0.041536	0.047842	0.052236	0.013058	1.286154	3
2	0.031551	0.112757	0.029798	0.013289	0.022557	0.006529	0.075188	6
3	0.000746	0.001462	0.00036	0.000484	0.000349	2.012521	0.000963	7
4	0.042593	0.152222	0.060498	0.071763	0.070638	0.048988	1.220082	4
5	0.092286	0.135308	0.104744	0.090368	0.093788	0.119434	1.496357	2
6	0.110428	0.177592	0.135444	0.122262	0.136527	0.088392	1.897336	1
7	0.118315	0.177592	0.11287	0.100999	0.074199	0.180678	1.134295	5

Step 4 and Step 5: Calculate divergence (D_j) value and Entropy weight (B_j) from Eqs. (4) and (5), respectively. Entropy weight is shown in Table (5).

Step 6: Using Eq. (6), the performance (p_i) of candidate materials (Table 6).

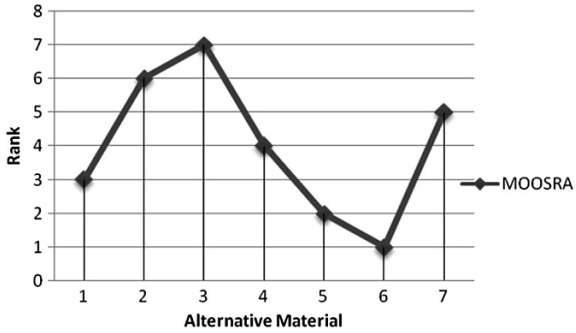

Fig. 1 Graph between rank and alternative material

4 Discussion and Conclusion

Selection and ranking are two critical steps in the material screening. In this paper, proposed methodology used in screen the best material for exhaust manifold. Ranking of material is shown in Table 6 is 3–6–7–4–2–1–5. Carburized steel is best and cast steel alloy worst material, respectively, for this case. Figure 1 shows between ranking of material and alternative material. This method is very simple and based on the simple ratio of beneficial and non-beneficial criteria represent output and input during decision making process by designers. It is observed that compared to other MADM methods such as ELECTRE, VIKOR, PROMETHEE, and EVAMIX, proposed method is simple and easy to understand.

References

1. Amiri, M., Zandieh, M., Soltani, R., Vahdani, B.: A hybrid multi-criteria decision-making model for firms competence evaluation. Expert Syst. Appl. **36**, 12314–12322 (2009)
2. Ashby, M.F., Brechet, Y.J.M., Cebon, D., Salvoc, L.: Selection strategies for materials and processes. Mater. Des. **25**, 51–67 (2004)
3. Bai, C., Sarkis, J.: Green supplier development: analytical evaluation using rough set theory. J. Clean. Prod. **18**(12), 1200–1210 (2010)
4. Brauers, W.K.M., Ginevicius, R.: Regional development in lithuania considering multiple objectives by the Moora method. Technol. Econ. Dev. Econ. **16**, 613–640 (2010)
5. Brauers, W.K.M., Zavadskas, E.K.: The Moora method and its application to privatization in a transition economy. Control Cybern. **35**(2), 445–469 (2006)
6. Fayazbakhsh, K., Abedian, A., Manshadi, B.D.: Introducing a novel method for materials selection in mechanical design using Z-transformation in statistics for normalization of material properties. Mat. Des. **30**, 4396–4404 (2009)
7. Cavallaro, F.: Fuzzy TOPSIS approach for assessing thermal-energy storage in concentrated solar power (Csp) systems. Appl. Energy **87**(2), 496–503 (2010)
8. Isaksson, C., Karlsson, F.: Indoor climate in low-energy houses—an interdisciplinary investigation. Build. Environ. **41**, 1678–1690 (2006)
9. Chan, F.T.S., Kumar, N.: Global supplier development considering risk factors using fuzzy extended AHP-based approach. Omega **35**, 417–431 (2007)
10. Chang, B., Chang, C.-W., Wu, C.-H.: Fuzzy DEMATEL method for developing supplier selection criteria. Expert Syst. Appl. **38**(3), 1850–1858 (2011)
11. Chatterjee, P., Athawale, V.M., Chakraborty, S.: Material's selection using complex proportional assessment and evaluation of mixed data methods. Mater. Des. **32**, 851–860 (2011)
12. Satty, T.L.: The analytic hierarchy process. McGraw-Hill, New York (1980)
13. Hwang, C.L., Yoon, K.: Multi criteria decision making: methods and applications, a state of art survey. Springer, New York (1981)
14. Kumar, R., Bhomik, C., Ray, A.: Selection of cutting tool material by TOPSIS method. In: National Conference on Recent Advancement in Mechanical Engineering (NCRAME-2013), NERIST, Itanagar, India. ISBN: 978-93-82880-71-4 (2013)
15. Kumar, R., Jagadish, A.R.: Selection of material: a multi-objective decision making approach. In: International Conference on Industrial Engineering (ICIE-2013), pp. 162–165. S.V. National Institute of Technology, Surat, India. ISBN: 978-93-83083-37-4 (2013)

16. Kumar, R., Jagadish, A.R.: Selection of cutting tool material: a holistic approach. In: 1st International Conference on Mechanical Engineering: Emerging Trends for Sustainability (ICMEETS-2014), pp. 447–452. M.A. National Institute of Technology, Bhopal, India. ISBN: 978-93-83083-45-9 (2013)
17. Rao, R.V., Patel, B.K.: A subjective and objective integrated multiple attribute decision making method for material selection. Mater. Des. **37**(10), 4738–4747 (2010)
18. Chatterjee, P., Chakraborty, S.: Material selection using preferential ranking methods. Mater. Des. **35**, 384–393 (2012)
19. Chen, C.C., Tseng, M.L., Lin, Y.H.: Using fuzzy DEMATEL to develop a causal and effect model of hot spring service quality expectation. In: IEEE International Conference on Industrial Engineering and Engineering Management, pp. 1004–1008 (2008)
20. Dagdeviren, M.: Decision making in equipment selection: an integrated approach with AHP and PROMETHEE. J. Intell. Manuf. **19**(4), 397–406 (2008)
21. Deng, Y.-M., Edward, K.L.: The role of materials identification and selection in engineering design. Mater. Des. **28**, 131–139 (2007)
22. Dweiri, F., Al-Oqla, F.M.: Material selection using analytical hierarchy process. Int. J. Comput. Appl. Technol. **26**, 182–189 (2006)
23. Edwards, K.L.: Selecting materials for optimum use in engineering components. Mater. Des. **26**, 469–474 (2005)
24. Karande, P., Chakraborty, S.: Application of multi-objective optimization on the basis of ratio analysis (MOORA) method for materials selection. Mater. Des. **37**, 317–324 (2012)
25. Kelemenis, A., Askounis, D.: A new TOPSIS-based multi-criteria approach to personnel selection. Expert Syst. Appl. **37**(7), 4999–5008 (2010)
26. Das, M.C., Sarkar, B., Ray, S.: Decision making under conflicting environment: a new MCDM method. Int. J. Appl. Sci. **5**(2), 2012 (2012)
27. Khorshidi, R., Hassani, A.: Comparative analysis between TOPSIS and PSI methods of materials selection to achieve a desirable combination of strength and workability in Al/SIC composite. Mater. Des. **52**, 999–1010 (2013)
28. Shanian, A., Savadogo, O.: TOPSIS multiple-criteria decision support analysis for material selection of metallic bipolar plates for polymer electrolyte fuel cell. J. Power Sources **159**, 1095–1104 (2006)

An Investigation into Use of Different Soft Artificial Intelligence Techniques in Mechanical Engineering Domain

Anubha Tiwari, Rajvardhan Jaideva and Sharad K. Pradhan

Abstract In the present era, of globalization and automation, artificial intelligence (AI) has come out as a better implement to solve many problems that require decision making. In this work, it has been tried to amalgamate the research work done related to application of soft computing techniques particularly in the area of mechanical engineering. A lot of researches have being carried out in this domain because it has been a pool of infinite scope for innovative works. This paper gives a quick view of the different applications of AI techniques, such as neural networks, fuzzy logic, neurofuzzy (NF), simulated annealing (SA), genetic algorithm (GA), genetic programming (GP), and data mining (DM), and provides a conscious view in the different paradigms of mechanical engineering where the soft computing techniques are separately used and even in combination with one another to perform certain tasks which if performed by human becomes a dreary task. Several applications of soft computing have been proposed in the literature to solve the problems related with complicated mechanical systems. It is felt that a review of the application in various mechanical areas would help to compare their main features and their relative advantages or limitations to allow choose the most suitable technique for a particular application and also throw light on aspects that needs further attention.

Keywords Soft computing · Artificial intelligence · Computer intelligence · Evolutionary computation

A. Tiwari (✉) · R. Jaideva · S.K. Pradhan
Department of Mechanical Engineering, NITTTR, Bhopal, Madhya Pradesh, India
e-mail: anuumishra@yahoo.com

R. Jaideva
e-mail: raj.jaideva@gmail.com

S.K. Pradhan
e-mail: spradhan@nitttrbpl.ac.in

K.N. Das et al. (eds.), *Proceedings of Fourth International Conference on Soft Computing for Problem Solving*, Advances in Intelligent Systems and Computing 335,
DOI 10.1007/978-81-322-2217-0_43

1 Introduction

Soft computing differs from conventional (hard) computing in that, unlike hard computing, it is tolerant of imprecision, uncertainty, partial truth, and approximation. In effect, the role model for soft computing is the human mind.

Hard computing, i.e., conventional computing requires a precisely stated analytical model and often a lot of computation time. Hard computing is based on binary logic, crisp systems, numerical analysis, and crisp software, but soft computing is based on fuzzy logic (FL), neural nets, and probabilistic reasoning. Although in hard computing, imprecision and uncertainty are undesirable properties, in soft computing, the tolerance for imprecision and uncertainty is exploited to achieve tractability, lower cost, high machine intelligence quotient (MIQ), and economy of communication. Hard computing requires programs to be written; soft computing can evolve its own programs.

The methods mentioned in this work can be dedicated to the so-called soft part of artificial intelligence (AI). The contrary "hard" part of AI consists of topics such as experts systems and formal logic and is looking for scientifically neat solutions rather than solving problems pragmatically.AI is a wide-ranging area of engineering and science which deals with improvement of system and incorporates features which are imitation of human intelligence. Soft computing indulges itself in making intelligent programs and even intelligent machines that make it an interdisciplinary field of engineering and science. Interdisciplinary because it go through many domains, not only computer science but also mathematics, neuroscience, psychology, statistics, mechanical engineering, economics, linguistics control theory and cybernetics, philosophy, and many more in the row. The acumen with which AI deals is generally human behavior-related issues such as problem solving, natural language processing, and perception and planning, adaptation and learning, and acting on the environment. An ample study of such problems that exist in AI milieu requires a clear-cut formulation of the problem so that thorough analysis can be carried out to get reasonable solutions [1].

2 Main Objectives of AI Techniques

The main objectives of AI research are as follows [2]:

- To comprehend human cognition.
- To provide lucrative automation of human being in intellectual tasks.
- To augment commercial intelligent in building systems to help humans sense wise.
- To support general problem-solving environment for solving an expansive range of real-world problem.
- To provide communication with people using natural language.

- To provide autonomy so that the intelligent systems can act on their own scheme.
- To train system in a way to gather its own data.
- To stock up information and know how to reclaim it.

3 Various AI Techniques

Listed below are the different techniques of AI:

- Artificial neural networks (ANN)
- FL
- Adaptive network-based fuzzy inference system (ANFIS)
- Evolutionary computation (EC)—based on the origin of the species

  GA
  Swarm intelligence (SI)
  Ant colony optimizations (ACO)

- GP
- SA
- NF
- DM
- Machine learning (ML)
- Support vector machines (SVM)
- Case-based reasoning (CBR)
- Cellular automata (CA)
- Multi-agent systems (MAS)
- Reinforced learning (RL)

4 Abilities

The different abilities and key features of the above-mentioned AI techniques have been tabulated in Table 1.

5 Existing Research Efforts

The application of various techniques of AI in the area of mechanical engineering has been summarized in the tables below:

Table 1 AI techniques have been tabulated

Abilities	ANN	FL	NF	GA	GP	SA	DM	MAS	RL	CBR
1. Decision making	✓	✓	✓		✓	✓				
2. Error compensation		✓		✓	✓	✓				
3. Optimization	✓	✓	✓	✓	✓	✓	✓	✓	✓	✓
4. Increase efficiency	✓	✓	✓	✓	✓				✓	✓
5. Trainable	✓									
6. Process control	✓							✓		
7. Accuracy	✓							✓		✓

5.1 Applications of Artificial Neural Network

Many research works have been done in the field of ANN. Scientists have made efforts in finding out the uses of ANN in the many fields. Here, Table 2 depicts various applications of ANN in mechanical engineering domain.

5.2 Applications of Genetic Algorithm

The Table 3 tabulates the areas of application of GA in the domain of mechanical engineering. Studies in the recent past have showed the wide-range applications of GA in many areas such as optimization of problem and error compensation.

5.3 Applications of Fuzzy Logic

FL has always been one of the favorite topics of researchers. For them, FL has the flexibility to adopt itself with any new techniques. The Table 4 presents the different applications and its contributions in the mechanical engineering domain.

Table 2 Neural network

Author	Contribution	Summary
Sterjovski et al. [3]	Use of artificial neural networks for modeling the mechanical properties of steels	• This paper highlights the effectiveness of 3 back-propagation models
		• Impact toughness of quenched and tempered pressure vessel steel exposed to multiple post-weld heat treatment (PWHT) cycles
		• Hardness of simulated heat-affected zone in pipe line and tap fitting after in-service welding
		• Hot ductility and strength of various micro-alloyed steels over the temperature range of slab straightening of continuous casting process
		• Economizes the experimental setup
Fines et al. [4]	Using artificial neural networks for compensation of machine tool positioning error	• Three architectures were developed to compensate machine tool positioning error
		• Lesser training required
Aysun et al. [5]	Using Taguchi design of experiment and artificial neural network model optimization of the wire electric discharge machining (EDM) process	• An experiment was performed with AISI-4340 steel to identify the main parameters affecting the surface roughness. Among them were
		–Open-circuit voltage
		–Pulse on time
		–Open voltage
		–Wire speed
		–Flushing pressure
		• Optimizing the process in wire EDM
Thomas et al. [6]	Classification of gas turbine sensor validation through artificial neural network	• A technique has been proposed which on training the artificial neural networks as classifier recognizes the sensor drift
		• Two types of gas turbines taken into consideration: One with single shaft Another one with twin-shaft machine
		• By this method, evaluation of sensors becomes accurate, aiming to minimize the need for calibration and avoid shutdowns
		• Detection of sensor drift
		• Cost-effective maintenance, increased availability, and reliability of power plant

(continued)

Table 2 (continued)

Author	Contribution	Summary
Brezak et al. [7]	Examined the flank wear regulation using artificial neural networks	• The objective was to maximize the allowed amount of tool wear rate within a predefined machining time, while simultaneously maintaining a high level of process productivity with the help of determination of a tool wear regulation model. The model constitutes of
		–Radial basis function NN controller
		–Modified dynamical neural network filter
		–Reduction found in control variable oscillations,
		–Control error in achieving the maximum allowed tool wear intensity, and
		–Estimation errors
Senatore et al. [8]	Piston ring friction losses prediction using artificial neural networks	• The proposed ANN model helps in identifying the factors with the prominent influence on the friction loss evolution
		• It can also be used for finding the combinations of inputs factors leading to the lowest average friction coefficient value
		• Comparison between the corresponding data obtained by the numerical algorithm and the ANN predicted values of the friction loss shows mutual agreement with a correlation coefficient of 0.9934
Presinkumar et al. [9]	In the prediction of wear losses for A390 aluminum alloy based on artificial neural network	• The pin-on-disk apparatus is used at room condition in order to test a material which is subjected to dry sliding wear
		• The experimental results were trained in an ANN program, and the results were compared with experimental values to evaluate the effects of
		–Load, sliding speed, time
		• The feed-forward back propagation neural network gave satisfactory agreement between the experimental and ANN results

(continued)

Table 2 (continued)

Author	Contribution	Summary
Midany et al. [10]	Enhancing the characteristics of manufactured product using artificial neural networks	• The target was to enhance the properties using a performance prediction model for the manufactured products. The two phases of the proposed approach are achieved by:
		–Enquiring how to decide the elements influencing the performance of the manufactured part
		–Explaining how to get edge from this predicted model in order to achieve the largest number of manufactured products which have better qualities through parts allocation to the matched assembled parts
Mahdavinejad et al. [11]	Optimization of milling parameters using artificial neural network and artificial immune system	• The proposed model helps to forecast the effective milling parameters of the work piece made of Ti-6Al-4 V for its final surface roughness. The parameters taken into consideration are
		–Cutting speed, depth of cut, feed per tooth
		• The lowest value should be assigned to feed rate, and different values should be taken for two variables as per the subjected condition in order to get extra finished surface
Lin et al. [12]	Analyses of composites machining using multiple regression and neural networks	• They contributed a model using
		–Generalized radial basis function (GRBF) neural networks and
		–Multiple regression
		For the purpose of analyses of composites (aluminum metal matrix composite)
		• Forecasting the attainment of tool wear is fairly accurate using force-wear equation derived from multiple regression analysis (MRA)
		• Further accuracy is achieved using neural network analysis keeping in mind that the functional dependency is nonlinear
		• GRBF neural network improves the accuracy of tool wear prediction because of the fact that it employs a linear activation function as the basis function

Table 3 Genetic algorithm

Author	Contribution	Summary
Elbeltagy [13]	A comparison of various optimization algorithms on a multi-level problem	• The study compares several strategies in order to combine fast evaluation of limited accuracy with a few accurate calculations
		• It has been concluded that a sequential strategy using cheap but inaccurate solution first allowed by a lesser number of intermediate solution before finally using a few calls to the fully accurate but most costly function proved to be best suitable technique
Nearchou [14]	Adaptive navigation of autonomous vehicles using evolutionary algorithms	• This paper contributed an adaptive navigation of a robot-like simulated vehicle making it capable to navigate freely in a constrained and unknown environment while performing a desired task
		• In order to measure the performance of the algorithm, it is demonstrated on problem with vehicles moving in two-dimensional grids and compared with that of a simple greedy algorithm and a random search technique
		• The comparative experimental results show a higher performance of the proposed algorithm versus that of two simple heuristics which are a random search technique and a greedy algorithm
Knosala [15]	Using genetic algorithm, a production scheduling problem is solved	A technique has been proposed for flexible manufacturing cell work scheduling with the aid of genetic algorithm and draft of code strings, which are used by this algorithm
		• In first case, it has been assumed that the cell works in optional mode that is every operation can be performed on every machine
		• In the second case, cell works in sequential mode that is the first operation is executed on the first machine, the second operation on the second machine and so on
		It has been summarized that the designed genetic algorithm used has come up correct with regard to time, schedules, but the optimality of solution is not guaranteed

(continued)

Table 3 (continued)

Author	Contribution	Summary
Rafiee et al. [16]	Generation of an identification system based on genetic algorithm	• The designed model investigates the type of gear failure of a gearbox system using artificial neural networks (ANN)
		• It is most suitable for practical implementations because of its short training duration and high accuracy
		• It has been concluded that MLP neural network of well-formed optimized structure has given a remarkable accuracy of 16:11:4 structure providing the capability to identify faults perfectly in 99 % of the circumstances
Filetin et al. [17]	Overview of the applied methods and results in predicting different properties of the heat-treatable steels and process parameters	• The combination of genetic algorithm and genetic programming has been proposed for definition of the relations between different variables
		• By means of neural network:
		–Coefficient of heat conductivity,
		–Tempering curve of tool steels,
		–Surface hardness of gas and
		–Plasma nitriding
		have been also successfully predicted
Jimenez et al. [18]	Designed a method of complete coverage path planning based on genetic algorithms technique	• Path planning problems involve
		–Computing or
		–Finding a collision-free path between two positions
		• Complete coverage path planning is a special type of path planning where a robot sweeps all area of free space in an environment, and they are not designed to optimize the process
		• Using cellular decomposition, the whole region was divided into two categories:
		–Sub-areas
		–Nodes
		• The results showed the feasibility and optimality of the proposed planner

Table 4 Fuzzy logic

Author	Contribution	Summary
Lee et al. [19]	Thermal error modeling of a horizontal machining center	• This paper highlights improvement made by thermal error model using of fuzzy logic strategy
		• This error model can be applied to any CNC machine tools
		• This model provides high speed and good accuracy
Majumdar et al. [20]	Using fuzzy reasoning and fuzzy analytic hierarchy process, risk analysis was carried out	• This paper consists of a risk assessment related to injuries occurring in many construction sites
		• These injuries were classified into minor, severe, and very severe
		• This model focuses on the safety of professionals
Rai [21]	Using the fuzzy logic-based prediction of performance and emission parameters for the LPG-diesel dual fuel engine	• This paper majorly focuses on the reduction of pollution using LPG-diesel dual fuel engine in order to lower down the emission of NITROGEN OXIDE (NOx) and smoke
		• A hybrid technique was used known as ANFIS system
		• This paper focuses on the engine performance and emission parameter as well like brake-specific energy consumption and brake thermal efficiency
Kwon [22]	Using the fuzzy neuron adaptive modeling to predict surface roughness under process variations in CNC turning	• This paper shows a model, which adapts the membership functions in accordance with the extent of the process variations, which is used to envisage the surface roughness
		• It is used for predicting the surface roughness
Jayaswal et al. [23]	The recent developments made in the field of neural networks, fuzzy logic, and wavelet transform in fault diagnosis.	• This paper gives the information about the topical developments in the field of fault diagnosis
		• This method of fault diagnosis is used by maintenance engineers for conditioning monitoring of rotating machines

(continued)

Table 4 (continued)

Author	Contribution	Summary
Healy [24]	A model based on the fuzzy logic sensor fault accommodation	• This paper has a fuzzy logic-based accommodation approach for future that will increase the value of the logical third channel in the control system's fault isolation and accommodation scheme
		• This approach is used in aircraft gas turbine engines
Singh [25]	Using fuzzy logic approach in the intelligent controller for mobile robot	• This paper shows an intelligent controller for mobile robot navigation algorithm
		• Simulation results confirmed the efficiency of the controllers
		• This paper shows an intelligent system which perform suitably in a vague environment
Kao [26]	Using the fuzzy logic control for the micro-hole electrical discharge machining	• In this study, a micro-hole electrical discharge machining (EDM) system was used with adaptive fuzzy logic control and the exactness piezoelectric stage was developed
		• This study also focuses on the stable and efficient micro-hole EDM drilling process
Jurado et al. [27]	Using the neural network techniques for the problems of tuning fuzzy controllers	• This paper describes specific technique which were developed and applied to the problem of tuning fuzzy controllers
		• One the main complications of these lab exercises is that they require resources
Daws [28]	Using fuzzy logic, an automated advisory material selection system was designed	• According to this paper, an automatically recommended material selection system is considered.
		• This design system is named as CAMS, and the objective of this system is to solve the problems of materials selection and evaluation
		• It is advantageous over existing systems that do not have decision modules

(continued)

Table 4 (continued)

Author	Contribution	Summary
Khabbaz et al. [29]	Using the fuzzy logic approach for metal casting selection process	• This paper shows an approach for dealing with the qualitative properties of materials and the fuzzy space
		• Used in metal casting process for right material selection
Xu [30]	An adaptive real-time fuzzy X-ray system was built for the solder joint inspection system	• This paper shows embedded software, Fuzzy Expert System for X-ray Inspection (FESXI), for the inspection of soldering defects in an electronic manufacturing process of Nokia networks
		• The FESXI software was useful in decreasing number of false alarms to prevent unnecessary rework and which increases the throughput time of production
Pourzeynali et al. [31]	Using fuzzy logic and genetic algorithms, an active control of high-rise building structures was developed	• This paper focuses to design and optimize the different parameters of the active tuned mass damper (ATMD) control scheme
		• This scheme was used for getting the improved results in the reduction of earthquake caused damage
		• The buildings were modeled as a shear frame and then the problem is solved
Mukherjee et al. [32]	Using intelligent fuzzy-based reactive power compensation for an isolated hybrid power system	• In this paper, an inaccessible wind–diesel hybrid power system model is well thought out for its online reactive power compensation
		• This paper also works on minimizing the gap between reactive power generation and its demand
Zaheeruddin et al. [33]	A fuzzy logic system was designed for noise-induced sleep disturbance	• In this paper, an attempt to build a fuzzy expert system for predicting the property of any annoyance made by noise that may be in the form of extent of its occurrence
		• This paper also shows the effect of noise on the sleep that varies according to the age of people

(continued)

Table 4 (continued)

Author	Contribution	Summary
Bayder et al. [34]	Using genetic programming, an automated generation of robust error recovery logic in assembly systems	• In this paper, using multi-level optimization in a "generate and test" type, an assembly line is modeled, and from the given error cases, a best way of error mending is investigated
		• This approach will not take much time for the generation of robust error recovery logic
Nada et al. [35]	Using fuzzy logic, for the quality prediction in the manufacturing system design	• This paper shows that a fuzzy inference system was used for modeling the relationship between manufacturing system design parameters and the product quality level
		• And also a composition capability zone is organized graphically.
		• And developed a system configuration that produces more than one product, and compared to standard six-sigma quality
Mitra et al. [36]	Using fuzzy attributes, evolutionary modular design of rough knowledge was prepared	• This paper integrates rough set theory with a fuzzy using algorithm, for tagging and set rule in soft computing
		• The genetic algorithm refines the fuzzification parameters such as network weight and then structure together, by optimizing a single fit function
Prabha et al. [37]	Using adaptive neuro-fuzzy inference system based on representing quality power factor for power quality	• In this paper, a quality power factor ANFIS RQPF is proposed
		• The ANFIS RQPF can symbolize an obligatory module for evaluating and collecting together the three power factors

Table 5 Simulated annealing

Author	Contribution	Summary
Cosola et al. [38]	A general framework for identification of hyper-elastic membranes with moré techniques and multi-point simulated annealing	• This paper presents a hybrid procedure for mechanical cataloging of hyper-elastic materials based on three techniques
		–Moiré technique
		–Finite element analysis
		–Global optimization
		• Feasibility, efficiency, and robustness were improved for both anisotropic and isotropic specimen
Genevese et al. [39]	Improving the global–local simulated annealing formulation for solving nonsmooth engineering optimization problems	• This paper focuses on the optimization algorithm that provides a better formulation of simulated annealing
		• This approach was much quicker than conventional simulated annealing
Gandhomi et al. [40]	Using genetic simulated annealing, an empirical model for shear capacity of RC deep beams was proposed	• This paper shows an empirical model to foresee the shear strength of RC deep beams
		• The model was created using an experimental catalog acquired from the literature
		• The proposed empirical model has the results which indicate that the projected empirical model was able in evaluating the shear strength of deep beams
Li et al. [41]	For 3D engineering layout design, a parallel simulated annealing algorithm was used based on functional feature tree modeling	• This paper was based on using multiple Markov chains
		• This algorithm increases computing competence by allocating computation load to networked computers
		• This approach was used in a real engineering application such as engine compartment layout design
Hwang et al. [42]	For engineering problems, improving real parameter of genetic algorithm with simulated annealing	• In this paper, an adaptive real parameter simulated annealing genetic algorithm (ARSAGA) is anticipated
		• Adaptive mechanisms were used to get the convergence speed

(continued)

Table 5 (continued)

Author	Contribution	Summary
Shen et al. [43]	Using the simulated annealing approach, a smart design was prepared for the assembly	• The core objective of this research is to widen a feasible optimization algorithm based on simulated annealing (SA) method
		• This algorithm was used to get feasible optimization solution
Barati [44]	Using a synergy between cellular automata and quasi-simulated annealing methods, a new approach of optimization problem for research reactors of fuel plate was used	• This paper presents an optimization technique which is a combination of cellular automata (CA) and quasi-simulated annealing (QSA)
		• These techniques were used in minimizing both the mass and deformation of fuel plate of a multi-purpose research reactor (MPRR)
Leite et al. [45]	Using parallel simulated annealing algorithm for getting the solution of the structural optimization problems	• In this paper, simulated annealing (SA) algorithm has demonstrated as a better technique for solving tricky combinatorial optimization problems
		• The evaluation of parallel schemes where the solution spaces may be very intricate and highly inhibited
Cagan et al. [46]	Using hierarchical models for general three-dimensional component layout, a simulated annealing-based algorithm was developed	• A well-organized simulated annealing based algorithm was used which optimizes the element layout.
		• This algorithm was used for the optimization of component layout
Dai et al. [47]	Using an improved genetic simulated annealing algorithm, an energy-efficient scheduling was done for flexible flow shop	• This paper focuses on to make mathematical model for the FFS problem based on an energy-efficient mechanism to solve a multi-objective optimization problem
		• Used in scheduling of the flow shop
Mirazaali et al. [48]	In tube hydro forming process, the application of simulated annealing method for the optimization of pressure and force loading	• In this paper, using simulated annealing optimization method, pressure and force loading paths in tube hydro forming process are investigated and optimized
		• The most important parameters in tube hydro forming are as follows:
		–Internal pressure
		–Force loading

(continued)

Table 5 (continued)

Author	Contribution	Summary
He et al. [49]	Using simulated annealing genetic algorithm, damage detection was made by an adaptive real parameter	• This paper demonstrates that the proposed algorithm is capable in identifying the flexural stiffness damage for beam-type structures under "free of noise" condition
		• This algorithm is mostly used in structural mechanics
Chen et al. [50]	Using a neural network integrated simulated annealing approach, the optimization of wire electrical discharge machining for pure tungsten is developed	• In this paper, the method of integrating back-propagation neural network (BPNN) and simulated annealing algorithm (SAA)
		• To solve problems in the field of manufacturing of pure tungsten profiles
		• This analyzes the difference of cutting velocity and surface finish
Nikbakhsh et al. [51]	Using simulated annealing for determination of the capacity of yard stations in a railway industry	• In this paper, a method was developed for optimization formulation and a solution route for the determination of capacity of rail yard stations
		• It uses a simulated annealing (SA) algorithm to solve the problem
Hui et al. [52]	Using an enhanced simulated annealing approach for the robot path planning	• Heuristic methods such as the genetic algorithm (GA)-based approaches were used
		• These methods have been investigated for robot path preparation in vibrant environments

5.4 Applications of Simulated Annealing

Table 5 highlights the various applications of SA in mechanical engineering.

5.5 Application of Other Techniques

There are some techniques other than the main highlighted techniques of AI which also works equivalently effective in many domains. Table 6 shows applications of some of these techniques in the mechanical engineering domain.

Table 6 Other AI techniques

Author	Contribution	Summary
Kusiak [53]	A structure for organizing and applying knowledge for decision making in manufacturing and service applications	• In this paper, basic concepts of data mining and machine learning have been highlighted
		• In order to build decision-making systems machine learning algorithms extract knowledge from vast data bases
		• The proposed approach has two phases
		• learning and
		• decision making
		• Making it suitable for system-on-a-chip applications
Dezelak et al. [54]	Using the machine learning technique to improve the springback modeling	• This paper highlights the machine learning (ML) approach to update the FEM for springback modeling
		• Springback is one of the more important factors that affect the quality of sheet metal forming products
		• It has been concluded that this technique of updating FEM using the combinations gives more accurate springback prediction compared to the solely FEM method
Wang et al. [55]	Based on multi-agent technique, a design on intelligent diagnosis system of reciprocating compressor was prepared	• This system builds the division of labor and cooperation of the different nature agents such as monitoring agent
		• It enhances the effectiveness of reciprocating compressor, condition monitoring, the rapidity of fault diagnosis, and the scalability of multi-agent systems also proving a steady functioning
Fu et al. [56]	Using case-based reasoning and multi-agents for cost collaborative management (CCM) in supply chain	• This study has two objectives:
		• To develop the multi-agents system for CCM.
		• To construct a novel framework model of cost collaborative management in supply chain based on the application of CBR
		• This study also develops a new method, which includes the four key steps:
		–Cost driver and problem identification

(continued)

Table 6 (continued)

Author	Contribution	Summary
		–Cost driver impact assessment and ranking
		–Decision of cost collaborative management actions
		–Optimization and solution
Yunlong et al. [57]	Based on the EMD complexity feature and least square support vector machines, a vibration fault diagnosis method was developed	• This paper presents a fault diagnosis method of centrifugal pump based on EMD complexity feature
		• In this paper, the empirical mode decomposition (EMD) method was used to decompose the vibration signals into a finite number of stationary intrinsic mode functions (IMF)
Faramarzi et al. [58]	Application of cellular automata technique in optimization of truss structures	• This paper presents a two-phase, hybrid, cellular automata–linear programming (CA–LP) method for both size and topology optimization of planar truss structures
		• The efficiency and effectiveness of this proposed algorithm is for the solution of topology and size optimization problems

6 Conclusion

The above study deals with the review of various applications of artificial intelligent techniques such as neural network, FL, SA, GP, GA, and DM in modeling mechanical systems. Based on the above literature, it can be concluded that these artificial intelligent techniques are very useful in various fields. Abilities of these techniques are quite relevant as well which includes decision making, optimization, and many more. In recent times, more emphasis is made on working with the soft computing techniques because of the fact that they reduce the work load and also provide better results.

References

1. Bourbakis, N.G.: Artificial Intelligence Methods and Applications. World Scientific Publishing Co., Singapore. ISBN 981-02-1057-4 (1992)
2. Akerkar, R.: Introduction to Artificial Intelligence. Prentice-Hall, New Jersey. ISBN 81-203-2864-7 (2005)
3. Sterjovski, Z., Nolan, D., Carpenter, K.R., Dunne, D.P., Norrish, J.: Artificial neural networks for modeling the mechanical properties of steels in various applications. J. Mater. Process. Technol. **170**, 536–544 (2005)

4. Fines, J.M., Agah, A.: Machine tool positioning error compensation using artificial neural networks. Eng. Appl. Artif. Intell. **21**, 1013–1026 (2008)
5. Sagbas, A., Kahraman, F.: Optimization of wire EDM process using Taguchi method and back propagation neural network. J. Eng. Archit. Fac. Eskisehir Osmangazi Univ. **25**(1), 1–18 (2012)
6. Palmé, T., Fast, M., Thern, M.: Gas turbine sensor validation through classification with artificial neural networks. Appl. Energy **88**, 3898–3904 (2011)
7. Brezak, D., Majetic, D., Udiljak, T., Kasac, J.: Flank wear regulation using artificial neural networks. J. Mech. Sci. Technol. **24**(5), 1041–1052 (2010)
8. Senatore, A., Ciortan, S.: An application of artificial neural networks to piston ring friction losses prediction. Mech. Testing Diagnosis **1**, 7–14 (2011). ISSN 2247–9635
9. Kumar, AJP., Singh, DKJ.: Artificial neural network-based wear loss prediction for A390 aluminum alloy. J. Theor. Appl. Inf. Technol, 961–964 (2008)
10. Midany, T.T., El-Baz, M.A., Abdelwahed, M.S.: Improve characteristics of manufactured products using artificial neural network performance prediction model. Int. J. Recent Adv. Mech. Eng (IJMECH) **2**(4) (2013)
11. Mahdavinejad, R.A., Khani, N., Fakhrabadi, M.M.S.: Optimization of milling parameters using artificial neural network and artificial immune system. J. Mech. Sci. Technol. **26**(12), 4097–4104 (2012)
12. Lina, J.T., Bhattacharyya, D., Kecmanb, V.: Multiple regression and neural networks analyses in composites machining. Compos. Sci. Technol. **63**, 539–548 (2003)
13. El-Beltagy, M.A.: A comparison of various optimization algorithm on a multi-level problem. Eng. Appl. Artif. Intell. **12**, 639–654 (1999)
14. Nearchou, A.C.: Adaptive navigation of autonomous vehicles using evolutionary algorithms. Artif. Intell. Eng. **13**, 159–173 (1999)
15. Knosala, R.: A production scheduling problem using genetic algorithm. J. Mater. Process. Technol. **109**, 90–95 (2001)
16. Rafiee, J., Arvani, F., Harifi, A., Sadeghi, M.H.: A GA-based optimized fault identification system using neural networks. Tehran International Congress on Manufacturing Engineering (TICME) (2005)
17. Filetin, T., Žmak, I., Lisjak, D., Novak, D., Landek, D.: The application of artificial intelligence methods in heat treatment. IFHTSE (2005)
18. Jimenez, P.A., Shirinzadeh, B., Nicholson, A., Alici, G.: Optimal area covering using genetic algorithms IEEE/ASME. In: International Conference on Advanced Intelligent Mechatronics, pp. 1–6. IEEE, Switzerland (2007)
19. Jin-Hyeon, Lee, Jae-Ha, Lee, Seung-Han, Yang: Thermal error modeling of a horizontal machining center using fuzzy logic strategy. J. Manuf. Process. **3**(2), 120–127 (2001)
20. Majumdar, D., Debnath, J., Biswas, A.: Risk analysis in construction sites using fuzzy reasoning and fuzzy analytic hierarchy process. In: International Conference of Computational Intelligence, Modeling Techniques and Applications (2013)
21. Rai, A., Kumar, N.S., Srinivasa Pai, P., Rao, B.R.: Fuzzy logic based prediction of performance and emission parameters of a LPG-diesel dual fuel engine. Int. Conf. Model. Optim. Comput. **38**, 280–292 (2012)
22. Kwon, Y., Fischer, G.W., Tseng, T.-L.: Fuzzy neuron adaptive modeling to predict surface roughness under process variations in CNC turning. J. Manuf. Syst. **21**(6), 440–450 (2002)
23. Jayaswal, P., Wadhwani, A.K.: Application of artificial neural networks, fuzzy logic and wavelet transform in fault diagnosis via vibration signal analysis. Aust. J. Mech. Eng. **7**(2), 157–171 (2009)
24. Healy, T.A., Kerr, L.J., Larkin, L.J.: Model based fuzzy logic sensor fault accommodation. J. Eng. Gas Turbines Power **120**(3), 533–536 (1998)
25. Singh, M.K., Parhi, D.R., Bhowmik, S., Kashyap, S.K.: Intelligent controller for mobile robot; fuzzy logic approach. In: 12th International Conference of International Association for Computer Methods and Advances in Geo-Mechanics (2008)

26. Kao, C.-C., Miller, S.F., Shih, A.J.: Fuzzy logic control of micro hole electrical discharge machining. J. Manuf. Eng. **130**(6) (2008)
27. Jurado, F., Caño, A., Ortega, M.: Department of Electrical Engineering, University of Jaén, Linares (Jaén), Spain
28. Daws, K.M., Al-Dawood, Z.I., Al-Kabi, S.H.: Fuzzy Logic Approach for Metal Casting Selection Process, vol. 3(3), pp. 162–167 (2009). ISSN 1995-6665
29. Sarfaraz Khabbaz, R., Manshadi Dehghan, B., Abedian, A., Mahmudi, R.: A Simplified Fuzzy Logic Approach for Material Selection in Mechanical Engineering Design, vol. 30(3) (2009)
30. Wei, Xu: Adaptive real time fuzzy X-ray solder joint inspection system. J. Manuf. Syst. **21**(2), 111–125 (2002)
31. Pourzeynali, S., Lavasani, H.H., Modarayi, A.H.: Active control of high-rise building structures using fuzzy logic and genetic algorithms. Eng. Struct. **29**(3), 346–357 (2009)
32. Banerjee, A., Mukherjee, V., Ghoshal, S.P.: Intelligent fuzzy based reactive power compensation of an isolated hybrid power system. Int. J. Electr. Power Energy Syst. **57**, 164–177 (2014)
33. Zaheeruddin, Z., Jain, V.K.: A fuzzy logic system for noise induced sleep disturbance. Published in the Journal of Experts System with Applications, vol. **40**(4) (2004)
34. Bayder Cem, M., Kazuhiro, Saitou: Automated generation of robust error recovery logic in assembly systems using genetic programming. J. Manuf. Syst. **20**(1), 55–68 (2001)
35. Nada, O.A., ElMaraghy, H.A., Waguih, H., ElMaraghy, W.H.: Quality prediction in the manufacturing system design. J. Manuf. Syst. **25**(3), 153–171 (2006)
36. Mitra, S., Mitra, P., Pal, S.K.: Evolutionary modular design of rough knowledge based network using fuzzy attributes. J. Neurocomputing **36**(1–4), 45–66 (2001)
37. Prabha Rathina, N., Marimuthu, N.S., Babulal, C.K.: Adaptive neuro fuzzy inference system based representative quality power factor for power quality assessment. Neurocomputing **73** (13–15), 2737–2743 (2010)
38. Cosola, E., Genovese, K., Lamberti, L., Pappalattere, C.: A general framework for identification of hyper-elastic membranes with moiré techniques and multi-point simulated annealing. Int. J. Solids Struct. **45**(24), 6074–6099 (2008)
39. Cosola, E., Genovese, K., Lamberti, L., Pappalattere, C.: Improved global–local simulated annealing formulation for solving non-smooth engineering optimization problems. Int. J. Solids Struct. **45**(1), 203–237 (2005)
40. Gandomi, A.H., Alavi, A.H., Shadmehri Mohammadzadeh, D., Sahab, M.G.: An empirical model for shear capacity of RC deep beams using genetic- simulated annealing. Arch. Civ. Mech. Eng. **13**(3), 354–369 (2013)
41. Li, N., Cha, J., Lu, Y.: A parallel simulated annealing algorithm based on functional feature tree modeling for 3D engineering layout design. Appl. Soft Comput. **10**(2), 592–601 (2010)
42. Hwang, S.-F., He, R.-S.: Improving real-parameter genetic algorithm with simulated annealing for engineering problems. Adv. Eng. Softw. **37**(6), 406–418 (2006)
43. Shen, H., Subic, A.: Smart Design for Assembly using the Simulated Annealing Approach. In: 2nd I*PROMS Virtual International Conference, pp. 419–424 (2006)
44. Barati, R.: A novel approach in optimization problem for research reactors fuel plate using a synergy between cellular automata and quasi-simulated annealing methods. Ann. Nucl. Energy **70**, 56–63 (2014)
45. Leite, J.P.B., Topping, B.H.V.: Parallel simulated annealing for structural optimization. Comput. Struct. **73**(1–5), 545–564 (1999)
46. Cagan, J., Degentesh, D., Yin, S.: A simulated annealing-based algorithm using hierarchical models for general three-dimensional component layouts. Comput. Aided Des. **30**(10), 781–790 (1998)
47. Dai, M., Tang, D., Giret, A., Salido, M.A., Li, W.D.: Energy-efficient scheduling for a flexible flow shop using an improved genetic-simulated annealing algorithm. Robot. Comput. Integr. Manuf: **29**(5), 418–429 (2013)

48. Mirzaali, M., Seyedkashi, S.M.H., Liaghat, G.H., Naeini Moslemi, H., Shojaee, G.K., Moon, Y.H.: Application of simulated annealing method to pressure and force loading optimization in tube hydro-forming process. Int. J. Mech. Sci. **55**(1) (2012)
49. He, R.-S., Hwang, S.-F.: Damage detection by an adaptive real-parameter simulated annealing genetic algorithm. J. Comput. Struct. **84**(31–32), 2231–2243 (2006)
50. Chen, H.-C., Lin, J.-C., Yang, Y.K., Tsai, C.-H.: Optimization of wire electrical discharge machining for pure tungsten using a neural network integrated simulated annealing approach. Expert Syst. Appl. **37**(10), 7147–7153 (2010)
51. Javadian, N., Sayarshad, H.R., Najafi, S.: Using simulated annealing for determination of the capacity of yard stations in a railway industry. Appl. Soft Comput. **11**(2), 1899–1907 (2011)
52. Hui, Miao, Yu-Chu, Tian: Dynamic robot path planning using an enhanced simulated annealing approach. J. Appl. Math. Comput. **222**(1), 420–437 (2013)
53. Kusiak, A.: Data mining: manufacturing and service applications. Int. J. Prod. Res. **44**(18–19), 4175–4191 (2006)
54. Dezelak, M., Pahole, I., Ficko, M., Brezocnik, M.: Machine learning for spring back modeling. Advances in Production Engineering and Management, vol. 17–26, pp. 1854–6250. ISSN (2012)
55. Wang F., Zhang, Y., Xu, Z., Wang, J., F, X.: Design on intelligent based system of reciprocating compressors based on multi agent systems. Int. Workshop Inf. Electron. Eng. Procedia Eng **17**, 3256–3261 (2012)
56. Fu, J., Fu, Y.: Case based reasoning and multi agents for cost collaborative management in supply chain. Int. Workshop Inf. Electron. Eng. Procedia Eng. **29**, 1088–1098 (2012)
57. Yunlong Z., Peng Z.: Vibration fault diagnosis of centrifugal pump based on EMD complexity feature and least square support vector machines. International Conference on Future Electrical Power and Energy Systems: Energy Procedia, vol. 17, pp. 939–945 (2012)
58. Faramarzi, A., Afshar, M.H.: Application of cellular automata to topology and size optimization of truss structures. Scientia Iranica (2012)

On Solving Multiobjective Quadratic Programming Problems in a Probabilistic Fuzzy Environment

Animesh Biswas and Arnab Kumar De

Abstract In this paper, a fuzzy goal programming (FGP) approach for solving fuzzy multiobjective quadratic chance-constrained programming (CCP) problem involving exponentially distributed fuzzy random variables (FRVs) is developed. In the proposed methodology, the problem is first converted into interval-valued quadratic programming problem using CCP technique and α-cut of fuzzy numbers. Then, using fuzzy partial order relations, the problem is converted into its equivalent deterministic form. The individual optimal value of each objective is found in isolation to construct the quadratic fuzzy membership goals of each of the objective. The quadratic membership goals are transferred into linear goals by applying piecewise linear approximation technique. A *minsum* goal programming (GP) method is then applied to both the linearized and quadratic model to achieve the highest membership degree of each of the membership goals in the decision-making context. Finally, a comparison is made on the two different approaches with the help of distance function. An illustrative numerical example is provided to demonstrate the applicability of the proposed methodology.

Keywords Fuzzy random variable · Fuzzy chance-constrained programming · Fuzzy exponential distribution · Fuzzy goal programming · Quadratic programming · Linear approximation

A. Biswas (✉)
Department of Mathematics, University of Kalyani, Kalyani 741235, India
e-mail: abiswaskln@rediffmail.com

A. Kumar De
Department of Mathematics, Academy of Technology, G.T. Road, Adisaptagram, Aedconagar, Hooghly 712121, India
e-mail: arnab7339@yahoo.co.in

K.N. Das et al. (eds.), *Proceedings of Fourth International Conference on Soft Computing for Problem Solving*, Advances in Intelligent Systems and Computing 335,
DOI 10.1007/978-81-322-2217-0_44

1 Introduction

From middle of the twentieth century, chance-constrained programming (CCP) is playing a major role in different real-life planning problems involving probabilistic uncertainties. In 1959, Charnes and Cooper [1] first introduced CCP technique for solving stochastic programming with random parameters associated with the problem. Different aspects of CCP technique were further investigated by Kataoka [2], Prekopa [3], and other researcher in the past.

In the process of deriving models of CCP, it is important to consider that the possible values of the random parameters under the occurrence of events as fuzzy numbers. Realizing the above fact, the concept of fuzzy CCP (FCCP) was introduced. FCCP problem is a CCP problem in the presence of ambiguous information. Many researchers like Liu [4], Luhandjula [5, 6], and others derived different methods to solve CCP problems. Most of the parameters of this type of problems involve fuzziness and randomness concurrently. In this paper, fuzziness and randomness are considered simultaneously in the form of fuzzy random variables (FRVs). The concept of FRVs was first introduced by Zadeh [7] and further developed by Kwakernaak [8] and Kratschmer [9] according to different requirements of measurability. Buckley [10–12] defined fuzzy probability using fuzzy numbers as parameters in probability density function and probability mass function. These fuzzy numbers are obtained from the set of confidence intervals. The approach of fuzzy probability theory developed by Buckley is different from his predecessors and also comfortable for computational point of view.

Goal programming (GP), introduced by Charnes and Cooper [13], is an efficient tool for solving multiobjective decision-making (MODM) problems having conflicting objectives. The main drawback of classical GP is that the aspiration levels of the goals need to be specified precisely in making a compromise decision. Also, the classical GP technique cannot capture directly the uncertainty arises due to the presence of chance constraints associated with the problems. Under this context, fuzzy goal programming (FGP) [14, 15] is used as a proficient technique for making decision in an imprecisely defined probabilistic MODM context. FGP method for solving CCP problems involving FRVs is recently studied by Biswas and Modak [16, 17]. Among the various types of probability distributions, exponential distribution plays an important role for its wide applications in queuing theory, reliability theory and reliability engineering, medical sciences and many other real-life decision-making areas. To the best of authors' knowledge, an efficient solution technique for solving multiobjective quadratic CCP (MOQCCP) problems following exponential distribution from the viewpoint of its potential use in different planning problems involving fuzzy parameters is yet to appear in the literature.

Further, it may found in a fuzzy MOQCCP (FMOQCCP) that objectives of the DMs are nonlinear in nature. To solve nonlinear objectives, different classical approaches have been developed in the past. The piecewise linear approximation method [18] is a linearization technique that is frequently used in a nonlinear decision-making situation. Since piecewise linear approximation technique

approximates functions in a piecewise manner, the error estimation becomes less in comparison with any other linear approximation techniques.

In the present study, piecewise linear approximation method has been used to solve fuzzy multiobjective quadratic CCP problems where the parameters are considered as fuzzy numbers. Also, the parameters in the right side of system constraints are taken as exponentially distributed FRVs. In the model formulation process, the problem is converted into deterministic problem using CCP technique, α-cut of fuzzy sets and fuzzy partial order relation. Solving each objective independently under the modified system constraints, the quadratic membership goals are formulated. Finally, a weighted *minsum* GP model is developed after linearizing the nonlinear goals for finding most compromise solution in the decision-making arena.

2 Fundamentals

In this section, some basic concepts on fuzzy number, triangular fuzzy number, α-cut, fuzzy inequality, and fuzzy probability that have been used in the model formulation process are discussed.

2.1 Fuzzy Number

A fuzzy set $\tilde{A}$ defined on the set of real numbers, $\mathbb{R}$, is said to be a fuzzy number if its membership function $\mu_{\tilde{A}}(x)$ satisfies the following characteristics:

(i) $\mu_{\tilde{A}} : \mathbb{R} \to [0, 1]$ is continuous.
(ii) $\mu_{\tilde{A}}(x) = 0$ for all $x \in (-\infty, a] \cup [d, \infty)$.
(iii) $\mu_{\tilde{A}}(x)$ is strictly increasing on $[a, b]$ and strictly decreasing on $[c, d]$.
(iv) $\mu_{\tilde{A}}(x) = 1$ for all $x \in [b, c]$ where $a \leq b \leq c \leq d$.

2.2 Triangular Fuzzy Number

A fuzzy number $\tilde{A} = (a, b, c)$ is said to be triangular fuzzy number if its membership function $\mu_{\tilde{A}}(x)$ is given by

$$\mu_{\tilde{A}}(x) = \begin{cases} 0 & \text{if } x < a \text{ or } x > c \\ \frac{x-a}{b-a} & \text{if } a \leq x \leq b \\ \frac{c-x}{c-b} & \text{if } b \leq x \leq c \end{cases}$$

2.3 α-cut of a Fuzzy Set

An α-cut of a fuzzy set $\tilde{A}$ is a crisp set, denoted by $\tilde{A}[\alpha]$ and defined by $\tilde{A}[\alpha] = \{x \in X : A(x) \geq \alpha, 0 \leq \alpha \leq 1\}$, where X represents the set on which the fuzzy set $\tilde{A}$ is defined.

2.4 Fuzzy Inequality

Let $F(\mathbb{R})$ be the set of all fuzzy numbers defined on $\mathbb{R}$. On $F(\mathbb{R})$, different types of partial order relations may be defined using α-cuts and defuzzification methods. According to Kaufmann and Gupta [19], a fuzzy partial order relation "$\gtrsim$" holds between two fuzzy numbers $\tilde{A}$ and $\tilde{B}$, denoted by $\tilde{A} \gtrsim \tilde{B}$, if and only if $a^L \geq b^L$ and $a^R \geq b^R$, where $\tilde{A}[\alpha] = [a^L, a^R]$ and $\tilde{B}[\alpha] = [b^L, b^R]$. The advantage of using this type of partial order relation is that it reduces mathematical computation.

2.5 FRV

Let X be a continuous random variable with probability density function $f(x, \theta)$, where θ is the parameter of the probability density function. If θ is uncertain in nature, then θ can be taken as a fuzzy number $\tilde{\theta}$. Then, the continuous random variable with parameter as fuzzy number $\tilde{\theta}$ is known as continuous FRV $\tilde{X}$ with fuzzy probability $\tilde{P}$. The probability density function of the continuous FRV $\tilde{X}$ is denoted by $f(x, \tilde{\theta})$ with the property $\int_{-\infty}^{\infty} f(x, \theta)\mathrm{d}x = 1; \theta \in \tilde{\theta}[\alpha]$.

With the deliberation of the above ideas, the FMOCCP model is derived in the following section.

3 Formulation of FMOQCCP Model

The general form of a fuzzy chance-constrained programming (FCCP) model with K objectives is presented as follows:

$$\begin{aligned}
&\text{Find } X(x_1, x_2, \ldots, x_n)\\
&\text{so as to Maximize } Z_k = \sum_{j=1}^{n} c_j^{(k)} x_j + \frac{1}{2}\sum_{j=1}^{n}\sum_{l=1}^{n} d_{jl}^{(k)} x_j x_l; \quad k = 1, 2, \ldots, K\\
&\text{subject to } \widetilde{Pr}\left(\sum_{j=1}^{n} \tilde{a}_{ij} x_j \lesssim \tilde{b}_i\right) \gtrsim \tilde{p}_i; \quad i = 1, 2, \ldots, m\\
&x_j \geq 0; j = 1, 2, \ldots, n; 0 \leq p_i \leq 1; p_i \in \tilde{p}_i[\alpha]
\end{aligned} \tag{1}$$

Here, $\tilde{b}_i$ is exponentially distributed FRVs with density function $f(b_i; \tilde{\theta}_i)$, $\tilde{\theta}_i$ is a fuzzy parameter, and $\tilde{p}_i$ are fuzzy numbers, $\gtrsim$ and $\lesssim$ represent greater than or equal and less than or equal, respectively, in fuzzy sense, which are fuzzy partial order relations.

As $\tilde{b}_i$ is exponentially distributed FRV, its probability density function is written as follows:

$$f\left(b_i; \tilde{\theta}_i\right) = \theta_i \mathrm{e}^{-b_i\theta_i}; \quad \theta_i \in \tilde{\theta}_i[\alpha]$$

where the support of $\tilde{b}_i$ is the set of nonnegative real numbers. Here, $\tilde{\theta}_i[\alpha]$ are the α-cut of fuzzy numbers $\tilde{\theta}_i$ whose support is the set of positive real numbers. On the basis of the above considerations, the equivalent deterministic model is derived in the following section.

3.1 Conversion to Deterministic Model

To convert the above problem to its equivalent deterministic form, the following methodology is adopted.

Let $\sum_{j=1}^{n} \tilde{a}_{ij} x_j = \tilde{u}_i$. Then $\widetilde{Pr}\left(\sum_{j=1}^{n} \tilde{a}_{ij} x_j \lesssim \tilde{b}_i\right) = \widetilde{Pr}(\tilde{u}_i \lesssim \tilde{b}_i)$. So its α-cut is given by [12]

$$\begin{aligned}
\widetilde{pr}\left(\tilde{u}_i \lesssim \tilde{b}_i\right)[\alpha] &= \left\{ \int_{u_i}^{\infty} f(b_i; \theta_i) \mathrm{d}b_i : \theta_i \in \tilde{\theta}_i[\alpha], u_i \in \tilde{u}_i[\alpha] \right\}\\
&= \left\{ \int_{u_i}^{\infty} \theta_i \mathrm{e}^{-b_i\theta_i} \mathrm{d}b_i : \theta_i \in \tilde{\theta}_i[\alpha], u_i \in \tilde{u}_i[\alpha] \right\}\\
&= \left\{ \mathrm{e}^{-\theta_i u_i} : \theta_i \in \tilde{\theta}_i[\alpha], u_i \in \tilde{u}_i[\alpha] \right\}
\end{aligned} \tag{2}$$

Here, the coefficients $\tilde{u}_i$, the parameter $\tilde{\theta}_i$ of the FRV $\tilde{b}_i$ and $\tilde{p}_i$ are all taken as triangular fuzzy numbers. Thus, $\tilde{u}_i$, $\tilde{\theta}_i, \tilde{p}_i$ are expressed as follows:

$$\tilde{u}_i = (u_i^L, u_i, u_i^R),\ \tilde{\theta}_i = (\theta_i^L, \theta_i, \theta_i^R),\ \tilde{p}_i = (p_i^L, p_i, p_i^R);\quad (i = 1, 2, \ldots, m)$$

Then, the α-cut of these fuzzy numbers is expressed as follows:

$$\begin{aligned}
\tilde{\theta}_i[\alpha] &= [\theta_i^L + (\theta_i - \theta_i^L)\alpha, \theta_i^R - (\theta_i^R - \theta_i)\alpha] \\
\tilde{u}_i[\alpha] &= [u_i^L + (u_i - u_i^L)\alpha, u_i^R - (u_i^R - u_i)\alpha] \\
\tilde{p}_i[\alpha] &= [p_i^L + (p_i - p_i^L)\alpha, p_i^R - (p_i^R - p_i)\alpha];\quad (i = 1, 2, \ldots, m)
\end{aligned}$$

Thus, using the above α-cuts, (2) can be written in the following form as follows:

$$\widetilde{Pr}(\tilde{u}_i \lesssim \tilde{b}_i)[\alpha] = \left[e^{-(\theta_i^R - (\theta_i^R - \theta_i)\alpha)(u_i^R - (u_i^R - u_i)\alpha)}, e^{-(\theta_i^L + (\theta_i - \theta_i^L)\alpha)(u_i^L + (u_i - u_i^L)\alpha)}\right]$$

Hence, the probabilistic constraints, $\widetilde{Pr}\left(\sum_{j=1}^{n} \tilde{a}_{ij} x_j \lesssim \tilde{b}_i\right) \gtrsim \tilde{p}_i$, in terms of α-cut are expressed as follows:

$$\begin{aligned}
&\left[e^{-(\theta_i^R - (\theta_i^R - \theta_i)\alpha)(u_i^R - (u_i^R - u_i)\alpha)}, e^{-(\theta_i^L + (\theta_i - \theta_i^L)\alpha)(u_i^L + (u_i - u_i^L)\alpha)}\right] \\
&\quad \geq [p_i^L + (p_i - p_i^L)\alpha, p_i^R - (p_i^R - p_i)\alpha] \\
&\text{i.e. } e^{-(\theta_i^R - (\theta_i^R - \theta_i)\alpha)(u_i^R - (u_i^R - u_i)\alpha)} \geq (p_i^L + (p_i - p_i^L)\alpha) \text{ and} \\
&\qquad e^{-(\theta_i^L + (\theta_i - \theta_i^L)\alpha)(u_i^L + (u_i - u_i^L)\alpha)} \geq (p_i^R - (p_i^R - p_i)\alpha) \\
&\text{i.e. } (\theta_i^R - (\theta_i^R - \theta_i)\alpha)(u_i^R - (u_i^R - u_i)\alpha) \leq -\ln(p_i^L + (p_i - p_i^L)\alpha) \text{ and} \\
&\qquad (\theta_i^L + (\theta_i - \theta_i^L)\alpha)(u_i^L + (u_i - u_i^L)\alpha) \leq -\ln(p_i^R - (p_i^R - p_i)\alpha); \\
&\qquad (i = 1, 2, \ldots, m)
\end{aligned}$$

$$\begin{aligned}
&\text{i.e. } \sum_{j=1}^{n} \left[a_{ij}^R - \left(a_{ij}^R - a_{ij}\right)\alpha\right] x_j (\theta_i^R - (\theta_i^R - \theta_i)\alpha) \leq -\ln(p_i^L + (p_i - p_i^L)\alpha) \text{ and} \\
&\qquad \sum_{j=1}^{n} \left[a_{ij}^L + \left(a_{ij} - a_{ij}^L\right)\alpha\right] x_j (\theta_i^L + (\theta_i - \theta_i^L)\alpha) \leq -\ln(p_i^R - (p_i^R - p_i)\alpha)
\end{aligned}$$

Hence, the deterministic model of the corresponding FMOQCCP model is derived as follows:

Find $X(x_1, x_2, \ldots, x_n)$

so as to Maximize $Z_k = \sum_{j=1}^{n} c_j^{(k)} x_j + \frac{1}{2}\sum_{j=1}^{n}\sum_{l=1}^{n} d_{jl}^{(k)} x_j x_l; \quad k = 1, 2, \ldots, K$

subject to

$$\begin{aligned}
&\sum_{j=1}^{n}\left[a_{ij}^R - (a_{ij}^R - a_{ij})\alpha\right] x_j\left(\theta_i^R - \left(\theta_i^R - \theta_i\right)\alpha\right) \leq -\ln(p_i^L + \left(p_i - p_i^L\right)\alpha) \\
&\sum_{j=1}^{n}\left[a_{ij}^L + \left(a_{ij} - a_{ij}^L\right)\alpha\right] x_j\left(\theta_i^L + \left(\theta_i - \theta_i^L\right)\alpha\right) \leq -\ln(p_i^R - \left(p_i^R - p_i\right)\alpha) \\
&x_j \geq 0; \quad (j = 1, 2, \ldots, n)(i = 1, 2, \ldots, m) 0 \leq \alpha \leq 1.
\end{aligned} \tag{3}$$

Now the above model is solved using FGP technique.

4 FGP Model Construction

In FGP, the membership goals are constructed to find the most commensurable solution in a MODM context. To find the membership goal of the objectives, the model is solved by considering each objective independently under the modified set of system constraints; the aspiration level of each objective is calculated in isolation.

Let $x_k^B = (x_{k1}^B, x_{k2}^B, \ldots, x_{kn}^B)$ be the point at which the kth objective Z_k; $(k = 1, 2, \ldots, K)$ attains its best value subject to the set of modified system constraints.

Using the best solutions $x_k^B = \left(x_{k1}^B, x_{k2}^B, \ldots, x_{kn}^B\right)$; $(k = 1, 2, \ldots, K)$, the value of all the objectives Z_k; $(k = 1, 2, \ldots, K)$ is calculated as follows: $Z_k^B = Z_k(x_k^B)$. Hence, a payoff matrix is constructed as follows:

$$\begin{array}{c} \\ x_1^B \\ x_2^B \\ \vdots \\ \vdots \\ x_K^B \end{array}
\begin{array}{c}
\begin{array}{cccc} Z_1(x) & Z_2(x) & \cdots & Z_K(x) \end{array} \\
\begin{bmatrix}
Z_1^B & Z_2(x_1^B) & \cdots & Z_K(x_1^B) \\
Z_1(x_2^B) & Z_2^B & \cdots & Z_2(x_2^B) \\
\vdots & \vdots & \vdots & \vdots \\
\vdots & \vdots & \vdots & \vdots \\
Z_1(x_K^B) & Z_2(x_K^B) & \cdots & Z_k^B
\end{bmatrix}
\end{array} \tag{4}$$

Then, the fuzzy goal of the kth objective is expressed as follows:

$$Z_k(x) \gtrsim Z_k^B; \quad \text{for } k = 1, 2, \ldots, K.$$

Thus the membership function for each of the objectives is written as follows:

$$\mu_{Z_k}(x) = \begin{cases} 0 & \text{if } Z_k \le Z_k^W \\ \frac{Z_k - Z_k^W}{Z_k^B - Z_k^W} & \text{if } Z_k^W \le Z_k \le Z_k^B \\ 1 & \text{if } Z_k \ge Z_k^B \end{cases} \tag{5}$$

where Z_k^W is calculated as follows: $Z_k^W = \min\{Z_k(x_1^B), Z_k(x_2^B), \ldots, Z_k(x_K^B)\}$ for $k = 1, 2, \ldots, K$.

In FGP model formulation process of the problem, the quadratic membership functions defined above are considered as flexible quadratic membership goals by introducing under-and over-deviational variables to each of them and thereby assigning the highest membership value (unity) as the aspiration level to each of them. Also, it is evident that full achievement of all the membership goals is not possible in a MODM context. So the under-deviational variables are minimized to achieve the goal values of objectives in the decision-making environment.

Thus, a FGP model is formulated as follows:

$$\begin{aligned} &\text{Find} \quad X(x_1, x_2, \ldots, x_n) \\ &\text{so as to} \quad \text{Min D} = \sum_{k=1}^{K_1} w_k d_k^- \\ &\text{and satisfy} \quad \frac{Z_k - Z_k^w}{Z_k^b - Z_k^w} + d_k^- - d_k^+ = 1 \quad \text{for } k = 1, 2, \ldots, K \\ &\sum_{j=1}^{n} \left[a_{ij}^R - (a_{ij}^R - a_{ij})\alpha\right] x_j \left(\theta_i^R - (\theta_i^R - \theta_i)\alpha\right) \le -\ln\left(p_i^L + (p_i - p_i^L)\alpha\right) \\ &\sum_{j=1}^{n} \left[a_{ij}^L + (a_{ij} - a_{ij}^L)\alpha\right] x_j \left(\theta_i^L + (\theta_i - \theta_i^L)\alpha\right) \le -\ln\left(p_i^R - (p_i^R - p_i)\alpha\right) \\ &x_j \ge 0; \quad (j = 1, 2, \ldots, n)\,(i = 1, 2, \ldots, m)\, 0 \le \alpha \le 1. \end{aligned} \tag{6}$$

where $w_{ik}^- \ge 0$ represents the numerical weights of the goals which are determined as follows:

$$w_{ik}^- = \frac{1}{(Z_k^b - Z_k^w)}.$$

The developed model (6) was solved to find the most satisfactory solution in the decision-making environment.

5 Linearization of the Quadratic Membership Goals

Since the membership goals are quadratic in nature, so a linearization technique, viz., piecewise approximation technique is applied to convert the quadratic goals into the linear form, and then, the developed model is solved to achieve the most

suitable solution in the decision-making arena. In piecewise approximation methodology, the quadratic membership goals are expressed with the form as follows:

$$\frac{\sum_{j=1}^{n} f_{kj}(x_j) - Z_k^W}{Z_k^B - Z_k^W} + d_k^- - d_k^+ = 1; \quad (k = 1, 2, \ldots, K) \tag{7}$$

Now the quadratic functions $f_{kj}(x_j)$ are linearized by taking the grid points $a_{jp}(p = 0, 1, \ldots, p_j)$ for the variable $x_j(j = 1, 2, \ldots, n)$. The variable x_j is expressed, by introducing a new variable, $y_{jp}; (p = 1, 2, \ldots, p_j)$, as $x_j = \sum_{p=0}^{p_j} a_{jp} y_{jp}$, where $\sum_{p=0}^{p_j} y_{jp} = 1$ with a_{j0} as a lower bound of the variable x_j which is obtained by solving each objective independently and a_{jp} as an upper bound of the variable x_j which is obtained by solving each objective independently. Then, piecewise approximated linear form of the quadratic function $f_{kj}(x_j)$ is expressed as follows:

$$F_{kj} = \sum_{p=0}^{p_j} y_{jp} f_{kj}(a_{jp}) \tag{8}$$

Using the above relation (8), the linear FGP model is presented as follows:

$$\begin{aligned}
&\text{Minimize } D = \sum_{k=1}^{K} w_k d_k^- \\
&\text{so as to satisfy } \frac{\sum_{j=1}^{n} F_{kj}(x_j) - Z_k^W}{Z_k^B - Z_k^W} + d_k^- - d_k^+ = 1; \quad (k = 1, 2, \ldots, K) \\
&\text{subject to } \sum_{j=1}^{n} \left[\left(a_{ij}^R - \left(a_{ij}^R - a_{ij} \right) \alpha \right) \left(\sum_{p=0}^{p_j} a_{jp} y_{jp} \right) \right] \left(\theta_i^R - \left(\theta_i^R - \theta_i \right) \alpha \right) \\
&\quad \leq -\ln\left(p_i^L + \left(p_i - p_i^L \right) \alpha \right) \\
&\sum_{j=1}^{n} \left[\left(a_{ij}^L + \left(a_{ij} - a_{ij}^L \right) \alpha \right) \left(\sum_{p=0}^{p_j} a_{jp} y_{jp} \right) \right] \left(\theta_i^L + \left(\theta_i - \theta_i^L \right) \alpha \right) \\
&\quad \leq -\ln(p_i^R - \left(p_i^R - p_i \right) \alpha) \\
&y_{jp} \geq 0; j = 1, 2, \ldots, n;\ i = 1, 2, \ldots, m;\ p = 1, 2, \ldots, p_j;\ 0 \leq \alpha \leq 1.
\end{aligned}$$

where $F_{kj}(x_j) = \sum_{p=0}^{p_j} y_{jp} f_{kj}(a_{jp})$.

At most two y_{jp} may be positive and if two are positive, they must be consecutive.

To ensure the above conditions, binary variable $Z_{jp}(j = 1, 2, \ldots, n;\ p = 0, 1, \ldots, p_j - 1)$ is to be introduced. The required restriction is then appeared as follows:

$$\begin{aligned} &y_{j0} \le Z_{j0}; \quad y_{jp} \le Z_{jp-1} + Z_{jp},\ (p = 0, 1, \ldots, p_j - 1); \\ &y_{jp_j} \le Z_{jp_j-1}; \quad \sum_{j=0}^{p_j-1} Z_{jp} = 1. \end{aligned} \tag{9}$$

Finally, the developed model (9) is solved to find the most satisfactory solution in the decision-making environment.

To illustrate the proposed approach, a numerical example is solved in the next section.

6 Numerical Example

This section demonstrates the efficiency of the proposed solution methodology using numerical examples. The following FCCP problem is considered as given below:

$$\begin{aligned} &\text{Maximize } Z_1 = 7x_1 + 3x_2 - 2x_1^2 - 2x_2^2 \\ &\text{Maximize } Z_2 = 8x_1 + 9x_2 - 3x_1^2 - 2x_2^2 \\ &\text{Maximize } Z_3 = 5x_1 + x_2 - x_1^2 - x_2^2 \\ &\text{Subject to } \widetilde{Pr}(\tilde{1}x_1 + \tilde{4}x_2 \lesssim \tilde{b}_1) \gtrsim \widetilde{0.90} \\ &\qquad \widetilde{Pr}(\tilde{1}x_1 + \tilde{1}x_2 \lesssim \tilde{b}_2) \gtrsim \widetilde{0.91} \\ &\qquad x_1, x_2 \ge 0 \end{aligned} \tag{10}$$

Here, $\tilde{b}_1$, $\tilde{b}_2$ are exponentially distributed FRVs and $\tilde{1}, \tilde{4}, \tilde{1}, \tilde{1}, \widetilde{0.90}, \widetilde{0.91}$ are all considered as triangular fuzzy numbers. The parameters $\tilde{\theta}_1 = \widetilde{0.03}, \tilde{\theta}_2 = \widetilde{0.05}$ of the FRVs are also assumed as triangular fuzzy numbers.

The above triangular fuzzy numbers are considered in the following respective form as follows:

$$\begin{aligned} &\tilde{1} = (0.90, 1, 1.05),\ \tilde{4} = (3.25, 4, 4.15),\ \tilde{1} = (0.85, 1, 1.1),\ \tilde{1} = (0.95, 1, 1.05), \\ &\widetilde{0.90} = (0.80, 0.90, 1),\ \widetilde{0.91} = (0.75, 0.91, 1.1),\ \widetilde{0.03} = (0.01, 0.03, 0.05), \\ &\widetilde{0.05} = (0.04, 0.05, 0.07). \end{aligned}$$

The α-cut of the above triangular fuzzy numbers are given by

$$\begin{aligned} &\tilde{1}[\alpha] = [0.90 + 0.1\alpha, 1.05 - 0.05\alpha],\ \tilde{4}[\alpha] = [3.25 + 0.75\alpha, 4.15 - 0.15\alpha], \\ &\tilde{1}[\alpha] = [0.85 + 0.15\alpha, 1.1 - 0.1\alpha],\ \tilde{1}[\alpha] = [0.95 + 0.05\alpha, 1.05 - 0.05\alpha], \\ &\widetilde{0.90}[\alpha] = [0.80 + 0.1\alpha, 1 - 0.1\alpha],\ \widetilde{0.91}[\alpha] = [0.75 + 0.16\alpha, 1.1 - 0.19\alpha], \\ &\widetilde{0.03}[\alpha] = [0.01 + 0.02\alpha, 0.05 - 0.02\alpha],\ \widetilde{0.05}[\alpha] = [0.04 + 0.01\alpha, 0.07 - 0.02\alpha]. \end{aligned}$$

Using the above α-cuts and applying chance-constrained methodology, the above model is reduced to the following form as follows:

$$\begin{aligned}
&\text{Maximize } Z_1 = 7x_1 + 3x_2 - 2x_1^2 - 2x_2^2\\
&\text{Maximize } Z_2 = 8x_1 + 9x_2 - 3x_1^2 - 2x_2^2\\
&\text{Maximize } Z_3 = 5x_1 + x_2 - x_1^2 - x_2^2\\
&\text{subject to}\\
&((0.90 + 0.1\alpha)x_1 + (3.25 + 0.75\alpha)x_2)(0.01 + 0.02\alpha) \leq -\ln(1 - 0.1\alpha)\\
&((1.05 - 0.05\alpha)x_1 + (4.15 - 0.15\alpha)x_2)(0.05 - 0.02\alpha) \leq -\ln(0.8 + 0.1\alpha)\\
&((0.85 + 0.15\alpha)x_1 + (0.95 + 0.05\alpha)x_2)(0.04 + 0.01\alpha) \leq -\ln(1.1 - 0.19\alpha)\\
&((1.1 - 0.1\alpha)x_1 + (1.05 - 0.05\alpha)x_2)(0.07 - 0.02\alpha) \leq -\ln(0.75 + 0.16\alpha)\\
&x_1, x_2 \geq 0; \quad 0 \leq \alpha \leq 1.
\end{aligned} \tag{11}$$

Now each nonlinear objective is considered independently and is solved with respect to the system constraints defined in (11) to find the individual optimal values of the objectives. The results are obtained as follows:

$Z_1^b = 4.87$ at $(x_1, x_2) = (1.443, 0.443)$; $Z_2^b = 9.875$ at $(x_1, x_2) = (1.060, 0.0.612)$ and $Z_3^b = 5.873$, at $(x_1, x_2) = (1.886, 0)$.

The payoff matrix is thus be constructed as follows: $\begin{bmatrix} 6.873 & 8.892 & 5.380 \\ 6.260 & 9.875 & 4.414 \\ 6.088 & 4.417 & 5.873 \end{bmatrix}$.

Then, the fuzzy goals of the objectives are found as follows:

$$Z_1 \gtrsim 6.873, \quad Z_2 \gtrsim 9.875, \quad Z_3 \gtrsim 5.873.$$

So constructing the quadratic membership goals of the respective objectives, the FGP model is constructed as follows:

$$\begin{aligned}
&\text{Minimize D} = 1.274d_1^- + 0.183d_2^- + 0.685d_3^-\\
&\text{so as to satisfy}\\
&\mu_{Z_1}(x) = 8.918x_1 + 3.822x_2 - 2.548x_1^2 - 2.548x_2^2 - 7.756 + d_1^- - d_1^+ = 1\\
&\mu_{Z_2}(x) = 1.464x_1 + 1.647x_2 - 0.549x_1^2 - 0.366x_2^2 - 0.808 + d_2^- - d_2^+ = 1\\
&\mu_{Z_3}(x) = 3.425x_1 + 0.685x_2 - 0.685x_1^2 - 0.685x_2^2 - 3.024 + d_3^- - d_3^+ = 1\\
&\text{subject to the system constraints defined in (11)}
\end{aligned} \tag{12}$$

Now the above FGP model is solved directly without linearization using *software* LINGO (Ver. 13) to find the compromise solution in the decision-making context. The solutions are achieved as $x_1 = 1.488,\ x_2 = 0.399$ with the achieved objective values $Z_1 = 6.866,\ Z_2 = 8.534$ and $Z_3 = 5.466$. The achieved membership values corresponding to the fuzzy goals are obtained as $\mu_1 = 0.99,\ \mu_2 = 0.75$ and $\mu_3 = 0.72$.

Again, the model is solved using piecewise approximation technique to the nonlinear membership goals as described below.

At first, each of the objectives is expressed as the sum of separable functions which are shown in Table 1.

The membership goals can now also be written as follows:

$$\begin{aligned} 1.274(f_{11}(x_1) + f_{12}(x_2) - 6.088) + d_1^- - d_1^+ &= 1 \\ 0.183(f_{21}(x_1) + f_{22}(x_2) - 4.417) + d_2^- - d_2^+ &= 1 \\ 0.685(f_{31}(x_1) + f_{32}(x_2) - 4.414) + d_3^- - d_3^+ &= 1 \end{aligned}$$

To linearize the functions using piecewise linear approximation technique, the set of grid points for the variables x_1 and x_2 is chosen as follows:

$$\{1.060, 1.473, 1.886\} \quad \text{and} \quad \{0, 0.153, 0.306, 0.459, 0.612\}.$$

Using the grid points on the above-mentioned membership goals with the methodology discussed in Sect. 5, the FGP model (12) is rewritten in the following form as follows:

$$\text{Minimize } Z = 1.274d_1^- + 0.183d_2^- + 0.685d_3^-$$

So as to satisfy

$$\begin{aligned} 1.274(F_{11}(x_1) + F_{12}(x_2) - 6.088) + d_1^- - d_1^+ &= 1 \\ 0.183(F_{21}(x_1) + F_{22}(x_2) - 4.417) + d_2^- - d_2^+ &= 1 \\ 0.685(F_{31}(x_1) + F_{32}(x_2) - 4.414) + d_3^- - d_3^+ &= 1 \end{aligned}$$

Table 1 Separable functions associated with the objectives

$f_{11}(x_1)$	$7x_1 - 2x_1^2$
$f_{12}(x_2)$	$3x_2 - 2x_2^2$
$f_{21}(x_1)$	$8x_1 - 3x_1^2$
$f_{22}(x_2)$	$9x_2 - 2x_2^2$
$f_{31}(x_1)$	$5x_1 - x_1^2$
$f_{32}(x_2)$	$x_2 - x_2^2$

Subject to

$$((0.90+0.1\alpha)(1.06y_{10}+1.473y_{11}+1.886y_{12})+(3.25+0.75\alpha)(0.153y_{21}+0.306y_{22}+0.459y_{23}+0.612y_{24}))(0.01+0.02\alpha)\leq -\ln(1-0.1\alpha)$$
$$((1.05-0.05\alpha)(1.064y_{10}+1.473y_{11}+1.886y_{12})+(4.15-0.15\alpha)(0.153y_{21}+0.306y_{22}+0.459y_{23}+0.612y_{24}))(0.05-0.02\alpha)\leq -\ln(0.8+0.1\alpha)$$
$$((0.85+0.15\alpha)(1.06y_{10}+1.473y_{11}+1.886y_{12})+(0.95+0.05\alpha)(0.153y_{21}+0.306y_{22}+0.459y_{23}+0.612y_{24}))(0.04+0.01\alpha)\leq -\ln(1.1-0.19\alpha)$$
$$((1.1-0.1\alpha)(1.06y_{10}+1.473y_{11}+1.886y_{12})+(1.05-0.05\alpha)(0.153y_{21}+0.306y_{22}+0.459y_{23}+0.612y_{24}))(0.07-0.02\alpha)\leq -\ln(0.75+0.16\alpha)$$

where

$$F_{11}=5.173\mathrm{y}_{10}+5.972\mathrm{y}_{11}+6.088\mathrm{y}_{12}$$
$$F_{12}=0.412\mathrm{y}_{21}+0.731\mathrm{y}_{22}+0.956\mathrm{y}_{23}+1.087\mathrm{y}_{24}$$
$$F_{21}=5.109\mathrm{y}_{10}+5.275\mathrm{y}_{11}+4.417\mathrm{y}_{12}$$
$$F_{22}=1.330\mathrm{y}_{21}+2.567\mathrm{y}_{22}+3.710\mathrm{y}_{23}+4.759\mathrm{y}_{24}$$
$$F_{31}=4.176\mathrm{y}_{10}+5.195\mathrm{y}_{11}+5.873\mathrm{y}_{12}$$
$$F_{32}=0.130\mathrm{y}_{21}+0.212\mathrm{y}_{22}+0.248\mathrm{y}_{23}+0.237\mathrm{y}_{24}$$

with

$$y_{10}+y_{11}+y_{12}=1$$
$$y_{20}+y_{21}+y_{22}+y_{23}+y_{24}=1$$
$$y_{10}\leq Z_{10};\ y_{11}\leq Z_{10}+Z_{11};\ y_{12}\leq Z_{11}$$
$$y_{20}\leq Z_{20};\ y_{21}\leq Z_{20}+Z_{21};\ y_{22}\leq Z_{21}+Z_{22};\ y_{23}\leq Z_{22}+Z_{23};\ y_{24}\leq Z_{23}$$

$y_{1p}\geq 0(p=0,1,2)$ and $y_{2p}\geq 0(p=0,1,2,3,4)$. Also the variables $Z_{1p}(p=0,1)$, $Z_{2p}(p=0,1,2,3)$ are binary variables and satisfy the following conditions

$$Z_{10}+Z_{11}=1$$
$$Z_{20}+Z_{21}+Z_{22}+Z_{23}=1.$$

Now solving the above model using *software* LINGO (Ver. 13), the solutions are found as

$x_1=1.473, x_2=0.413$ with objective values $Z_1=6.869$, $Z_2=8.651$ and $Z_3=5.438$.

Table 2 Result comparisons of two techniques

	Solution points	Objective values	Membership values	Euclidean distance
Without linearization	$x_1 = 1.488$	$Z_1 = 6.866$	$\mu_1 = 0.99$	$d = 0.38$
	$x_2 = 0.399$	$Z_2 = 8.534$	$\mu_2 = 0.75$	
		$Z_3 = 5.466$	$\mu_3 = 0.72$	
Using piecewise linear approximation method	$x_1 = 1.473$	$Z_1 = 6.869$	$\mu_1 = 0.99$	$d = 0.37$
	$x_2 = 0.413$	$Z_2 = 8.651$	$\mu_2 = 0.78$	
		$Z_3 = 5.438$	$\mu_3 = 0.70$	

The solutions achieved through piecewise linearization method and without using any linearization technique are summarized in the following Table 2. The superior solution is measured using Euclidean distance function [20] for group decision making, which is given by $d = \{\sum_{k=1}^{2}(1-\mu_k)^2\}^{\frac{1}{2}}$.

The comparison reflects that better solution is obtained in the process of piecewise linear approximation method than without using linearization technique.

7 Conclusions

The aim of this paper was to show the application of fuzzy exponential random variables to a fuzzy multiobjective quadratic programming problem with some probabilistic constraints. The methodology captures both types of uncertainties such as fuzziness and randomness simultaneously which are frequently occurred in the model formulation process of any decision-making problem. The proposed method can be extended to solve fuzzy multiobjective quadratic programming problems with other types of probability distributions. The method can also be adapted to hierarchical decision-making environment with multiplicity of objectives. However, it is hoped that the proposed methodology may open up new vistas into the way of making decision in a fuzzily defined probabilistic decision-making arena.

Acknowledgments The authors are thankful to the anonymous reviewers for their valuable comments and suggestions in improving the quality of the paper.

References

1. Charnes, A., Cooper, W.W.: Chance-constrained programming. Manage. Sci. **6**, 73–79 (1959)
2. Kataoka, S.: A stochastic programming model. Econometrica **31**, 181–196 (1963)
3. Prekopa, A.: Contribution to the theory of stochastic programming. Manage. Sci. **4**, 202–221 (1973)
4. Liu, B., Iwamura, K.: Chance constrained programming with fuzzy parameters. Fuzzy Sets Syst. **94**, 227–237 (1998)

5. Luhandjula, M.K.: Linear programming under randomness and fuzziness. Fuzzy Sets Syst. **10**, 45–55 (1983)
6. Luhandjula, M.K.: Mathematical programming in the presence of fuzz quantities and random variables. J. Fuzzy Math. **11**, 27–39 (2003)
7. Zadeh, L.: Probability measures of fuzzy events. J. Math. Anal. Appl. **23**, 421–427 (1968)
8. Kwakernaak, H.: Fuzzy random variable—I definitions and theorems. Inf. Sci. **15**, 1–29 (1978)
9. Kratschmer, V.: A unified approach to fuzzy random variables. Fuzzy Sets Syst. **123**, 1–9 (2001)
10. Buckley, J.J.: New approach and applications. Fuzzy probabilities. Physica Verlag, Heidelberg (2003)
11. Buckley, J.J., Eslami, E.: Uncertain probabilities—II. Soft Comput. **8**, 193–199 (2004)
12. Buckley, J.J., Eslami, E.: Uncertain probabilities—III. Soft Comput. **8**, 200–206 (2004)
13. Charnes, A., Cooper, W.W.: Goal programming and multiple objective optimizations. Euro. J. Opl. Res. **1**, 39–54 (1977)
14. Hannan, E.L.: Linear programming with multiple fuzzy goals. Fuzzy Sets Systs. **6**, 235–248 (1980)
15. Narasimhan, R.: On fuzzy goal programming—some comments. Dec. Sci. **11**, 532–538 (1980)
16. Biswas, A., Modak, N.: Using fuzzy goal programming technique to solve multiobjective chance constrained programming problems in a fuzzy environment. Int. J. Fuzzy Syst. Appls. **2**, 71–80 (2012)
17. Biswas, A., Modak, N.: A fuzzy goal programming method for solving chance constrained programming with fuzzy parameters. Comm. Comp. Inform. Sci. **140**, 187–196 (2011)
18. Bazaraa, M.M., Sherali, H.D., Shetty, C.M.: Nonlinear Programming Theory and Algorithms. Wiley, New York (1993)
19. Kaufmann, A., Gupta, M.M.: Introduction to fuzzy arithmetic. Van Nostrand Reinhold (1985)
20. Yu, P.L.: A class of solutions for group decision problems. Manage. Sci. **19**, 936–946 (1973)

Partial Commutation on Some Classes of 2D Picture Languages

T. Kamaraj, D.G. Thomas, T. Robinson and A.K. Nagar

Abstract The concept of partial commutation and traces on strings has been recently extended to rectangular picture arrays and languages, motivated by the two-dimensional patterns which appear in studies concerning parallel computing and image analysis. The closure property of Siromoney matrix languages (SML) under partial commutation is already studied. In this paper, we consider partial commutation on a generalization of SML languages and Siromoney array languages (SAG) and establish some interesting results. Also, we examine the partial commutativity applied on some higher classes of 2D picture languages generated by Regional tile rewriting grammars and Prusa grammars. We extend partial commutation concept to hexagonal pictures also.

Keywords Array grammar · Partial commutation · Regional tile rewriting grammars · Prusa grammars · Hexagonal pictures

1 Introduction

A two-dimensional language (picture language) is a set of rectangular arrays of patterns which appear in the studies concerning parallel computing and image analysis. A number of rectangular picture generating mechanisms such as

T. Kamaraj (✉)
Department of Mathematics, Sathyabama University, Chennai 600119, India
e-mail: kamaraj_mx@yahoo.co.in

D.G. Thomas · T. Robinson
Department of Mathematics, Madras Christian College, Chennai 600059, India
e-mail: dgthomasmcc@yahoo.com

T. Robinson
e-mail: robin.mcc@gmail.com

A.K. Nagar
Department of Computer Science, Liverpool Hope University, Hope Park Liverpool, UK
e-mail: nagara@hope.ac.uk

K.N. Das et al. (eds.), *Proceedings of Fourth International Conference on Soft Computing for Problem Solving*, Advances in Intelligent Systems and Computing 335,
DOI 10.1007/978-81-322-2217-0_45

two-dimensional array grammars (AGs) and automata have been introduced in the literature [1, 2, 7, 8, 10, 11]. Siromoney matrix grammar (SMG) [10] is one of the earliest array models which used simple sequential and parallel rules for generating rectangular picture languages. AG, introduced by Siromoney et al. [11], is a generalization of SMG which overcomes the disadvantage of SMG in not maintaining the proportion between rows and columns of rectangular pictures generated. Row and column catenation operators are used in the sequential phase of generation of AG.

Based on the behavior of the elementary net theory, Mazurkiewicz [4] introduced the concept of partial commutation and traces on strings as a formal approach of analyzing the concurrent systems. An extension of partial commutation to two-dimensional rectangular arrays has been recently attempted [3], and closure of local [2] and Siromoney matrix languages (SML) [10] under partial commutation have been discussed.

In this paper, we consider generalization of SML languages: Siromoney array languages (SAL) [11] which are unlike SML may contain pictures of given proportion and traditional kolam patterns. We establish some interesting results on closure of some classes of AL under partial commutation. We also consider class of context-free (CF) picture languages generated by Regional tile rewriting grammars [5] and Prusa grammars [6], under partial commutation, and present some closure results. Also, we extend the notion of trace on rectangular arrays to hexagonal arrays and languages and examine whether the hexagonal language obtained by applying partial commutation on a hexagonal local picture language is hexagonal local or not.

2 Preliminaries

In this section, we recall the notions of picture languages, array operations, and Siromoney AGs [11].

Definition 1 If Σ is an alphabet set, then Σ^* denotes the collection of all horizontal sequence of letters from Σ and $\Sigma^+ = \Sigma^* - \{\epsilon\}$, where ε is an empty element. Σ_* denotes the set of all vertical sequences of letters from Σ.

Definition 2 A two-dimensional string (or a picture) over an alphabet Σ is a rectangular array of elements of Σ. The set of all two-dimensional strings over Σ is denoted by Σ^{**}. $\Sigma^{++} = \Sigma^{**} - \{\Lambda\}$, where Λ is the empty picture. For $h, k \geq 0$, $\Sigma^{(h,k)}$ denotes the set of pictures of size (h, k). A two-dimensional language L over Σ is a subset of Σ^{**}. A picture p of size (2, 2) is called a tile. If $p \in \Sigma^{**}$, then $\hat{p}$ is the array obtained by surrounding p with a special boundary symbol $\# \notin \Sigma$.

Definition 3 Row and column catenations are partial operations on arrays denoted by $\circ$ and $\square$. If $p, q \in \Sigma^{(k,*)}$ (resp. $p, q \in \Sigma^{(*,\ell)}$) $p \square q$ (resp. $p \circ q$) is the horizontal (resp. vertical) juxtaposition of p and q. With $(p)^n$ (resp $(p)_n$) is denoted the horizontal (resp. vertical) juxtaposition of n copies of p. If L_1 and L_2 are two array

languages over Σ, then the column catenation of L_1, L_2, denoted as $L_1 \square L_2$, is a language defined by $L_1 \square L_2 = \{p \square q / p \in L_1 \text{ and } q \in L_2\}$. The row catenation, $L_1 \circ L_2$, can be defined in the similar notion.

Definition 4 AG is 4 tuple $\langle V, T, P, S \rangle$, where $V = N \cup I$, N is a finite set of nonterminals, I is a finite set of Intermediates, T = a finite set of terminals, $P = P_1 \cup P_2 \cup P_3$, P_1 is the finite set of nonterminal rules, P_2 is the finite set of intermediate rules, and P_3 is the finite set of terminal rules. $S \in N$ is the start symbol. P_1 is a finite set of ordered pairs (A, B) (written $A \rightarrow B$), A and B in $(N \cup I)^+$ or $A, B \in (N_1 \cup N_2)_+$. The rules of P_1 may be either context sensitive (CS) or CF or regular (R). P_2 is the set of ordered pairs (A, B) such that each intermediate K in I generates an intermediate matrix language LK (may be CS, CF, R) using the sequence of elements of P_2, P_3 the finite set of ordered pairs (E, F), E in $(N \cup I)$, and F in T^{++}.

A SAG is called $(R{:}R)$AG if P_1 rules are regular (R) and all the intermediate languages are R. An AG is called $(R : \text{CF})$ if P_1 rules are R and at least one intermediate language is CF. An AG is called $(R : \text{CS})$ if P_1 rules are R and at least one intermediate language is CS. Similarly, all other six $(X : Y)$SAG are defined, where $X \in \{\text{CF}, \text{CS}\}$ and $Y \in \{R, \text{CF}, \text{CS}\}$. A language generated by any $(X : Y)$ AG grammar is denoted by $(X : Y)$AL.

Derivation proceeds as follows: Starting from S, nonterminal rules are applied without any restriction as in a string grammar, till all the nonterminals are replaced, introducing parentheses whenever necessary. Now replace for each intermediate A in I elements from the intermediate language LA, subject to the conditions imposed by row or column catenations. The replacements start from the innermost parenthesis and proceeds outward. The derivation comes to an end if the condition for $\circ$ or $\square$ is not satisfied.

3 Partial Commutation on Array Languages

In this section, we recall the notions of partial commutation on arrays [3] and give some examples.

Definition 5 Let Σ be an alphabet and $I \subseteq \Sigma \times \Sigma$ be an independent relation on Σ and $p \in \Sigma^{**}$. The row partial commutation mapping $\phi_R{:}I \rightarrow I$ is defined as $\phi_R(\begin{array}{cc} a & b \end{array}) = (\begin{array}{cc} b & a \end{array})$ and $\phi_R(\begin{array}{cc} b & a \end{array}) = (\begin{array}{cc} a & b \end{array})$ for $(a, b) \in I$, i.e., a and b commute with each other. A row partial commutation is also denoted by $(\begin{array}{cc} a & b \end{array}) \leftrightarrow (\begin{array}{cc} b & a \end{array})$.

It is applied on any row of p replacing ab by ba and vice versa. The set of all equivalence classes obtained by row partial commutation is a trace language. Let ϕ_R be the row partial commutation mapping such that $\phi_R(p) = [p]$. If $L \subseteq \Sigma^{**}$, then $\phi_R(L) = \{[p] | p \in L\}$.

Definition 6 Let Σ be an alphabet and $I \subseteq \Sigma \times \Sigma$ be an independent relation on Σ and $p \in \Sigma^{**}$. The column partial commutation mapping $\phi_C{:}I \to I$ is defined as $\phi_C\begin{pmatrix} a \\ b \end{pmatrix} = \begin{pmatrix} b \\ a \end{pmatrix}$ and $\phi_C\begin{pmatrix} b \\ a \end{pmatrix} = \begin{pmatrix} a \\ b \end{pmatrix}$. For $(a, b) \in I$. It is also denoted by $\begin{pmatrix} a \\ b \end{pmatrix} \to \begin{pmatrix} b \\ a \end{pmatrix}$. It is applied on any column of $p \in \Sigma^{**}$. The equivalence class of p obtained by column partial commutation is a trace denoted by $[p]$. Then, the trace of L is $\phi_C(L) = \{[p]/p \in L\}$, where $L \subset \Sigma^{**}$.

Example 1 Consider the language L_1 of $m \times n$ arrays $(m > 1, n > 1)$ on $\Sigma = \{\bullet, x\}$ describing the L tokens of all sizes with equal arms, i.e., L_1 contains pictures of the form

$$\begin{matrix} x & \bullet & \bullet \\ x & \bullet & \bullet \\ x & x & x \end{matrix}$$

If we apply row partial commutation $(x \quad \bullet) \leftrightarrow (\bullet \quad x)$, then

$$\phi_R(L_1) = \left\{ \begin{matrix} x & \bullet \\ x & x \end{matrix}, \begin{matrix} x & \bullet & \bullet \\ x & \bullet & \bullet \\ x & x & x \end{matrix}, \begin{matrix} x & \bullet & \bullet & x \\ x & \bullet & \bullet & \bullet \\ x & x & x & x \end{matrix}, \begin{matrix} x & \bullet & \bullet & \bullet & x \\ x & \bullet & \bullet & \bullet & \bullet \\ x & x & x & x & x \end{matrix}, \begin{matrix} x & \bullet & \bullet & \bullet & \bullet & x \\ x & \bullet & \bullet & \bullet & \bullet & \bullet \\ x & x & x & x & x & x \end{matrix}, \ldots \right\}$$

Example 2 The language L_2 of squares over $\Sigma = \{0, 1\}$ such that the principal diagonal elements are '1' and remaining elements are all '0', i.e.,

$$L_2 = \left\{ \begin{matrix} 1 & 0 \\ 0 & 1 \end{matrix}, \begin{matrix} 1 & 0 & 0 \\ 0 & 1 & 0 \\ 0 & 0 & 1 \end{matrix}, \ldots \right\}$$

By applying the row commutativity $(0 \quad 1) \leftrightarrow (1 \quad 0)$ to each element of L, we get $\phi_R(L_2) = \left\{ \begin{matrix} 1 & 0 \\ 0 & 1 \end{matrix}, \begin{matrix} 1 & 0 & 1 \\ 0 & 1 & 0 \\ 1 & 0 & 1 \end{matrix}, \begin{matrix} 1 & 0 & 0 & 1 \\ 0 & 1 & 0 & 0 \\ 0 & 0 & 1 & 0 \\ 0 & 0 & 0 & 1 \end{matrix}, \begin{matrix} 1 & 0 & 0 & 0 & 1 \\ 0 & 1 & 0 & 0 & 0 \\ 0 & 0 & 1 & 0 & 0 \\ 0 & 0 & 0 & 1 & 0 \\ 0 & 0 & 0 & 0 & 1 \end{matrix}, \ldots \right\}$

Example 3 Consider the language $L_3 = \left\{ \begin{matrix} a & b & c \end{matrix}, \begin{matrix} a & b & c \\ a & b & c \end{matrix}, \begin{matrix} a & b & c \\ a & b & c \\ a & b & c \end{matrix}, \ldots \right\}$.

By applying column partial commutation $\begin{pmatrix} a \\ b \end{pmatrix} \leftrightarrow \begin{pmatrix} b \\ a \end{pmatrix}$, we get $\phi_C(L_3) = L_3$.

Example 4 By applying column partial commutation $\begin{pmatrix} x \\ \bullet \end{pmatrix} \leftrightarrow \begin{pmatrix} \bullet \\ x \end{pmatrix}$ on the language in the Example 1,

$$\phi_C(L_1) = \left\{ \begin{matrix} x & \bullet & x & x \\ x & x & x & \bullet \end{matrix}, \begin{matrix} x & \bullet & \bullet & x & \bullet & \bullet & x & x & \bullet & x & x & \bullet \\ x & \bullet & \bullet & x & x & \bullet & x & \bullet & \bullet & x & \bullet & x \\ x & x & x & x & \bullet & x & x & \bullet & x & x & \bullet & \bullet \end{matrix}, \ldots \right\}$$

4 Results on Array Languages Under Partial Commutation

In this section, we examine the partial commutation applied on languages generated by some classes of Siromoney AGs, Regional tile rewriting grammars [5] and Prusa grammars [6].

Proposition 1 *There exists a picture language* $(R{:}R)\mathrm{AL}$ L *such that* $\phi_C(L)$ *is not a* $(R:R)\mathrm{AL}$.

Proof Consider the language L_1 describing L tokens on $\{\bullet, x\}$ with equal arms, given in Example 1. This language can be generated by the $(R:R)\mathrm{AG}$, $G = \langle V, T, P, S\rangle$ $V = N \cup I$, $N = \{S\}$, $I = \{I_1, I_2\}$, $T = \{x, \bullet\}$, $P_1 = \{S \rightarrow (I_1 \circ S)\,\square\, I_2\}$, $P_3 = \left\{ S \rightarrow \begin{matrix} x & \bullet \\ x & x \end{matrix} \right\}$,

$$L_{I_1} = \{\, x \quad (\bullet)^n / n \geq 1\}, \quad L_{I_2} = \left\{ \begin{matrix} (\bullet)_n \\ x \end{matrix} / n \geq 1 \right\}.$$

But $\phi_C(L_1)$ (given in Example 1) cannot be generated by an $(R:R)\mathrm{AG}$. Suppose there exists an $(R:R)\mathrm{AG}$ to generate $\phi_C(L_1)$, then the corresponding P_3 should have an additional rule $S \rightarrow \begin{matrix} x & x \\ x & \bullet \end{matrix}$ and infinite number of terminal rules whose left part is not involving S and the right part is involving square picture over $\{x, \bullet\}$ containing at least one column consisting of all $\bullet$'s, which is not possible. □

Proposition 2 *There exists a picture language* $(R{:}R)\mathrm{AL}$ L *such that* $\phi_C(L)$ *is also a* $(R:R)\mathrm{AL}$.

Proof The language L_3 in Example 3 can be generated by an $(R{:}R)$ AG, $G = \langle V, T, P, S\rangle$, where $V = N \cup I$, $N = \{S\}$, $I = \{A\}$, $T = \{x, \bullet\}$, $P_1 = \{S \rightarrow A \circ S\}$, $P_3 = \{S \rightarrow a \quad b \quad c\}$ $L_A = \{\, a \quad b \quad c\,\}$. Since $\phi_C(L_3) = L_3$, $\phi_C(L_3)$ is also a $(R:R)\mathrm{AL}$. □

Proposition 3 *There exists a picture language* $(\mathrm{CF}:R)\mathrm{AL}$ L *such that* $\phi_C(L)$ *is not a* $(\mathrm{CF}:R)\mathrm{AL}$.

Proof Consider the language L_4 describing digitized forms of English letter T, made of x's in the back ground of $\bullet$'s with the three arms of T with same length. This language can be generated by a $(\mathrm{CF}:R)$ AG, $G = \langle V, T, P, S\rangle$ $V = N \cup I$, $N = \{S, S_1\}$, $I = \{A, B, C, D\}$, $T = \{x, \bullet\}$, $P_1 = \{S \rightarrow (A \circ S_1)\,\square\, B\,\square\, (A \circ S_1)$, $S_1 \rightarrow (S_1 \circ C)\,\square\, D\}$, $P_3 = \{S_1 \rightarrow \bullet\}$, $L_A = \{(x)^n / n \geq 1\}$, $L_B = \{(x)_{n+1} / n \geq 1\}$, $L_C = \{(\bullet)^n / n \geq 1\}$, and $L_D = \{(\bullet)_{n+1} / n \geq 1\}$. But $\phi_C(L_3)$ cannot be generated by any $(\mathrm{CF}:R)\mathrm{AG}$. Since the letter T is superimposition of two inverted L tokens in opposite directions, to generate $\phi_C(L_3)$, P_3 should have (as in Proposition 1) infinite number of terminal rules whose left part is not involving S_1 and the right part is involving square picture over $\{x, \bullet\}$, containing at least one column consisting of all $\bullet$'s, which is not possible.

Since $(R{:}R)$AL is a proper subset of $(\mathrm{CF}{:}R)$AL, from Proposition 2, we have the following result immediately. □

Proposition 4 *There exists a picture language* $(\mathrm{CF}:R)$AL L *such that* $\phi_C(L)$ *is also a* $(\mathrm{CF}:R)$AL.

Remark 1 We can also have example on $(\mathrm{CS}{:}R)$AL by constructing $(\mathrm{CS}{:}R)$AG, G with the nonterminal rules to generate $\{A^nB^nC^n/n \geq 1$, where A, B, C are the intermediates$\}$ and let $L_A = \{(x)_m/m \geq 1\}, L_B = \{(y)_m/m \geq 1\}, L_C = \{(z)_m/m \geq 1\}$. Again, it is easy to show that $\phi_C(L)$ cannot be generated by any $(\mathrm{CS}{:}R)$AG.

Remark 2 We can also have examples on $(X{:}Y)$AL, where $X \in \{R, \mathrm{CF}, \mathrm{CS}\}$ and $Y \in \{\mathrm{CF}, \mathrm{CS}\}$ (Lemma 2.6, [11]) such that $\phi_C(L)$ cannot be generated by $(X{:}Y)$AG.

Theorem 1 *If* L *is a* $(X{:}Y)$AL, *then* $\phi_C(L)$ *need not be a* $(X{:}Y)$AL, *where* $X, Y \in \{R, \mathrm{CF}, \mathrm{CS}\}$.

Proof The proof is obvious from the Propositions 1, 2, 3, 4 and Remarks 1, 2.

If we choose the languages as the languages considered in Theorem 1 but containing pictures with 90° rotation, then it is easy to prove the following result. □

Theorem 2 *If* L *is a* $(X{:}Y)$AL, *then* $\phi_R(L)$ *need not be a* $(X{:}Y)$AL, *where* $X, Y \in \{R, \mathrm{CF}, \mathrm{CS}\}$.

Now we study the partial commutativity applied on some rich classes of 2D picture languages generated by regional tile grammars (RTG) [5] and Prusa grammars (PG) [6]. Prusa grammars are the formalisms that extend the CF AG by admitting rules in which nonterminal symbols can be substituted with rectangular pictures. RTG performs an isometric derivation process for which homogeneous subpictures are replaced with isometric pictures of the local language defined by the right part of the rules. In the following, we denote by $\pounds(X)$ the family of all languages generated by the device X. Also, we use the notation $[[p]]$, to denote the set of all tiles contained in a picture p.

Theorem 3 *If* $L \in \pounds(\mathrm{RTG})$, *then* $\phi_C(L)$ *need not be a member of* $\pounds(\mathrm{RTG})$

Proof The language L_2 of Example 2 consisting of squares over $\Sigma = \{0, 1\}$ such that the principal diagonal elements are '1' and remaining elements are all '0' can be generated by RTG $G = <\Sigma, N, S, R>$, where $N = \{S, A, B, A', B', C, U, V, W\}$ $\Sigma = \{0, 1\}$ and R consists of variable size rules as

$$S \rightarrow \left[\left[\begin{array}{ccccc} \# & \# & \# & \# & \# \\ \# & S & S & A & \# \\ \# & S & S & A & \# \\ \# & B & B & C & \# \\ \# & \# & \# & \# & \# \end{array}\right]\right] \Big/ \left[\left[\begin{array}{cccc} \# & \# & \# & \# \\ \# & S & U & \# \\ \# & V & W & \# \\ \# & \# & \# & \# \end{array}\right]\right],$$

$$A \rightarrow \left[\begin{bmatrix} \# & \# & \# \\ \# & A & \# \\ \# & A & \# \\ \# & A' & \# \\ \# & \# & \# \end{bmatrix}\right], \quad B \rightarrow \left[\begin{bmatrix} \# & \# & \# & \# & \# \\ \# & B & B & B' & \# \\ \# & \# & \# & \# & \# \end{bmatrix}\right]$$

and the variable fixed size rules as: $S, W, C \rightarrow 1$ and $A, A'B, B'U, V \rightarrow 0$. Now $\phi_C(L_2)$ cannot be generated by any RTG G. To maintain the square shape of pictures of $\phi_C(L_2)$, the variable size rules should be constructed in a similar manner to that of G. But all fixed size rules should have the right part as either 0 or 1. But this lead to the generation of the picture $\begin{matrix} 0 & 0 \\ 0 & 0 \end{matrix}$, but such a picture is not in $\phi_C(L_2)$.

Since L_2 consists of all symmetrical pictures, if we consider the row partial commutation on L_2, we get $\phi_R(L_2) = [\phi_C(L_2)]^t$. Hence, we have an immediate result. □

Theorem 4 *If $L \in$ £(RTG), then $\phi_R(L)$ need not be a member of* £(RTG).

Theorem 5

1. *If $L \in$ £(PG), then $\phi_C(L)$ need not be a member of* £(PG)
2. *If $L \in$ £(PG), then $\phi_R(L)$ need not be a member of* £(PG).

Proof The language L_2 of squares over $\{1, 0\}$, in Example 2, can be generated by a Prusa grammar, $G = (N, T, P, S)$, where $N = \{S, H, V\}, T = \{a\}$,

$$P : \left\{ S \rightarrow \begin{matrix} 1 & H \\ V & S \end{matrix}, \quad H \rightarrow 0H/0, \quad V \rightarrow \begin{matrix} 0 \\ V \end{matrix} / \quad 0, \quad S \rightarrow \quad 1 \right\}$$

Since $\mathcal{L}(\text{PG}) \subset \mathcal{L}(\text{RTG})$ [5, Proposition 8] and $\phi_C(L_2)$ is not in $\mathcal{L}(\text{RTG})$, $\phi_C(L_2)$ is not in $\mathcal{L}(\text{PG})$ also. In a similar argument, we can show that $\phi_R(L_2)$ is not in $\mathcal{L}(\text{PG})$. □

5 Partial Commutation on Hexagonal Arrays

In this section, we extend the notion of trace on rectangular arrays to hexagonal arrays and languages.

First, we review the notions of formal language theory relating to hexagonal pictures and languages [9] and hexagonal local languages [1].

Let Σ be a finite alphabet of symbols. A hexagonal picture p over Σ is a hexagonal array of symbols of Σ. A p-hexagonal array is a six-sided convex hexagonal array whose opposite sides are parallel. A b-hexagonal array is an equiangular p-hexagonal array whose opposite sides are equal. Σ^{**H} denotes the set of all b-hexagonal arrays over the symbols alphabet Σ. With respect to a triad of

triangular axes x, y, z, i.e., 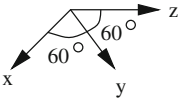

the coordinates of each element of a hexagonal picture can be fixed. $\Sigma^{(\ell,m,n)H}$ denotes the set of hexagonal pictures of size (ℓ, m, n), i.e., having ℓ elements on the side along x axis, m elements on the side along y axis, and n elements on the side along z axis. If $p \in \Sigma^{**H}$, then $\hat{p}$ is the hexagonal array obtained by surrounding p with a special boundary symbol $\#\notin\Sigma$. Given a hexagonal picture p of size (ℓ, m, n) for $g \leq \ell$, $h \leq m$, and $k \leq n$, we denote by $B_{g,h,k}(p)$ the set of all hexagonal subpictures of p of size (g, h, k). Each member of $B_{2,2,2}(p)$ is called a hexagonal tile.

Let Γ be a finite alphabet. A hexagonal picture language $L \subseteq \Gamma^{**H}$ is called local if there exists a finite set Δ of hexagonal tiles over $\Gamma \cup \{\#\}$ such that $L = \{p \in \Gamma^{**H} / B_{2,2,2}(\hat{p}) \subseteq \Delta\}$. The family of local hexagonal picture languages will be denoted by HLOC.

Definition 7 Let Σ be an alphabet and $I \subseteq \Sigma \times \Sigma$ be an independent relation on Σ and $p \in \Sigma^{**H}$. The x-directional partial commutation mapping $\phi_x{:}I \to I$ is defined as $\phi_x\begin{pmatrix} & a \\ b & \end{pmatrix} = \begin{pmatrix} & b \\ a & \end{pmatrix}$ and $\phi_x\begin{pmatrix} & b \\ a & \end{pmatrix} = \begin{pmatrix} & a \\ b & \end{pmatrix}$ for all $(a, b) \in I$, i.e., a and b in the x-direction commute with each other. A x-directional partial commutation is denoted by $\begin{pmatrix} & a \\ b & \end{pmatrix} \leftrightarrow \begin{pmatrix} & b \\ a & \end{pmatrix}$. It is applied on any x-directional string of a hexagon p replacing ab by ba and vice versa. The equivalence class of p obtained by x-directional partial commutation is a trace, denoted by $[p]_x$ or $\phi_x(p)$. The set of all equivalence classes obtained by x-directional partial commutation on a hexagonal language L, denoted by $\phi_x(L)$, is a trace language. If $L \subseteq \Sigma^{**H}$, then $\phi_x(L) = \{[p]_x | p \in L\}$.

Definition 8 Let Σ be an alphabet and $I \subseteq \Sigma \times \Sigma$ be an independent relation on Σ and $p \in \Sigma^{**H}$. The y-directional partial commutation mapping $\phi_x{:}I \to I$ is defined as $\phi_y\begin{pmatrix} a & \\ & b \end{pmatrix} = \begin{pmatrix} b & \\ & a \end{pmatrix}$ and $\phi_y\begin{pmatrix} b & \\ & a \end{pmatrix} = \begin{pmatrix} a & \\ & b \end{pmatrix}$ for all $(a, b) \in I$, i.e., a and b in the y-direction commute with each other. A y-directional partial commutation is denoted by $\begin{pmatrix} a & \\ & b \end{pmatrix} \leftrightarrow \begin{pmatrix} b & \\ & a \end{pmatrix}$. It is applied on any y-directional string of a hexagon p replacing ab by ba and vice versa. The equivalence class of p obtained by y-directional partial commutation is a trace, denoted by $[p]_y$ or $\phi_y(p)$. The set of all equivalence classes obtained by y-directional partial commutation on a hexagonal language L, denoted by $\phi_y(L)$, is a trace language. If $L \subseteq \Sigma^{**H}$, then $\phi_y(L) = \{[p]_y | p \in L\}$.

Definition 9 Let Σ be an alphabet and $I \subseteq \Sigma \times \Sigma$ be an independent relation on Σ and $p \in \Sigma^{**H}$. The z-directional partial commutation mapping $\phi_z{:}I \to I$ is defined as $\phi_z(\begin{matrix} a & b \end{matrix}) = (\begin{matrix} b & a \end{matrix})$ and $\phi_z(\begin{matrix} b & a \end{matrix}) = (\begin{matrix} a & b \end{matrix})$ for all $(a, b) \in I$, i.e., a and b in

the z-direction commute with each other. A z-directional partial commutation is denoted by $(a \quad b) \leftrightarrow (b \quad a)$. It is applied on any z-directional string of a hexagon p replacing ab by ba and vice versa. The equivalence class of p obtained by z-directional partial commutation is a trace, denoted by $[p]_z$ or $\phi_z(p)$. The set of all equivalence classes obtained by z-directional partial commutation on a hexagonal language L, denoted by $\phi_z(L)$, is a trace language. If $L \subseteq \Sigma^{**H}$, then $\phi_z(L) = \{[p]_z | p \in L\}$.

Example 5 Consider the hexagonal language over $\{0, 1\}$,

$$L_5 = \left\{ \begin{array}{ccccccccccccccccc} & & & & & & & & 1 & & 0 & & 0 & & & & \\ & & 1 & & 0 & & & 0 & & 0 & & 1 & & 0 & & & \\ 0 & & & 0 & & & 1,0 & & 1 & & 0 & & 0 & & & 1,\ldots \\ & & 1 & & 0 & & & 0 & & 0 & & 1 & & 0 & & & \\ & & & & & & & & 1 & & 0 & & 0 & & & & \end{array} \right\}$$

This language is in HLOC, as we can find the set of hexagonal tiles θ over $\{0, 1\} \cup \{\#\}$ as $\theta =$

$$\left[\left[\left[\begin{array}{ccccccccccccccccc} & & & & \# & \# & \# & \# & \# & \# & & & & & & & \\ & & & \# & 1 & 0 & 0 & 0 & 0 & \# & & & & & & & \\ & & \# & 0 & 0 & 1 & 0 & 0 & 0 & \# & & & & & & & \\ & \# & 0 & 1 & 0 & 0 & 1 & 0 & 0 & \# & & & & & & & \\ \# & 0 & 0 & 0 & 0 & 0 & 0 & 0 & 1 & 0 & \# & & & & & & \\ \# & 0 & 0 & 1 & 0 & 0 & 0 & 0 & 0 & 1 & \# & & & & & & \\ \# & 0 & 0 & 0 & 0 & 0 & 0 & 1 & 0 & \# & & & & & & & \\ & \# & 0 & 1 & 0 & 0 & 1 & 0 & 0 & \# & & & & & & & \\ & & \# & 0 & 0 & 1 & 0 & 0 & 0 & \# & & & & & & & \\ & & & \# & 1 & 0 & 0 & 0 & 0 & \# & & & & & & & \\ & & & & \# & \# & \# & \# & \# & \# & & & & & & & \end{array}\right]\right]\right]$$ such that

$L_5 = L(\theta)$.

If we apply the x-directional partial commutation $\begin{pmatrix} & 1 \\ 0 & \end{pmatrix} \leftrightarrow \begin{pmatrix} & 0 \\ 1 & \end{pmatrix}$ on pictures of L_5, we have $\phi_x(L_5) = \left\{ \begin{array}{ccccccccccccccccc} & & 1 & & 0 & & & 0 & & 0 & & 1 & & 0 & & & \\ 0 & & & 0 & & & 1,1 & & 0 & & 1,0 & & 1 & & & 1,\ldots \\ & & 1 & & 0 & & & 1 & & 0 & & 0 & & 0 & & & \end{array} \right\}$.

$\phi_x(L_5)$ cannot be in HLOC, for if it is local hexagonal, then there exists a set of hexagonal tiles θ' such that $L(\theta') = \phi_x(L_5)$. Since $\begin{array}{ccccccccc} & & & 0 & & 0 & & 0 & \\ & 0 & & 0 & & 0 & & 0 & \\ 1 & & 0 & & 0 & & 0 & & 0 \\ & 1 & & 0 & & 0 & & 0 & \\ & & 1 & & 1 & & 1 & & \end{array}$ and $\begin{array}{ccccccccc} & & & 1 & & 1 & & 1 & \\ & 0 & & 0 & & 0 & & 1 & \\ 0 & & 0 & & 0 & & 0 & & 1 \\ & 0 & & 0 & & 0 & & 0 & \\ & & 0 & & 0 & & 0 & & \end{array}$ are in $\phi_x(L_5)$, θ' should contain the tiles

$$\begin{array}{ccc} \# & \# & \\ \# & 0 & 0, \\ 0 & 0 & \end{array} \quad \begin{array}{ccc} \# & \# & \\ 0 & 0 & \# \\ 0 & 0 & \end{array}, \quad \begin{array}{ccc} & \# & \\ 0 & 0 & \# \\ 0 & \# & \end{array}, \quad \begin{array}{ccc} 0 & 0 & \\ 0 & 0 & \# \\ \# & \# & \end{array},$$

$$\begin{array}{ccc} 0 & 0 & \\ \# & 0 & \# \\ & \# & \end{array}, \quad \begin{array}{ccc} & \# & 0 \\ \# & 0 & 0 \\ & \# & \# \end{array} \text{ and } \begin{array}{ccc} & 0 & 0 \\ 0 & 0 & \\ 0 & 0 & \end{array}$$

This implies that the hexagonal picture $\begin{array}{ccc} & 0 & \\ 0 & & 0 \\ & 0 & \end{array}$ is in $L(\theta')$, but such a picture is not in the language $\phi_x(L_5)$.

Since L_5 is having symmetrical hexagonal pictures, we can easily observe that $\phi_y(L_5)$ and $\phi_z(L_5)$ are also not in HLOC.

Hence, we can state the following immediately.

Theorem 6 *Suppose ϕ is a x-directional (y-directional, z-directional) partial commutation mapping and θ is a finite hexagonal tile set over the alphabet $\Gamma \cup \{\#\}$. If L is local hexagonal, then $\phi(L)$ need not be local hexagonal.*

6 Conclusion

In this work, we have considered row partial commutation ϕ_R and column partial commutation ϕ_C on some classes of Siromoney array languages and classes of languages generated by Regional tile rewriting grammars and Prusa grammars and studied the closure properties under ϕ_C and ϕ_R. We also extended the notion of partial commutation and traces to hexagonal arrays and languages, and under which, HLOC languages are examined. The question of whether there exists a proper subset of above classes of languages which are closed under partial commutation is interesting and can be analyzed further. Application of partial commutation on 2D languages for analyzing concurrent schemes or actions is explored in the future.

References

1. Dersanambika, K.S., Krithivasan, K., Martin-Vide, C., Subramanian, K.G.: Local and recognizable hexagonal picture languages. Int. J. Pattern Recogn. Artif Intell. **19**(7), 853–871 (2005)
2. Giammarresi, D., Restivo, A.: Two-dimensional languages. In: Handbook of Formal Languages, vol. 3, pp. 215–226. Springer, Berlin (1997)

3. Kamaraj, T., et al.: Partial commutation on array languages. In: Barneva, R.P., et al. (eds.) IWCIA 2012, LNCS 7655, 196–208. Springer, Berlin, Heidelberg (2012)
4. Mazurkiewicz, A.: Introduction to trace theory. In: Diekert, V., Rozenberg, G. (eds.) The Book of Traces, pp. 3–41. World Scientific Publishers, Singapore (1995)
5. Pradella, M., Cherubini, A., Crespi-Reghizzi, S.: A unifying approach to picture grammars. Inf. Comput. **209**, 1246–1267 (2011)
6. Prusa, D.: Two-dimensional Languages. Ph.D. thesis. Charles University in Prague, Prague (2004)
7. Rosenfeld, A.: Picture Languages: Formal Models for Picture Recognition. Academic Press, New York (1979)
8. Rosenfeld, A., Siromoney, R.: Picture languages—a survey. Lang. Des. **1**, 229–245 (1993)
9. Siromoney, G., Siromoney, R.: Hexagonal arrays and rectangular blocks. Comp. Graph. Image Process. **5**, 353–381 (1976)
10. Siromoney, G., Siromoney, R., Krithivasan, K.: Abstract families of matrices and picture languages. Comp. Graph. Image Process. **2**, 284–307 (1972)
11. Siromoney, G., Siromoney, R., Krithivasan, K.: Picture languages with array rewriting rules. Inf. Control **22**, 447–470 (1973)

Dynamic Stability Enhancement of Power System Using Intelligent Power System Stabilizer

Swati Paliwal, Piyush Sharma and Ajit Kumar Sharma

Abstract The destabilizing effect of high gain in voltage regulators persists in power system. The power oscillations of small magnitude and high frequency, which often persisted in power system, present the limitation to the amount of power transmitted within the system. In this paper, a linearized Heffron–Phillips model of a single machine infinite bus (SMIB) is developed using different controllers like fuzzy logic power system stabilizer (FPSS), PID controller, particle swarm optimization (PSO)-based PID controller for analyzing the stability enhancement in power system. For FPSS, speed deviation and acceleration deviation are taken as inputs. Comparison of the effectiveness (steady-state error, ess, overshoot (Mp), and settling time (ts) for a different controller has been done. The performance of the SMIB system using FPSS has been analyzed when comparing with conventional controllers used in SMIB. Similarly the PSO is done using different iterations on conventional PID controller. The results of the simulation show that for low frequency oscillations, FPSS is more effective in damping compared to conventional controllers, and similarly PSO-based PID controller is more effective than a conventional PID controller.

S. Paliwal (✉)
Electrical and Electronics Engineering Department, Amity University, Noida, India
e-mail: swatipaliwal03@gmail.com

P. Sharma
Electrical Engineering Department, SS College of Engineering, Udaipur, Rajasthan, India

A.K. Sharma
Electrical and Electronics Engineering Department, Northern India Engineering College, Delhi, India
e-mail: piyushsharma034@gmail.com

A.K. Sharma
e-mail: ajit.sharma@niecdelhi.ac.in

K.N. Das et al. (eds.), *Proceedings of Fourth International Conference on Soft Computing for Problem Solving*, Advances in Intelligent Systems and Computing 335,
DOI 10.1007/978-81-322-2217-0_46

Keywords Heffron–Phillips model · Power system stabilizer · Fuzzy logic power system stabilizer · Reduced rule fuzzy logic power system stabilizer · Controller · Membership functions · PID controller and particle swarm optimization

1 Introduction

Stability of electric power system is one of the most significant concerns in any electric power system network. This can be traced from the fact that in steady state, the average electrical speed of the generators must be in synchronism. The power system may be broadly defined as that property of power system that enables it to remain in a state of operating equilibrium under normal operating condition and to regain an acceptable state of equilibrium after being subjected to a disturbance.

Power system stability [1] can be classified into: Transient stability and Small signal stability. Transient stability of a system was conventionally suppressed using automatic voltage regulator (AVR), has the electric system, and has been seen with oscillations of frequencies ranging from 0.1 to 2 Hz. These regulators have high gain leading to destabilizing effect on power system and also these are designed for specific operating condition hence limiting to specific level of performance [2]. The solution to this problem is provided by using different controllers like fuzzy logic controller, PID controller. This paper also investigates the optimization in PID controller through particle swarm optimization (PSO) technique using different iterations. Under PSO technique, the best probabilities are considered for PID controllers. Fuzzy logic [3–5] has the features of simple concept, easy implementation, and computational efficiency. This provides an easy method to draw the definite conclusion from hazy, uncertain, or inexact information. Also, the PID controller has the ability to reduce both peak overshoot as well as the settling time of a system. So in this paper, the fuzzy logic-based power system stabilizer model and PID controller are evaluated on a single machine infinite bus (SIMB) power system, and then, the performance of conventional power system stabilizer (CPSS), fuzzy logic-based power system stabilizer (FPSS) is compared, also there will be a comparison between the PID controller together with PSO-based PID controller.

2 Modeling of Power System

Synchronous generators from the principle source of electric energy in power system. SMIB system consists of a synchronous machine connected to an infinite bus through a transmission line (Fig. 1).

Figure 2 shows the block diagram of SMIB power system model. This diagram was developed by Heffron and Phillips so to represent a single synchronous generator connected to the grid through a transmission line. Heffron–Phillips model

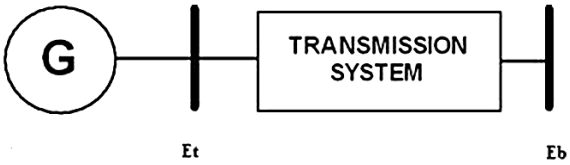

Fig. 1 Single machine infinite bus system (SMIB)

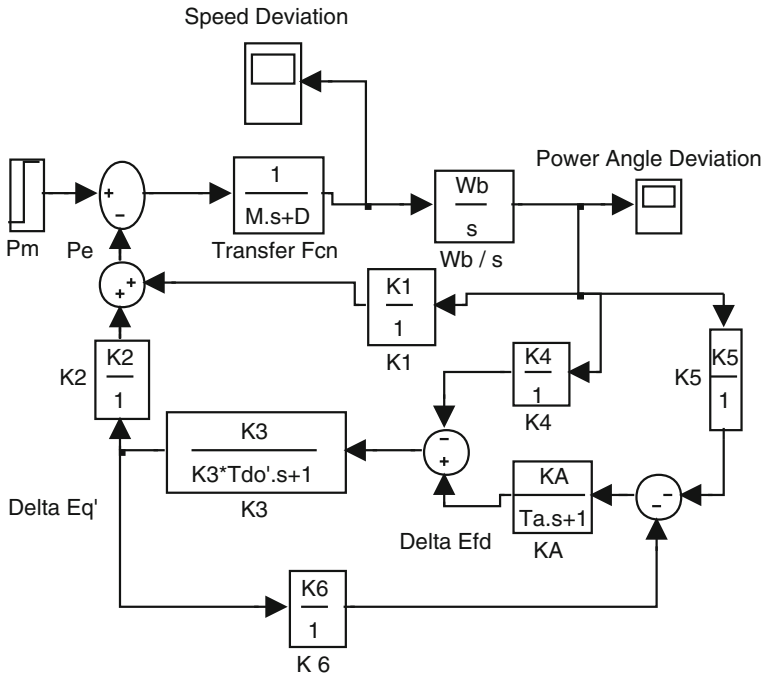

Fig. 2 MATLAB/SIMULINK model of Heffron and Phillips without controller

[6] is a linear model. It is quite accurate for studying LFOs and stability of power systems. It has also been successfully used for designing classical power system controllers, which are still active in most power utilities.

3 Controllers

Controller is a gadget fabricated in a chip form, analogue electronics, or computer that supervise and actually alters the working conditions after checking the errors of a considered dynamical system. This paper deals with different types of power system controllers discuss below.

3.1 Conventional Power System Stabilizer (CPSS)

The power system stabilizer (PSS) is used to provide a sufficient damping to electromechanical oscillations in SMIB energy system. So CPSS [7–11] is used to achieve desired transient behavior and low steady-state error. The input to controller is speed deviation $(\Delta\omega)$. The PSS as represented in Fig. 3 has three components. They are phase compensation block, signal washout block, and gain block.

The controller gain Ks is an important factor as the damping provided by the PSS increases in proportion to an increase in the gain up to a certain critical gain value, after which the damping begins to decrease. The phase compensator block is used to make the system "settle down" quickly. The outcome value of the controller has to be gradually drawn toward zero in steady-state condition. Therefore, a washout transfer function [Tw.S/(Tw.S+1)], which has a steady-state gain zero is used. The value of washout time constant Tw, may be in the range of 1–20 s.

3.2 Fuzzy Logic Controlled Power System Stabilizer (FPSS)

The fuzzy power system stabilizer is a two-input component which have single output. These inputs are angular speed deviation and angular acceleration while output of fuzzy logic controller is a voltage signal.

3.2.1 Fuzzy Logic Control System

Concept of fuzzy logic has been given by Lotfi Zadeh in 1965. This logic is used in many applications in the industry because of some advantages: simple and faster tactic, reduce a propose enlargement cycle, simple to execute, reduce hardware cost, improve the control performance, simplify design convolution. So it is used as a controller in a power system as a fuzzy power system stabilizer [12–20]. The designing process is carried out with the help of MATLAB 2009a. A fuzzy controller comprises of three stages: fuzzification, fuzzy rule, and defuzzification (Table 1).

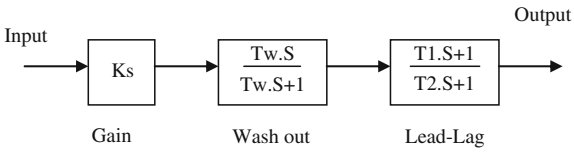

Fig. 3 Structure of conventional lead-lag controller

Table 1 49 Rule base of fuzzy logic controller

	Acceleration						
	NH	NM	NS	ZR	PS	PM	PH
NH	NH	NH	NH	NH	NM	NM	NS
NM	NH	NM	NM	NM	NS	NS	ZR
NS	NM	NM	NS	NS	ZR	ZR	PS
ZR	NM	NS	NS	ZR	PS	PS	PM
PS	NS	ZR	ZR	PS	PS	PM	PM
PM	ZR	PS	PS	PM	PM	PM	PH
PH	PS	PM	PM	PH	PH	PH	PH

Membership functions are used to adapt the fuzzy standards between 0 and 1 for both input and output values (Figs. 4 and 5).

3.3 PID Controller

The PID control algorithm is a robust and simple algorithm that is widely used in the industry. The algorithm has sufficient flexibility to yield excellent results in a wide variety of applications and has been one of the main reasons for the continued use over the years. As the name suggests, PID algorithm consists of three basic coefficients; proportional, integral, and derivative which are varied to get optimal response (Fig. 6).

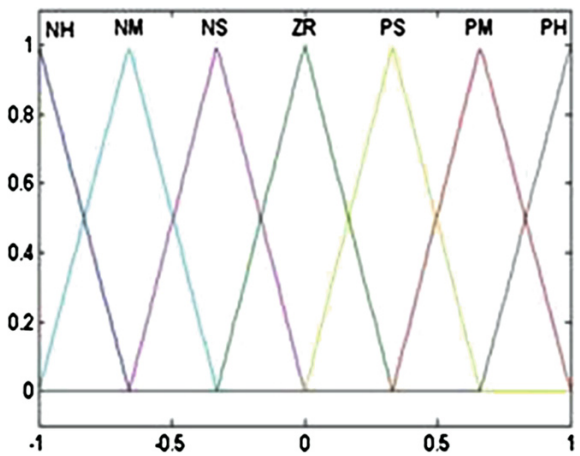

Fig. 4 Membership functions for fuzzy controller for input and output variables

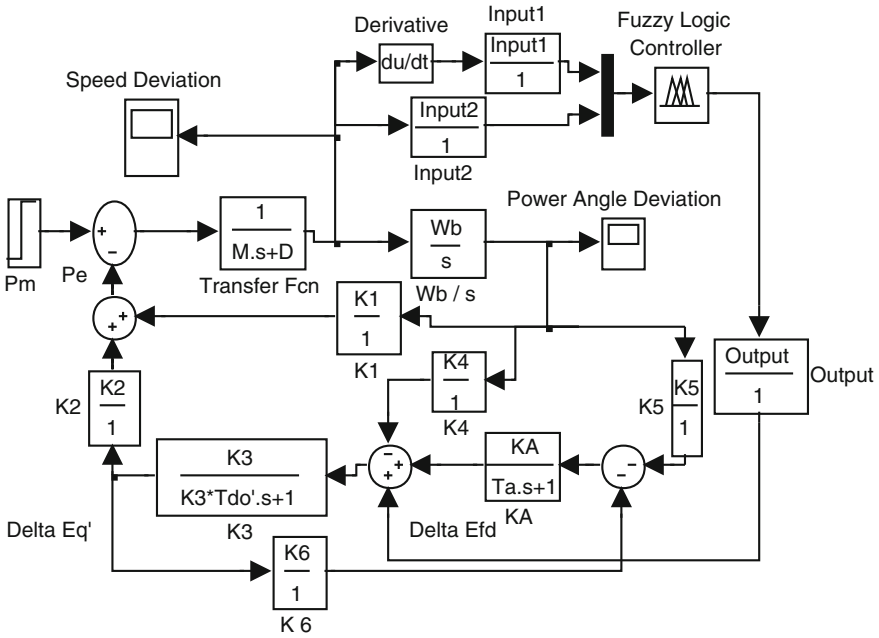

Fig. 5 Shows the Heffron–Phillips MATLAB/SIMULINK model of single machine infinite bus (SMIB) equipped with FLC

3.4 Particle Swarm Optimization

PSO concept is attributed to Kennedy (social-psychologist) and Russell Eberhart (electrical engineer) in 1995. PSO is an artificial intelligence technique for finding approximate solutions toward extremely difficult or impossible numeric maximization and minimization problems. This candidate-based Stochastic optimization technique is motivated by social behavior of Fish Schooling and swarming theory. It uses a number of agents (particles) that constitute a swarm moving around in the search space looking for the best solution. In this paper, PSO technique is applied so that using different iterations, we analyzed the stability enhancement conditions at each particular interval with accuracy. The PSO technique gives more accurate results than a conventional PID controller.

Figure 7 shows the flow chart of PSO technique which shows how the selection of different parameters is done and generates the best initial fitness parameters (Fig. 8).

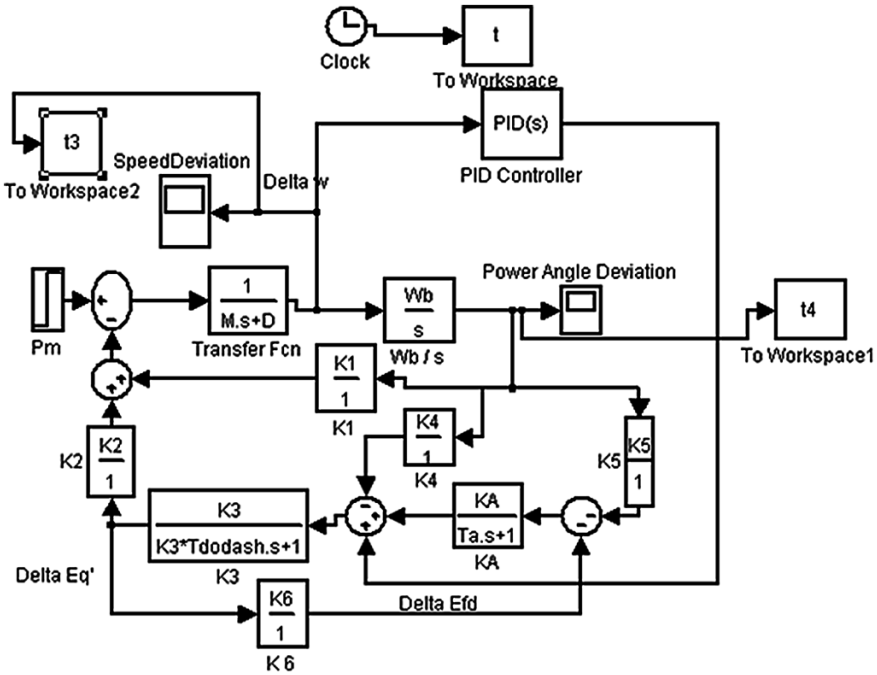

Fig. 6 MATLAB/SIMULINK model plant controlled by small perturbed PID controller

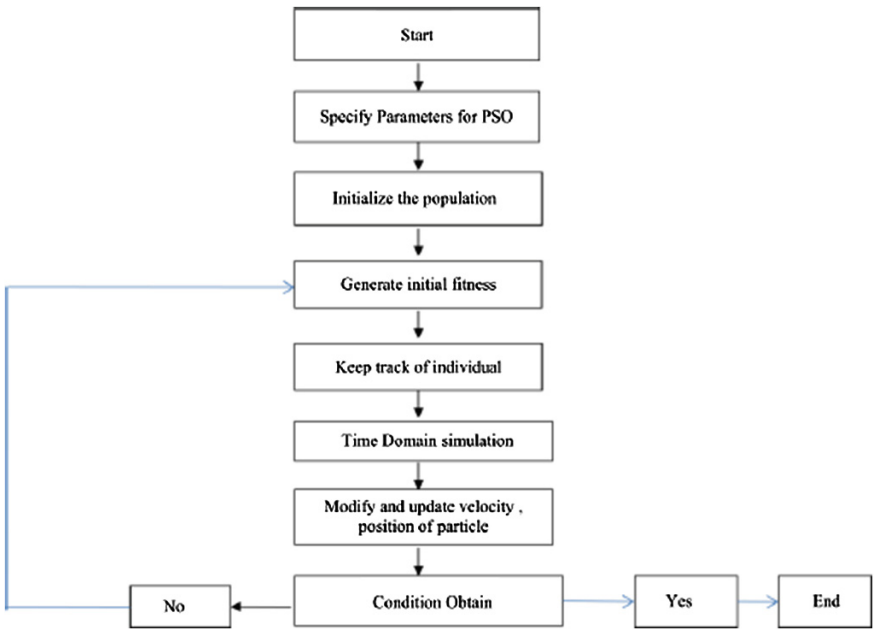

Fig. 7 Flowchart of particle swarm optimization

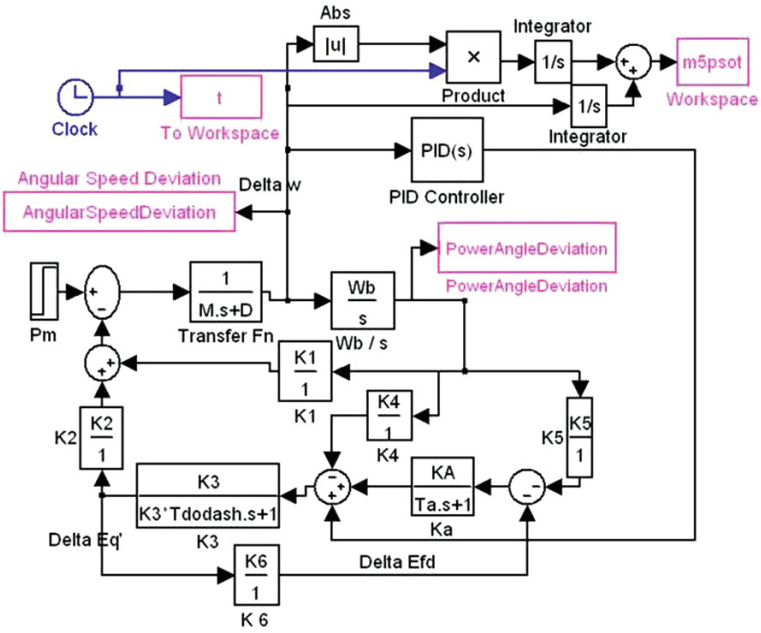

Fig. 8 MATLAB/SIMULINK model plant controlled by PSO-based PID controller

4 Simulation Results

Figures 9, 10, 11, 12 and 13 show the speed deviation ($\Delta\omega$), power angle deviation ($\Delta\delta$) of the SMIB system without controller, controlled by conventional controller, FLC, PID-based controller, and PSO-based PID, respectively. The system parameters (a) Speed deviation ($\Delta\omega$) (b) Power angle deviation ($\Delta\delta$) of generator obtained with the proposed controllers are given in Table 2. The outputs of SMIB system without PSS (a) Speed deviation ($\Delta\omega$) (b) Power angle deviation ($\Delta\delta$) of generator are shown in Fig. 9. The responses clearly show that system has large overshoot (Mp) and large settling time (ts), and error steady state 0 and 2 for speed deviation and power angle, respectively.

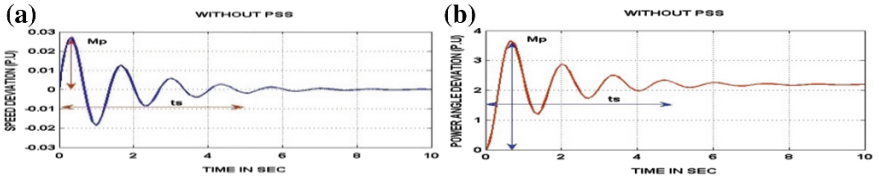

Fig. 9 Output of SMIB system without PSS **a** speed deviation ($\Delta\omega$) **b** power angle deviation ($\Delta\delta$) of generator

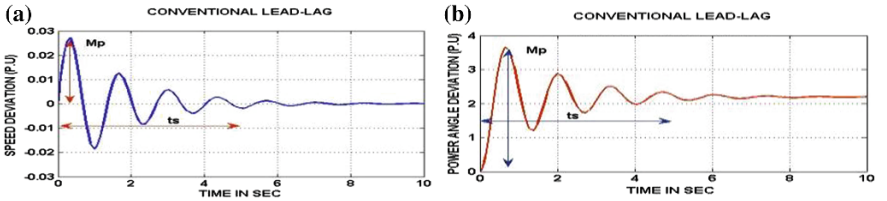

Fig. 10 Output of SMIB system conventional lead-lag PSS **a** speed deviation ($\Delta\omega$) **b** power angle deviation ($\Delta\delta$) of generator

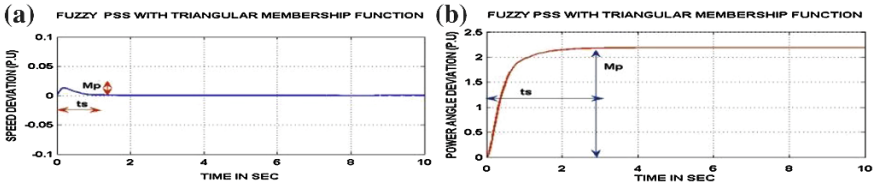

Fig. 11 Output of SMIB system fuzzy PSS for triangular membership function **a** speed deviation ($\Delta\omega$) **b** power angle deviation ($\Delta\delta$) of generator

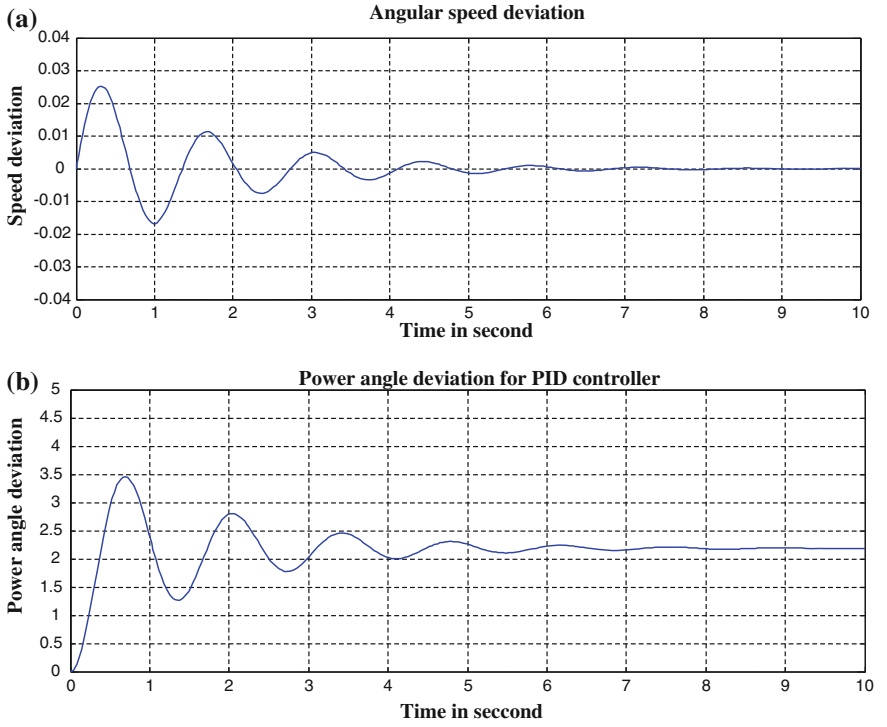

Fig. 12 Output of SMIB system with PID controller **a** speed deviation ($\Delta\omega$) **b** power angle deviation ($\Delta\delta$) of generator

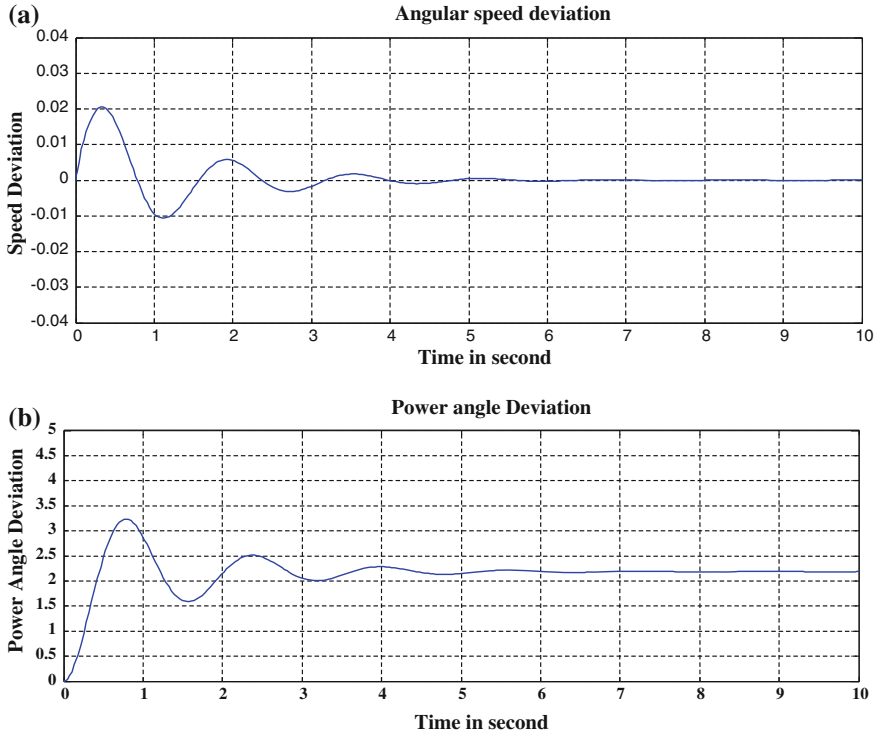

Fig. 13 Output of SMIB system with PID PSO **a** speed deviation ($\Delta\omega$) **b** power angle deviation ($\Delta\delta$) of generator

The outputs of SMIB systems with conventional PSS (a) speed deviation ($\Delta\omega$) (b) power angle deviation ($\Delta\delta$) of generator are shown in Fig. 10. The responses show that system has still larger overshoot (Mp) and larger settling time (ts), and error steady state 0 and 2 for speed deviation and power angle, respectively. This can be further improved by fine tuning of controller parameters.

The outputs of SMIB system with Fuzzy PSS for a triangular membership function (a) speed deviation ($\Delta\omega$) (b) power angle deviation ($\Delta\delta$) of generator are shown in Fig. 11. The responses show that system has smaller overshoot (Mp) and smaller settling time (ts), and error steady state 0 and 2 for speed deviation and power angle, respectively. So performance improved by using Fuzzy PSS. This can be further improved by fine tuning of controller parameters.

The outputs of SMIB system with PID controller (a) speed deviation ($\Delta\omega$) (b) power angle deviation ($\Delta\delta$) of generator are shown in Fig. 12. The responses clearly show that system has small overshoot (Mp), small settling time (ts), and error steady state for speed deviation is zero and 2 for Power angle. This can be further improved by fine tuning of controller parameters.

Table 2 System parameters with different controller

S. no.	System parameter	With conventional PSS controller	Fuzzy PSS for triangular membership function	PID controller	PID PSO controller
1	Speed deviation ($\Delta\omega$)	Large overshoot (Mp), peak value = 0.049 pu, large settling time (ts), ess = 0	Smaller overshoot (Mp), peak value = 0.037 pu, smaller settling time (ts), ess = 0	Smaller overshoot (Mp), peak value = 0.0276 pu, smaller settling time (ts), ess = 0	Smaller Max. overshoot, Mp = 0.020 pu, smaller settling time (ts), ess = 0
2	Power angle deviation ($\Delta\delta$)	Large overshoot (Mp), peak value = 4.5 pu, large settling time (ts), ess= 2	Smaller overshoot (Mp), peak value = 3.9 pu, smaller settling time (ts), ess = 2.01	Smaller overshoot (Mp), peak value = 3.5 pu, smaller settling time (ts), ess = 2.02	Smaller Max. overshoot. Mp = 3.37 pu small settling time (ts), ess = 2.01

The outputs of SMIB system with PSO-based PID controller (a) speed deviation (Δω) (b) Power angle deviation (Δδ) of generator are shown in Fig. 13. The responses clearly show that system has smaller overshoot (Mp), smaller settling time (ts) as compare to PID controller, and error steady state for speed deviation is zero and 2 for Power angle.

5 Conclusion

In this paper, initially the effectiveness of power system stabilizer is reviewed. The proposed method has been simulated on a SMIB energy system with FLC, PID controller, and conventional controller using complete state space model. The MATLAB/SIMULINK simulation results showed that in the presence of small disturbances in the system, fuzzy controller is more effective as compared to the conventional controller, and also, PSO-based PID controller is also more effective than PID controller. The fuzzy logic power system stabilizer (FPSS) gives zero steady-state error, smaller overshoot, and settling time as compared to conventional power system stabilizer.

Appendix

Parameter Values

Generator: $M = 7.0$ s, D = 0, $X_d = 1.8$, $X_q = 1.76$, $X'_d = 0.3$, $T'_{do} = 7.2940$, $\omega_b = 314$

Exciter: (IEEE Type ST1): $K_A = 200$, $T_A = 0.02$ s, $T_1 = 0.154$, $T_2 = 0.033$, $K_S = 9.5$, $T_W = 1.4$, $K_1 = 0.7636$, $K_2 = 0.8644$, $K_3 = 0.3231$, $K_4 = 1.4189$, $K_5 = 0.1463$, $K_6 = 0.4167$, $K_p = 278.65$, $K_i = 271.41$, $K_d = 18.14$.

References

1. Kundur, P.: Power System Stability and Control. McGraw-Hill, New York (1994)
2. Gupta, N., Jain, S.K.: Comparative analysis of fuzzy power system stabilizer using different membership functions. Int. J. Comput. Electr. Eng. **2**(2) (2010)
3. Zadeh, L.A.: Outline of a new approach to the analysis of complex systems and decision processes. IEEE Trans. Syst. Man Cybern. **3**, 28–44 (1973)
4. Zadeh, L.A.: A theory of approximate reasoning. In: Hayes, J.E., Mikulich, L.I. (eds.) Machine Intelligence, pp. 149–196, Ellis Horwood/Wiley, New York, (1979)
5. Zadeh, L.A.: A rationale for fuzzy control. Transactions of the ASME, Series G (USA). J. Dyn. Syst. Meas. Contr. **94**, 3–4 (1974)
6. Gurrala, G., Sen, I.: A modified Heffron-Phillip's model for the design of power system stabilizers. In: Power System Technology and IEEE Power India Conference, 2008. Joint International Conference on POWERCON 2008, pp. 1–6, Oct 2008

7. Larsen, E., Swann, D.: Applying power system stabilizers part i, ii, iii: practical considerations. IEEE Trans. Power Apparatus Syst. **PAS-100**(6), 3034–3046 (1981)
8. Laskowski, T., DeMello F.P., Nolan, P.J., Undrill, J.: Coordinated application of stabilizers in multimachine power system. In: Proceedings of the 21st Annual North-American Power Symposium, vol. 9–10, pp. 175–184 (1989)
9. Vournas, C., Mantzaris, J.: Application of PSS modeling to stabilizer design for inter area oscillations. IEEE Trans. Power Syst. **25**(4), 1910–1917 (2010)
10. Watson, W., Manchur, G.: Experience with supplementary damping signals for generator static excitation systems. IEEE Trans. Power Apparatus and Syst. **PAS-92**(1), 199–203 (1973)
11. Radman, G., Smaili, Y.: Performance evaluation of pid power system stabilizer for synchronous generator. In: IEEE Conference Proceedings Southeastcon '88, pp. 597–601 (1988)
12. Lin, Y.: Systematic approach for the design of a fuzzy power system stabilizer. In: Power System Technology, 2004. 2004 International Conference on PowerCon 2004, vol. 1, pp. 747–752, Nov 2004
13. Roosta, A., Khorsand, H., Nayeripour, M.: Design and analysis of fuzzy power system stabilizer. In: Innovative Smart Grid Technologies Conference Europe (ISGT Europe), 2010 IEEE PES, pp. 1–7, Oct 2010
14. Taher, A., Shemshadi S.A.: Design of robust fuzzy logic power system stabilizer. World Acad. Sci. Eng. Technol. **27** (2007)
15. Kothari, M., Kumar, T.: A new approach for designing fuzzy logic power system stabilizer. In: International Power Engineering Conference, 2007. IPEC 2007, pp. 419–424, Dec 2007
16. Hussein, T., Saad, M., Elshafei, A., Bahgat, A.: Damping inter-area modes of oscillation using an adaptive fuzzy power system stabilizer. In: 2008 16th Mediterranean Conference on Control and Automation, pp. 368–373, June 2008
17. Gupta, R., Bandyopadhyay, B., Kulkarni, A.: Design of power system stabiliser for single-machine system using robust periodic output feedback controller. IEEE Proc. Gener. Transm. Distrib. **150**(2), 211–216 (2003)
18. Dobrescu, M., Kamwa, I.: A new fuzzy logic power system stabilizer performances. In; Power Systems Conference and Exposition, 2004. IEEE PES, vol. 2, pp. 1056–1061, Oct 2004
19. Dysko, A., Leithead, W., O'Reilly, J.: Enhanced power system stability by coordinated PSS design. IEEE Trans Power Syst. **25**(1), 413–422 (2010)
20. Gupta, R., Sambariya, D., Gunjan, R.: Fuzzy logic based robust power system stabilizer for multimachine power system. In: Industrial Technology, 2006. IEEE International Conference on ICIT 2006, pp. 1037–1042, Dec 2006
21. Tayal, V.K., Lather, J.S.: Digital simulation of reduced rule fuzzy logic power system stabilizer for analysis of power system stability enhancement. Int. J. Comput. Appl. **47**(7), 888–975 (2012)
22. Tayal, V.K., Lather, J.S., Sharma, P., Sinha, S.K.: Power system stability enhancement using fuzzy logic based power system stabilizer. In: Proceedings of the Third International Conference on Soft Computing for Problem Solving, Advances in Intelligent Systems and Computing, vol. 258, pp. 55–68 (2014)
23. Hong, T.P., Lee, C.: Induction of fuzzy rules and membership functions from training examples. Fuzzy Sets Syst. **84**, 33–47 (1996)
24. Rose, T.J.: Fuzzy Logic with Engineering Applications. McGrawHill. Inc, New York (1997)

An Analytical Study of Ordered Weighted Geometric Averaging Operator on Web Data Set as a MCDM Problem

Ankit Gupta and Shruti Kohli

Abstract Ordered weighted aggregation operators were introduced in the year 1988 and since then have been used in a wide variety of applications. This paper is an attempt to use a special variant of OWA operator—ordered weighted geometric averaging operator for regression analysis. Regression analysis is used to formulate a suitable business model based on the past performances of the company/organization and is an integral component of data mining techniques. Various regression algorithms have been proposed in the literature. In this paper, a multi-criteria decision-making problem is being formulated using some of these regression algorithms on a real-time industrial web data followed by the analysis of using one the OWA operators on its results.

Keywords Multi-criteria decision making · Ordered weighted operator · Regression

1 Introduction

The concept of multi-criteria decision making (MCDM) was introduced in mid-60s and has been an active area of research especially for decision making and system engineering [1, 2]. It has established itself as a useful consortium of methodologies to solve various complex decision-making problems consisting of multiple attributes and criterion and hence being utilized in number of practical applications [3].

A. Gupta (✉) · S. Kohli
Birla Institute of Technology, Mesra, Ranchi, India
e-mail: theankit@yahoo.com

S. Kohli
e-mail: shruti@bitmesra.ac.in

K.N. Das et al. (eds.), *Proceedings of Fourth International Conference on Soft Computing for Problem Solving*, Advances in Intelligent Systems and Computing 335,
DOI 10.1007/978-81-322-2217-0_47

Erkan et al. [4] have described a MCDM problem as '*...a branch of general class of operation research models that deals with the decision making problems under the presence of a number of decision making criteria*'.

The classic MCDM prescribes different ways of ranking, evaluating, and then selecting the most favorable and suitable alternative from a set of feasible ones which are characterized by multiple, usually conflicting criteria [1, 5]. The fundamental components of a MCDM problem are set of 'n' criteria, $C = \{C_1, C_2, \ldots, C_n\}$, set of '$m$' decision makers, $DM = \{DM_1, DM_2, \ldots, DM_m\}$, and a set of possible 'p' alternatives, $X = \{X_1, X_2, \ldots, X_p\}$.

Velasquez et al. [6] have classified various MCDM approaches into eleven categories, namely (i) multi-attribute utility theory, (ii) analytic hierarchy approach, (iii) fuzzy set theory, (iv) case-based reasoning, (v) data envelopment analysis, (vi) simple multi-attribute rating technique, (vii) goal Programming, (viii) ELECTRE, (ix) PROMETHEE, (x) simple additive weighting and (xi) technique for order of preference by similarity to ideal solution.

Most of the MCDM theory and approaches were developed in line with the development of uncertainty and chaos theory [7] and thus fuzzy set theory introduced by Zadeh [8] emerged as one of the effective methodology for solving MCDM problem especially when the problem is vague or imprecise. The fusion of MCDM and fuzzy set theory is known as fuzzy MCDM [9].

One of the earliest examples of fuzzy-based MCDM problem was to evaluate the creditworthiness of credit card application in Germany [10].

An important MCDM problem proposed in the last decade was for selecting applicants for a PhD program in any educational or research institution. The problem was investigated by various authors [11–13]. Carlsson et al. [13] tried to solve it with the help of ordered weighted averaging operator proposed by Yager [14]. Renata et al. [15] compared the effect of using various fuzzy aggregation operators like Sugano integral [16], Leximin ordering [17], ordered weighted maximum and minimum operators [16], Quasi linear means [18], on this problem.

In this paper, a MCDM regression problem based on fuzzy set theory is being formulated where a variant of ordered weighted operator, namely ordered weighted geometric averaging operator is used to aggregate the outcome of results obtained by using various regression techniques and then analyzes the aggregated result thus obtained on parameter—'average error'.

The rest of the paper is as follows: Sect. 2 will give some insight of OWA and ordered weighted geometric averaging operator along with the approaches for determining `Weights`, Sect. 3 will provide a brief overview of data mining and regression and the relevance of this experiment, Sect. 4 will describe the data set and modeling of regression problem into MCDM problem followed by result analysis, and Sect. 5 will conclude the paper with some future direction of this work.

2 Averaging Operators and Weights

2.1 Ordered Weighted Averaging Operator

Ordered weighted averaging operators were introduced in 1988 by Yager [14] as a possible solution to aggregation of different criteria. Many variants of this operator were introduced subsequently.

In these operators, coefficients are not associated directly with a particular attribute but rather to an ordered position.

Definition 1 An OWA operator of dimension n is a function $\phi : R^n \rightarrow R$ that has associated with a set of weights or weighing vector $W = (w_1, \ldots, w_n)$ such that $w_i \in [0, 1]$ and $\sum_{i=1}^{n} w_i = 1$ and is defined to aggregate a list of values p_1, …, p_n according to the following expression

$$\phi(p_1, \ldots, p_n) = \sum_{i=1}^{n} w_i \cdot q_i \tag{1}$$

being q_i the ith largest value in the set (p_1, …, p_n).

2.2 The Ordered Weighted Geometric Averaging Operator (OWGO)

Inspired from [14], Xu et al. [19] proposed two different variants of OWA operators, namely descending ordered weighted geometric averaging operator (DOWGA) and ascending ordered weighted geometric averaging operators (AOWGA). The importance of ordered weighted geometric operators in MCDM was highlighted in [20].

Definition 2 A DOWGA operator of dimension n is a mapping $g : R^{+^n} \rightarrow R^+$ that has associated with a weighting vector $w = (w_1, w_2, \ldots, w_n)^{\mathrm{T}}$, with $w_i \in [0, 1]$ and $\sum_{i=1}^{n} w_i = 1$, such that

$$g(\alpha_1, \alpha_2, \ldots, \alpha_n) = \prod_{j=1}^{n} b_j^{w_j} \tag{2}$$

where b_j is the jth largest of the α_i $(i = 1, 2, \ldots, n)$.

Here, the elements b_j $(j = 1, 2, \ldots, n)$ mentioned above are arranged in descending order as

$$b_1 \geq b_2 \geq \cdots \geq b_n$$

Definition 3 An AOWGA operator of dimension n is a mapping $h: R^{+^n} \rightarrow R^+$ that has associated with it a weighing vector $w = (w_1, w_2, \ldots, w_n)^T$, with $w_i \in [0, 1]$ and $\sum_{i=1}^{n} w_i = 1$ such that

$$h(\alpha_1, \alpha_2, \ldots, \alpha_n) = \prod_{j=1}^{n} d_j^{w_j} \tag{3}$$

Here, the d_j is the jth smallest of the α_i $(i = 1, 2, \ldots, n)$, and the elements d_j $(j = 1, 2, \ldots, n)$ are arranged in ascending order $b_1 \leq b_2 \leq, \ldots, \leq b_n$.

Various fuzzy averaging operators have proved their usefulness in variety of application areas such as neural networks, database systems, fuzzy logic controllers, location-based services, decision making, expert systems, market Research, data mining, linguistic quantified proposition, mathematical programming, and lossless image compression [19, 21].

2.3 Weights

As discussed in earlier sections, `weights` are important for solving any equations while using a variant of ordered weighted averaging operator.

There are various ways by which `weights` can be obtained and can be categorized as [21]:

- the programming based approach
- the experience (learning based approach)
- the analytic formula based approach
- the quantifier-guided approach

Various methods of determining weights are dependent on maximizing/minimizing *dispersion* or *degree of orness*.

For example, Hagan [22] proposed an approach for finding *weights* as:

$$\text{Maximize} - \sum_{i=1}^{n} w_i \ln w_i \tag{4}$$

Subject to

$$\frac{1}{(n-1)} \sum_{i=1}^{n} (n-1) w_i = \alpha, \quad 0 \leq \alpha \leq 1 \tag{5}$$

and

Table 1 Weights obtained using LSOWA approach for different degree of orness

wt.	0*	0.1*	0.2*	0.3*	0.4*	0.5*	0.6*	0.7*	0.8*	0.9*	1.0*
w_1	0	0	0	0.04	0.12	0.2	0.28	0.36	0.46	0.6333	1
w_2	0	0	0.04	0.12	0.16	0.2	0.24	0.28	0.32	0.3333	0
w_3	0	0.0333	0.18	0.20	0.20	0.2	0.20	0.20	0.18	0.0333	0
w_4	0	0.3333	0.32	0.28	0.24	0.2	0.16	0.12	0.04	0	0
w_5	1	0.6333	0.46	0.36	0.28	0.2	0.12	0.04	0	0	0

* α

$$\sum_{i=1}^{n} w_i = 1, \quad 0 \le w_i \le 1,\ i = 1, \ldots, n$$

Fuller et al. [23] transform the above equation using Lagrange multiplier into a polynomial equation and then solved to find the optimal weighting vector as

$$w_1[(n-1)\alpha + 1 - nw_1]^n = ((n-1)\alpha)^{n-1}[((n-1)\alpha - n)w_1 + 1] \tag{6}$$

$$w_n = \frac{((n-1)\alpha - n)w_1 + 1}{(n-1)\alpha + 1 - nw_1} \tag{7}$$

$$w_j = \sqrt{[n-1]w_1^{n-j}w_n^{j-1}} \tag{8}$$

Ahn [21] used least-squared OWA methods to determine OWA Operator weights. Ahn proposed three different methods to calculate OWA weights, namely

1. The LSOWA and minimax disparity approach. This paper uses this approach for weights consideration as a pilot case basis. The equation to calculate weights is

$$w_i = \frac{1}{n} + \frac{6(2i - n - 1)}{n(n+1)}(0.5 - \alpha) \tag{9}$$

2. The goal programming approach
3. The product of weight approach

`Weights` for five parameters, obtained using Eq. 9, are consolidated in Table 1.

3 Data Mining and Regression

3.1 Data Mining

Data mining is a term frequently used to mine the appropriate information from a group of structured or unstructured data. This process includes convenient extraction of patterns from a group of data which exhibits some kind of knowledge [24].

Earlier, data mining was used as one of the many steps of the knowledge discovery process, but later many researchers have started using data mining as synonyms of the knowledge process [25]. Data mining can be done using association rules, regression analysis, clustering analysis, and deviation detection, etc.

3.2 Regression Analysis

Regression analysis is used to predict the future business direction based on the past performance. The output of a regression analyzer is in the form of a model which can depict future trends if the future data set is somehow similar to the past data. Companies rely heavily on regression analysis to make future business or strategic strategies [26].

Last 10 years has seen a tremendous growth in the number of online shopping portals. These companies have to compete in a highly competitive and intense market. This scenario signifies the relevance of regression analysis for the companies. One of the main objective of these companies is to find a suitable futuristic model with the help of regression based on some input attribute. As this market is still in its native state, most of the time these companies lack a good amount of historical data for the regression purpose. Besides this, these have to deal with the online users who are mostly unfamiliar with the system and most of the time uncertain about their needs [27]. Both of these problems finally result in company's web log as a highly flexible and lesser amount of data to work upon.

The experimental work in this paper is based on this kind of new, vague, and imprecise data. This work is an extension of our earlier work [28] where we have analyzed the effect of various regression techniques on such kind of data sets where we tried to find out the best regression algorithm on such kind of data.

Yager [29] introduced OWA operator in regression analysis in the year 2010 and showed that the use of OWA operator can reduce the outliers (typical data that do not follow the regression models) to a great extent.

4 Experiment

4.1 Experimental Setup

This experiment makes use of traces of real-time industrial web data, obtained from a mid-size company using web analytical tool, and is given in Table 2.

Company considers `Page_views` as an 'asset' and wants to generate a regression model keeping `Page_views` as a dependent variable. Initially, 5 different kind of regression techniques were used namely (i) linear Regression, (ii) SMO regression, (iii) SMO regression with normalization, (iv) SMO regression

Table 2 Data set obtained using web analytics

Month	ST[a]	BAS[b]	PPC[c]	REM[d]	VU[e]	PV[f]
April 2011	1,000	0	$650	0	100	20,000
May 2011	5,000	0	$2,500	0	141	100,000
June 2011	10,000	0	$3,000	0	90	200,000
July 2011	12,500	0	$1,600	896	50	250,000
August 2011	15,000	0	$1,550	1,002	172	300,000
September 2011	21,000	$6,234	$3,500	1,788	300	400,000
October 2011	31,000	$1,1232	$5,600	2,381	310	550,000
November 2011	38,000	$7,439	$3,900	2,979	310	650,000
December 2011	40,000	$2,389	$1,100	2,987	0	700,000
January 2012	47,000	$7,823	$3,900	2,916	54	800,000
February 2012	56,000	$9,372	$5,000	3,272	410	900,000
March 2012	75,000	$18,782	$10,500	3,987	410	1,150,000
April 2012	95,000	$18,378	$11,000	4,876	415	1,300,000
May 2012	109,000	17,283	$7,500	5,498	500	1,475,000
Jun 2012	145,000	$35,986	$19,500	5,007	510	1,900,000

[a] Subscriber total
[b] Banner Ad spend
[c] Pay per click
[d] Reminder emails sent
[e] Videos upload
[f] Page views

with standardization, and (v) additive regression. WEKA [30] tool has been used (a data mining and machine learning tool) to generate regression model. The output values of the expected `Page_views`, thus obtained from different regression techniques, are consolidated in Table 3.

4.2 Modeling Problem into MCDM Problem

As discussed in Sect. 2, OWA operator needs some input values to aggregate. In this experiment, predicted output value of each individual regression technique (row wise) has been provided for individual level of aggregation. For example, from the first row of Table 3, we obtained:

$$(82075, 54318, 51677, 34053, 31066)$$

and it became the first level of input to the aggregation function. To be able to use it with DOWGA operator (Eq. 2), next step is to calculate various values from the above set in decreasing order as, a_1 (element having maximum value in the above set) is 82075, a_2 (second highest number) is 54318, a_3, a_4, and a_5 (third, fourth, and fifth highest number from the above set) are, respectively, 51677, 34053, and

Table 3 Predicted output using various techniques

LR[a]	SMON[b]	SMOS[c]	SMO[d]	ADRE[e]	DOWGA[f]	AOWGA[g]
82,075	54,318	51,677	34,053	31,066	47,574	47,574
122,368	97,317	100,028	131,724	115,360	112,600	112,600
172,733	150,549	156,728	200,000	223,833	178,743	178,743
258,909	260,284	261,642	280,052	223,833	256,267	256,267
291,308	258,030	259,821	285,896	223,833	262,642	262,642
405,251	409,121	399,979	390,942	544,198	426,477	426,477
546,349	591,375	577,329	550,000	544,198	561,532	561,532
657,569	667,621	660,063	662,888	690,501	667,624	667,624
678,259	699,142	699,389	700,000	688,933	693,091	693,091
743,938	785,714	782,411	768,048	773,227	770,524	770,524
858,830	819,846	87,285	831,864	690,501	801,393	801,393
1,098,891	1,144,763	1,137,599	1,150,000	1,310,243	1,166,116	1,166,116
1,360,869	1,334,870	1,385,749	1,436,100	1,310,243	1,364,883	1,364,883
1,544,234	1,474,142	1,475,022	1,475,000	1,437,929	1,480,867	1,480,867
1,873,442	1,900,859	1,901,074	1,900,000	1,887,096	1,892,462	1,892,462

[a] Linear regression
[b] SMO regression with normalization
[c] SMO regression with standardization
[d] SMO regression
[e] Additive regression
[f, g] Regression result with DOWGA and AOWGA operator with $\alpha = 0.5$ using LSOWA approach

31066. Similarly, other alternative values for the different `Page_views` i.e., (b_1, …, b_5) till (o_1, …, o_5) can be calculated from each individual row of the Table 3.

To use it with `AOWGA` operator (Eq. 3), various values can be calculated in increasing order as, A_1 (Lowest value from the set) is 31066. In the same way, A_2, A_3, A_4, A_5 can be obtained as 34053, 51677, 54318, 82075, respectively. Similarly, other alternative values obtained using this operator for different `Page_views` i.e., (B_1, …, B_5) till (O_1, …, O_5) can be calculated from each individual row of the Table 3.

For an initial phase of study, this problem is being solved with `DOWGA operator` (Eq. 2) and `AOWGA operator` (Eq. 3) while keeping the value of $\alpha = 0.5$ (as $\alpha = 0.5$ is considers as the global optimal value for the dispersion of all OWA operators of dimension 'n' [23]). `Weight`, for $\alpha = 0.5$, has been taken from Eq. 9 (consolidated in Table 1) as {0.2, 0.2, 0.2, 0.2, 0.2}. The first level of alternative can be obtained using `DOWGA` operator:

$$a_1^{0.2} \cdot a_2^{0.2} \cdot a_3^{0.2} \cdot a_4^{0.2} \cdot a_5^{0.2} = 47,574$$

and using AOWGA operator:

$$A_1^{0.2} \cdot A_2^{0.2} \cdot A_3^{0.2} \cdot A_4^{0.2} \cdot A_5^{0.2} = 47,574$$

as shown in Table 3 (Column 6, 7). It is worth noticing that the values obtained using both operators are identical. It is because of the use of same value of weight for $\alpha = 0.5$.

4.3 Result Analysis

Figure 1 demonstrates the difference between 5 different regression techniques with DOWGA operator with $\alpha = 0.5$.

This figure clearly indicates that use of ordered weighted geometric operator has significantly reduced the *outlier* values, which is considered as a positive characteristic of any regression techniques and the result is comparatively more close to the actual value, i.e., Page_views.

Inspired by this result, this experimental work was extended further by inducting various weights for different α value from Table 1 into this experiment.

Table 4 consolidated the 'error percentage' obtained from using various values of α along with corresponding weights. As can be seen from the 'average error' output from the table, both operator DOWGA and AOWGA showing almost symmetrical pattern. While DOWGA operator displaying a pattern of increasing value in 'average error' with increasing α, AOWGA operator is indicating decreasing 'average error' value with increasing α. Figure 2 represents a graphical overview of the same using DOWGA operator only. As evident from Table 4 and Fig. 2, increasing value of α from 0 to 1 has an significant effect on the error percentage. Apart from values for

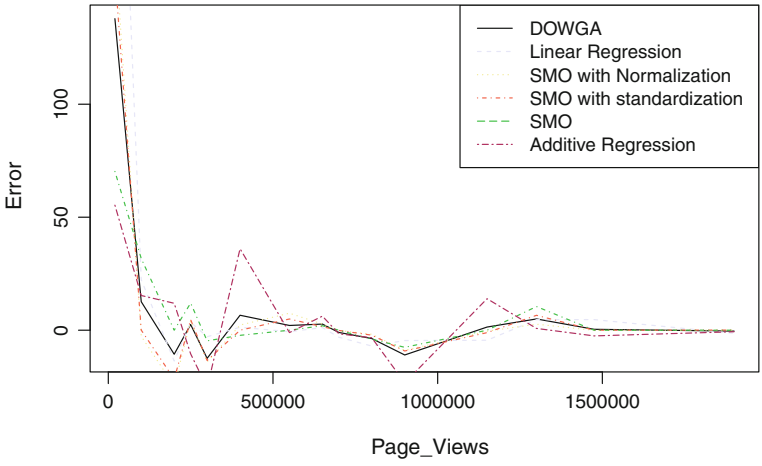

Fig. 1 Error percentage using different regression approach with DOWGA operator with $\alpha = 0.5$

Table 4 Error percentage w.r.t page_views using different α values

DOWGA operator							AOWGA operator					
α =	0	0.2	0.4	0.6	0.8	1	0	0.2	0.4	0.6	0.8	1
	55.33	−91.95	116.01	161.94	219.42	310.37	310.37	−89.28	161.94	116.01	79.26	55.33
	−2.68	−96.74	9.02	16.29	24.24	31.72	31.72	−96.38	16.29	9.02	2.16	−2.68
	−24.72	−97.78	−14.26	−6.84	1.57	11.91	11.91	−97.47	−6.84	−14.26	−20.94	−24.72
	−10.46	−97.59	0.644	4.405	7.83	12.02	12.02	−97.49	4.40	0.64	−3.01	−10.46
	−25.38	−97.98	−14.63	−10.22	−5.90	−2.898	−2.89	−97.84	−10.22	−14.63	−19.0	−25.38
	−2.26	−97.91	3.74	9.57	16.32	36.05	36.05	−97.78	9.578	3.74	−0.72	−2.26
	−1.05	−98.10	1.19	3.006	4.98	7.523	7.523	−98.05	3.0	1.19	−0.506	−1.05
	1.16	−98.17	2.26	3.161	4.13	6.231	6.23	−98.15	3.16	2.26	1.49	1.165
	−3.10	−98.25	−1.29	−0.677	−0.12	−0.001	−0.01	−98.23	−0.67	−1.29	−1.96	−3.10
	−7.00	−98.35	v4.17	−3.191	−2.29	−1.786	−1.78	−98.33	−3.19	−4.17	−5.20	−7.00
	−23.27	−98.51	−12.55	−9.325	−6.51	−4.575	−4.57	−98.45	−9.32	−12.55	−15.86	−23.27
	−4.445	−98.49	−0.05	2.884	6.05	13.93	13.93	−98.45	2.88	−0.05	−2.48	−4.44
	0.78	−98.50	4.06	5.923	7.84	10.47	10.47	−98.46	5.92	4.06	2.31	0.788
	−2.51	−98.59	v0.17	0.975	2.13	4.69	4.69	−98.58	0.97	−0.17	−1.18	−2.51
	−1.39	−98.69	−0.54	−0.251	0.01	0.05	0.05	−98.69	−0.25	−0.54	−0.86	−1.39
ML[x]	55.33	−91.95	116.015	161.948	219.425	310.375	310.375	−89.283	161.948	116.015	79.268	55.33
NL[y]	−25.389	−98.699	−14.63	−10.22	−6.516	−4.575	−4.575	−98.693	−10.22	−14.63	−20.948	−25.389
AE[z]	−3.40	−97.71	5.95	11.84	18.64	29.04	29.04	−97.44	11.84	5.95	.89	−3.40

[x] Maximum limit
[y] Minimum limit
[z] Average error

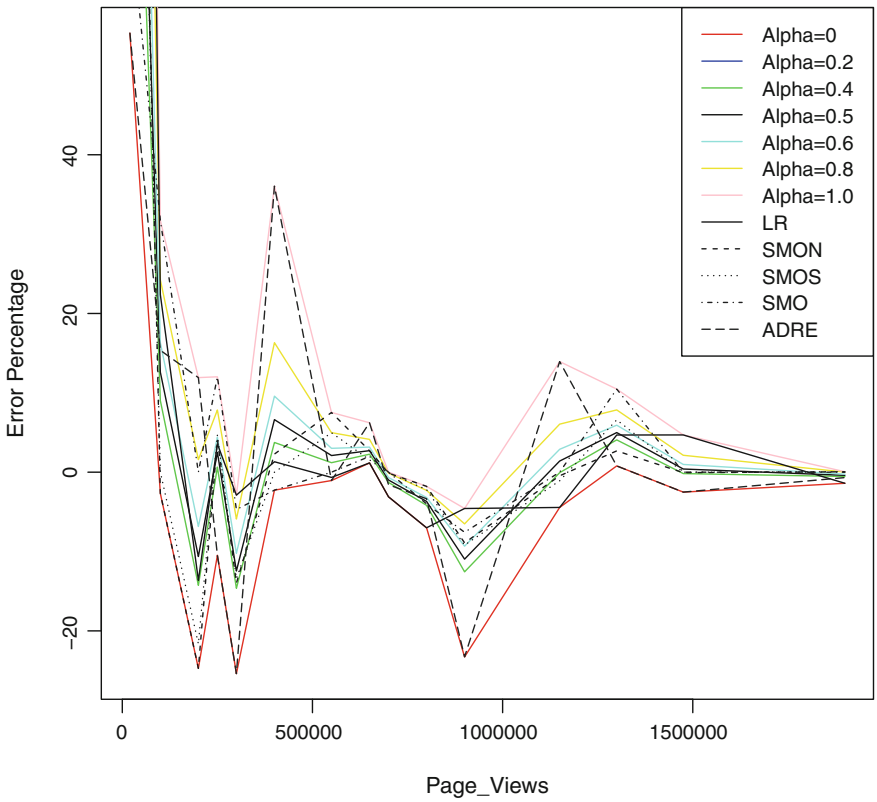

Fig. 2 Comparison of error % varying α

$\alpha = 0.2$, all other values lie very close to the actual and idealistic values and showing an decreasing trend for the error percentage. The most optimized result, using DOWGA operator, is obtained using $\alpha = 0$ and $\alpha = 0.4$. In case of AOWGA operator, optimized result is obtained using $\alpha = 0.8$ and $\alpha = 1.0$. When maximum and minimum limit of error percentage is taken into account, `DOWGA` operator is displaying most suitable range at $\alpha = 0$ while AOWGA operator is displaying it for $\alpha = 1$.

More formally, it can be said (most of the cases) that for `DOWGA` operator and `weights` obtained from `LSOWA` approach:

$$\text{AE} \propto \alpha \tag{10}$$

Similarly, for `AOWGA` operator:

$$\text{AE} \propto \frac{1}{\alpha} \tag{11}$$

where AE = 'average error'.

5 Conclusion and Future Work

In this Paper, variants of OWO operator—decreasing ordered weighted geometric averaging operator (DOWGA) and AOWGA are used for solving a MCDM problem. First, a regression problem into a MCDM problem was formulated and then it was solved with DOWGA operator and AOWGA operator while taking weights from LSOWA approach. As evident from the preceding section, use of these fuzzy averaging operator was able to reduce the outliers in the web data at a significant level for some values of α and for a particular type of weights and the resulting result was more close to the original values. With the result of this pilot case study, this work can be extended to other variants of OWA operators along with different techniques of finding weights. The future work includes the study of effects of using different weights with different operators and its effect on web data as MCDM problem. The future work also plans to propose a formal mathematical model for this integration of OWA operators with regression techniques.

Acknowledgment This work has been partially funded under Grant F.No. 42-134/2013(SR) in the Major Research Project Scheme of University Grant Commission, India.

References

1. Yoon, K.P., Hwang, C.L.: Multiple Attribute Decision Making: An Introduction, vol. 104. Sage Publications, Thousand Oaks (1995)
2. Peng, Y., Kou, G., Wang, G., Shi, Y.: FAMCDM: A fusion approach of MCDM methods to rank multiclass classification algorithms. Omega **39**(6), 677–689 (2011)
3. Yu, X., Xu, Z., Ma, Y.: Prioritized multi-criteria decision making based on the idea of PROMETHEE. Procedia Comput. Sci. **17**, 449–456 (2013)
4. Erkan, T.E., Royendegh, B.D.: Curriculum change parameters determined by multicriteria decision making. In: 5th World Conference on Educational Sciences-WCES 2013
5. Yager, R.R., Rybalov, A.: Full reinforcement operators in aggregation techniques. IEEE Trans. Syst. Man Cybern. Part B Cybern. **28**(6), 757–769 (1998)
6. Velasquez, M., Hester, P.T.: An analysis of multi-criteria decision making methods. Int. J. Oper. Res. **10**, 56–66 (2013)
7. Abdullah, L.: Fuzzy multi criteria decision making and its applications: a brief review of category. Procedia-Soc. Behav. Sci. **97**, 131–136 (2013)
8. Zadeh, L.A.: Outline of a new approach to the analysis of complex systems and decision process. IEEE Trans. Syst. Man Cybern. **3**, 28–44 (1999)
9. Carlsson, C., Fullr, R.: Fuzzy multiple criteria decision making: recent developments. Fuzzy Sets Syst. **78**(2), 139–153 (1996)
10. Zimmermann, H.J.: Fuzzy Set Theory and Its Applications Second, Revised Edition. Kluwer Academic Publishers, Dordrecht (1992)
11. Davey, A., Olson, D., Wallenius, J.: The process of multiattribute decision making: a case study of selecting applicants for a Ph.D. program. Eur. J. Oper. Res. **72**(3), 469–484 (1994)
12. Bordogna, G., Fedrizzi, M., Pasi, G.: A linguistic modeling of consensus in group decision making based on OWA operators. IEEE Trans. Syst. Man Cybern. Part A Syst. Hum. **27**(1), 126132 (1997)

13. Carlsson, C., Fuller, R.: OWA operators for doctoral student selection problem. In: Yager, R. R., Kacprzyk, J. (eds.) The Ordered Weighted Averaging Operators: Theory, Methodology and Applications, pp. 167–178. Kluwer Academic Publishers, Boston (1997)
14. Yager, R.R.: On Ordered weighted averaging aggregation operators in multicriteria decision making. IEEE Trans. Syst. Man Cybern. **18**(1), 183–190 (1988)
15. Smolkov, R., Wachowiak, M.P.: Aggregation operators for selection problems. Fuzzy Sets Syst. **131**(1), 23–34 (2002)
16. Sugeno, M.: Theory of fuzzy integrals and its applications, Ph.D. thesis, Tokyo Institute of Technology, Tokyo (1974)
17. Dubois, D., Fargier, H., Prade, H.: Refinement of the maximin approach to decision making in a fuzzy environment. Fuzzy Sets Syst. **81**, 103–122 (1996)
18. Marichal, J.L.: Aggregation operators for multicriteria decision aid. Ph.D. Dissertation, University De Liege, Liege (1999)
19. Xu, Z.S., Da, Q.L.: The ordered weighted geometric averaging operators. Int. J. Intell. Syst. **17**, 709–716 (2002)
20. Herrera, F., Herrera-Viedma, E.: A study of the origin and uses of the ordered weighted geometric operator in multicriteria decision making. Int. J. Intell. Syst. **18**, 689–707 (2003)
21. Ahn, B.S.: Some remarks on the LSOWA approach for obtaining OWA operator weight. Int. J. Intell. Syst. **24**, 1265–1279 (2009)
22. Hagan, O.: Aggregating template or rule antecedent in real time expert system with fuzzy set logic. In: Proceedings 22nd Annual IEEE Asilomar Conference on Signals, Systems, Computers. Pacific Grove, CA, pp. 81–89 (1988)
23. Fuller, R., Majlender, P.: An analytic approach for obtaining maximal entropy OWA operator weights. Fuzzy Sets Syst. **124**, 53–57 (2001)
24. Han, J., Kamber, M.: Data Mining Concepts and Techniques, 2nd edn. Morgan Kauffman Publisher, Los Altos (2006)
25. Mariscal, G., Marban, O., Fernandez, C.: A survey of data mining and knowledge discovery process models and methodologies. Knowl. Eng. Rev. **25**(2), 137–166 (2010)
26. Kohli, S., Gupta, A.: Analysis of Aggregation operators in regression analysis. In: International Workshop on Machine Learning and Text Analytics, New Delhi, pp. 15–23 (2013)
27. Kohli, S., Gupta, A.: A survey on web information retrieval inside fuzzy framework. In: Proceedings of the Third International Conference on Soft Computing for Problem Solving. Springer, Berlin (2014)
28. Kohli, S., Gupta, A.: Analysis of regression techniques for improved information extraction from real-time industrial dataset. Int. J. Data Min. Emerg. Technol. **3**(2), 51–57 (2013)
29. Yager, R.R., Beliakov, G.: OWA operators in regression problems. IEEE Trans. Fuzzy Syst. **18**, 106–113 (2010)
30. Hall, M., Frank, E., Holmes, G., Pfahringer, B., Reutemann, P., Witten, I.: The WEKA data mining software: an update. SIGKDD Explor. **11**(1), 10–18 (2009)

A Niching Co-swarm Gravitational Search Algorithm for Multi-modal Optimization

Anupam Yadav and Joong Hoon Kim

Abstract In this paper, a Niching co-swarm gravitational search algorithm (CoGSA) is designed for solving multi-modal optimization problems. The collective approach of Gravitational Search Algorithm and differential evolution (DE) is used to solve multi-modal optimization problems. A set of twelve multi-modal problems are taken from a benchmark set of CEC 2013. An experimental study has been performed to evaluate the availability of CoGSA over these twelve problems. The performance is measured in an advanced way. It has been observed that CoGSA provides good solution for multi-modal optimization problems.

Keywords Gravitational search algorithm · Differential evolution · Multi-modal · Optimization

1 Introduction

Optimization is a process of obtaining the optimal solution of an objective function subject to a set of constraints. Mathematically, an optimization problem can be defined as follows:

$$\text{Optimize } F(x), \quad x = [x_1, x_2, x_3, \ldots, x_D], \tag{1}$$

subject to a set of inequality constraints

$$P_j(x) \leq 0, \quad j = 1, 2, 3, \ldots q, \tag{2}$$

A. Yadav (✉) · J.H. Kim
School of Civil, Environmental and Architectural Engineering,
Korea University, Seoul 136-713, South Korea
e-mail: anupuam@gmail.com

K.N. Das et al. (eds.), *Proceedings of Fourth International Conference on Soft Computing for Problem Solving*, Advances in Intelligent Systems and Computing 335,
DOI 10.1007/978-81-322-2217-0_48

as well as equality constraints

$$Q_j(x) = 0, \quad j = q+1, q+2, \ldots m, \tag{3}$$

where $F(x)$ is called the objective function and the constraints are identified with the help of $P_j(x)$ and $Q_j(x)$. Based on the nature of the function $F(x)$, $P_j(x)$, and $Q_j(x)$, the optimization problem can be classified in several ways. Their classifications depend on the characteristics of the functions involved in the problem such as the influence of objective function, the number of variables, nonlinearity of the functions etc. The nature of the function $F(x)$ determines the uni-modal or multi-modal nature of the problem. In the real world, a majority of the problems are multi-modal in characteristics. The multi-modal problems are having more than one global solution and multiple local optima. While solving the multi-modal optimization problems, the main objective of the optimization algorithms is to determine all possible global optima and improve the solution as much as possible. Enormous effort has been made to develop the optimization techniques that can deal with multi-modal optimization problems. The techniques which deal with multi-modal optimization problems are generally referred as niching methods. Many niching methods are proposed in literature such as crowding based differential evolution (DE) [1], CLPSO [2], SHPSO [3], Bi-objective DE [4], distance based PSO [5], and Niching PSO [6]. The scientific community still needs a better solver for multi-modal optimization problems. Because all these methods mentioned here are aimed to solve the low-dimensional multi-modal problems e.g. dimension 2 or 3. So, this could be a strong motivation for developing an efficient optimization algorithm for solving the multi-modal optimization problems on a high scale.

In this article, recently proposed co-swarm gravitational search algorithm (CoGSA) [7] is redesigned for the purpose of obtaining the global optima of multi-modal optimization problems. The efficient performance of CoGSA over some multi-modal optimization problems as discussed by Yadav and Deep [7] inspired to redesign it solely as a niching method. The objective of this algorithm is set to determine the all possible global optima of a multi-modal optimization problem. To judge the suitability of the proposed algorithm, twelve benchmark problems on multi-modal optimization are tested which are recently proposed in CEC 2013 [8]. A set of performance measure is used to discuss the results and the availability of the algorithm.

2 Co-swarm Gravitational Search Algorithm (Co-GSA)

The Co-Swarm Gravitational Search Algorithm [7] is designed by hybridizing the Gravitational Search Algorithm [9] with DE [10]. The main motivation was to use the simultaneous advantages of the GSA as well as DE. The hybridization became more interesting because the working principle of GSA is based on Newton's Laws of motion and the effective force of attraction among the masses, whereas DE works

on the very basic principle of human evolution. The CoGSA follows the following steps, let $(X_1^t, X_2^t, \ldots, X_{ps}^t)$ be the initial population. This population will be processed to both the algorithms separately. The calculated acceleration of the particle from GSA will be utilized to calculate the velocity of the particle in each iteration using Eq. 4. Later on the position of the particle will be updated using the position update Eq. 5

$$V_i^{t+1} = \omega V_i^t + ac_i^t + c * \text{rand}() \times (u_i^t - X_i^t) \tag{4}$$

$$X_i(t+1) = V_i^{t+1} + X_i^t \tag{5}$$

The exhaustive algorithm of the CoGSA is explained in Table 1.

Table 1 The pseudo code of the CoGSA algorithm

Co-Swarm Gravitational Search Algorithm
Step (1) Initialization
Randomly initialize all the particles $(X_1^t, X_2^t, ..., X_{ps}^t)$ in $[X_{min}, X_{max}]^D$.
Initialize velocity $(V_1^t, V_2^t, ..., V_{ps}^t)$
set iteration t=0
While$(t < itermax)$
Step (2) Reproduction and Updation
Evaluate the fitness values $(fit_1^t, fit_2^t, ..., fit_{ps}^t)$ of X.
for $i = 1 : ps$
Mutation
$v_i^t = X_{1i}^t + F(X_{2i}^t - X_{3i}^t)$
Crossover
Evaluate u_i^t using crossover
Apply Gravitational Search Algorithm
$G^t = G^{t_0} \times \exp((-\alpha \frac{iter}{itermax}))$
for $j = 1 : ps$ $F_{ij}^t = G^t \times \frac{M_{pi}^t \times M_{aj}^t}{R_{ij}^t} \times (X_i^t - x_j^t)$
$R_{ij}^t = \|X_i^t, X_j^t\|_2$
end **for**
Calculate acceleration
$ac_i^t = \frac{F_i^t}{M_{ii}^t}$
Step (3) Velocity and position update equation
$V_i^{t+1} = \omega \times V_i^t + ac_i^t + rand() \times (u_i^t - X_i^t)$
$X_i^{t+1} = V_i^{t+1+X_i^t}$
end of **for**
t=t+1
end of **while**

3 Benchmark Functions

- F_1: Five-Uneven-Peak Trap

$$F_1(x) = \begin{cases} 80(2.5 - x), & \text{for } 0 \le x < 2.5, \\ 64(x - 2.5), & \text{for } 2.5 \le x < 5.0, \\ 64(7.5 - x), & \text{for } 5.0 \le x < 7.5, \\ 28(x - 7.5), & \text{for } 7.5 \le x < 12.5, \\ 28(17.5 - x), & \text{for } 12.5 \le x < 17.5, \\ 32(x - 17.5), & \text{for } 17.5 \le x < 22.5, \\ 32(27.5 - x), & \text{for } 22.5 \le x < 27.5, \\ 80(x - 27.5), & \text{for } 27.5 \le x \le 30. \end{cases} \tag{6}$$

  where $x \in [0, 30]$, No. of global optima: 2, No. of local optima: 3.
- F_2: Equal Maxima

$$F_2(x) = \sin^6(5\pi x). \tag{7}$$

  where $x \in [0, 1]$, No. of global optima: 5, No. of local optima: 0.
- F_3: Uneven Decreasing Maxima

$$F_3(x) = \exp\left(-2\log(2)\left(\frac{(x - 0.08)}{0.854}\right)^2\right)\sin^6\left(5\pi\left(x^{3/4} - 0.05\right)\right). \tag{8}$$

  where $x \in [0, 1]$, No. of global optima: 1; No. of local optima: 4
- F_4: Himmelblau

$$F_4(x, y) = 200 - (x^2 + y - 11)^2 - (x + y^2 - 7)^2. \tag{9}$$

  where $x, y \in [-6, 6]$, No. of global optima: 4, No. of local optima: 0.
- F_5: Six-Hump Camel Back

$$F_5(x, y) = -4\left[\left(4 - 2.1x^2 + \frac{x^4}{3}\right)x^2 + xy + \left(4y^2 - 4\right)y^2\right]. \tag{10}$$

  where $x \in [-1.9, 1.9]$; $y \in [-1.1, 1.1]$, No. of global optima: 2, No of local optima: 2.
- F_6: Shubert

$$F_6(x) = -\prod_{i=1}^{D}\sum_{j=1}^{5} j\cos[(j + 1)x_i + j]. \tag{11}$$

  where $x_i \in [-10, 10]^D$, No. of global optima: $D \cdot 3^D$ and multiple local optima.

- F_7: Vincent

$$F_7(x) = \frac{1}{D}\sum_{i=1}^{D} \sin(10\log(x_i)). \tag{12}$$

where $x_i \in [0.25, 10]^D$, No. of global optima: 6^D, No. of local optima: 0.

- F_8: Modified Rastrigin

$$F_8(x) = -\sum_{i=1}^{D}()10 + 9\cos(2\pi k_i x_i). \tag{13}$$

where $x_i \in [0, 1]^D$, No. of global optima: $\prod_{i=1}^{D} k_i$, No. of local minima: 0. functions F_9, F_10, F_11 and F_12 are composition functions of Griewank's function, Weierstrass function, Rastrigin function and sphere function, see in details [8].

4 Determination of All Global Optima

All the functions from F_1 to F_{12} are optimized using CoGSA technique. The target is to discover each global optima of the problem. The success of the algorithm will be based on the maximum number of global optima discovered by it in a course of experiment. To count the number of global optima covered by the algorithm, a sorting method is followed as suggested by Li et al. [8]. The algorithm for counting the number of global optima located by algorithm is presented in Table 2. This table shows the algorithm which will be invoked after each experiment, and it will determine the total number of global optima located. This algorithm takes the input of the final population in a sorted (L_{sorted}) form of their fitness value. A set S is considered which will store the individual global optima discovered during the

Table 2 The algorithm for counting the located global minima

L_{sorted}: A sorted list of the final population in order of their decreasing fitness value.
S: A set of the unique global optima discovered at the end of the experiment.
Set $S = \phi$;
while not reaching the end of L_{sorted};
for all $s \in S$
if $d(s, p) \leq r$ (niching radius)
$L_sorted++$;
else
$S = S \cup \{p\}$;(f(p)=L)
end
end
end

course of experiment. Initially, the set S set to be an empty set. A niching radius (r) is defined which is a minimum distance between all the global optima. If the distance between two solutions is less than r then it will be considered that both the solutions have discovered the same global optima. Finally, the set S has all those solutions which are at a distance more than the niching radius and the cardinality of the set S will give the total number of discovered global optima.

5 Performance Measures

The idea of peak ratio (PR) [8] and success rate (SR) are considered for the measuring the efficiency of the optimization algorithm. The PR measures the average percentage of all known global optima found over multiple runs:

$$\mathrm{PR} = \frac{\sum_{i=1}^{\mathrm{NR}} \mathrm{NPF}_i}{\mathrm{NKP} * \mathrm{NR}} \tag{14}$$

where NR is the total number of runs, NKP is the number of known global optima, and NPF_i is the number of global optima found in the end of the ith run. SR is defined as

$$\mathrm{SR} = \frac{\mathrm{NSR}}{\mathrm{NR}}, \tag{15}$$

SR measures the percentage of successful runs.

6 Experimental Setup

The evaluation of CoGSA is done based on the performance measures discussed in the previous section. The parameter values (Table 3) are considered for evaluation of the PR and SR. Table 4 provides the niching radius for each problem.

Table 3 Parameter values

ω	c	ps	F	CR	$itermax$	NR
0.9	1.49618	30	0.7	1.1	4000	50

Table 4 Niching radius(r) for each function

Function	$F_1(1D)$	$F_2(1D)$	$F_3(1D)$	$F_4(2D)$	$F_5(2D)$	$F_6(3D)$
Niching radius(r)	0.01	0.01	0.01	0.01	0.5	0.5
Function	$F_7(3D)$	$F_8(2D)$	$F_9(2D)$	$F_{10}(2D)$	$F_{11}(10D)$	$F_{12}(10D)$
Niching radius(r)	0.2	0.01	0.01	0.01	0.01	0.01

7 Experimental Results

The results of the experiments are listed in Tables 5 and 6. Both the tables present a comparative analysis of the PR and SR. The results of the CoGSA are compared with the results of GSA [9] and DE [10]. Higher the value of PR shows the good capability of the algorithm to cover all the peaks. Table 6 shows the SR of the algorithm. The SR value '1' shows the algorithm has successfully determined all the peaks in all runs. The results of CoGSA are compared with the results of GSA and DE over five levels of accuracy starting with error tolerance 0.1–0.00001 for both peak ration and SR. It can be observed that the behavior of the algorithms is alike on the accuracy level 0.1 and as we choose a higher level of accuracy the performance of CoGSA is better than GSA and DE in terms of PR and SR.

Table 5 Peak Ratio of the algorithms GSA, DE, and CoGSA with different accuracy levels

Method	F_1	F_2	F_3	F_4	F_5	F_6	F_7	F_8	F_9	F_{10}	F_{11}	F_{12}
Accuracy level: 0.1												
DE	1.00	0.80	1.00	0.25	1.00	0.10	0.11	0.00	0.00	0.25	0.17	0.13
GSA	1.00	0.80	1.00	0.25	1.00	0.10	0.11	0.00	0.00	0.25	0.00	0.00
CoGSA	1.00	1.00	1.00	0.25	1.00	0.90	0.03	0.01	0.00	0.25	0.17	0.13
Accuracy level: 0.01												
DE	1.00	0.40	1.00	0.22	1.00	0.00	0.00	0.00	0.03	0.01	0.02	0.01
GSA	1.00	0.35	1.00	0.21	1.00	0.00	0.00	0.00	0.00	0.00	0.00	0.00
CoGSA	1.00	0.80	1.00	0.25	1.00	0.81	0.03	0.00	0.00	0.25	0.17	0.13
Accuracy level: 0.001												
DE	1.00	0.40	1.00	0.22	1.00	0.00	0.00	0.00	0.03	0.01	0.02	0.01
GSA	1.00	0.35	1.00	0.21	0.75	0.00	0.00	0.00	0.00	0.00	0.00	0.00
CoGSA	1.00	0.40	1.00	0.25	1.00	0.56	0.03	0.00	0.05	0.25	0.17	0.13
Accuracy level: 0.0001												
DE	1.00	0.40	1.00	0.20	1.00	0.00	0.00	0.00	0.00	0.01	0.02	0.01
GSA	1.00	0.35	1.00	0.20	0.70	0.00	0.00	0.00	0.00	0.00	0.00	0.00
CoGSA	1.00	0.40	1.00	0.25	1.00	0.56	0.03	0.00	0.00	0.17	0.17	0.13
Accuracy level: 0.00001												
DE	1.00	0.40	1.00	0.20	1.00	0.00	0.00	0.00	0.00	0.01	0.02	0.01
GSA	1.00	0.30	1.00	0.15	0.10	0.00	0.00	0.00	0.00	0.00	0.00	0.00
CoGSA	1.00	0.40	1.00	0.25	1.00	0.80	0.03	0.00	0.00	0.17	0.17	0.13

Table 6 Success rate of the algorithms GSA, DE, and CoGSA with different accuracy levels

Method	F_1	F_2	F_3	F_4	F_5	F_6	F_7	F_8	F_9	F_{10}	F_{11}	F_{12}
Accuracy level: 0.1												
DE	1.00	0.20	1.00	0.00	1.00	0.00	0.00	0.00	0.00	0.25	0.17	0.13
GSA	1.00	0.20	1.00	0.00	1.00	0.00	0.00	0.00	0.00	0.25	0.00	0.00
CoGSA	1.00	1.00	1.00	0.00	1.00	0.20	0.00	0.00	0.00	0.25	0.17	0.13
Accuracy level: 0.01												
DE	1.00	0.10	1.00	0.00	1.00	0.00	0.00	0.00	0.00	0.01	0.02	0.01
GSA	1.00	0.00	1.00	0.00	1.00	0.00	0.00	0.00	0.00	0.00	0.00	0.00
CoGSA	1.00	0.60	1.00	0.00	1.00	0.20	0.00	0.00	0.00	0.25	0.17	0.13
Accuracy level: 0.001												
DE	1.00	0.00	1.00	0.00	1.00	0.00	0.00	0.00	0.00	0.01	0.02	0.01
GSA	1.00	0.00	1.00	0.00	0.00	0.00	0.00	0.00	0.00	0.00	0.00	0.00
CoGSA	1.00	0.00	1.00	0.00	1.00	0.20	0.00	0.00	0.00	0.25	0.17	0.13
Accuracy level: 0.0001												
DE	1.00	0.00	1.00	0.00	1.00	0.00	0.00	0.00	0.00	0.01	0.02	0.01
GSA	1.00	0.00	1.00	0.00	0.10	0.00	0.00	0.00	0.00	0.00	0.00	0.00
CoGSA	1.00	0.00	1.00	0.00	1.00	0.20	0.00	0.00	0.00	0.17	0.17	0.13
Accuracy level: 0.00001												
DE	1.00	0.00	1.00	0.00	1.00	0.00	0.00	0.00	0.00	0.01	0.02	0.01
GSA	1.00	0.00	1.00	0.00	0.00	0.00	0.00	0.00	0.00	0.00	0.00	0.00
CoGSA	1.00	0.00	1.00	0.00	1.00	0.20	0.00	0.00	0.00	0.17	0.17	0.13

8 Conclusion

In this article, a recently proposed CoGSA algorithm is redesigned to solve multi-modal optimization problems. A recent and advance set of benchmark problems is considered to judge the behavior of the CoGSA. The experimental studies are performed on 12 multi-modal functions with a varied level of difficulties. The results of CoGSA are compared with GSA and DE over two performance measures on different level of accuracies. It is observed that the performance of CoGSA is good over multi-modal functions. The experimental results recommend CoGSA as a good muti-modal optimizer. In future, a more the algorithm can be used for some real life multi-modal optimization problems.

Acknowledgment This work was supported by the National Research Foundation of Korea (NRF) grant funded by the Korean government (MSIP) (No. 2013R1A2A1A01013886).

References

1. Thomsen, R.: Multimodal optimization using crowding-based differential evolution. In: Evolutionary Computation, 2004. CEC2004. Congress on, IEEE, vol. 2, pp. 1382–1389 (2004)
2. Liang, J.J., Qin, A.K., Suganthan, P.N., Baskar, S.: Comprehensive learning particle swarm optimizer for global optimization of multimodal functions. Evol. Comput. IEEE Trans. **10**(3), 281–295 (2006)
3. Yadav, A., Deep, K.: Shrinking hypersphere based trajectory of particles in PSO. Appl. Math. Comput. **220**, 246–267 (2013)
4. Deb, K., Saha, A.: Multimodal optimization using a bi-objective evolutionary algorithm. Evol. Comput. **20**(1), 27–62 (2012)
5. Qu, B.-Y., Suganthan, P.N., Das, S.: A distance-based locally informed particle swarm model for multimodal optimization. IEEE Trans. Evol. Comput. **17**(3), 387–402 (2013)
6. Qu, B.-Y., Liang, J.J., Suganthan, P.N.: Niching particle swarm optimization with local search for multi-modal optimization. Inf. Sci. **197**, 131–143 (2012)
7. Yadav, A., Deep, K.: A novel co-swarm gravitational search algorithm for constrained optimization. In: Proceedings of the Third International Conference on Soft Computing for Problem Solving, pp. 629–640. Springer, Berlin (2014)
8. Li, X., Engelbrecht, A., Epitropakis, M.G.: Benchmark functions for CEC'2013 special session and competition on niching methods for multimodal function optimization. Evolutionary Computation and Machine Learning Group, RMIT University, Melbourne Tech. Rep. (2013)
9. Rashedi, E., Nezamabadi-Pour, H., Saryazdi, S.: GSA: a gravitational search algorithm. Inf. Sci. **179**(13), 2232–2248 (2009)
10. Storn, R., Price, K.: Differential evolution–a simple and efficient heuristic for global optimization over continuous spaces. J. Global Optim. **11**(4), 341–359 (1997)

Comparing Rapid Sort with Some Existing Sorting Algorithms

Heisnam Rohen Singh and Mriganka Sarmah

Abstract Sorting is arranging a collection of elements either in ascending or descending order. There are various applications of sorting algorithm in every field of computer science. Already there exist different sorting algorithms with different complexities. In worst case, the best known complexity is O ($n$log n). We have an algorithm called RAPID SORT and analyzed in detail and also compared with some of the existing algorithm like the Quick Sort, Merge sort, Bubble sort, Insertion sort, and selection sort. This algorithm is much better for closely related datasets. This algorithm is very efficient to sort the elements in reverse order.

Keywords Sorting · Complexity · Worst case · Reverse order

1 Introduction

1.1 Sorting

It is nothing but arranging a collection of elements in a sequence, i.e., either ascending or descending order. There are a lot of applications of sorting where data need to be arranged. For example, the details of the students in a class can be easily analyzed if the student's name can be arranged in alphabetical order or the students are arranged according to their roll number. So, to arrange them, the sorting algorithm can be used. Already there exists lots of sorting algorithm like Quick sort, Merge sort, Insertion sort, and Radix sort.

H.R. Singh (✉) · M. Sarmah
Department of Computer Science and Engineering, Assam Down Town University, Guwahati, India
e-mail: rohenheisnam87@gmail.com

M. Sarmah
e-mail: sarmah_mriganka@rediffmail.com

K.N. Das et al. (eds.), *Proceedings of Fourth International Conference on Soft Computing for Problem Solving*, Advances in Intelligent Systems and Computing 335,
DOI 10.1007/978-81-322-2217-0_49

1.2 Analysis of Algorithm

In order to find which algorithm is better than other, we need to compare these algorithms. To compare, the complexity of these algorithms needs to be calculated.

There are two types of complexity. They are as follows:

Space complexity: It gives the total amount of memory required to perform the algorithm.

Time complexity: It gives the total amount of time required to perform the algorithm.

Nowadays, time complexity is much more important than the space complexity, but there, we have a brief comparison of the space complexity also. Mostly, when we talk about the complexity, we mean time complexity as the memory becomes very cheap. Comparing the amount of time taken by algorithm is a difficult task. One way of comparing is based on the exact running time of all algorithms, but it depends upon processor and language used. Even if the processor and language are same, calculating the exact time is difficult as CPU utilization may be different.

The time complexity is dependent on the number of input. So, it is expressed in terms of number of input or input size. Two algorithms can be compared by using the rate of growth function, $f(n)$ of the algorithms expressed in terms of number of input n. The algorithm with lesser rate of growth function is better than the other. If the rate of growth function is high as the number of input increases, the number of operation also increases.

2 Existing Sorting Algorithm

There are lots of sorting algorithms. Some of the common sorting algorithms are given here.

Bubble sort [1, 2]: In this algorithm, the largest elements are pushed back to one end of the sequence. It compares the two consecutives elements: If the second element is smaller than the first one, the two elements are swapped and the larger element is pushed at back. It continues doing this for each pair of adjacent elements to the end of the dataset. It is continue till no swapping is done.

Insertion sort [3, 4]: This algorithm is just like the technique of arranging cards in card playing. It works by taking elements one by one from the list and inserting them in their correct position into a new sorted sequence.

Selection sort [5, 6]: In this sorting algorithm, the smallest element from list is found and swapped with the first element. The second smallest is swapped from second element. These are repeated until all elements are sorted.

Quick sort [7, 8]: In this algorithm, an element is chosen as pivot element, and in each step, the exact position of the pivot element is found. A pivot partitions the elements into two parts: One part consists of all elements less than the pivot, and the

other consists of all elements greater than pivot. The same step is repeated for each partition.

Merge sort [9, 10]: This algorithm is based on divide and conquer technique. The lists of elements are divided into smaller sorted list. And these small sorted lists are merged into single sorted list.

3 Algorithm

We assume we are sorting an array in ascending order.

Begin
From an Array of n numbers find the *minimum(A)* and *maximum(A).*
insert *minimum(A)* at the beginning and *maximum(A)* at the end.
Set lower_bound=0, upper_bound=Last
/*lower_bound points to the recent most element on left side. upper_bound points to the recent most element on right side*/
Get next_number.
Dist(lb)=abs(minimum(A) - next_number)
Dist(ub)=abs(maximum(A) - next_number)
/*steps : To find out the proximity towards either of the far ends*/
If Dist(lb) <Dist(ub)
Insert *next_number* to the right of *lower_bound*
Else
Insert *next_number* to the left of *upper_bound*
Set tempLB=*lower_bound*, tempUB=*upper_bound*
While (*next_number* < A[tempLB])
/*finding the position of the number in lower half*/
Insertion _Sort(*next_number*, A[tempLB])
tempLB++ /*Resetting the lower_bound*/
While(*next_number* < A[tempUB]
/*finding the position of the number in upper half*/
Insertion_Sort(*next_number* , A[tempUB]))
tempUB-- /*Resetting the upper_bound*/
Repeat for all remaining elements.
End

4 Rapid Sort

In this sorting first, the minimum and maximum elements from the sequence are found and placed in extreme ends of the sequence. These ends are marked as lower bound and upper bound; that is, minimum and maximum elements are put at lower bound and upper bound, respectively.

Consider the following sequence of element.

4	5	12	1	14	7	8	20	6	3

In the above example, the minimum element is 1 and maximum element is 20. So 1 is put in the first mark by lower bound, and the element 20 is put at last, mark as upper bound.

low_bnd upp_bnd

1	5	12	4	14	7	8	3	6	20

The other remaining elements in the sequence are placed alongside *the nearer* extreme end which is calculated by comparing the absolute values of |*minimum—element*| and |*maximum—element*|.

If the element is nearer to the lower bound, the element is put in position (lower_bound + 1) and lower bound is set to the new element position, i.e., (lower_bound + 1); otherwise, the upper bound is set to the new element position (upper_bound − 1).

In the example, the next element is 5 and the element is nearer to the element in lower bound. Hence, the element 5 is placed alongside lower bound. Lower bound is reset to second position.

low_bnd upp_bnd

1	5	12	4	14	7	8	3	6	20

Next element 12 has distance of 11 from minimum and 6 from maximum; hence, it was placed alongside upper bound. The upper_bound is reset to ninth position.

low_bnd upp_bnd

1	5	6	4	14	7	8	3	12	20

Element 6 has distance of 5 from minimum and 12 from maximum; hence, it was placed alongside lower_bound. This number 6 is compared with the element in

lower_bound, i.e., 5. As 6 is larger than 5, the position of 6 is found and lower_bound is reset.

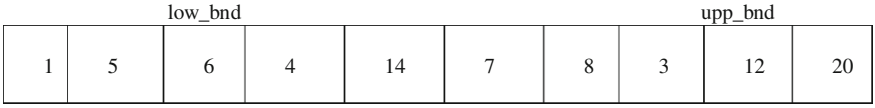

Number 4 has distance of 3 from minimum and 16 from maximum; hence, it was placed along side lower_bound. After that, the exact position of the new element 4 is found by comparing in lower half. lower_bound is reset to next position.

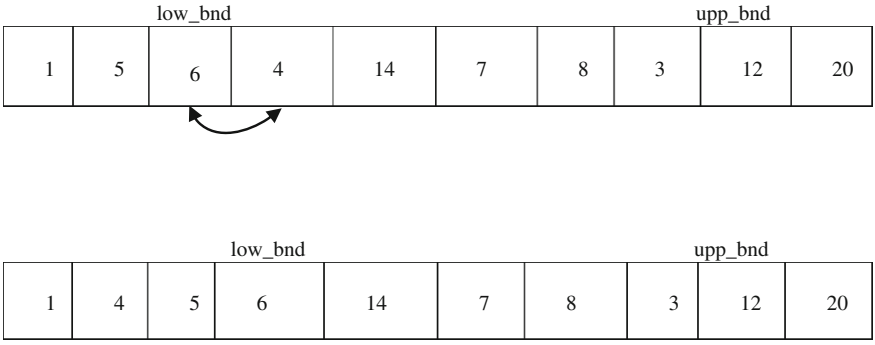

For element 14, place near upper_bound after finding the exact position.

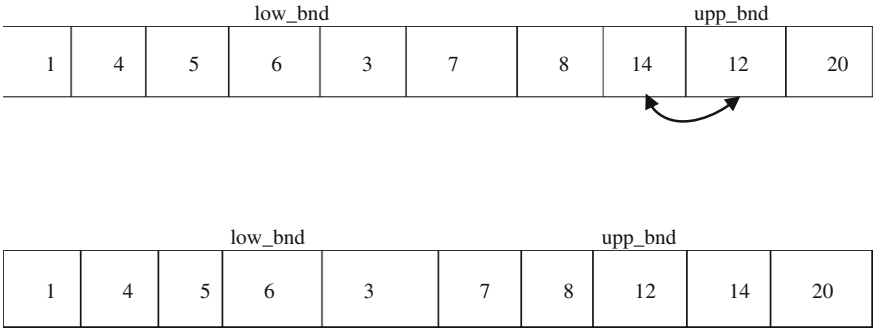

For element 3, the scenario is as shown below.

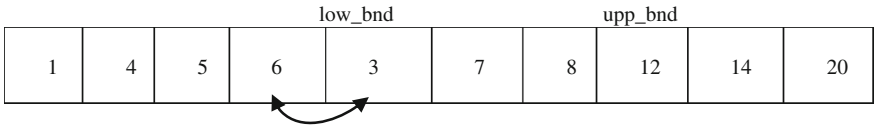

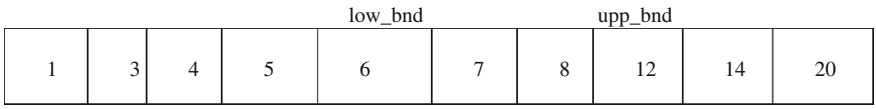

Similarly, for elements 7 and 8, the exact position can be found. And at last, the *lower_bound and upper_bound* will differ by 1 at that moment the operation is stopped.

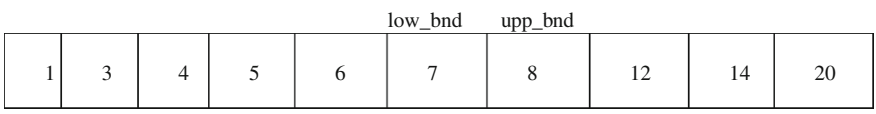

In this algorithm, for each element after finding the nearer end, the exact position needs to be found. To find the position, linear search with order of time $O(n)$ [11, 12] or binary search [13, 14] with order of time $O(\log n)$ can be used. And in positioning, the element shifting of the elements may be involved. To overcome this shifting, different data structure like linked list [15] can be used. In that, shifting can be just changing nearly one link, resulting in a time order of $O(1)$. Our algorithm *The Rapid Sort* can be further improved to be more efficient implementing linked lists. However, for reversing an entire list of closely related data elements, the order of time complexity is $O(n)$. Thus, the worst case may be said to be resulting in $O(n)$ which is speedy.

5 Results and Discussion

The experiment was performed using the linear data structure array. The datasets are generated using the C inbuilt rand() function. This algorithm is compared with the common existing algorithm like bubble sort, insertion sort, quick sort, and merge sort. The complexity of the algorithm depends mostly upon the number of comparisons to do the sorting. So, in this, the numbers of comparison of various

algorithms are compared and are shown in the following figure. This experiment is fully programmed using Turbo C in a Windows 7 platform. The elements were generated using rand() function of the Turbo C library (Figs. 1, 2, 3, 4, 5 and Table 1).

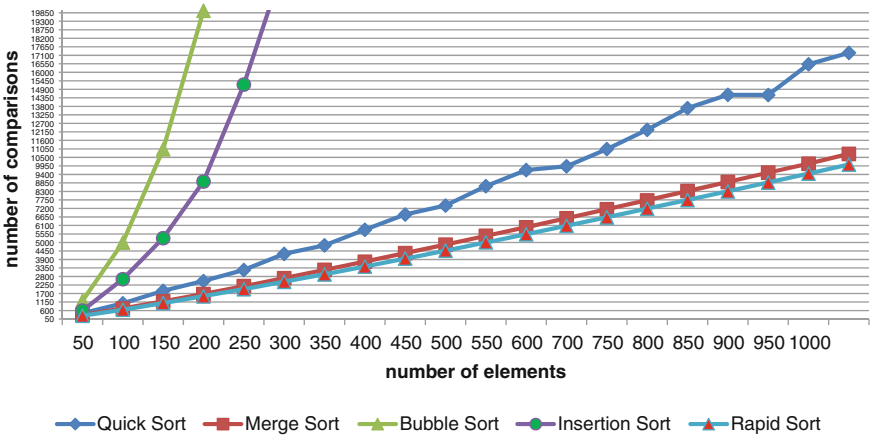

Fig. 1 Number of elements versus number of comparisons

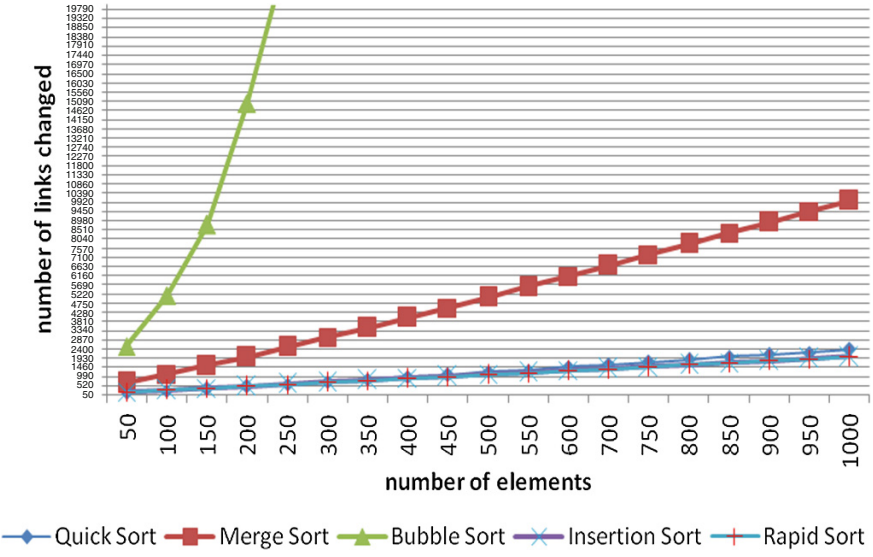

Fig. 2 Number of elements versus number of links exchanged

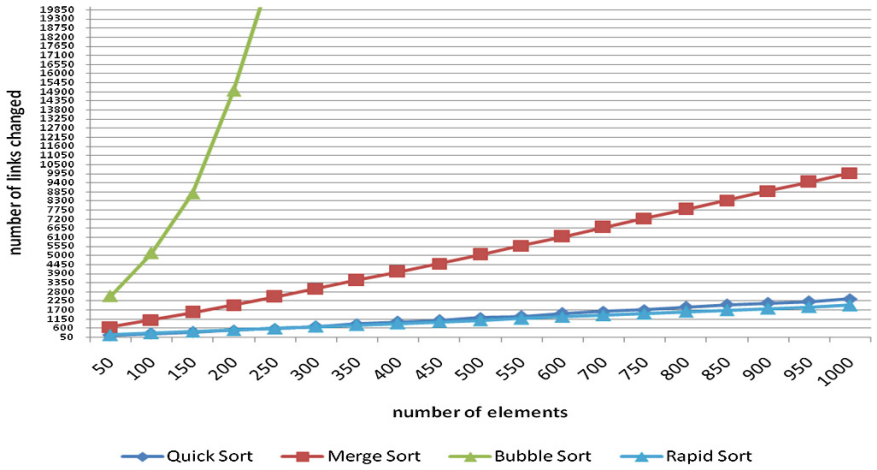

Fig. 3 Number of elements versus number of links exchanged

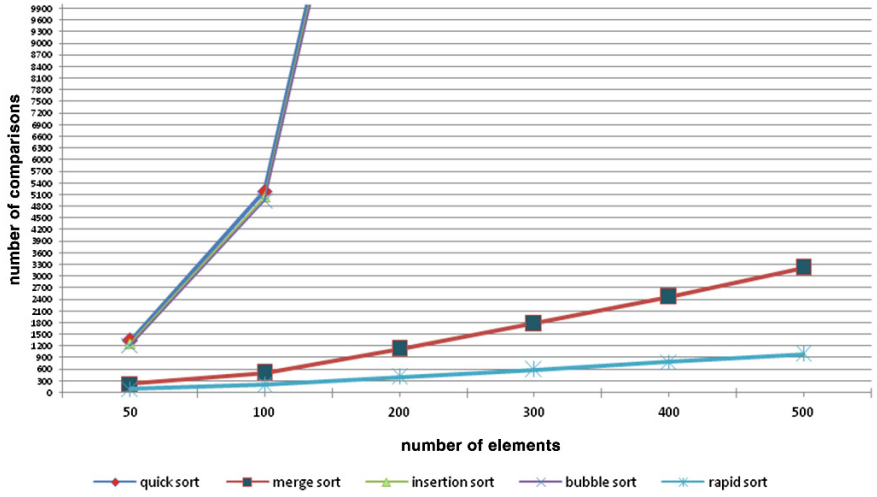

Fig. 4 Number of comparisons to reverse a list of elements

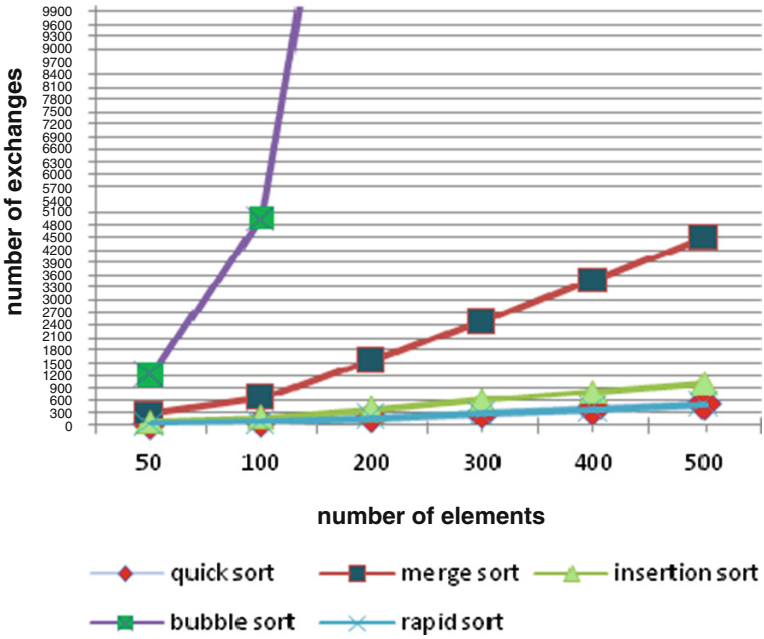

Fig. 5 Number of exchanges to reverse a list of elements

Table 1 Number of link exchanged

Number of elements	Quick sort	Merge sort	Bubble sort	Insertion sort	Rapid sort
50	166	672	2,529	198	183
100	252	1,094	5,129	298	282
150	359	1,544	8,744	398	381
200	469	1,994	14,961	498	481
250	579	2,488	22,704	598	580
300	697	2,988	30,050	698	678
350	845	3,488	39,659	798	777
400	969	3,988	49,172	898	877
450	1,068	4,488	60,747	998	976
500	1,234	5,026	75,150	1,098	1,076
550	1,302	5,576	87,414	1,198	1,175
600	1,484	6,126	105,090	1,298	1,275
700	1,604	6,676	120,655	1,398	1,375
750	1,713	7,226	140,121	1,498	1,475
800	1,859	7,776	160,480	1,598	1,575
850	2,003	8,326	177,045	1,698	1,675
900	2,105	8,876	198,048	1,798	1,775
950	2,205	9,426	223,415	1,898	1,875
1,000	2,366	9,976	248,531	1,998	1,975

6 Conclusion

Based on the experience, charts and graphs are shown above with the number of comparisons and number of link exchanges with the number of inputs for different sorting algorithms. It has been found that our algorithm is better than the existing sorting algorithm as the number of exchanges and comparisons is lesser.

To reverse a list, *Rapid Sort* performs the task faster.

References

1. Langsam, Y., Augenstein, M.J., Tenenbaum, A.M.: Data Structures Using C and C++, pp. 355–358. Pearson Prentice Hall, New Delhi (2007)
2. Astrachan, O.: Bubble sort: an archaeological algorithmic analysis. SIGCSE 2003 Hannan Akhtar. Available at: http://www.cs.duke.edu/~ola/papers/bubble.pdf
3. Robert, S.: Algorithms, (chapter 8, p. 95). Addison-Wesley, MA (1983)
4. Langsam, Y., Augenstein, M.J., Tenenbaum, A.M.: Data Structures Using C and C++, pp. 381–382. Pearson Prentice Hall, New Delhi (2007)
5. Langsam, Y., Augenstein, M.J., Tenenbaum, A.M.: Data Structures Using C and C++, pp. 367–368. Pearson Prentice Hall, New Delhi (2007)
6. Srivastava, S.K., Srivastava, D.: Data Structures Through C in Depth, pp. 421–424. BPB Publication, New York (2011)
7. Cormen, T.H., Leiserson, C.E., Rivest, R.L., Stein, C.: Introduction to Algorithms, 2nd edn., pp. 145–148. PHI
8. Srivastava, S.K., Srivastava, D.: Data Structures Through C in Depth, pp. 358–364. BPB Publication, New York (2007)
9. Horowitz, E, Sahni, S, Rajasekaran, S.: Fundamentals of Computer Algorithms, pp. 159–167. University Press (2009)
10. Srivastava, S.K., Srivastava, D.: Data Structures Through C in Depth, pp. 434–444. BPB Publication, New York (2011)
11. Langsam, Y., Augenstein, M.J., Tenenbaum, A.M.: Data Structures Using C and C++, pp. 403–405. Pearson Prentice Hall, New Delhi (2007)
12. Srivastava, S.K., Srivastava, D.: Data Structures Through C in Depth, pp. 472–473. BPB Publication, New York (2011)
13. Langsam, Y., Augenstein, M.J., Tenenbaum, A.M.: Data Structures Using C and C++, pp. 410–413. Pearson Prentice Hall, New Delhi (2007)
14. Srivastava, S.K., Srivastava, D.: Data Structures Through C in Depth, pp. 473–476. BPB Publication, New York (2011)
15. Langsam, Y., Augenstein, M.J., Tenenbaum, A.M.: Data Structures Using C and C++, pp. 202–207. Pearson Prentice Hall, New Delhi (2007)

An Ensemble Wrapper Feature Selection for Credit Scoring

Waad Bouaguel and Mohamed Limam

Abstract In this paper, we address the problem of credit scoring (CS) as a feature selection problem. More specifically, we use wrapper feature selection methods to identify features that contain the most relevant information to distinguish good loan applicants from bad loan applicants. Wrapper feature selection approaches are widely used to select a small subset of relevant features from a dataset. However, wrappers suffer from the fact that they only use a single classifier in the evaluation process and each classifier is of a different nature and will have its own biases. Hence, this paper investigates the effects of using different classifiers for wrapper feature selection. A new ensemble method for feature selection is then proposed and evaluated on four credit datasets, and results illustrate that combining classifiers improves the performance of scoring models.

Keywords Wrapper · Feature selection · Credit scoring

1 Introduction

Credits' granting is a fundamental question for which every credit institution is confronted and one of the most complex tasks that it has to deal with. The set of decision models and their underlying methods that serve lenders in granting consumer credit are called credit scoring (CS) [1]. The CS task is based on analyzing and judging a large amount of receipts credits' requests. Typically, CS databases are often large and characterized by redundant and irrelevant features. With so many

W. Bouaguel (✉) · M. Limam
LARODEC, ISG, University of Tunis, Tunis, Tunisia
e-mail: bouaguelwaad@mailpost.tn

M. Limam
e-mail: mohamed.limam@isg.rnu.tn

M. Limam
Dhofar University, Salalah, Oman

K.N. Das et al. (eds.), *Proceedings of Fourth International Conference on Soft Computing for Problem Solving*, Advances in Intelligent Systems and Computing 335,
DOI 10.1007/978-81-322-2217-0_50

features, classification methods become more computational demanding. This difficulty can be solved using feature selection methods. This process involves not only a predefined cutoff on the number of features that can be considered when building a credit model, but also the choice of appropriate features based on their relevance to the study [2]. Further, it is often the case that finding the correct subset of predictive features is an important problem in its own right.

Many feature selection methods are proposed in literature such as filter and wrapper methods [3]. Filter methods select the best features by evaluating the fundamental properties of data, making them fast and simple to implement. Wrapper methods select the best features according to the classifier accuracy, making results well matched to the predetermined classification algorithm.

Choosing between filter and wrapper methods is not an easy task, since it depends on numerous factors. Feature selection methods could be compared according to different purposes; for general purpose of irrelevancy removal, filters are good choices as they are unbiased and fast. On the other hand, to improve the classification performance, wrappers should be preferred over filters since they are more appropriate to the classification tasks.

Notice that the main idea of wrapper feature selection is to remove unwanted features from the data by using the predictive accuracy of a particular classifier. It has been shown that wrappers generally outperform filters [4] in terms of accuracy since they are tuned to the specific interactions between the classifier and the dataset. However, wrapper methods have practical and theoretical limitations [5]. Wrappers typically lack generality since the resulting subset of features is tied to the bias of the classifier used in the evaluation function.

Using a single classifier in the wrapper process may favor one candidate subset over the others. In fact, the difference in biases and assumptions of each classifier may influence the final result in term of accuracy and execution time [6]. According to [5], when a classifier used for evaluation is changed, the set of kept features will change, and as a result, different levels of accuracy are obtained, inducing a lack of generality in the produced model. The level of complexity of the classifier is also a fundamental factor to be investigated. In theory, when a complex classifier is used, it may take much longer to choose the best subset of features than a classifier which is considered to be simple. For example, when support vector machines (SVM) is used as an evaluation function in the process of finding the best features subset, it may take more time to identify the most relevant features than using logistic regression (LR) or K-nearest-neighbor (KNN).

The number of classifiers used in the combination framework may also affect the evaluation process. If a small number of classifiers is used, it is likely that we obtain a good set of relevant features given the high level of harmony among classifiers. However, if a high number of classifiers is used, we may end up getting fewer relevant features. This is true to find that the level of agreement between the classifiers will probably be low since more classifiers are required to agree on the relevance of a feature.

Based on the important limitation of using a single classifier, we consider using more than one classifier within wrapper feature selection framework. Consequently, we may notably improve the general accuracy. In fact, we look for mutually approved sets of significant features. Such sets will possibly give higher classification accuracies and reduce the biases of individual classifiers.

This paper is organized as follows. Section 2 describes our proposed approach, which is formed of two parts. In the first part, we perform a primary dimensionality reduction step based on a similarity study. Then in the second part, we discuss the effects of using multiple classifiers in the evaluation process. Experimental investigations and results on four datasets are given in Sect. 3, and finally in Sect. 4, conclusions are drawn.

2 New Approach for Wrapper Feature Selection Combining Multiple Classifiers

In this section, we propose a novel approach for wrapper feature selection. At first, primary dimensionality reduction step is conducted on the original feature space based on similarity study with the prior knowledge. This step is used in order to reduce the search space. The final step is to study the evaluation process of wrapper feature selection and the effect of using multiple classifiers with different and same nature.

2.1 Primary Dimensionality Reduction Step: Similarity Study

The search strategy determines new candidate subsets of features; the learning algorithm has to be applied to each candidate subset in order to produce reliable results. The time used to train the classifier is the dominating factor in terms of computational time [7]. Since the used learning machine is considered a black box, it is not possible to optimize within the classifier without losing generality. Therefore, we aim to minimize the number of classifier evaluation by reducing the number of features which will reduce the number of candidate subsets without a significant increase of the risk of missing important feature subsets.

The first step of our proposed approach is designed specifically to select less redundant features without sacrificing the quality. Redundancy is measured by a similarity measure between a preselected set of features and the remaining features in the dataset. In this step, we enhance an existing set of preselected features by adding additional features that complement the existing set but still with strong predictive power.

In CS, we may already have a set of features preselected with prior information. In fact, experts in banks have years of experience on some particular category of credit and knowledge about which features are more important. This knowledge is generally obtained by years of use of classical feature selection methods. Thus, a

possible improvement of the exhaustive search is to use the prior knowledge and to eliminate redundant features before generating the candidate subsets. Since our goal is to take advantage of any additional information about the feature, we may want to select a set of features complementary to those preselected by bank experts. We study the effect of using prior information on relevant feature complexity.

First, we split the features set in two sets. The first one regroups a set of features that were assumed to be more relevant according to some prior knowledge. The second set contains the remaining ones. Once the two sets are obtained, we conduct a similarity study and a similarity matrix is constructed. In this step, the mutual information (MI) is chosen as a similarity measure given its efficiency. Then, we take each feature from the remaining set and we investigate its level of similarity with the features of the first set. If the similarity is over 80 %, the evaluated feature is eliminated, else it is retained for further examination.

2.2 Evaluation Step: Effects of Using Multiple Classifiers

In this step, we concentrate on the evaluation process. Once all candidate feature's subsets are generated, the chosen learning algorithm is used as evaluation function, choosing the most appropriate classifier depends on many factors as the context of the study. Many classification methods were proposed to deal with the credit worthiness problem on the basis of information from past applicants. The most common statistical methods to evaluate applicants' solvability are LR and discriminant analysis (DA) [8]. Unfortunately, these two methods need some fundamental assumptions on data [9]. In addition to traditional methods, different machine learning and artificial intelligence methods have been used, such as decision trees (DT), artificial neural networks (ANN), and SVM.

Each one of these individual methods produce a single discrimination rule, and each of them has some qualities and restrictions which may influence the feature evaluation process. No one can confirm for sure the superiority of one classifier on another. Rather than to try to optimize the accuracy of one classifier, it is better to integrate multiple classifiers. This approach has been recognized to be successful and achieves better performance and higher precision of predictability in the learning process [10, 11]. Here, the same ensemble concept is adopted in the feature evaluation process as part of the preprocessing course.

The chosen algorithms in this study are representative of the most popular family of classifier models that were selected to form committees of experts, in order to test various classifier combination schemes. Among the most popular classifier models, four were selected, namely DT, SVM, KNN, and ANN. Therefore, this section focuses only on the general aspect of each family. As detail, algorithms are not the main concern of this paper, only conceptual description of the algorithms is given in Table 1.

Two different classifier combination approaches are used within the wrapper evaluation process, namely the same-type approach and the mixed-type approach. The same-type approach combines classifiers from the same family and uses them

Table 1 General properties of some classification algorithms

	Classification algorithms				
		DT	SVM	ANN	KNN
Assumptions	Numeric variables				Yes
	Normally distributed variables				
	Equal covariance matrices				
	Problem of interaction				
	Problem of multicollinearity				
	Normalization of variables		Yes		Yes
	Sensitive to class proportions	Yes		Yes	Yes
Output	Score	Yes		Yes	Yes
	Class	Yes	Yes	Yes	Yes

within the wrapper framework to select the relevant features. For example, classifiers belonging to SVM family are combined together. The mixed-type approach combines classifiers from different families.

The same-type combinations use classifiers from the four different families discussed before. More precisely, two classifiers from DT family, two from ANN family, and one from KNN family is used with two different number of neighbors $K = 1$ and $K = 5$, and one classifier is used from SVM family. The chosen SVM classifier is used with two different kernels, namely the polynomial and radial basis function kernel. In this way, features that are related to both linear aspects and nonlinear aspects can be identified. All considered classifiers are summarized in Table 2.

By using the second arrangement approach, we investigate how classifiers from different families work together and how their interaction affects features' selection. Classifiers are combined using an exhaustive approach so that each classifier is used with every other classifier from a different nature. This leads to the construction of a total of 24 2-classifier mixed-type combinations (see Table 3). In this way, both approaches help us obtain a complete picture of the effects of the nature of classifiers on feature selection.

Traditionally, the approach used to build a multi-classifiers system is to experimentally compare the performance of several classifiers and select the best one. However, many alternative approaches based on combining multiple classifiers have emerged over recent years [12]. There are basically two classifier combination scenarios. In the first, all classifiers use the same representation of the input example. In this case, each classifier, for a given input example, produces an estimate of the same posteriori class probability. In the second scenario, each

Table 2 Summary of used classifiers within each family

DT	ANN	KNN	SVM
J48	Multilayer perceptron (MP)	$K = 1$ (1NN)	Polynomial (SVMP)
Random forest (RF)	Voted perceptron (VP)	$K = 5$ (5NN)	Radial (SVMR)

Table 3 Summary of the possible combination of all classifiers, where the number of classifiers to be combined is two

Possible combinations
(J48 + SVMP), (J48 + SVMR), (J48 + MP), (J48 + VP), (J48 + 1NN),
(J48 + 5NN), (RF + SVMP), (RF + SVMR), (RF + MP), (RF + VP),
(RF +1NN), (RF + 5NN), (SVMP + MP), (SVMP + VP), (SVMP + 1NN),
(SVMP + 5NN), (SVMR + MP), (SVMR + VP), (SVMR + 1NN),
(SVMR + 5NN), (MP + 1NN), (MP + 5NN), (VP + 1NN), (VP + 5NN)

classifier uses its only representation of the input example. For multiple classifiers using distinct representations, many existing schemes can be considered, where all the representations are used jointly to make a decision. We can derive the commonly used classifier combination schemes such as the product rule, average rule, minimum rule, maximum rule, and majority voting schemes.

The simplest and most common way for aggregation is to use a simple arithmetic mean, also known as the average. This operator is interesting because it gives an aggregated value that is smaller than the greatest argument and bigger than the smallest one. Then, the resulting aggregation is "a middle value". This property is known as the compensation property. The minimum and the maximum are also basic aggregation operators. The minimum gives the smallest value of a set, while the maximum gives the greatest one [13]. Majority vote is also a common classifier combination method, particularly used in classifier ensembles when the class labels of the classifiers are crisp [12]. In general, majority voting is a simple method that does not require any parameters to be trained or any additional information for later results.

3 Experimental Investigations

3.1 Datasets Description and Performance Measures

The adopted herein datasets used for evaluation are four real-world datasets: two datasets from the UCI repository of machine learning databases: Australian and German credit datasets (http://archive.ics.uci.edu/ml/datasets.html), a dataset from a Tunisian bank, and the HMEQ dataset. Table 4 displays the characteristics of these datasets.

We considered information retrieval measures for the four datasets when the linear SVM was applied as a classifier on the selected set of features using the ensemble wrapper approach by tenfold cross-validation. The precision, recall, F-measure, and ROC area of feature subsets selected from different combinations are given in Tables 5, 6, 7, and 8, where the best results are shown in bold.

Table 4 Summary of datasets used for evaluating the feature selection methods

Names	Australian	German	HMEQ	Tunisian
Total instances	690	1,000	5,960	2,970
Nominal features	6	13	2	11
Numeric features	8	7	10	11
Total features	14	20	12	22
Number of classes	2	2	2	2

3.2 Results and Discussion for the Same-Type Approach

Looking to the results produced by DT family, we notice that the J48 classifier achieves in most cases the best individual results for the German, HMEQ, and the Tunisian datasets, expect for the Australian dataset where the individual results produced by SVM were slightly better. The good performance of the wrapper using DT classifiers is guided by the nature of this family which is well known for its highly accurate performance on financial data. A closer look at Tables 5, 6, 7, and 8 shows that results are much better within the combination process.

When some DT algorithms adopt local search strategy, others are global optimized algorithms. Then, combing a set of DT algorithms may avoid some of their drawbacks, and the experimental results demonstrate that combination results are more effective than individual ones. As expected, combination schemes have approximately the same performance. The product, minimum and the maximum rules, seems to have the best precision rates, while the average rule and the majority vote rule give the best recall and ROC area for DT family.

Going over the results presented in Tables 5, 6, 7, and 8, we notice some differences among the individual results of polynomial and radial SVM. For the four datasets, we notice that the performance with the radial SVM is slightly better. This result is due to the nature of the two kernels. In general, the polynomial kernel looks for linear characteristics within datasets, while the radial kernel identifies linear and non-linear aspects of the datasets.

Overall, we notice that the same-type combinations with SVM improve the performance, meaning that the selected features within the combination process are more suitable for the CS task. Tables 5, 6, 7, and 8 show how the model performance changes with the different combination rules. We notice that the four performance measures increase with the combination. In fact, majority vote, minimum, and average rule combination give significantly higher ROC area and *F*-measure.

Table 5 Performance comparison of the new wrapper method and the other feature selection methods for the Australian dataset

	Precision	Recall	*F*-Measure	ROC area
	Decision tree			
J48	0.867	0.855	0.855	0.862
RF	0.863	0.851	0.851	0.858
Average	0.782	**0.925**	0.848	0.863
Product	0.864	0.852	0.853	0.859
Maximum	**0.930**	0.794	**0.856**	0.859
Minimum	0.866	0.855	0.855	0.862
Majority vote	0.782	0.922	0.846	**0.865**
	Support vector machine			
SVMP	0.921	0.794	0.853	0.855
SVMR	**0.930**	0.799	**0.860**	0.862
Average	0.787	**0.925**	0.850	**0.864**
Product	0.866	0.855	0.855	0.861
Maximum	0.859	0.848	0.848	0.856
Minimum	0.927	0.794	0.855	0.858
Majority vote	0.781	0.915	0.848	0.857
	Artificial neural network			
MP	0.860	0.849	0.850	0.856
VP	0.859	0.848	0.848	0.855
Average	0.862	0.851	0.851	0.857
Product	0.783	**0.919**	**0.861**	**0.860**
Maximum	0.862	0.851	0.851	0.857
Minimum	0.862	0.851	0.851	0.857
Majority vote	**0.864**	0.853	0.854	0.858
	K-Nearest neighbor			
1NN	**0.865**	0.852	**0.852**	0.860
5NN	0.859	0.848	0.848	0.855
Average	0.812	**0.890**	0.849	0.877
Product	0.811	0.866	0.838	**0.883**
Maximum	0.820	0.880	0.849	0.875
Minimum	0.824	0.823	0.822	0.876
Majority vote	0.853	0.851	0.851	0.882

Tables 5, 6, 7, and 8 show that KNN classifiers give always better results when the size of the dataset does not exceed 1,000 instances as is the case for the German (1,000 instances) and Australian (690 instances) datasets. For these datasets, KNN combinations give higher classification performance than using the combination from other families.

Table 6 Performance comparison of the new wrapper method and the other feature selection methods for the German dataset

	Precision	Recall	*F*-Measure	ROC area
	Decision tree			
J48	0.735	0.750	0.723	**0.635**
RF	0.686	0.716	0.665	0.570
Average	0.740	0.930	0.824	0.583
Product	0.732	0.933	0.820	0.568
Maximum	0.741	0.930	0.825	0.585
Minimum	**0.744**	0.929	**0.826**	0.591
Majority vote	0.740	**0.934**	**0.826**	**0.635**
	Support vector machine			
SVMP	0.490	0.700	0.576	0.500
SVMR	**0.708**	**0.728**	**0.709**	**0.627**
Average	0.695	0.722	0.678	0.583
Product	0.682	0.714	0.664	0.568
Maximum	0.697	0.723	0.680	0.585
Minimum	0.702	0.726	0.685	0.591
Majority vote	0.699	0.724	0.679	0.584
	Artificial neural network			
MP	0.719	0.738	0.717	0.634
VP	0.703	0.726	0.701	0.614
Average	**0.769**	0.896	0.827	0.634
Product	**0.769**	0.894	0.825	**0.645**
Maximum	0.758	0.894	0.820	0.643
Minimum	0.717	0.737	0.712	0.625
Majority vote	0.764	**0.904**	**0.828**	0.625
	K-Nearest neighbor			
1NN	0.699	0.724	0.677	0.582
5NN	0.691	0.718	0.688	0.598
Average	0.745	0.917	0.822	0.592
Product	0.739	**0.937**	**0.826**	**0.601**
Maximum	**0.749**	0.899	0.817	0.597
Minimum	0.745	0.917	0.822	0.592
Majority vote	0.742	0.914	0.819	0.587

From Tables 5, 6, 7, and 8, we notice that as with the combination from other classifier families, the final result has improved using ANN combinations. ANN classifiers are made out of neurons and are excellent to extract information from a

Table 7 Performance comparison of the new wrapper method and the other feature selection methods for the HMEQ dataset

	Precision	Recall	*F*-Measure	ROC area
	Decision tree			
J48	0.859	0.864	0.844	0.795
RF	0.857	0.860	0.838	0.785
Average	0.867	0.982	**0.921**	0.793
Product	0.863	**0.983**	0.918	0.787
Maximum	**0.914**	0.899	0.906	**0.809**
Minimum	0.855	0.852	0.853	0.806
Majority vote	0.868	0.979	0.920	0.797
	Support vector machine			
SVMP	0.633	0.796	0.705	0.555
SVMR	**0.843**	0.804	0.724	0.619
Average	0.827	0.977	0.896	0.701
Product	0.809	0.815	0.759	0.662
Maximum	0.816	0.822	0.774	0.683
Minimum	0.800	0.819	0.778	**0.691**
Majority vote	0.824	**0.987**	**0.898**	0.682
	Artificial neural network			
MP	0.693	0.638	0.664	0.677
VP	0.81	0.827	0.789	0.607
Average	0.868	0.871	0.869	0.877
Product	0.835	**0.977**	**0.902**	0.602
Maximum	0.811	0.829	0.793	0.734
Minimum	0.838	0.974	0.901	0.732
Majority vote	**0.911**	0.930	0.920	**0.879**
	K-Nearest neighbor			
1NN	0.852	0.837	0.791	0.803
5NN	0.837	0.824	0.766	0.812
Average	0.821	**0.998**	0.901	**0.891**
Product	0.850	0.825	0.766	0.881
Maximum	**0.889**	0.997	**0.940**	0.889
Minimum	0.821	0.996	0.900	0.842
Majority vote	0.832	0.996	0.907	0.844

dataset. During the training process, ANN can be used to map an input to desired output, classify data or learn patterns. Hence, ANN can also be used to perform indirectly feature selection.

Table 8 Performance comparison of the new wrapper method and the other feature selection methods for the Tunisian dataset

	Precision	Recall	*F*-Measure	ROC area
	Decision tree			
J48	0.722	0.850	0.781	0.597
RF	0.797	0.846	0.801	**0.695**
Average	0.858	0.985	0.917	0.652
Product	0.859	0.985	0.918	0.655
Maximum	**0.866**	0.985	**0.921**	0.653
Minimum	0.861	**0.986**	0.919	0.644
Majority vote	0.858	0.987	0.917	0.649
	Support vector machine			
SVMP	0.722	0.850	0.781	0.500
SVMR	0.797	0.837	0.805	0.566
Average	**0.861**	0.962	0.909	**0.666**
Product	0.710	0.842	0.770	0.500
Maximum	0.860	**0.968**	**0.911**	0.563
Minimum	0.798	0.839	0.803	0.661
Majority vote	0.859	**0.968**	0.910	0.656
	Artificial neural network			
MP	0.802	0.843	0.800	0.577
VP	0.826	0.857	0.816	0.562
Average	0.856	0.979	0.913	0.677
Product	0.865	**0.984**	**0.921**	0.659
Maximum	0.867	0.975	0.918	0.668
Minimum	**0.888**	0.855	0.871	**0.731**
Majority vote	0.866	0.981	0.920	0.657
	K-Nearest neighbor			
1NN	0.785	0.843	0.794	0.680
5NN	0.792	0.844	0.800	0.685
Average	0.855	0.977	0.912	**0.775**
Product	0.852	0.993	0.917	0.756
Maximum	0.864	0.925	0.893	0.746
Minimum	0.863	0.932	0.896	0.704
Majority vote	**0.866**	**0.985**	**0.921**	0.753

3.3 Results and Discussion for the Mixed-Type Approach

Because of the large number of combinations, the mixed-type approach is examined using the Australian dataset and results are summarized in Table 9. Table 9 gives the following:

- The measured F-measure for the features generated by different combinations
- The mean number of evaluated subsets, that is, the first number between the parentheses in the table, and the associated mean number of selected features, that is, the second number between the parentheses.

Table 9 shows that combining DT classifiers with ANN or KNN classifiers generally yields the lowest *F*-measure (RF + MP, RF + VP, RF + 5NN, J48 + 1NN), and this is due to the difference in nature between these three types of classifiers. Actually, ANN classifiers identify relationships between features based on the available prior knowledge about the actual features in the dataset. However, KNN classifiers select the most relevant features with the closest distance to a set of specified features called neighbors. For this family, the resulting features depend of the number of chosen neighbors. DT classifiers nature is very dissimilar to the nature of ANN and KNN. In fact, they use a statistical measure to evaluate the relevance of features.

Results of Sect. 3.2 show that when the same-type arrangement approach is used, DT classifiers give nearly the best results. Table 9 shows that it is not the case when classifiers from this family are combined with classifiers from other families.

Table 9 Total number of evaluated subsets and selected features by 2-classifier mixed-type combinations and associated *F*-measure rates for the Australian dataset

Lowest *F*-measure lies between 0.847 and 0.855	Intermediate *F*-measure lies between 0.856 and 0.859	Highest *F*-measure lies between 0.860 and 0.874
j48 + 1NN (79, 3)	J48 + SVMP(106, 4)	J48 + MP(116, 7)
RF + SVMR(82, 2)	J48 + SVMR(106, 4)	RF + SVMP(79, 3)
RF + MP(111, 6)	J48 + VP(120, 7)	RF + 1NN(96, 4)
RF + VP(104, 5)	j48 + 5NN(105, 4)	SVMP + VP(88, 4)
RF + 5NN(96, 4)	SVMP + MP(112, 5)	SVMP + 1NN(79, 3)
SVMP + 5NN(116, 6)	SVMR + MP(112, 7)	MP + 5NN(121, 7)
SVMR + 1NN(79, 3)	SVMR + VP(116, 7)	VP + 5NN(117, 7)
SVMR + 5NN(127, 9)		
MP + 1NN(107,6)		
VP + 1NN(127,6)		

4 Conclusion

In this study, we developed an ensemble wrapper feature selection approach for a CS application. The proposed approach is composed of two stages. In the first one, we performed a dimensionality reduction using bank experts' knowledge on features where we eliminate redundant features before generating the candidate subsets. In the second stage, the generated subsets were evaluated using a multi-classifiers process involving two arrangement approaches, namely the same-type and mixed-type approach. From the two stages, we show that the use of prior information on relevant features effectively induces a significant gain in complexity with improved generalization. Also, we have shown that the nature of classifiers has an important effect on wrapper feature selection results. While this paper offers a promising take on wrapper approach, there are still improvement possibilities that need to be discussed as the role of number of classifiers in the ensemble feature selection.

References

1. Zhang, D., Zhou, X., Leung, S.C.H., Zheng, J.: Vertical bagging decision trees model for credit scoring. Expert Syst. Appl. **37**, 7838–7843 (2010)
2. Fernandez, G.: Statistical Data Mining Using SAS Applications. Chapman & Hall/CRC, London. Data Mining and Knowledge Discovery. Taylor and Francis, London (2010)
3. Rodriguez, I., Huerta, R., Elkan, C., Cruz, C.S.: Quadratic programming feature selection. J. Mach. Learn. Res. **11**, 1491–1516 (2010)
4. Liu, Y., Schumann, M.: Data mining feature selection for credit scoring models. J. Oper. Res. Soc. **56**, 1099–1108 (2005)
5. Chrysostomou, K.A.: The role of classifiers in feature selection: number vs nature. Ph.D. thesis, School of Information Systems, Computing and Mathematics, Brunel University (2008)
6. Chrysostomou, K., Chen, S.Y., Liu, X.: Combining multiple classifiers for wrapper feature selection. Int. J. Data Min. Modell. Manage. **1**, 91–102 (2008)
7. Schaffernicht, E., Stephan, V., Groß, H.M.: An efficient search strategy for feature selection using chow-liu trees. In: Proceedings of the 17th International Conference on Artificial Neural Networks. ICANN'07, Springer, Berlin, pp. 190–199 (2007)
8. Paleologo, G., Elisseeff, A., Antonini, G.: Subagging for credit scoring models. Eur. J. Oper. Res. **201**, 490–499 (2010)
9. Šušteršič, M., Mramor, D., Zupan, J.: Consumer credit scoring models with limited data. Expert Syst. Appl. **36**, 4736–4744 (2009)
10. Hsieh, N.C., Hung, L.P.: A data driven ensemble classifier for credit scoring analysis. Expert Syst. Appl. **37**, 534–545 (2010)
11. Chen, F.L., Li, F.C.: Combination of feature selection approaches with svm in credit scoring. Expert Syst. Appl. **37**, 4902–4909 (2010)
12. Kuncheva, L.I., Bezdek, J.C., Duin, P.W.: Decision templates for multiple classifier fusion: an experimental comparison. Pattern Recogn. **34**, 299–314 (2001)
13. Kittler, J.: Combining classifiers: a theoretical framework. Pattern Anal. Appl. **1**, 18–27 (1998)

Author Index

K.N. Das et al. (eds.), *Proceedings of Fourth International Conference on Soft Computing for Problem Solving*, Advances in Intelligent Systems and Computing 335,
DOI 10.1007/978-81-322-2217-0